

AD-A286 481

ISBN 0-805-0422-0



Volume 105 Number 6 December 1993

DTIC
ELECTED
NOV 1 4 1994
S G D

Special Issue on
Solar Energy and
Applied Photochemistry

Chemical Sciences

Proceedings of the Indian Academy of Sciences

Chemical Sciences

Editor

V Krishnan

Indian Institute of Science, Bangalore

Associate Editor

S Chandrasekaran

Indian Institute of Science, Bangalore

Editorial Board

- J C Chandrasekhar (*Indian Institute of Science, Bangalore*)
N Chandrasekhar (*University College, St. George's Hospital, Madras*)
M K Chaudhuri (*North Eastern Hill University, Shillong*)
M Chowdhury (*Indian Institute of Technology, Kanpur*)
B M Deb (*Indian Institute of Technology, Kharagpur*)
G R Deshpande (*University of Mumbai, Mumbai*)
K N Ganesh (*University College, St. George's Hospital, Madras*)
A K Lal (*Indian Institute of Technology, Kharagpur*)
J P Mittal (*Indian Institute of Technology, Kharagpur*)
A S N Murthy (*Indian Institute of Technology, Kharagpur*)
V N R Pillai (*Maulana Azad National Urdu University, Hyderabad*)
C N R Rao (*Indian Institute of Science, Bangalore*)
S Ramakrishnan (*Indian Institute of Technology, Madras*)
N Satyamurthy (*Indian Institute of Technology, Kharagpur*)
R P Sharma (*Indian Institute of Technology, Kharagpur*)

Editor of Publications of the Academy

C N R Rao

Indian Institute of Science, Bangalore

Subscription Rates

For 1981 volume

All countries except India	Rs 100	Rs 100	Rs 100
Postage: India, Airmail: All countries	Rs 100	Rs 100	Rs 100
India	Rs 100	Rs 100	Rs 100

All correspondence regarding editorial matters should be addressed to the **Editor**, **Chemical Sciences Department**, **Indian Institute of Science**, **Bangalore 560012**.

The Corrections

Editorial Office

Indian Academy of Sciences, **15, Bengaluru Road**
Postbox number 2852, **560001**
Bangalore 560012

*Telephone: 222111-14-16-18
Telex: 346-111-121-15
Telex: 346-111-121-16*

© 1981 by the Indian Academy of Sciences. All rights reserved.

Notes: - The papers in all parts are presented in the one issue of every volume.

DRAFT SF 298

1. Report Date (dd-mm-yy) 01-12-93	2. Report Type Proceedings	3. Dates covered (from... to) 6-11 January 1993		
4. Title & subtitle Second International Conference on Solar Energy Storage and Applied Photochemistry			5a. Contract or Grant # N00014-93-J-3007	
			5b. Program Element #	
6. Author(s) V. Krishnan, editor			5c. Project # 8202	
			5d. Task # EUR	
			5e. Work Unit #	
7. Performing Organization Name & Address Ain Shams University, Abbasia Department of Chemistry Faculty of Science Cairo, Egypt		8. Performing Organization Report #		
9. Sponsoring/Monitoring Agency Name & Address Office of Naval Research Europe PSC 802 BOX 39 FPO AE 09499-0700		10. Monitor Acronym ONREUR		
		11. Monitor Report #		
12 Distribution/Availability Statement A				
13 Supplementary Notes				
14 Abstract This issue brings together papers presented at the Second International Conference on "Solar Energy Storage and Applied Photochemistry" held at Cairo in January 1993. The topics covered by the many papers are of importance in solar energy conversion, storage and photochemical applications.				
15 Subject Terms solar energy storage, applied photochemistry				
16. Report Classification UNCLASS			17. Abstract Classification UNCLASS	18. This Page UNCLASS
19. Limitation of Abstract Unlimited	20. # of Pages 421	21. Responsible Person (Name and Telephone #) Mike Shear, 011-44-71-514-4921		

Editor's Note

This issue brings together papers presented at the Second International Conference on "Solar Energy Storage and Applied Photochemistry" held at Cairo in January 1993. The topics covered by the many papers are of importance in solar energy conversion, storage and photochemical applications. Special thanks are due to M A El Sayed and M S A Abdel Mottaleb for editing the manuscripts for publication.

V KRISHNAN

Accession For	
NTIS	CRA&I
DTIC	TAB
Unannounced	
Justification	
By _____	
Distribution:/	
Availability Codes	
Dist	Avail and/or Special
A-1	

CSK
94-34960



DTIC QUALITY INSPECTED 6

94 11 0 141

Solar Energy and Applied Photochemistry

Foreword

This volume contains papers based on lectures delivered at the Second International Conference on Solar Energy Storage and Applied Photochemistry which was held in Cairo, January 6-11, 1993. The conference was hosted by Ain Shams University (ASU) under the auspices of President Mubarak.

The development and application of chemical reactions occurs across and between scientific disciplines and photoinduced chemical processes are no exception. Thus conferences concerned with photochemistry attract a range of contributions from several scientific disciplines. The common goal is to understand and use photochemically induced molecular changes. The breadth of the scientific interests represented in this conference was considerable, reflecting the fact that solar energy storage and its conversion have many facets including photovoltaic processes, semiconductor-driven chemical devices, waste water treatment, fuel generation and the synthesis of compounds using near ultraviolet or visible radiation.

The conference attracted one hundred foreign photoscientists in different disciplines from twenty-four countries who are dedicated to the task of utilising solar energy in one way or another. This conference enabled many young Egyptian scientists to interact with international experts and thereby helped in establishing new national photochemical activities.

It is a great pleasure to thank the authorities of Ain Shams University and the Faculty of Science and all colleagues in the Department of Chemistry (the host institution). We also wish to acknowledge all those whose sincere advice and fund raising have contributed to making this conference a tremendous success. We wish to acknowledge, in particular, the assistance received from the Ministry of International Cooperation, Ministry of Petroleum & Mineral Resources, Ministry of Education and Ministry of Scientific Research, Supreme Council of Universities, International Center for Science and High Technology (ICS/IIC/ICTP), Trieste, Italy and the European Office of the US Naval Research.

SABRY ABDEL-MOTTALEB (Ain Shams University)
MOSTAFA EL-SAYED (University of California at Los Angeles)

Strategies for solar fuel generation

HELmut TRIBUTSCH

Hahn-Meitner-Institut, Dept. Solare Energetik, D-14109 Berlin, Germany

Abstract. Solar production and use of fuels (hydrogen, reduced carbon compounds) is an integral part of any large scale solar energy strategy. Technically, the most promising pattern of implementation is the decentralised generation of photovoltaic energy on buildings, interconnection with the public electricity grid and centralized electrolytic generation of fuels. A complementary strategy could be solar electrochemical generation of simple inorganic energy carriers (e.g. Fe^{2+} from Fe^{3+}) which serve as the energy source for bacteria (e.g. *Thiobacillus ferrooxidans*), which fix carbon dioxide via the Calvin cycle. Direct photoelectrochemical generation of solar fuels (in analogy to photosynthesis) is a complex frontier with many unsolved problems, some of which are discussed. The most promising route appears to be development of photoactive transition metal electrocatalysts, which are able to induce interfacial coordination chemical mechanisms. In addition, it may be necessary to develop far-from-equilibrium electrochemical mechanisms to facilitate cooperative electron transfer processes during photocatalysis.

At the long term, solar fuel generation may gradually become economical with increasing consideration of social and environmental costs in the price of fossil energy.

Keywords. Solar fuel generation, photovoltaic energy, centralized electrolytic generation, solar electrochemical generation

1. Natural and artificial photosynthesis

The generation of energy-rich chemical compounds, by solar-driven mechanisms in photosynthesis, is the basis for higher forms of life on earth and a model for artificial attempts to produce solar fuels. The photosynthetic process itself is composed of several steps. They include harvesting of light through light-scattering processes and non-imaging optical light concentration, non-radiative energy transfer within assemblies of chlorophyll molecules and the supply of excitation energy to photosynthetic reaction centers. The excited state produces a sensitization-type of electron injection into the electron-transfer chain and electron transfer across the photosynthetic membrane. This electron transport leads to the generation of reduced energy-carrying chemical species (NADPH) and simultaneously also to a proton transfer across the membrane in the opposite direction. The illuminated photosynthetic membrane thus not only produces photoinduced currents and potentials but also behaves like a combined electron- and ion-conductor able to undergo topotactic redox reactions. This means that illumination leads to the insertion and transport of ions. The proton gradient produced between the inside and the outside of the photosynthetic membrane stores energy which is used to drive a proton current across a reversible ATPase which leads to the synthesis of ATP from ADP. The energy-rich compounds ATP and NADPH are then used to fix carbon dioxide for the production of carbon

compounds as a source of energy and materials. The basis of photoinduced electron transport is the transfer of electrons from water to NADP^+ . This photoinduced water-splitting mechanism leading to the liberation of molecular oxygen and to the formation of the hydrogen species bound to an energy-carrying molecule is the key solar energy conversion process on earth. Life only became possible through evolution of an efficient photocatalytic center for oxygen evolution from water. To evolve one molecule of molecular oxygen four electrons have to be transferred from water. Since radical intermediates have to be avoided for energetic reasons, all four electrons have to be transferred close to the thermodynamic redox potential of $E_0 = 1.23 \text{ V}$ (NHE). This is only possible in a highly specialized molecular enzymatic complex, which controls intermediates in an extremely precise way. The water-oxidizing manganese complex in photosynthesis contains two pairs of manganese centers in close proximity. Its exact structure and function is not yet known.

Experimentally, and with synthetic and typically inorganic materials, most elementary steps occurring in photosynthetic membranes can be qualitatively reproduced (Tributsch 1990). They include radiationless energy transfer between dye assemblies, electron injection through sensitization (into oxide semiconductors), conversion of light into electrochemical energy (with semiconductors), photogeneration of reduced species (at semiconductor electrodes), photoinduced ion insertion and transport (at combined

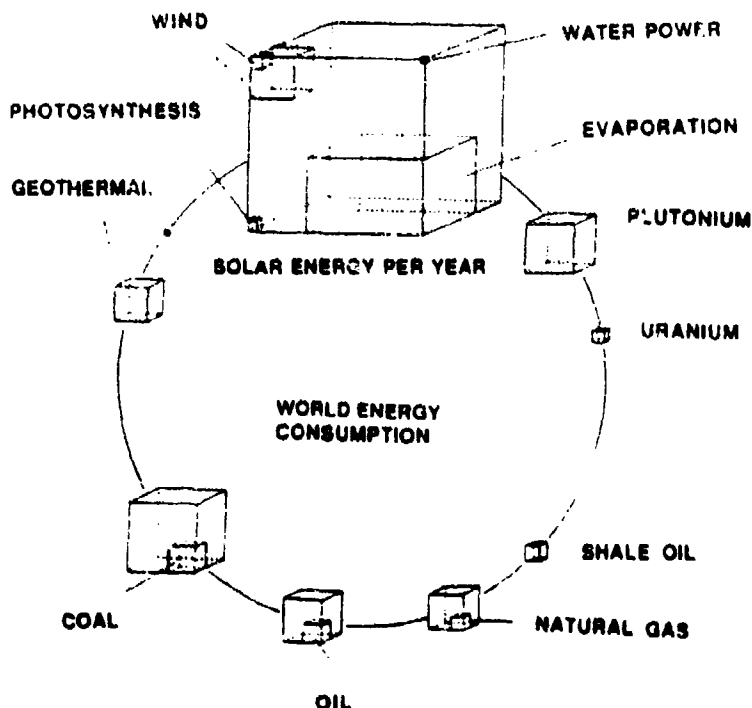


Figure 1. Cubes compare total energy available from different sources with solar energy incident on earth during one year. At the center is shown the world energy consumption.

semiconducting electron- and ion-conducting materials) as well as photocatalysis of oxygen evolution from water (which up to now is energetically not yet efficient).

The key reason why we cannot yet reproduce photosynthesis artificially for technical applications is our inability to produce stable solid-liquid junctions and to provide complicated photoactive materials at reasonable prices. Since self-organization mechanisms and highly complex bioorganic reactions are not yet technically accessible for artificial photosynthesis, simpler technical pathways must be developed. Key elements are inorganic materials, which are thermodynamically and kinetically stable under illumination and polarization. Since cheap and efficient complex-organic catalysts are not available, highly catalytic metals, deposited on semiconductors, must be considered for fuel generation. This means that our inability to deal properly with the complexity and instability of organic molecules and materials forces us to adopt strategies in which the principles of energy conversion are equivalent to the biological ones but the materials are very different. In addition, technical applications aim at much higher energy conversion efficiencies than biological systems, which typically do not specialize in energy conversion but simultaneously also optimize other functions. There is no doubt that large-scale utilization of solar energy is an attractive and reasonable long-term option for mankind. Figure 1 shows that the solar energy incident on earth during one year exceeds the total energy available from all other energy forms, including fossil and nuclear energy via plutonium breeding.

2. Efficiency considerations

The most efficient green plants (C₄-plants like sugarcane or corn) produce, during their most productive season, biomass with a solar energy efficiency of 2-4%. Averaged over a farming year, however, not more than 0.5% solar energy efficiency can be expected. As plants also consume energy for their living processes, the real energy conversion efficiency could be higher by a factor of two. Since a mechanism leading to energy storage always consumes energy, the primary energy conversion efficiency in the most efficient plants may reach 10% in the most efficient season.

From thermodynamic calculations we know that photon-absorbing materials may produce a solar energy conversion efficiency of up to 31%, depending on their band gap or absorption gap (figure 2). The best evidence that this can reasonably well be approached is given by the highly developed electronic materials silicon and gallium arsenide. Solar energy conversion devices made of silicon with its energy gap of $E_g = 1.1\text{ eV}$ may have a theoretical energy conversion efficiency limit of 27%, while 24% has been achieved in the laboratory. Gallium arsenide solar cells with an energy gap of approximately $E_g = 1.5\text{ eV}$ have a theoretical energy conversion efficiency of close to 30%, while 27% has been reached in the laboratory. Several solar energy absorbing materials arranged into a cascade reach theoretical solar energy conversion efficiencies beyond 50%, which suggests that at the long term practical solar energy conversion efficiencies of the order of 40% may be expected.

Energy is always lost during energy storage in chemicals such as hydrogen. However, for water photoelectrolysis with a tandem solar cell, a theoretical energy conversion efficiency of 27% and a practical one of 20% have been estimated (Bolton *et al* 1985). This means, that well-developed technical solar energy systems for the production of chemical energy could become more efficient by a factor of 40 than agricultural

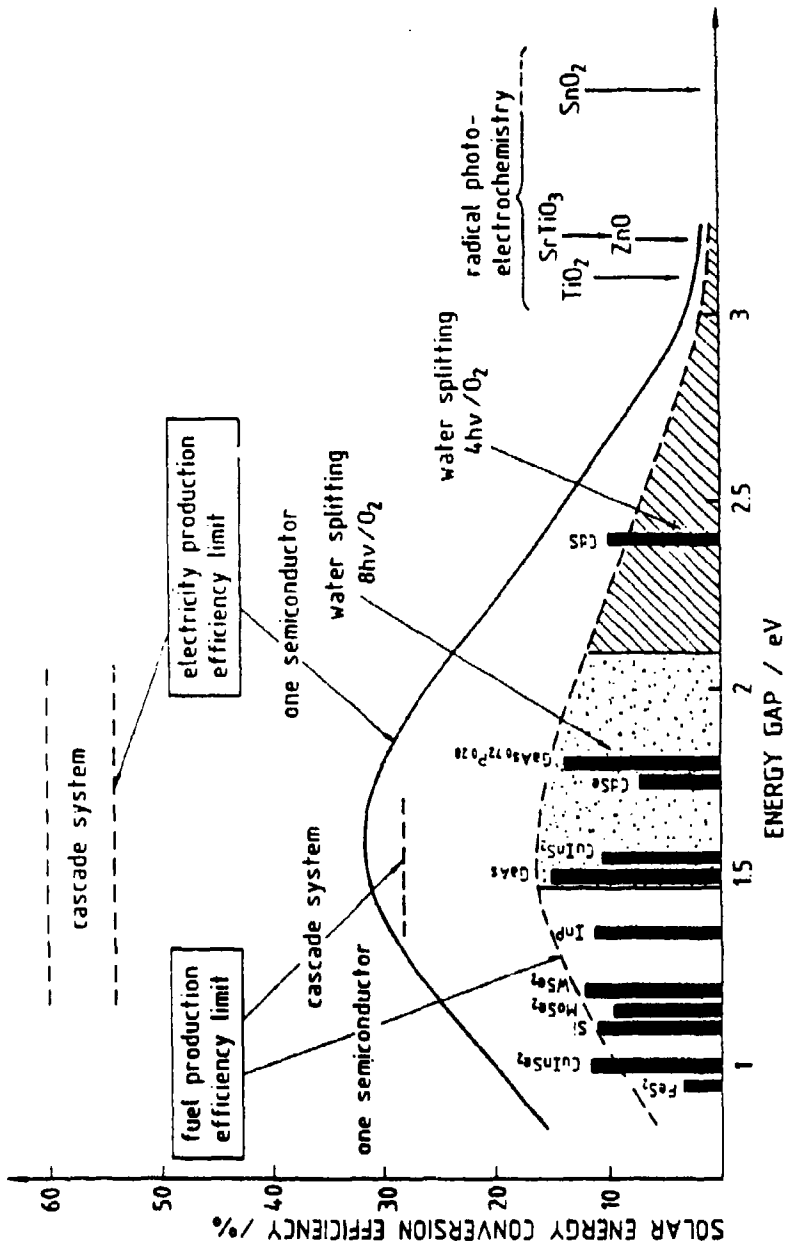


Figure 2. Thermodynamic solar energy conversion efficiencies for photoactive materials (dependent on the energy gap) and of materials arranged in a cascade. In addition, the approximate efficiency limits for solar fuel production and for water splitting with 4 and 8 photons per oxygen molecule are given. The black bars indicate experimental efficiencies of electricity-producing photoelectrochemical cells.

ones (0.5% as yearly average). These considerations clearly show the promise of technical systems for solar fuel generation, which should motivate on-going research.

3. Strategies for solar fuel generation

3.1 Photovoltaic-electrochemical generation of hydrogen from water and of carbon compounds from carbon dioxide

The technically most straightforward way for solar fuel generation is photovoltaic generation of electricity for the production of chemicals by electrochemical syntheses. The classical technical vision of solar pioneers are huge photovoltaic installations in the deserts, which produce electricity for the electrolysis of seawater. A practical obstacle is at present the high cost of photovoltaic electricity which still is ten times as expensive as electricity produced from fossil fuels. However, photovoltaic energy will become cheaper with mass production and improved manufacturing techniques. It may also be expected that social costs of fossil energy, including political and environmental costs, health consequences and greenhouse effects, which are significant, may gradually be added to increase the prize of fossil energy. Recently, the concept of huge centralized photovoltaic power stations has seen a gradual transformation. It became apparent, that – especially in countries with much sunshine – most photovoltaic energy needed could be produced by photovoltaic panels installed on houses, in villages and cities. Small electrical inverters, directly integrated into the panels would convert the direct photocurrent immediately into alternating current which could be coupled into the public electricity grid. In fact, such inverter-equipped panels could directly be plugged in into the grid and during sunshine would only cause the electricity counter to invert the movement and count the negative consumption (equivalent to production). The advantage of such a decentralized, grid-connected photovoltaic system would be that the installation would be simple and flexible and electrical losses would be relatively small. Inconvenient and expensive direct current installations, such as thick cables, could also be avoided. The electrical energy could conveniently be used in centralized installations for hydrogen production for chemical use or for electricity generation in fuel cell power plants (figure 3). Energy self-sufficient solar houses can produce hydrogen directly under pressure to avoid compression for hydrogen storage. A problem, concerning electrode degradation as a consequence of a highly irregular energy supply for water electrolysis could be surmounted by applying a bias potential to the electrodes during intervals without solar energy. Electrode corrosion could in this way be avoided with just a small sacrificial loss of energy.

Electricity can, of course, also be used for direct reduction of carbon dioxide. Recently, much effort has been made to develop metallic electrodes for the generation of alcohol, methane or other chemical energy carriers from carbon dioxide (Azuma *et al* 1990). Pure copper electrodes turned out to be catalytically the most active material. However, inhibition by intermediates, limited selectivity of the electrodes and toxic side products (carbon monoxide) remain a problem. Additional complications are that relatively high overpotentials have to be applied, that catalysis is limited to comparatively small current densities and that for the applied electrode potentials hydrogen evolution is an efficiency reducing competitive reaction.

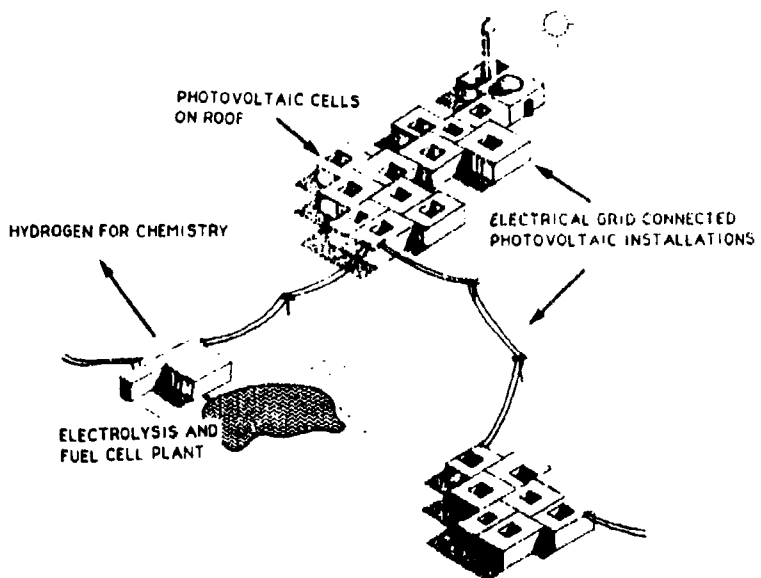


Figure 3. Picture showing decentralized photovoltaic energy production on houses, interconnection with the alternating current grid and centralized hydrogen production and reutilization.

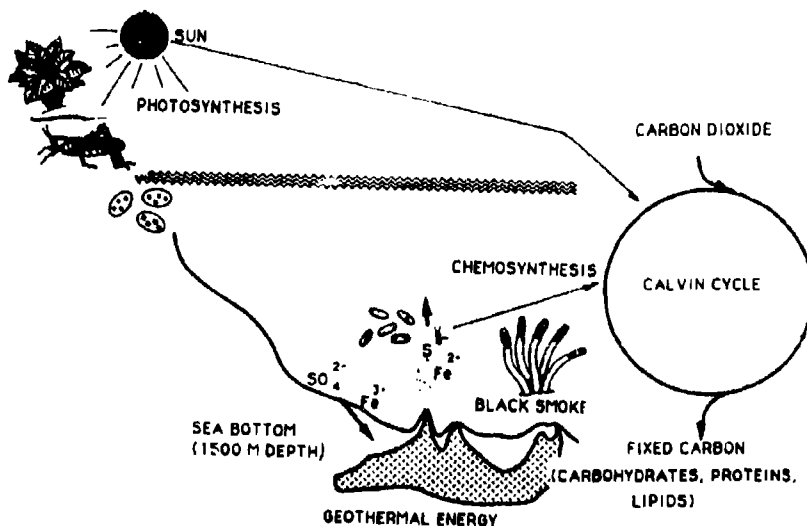


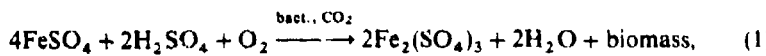
Figure 4. Photosynthesis as well as geothermally powered chemosynthesis can lead to the build-up of carbon compounds via the Calvin cycle.

In principle, it is possible to isolate biological enzymes which are active in carbon dioxide reduction and to immobilize them on electrodes. But it turns out to be very difficult to keep the immobilized enzymes active for a reasonably long time period.

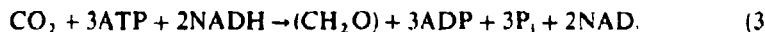
3.2 Photovoltaic-electrochemical or photoelectrochemical generation of simple energy carriers (e.g. Fe(II)) from Fe(III), which provide the energy source for carbon dioxide fixating bacteria

Photosynthesis is not the only energy basis sustaining biological ecosystems on earth. Chemosynthesis can also support life and also leads to fixation of carbon dioxide for living activities and biomass formation. Well-known examples are submarine ecosystems existing around so-called black smokers, which are powered by geothermal energy and liberate reduced species (e.g. Fe(II)), sulfur and sulfides (figure 4).

Bacteria like *Thiobacillus ferrooxidans* use the inorganic chemical energy as their only energy source to drive carbon dioxide fixation. In addition they only need a few salts for the supply of chemical elements and an acid environment ($pH < 3$) to avoid precipitation of $Fe_2(SO_4)_3$. These bacteria are approximately $1\text{ }\mu\text{m}$ long, of oval shape and are equipped with a rotating flagellum for propagation. They, in fact, use the same Calvin cycle as plants for carbon dioxide fixation and biomass formation but use inorganic chemical energy instead of photon energy as primary energy source. Depending on whether the bacteria use Fe^{2+} or a sulfide (FeS_2) as the energy source, the energy converting chemical reaction can be written as follows.



Biomass formation is based on the fixation of carbon dioxide according to the Calvin cycle:



Both the energy carriers ATP and NADH are generated by the energy liberated during Fe^{2+} oxidation (7.84–5.89 kcal/mol between pH 1.5 and 3) and sulfide oxidation respectively (≈ 200 kcal/mol for a disulfide). 118 kcal/mol of energy is needed for the reduction of carbon dioxide.

The strategy of using solar energy for the synthesis of simple energy carriers consumed by chemoautotrophic bacteria has been discussed in some detail (Tributsch 1979, 1982, 1989). In the simplest technical set-up (figure 5), solar energy is used to generate Fe^{2+} and oxygen in an electrochemical cell either by photovoltaic or photoelectrochemical energy. These two chemical species are sufficient to activate the Calvin cycle via the bacterial metabolism which is able to fix carbon dioxide. 19 Fe^{2+} ions must be oxidized for the fixation of one CO_2 molecule. In addition, the bacteria (*Thiobacillus ferrooxidans*) only need some inorganic minerals and trace elements, which has been confirmed in many cultivation experiments (Kelly *et al* 1977).

It is thus sufficient to generate Fe^{2+} and O_2 by photovoltaic or photoelectrochemical processes to provide the basis for continuous growth and continuous carbon dioxide fixation by bacterial culture. This process is simple and efficient since the required

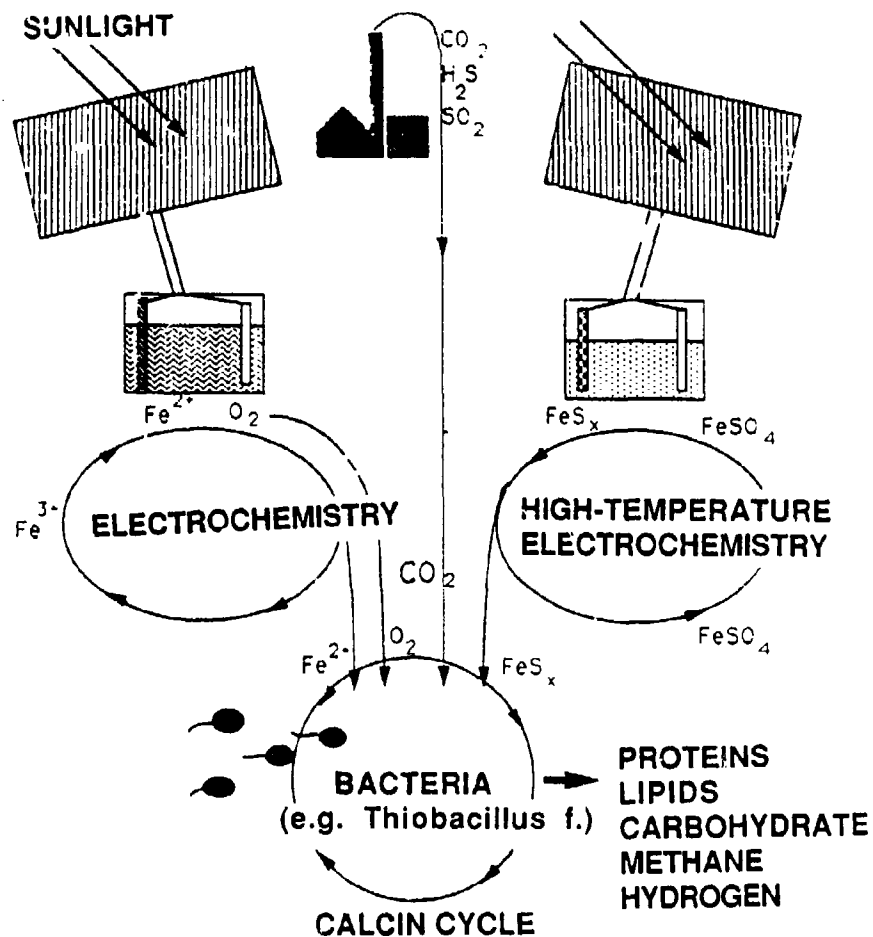


Figure 5. Solar electrochemical and thermoelectrochemical generation of chemical energy carriers (Fe^{2+} , FeS_2) for bacterial biomass production.

electrode materials (noble metals and RuO_2) are available and the bacteria rapidly reproduce in presence of the energy source. The real growth yield (gram dry weight per gram atom Fe^{2+}) has been determined for continuous cultures to be 1.33, corresponding to an energy efficiency for CO_2 fixation of $\eta_k = 78.8\%$ (Kelly *et al* 1977). Since bacterial life processes themselves consume energy, the real efficiency is reduced to $\eta_{eff} = 47\%$ (corresponding to a real growth yield of 0.8).

Considering an efficiency of $\eta_{el} = 80\%$ for the photovoltaic generation of Fe^{2+} in an electrochemical cell, it is found that the total efficiency $\eta = \eta_k \eta_{eff} \eta_{el}$ for carbon dioxide fixation would be approximately one third of the photovoltaic energy conversion efficiency. This means that for a solar cell with 15% solar energy conversion efficiency the efficiency of carbon dioxide fixation would be approximately $\eta = 5.6\%$. This is higher than the efficiency of photosynthetic carbon dioxide fixation. If sulfide

compounds could be synthesized from sulfate by solar-powered electrochemical processes, these sulfides could, of course, also serve as energy carriers for the bacterial energy cycle. The energy density of sulfide/sulfate-based solar-powered biomass production systems would be significantly higher, since the bacteria can gain much more energy from sulfide oxidation.

3.3 The direct photoelectrocatalytical generation of solar fuels with especially tailored photoactive semiconductor electrodes

The most fascinating and ambitious strategy for the production of chemicals with solar energy is the direct photoelectrochemical synthesis with catalytic electrodes. It is an interfacial molecular photoelectrochemical approach which follows, with new materials, the principle of the photosynthetic mechanism applied in the thylacoide membranes of plants. In this approach, electrode materials have to be identified, which not only temporarily store excitation-energy (semiconductors with an energy gap appropriate for harvesting solar energy), but which also photoreact in a way which facilitates the formation of chemical products which store energy. A key target has been photoelectrochemical water splitting, which can be separated into a cathodic hydrogen-evolution step and an anodic oxygen-evolution step. Hydrogen evolution is a kinetically simple reaction and can quite easily be accomplished using metal catalyst particles (e.g. Pt, Pd, Ni) on photoactive electrodes. Oxygen evolution, however, is a complicated multielectron-transfer reaction and remains the real problem in the water-splitting reaction. Many strategies have been tried to accomplish photoelectrolysis of water including the use of oxides with large energy gaps, of semiconductors which are covered by stable thin-oxide films, catalytic metals or catalytic polymers (for a review see Tributsch 1989b). Much research has been directed into the photoreaction of TiO_2 and related large gap oxides (e.g. $SrTiO_3$) with water. Even though the photoelectrochemistry of these materials is very interesting, it has not really advanced our knowledge on water splitting with visible light. The oxidation potential (quasi-Fermi level for holes) at UV-illuminated TiO_2 interfaces is so positive that OH-radicals can be generated by direct oxidation of OH^- . This is the basis of a radical photoelectrochemistry which also allows evolution of oxygen. Such a process is interesting for the degradation of organic waste compounds (Fox 1989), but energetically not favourable for water splitting using visible light.

Our strategy for the photoelectrochemical production of chemicals has been to provide photoelectrodes which allow light-induced interfacial coordination chemical mechanisms to proceed via transition metal states (figure 6). Many transition metal compounds with energy bands derived from transition metal *d*-states have been investigated (table 1). Generally it turns out that an anodic photoreaction with water is possible when photogenerated holes are provided for the interfacial reaction via a semiconductor valence band derived from *d*-states. However, the transition metal must be able to reach a sufficiently high oxidation state for oxygen evolution (e.g. Pt, Ru, Re, Ir). If this is not the case as with Fe in FeS_2 , the oxygen is transferred to the sulfur for sulfate formation. The oxidation of the chalcogen is favoured when changing from a sulfide to a selenide and telluride (e.g. in RuX_2 -compounds) due to an increasing overlap of chalcogenide *p* states with valence band *d*-states.

Water photooxidation to molecular oxygen is efficient when the valence-band edge is made up of pure *d-s*-states (Jaegermann and Tributsch 1988). There is no doubt that

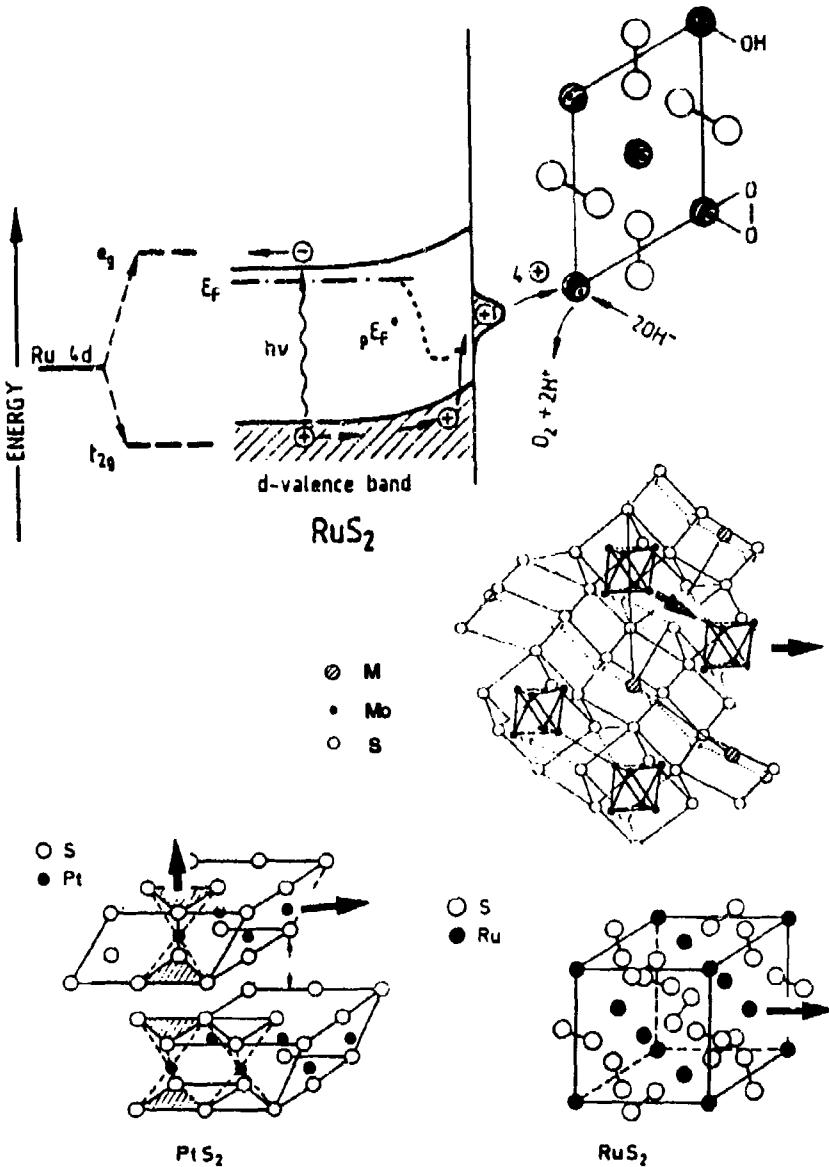


Figure 6. Schematic representation of material research strategy based on d -band semiconductors, which permit a photoinduced interfacial coordination chemistry. The path of photoinduced holes (arrows) in layer-type, pyrite-type and cluster-type transition metal compounds is indicated.

Table 1. Comparison of solid-state chemical and photoelectrochemical properties of different semiconducting d-band materials

Compounds	Me-Me distance (Å)	Energy gap (eV)	Oxidation state of metal	Photocatalysis products
MoS ₂	1.2	1.1	Medium	O ₂ , MoO ₄ ²⁻ , SO ₄ ²⁻
MoSe ₂	1.3	1.1	Medium	MoO ₄ ²⁻ , SeO ₄ ²⁻
WS ₂	1.2	1.15	Medium	O ₂ (*) WO ₄ , SO ₄ ²⁻
WSe ₂	1.3	1.2	Medium	WO ₄ , SeO ₄ ²⁻
PtS ₂	3.6	0.95	High	O ₂
RuS ₂	1.9	1.25	High	O ₂
RuSe ₂	4.15	< 1	High	O ₂ (90%), RuO ₄ , SO ₄ ²⁻
RuTe ₂	4.5	< 1	High	O ₂ (10%), RuO ₄ , SO ₄ ²⁻
FeS ₂	3.8	0.95	Low	SO ₄ ²⁻ , Fe ²⁺
IrS ₂	4.3	< 1	High	O ₂ (m.)
ReS ₂	2.6-2.9	1.4	High	Re ₂ O ₇ , O ₂
RuP ₂	2.8	1.67	High	RuO ₄ , O ₂ , PO ₄ ³⁻
RuPS	~3.8	1.2	High	SO ₄ ²⁻ , PO ₄ ³⁻
Ru ₂ Mo ₄ Se ₉	~2.7	~1.3	High	SeO ₄ ²⁻ , MoO ₄ ²⁻

a photoinduced interfacial coordination complex is formed with water. Ion-scattering experiments have indeed confirmed that electron donors like I⁻, Br⁻ or OH⁻ interact with the interfacial metal centers of the electrode. Attachment of suitable metal ligands to these interfaces (e.g. CN, CO, pyrazine) improves photoinduced interfacial electron transfer (Schubert and Tributsch 1990; Büker *et al* 1993) which supports the picture of metal-centered interfacial coordination photoelectrochemistry.

For a long time it remained a puzzle why van der Waals surfaces of layer-type transition metal dichalcogenides with d-band structure are photocatalytically active even though the surface-atom layer is made up of chalcogen atoms. Potential-assisted water photooxidation to molecular oxygen has not only been observed for PtS₂ (Tributsch and Gorochov 1981), though with a high overpotential typical for platinum, but also for freshly cleaved MoS₂ for the first 6–8 hours after starting the experiments. For MoS₂ the water oxidation to molecular oxygen, measured by polarographic techniques, gradually changes to molybdenum sulfate formation and corrosion (Tributsch 1977). This latter reaction is facilitated at edge sites of the material, which expose dangling bonds. It may be concluded that water oxidation to molecular oxygen is even possible with a comparable modestly active catalytic metal such as molybdenum, as long as there are no dangling bonds in the environment which could react with intermediate species such as surface-bound oxygen. However, it was unclear how water molecules could have access to the molybdenum d-states through a monolayer of sulfur. Recently, high resolution tunnelling electron microscopic pictures performed at TaSe₂ have clearly shown that the Mo-dz² charge-density contours are visible besides those of the surface sulfur atoms. Atoms at two different levels are sensed by the tunnelling tip. The transition-metal charge density does protrude upward between the sulfur charge density so that it is accessible for reactants from the electrolyte and for chemical interaction (Haneman and Tributsch 1993).

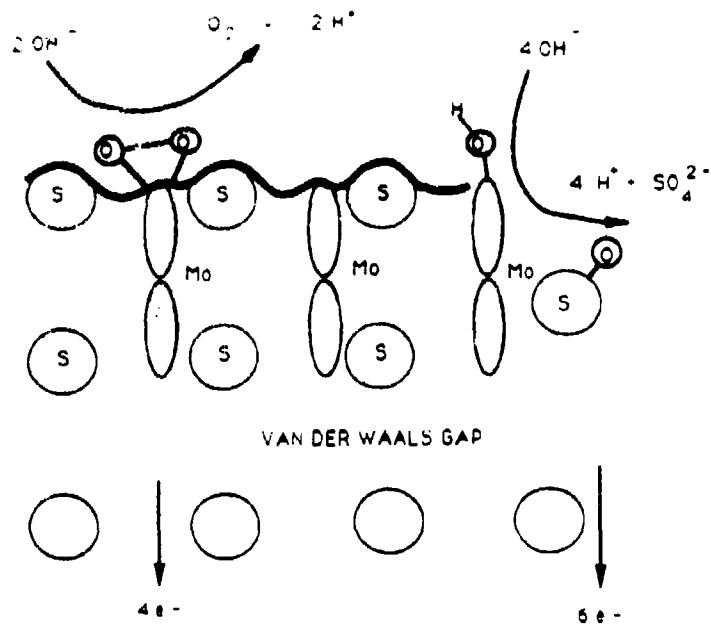


Figure 7. Scheme of charge density profile at van der Waals surface of a layer-type semiconductor (MoS_2 , PtS_2) showing accessibility of metal d_{2z^2} orbitals for interaction with water. An edge site, where corrosion occurs, is also shown.

This explains, why potential-assisted photoinduced oxygen evolution was observed at freshly cleaved MoS_2 surfaces. The lack of dangling bonds at the van der Waals surface kept the Mo-peroxo complex sufficiently stable for oxygen evolution.

This confirms that photoelectrochemical interaction of water with transition metals is the key to water oxidation to molecular oxygen. As long as the peroxo-type complex can be stabilized and side reactions are largely suppressed, oxygen may be liberated even with a modestly active transition metal. However, as soon as side reactions with increase of step-site formation (exposed dangling bonds) dominate, sulfate formation and corrosion result. This means that we need not only form a suitable transition metal complex with water photoelectrochemically but have also to provide for a suitable chemical environment. Transition metals which allow the formation of high oxidation states (Ru, Pt, Ir) do not seem to readily shift oxygen from their peroxo complex to the sulfur. Therefore photoreactions lead to oxygen evolution when these metal centers are active on d -type sulfide semiconductor surfaces. The compound RuS_2 turned out to be very efficient for photoinduced potential-assisted oxygen evolution (up to 40% quantum efficiency observed (Collet *et al* 1993)) and kinetically very stable (not dissolved by aqua regia). However, when in ruthenium disulfide one sulfur atom is replaced by phosphorus, so that the semiconducting compound RuPS is formed, corrosion is significantly increased (Fleming and Tributsch 1993). The reason may be the ease with which oxygen can be transferred to phosphorus to form soluble phosphate. The molecular basis of interfacial photoreactivity of RuS_2 for

water oxidation to molecular oxygen is presently investigated with new techniques and with systematic material modifications. It turns out that the electrical field in the Helmholtz-layer contributes to the efficiency of oxygen evolution (Alonso Vante *et al* 1993). Electronically degenerate samples which produce a significant potential drop in the double layer show improved oxygen evolution, which indicates that a potential-dependent activation barrier may be controlling the reaction. Since proton exchange between the surface and the electrolyte participates in the oxygen-evolution process, this ion-transfer mechanism (e.g. desorption of protons as steps leading to the formation of an interfacial peroxy complex) may be rate determining (Alonso Vante *et al* 1993). The requirement of an interfacial electrical field for photoinduced water oxidation would be an important restriction for semiconducting oxygen evolution electrodes.

To improve the catalytic activity of materials for photoinduced multielectron-transfer, semiconducting *d*-band materials were developed which provide clusters of transition metals as reservoirs and interfacial coordination centers for reactants (Alonso Vante and Tributsch 1986). Most of these are of the type $M_xMo_{6-x}X_8$, MMo_6X_8 , or $Re_6X_8Y_2$ (M = metal; X = S, Se; Y = Cl, Br) and permit insertion of additional metal atoms into channels between transition metal clusters. At such interfaces with clustered transition metal centers, interfacial complexes, which can accommodate several electrons needed for multielectron-transfer catalysis, are expected. It turns out that oxygen-reduction and hydrogen-evolution in acid solution at semiconducting electrodes of the type $Ru_2Mo_4Se_8$ are as efficiently catalyzed as at platinum electrodes (Alonso Vante and Tributsch 1986; Alonso Vante *et al* 1989). A systematic variation of metals inserted into cluster materials showed that cooperative interaction between metal atoms is important for multielectron transfer. However, the proximity of another atom is not important for hydrogen evolution, since the individually most active catalytic element, present in the semiconductor interface, is involved in hydrogen evolution catalysis.

Even though cluster compounds with reasonably good photoeffects could be developed and have demonstrated photoinduced oxygen-reduction behaviour (Fischer *et al* 1993) with high photocatalytic activity, they have not yet shown sufficient stability for anodic photoprocesses. It turned out that anodic metal oxide formation by less noble metals (e.g. Mo) leading to soluble oxidation products is a limiting side reaction. Cluster compounds, on the other hand, now already appear to be catalytically very favourable for cathodic multielectron reactions.

Interfacial coordination chemical mechanisms may be a precondition for photoelectrolysis of water but cannot guarantee a low overpotential. The overpotential needed will largely be determined by the energetic position and the stepwise dynamic transformation of electronic states of the interfacial coordination complexes formed. However, transition metal clusters serve as reservoirs for electrons and the energetic variation of states in complexes formed during multielectron transfer with these is more restricted, which is an energetic advantage.

3.4 Irreversible, nonlinear thermodynamics - a key to efficient kinetics and stability of fuel producing interfaces?

Several arguments indicate that autocatalysis and dynamic structural changes during electron transfer are additionally needed for energy efficiency during multi-electron

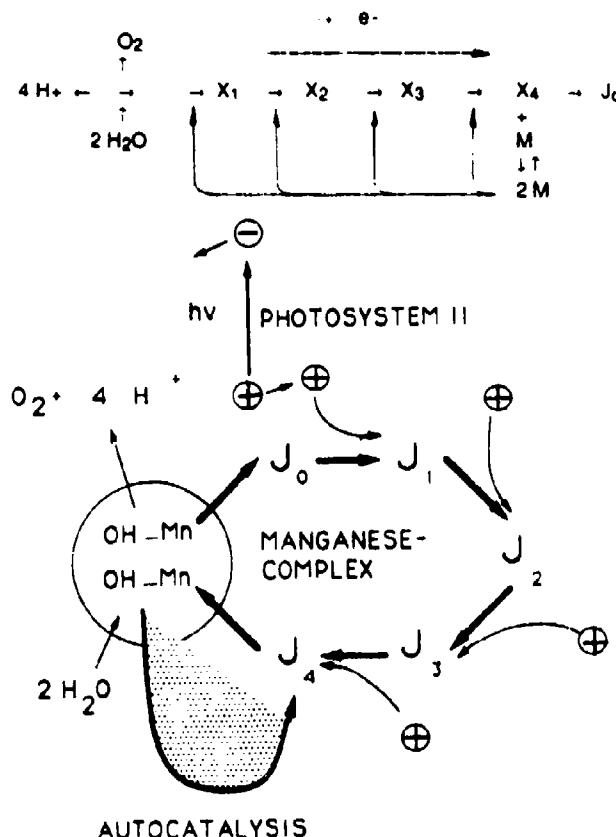


Figure 8. Reaction pathway with nonlinear autocatalytic feedback (above) and proposed function of the manganese-containing oxygen-evolution center of photosynthesis (below).

transfer reactions. In order to avoid successive transfers of electrons with all the difficulty of controlling the energetic properties of intermediates, it may be attempted to transfer electrons collectively in a cooperative way. This concept is new and goes beyond classical electron transfer theory, which only knows successive electron transfer steps. A key element of cooperation within the framework of irreversible thermodynamics is autocatalysis. When the first electron is transferred it must form an intermediate state which exerts a feedback upon the second, third or following electrons. Model calculations indeed show that a "slaving" of degrees of freedom can occur which theoretically proves cooperative electron transfer (Pohlmann and Tributsch 1992; Tributsch and Pohlmann 1992). It can intuitively be understood in analogy to photon emission, which by feedback mechanisms (stimulated emission) turns into coherent laser light. Calculations show that onset of cooperation is accompanied by a breakdown of the activation barrier. In practice, this irreversible thermodynamic approach to multielectron transfer and chemical fuel generation means that very specific electronic-dynamic conformation changes must occur during the process. It may perhaps proceed in the above-mentioned cluster compounds during multielectron

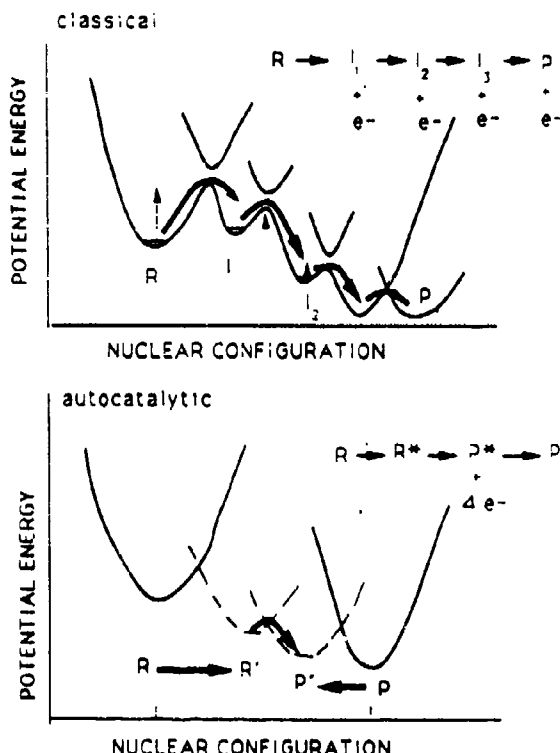


Figure 9. Potential energy-nuclear configuration diagrams of multielectron transfer reaction for classical (above) and proposed cooperative electron transfer (below).

transfer since the volume of the clusters is increased when electrons are extracted. Model calculations show that nonlinear feedback is needed for cooperative electron transfer.

Water photoelectrolysis – as it occurs in photosynthesis – is an energetically extremely efficient process since it occurs very close to the reversible thermodynamic oxidation potential of water ($E_0 = 1.23$ V) and may thus be considered to be a phenomenon of nonlinear irreversible thermodynamics. The accumulation of four photogenerated holes in the manganese complex may proceed in the conventionally described way, however, during transition of the state J_4 to J_0 (which is accompanied by oxygen evolution), the first electron extracted from water must induce an autocatalytic feedback inducing an increase of the transfer rate of the second and the following electrons for inducing cooperative electron transfer. A key problem in this new approach to multielectron transfer catalysis is to understand and properly handle autocatalytic reactions.

Figure 9 compares classical stepwise multielectron transfer with cooperative electron transfer triggered by nonlinear autocatalysis. In this way new nuclear configurations for both the reactant and the product are formed which dramatically reduce activation barriers. It can be imagined that an autocatalytic configuration pathway can be exploited to reach a much more favourable electron-transfer situation.

Cooperation in catalysis of fuel production may not be the only irreversible process of a new kind to be explored for solar fuel production. It is well known that biological membranes are unstable when extracted from biological systems and it is well known that artificial photoelectrochemical cells have problems with instability. The key strategy which nature employs to stabilize fragile structures is the export of entropy (increase of order) through cooperative mechanisms, based on autocatalytic processes. The entropy of a critical system is maintained by channelling entropy production of the irreversible system through uncritical pathways and by repairing damage. We call the phenomenon self-organization. We may have to learn about it to handle the stability problems of photoelectrodes.

4. Discussion

We have seen that initiatives towards solar-fuel production meet several frontiers. One is of political nature. As long as fossil fuels are sold at such low prices without taking into account the real social costs and long-term environmental degradation including the greenhouse effect, fuel from solar energy will not be able to compete. We should nevertheless make efforts to develop solar-fuel technologies because sooner or later mankind will realize that it is not possible to cheat nature and time. Fossil fuels are in fact "borrowed biomass", for which we should pay interest because accumulating carbon dioxide will have to be recycled by photosynthetic processes. This interest (or carbon dioxide tax), should be used to counteract the greenhouse effect by reforestation, energy-efficient architecture, introduction of solar energy technology and energy saving.

The second frontier is a strategic one. Transition to solar energy utilization should be a gradual one and should, to a large extent, guarantee the advantages of modern technology. It should also not threaten the survival of cities with high densities of population. It is my feeling that the most convenient approach to large scale solar fuel production would be the strategy sketched in figure 3: Photovoltaic systems installed in large numbers on buildings, over otherwise-used land and in small photovoltaic plants, which are interconnected with the public electricity grid, will supply most of the electrical energy. Surplus electrical energy will be extracted from the grid in special electrolysis plants for hydrogen production. This hydrogen can be stored to be reconverted to electrical energy via fuel cells. It can also be used for the chemical industry or its energy stored in the form of methanol or ammonia after combining it with carbon dioxide and nitrogen respectively for further use.

An alternative and complementary strategy for chemical-fuel generation from solar energy could be based on the photovoltaic electrochemical generation of a simple inorganic energy carrier such as Fe^{2+} (from Fe^{3+}). In the presence of oxygen it is the only energy carrier needed for carbon dioxide fixating bacteria, which provide high quality biomass containing proteins, carbohydrates and lipids. The solar energy efficiency of this biomass route based on chemosynthetic bacteria exceeds natural photosynthetic energy conversion efficiency. This strategy, which can also be based on a sulfide-sulfate energy cycle, could in fact become the background of an entirely artificial type of agriculture, practicable on infertile desert land.

The third frontier is the microscopic, molecular photoelectrochemical one, which aims at direct photoinduced water splitting or carbon dioxide fixation. This route

closely follows the strategy applied in green plants, but must, for the near future, rely on significantly less complicated materials and processes. Much research is still needed to produce energy-storing chemicals through such direct interfacial photocatalytical mechanisms. We have shown that a material research strategy towards photoelectrodes able to induce interfacial coordination chemical reactions with water or other reactants for multielectron transfer mechanisms is very promising. Water can indeed be photo-oxidized to oxygen with high quantum efficiency. However, the overpotential cannot easily be controlled and limited to low values.

Here we have introduced a new strategy to improve the kinetics of fuel generation. The feasibility of cooperative electron transfer has been theoretically demonstrated. The catalyst must be able to exert feedback reactions on subsequent electron transfer steps during electron transfer. This means that it must have the property to induce autocatalytic processes. Such mechanisms belong to nonlinear irreversible thermodynamics. This is a field we consider of great challenge for photoelectrochemistry since it provides mechanisms which can extract entropy or increase order locally at the expense of general entropy production. Entropy export would be helpful both for stabilizing energy-converting electrode interfaces and for the photosynthesis of complicated molecules. Nature has skilfully exploited the potential of far-from-equilibrium mechanisms and it may be that for improved solar generation of fuels we also will have to learn to handle them.

References

- Alonso Vante N, Collet H and Tributsch H 1993 *J. Phys. Chem.* **97** 738
Alonso Vante N, Schubert B and Tributsch H 1989 *Mater. Chem. Phys.* **22** 281
Alonso Vante N and Tributsch H 1986 *Nature (London)* **323** 431
Azuma M, Hoshimoto K, Hiramoto M, Watanabe M and Sakata T 1990 *J. Electrochem. Soc.* **137** 1772
Bolton R J, Strickler S J and Connolly J S 1985 *Nature (London)* **316** 495
Buker K, Vante N A and Tributsch H 1993 (to be published)
Collet H, Alonso Vante N and Tributsch H 1993 (to be published)
Fischer C, Alonso Vante N and Tributsch H 1993 (to be published)
Fleming I G and Tributsch H 1993 *J. Electrochem. Soc.* (to be published)
Fox M A 1989 In *Photocatalysis* (eds) N Serpone and E Pelizzetti (New York: J Wiley & Sons) p. 431 (see also additional contributions in this volume)
Haneman D and Tributsch H 1993 *Chem. Phys. Lett.* (in press)
Jaegermann W and Tributsch H 1988 *Prog. Surf. Sci.* **29** 1
Kelly D P, Eccleston M and Jones C A 1977 In *Conference on Bacterial Leaching* (eds) H G Schlegel and J Barnes (Göttingen: Verlag Chemie)
Pohlmann L and Tributsch H 1992a *J. Theor. Biol.* **156** 63
Pohlmann L and Tributsch H 1992b *J. Theor. Biol.* **199** 443
Schubert B and Tributsch H 1990 *Inorg. Chem.* **29** 5042
Tributsch H 1977 *Z. Naturforsch.* **32** 361
Tributsch H 1979 *Nature (London)* **281** 555
Tributsch H 1982 *Aeronaut. Astronaut.* **20** 6
Tributsch H 1989a In *Photoconversion processes for energy and chemicals* (eds) D O Hall, G Grassi (New York, London: Elsevier) p. 283
Tributsch H 1989b In *Photocatalysis* (eds) N Serpone and E Pelizzetti (New York: J Wiley & Sons) p. 336
Tributsch H 1990 In *Proceedings of the 1st World Renewable Energy Conference, Energy and the Environment in the 1990s* (ed.) A M Sayigh, vol. 3, p 1447
Tributsch H and Gorochov O 1981 *Electrochim. Acta* **27** 215
Tributsch H and Pohlmann L 1992 *Chem. Phys. Lett.* **188** 338

Photobiotechnology: Application of photosynthesis to the production of renewable fuels and chemicals

E GREENBAUM

Chemical Technology Division, Oak Ridge National Laboratory, P. O. Box 2008, Oak Ridge, TN 37831-6194, USA

Abstract. Sustained hydrogen photoevolution from *Chlamydomonas reinhardtii* and *C. moewusii* was measured under an anoxic, CO₂-containing atmosphere. It has been discovered that light intensity and temperature influence the partitioning of reductant between the hydrogen photoevolution pathway and the Calvin cycle. Under low incident light intensity ($1\text{--}3 \text{ W m}^{-2}$) or low temperature ($\approx 0^\circ\text{C}$), the flow of photosynthetic reductant to the Calvin cycle was reduced, and reductant was partitioned to the hydrogen pathway as evidenced by sustained H₂ photoevolution. Under saturating light (25 W m^{-2}) and moderate temperature ($20 \pm 5^\circ\text{C}$), the Calvin cycle became the absolute sink for reductant with the exception of a burst of H₂ occurring at light on. A novel photobiophysical phenomenon was observed in isolated spinach chloroplasts that were metalized by precipitating colloidal platinum onto the surface of the thylakoid membranes. A two-point irradiation and detection system was constructed in which a continuous beam helium-neon laser ($\lambda = 632.8 \text{ nm}$) was used to irradiate the platinized chloroplasts at varying perpendicular distances from a single linear platinum electrode in pressure contact with the platinized chloroplasts. No external voltage bias was applied to the system. The key objective of the experiments reported in this report was to measure the relative photoconductivity of the chloroplast-metal composite matrix.

Keywords. Photobiotechnology; photosynthesis; hydrogen; oxygen; platinized chloroplasts; water splitting.

1. Introduction

1.1 Hydrogen production

Hydrogen photoevolution by unicellular algae was first demonstrated by Gaffron and Rubin (1942). Since their pioneering discovery, the reducing power driving sustained hydrogen photoevolution under anaerobiosis has been shown to be primarily derived from the water-splitting reaction of photosystem II (Bishop *et al* 1977). In green algae, an oxygen-labile hydrogenase couples the oxidation of reduced ferredoxin with hydrogen evolution. Hydrogenase is a critical catalyst for a number

'The submitted manuscript has been authored by a contractor of the US Government under contract No. DE-AC05-84OR21400. Accordingly, the US Government retains a nonexclusive, royalty-free license to publish or reproduce the published form of this contribution, or allow others to do so, for US Government purposes.'

of single and multistep reactions. Experimental conditions determine which reactions proceed (Bishop *et al* 1977; Senger and Bishop 1979).

Light activated:

- (1) Photoreduction: $\text{CO}_2 + 2\text{H}_2 + \text{light} \rightarrow \text{CH}_2\text{O} + \text{H}_2\text{O}$,
- (2) H_2 photoproduction: $\text{XH}_2 + \text{light} \rightarrow \text{X} + \text{H}_2$.

Thermally activated:

- (3) Oxy-hydrogen reaction: $2\text{H}_2 + \text{O}_2 \rightarrow 2\text{H}_2\text{O}$,
- (4) Dark CO_2 fixation: $\text{CO}_2 + \text{H}_2 + \text{energy} \rightarrow \text{CH}_2\text{O} + \text{H}_2\text{O}$,
- (5) H_2 production: $\text{RH}_2 \rightarrow \text{R} + \text{H}_2$,
- (6) H_2 uptake: $\text{R} + \text{H}_2 \rightarrow 2\text{H}_2$.

In the absence of CO_2 , the absolute light-saturated rate of electron transport is greatly reduced. Under these experimental conditions hydrogen evolution is the main pathway for the utilization of photoproduced reductant. The steady-state ratio for H_2 to O_2 evolution is usually close to two, indicating that essentially all electrons generated by the biophotolysis of water are expressed as H_2 (Greenbaum 1984; Ward *et al* 1985). If CO_2 is available sustained hydrogen photoproduction does not occur (Gaffron and Rubin 1942; Stuart and Gaffron 1972). Gaffron and Rubin (1942) demonstrated that under anaerobic conditions dinitrophenol inhibited CO_2 reduction in *Scenedesmus* and allowed hydrogen photoproduction to occur in the presence of CO_2 . Similarly, glucose and carbonyl cyanide-*m*-chlorophenylhydrazone stimulated H_2 photoevolution in the presence of CO_2 (Kaltwasser *et al* 1969). Those experiments suggested the coexistence of two reductant sinks, with the Calvin cycle being the primary sink in the presence of CO_2 and the hydrogen pathway serving as an alternate sink that functioned when CO_2 was absent or when the activity of the Calvin cycle was inhibited.

Stuart and Gaffron (1972) approached the problem of dual, competitive pathways using a closed system and chemical inhibitors. However, a closed-system approach is severely limited in the useful information that can be obtained. For example, uniform conditions are impossible to maintain for the duration of an experiment because the organisms modify their environment by liberating O_2 and H_2 and consuming CO_2 . This situation leads to non-steady-state conditions that stimulate several of the aforementioned hydrogenase mediated reactions, thereby greatly complicating the interpretation of experimental results. The experiments described in this review have taken a new approach to this problem. First, continuous gas flow was used; this prevented O_2 inactivation of hydrogenase resulting from the accumulation of O_2 , which occurred in closed systems such as those used in most other studies of anaerobic photosynthesis. Second, continuous flow also removed photoproduced H_2 and O_2 so that the oxy-hydrogen and photoreduction reactions, photorespiration, and respiration did not occur. Third, the concentration of CO_2 was maintained at a constant level by bubbling an $\text{He}-\text{CO}_2$ gas mixture through the sample instead of supplying CO_2 from finite bicarbonate or gas phase source (Gaffron and Rubin 1942; Healey 1970; Stuart and Gaffron 1972; Gfeller and Gibbs 1985). Fourth, the ability to perform long-term experiments in which all measured reactions were driven into steady-state provided additional information not available previously. The coexistence of two pathways that directly utilize photogenerated reductant provides a unique opportunity to experimentally examine the kinetic competition between the pathways for reductant and the regulatory mechanisms that work to control and balance the

activities of the Calvin cycle, the hydrogen pathway, and the photosynthesis. The key discovery of this report is control of partitioning of photogenerated reductant between the hydrogen pathway and the Calvin cycle, by variable light intensity and temperature.

1.2 Photoconductivity

Photosynthesis is vectorial photochemistry. Light quanta that are captured in photosynthetic reaction centers initiate a primary electron transfer reaction, resulting in spatial separation of electrostatic charge across the photosynthetic membrane. The vectorial nature of photosynthesis lies in the intrinsic orientation of the reaction centers embedded in the membranes. Electron flow is from the inner membrane surface of the flattened sac-like vesicles to the outer surface (Amesz 1987). In normal photosynthesis, electrons from the reducing end of photosystem I are used for the enzymatic reduction of NADP^+ to NADPH. This reduction is mediated by ferredoxin and ferredoxin NADP-reductase. NADPH serves as the electron carrier to the Calvin cycle for the enzymatic reduction of atmospheric carbon dioxide to plant matter.

It has been shown that colloidal platinum can be precipitated onto the surface of photosynthetic membranes so that water is photobiocatalytically split into molecular hydrogen and oxygen upon illumination with light of any wavelength in the chlorophyll absorption spectrum (Greenbaum 1985). Since no electron mediator such as ferredoxin or methyl viologen was present, the colloidal platinum must have been precipitated sufficiently close to the photosystem I reduction site to allow interfacial electron transfer from the membrane to the platinum. The presence of a reticulated network of platinum particles embedded in the chloroplast matrix suggests that metal-like properties can, at least partially, be imparted to the chloroplasts. In this work, the relative photoconductivity of the material was measured by the flow of photocurrent in the plane of the entrapped platinized chloroplasts of uniform thickness from the point of laser irradiation to the linear platinum wire electrode.

2. Results

2.1 Hydrogen production

Under anaerobic conditions in the absence of CO_2 , the ratio of light-saturated, steady-state H_2 and O_2 photoevolution by *C. reinhardtii* approached two. However, when CO_2 was introduced, photosaturated O_2 evolution increased dramatically and light-driven H_2 evolution ceased, except for a transient burst that occurred when the light was turned on. These observations were consistent with those of Stuart and Gaffron (1972).

The 5–10-fold increase in light-driven O_2 production corresponded with the typical increase attributed to the bicarbonate effect on PS II activity (Vermaas and Govindjee 1981). The lack of sustained H_2 photoevolution suggested that CO_2 also affected the activation of the Calvin cycle because CO_2 is well known to activate RuBP Carboxylase by providing substrate and positive effector (Lorimer *et al* 1976). The Calvin cycle provided a faster kinetic sink for reductant than the H_2 pathway thereby eliminating H_2 photoevolution under conditions where photosynthesis and the Calvin cycle were fully activated.

2.2 Hydrogenase activity in the presence of CO_2

Dark hydrogen evolution and the burst of H_2 accompanying 'light on' in the presence of CO_2 indicated that hydrogenase activity was not adversely affected by CO_2 , or the high O_2 photoevolution rate in the continuous flow experimental system. The yield of H_2 represented by the burst at 'light on' was about 25 nmol for the cell suspension containing 50 μg Chl. Normalizing the data to 1 mg of Chl, the H_2 yield from the burst was 500 nmol/mg Chl. By measuring the H_2 yield associated with the burst in other, similar experiments, the yield was found to be variable, ranging from 200 to 1000 nmol/mg Chl (data not shown). This information allowed an estimation of the number of reducing equivalents contributed by each photosynthetic electron transport chain for the transient burst. The following calculation was based on the data normalized to 1 mg Chl.

$$500 \times 10^{-7} \text{ mol H}_2 / (1.1 \times 10^{-6} \text{ mol Chl}/500 \text{ mol Chl/mol photosynthetic electron transport chains}) = 227 \text{ mol H}_2/\text{mol electron transport chain.}$$

With 2 electrons per H_2 , a total of 454 electrons were spent in the burst of H_2 . This number far exceeds $\approx 5\text{--}20$ reducing equivalents per electron transport chain stored in a completely reduced plastoquinone pool (Joliot 1965; Forbush and Kok 1968; Stiehl and Witt 1969; Greenbaum 1979).

To determine the source of the reductant driving the burst of H_2 at light-on in the presence of CO_2 , an ethanolic solution of DCMU was added to the algal cells to give a final DCMU concentration of 15 μM . This level of DCMU completely eliminated the burst of H_2 at light-on as well as O_2 photoevolution (data not shown). However, sustained light-driven H_2 evolution was observed for a few hours after the addition of DCMU demonstrating that stored reductant can be used for light-driven H_2 photoevolution.

2.3 The effect of light intensity on H_2 and O_2 photoevolution

Light intensity was varied from 0 to 25 W m^{-2} . Under low-light conditions, sustained H_2 photoevolution was detected with the maximum ratio of H_2 to O_2 being about one at 0°C, sustained, albeit low, H_2 photoproduction was observed even at the highest light intensity.

In the absence of CO_2 at 20°C and at various light intensities, H_2 and O_2 were coevolved with a hydrogen-to-oxygen ratio of about 2, as previously reported (Greenbaum 1984). The yield of H_2 and O_2 at 0°C was similar to that seen at 20°C, and the stoichiometry of H_2 -to- O_2 was ≈ 2 .

2.4 The effect of temperature on H_2 and O_2

Light-driven H_2 production was measured at temperatures ranging from 0 to 40°C. Pretreatment of the algae had a significant effect on O_2 and H_2 photoevolution. The cells adapted to changes in temperature by shifting their optimal photoproduction temperature. For example, cells held overnight at 0°C showed higher O_2 yields at 5°C than cells taken from 20 to 5°C within 2 h and assayed immediately. After cooling to 0°C, the algae were assayed for 1 h then the temperature was raised by 5°C and the same algae were assayed for 1 h followed by another 5°C temperature adjustment.

and 1 h assay until 40°C was reached. The temperature changes required less than 5 min each and the steady-state rate of photoevolution was then measured after 1 h of irradiation.

At 0°C steady-state H₂ and O₂ photoevolution occurred in the presence of CO₂. The ratio of H₂ to O₂ was about 1.2, indicating that the hydrogen pathway was not the sole pathway for reductant utilization. Under these conditions, competition for reductant evidently existed between the Calvin cycle and the H₂ pathway. Moderate temperatures (> 5 and < 30°C) caused the cessation of H₂ photoevolution; however, at warmer temperatures (> 30°C), a small portion of the photogenerated reductant was shunted to the hydrogen pathway.

In the absence of CO₂, the H₂-to-O₂ photoevolution ratio remained close to 2 until the temperature rose to > 25°C. At warmer temperatures, the H₂-to-O₂ ratio significantly exceeded 2, suggesting that additional reductant was being supplied from a source other than PS II. The alternative source, which may enter the photosynthetic electron transport chain through the plastoquinone pool (Diner and Mauzerall 1973; Gfeller and Gibbs 1985; Peltier *et al.* 1987), was light driven since H₂ photoevolution fell to zero when the light was turned off.

2.5 Photoconductivity

Table 1 presents data for four platinum concentrations. A 5-ml suspension of spinach chloroplasts (containing 3 mg of chlorophyll) was used. Platinization of chloroplasts is feasible because hexachloroplatinate can be converted to metallic platinum at pH 7 and room temperature (Anderson 1975). These are experimental conditions that preserve photoactivity of the isolated chloroplasts. The platinized chloroplasts were entrapped on a thin, fiberglass filter pad (Millipore, AP40) and were moistened with Walker's assay medium (Walker 1980), in which the chloroplasts were suspended. The fiberglass filter pad was 0.3 mm thick, had an active filtration area of 10.4 cm², and contained no binder resins. The thickness of the chloroplast film was estimated to be between 0.01 and 0.1 mm. A silver-silver chloride reference electrode was placed

Table 1. Vectorial photocurrents and electron-transfer distances in platinized chloroplasts as a function of platinum loading.

Line no.	I ₀ ^a nA	D _{max} , mm	[Pt] ^b , mg/ml
1	0	0	0.24
2	0	0	0.49
3	3.6	2.3	0.97
4	7.8	3.4	1.94

^aI₀ is defined as the measured photocurrent when D = 0. This corresponded to the laser beam position when it was directly over the near electrode and was the maximum current measured in each run.

^bAqueous-phase platinum concentration from which the platinum precipitation step was performed. Lines 1 and 2 are the average of two runs each. Line 3 is the average of three runs. Line 4 is the average of six runs.

in pressure contact with the filter; a straight, single, platinum wire of 0.2 mm diameter was placed in pressure contact with the entrapped platinized chloroplasts. The electrodes, platinized chloroplasts, and filter paper were held together with lucite plates and compression screws. To prevent the electrochemistry of atmospheric oxygen from interfering with the cathode reactions by providing an alternative electron pathway, the entire assembly was placed in a small glass chamber sealed with an O-ring. The O-ring was pierced to allow the passage of two narrow-diameter wires for establishing electrical contact with the electrodes. Premoistened helium gas flowed through the chamber to flush out atmospheric oxygen. After about 45 min, the oxygen concentration of the chamber was below 3 ppm as measured by a calibrated Hersch electrogalvanic cell. Calibration was achieved with an in-line electrolysis cell and Faraday's law of electrochemical equivalence.

The platinum precipitation step was performed in a water-jacketed reactor cell containing 8.0 ml of suspension maintained at 20°C. Molecular hydrogen was passed over the head space of the reactor while a teflon-coated magnetic stirrer was used to gently stir the chloroplast suspension in a neutral hexachloroplatinate solution. Purge times of 30 to 60 min were used. After incubation and precipitation, the reactor chamber was opened to air, the contents were filtered onto the filter pad, and the cell was assembled as described previously. This coprecipitation step was essential.

The novel observation in this research is the effect of the precipitated platinum on the photoconductivity of the chloroplast matrix. Each data point represented a steady-state flow of current. Although steady-state was achieved within a few minutes of each change in the laser beam position, sustained photocurrent could be observed for hours. Each data point represents a dwell time of 15 to 20 min.

The photocurrent had a maximum value when the laser beam was directly over the platinum wire. Although the laser beam was partially blocked by the wire electrode when the beam was positioned directly over it, this loss of light was not sufficient to cause a drop in photocurrent. This observation is reasonable since the diameter of the laser beam is larger than the diameter of the platinum wire electrode. Also, the close physical proximity of the laser light and wire on the umbral periphery of the wire provided for efficient charge collection. The extent to which the laser beam could be moved from the wire and still generate measurable photocurrent depended on the concentration of the solution from which the platinum was precipitated. Table 1 is a summary of the data of initial currents and maximum distances that were observed for varying distances.

3. Discussion

3.1 Hydrogen production

These results establish the coexistence of two competitive pathways for photosynthetically generated reductant and support the findings of Gaffron and coworkers that under anaerobiosis and CO₂, inhibitors of photophosphorylation and carbon reduction stimulate H₂ photoevolution in microalgae. Light and temperature physically accomplished a result similar to that achieved by the chemical inhibitors used in prior research (Gaffron and Rubin 1942; Stuart and Gaffron 1972). Under low light intensities the activity of many Calvin cycle enzymes is known to be reduced

(Buchanan 1980), resulting in an imbalance between the number of reducing equivalents generated by photosynthetic water splitting and the number consumed for carbon reduction. At least part of the excess was expressed as H₂ via the hydrogen pathway. Similarly, both high and low temperature caused a disparity between production and demand, again leading to the expression of H₂. Based on these observations and those of Gaffron and colleagues (Gaffron and Rubin 1942; Stuart and Gaffron 1972), any event that selectively impairs the demand of the Calvin cycle for reductant should lead to the expression of the excess reducing equivalents as H₂. The experimental conditions lead to a relative imbalance between reductant demand by the Calvin cycle and reductant supply by photosynthetic water splitting. The results suggest that the activity of the photosynthetic electron transport chain and the photosystems was less sensitive to low temperatures and light regulation than the Calvin cycle. The fact that H₂ photoevolution rates under He were comparable at both 20 and 0°C indicated that hydrogenase was not limiting at the lower temperature.

Hydrogen evolution in the dark was accounted for by the dark hydrogen production reaction (Healey 1970). The burst of H₂ at light-on represented H₂ photoevolution. The reductant expended in the burst may be from at least three different sources: (1) electrons may be released from the completely reduced plastoquinone pool. One complete release would account for about 10 hydrogen molecules per photosynthetic electron transport chain, assuming 20 PQ/pool. (2) Electrons may be released from a stored pool of reductant other than the plastoquinone pool although this reductant may enter the photosynthetic electron transport chain via the plastoquinone pool (Diner and Mauzerall 1973; Greenbaum 1984; Gfeller and Gibbs 1985; Peltier *et al* 1987). (3) Hydrogen photoproduction may be directly driven by the biophotolysis of water. Since the amount of reductant necessary to give a hydrogen burst of the measured magnitude must equal about 450 electrons, the plastoquinone pool cannot be the sole source of reductant. An alternative pool, biophotolysis of water, or both may contribute to the transient burst. Inhibition of O₂ evolution with DCMU eliminated the burst of H₂ at light-on indicating that the burst was driven by the biophotolysis of water. However, the observation of sustained light-driven H₂ production in the absence of O₂ photoevolution indicated that stored reductant was entering the photosynthetic electron transport system under these conditions. The most likely explanation for the burst of H₂ upon illumination is a time delay between photosynthetic reductant production and activation of light regulated Calvin cycle enzymes. During the lag time, reductant is partitioned to the H₂ pathway. However, the possibility that electrons from an alternative source contribute to the burst cannot be completely excluded since H₂ evolution was observed in the presence of DCMU.

In conclusion, the coexistence of two competitive pathways for photogenerated reducing equivalents has been demonstrated in *C. reinhardtii* and *C. moewusii* adapted for H₂ evolution in the presence of CO₂. The experimental manipulation of electron partitioning between the two pathways, using the physical parameters of light and temperature, indicates that the pathways coexist under certain experimental conditions. These pathways provide the organisms with a mechanism to avoid becoming 'over reduced' under circumstances where reductant availability exceeds demand. These experiments also demonstrate that the flow of photogenerated reductant can be partially and reversibly switched from carbon fixation to hydrogen evolution for the production of a high-energy, inorganic compound by simply changing conditions in the physical environment.

3.2 Photoconductivity

The origin of the photocurrent can be understood as follows: It has previously been shown that colloidal platinum can make electrical contact with the reducing end of photosystem I of photosynthesis. This contact was demonstrated by (1) the photo-catalytic evolution of molecular hydrogen and (2) the observation of photocurrent in a sandwichlike photobioelectrochemical cell (Greenbaum 1989). Upon illumination, the platinum electrode in pressure contact with the platinized chloroplasts swung negative with respect to the silver-silver chloride electrode that was in pressure contact with the electrolyte-impregnated filter pad. No external bias was placed on the electrodes to force the direction of photocurrent flow.

A reasonable model for these results, based on the generally accepted structure of photosynthetic membranes (Marder and Barber 1989), is that colloidal platinum precipitated onto the external surface of the thylakoid membranes forms an isopotential surface whose distance is determined by the connectivity of the reticulated colloidal particles that are the metallic component of the chloroplast-metal composite matrix. This distance is a statistical parameter whose average value is determined by the nature of the platinum precipitation process. When platinum is precipitated, it does so in a nonspecific manner on the external surface of the thylakoid membrane. There is, however, an electrostatic between the negative charge of the hexachloroplatinate ions and the local positive charge of the lysine residues constituting part of the polypeptides of the photosystem I proteins (Colvert and Davis 1983).

The experimental system described in this work differs qualitatively from prior research performed with photosynthesis-based bioelectrochemical cells that utilized various organelles and components to generate photocurrents. Examples of prior research include chlorophyll liquid crystals (Aizawa *et al* 1978, 1979), pigmented bilayer membranes (Tien 1976), chloroplasts (Haehnel and Hochheimer 1979), chloroplast membranes (Allen *et al* 1974; Allen and Crane 1976; Allen 1977), algae (Ochiai *et al* 1980), and photosynthetic bacterial reaction centers (Janzen and Seibert 1980). For example, a photosystem II-enriched submembrane fraction in a photo-electrochemical cell operated in potentiostatic mode was used by Lemieux and Carpentier (1988) to generate photocurrents. The cell included artificial electron acceptors acting as charge transfer mediators between the photosynthetic membrane and the working electrode. Trissl and Kunze (1985) took another approach to generating and measuring photoelectric signals; they studied primary electrogenic reactions in chloroplasts probed by picosecond flash-induced dielectric polarization. Seibert and Kendall-Tobias (1982) measured photoelectrochemical properties of electrodes coated with photoactive-membrane vesicles isolated from photosynthetic bacteria. In their work, chromatophores isolated from the photosynthetic bacterium *Rhodopseudomonas sphaeroides* R-26 were prepared as a film on tin oxide electrodes, and the response to red light was examined in a liquid-junction photoelectrochemical cell. Alexandrowicz and Berna (1980) measured photovoltages in chloroplast extract bilayer membranes stimulated by micromolar amounts of oxidants and reductants.

The distinguishing feature of the work presented in this paper is that the planar composite matrix of precipitated platinum and chloroplast membranes is the conductive medium. That is to say, unlike chloroplast suspensions coupled to electrodes by redox-active mediators (there are no mediators in the preparation) or chloroplast preparations or films in close physical proximity to the electrodes, the composite

photobioelectronic material itself is the photoconductive pathway. It was demonstrated that the concentration of the solution from which the platinum was precipitated directly affects the relative photoconductivity of the sample.

In conclusion, it has been demonstrated that electrical contact with the reducing end of photosystem I was achieved by precipitating colloidal platinum in the presence of isolated chloroplasts. The presence of the platinum had a significant effect on the photoconductivity of the metal-biological composite material. This work is technologically significant because the photosynthetic reaction centers are nanometer structures with picosecond switching times. This work demonstrates that the electron transport chain of photosynthesis can be electrically contacted and that the larger structural matrix of the platinized chloroplasts demonstrates enhanced photoconductivity.

Acknowledgements

I thank S L Blankinship and C V Tevault for technical support and D J Weaver and S A Hoglund for secretarial support. This research was supported by the US Department of Energy and Pittsburgh Energy Technology Center. Oak Ridge National Laboratory is managed by Martin Marietta Energy Systems, Inc., for the US Department of Energy under contract DE-AC-05-84OR21400.

References

- Aizawa M, Hirano M and Suzuki S 1978 *J. Memb. Sci.* **4** 251
Aizawa S, Hirano M and Suzuki S 1979 *Electrochim. Acta* **24** 89
Alexandrowicz G and Berns D S 1980 *Photobiochem. Photobiophys.* **1** 353
Allen M J 1977 in *Living systems as energy converters* (eds) R Buret, M J Allen and J P Massue (New York: North Holland) pp. 271-274
Allen M J and Crane A E 1976 *Bioelectrochem. Bioenerg.* **3** 85
Allen M J, Curtis J A and Kerr M W 1974 *Bioelectrochem. Bioenerg.* **1** 408
Amesz J (ed.) 1987 *Photosynthesis* (Amsterdam: Elsevier)
Anderson J R 1975 *Structure of metallic catalysts* (New York: Academic Press)
Bishop N I, Frick M and Jones L W 1977 In *Biological solar energy conversion* (eds) A Mitsui, S Miyachi, A San Pietro and S Tamura (New York: Academic Press) pp. 3-22
Buchanan B B 1980 *Annu. Rev. Plant. Physiol.* **31** 341
Colvert K K and Davia D J 1983 *Arch. Biochem. Biophys.* **225** 936
Diner B and Mauzerall D 1973 *Biochim. Biophys. Acta* **305** 329
Forbush B and Kok B 1968 *Biochim. Biophys. Acta* **162** 243
Gaffron H and J Rubin 1942 *J. Gen. Physiol.* **26** 219
Gfeller R P and Gibbs M 1985 *Plant Physiol.* **77** 509
Greenbaum E 1979 *Sol. Energy* **23** 315
Greenbaum E 1984 *Photobiochem. Photobiophys.* **8** 323
Greenbaum E 1985 *Science* **230** 1373
Greenbaum E 1989 *Bioelectrochem. Bioenerg.* **21** 171
Hachnel W and Hochheimer H J 1979 *Bioelectrochem. Bioenerg.* **6** 563
Healey F P 1970 *Plant Physiol.* **45** 153
Janzen A F and Seibert M 1980 *Nature (London)* **286** 584
Joliot P 1965 *Biochem. Biophys. Acta* **102** 116
Kaltwasser H, Stuart T S and Gaffron H 1969 *Planta* **89** 309
Lemieux S and Carpentier R 1988 *J. Photochem. Photobiol.* **B2** 221

- Lorimer G, Badger M R and Andrews T J 1976 *Biochemistry* **15** 529
Marder J B and Barber 1989 *J. Plant. Cell Environ.* **12** 595
Ochiai H, Shibata H, Sawa Y and Katoh T 1980 *Proc. Natl. Acad. Sci. USA* **77** 2442
Peltier G, Ravenel J and Vermeglio A 1987 *Biochim. Biophys. Acta* **893** 83
Seibert M and Kendall-Tobias M W 1982 *Biochim. Biophys. Acta* **681** 504
Senger H and Bishop N I 1979 *Planta* **145** 53
Stiehl H H and Witt H T 1969 *Z. Naturforsch.* **246** 1588
Stuart T S and Gaffron H 1972 *Plant Physiol.* **50** 136
Tien H T 1976 *Photochem. Photobiol.* **24** 97
Trissl H W and Kunze U 1985 *Biochim. Biophys. Acta* **806**, 136
Vermaas W F J and Govindjee 1981 *Proc. Indian Natl. Sci. Acad.* **B47** 581
Walker D A 1980 *Methods Enzymol.* **69** 94
Ward B, Reeves M E and Greenbaum E 1985 *Biotechnol. Bioeng. Symp.* **15** 501

Gold-platinum bimetallic cluster catalysts for visible light-induced hydrogen production from water

NAOKI TOSHIMA* and TETSU YONEZAWA

Department of Industrial Chemistry, Faculty of Engineering, The University of Tokyo,
Hongo, Bunkyo-ku, Tokyo 113, Japan

Abstract. Simultaneous reduction of two kinds of noble metal ions by refluxing in alcohol in the presence of poly(*N*-vinyl-2-pyrrolidone) can generally give polymer-protected bimetallic clusters with a core structure. The structures of the clusters were determined by the EXAFS measurements. On the other hand, it is known that micelle-protected platinum clusters work as good catalysts for visible light-induced hydrogen production from water in a system of EDTA/Ru(bpy)₃²⁺/methyl viologen. The stable dispersions of polymer- and micelle-protected gold/platinum bimetallic clusters were prepared by alcohol- and photo-reduction, respectively. The dispersions prepared by photoreduction in the presence of micelle are mainly composed of the mixtures of monometallic gold and platinum clusters, which cannot work as more active catalysts than monometallic platinum clusters. In contrast, the dispersions prepared by alcohol-reduction in the presence of polymer are composed of Au/Pt bimetallic clusters with a "Pt-surrounded Au-core" structure, which are more active catalysts than the monometallic Pt clusters as catalysts for the hydrogen production.

Keywords. Bimetallic cluster; platinum; hydrogen production; catalysts; solar energy storage; electron transfer.

1. Introduction

Production of hydrogen and oxygen from water by using visible light energy has been a dream for mankind for artificial photosynthesis (see for example, Yamada *et al* 1983). Production of hydrogen by visible light irradiation in the system of EDTA/Ru(bpy)₃²⁺/methyl viologen/Pt is a kind of model for such artificial photosynthesis (figure 1). Although this system uses a sacrificial electron donor, EDTA, the production of hydrogen by visible light irradiation is an uphill reaction. In this system, platinum has been used as a catalyst for the production of hydrogen. Colloidal platinum is superior to other platinum catalysts like platinum black and conventional platinum catalysts because of its high specific surface area and transparency with respect to visible light.

More than a decade ago, we developed a convenient method to prepare colloidal dispersions of noble metals (Hirai *et al* 1978; Hirai and Toshima 1986). Refluxing of the solution of noble metal ions in alcohol without additives usually results in the formation of black precipitate which is the reduced metal. However, the addition of

*For correspondence

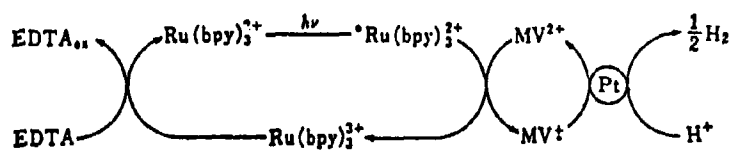


Figure 1. Visible light-induced hydrogen production in a system of Pt colloid/methyl viologen/ruthenium complex/EDTA (sacrificial reagent).

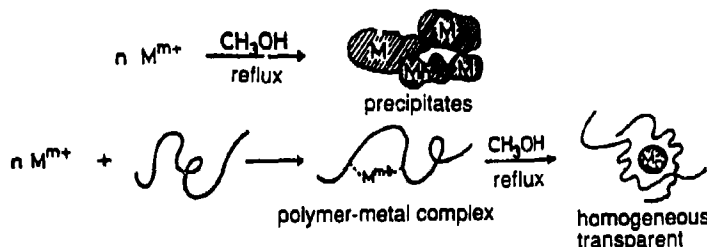


Figure 2. Schematic illustration of reduction of metal ions by refluxing in methanol in the absence and presence of poly(*N*-vinyl-2-pyrrolidone).

a water-soluble polymer, especially poly(*N*-vinyl-2-pyrrolidone), to the solution before reduction results in polymer-metal complexes which produce the homogeneous and transparent colloidal dispersion of noble metals on refluxing as illustrated in figure 2. Colloidal dispersions thus prepared contain metal clusters which are small in size and of narrow size distribution. They are stable and active as catalysts for months. The size of the clusters can be controlled by the reaction conditions, such as the type of alcohol or polymer used, and the concentration of the metal ions or alcohols. The colloidal dispersion of platinum clusters prepared by this method has been applied to the catalyst for the system shown in figure 1, indicating an interesting size effect of the Pt-clusters upon the catalytic activity (Toshima *et al* 1981).

More sophisticated platinum catalysts have been developed by using surfactants (Toshima *et al* 1988). Thus, visible-light irradiation of the aqueous solution of hexachloroplatinic acid containing surfactant micelles gave a colloidal dispersion of platinum clusters protected by micelles. If the surfactant has a terminal olefin, UV-irradiation in the presence of an initiator or γ -ray irradiation polymerizes the surfactant molecules to form polymerized micelle-protected platinum clusters. When the platinum clusters thus prepared are used as catalysts for visible light-induced hydrogen production in the system of figure 1, the presence of the hydrophobic micellar phase in a hydrophilic aqueous medium can promote effective charge separation (figure 3).

Against this background, we would like to present here the preparation and characterization of bimetallic clusters, and the application of gold/platinum bimetallic clusters to the visible light-induced hydrogen production from water.

2. Preparation and characterization of colloidal dispersions of bimetallic clusters

Colloidal dispersions of bimetallic clusters can be easily prepared by refluxing the mixed solution of both metal ions in alcohol in the presence of poly(*N*-vinyl-2-

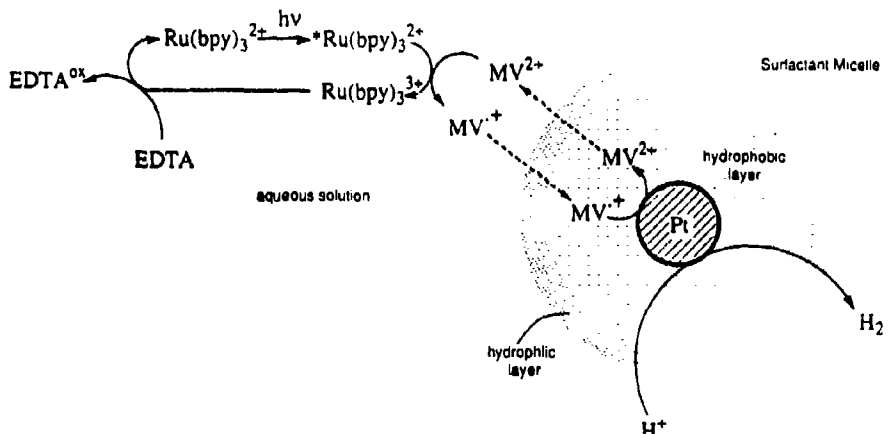


Figure 3. Schematic illustration of effective visible light-induced hydrogen production by using micelle-protected Pt clusters as catalyst.

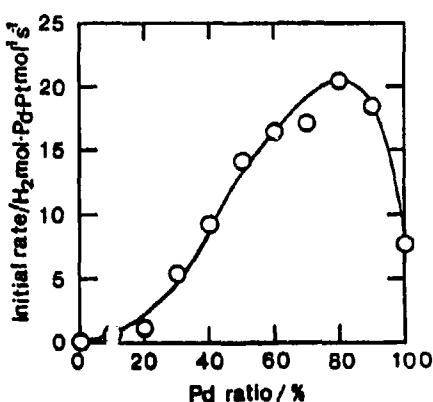


Figure 4. Dependence upon the metal composition of the catalytic activity of Pd/Pt bimetallic clusters for partial hydrogenation of 1,3-cyclooctadiene.

pyrrolidone) (PVP). For example, the solution of PdCl_2 and H_2PtCl_6 in ethanol/water (1/1, v/v) in the presence of the PVP was refluxed for 1 h, resulting in colloidal dispersions of the Pd/Pt bimetallic clusters (Toshima *et al* 1989). The bimetallic clusters are smaller in size and narrower in size distribution than monometallic platinum or palladium clusters. The Pd/Pt bimetallic clusters thus prepared were used as catalysts for partial hydrogenation of 1,3-cyclooctadiene to cyclooctene. The dependence of catalytic activity on the metal composition (figure 4) indicates that the Pd/Pt bimetallic cluster at a Pd concentration of 80%, i.e., Pd/Pt (4/1), has the highest activity, about 3 times that of the monometallic palladium cluster (Toshima *et al* 1989).

The structure of Pd/Pt (4/1) bimetallic clusters has been determined by using an EXAFS technique (Toshima *et al* 1990, 1991; Harada *et al* 1992). Four kinds of coordination numbers obtained from EXAFS measurements for Pd/Pt (4/1) clusters

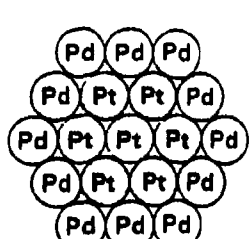


Figure 5. Model for Pd/Pt (4/1) bimetallic clusters.

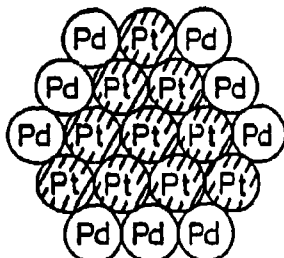


Figure 6. Model for Pd/Pt (1/1) bimetallic clusters.

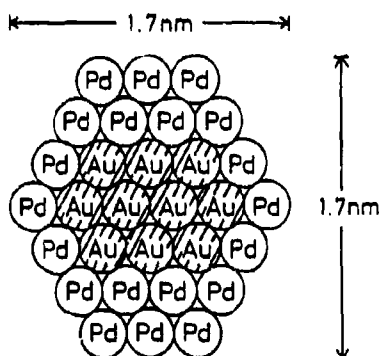


Figure 7. Model for Au/Pd (1/4) bimetallic clusters.

can be compared with those calculated for the model structure shown in figure 5, indicating that the Pd/Pt (4/1) cluster has a "Pd-surrounded Pt-core" structure. Even though the Pd/Pt ratio is varied, the Pt-core structure is maintained. Thus, the Pd/Pt (1/1) cluster has the structure shown in figure 6. In this structure, some of the Pd atoms located on the surface of the Pd/Pt (4/1) cluster have been replaced by Pt atoms, but the other Pd atoms still remain on the surface forming islands.

Au/Pd bimetallic clusters were also prepared by the same method as described above. Their structures were analyzed by the EXAFS technique again. Thus, the Au/Pd (1/4) bimetallic cluster was shown to be a Pd-surrounded Au-core as shown in figure 7 (Toshima *et al.* 1992). In a similar way, the Rh/Pt (1/1) bimetallic cluster has been determined to be an assembly of microclusters with Rh-surrounded Pt-core structure.

From these results, it can be concluded that there is a tendency for noble metals to form the inner core thus: (inner) Au > Pt > Pd > Rh (outer). This tendency could be attributed to the coordination ability of the metal to the PVP which surrounds the metal cluster for protection.

3. Colloidal dispersion of Au/Pt bimetallic clusters

Colloidal dispersions of Au/Pt bimetallic clusters were prepared by simultaneous photoreduction of HAuCl_4 and H_2PtCl_6 in water in the presence of nonionic sur-

factants C₁₂EO and by simultaneous alcohol reduction of HAuCl₄ and H₂PtCl₆ in ethanol/water in the presence of the water-soluble polymer, poly(N-vinyl-2-pyrrolidone) (PVP). The former method was used to obtain micelle-protected Au/Pt bimetallic clusters and the latter, to obtain polymer-protected Au/Pt bimetallic clusters. These clusters used for catalysis of visible light-induced hydrogen production from water in the system EDTA/Ru(bpy)₃²⁺/methyl viologen.

3.1 Photoreduction system

The degassed solution of H₂PtCl₆ and HAuCl₄ in water in the presence of polyethylene glycol monolaurate (C₁₂EO) was irradiated by visible light under argon for 4 h, resulting in reddish-brown solution. The bimetallic dispersion samples thus obtained were used as the catalyst for visible light-induced hydrogen production. The results are shown in figure 8, along with those of physical mixtures of monometallic Au and Pt clusters prepared separately by the same method, and those of the monometallic Pt clusters at concentrations equal to the Pt fraction of the Au/Pt bimetallic clusters. The comparison of these three kinds of catalysts indicates that the physical mixtures have the same activities as those of the monometallic Pt clusters, which means that the coexisting Au clusters have no effect on the catalytic activity of the monometallic Pt clusters. On the other hand, the Au/Pt bimetallic samples result in slightly higher catalytic activities than monometallic Pt clusters or mixtures. The increase in the activity is not as large as expected. This is actually because Au/Pt bimetallic samples are mainly composed of monometallic Pt and monometallic Au clusters, and contain the Au/Pt bimetallic clusters only in small fractions. This is confirmed by comparing the particle size distribution of the Au/Pt(3/2) bimetallic sample with that of monometallic Au clusters. Thus, in the Au/Pt bimetallic sample, the large particles are mainly composed of Au clusters and the small particles are the Pt clusters. Some particles in the intermediate size range are probably the Au/Pt bimetallic clusters.

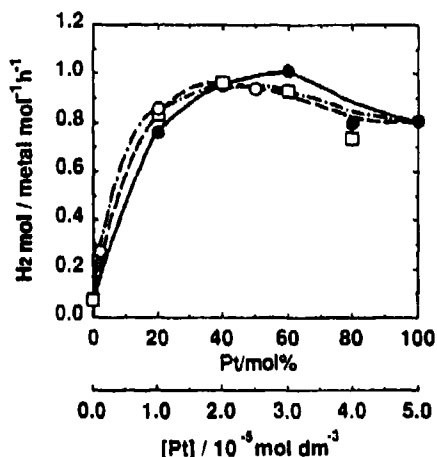


Figure 8. Visible light-induced hydrogen production catalyzed by C₁₂EO-protected Au/Pt bimetallic clusters (●), physical mixtures of monometallic Au and Pt clusters (◻), and monometallic Pt clusters at concentrations equal to the Pt fraction of Au/Pt bimetallic clusters (○).

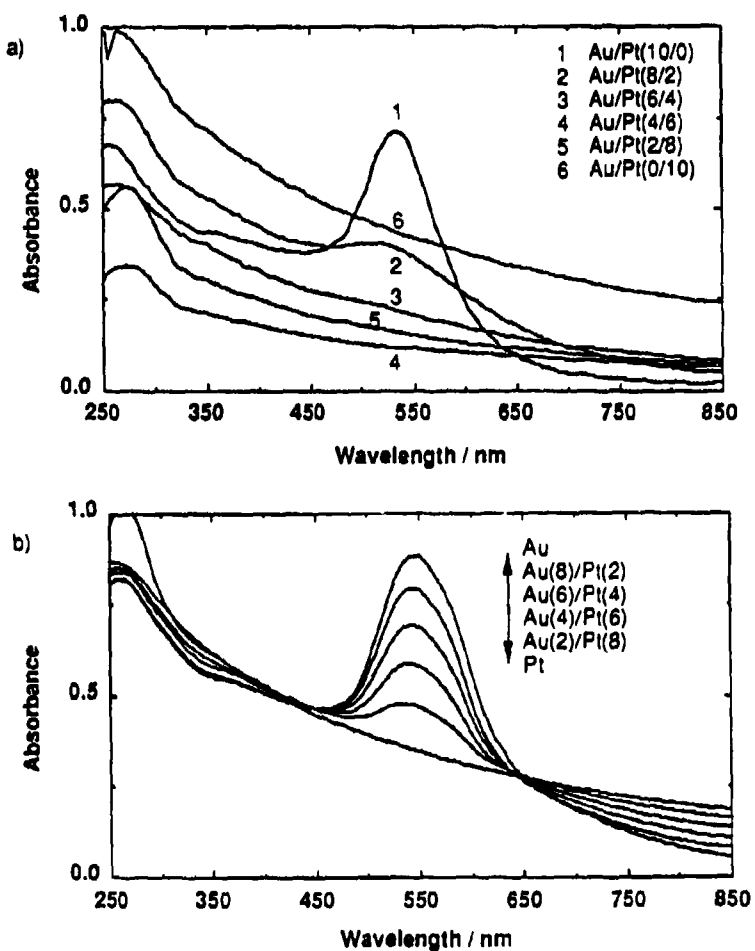


Figure 9. UV-Vis absorption spectra of (a) PVP-protected Au/Pt bimetallic clusters and (b) mixtures of Au and Pt monometallic clusters.

The same conclusion can be drawn by comparing the UV-Vis absorption spectra of the Au/Pt bimetallic samples with those of the physical mixtures. The physical mixtures always have the absorption peak at about 545 nm, which is attributed to the plasma absorption of Au, the peak height of which corresponds to the fraction of Au clusters in the mixtures. The micelle-protected Au/Pt bimetallic samples also have the same absorption peaks, although the peak height is not as high as that of the mixtures.

3.2 Alcohol-reduction system

The solution of H_2PtCl_6 and HAuCl_4 in water/ethanol (1/1, v/v) in the presence of poly(N-vinyl-2-pyrrolidone) (PVP) was heated to refluxing under argon for 2 h,

resulting in a dark brownish solution (Toshima and Yonezawa 1992). The dispersions thus obtained are composed of small metal particles with rather narrow size distribution, as shown by observation with a transmission electron microscope (TEM).

The UV-Vis absorption spectra of a series of PVP-protected Au/Pt bimetallic clusters, shown in figure 9a, are quite different from those of the mixtures of monometallic Au and Pt clusters (figure 9b) and those of the C₁₂EO-protected Au/Pt

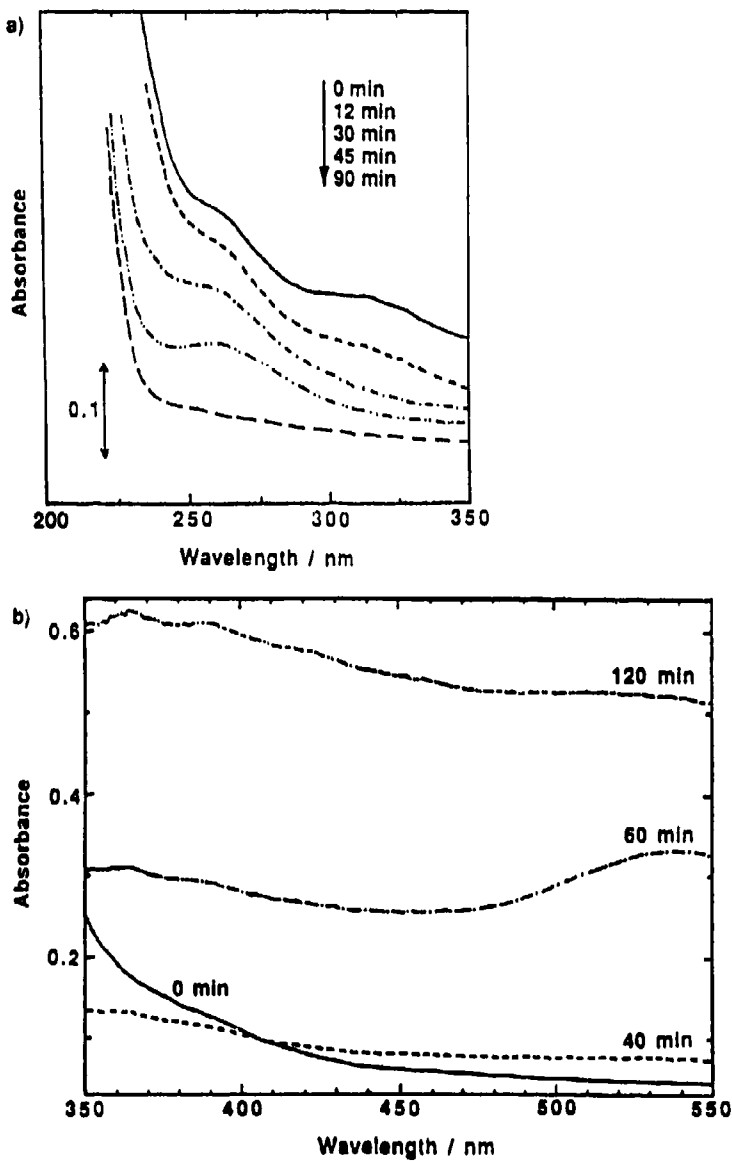


Figure 10. *In situ* UV-Vis absorption spectra during the reduction of a 1/1 mixture of HAuCl₄ and H₃PtCl₆ in ethanol/water (1/1) in the presence of PVP. $\lambda < 350$ nm (a) and > 350 nm (b).

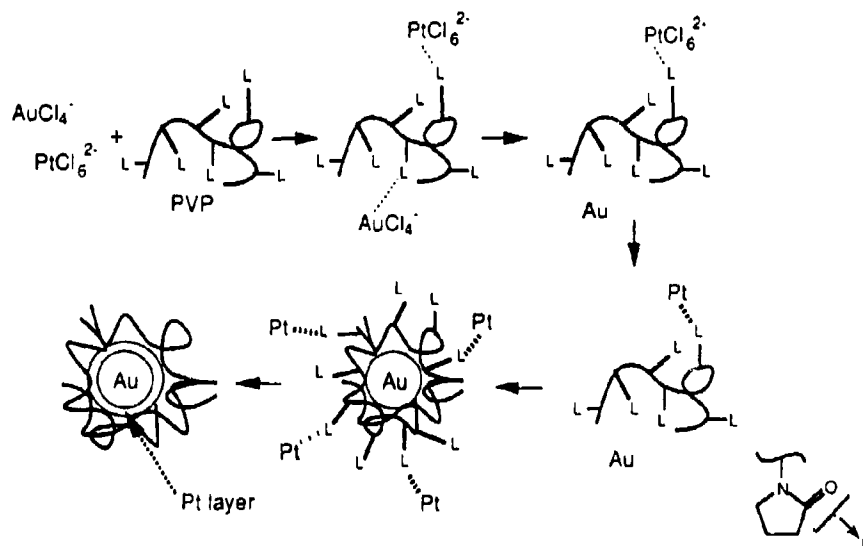


Figure 11. Schematic illustration of the formation by alcohol reduction of PVP-protected Au/Pt bimetallic clusters.

clusters. Thus, the plasma absorption of Au decreases quickly with increase of Pt fraction in the Au/Pt bimetallic clusters and completely disappears at $\text{Au/Pt} = 3/2$. This demonstrates that enough Au atoms are not located on the surface of the Au/Pt (3/2) bimetallic cluster particle to show plasma absorption. In other words, the Au/Pt (3/2) cluster particle is mainly covered by Pt atoms, and the Au atoms are located near the centre of the bimetallic cluster particle, forming an Au core.

The Pt-surrounded Au-core structure is supported by the *in situ* UV-Vis absorption spectra during the reduction of a 1/1 mixture of HAuCl_4 and H_2PtCl_6 in the presence of PVP. As shown in figure 10, the spectrum changes with refluxing time. The change starts at the disappearance of the peak at about 310 nm, due to Au(III) ions. Second, the peak at about 260 nm, attributed to Pt(IV) ions, decreases, and third, the plasma absorption at 545 nm appears, indicating the formation of Au microclusters. At the last, however, plasma absorption disappears and the absorption at whole wavelength increases, suggesting the formation of Pt clusters. Thus, the Au microcluster is covered by Pt atoms forming particles with Pt atoms over the whole surface.

The process of formation of PVP-protected Au/Pt bimetallic clusters by alcohol reduction is schematically shown in figure 11, by which the mechanism of formation of the Pt-surrounded Au-core structure can be understood. The importance of the coordination ability of PVP should be emphasized again in this case. The stronger coordination of PVP to Pt atoms as compared to Au atoms could control the order of aggregation of the atoms, resulting in the Au core and then the Pt shell.

The PVP-protected Au/Pt bimetallic clusters were used as catalysts for visible light-induced hydrogen production. The results are shown in figure 12 for a total metal concentration of $7.5 \times 10^{-6} \text{ mol dm}^{-3}$. Comparison of the catalytic activity of the bimetallic clusters with that of monometallic Pt clusters indicates that Au/Pt bimetallic clusters have higher activity than the monometallic Pt clusters. This is

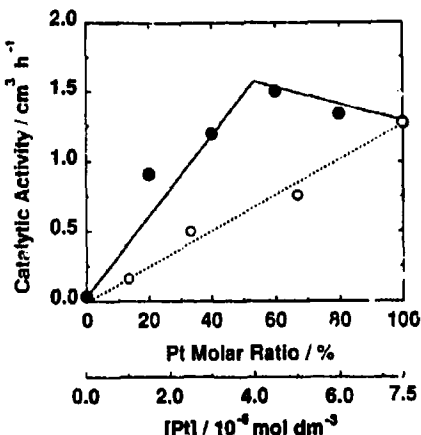


Figure 12. Catalytic activity depending on the metal composition and Pt concentration, respectively, of visible light-induced hydrogen production catalyzed by PVP-protected Au/Pt bimetallic clusters (●) and monometallic Pt clusters (○).

probably because of the ligand effect of the Au core on the Pt shell in the Au/Pt bimetallic cluster particles. In other words, the Pt atoms on the surface of the bimetallic clusters could be rich in electron density by localization of electrons from the inner Au to the outer Pt because of the difference in electron affinities or ionization potentials of Au and Pt atoms.

4. Conclusions

- (1) Alcohol reduction of mixtures of two kinds of noble metal ions in the presence of poly(N-vinyl-2-pyrrolidone) can produce poly(N-vinyl-2-pyrrolidone)-protected bimetallic clusters with a core structure, although photoreduction of the same mixtures in the presence of micelles produces the complex mixtures.
- (2) A common tendency has been observed for the metal which favors the inner core in the bimetallic clusters prepared by alcohol reduction in the presence of poly(N-vinyl-2-pyrrolidone); (inner) Au > Pt > Pd > Rh (outer).
- (3) Visible light-induced hydrogen production in a system of EDTA/Ru(bpy)₃²⁺/methyl viologen/metal catalyst cannot be accelerated by the coexistence of Pt and Au clusters, but can be accelerated by Au/Pt bimetallic clusters with a "Pt-surrounded Au-core structure".

Acknowledgements

The authors express their sincere thanks to Dr M Harada, by whom part of the present work was done, and Drs K Adachi and S Fukuda for their advice on TEM measurements. Financial support by a special grant from The Asahi Glass Foundation, and by Grants-in-Aid for Scientific Research in Priority Areas of "Macromolecular

Complexes" and "Non-equilibrium Process in Solutions" from the Ministry of Education, Science and Culture, Japan are acknowledged.

References

- Harada M, Asakura K, Ueki Y and Toshima N 1992 *J. Phys. Chem.* **96** 9730
Hirai H, Nakao Y and Toshima N 1978 *J. Macromol. Sci. Chem.* **A12** 1117
Hirai H and Toshima N 1986 *Tailored metal catalysts* (ed.) Y Iwasawa (Dordrecht: Reidel) pp. 87-140
Toshima N, Harada M, Yamazaki Y and Asakura K 1992 *J. Phys. Chem.* **96** 9927
Toshima N, Harada M, Yonezawa T, Kushihashi K and Asakura K 1991 *J. Phys. Chem.* **95** 7448
Toshima N, Kuriyama M, Yamada Y and Hirai H 1981 *Chem. Lett.* 793
Toshima N, Kushihashi K, Yonezawa T and Hirai H 1989 *Chem. Lett.* 1769
Toshima N, Takahashi T and Hirai H 1988 *J. Macromol. Sci. Chem.* **A25** 669
Toshima N and Yonezawa T 1992 *Makromol. Chem., Macromol. Symp.* **59** 281
Toshima N, Yonezawa T, Harada M, Asakura K and Iwasawa Y 1990 *Chem. Lett.* 815
Yamada A, Toshima N and Kaneko M (eds) 1983 *Photoenergy conversion* (Tokyo: Sci. Soc. Press)

Light-induced hydrogen production using waste compounds as sacrificial electron donors

CHRISTIAN KÖNIGSTEIN and RUPERT BAUER*

Institute of Physical Chemistry, Technical University Vienna, Getreidemarkt 9/156, A-1060 Vienna, Austria

Abstract. Systems for the conversion and chemical storage of solar energy are usually based on photo-induced electron transfer reactions from an excited sensitizer to an electron acceptor (i.e. an electron relay compound). We have investigated the photo- and electrochemical properties of two novel electron relay compounds: 1,1",1"-trimethyl[4,2;4',4"; 6,4"]quaterpyridinium trichloride (**1**) and 1,1',1",1"-tetramethyl[4,2'; 4',4"; 6,4"]quaterpyridinium tetrachloride (**2**). When solutions containing Ru(bpy)₃Cl₂ or Zn-porphyrin (as photosensitizer), compound **1** or **2** and EDTA (as sacrificial electron donor) are irradiated by visible light ($\lambda > 400$ nm), only the formation of reduced relay compound **1** occurs. Addition of platinum catalyst to such solutions with compound **1** leads to the formation of hydrogen. Quantum yields are in the range of 5%, calculated for absorbed light. Using other sacrificial electron donors such as alcohol or glucose (or waste compounds like 4-chlorophenol) did not result in hydrogen evolution. However, **1** and **2** are reduced by these sacrificial electron donors in the absence of an additional photosensitizer, when near UV irradiation light ($\lambda > 280$ nm) is used. Quantum yields for hydrogen production with compound **1** are about 2%, calculated for absorbed light out of GC-measurements from H₂ in the gas phase above the irradiated solution. The photo- and electrochemical properties of compounds **1** and **2** are discussed.

Keywords. Electron transfer; photo-induced hydrogen production; radicals; electron relays; relay sensitizer.

1. Introduction

Conversion and chemical storage of solar energy has become more interesting since problems of environmental pollution and greenhouse warming increased. Different approaches have been made for the conversion of light. Besides the production of hydrogen by photovoltaic cells (generating electricity), combined with the electrolysis of water, direct hydrogen production by the direct light driven splitting of water has attracted much attention (Harriman and West 1982; Pelizzetti and Schiavello 1991).

Such systems are based usually on photo-induced charge separation.



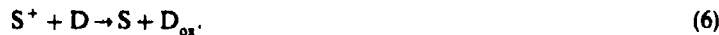
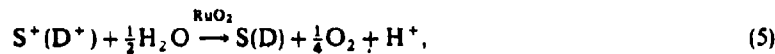
* For correspondence

After excitation (1) a photosensitizer (S^*) releases an electron (2) to an electron-accepting molecule (electron relay, R) or receives an electron (3) from an electron donor (D).

In the presence of a suitable catalyst (e.g. platinum) the reduction of water can be achieved either by the reduced relay radical R^- or the reduced sensitizer A^- to give H_2 :



The reduction of the oxidized sensitizer S^+ (or the oxidized electron donor D $^+$) can be done either by oxidizing water to oxygen (5) or in the presence of a sacrificial electron donor D. In this case, the oxidation of the electron donor is irreversible in reaction (3) or (6):



For practical applications, the use of sacrificial electron donor is of interest, only if it is cheap or a waste product of some other reaction.

The utilization of a (organic) compound as such a donor is strongly limited by the redox potentials of the sensitizer in its ground and excited state(s).

Since the oxidation potentials of widely used sensitizers (e.g. Ru(bpy) $_3^{2+}$: $E_0^{2+/3+} = 1.27$ V, $E_0^{4+/5+} = 0.8$ V vs. NHE) lie in the region of +1.5 V, we tried to find other substances with more positive oxidation potentials (in their excited states).

2. Experimental details

Compounds 1 and 2 (see figure 1) were prepared according to Eichinger *et al* (1987) and Bauer and Königstein (1991). *Tris* (2,2'-bipyridyl) ruthenium(II)chloride. 6 H₂O (= Ru(bpy) $_3^{2+}$, Janssen) and methyl viologen (= MV $^{2+}$, Aldrich) were used without further purification.

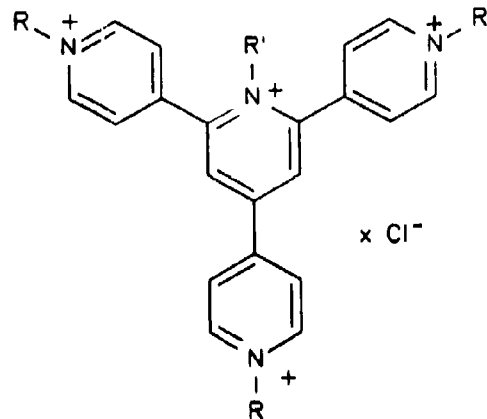


Figure 1. Compounds 1 and 2: 1: R = -CH₃, R' = -, x = 3; 2: R = R' = -CH₃; x = 4.

H₂-production: Argon-purged solutions [containing 1 ml relay (compound 1 or 2, $c_0 = 10^{-2}$ mol/l), 0.5 ml acetate buffer ($c_0 = 1$ mol/l), 1 mol sacrificial electron donor (EDTA, 2-propanol or glucose, $c_0 = 0.1$ mol/l), 0.3 ml Pt-catalyst ($c_0 = 109$ mg/l prepared according to Bauer and Königstein (1991)) and 0.2 ml water] were irradiated by a Hg high pressure lamp (photon flux: $I_0 = (2.1 \pm 0.2) \times 10^{16}$ photons s⁻¹ cm⁻², calculated from 280 to 580 nm, measured by ferrioxalate actinometry).

Solutions with Ru(bpy)₃²⁺ or proflavine as sensitizer consisting of 0.3 ml sensitizer ($c_0 = 5 \times 10^{-3}$ mol/l), 0.6 ml relay (methyl viologen, compound 1 or 2, $c_0 = 10^{-2}$ mol/l), 0.5 ml acetate buffer ($c_0 = 1$ mol/l), 0.5 ml 2-propanol, 0.3 ml platinum catalyst ($c_0 = 109$ mg/l) and 0.8 ml water were irradiated with visible light (400 nm cut-off-filter, 250 W-tungsten halide filament lamp, photon flux: $I_0^{400-580\text{ nm}} = (3.33 \pm 0.05) \times 10^{17}$ photons s⁻¹ cm⁻²).

The H₂-concentration in the gas phase was determined by GC-analysis (Carlo Erba Instruments: GC 6000, with HWD-detector 430, column: 2 m packed iron steel column, filled with 5 Å molecular sieve, carrier: N₂(99.999%)).

Spectroscopy and fluorescence: All absorption spectra were recorded with a Hitachi 220 spectrophotometer. Fluorescence and excitation spectra were monitored with a Perkin Elmer LS 50 fluorescence spectrophotometer. As solvents, water (twice distilled) and acetonitrile (p.A.) were used. The concentration was 10⁻³ mol/l, in acetonitrile BF₄⁻ was used as counter ion (instead of Cl⁻).

Cyclovoltammetry: Measurements with compound 1 were reported in Bauer *et al* (1992); those of 2 were done with a Polarograph VA663 (Metrohm AG) equipped with a Scanner VA E612 and Polarecord E506 reference electrode: Ag/AgCl; acetonitrile solution (working electrode: hanging mercury drop); supporting electrolyte: (0.1 mol/l tetrabutyl ammonium perchlorate (TBAP, electrochemical grade), concentration of compound 2: $c = 2 \times 10^{-4}$ mol/l; scan speed: $v_s = 50$ mV/s–200 mV/s.

3. Results and discussion

Out of phosphorescence measurements the 0–0 transition energy of Ru(bpy)₃²⁺ is calculated to be 2.1 eV. With its ground state redox potentials at $E_0^{2+/3+} = +1.27$ V vs. NHE, and $E_0^{+/2+} = +0.8$ V vs. NHE, those of the excited triplet state are $E_0^{2+*/3+} = 0.84$ V and $E_0^{+/2+*} = 0.84$ V (vs. NHE) (Juris *et al* 1988). So the maximum oxidation power of Ru(bpy)₃²⁺ is 1.27 V (in the ground state). Only a small number of organic compounds (soluble in water) are known, which can be oxidized at this potential (e.g. EDTA, triethanol amine,...). Alcohols, acids (Kolbe photoreaction!) need a more positive potential for their use as sacrificial electron donor agents.

Light-induced hydrogen production experiments with aqueous solutions of Ru(bpy)₃²⁺ (as photosensitizer), methyl viologen (MV²⁺) or compound 1 (as electron relay substance), platinum catalyst, acetate buffer and EDTA gave H₂ with quantum yields of 15 and 4% for MV²⁺ and 1, respectively (calculated for absorbed light, Bauer and Königstein 1991, 1993). Using compound 2 instead of MV²⁺ or 1 as electron relay compound, no H₂ could be produced. Since the first reduction potential of 2 ($E_0^{2+} = -1.15$ V vs. NHE, see table 1) is more negative than that of Ru(bpy)₃^{2+*} ($E_0^{2+*/3+} = -0.84$ V vs. NHE) no electron transfer can occur from the excited sensitizer to the electron relay according to (2).

Table 1. Data on compounds 1 and 2.

Relay sensitizer compound	$\lambda_{\text{max}}^{\text{fl}}$ [nm]	$E_{\text{pH}=0}$ [mV]	$dE/d\text{pH}$ [mV]	$E^{R^+/R3+e}$ [V]	ΔE^{0-0} [eV]	$\Phi_{(1/2)\text{H}_2}$ [%]
1	372	-344	-24	2.87	3.33	2
2	434	-1150 ^a	—	1.71	2.86	—

$E_{\text{pH}=0}$ extrapolated values from Bauer and Königstein (1991); all potentials vs. NHE;
 $dE/d\text{pH}$ measured with CV at different pH values ($\text{pH} = 3 - 13$) (Bauer and Königstein 1991); $E_{\text{pH}} = E_{\text{pH}=0} + dE/d\text{pH} \times \text{pH}$;
 $\lambda_{\text{max}}^{\text{fl}}$ maximum of fluorescence emission;
 $E_0^{R^+/R3+e}$ redox potentials ($\text{pH} = 7$) of the excited states for the reaction:
 $R^{3+e} + 2e^- \rightarrow R^+$;
 ΔE^{0-0} zero-zero transition energy, calculations from $\lambda_{\text{max}}^{\text{fl}}$;
 $\Phi_{(1/2)\text{H}_2}$ quantum yields for H_2 production (for absorbed light, from 280–360 nm);
^a electrochemical measurements of compound 2 were performed in acetonitrile in the absence of protons.

Hydrogen production experiments with other organic sacrificial electron donors (e.g. 2-propanol, glucose, 4-chlorophenol) failed due to unsuitable redox potentials, as described above.

We have shown earlier (Bauer and Königstein 1990, 1991, 1993) that 1,1",1"-trialkyl[4,2';4',4";6',4"]quaterpyridinium trichlorides can act both as photosensitizers and electron relays when excited by near UV light ($\lambda > 280$ nm). Excitation maxima in aqueous solutions for compound 1 were found at 300 and 340 nm (Eichinger *et al* 1987; Bauer and Königstein 1991).

Fluorescence measurements of aqueous solutions of 2 ($c = 10^{-3}$ mol/l, counter ion: ClO_4^-) gave emission maxima at 370, 569 and 722 nm. Excitation maxima for the luminescence at 370 nm could be observed at 346 nm and for the yellow green emission (569 nm) at 392 and 460 nm (figure 2).

The results are in good agreement with those obtained for other derivatives in the series of the 1,1",1"-trialkyl[4,2';4',4";6',4"]quaterpyridinium trichlorides (Eichinger *et al* 1987; Bauer and Königstein 1991).

Emission properties of both compounds 1 and 2 in acetonitrile were a little different from the results in aqueous solutions, reported above. An additional emission band appears at 427 nm (1) and 429 nm (2) with excitation maxima at 367 nm (1) and 378 nm (2) (see figure 3).

Electrochemical measurements of 2 in acetonitrile gave as a result two reversible reduction steps at -1.15 and -1.33 V (vs. NHE). The shift to more negative potentials compared with 1 is attributed to the fourth methyl group in 2.

Calculating the 0-0 transition energies out of the fluorescence measurements (Juris *et al* 1988) of aqueous solutions (see figure 2 and table 1), we found $\Delta E^{0-0} = 3.33$ and 3.35 eV for 1 and 2, respectively. The redox potentials of their excited states are obtained with their ground state redox potentials of $E_0^{(1)} = -0.51$ V (vs. NHE, $\text{pH} = 7$), and $E_0^{(2)} = -1.15$ V (vs. NHE) from cyclic voltammetry (CV): $E_0^* = +2.82$ and $+2.20$ V (vs. NHE) for 1 and 2, respectively (see table 1). This is much more positive than the potential which can be reached by $\text{Ru}(\text{bpy})_3^{2+}$.

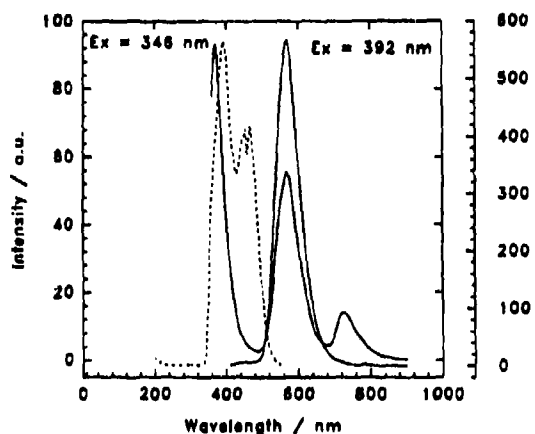


Figure 2. Fluorescence (—) and excitation spectra (-----) of compounds 2 in water.

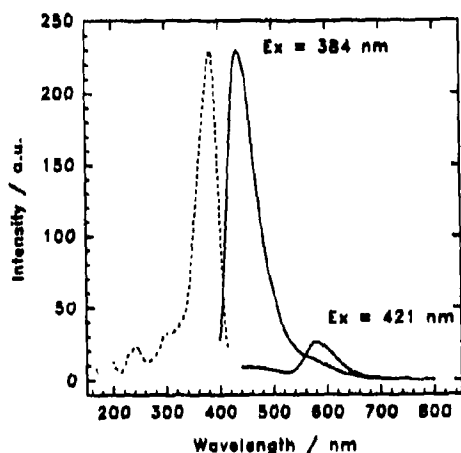


Figure 3. Fluorescence (—) and excitation spectra (-----) of compounds 2 in acetonitrile.

Excitation of aqueous solutions, containing compound 1 or 2, phosphate buffer ($\text{pH} = 7$) and a sacrificial electron donor (EDTA, glucose or 2-propanol), with near UV light ($\lambda > 280 \text{ nm}$) resulted in the formation of reduced relay molecules and the oxidation of organic compounds. In contrast, $\text{Ru}(\text{bpy})_3^{2+}$ was successfully used as photosensitizer only in combination with EDTA as sacrificial electron donor.

In the presence of a platinum catalyst hydrogen could be detected in the gas phase above the solution. The quantum yield was calculated for absorbed light to be: $\Phi_{(1/2)\text{H}_2} = 2\%$ for compound 1. However compound 2 was not able to produce H_2 under these conditions.

Using waste water containing 100 ppm 4-chlorophenol as sacrificial electron donor agent for photoinduced H_2 -formation with compound 1 or 2 did not succeed, although thermodynamically allowed.

A high excess of the electron-donating substance is necessary to obtain sufficiently fast reaction rates. In case of glucose and 2-propanol the initial sacrificial donor concentration was five times the concentration of 1 and 2, respectively.

4. Conclusion

Both compounds 1 and 2 were found to be able to undergo reversible redox processes. The first reduction potentials were determined by cyclic voltammetry $E_0 = -0.51$ and -1.15 V (at $\text{pH} = 7$, vs. NHE) for 1 and 2, respectively. Fluorescence measurements of aqueous solutions showed that both compounds gave blue luminescence emission with its maxima at 372 nm (1) and at 370 nm (2), when excited by near UV-light ($\lambda^{\text{Ex}} = \sim 340\text{ nm}$). With 0-0 transition energies (from the emission properties) of 3.33 eV (1) and 3.35 eV (2), redox potentials of the excited states were calculated: $E^{*(1)} = 2.82\text{ V}$ and $E^{*(2)} = 2.20\text{ V}$ ($\text{pH} = 7$, vs. NHE). These values are much more positive than the redox potentials of $\text{Ru}(\text{bpy})_3^{2+}$ (0.8 V excited or 1.27 V ground state vs. NHE, respectively). Hydrogen production experiments showed that organic compounds in excess can act as sacrificial electron donors with 1 or 2 (as relay-sensitizers).

Acknowledgements

We wish to thank Professor Dr. Karl Eichinger, of the Institute of Organic Chemistry, for the synthesis of the relay compounds, and for very stimulating discussions. Furthermore, the financial support of the Fonds zur Förderung der Wissenschaftlichen Forschung (Project number 8346) is gratefully acknowledged.

References

- Bauer R, Hofstädler K and Königstein Ch 1992 *Proc. Indian Acad. Sci. (Chem. Sci.)* **104** 265
Bauer R and Königstein Ch 1990 in *Hydrogen energy progress VIII* (eds) T N Veziroglu and P K Takahashi (New York: Pergamon)
Bauer R and Königstein Ch 1991 *J. Photochem. Photobiol. A* **59** 61
Bauer R and Königstein Ch 1993 *Int. J. Hydrogen Energy* **18** 205
Eichinger K, Nussbaumer P and Vytlacil R 1987 *Spectrochim. Acta A* **43** 731
Harriman A and West M A (eds) 1982 *Photogeneration of hydrogen* (London: Academic Press)
Juris A, Balzani V, Barigelli F, Campagna S, Belser P and von Zelewsky A 1988 *Coord. Chem. Rev.* **84** 85
Pelizzetti E and Schiavello M (eds) 1991 *Photochemical conversion of solar energy* (Amsterdam: Kluwer)

What's new in stereophotolithography?

J C ANDRE*, S CORBEL and J Y JEZEQUEL

GdR "Optical Instrumentation" CNRS, ENSIC-INPL, BP451-F 54001 Nancy Cedex,
France

Abstract. Laser stereophotolithography is a technology which allows the space-resolved phototransformation of a product. In this paper we describe the different basic processes with their limits. We present several ways to override these limits and discuss new application areas.

Keywords. Stereophotolithography; space-resolved phototransformation.

1. Introduction

First generation stereophotolithography (SPL) deals with the manufacture of three-dimensional objects. They are made by space-resolved laser-induced polymerization. As a matter of fact, one uses a layer-by-layer process (photolithography) which allows the manufacture of objects (stereo). This scientific field, which is widely open to industrial application (design, prototyping, scale models etc.), is still restricted by the quality of the materials: volume shrinkage, warping, hardness, mechanical properties etc. All this defines a wide research area in connection with the making of new photoconvertible materials by the association of monomers, the addition of fillers and new photochemical initiators.

It is, for example, possible to override the limits of this technology, induced by volume variations, by modifying the manufacture process to take them into account beforehand. Also, since we aimed at manufacturing pieces fit for use, we developed a "second generation" technique that we describe in this paper.

In other respects, several different domains of application exist and every one of them needs specific materials as well as specific processes. They can be the manufacture of optical pieces, microtechnological objects, scale models etc. This proves that the market for stereophotolithography must expand and find application areas in specific domains. Out of this description, the use of new principles in photochemical initiation allows the possibility of 3D information systems.

In this paper, we shall recall the bases of the "first generation" stereophotolithography, show its limits and consider solutions to reach better results. These improvements will come from the materials and/or the processes.

* For correspondence

2. Recalls on the laser stereolithography

We have developed, along with others, a process which makes three-dimensional objects by polymerizing a liquid monomer using a laser energy source (Andre *et al* 1990). The laser beam can be focused precisely on a liquid so that a liquid/solid photochemical transformation can be achieved. The advantages over the traditional techniques are that a mould is no longer necessary, the shape of the object can be totally arbitrary and wear of the tool is not needed.

Here, we show how three-dimensional objects can be created by using computer-aided design. In the current stage, this new technique, which has led to very promising results, is limited by the choice of materials, and the traditional CAD has to be thus adapted. After discussing briefly the manufacture of objects by computer-aided laser polymerization, the coupling between the adapted CAD and the choice of materials is shown. The applications of this new technique are not all known yet; however, future progress will depend on the ability of specialists in the fields of materials engineering, photochemistry and computer-aided design to work together.

2.1 Brief review of photopolymerization methods

If a sufficient number of photons is absorbed per volume unit, unstable species are created and the liquid monomer polymerizes into a solid which is not soluble in the liquid monomer.



The above simplified mechanism shows that two main difficulties have to be surmounted: the local light absorption and the choice of materials. If these two main difficulties are only partially mastered, a modification of the computer-aided design becomes necessary.

2.1a Light absorption: Two excitation techniques have been proposed so far: multiphotonic absorption and monophotonic absorption. For now, the second seems more efficient for industrial applications.

The theoretical basis is the Beer-Lambert law. A light beam is incident on z , the concentration C_a is such that the light absorption during dt produces a polymerization of the monomer between z and $z + \Delta z$. If the beam radius is Δr , the polymerized voxel volume is $\pi \Delta r^2 \Delta z$.

Successive layers of thickness, Δz , are made. This is shown qualitatively in figure 1. Starting from the base which contains a layer of thickness Δz , the laser beam is displaced in the xy plane in order to solidify the $z = 0$ plane. Afterwards, a new layer of monomer is added and the process is repeated. An object can be made with just one laser. The laser beam is guided into the reactor containing the monomer. The guide must be very loosely attached to the created voxel otherwise deformation or rupture is possible. Several techniques enabling this exist. In all monophotonic processes, the object coordinates stored in the computer are given in the form $z = f(x, y)$.

2.1b Materials: Unless some special mechanical property of the object is desired, the liquid monomers should have the following characteristics: rapid reaction rate

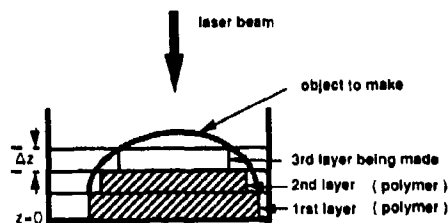


Figure 1. Principle of the layer-by-layer space-resolved polymerization.

and lowest possible viscosity in order to reduce the time needed per layer and to limit hydrodynamic side effects caused by the guide displacement. Monomers M having such properties are mainly in the epoxy or acrylate groups. Photochemists know well how to initiate and control the reactions using these species. When a monomer is polymerized, a volume variation is observed due to the photoreaction. This has various consequences. A polymerized voxel, which is not sustained and whose density is higher than that of the liquid, will tend to sink to the bottom unless held by surface tension forces. The manufactured object may thus acquire dimensions other than the ones specified. Furthermore, the object can deform.

In order to remedy these difficulties, materials which do not shrink and which have the properties mentioned earlier have to be searched for (*cf* § 3). These materials exist but their viscosity is often too high. Another solution is to adapt the computer-aided design in order to limit memory effects induced by the polymerization.

The principle consists in polymerizing voxels that are separated one from the other. The volume variation of each element occurs independently and then the interstices separating the voxels are polymerized. Since the laser has to be continuously displaced, a galvanometric mirror controlled by a computer should be used.

2.2 Basis of a laser CAD machine

2.2a The machine: The monophotonic process described earlier is split into several sub-systems which are:

- the computer system which includes the computer which receives the CAD data from another system. The computer system adapts the data to define the optimum laser beam displacement;
- the photochemical reactor;
- the laser;
- a motor-driven optical mechanical unit with several degrees of freedom which shapes the light beam and then deflects it into the monomer to be polymerized;
- a motor-driven system which moves the object along the z axis.

2.2b CAD software: In our case, the objects to be made are solids, either filled or hollow. Furthermore, great care must be taken in their manufacture since they are intended to be duplicated. A model is the more realistic that it accounts for the greater number of constraints of the object.

The system configuration must be able to use CAD software which is commercially available. The interface must be conceived and should:

- verify that the object can be made;
- choose the best manufacturing order;
- decompose the object into voxels;
- predict and impede object deformation;
- command the whole process.

We have previously shown that it is not acceptable to create voxels that are independent of the partially created object.

As indicated before, the object can be manufactured at z by laser-induced polymerization on the whole or part of the surface. The polymerization time is proportional to h^3 for an object of size h and proportional to h^2 if only the surface is polymerized. It may be advantageous to polymerize the surface of the object only plus several elements inside it to increase its rigidity.

After taking the object out of the reactor, it contains liquid monomer. It can be used as such or a more complete polymerization can be obtained in an annex system. One must take into account that in this latter case, the object can deform due to shrinkage. The definition of the points where the object must be reinforced could be interesting. All these technical difficulties can be solved by adapting existing CAD software or by carefully choosing the materials used.

2.2c Optical mechanics: Carboxylic components are the most well-known and the most efficient photochemical reaction initiators. Their absorption spectra are centred



Figure 2. Object manufactured by laser stereophotolithography.

at 350 nm. A laser which emits in this spectral zone is usable (He/Cd, Ar⁺ etc.). Other compounds to initiate the reaction are available in the visible and the infrared regions.

When using z-axis displacement to guide the light beam, it is preferable to use stages moved by a computer-controlled step-by-step motor. For a system using the superposition of layers on the partially realized object, and in order to reduce manufacture time, it is advised to use displacement systems with very small inertia, for example, computer-controlled galvanometric mirrors.

This technique allows the manufacture of objects having a satisfying shape and quality (cf figure 2). Nevertheless, as already said, it is necessary to improve the process to make it completely satisfactory. The following paragraphs describe several ways to improve this process.

3. Improvement of first generation processes

It is clear that we must first improve the qualities of the materials. We arranged them in the following decreasing order of importance:

- volumic shrinkage;
- viscosity;
- mechanical and thermal properties;
- resins with fast reaction kinetics.

Since so far it has been impossible to obtain no volume variation between the monomer and the polymer when the monomer is viscous, we had to present the following modifications.

3.1 Improvement of the resins used in stereophotolithography (SPL)

It is necessary to use a resin whose shrinkage is as small as possible to avoid volume deformations and shear stresses in the objects manufactured by SPL.

Experiments prove that when we use oligomers instead of monomers, the shrinkage decreases. But since at the same time the viscosity of the liquid increases appreciably, this limits the interest of the process beyond some value (several Pa.s typically).

Table I. Principal resins used in SPL commercially available in Europe.

Resin	Density	Viscosity (Pa.s) (at T °C)	Appearance	Elongation before break (%)*	1% secant modulus (MPa)*	Shrinkage (%)
XB 5081	1.14	1.8-3.6 (30)	Transparent	2-3	2500-3500	5.2
XB 5134	1.12	1.6-2 (30)	Slightly opaque	10	800-1100	
Somos 3100	1.13	1.5 (25)	Amber transparent	15	800-900	6.2
Somos 2100	1.16	5.3 (25)	Milky white opaque	12	30-40	
Diacryl 103	1.12	1.0-1.4 (25)	Transparent	1.2		6.2

*Characteristics measured with products post-cured by fluorescent or UV light

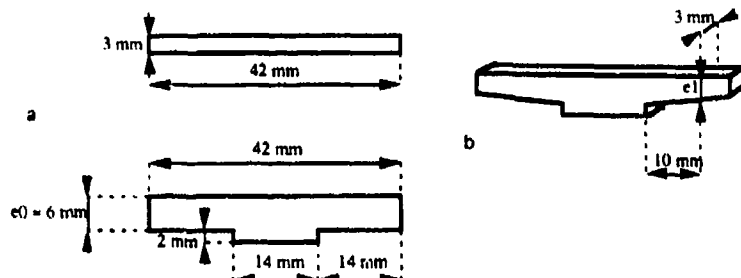
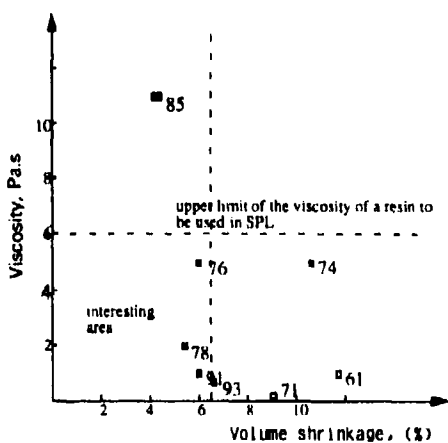


Figure 3. Test piece and bend coefficient. (a) Test piece. (b) Test piece manufactured by SPL.



c : resin having a bend coefficient of $c \%$. The higher this coefficient is, the darker the square is.

Figure 4. Influence of the viscosity and of the shrinkage on the bend coefficient c .

In table 1 are presented the characteristics of several resins commonly available commercially and used in Europe. They have small shrinkage ratios (between 5 and 6% usually).

Beside this shrinkage problem, it would be interesting to correlate the type of the resin with the global deformation of a test piece such as the one presented in figure 3. These deformations occur after polymerization by SPL.

To compare various resins, we measure the thickness e_1 , 10 mm away from the base of the piece (cf figure 3). We define the bend coefficient c (in %) as the ratio:

$$c = (e_1/e_0) \cdot 100,$$

where e_0 is the expected thickness of the piece. The closer c is to 100, the more precise is the piece.

By changing the composition of the reactive medium (a mixture of several acrylic oligomers to have fast reaction kinetics), we have not managed as yet to reach

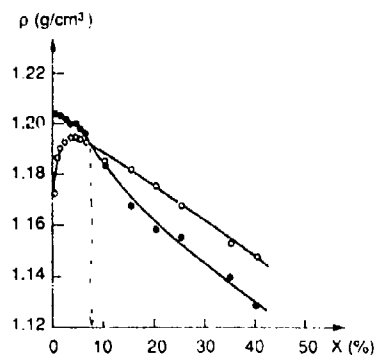


Figure 5. Specific gravity of the epoxy/PSS system before (○) and after (●) polymerization versus the PSS ratio.

shrinkage ratios smaller than 5% (*cf* figure 1). By a trial-and-error method, we made a resin (EOS-SPM) (Andre *et al* 1991), composed of aliphatic methane with carbonate acrylic which has not only these volume properties, but also reasonable mechanical characteristics.

Taking these results into account, a natural way to modify the characteristics of the reactive medium is to add charges in it. They limit the proportion of reactive medium per volume unit and then should induce smaller shrinkages. We experimentally found that the shrinkage decreases linearly with the charge ratio when the charge is not porous. This means that it can never be equal to zero. On the contrary, we experimentally proved that it was possible to obtain the same density for the monomer and the polymer (*cf* figure 5) when we used porous charges.

This method of research is very attractive as long as the resin viscosity does not exceed several pascals and as long as the sedimentation of the charge can be neglected. This implies the use of charges whose sizes are very small (Karrer *et al* 1992).

This short summary of the materials side of the process show that it is possible to improve the geometrical characteristics of an object manufactured by SPL by using proper compositions of the reactive medium. Nevertheless, it is still necessary to carry on investigations in this area, and this is why it remains one of our research fields of interest.

3.2 Improvement of the process

To improve the process, investigations can be developed in two directions: the improvement of the process itself and the improvement of the polymerization ratio to avoid a post-phototransformation.

Layerwise photopolymerization generally uses the principle of a polymerization by voxels which are independent from the others: in a given layer, the liquid-to-solid phototransformation is carried out on voxels which are individually affected by the shrinkage effect. Then, a second pass of actinic light allows the voxels to be sealed together so as to generate the final profile of the object. In doing so, the overall deformation is the result of reduced volume shrinkages corresponding to the association of the solid voxels with the others (*cf* figure 6).

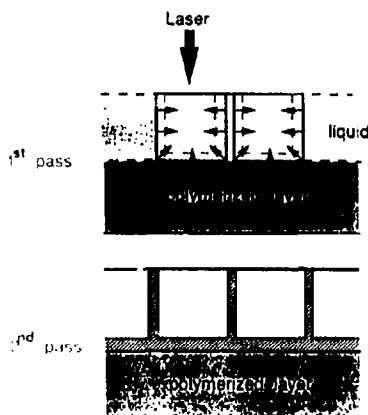


Figure 6. Principle of a space and time-resolved irradiation reducing the volume shrinkage.

A second improvement can come from research on materials having a high photopolymerization ratio, to avoid postpolymerizations in particular, which are very often the cause of global deformations. This postpolymerization is necessary when:

- the progress of the reaction is such that one is beyond the gel point. The mechanical properties of the object are satisfactory but complete polymerization is not yet achieved.
- only a part of the object being manufactured is photopolymerized in order to reduce the time of manufacture.

In table 2 we collected the conversion ratios of several commercialized acrylic resins that we measured.

Table 2. Experimental conversion ratio measurements for several commercialized resins.

Resins	Average conversion ratios (%)	Energy density (mJ. cm ⁻²)
Mixture of 50% Ebecryl 7100 50% C1993	98	81.8
C1993	76	81.8
Ebecryl 3200	84	81.8
Mixture of 50% Ebecryl 3703 50% C1993	90	20
Mixture of 50% Ebecryl 3703 50% Ebecryl 7100	92	20
Ebecryl 140	46	94.6
Eos SPM	91	88
Ebecryl 7100	96	16
Diacryl 103	47	16

3.3 Conclusions

We have qualitatively shown here the need to modify both the process and the photo-transformable materials to improve the "first generation" stereophotolithography. Other principles can be considered to manufacture prototype pieces and the actually existing technology must still be improved to fill the market which could be its own.

4. Second generation stereophotolithography

The choice of naming this technology "second generation SPL" only deals with the fact that the object is self-sustained during its manufacture. It means that the nature and the reactivity of the materials are not taken into account in this definition. But in the following descriptions, it will on the contrary be natural to make a distinction between physical processes and chemical processes.

4.1 Physical processes

The basic principle of this process is the use of the powder of a material which can either melt or sinter. This material can be a polymer, a ceramic powder, metal powders etc. The choice of the material is much wider in that case because the imposed conditions are the following:

- the material must absorb light;
- the light energy must be high enough to melt or to sinter the powder;
- the adhesiveness between the particles of powder must be strong enough to obtain a solid object.

The principle of how it works is shown in figure 7.

4.1a Principle of the manufacture of a layer: Let us assume that the piece has been manufactured up to height h . We make the mobile sustaining plate go down at a

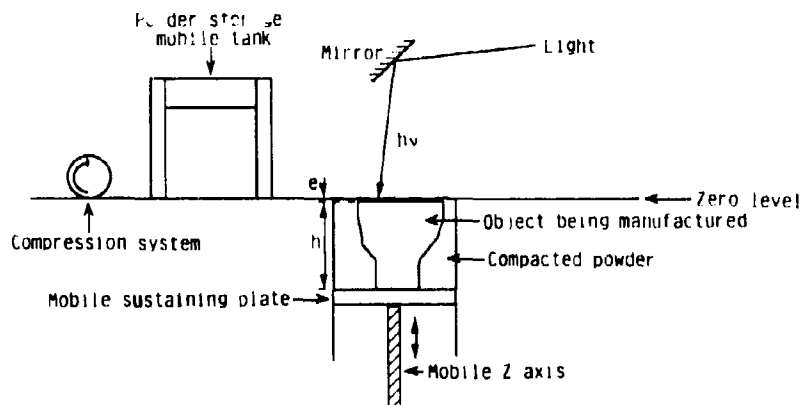


Figure 7. Schematic block diagram of a second generation SPL process using powder materials.

distance e' from the zero level, slightly larger than the desired thickness e . In a second step, we slide the powder storage mobile tank over the sustaining plate. This translation of the storage tank fulfills two purposes: bringing in material and scraping the open surface of the reactor.

To bring the particles of powder closer together, we can move up the plate by a height of $(e' - e)$ and compact the material to a maximum by the compression system. This more compact material leads to smaller shrinkages. The choice of the powder is very important for obtaining the smallest possible deformations. For example, the use of particles of different sizes could be a way to again increase the compactness.

In a third step – now that the new layer, e thick, is ready – we can induce the phototransformation of the material by melting or sintering the powder. The expected space resolution depends on several parameters:

- the power of the laser;
- the resolution of the beam at the surface of the layer (one must in particular pay attention to the problems of reflection and of diffusion of the light which can be harmful to the eyes. The users of such apparatus must carefully read the safety notices about laser sources);
- the local distribution of the particles;
- the volumic and surface heat transfer coefficients;
- the thermal evolution of the material, from a pulverized state to a continuous state when melting occurs;

among others.

However, this technology in principle presents important advantages because the manufacture of an object made of different materials is highly simplified (*cf* figure 8).

When the manufacture of the part is achieved the part lies inside a compact matrix. The binding material is removed by a proper solvent – which can be water – and the powder that has not been irradiated is easily taken away.

We define the object inside the matrix as a 3D latent image and the removal of the non-irradiated powder as the development of this 3D image.

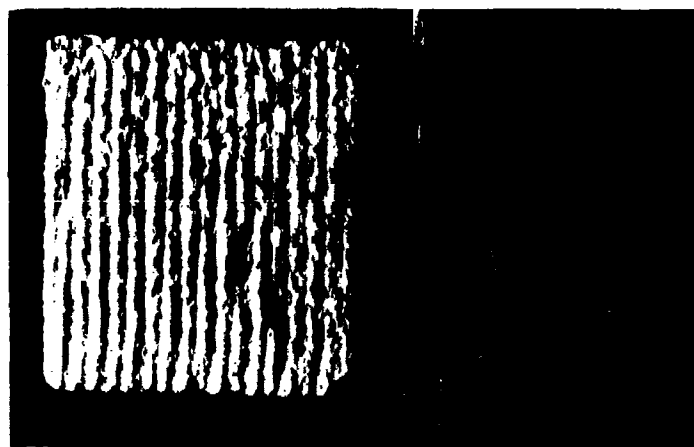


Figure 8. Piece manufactured by the space-resolved laser sintering of alumina powder.

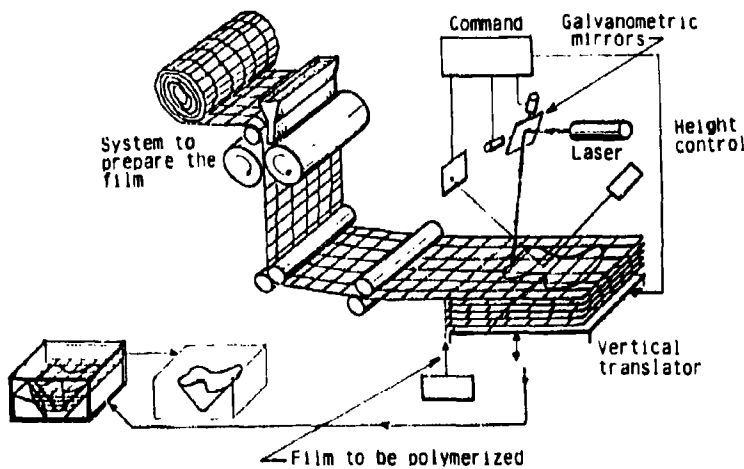


Figure 9. Second generation SPL apparatus using composite materials.

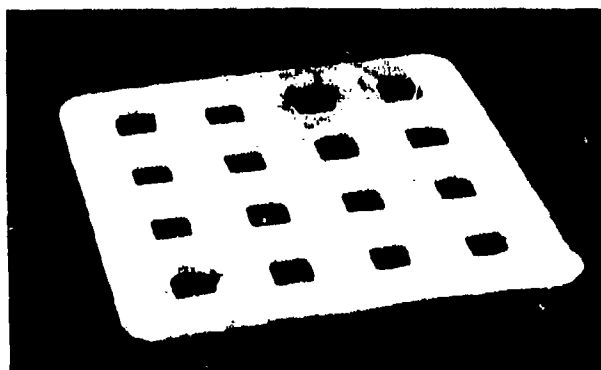


Figure 10. Object manufactured by a second generation SPL process.

4.2 Chemical processes

In the "bidimensional" lithography used in offset or in electronics, one uses photo-sensitive resins which are rendered insoluble by irradiation whereas the unirradiated resin remains soluble in some solvent. This technique can schematically be compared to the photoreticulation of a part of the material, and we can apply the technique described in figure 7 to manufacture 3D objects: since the irradiated resin becomes insoluble, one only has to plunge the matrix into an appropriate solvent to develop the object.

Another method to manufacture objects by a second generation SPL process is to use a reinforced material made of wire netting embedded in a resin (with a possible added charge to try to minimise shrinkage). The principle of this process is depicted in figure 9, and figure 10 is a photograph of an elementary object manufactured by this technique.

When the object is achieved, the un-irradiated resin is removed by a solvent, as usual, and we get an object which is completely associated to the wire netting. The netting external to the object is destroyed by chemical treatment such as its dissolution by an acid or a base.

5. Other processes - technological application fields

This paper would become much too long if we described all the fields where a space resolved light absorption could be used to manufacture 3D objects. We shall nevertheless mention several attempts which have already been partly investigated.

5.1 Information storage and third generation SPL

The basic principle is the multiphonic absorption of light, either sequentially or simultaneously. Even if this process has not yet found any application in laser computer-aided design and manufacturing after the interesting research of the Battelle Institute, it should be possible to use it – as it is already the case with the photoablation processes (Andre 1991) to store information in 2D or even 3D.

5.2 Optical-component manufacture

One can focus a laser beam on a monomer to photopolymerize it and to manufacture optical components that way: for example microlenses, lenses or optical fibres (Brulle 1992). As an example, figure 11 depicts a process to manufacture optical fibres by space-resolved photopolymerization.

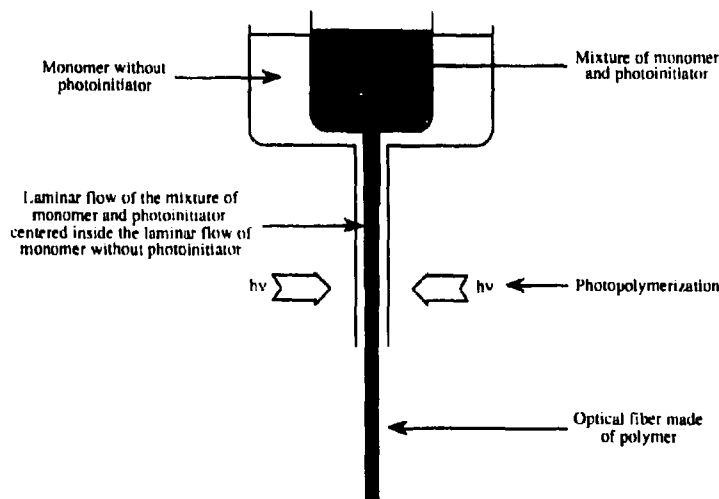


Figure 11. Manufacture of polymer optical fibres by the photopolymerization of a laminar flow of monomer.

5.3 SPL and microtechniques

A new market which needs the manufacture of micro-objects is coming up: micro-motors, active microsystems, microresonators etc. Studies on photonic systems able to manufacture active microobjects by SPL is of great interest because it opens up the possibility of making them automatically, via collective processes. These studies are far from completion but several technologies, based on the ones we described in this paper or on others (Meermann 1992), have already provided very encouraging results.

5.4 2D photography

The idea of combining the transformation of a material with its colouring, at least on the surface of the object, should allow the manufacture of 3D photographs. Since these studies are still under progress, we cannot describe them as yet.

6. Conclusions

Laser stereophotolithography is a recent technology which has been commercialized. It has not yet realised its entire potential, even if we do visualize some of them. If it is true that this technology will not probably take the place of all computer-aided tooling techniques, it is also true that all its applications are not yet known. To know them, it is necessary to undertake pluridisciplinary studies getting together photo-chemists, specialists in material sciences, automatics, informatics and possible users. This is a difficult but very stimulating activity, and we expect to persist in doing it.

References

- Andre J C 1991 Microstéréophotolithographie. In *Recherches en Microtechniques: réalités et perspectives*. Institut des Microtechniques Ed., Besançon, France. pp. 73-88
Andre J C, Balme F, Corbel S, Vanoeuvre F and Langer H 1991 Lichthärt bares Kunststoffmaterial, Deutscherpatent 413 83 09
Andre J C, Corbel S, Nonnenmacher F, Schaeffer P and Cabrera M 1990 Computer aided manufacture of three-dimensional objects in Industrial Photo-chemistry - B, 475-95, ENSIC Ed. Nancy - France
Brulle Y 1992 *Photonical processes for optics*. Ph D thesis, Nancy, France
Karrer P, Corbel S, Andre J C and Lougnot D J 1992 Shrinkage effects in photopolymerizable resins containing filling agents: Application to stereophotolithography. *J. Polym. Sci.* **304** 2715
Meermann H 1992 Eiffeltower mit dem Laser gebaut. In MPG Presse Information, München-BDR, PRI C 3/92 (12)

Purification of drinking water by irradiation. A review

NIKOLA GETOFF

Institut für Theoretische Chemie und Strahlenchemie, der Universität Wien und Ludwig Boltzmann Institut für Strahlenchemie und Strahlenbiologie, Währingerstr. 38, A-1090 Wien, Austria

Abstract. The present review deals with the possibilities of water purification by UV-light, solar energy in combination with catalysts (e.g. $n\text{-TiO}_2$), as well as by using ionizing radiation (e.g. high energy electrons or γ -rays). The various methods are illustrated by typical examples concerning the degradation of aliphatic and aromatic halogenated pollutants in water. Some probable reaction mechanisms initiated by light or ionizing radiation are also given.

Keywords. Water purification; pollutants; degradation; photolysis; radiolysis.

1. Introduction

Water is the most important life factor for all living systems. As a consequence of the rapid development of various industries, the application of fertilizer, pesticides etc. in modern agriculture, the production and combustion of fossil fuels etc., there has been a strong overloading of water resources. On the other hand, the chlorination of drinking water (containing humic substances) for the purpose of disinfection leads to the formation of a number of toxic compounds (Rock 1974; Hutzinger *et al* 1982; Getoff 1986a). Hence, a subsequent purification of the water, e.g. by filtration through activated carbon, is necessary.

Careful investigations by various laboratories in the recent years proved that biological resistant pollutants in water can be decomposed by UV-light, solar energy in the presence of special catalysts, e.g. $n\text{-TiO}_2$, and ionizing radiation. All these three possibilities are later illustrated by examples and critically discussed. Based on the present state-of-the-art a comparison between them is made with respect to their technical application.

2. Photoinduced degradation of water pollutants

2.1 Using VUV- and UV-light

In the last decades, a number of papers have been published about the photoinduced decomposition of water pollutants. Only some of them will be briefly mentioned in the frame of this review, since further papers on nearly the same topics are also on the programme.

Naturally, a direct photochemical degradation can be achieved only when the incident light (vacuum-UV-quanta: $\lambda < 200\text{ nm}$ or UV-light: $\lambda > 200\text{ nm}$) is absorbed by the

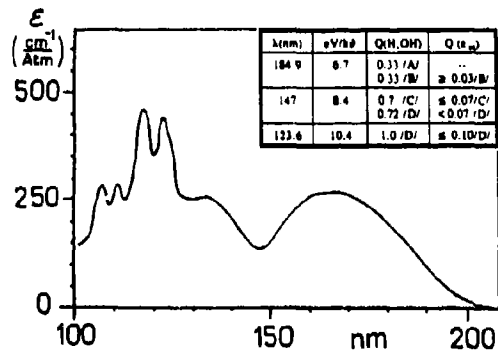


Figure 1. Absorption spectrum of water (Watanabe and Zelikoff 1953). Inset: Quantum energy (eV/hν) and quantum yields (Q) of the primary products of water photolysis with VUV-light at 123.6, 147 and 184.9 nm. (A) Dainton and Fowles 1965b; (B) Getoff 1968b; (C) Sokolov and Stein 1966; (D) Getoff and Schenck 1968.

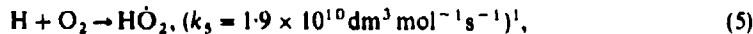
pollutant in question. As sources for VUV-light, low pressure Hg-lamps emitting simultaneously $\lambda = 184.9$ nm (10%) and 253.7 nm (100%) are mostly used. For UV-light the same lamps were equipped with a Vycor-filter for absorption of the 184.9 nm-line, as well as medium pressure Hg-lamps, emitting several lines in the range of 250 to 578 nm.

2.1a *Water photolysis:* Figure 1 shows the absorption spectrum of water as well as the quantum yield (Q) of H, OH and e_{aq}^- of the primary products of water photolysis for three VUV-lines. The light at 123.6 and 147 nm can be produced by electrodeless special lamps (Getoff 1968a; Getoff and Schenck 1968). The VUV-light at these two wavelengths is at present of no practical interest, but is rather important with respect to the ozone chemistry in the upper atmosphere.

As can be seen from figure 1, the VUV-line at 184.9 nm is absorbed by water and hence it can be photolytically decomposed:



The free radicals so produced, OH, H and e_{aq}^- (solvated electrons), can initiate the decomposition reactions of water pollutants. In the presence of air, both H and e_{aq}^- are converted into peroxy-radicals.



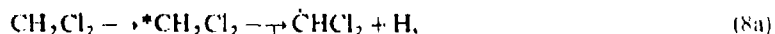
¹If not otherwise specified, the constants used (k) are taken from Buxton *et al* (1988).

The HO_2 species are in general more reactive than the O_2^- ones. The absorbed energy per quantum at 184.9 nm is: $E = 6.7 \text{ eV}/\text{hv}$, which was taken as basis for calculation of the "photochemical" G-values² of: $G_{ph}(\text{H}, \text{OH}) = 4.92$ and $G_{ph}(\text{e}_{aq}^-) \leq 0.45$ at pH 7.

In the following the photoinduced decomposition of dichloromethane and tetrachloroethylene in aqueous solution as representatives of halogenated aliphatic pollutants are briefly discussed.

2.1b Dichloromethane: This compound is studied in the presence of air in neutral aqueous solutions as a model for the halogenated, simple aliphatic compounds (Cietoff 1991, and references therein). Its major absorption lies in the VUV-range (see figure 2). Hence, using VUV-light of 184.9 nm, both processes - direct electronic excitation of the substrate as well as photolysis of water - take place simultaneously. The yield of the photoinduced Cl-cleavage is determined as a function of the absorbed light energy and is taken as an indicator of the decomposition process. This dependence is shown in figure 2. It is obvious that up to a VUV-dose of about $3.9 \times 10^{16} \text{ J} \cdot \text{ml}^{-1}$ the formation of Cl^- ions is linear with absorbed energy and later on tends to a saturation value.

In addition to the photolysis of water (reactions (1) to (4)), a direct excitation of CH_2Cl_2 by the 184.9 nm VUV-light also takes place:



The H-atoms are scavenged by O_2 , according to reaction (5), resulting in HO_2 radicals which are converted into O_2^- species (see reactions (5) to (7)). Both transients, $\dot{\text{C}}\text{HCl}_2$ and CH_2Cl react with oxygen and the resulting peroxy-radicals subsequently lead

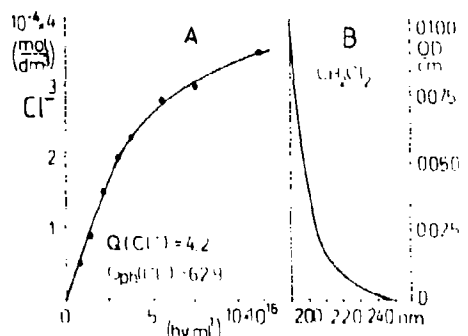


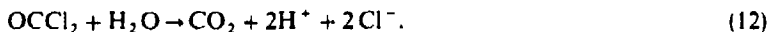
Figure 2. (A) Photoinduced Cl-cleavage from aqueous air-saturated $2 \times 10^{-4} \text{ mol} \cdot \text{dm}^{-3}$ CH_2Cl_2 using $\lambda_{max} = 184.9 \text{ nm}$. (B) Absorption spectrum of $10^{-4} \text{ mol} \cdot \text{dm}^{-3}$ CH_2Cl_2 in water ($\text{pH} \sim 7$).

²G-value = number of formed or decomposed molecules per 100 eV absorbed energy. For conversion to SI-units multiply the G-value by 0.10164 to obtain $G(x)$ in $\mu\text{mol} \cdot \text{l}^{-1}$. Initial G-value (G_i) = yield before the degradation of final product occurs.

to degradation of the pollutant (Getoff 1991):



Phosgene (OCCl_2) is formed as an intermediate, but it is not stable in aqueous solution and hydrolyzes (Asmus *et al* 1985; Getoff 1989b).



It has been shown (Packer *et al* 1980; Alfassi *et al* 1987) that by increasing the number of halogen atoms in the molecule also, the reactivity of the peroxy radical is enhanced. Therefore, it is expected that the O_2CHCl_2 species are stronger in reacting with organic compounds than $\text{O}_2\text{CH}_2\text{Cl}$:

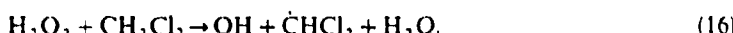
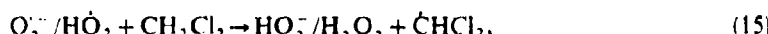


The OH radicals from the water photolysis at 184.9 nm (reactions (1) and (4)) as well as those from reactions (9) to (11) can also react with CH_2Cl_2 , whereas the H atoms resulting from reactions (1) as well as e_{aq}^- from reaction (3) are converted into O_2^- species (reactions (5) to (7)). Hence,



$$k_{\text{cat}} = 0.9 \times 10^8 \text{ dm}^3 \text{ mol}^{-1} \text{ s}^{-1}$$

The two species, CHCl_2 and CH_2Cl , are involved in the above reactions (10) and (11) followed by reactions (12) and (13). Finally, the peroxy radicals, O_2^- and/or HO_2 , as well as H_2O_2 , also contribute to the decomposition process of the substrate, e.g.:



OH and $\dot{\text{C}}\text{HCl}_2$ radicals are consumed as discussed above. Based on the yield of Cl^- ions the quantum yield, (Q), as well as the "photochemical" G -value of the Cl^- ions were calculated and are given in figure 2 as an insert. The very high degradation yield obtained is due to the chain reactions initiated by the OH radicals which are generated in reactions (9) to (11) and then converted into CHCl_2 and $\dot{\text{C}}\text{H}_2\text{Cl}$ transients, (14a) and (14b). The propagation reactions are (10), (11), (13), (14a) as well as (14b).

2.1c Tetrachloroethylene: This pollutant has been chosen as representative of the halogenated ethylenes. Its absorption spectrum with $\lambda_{\text{max}} = 203 \text{ nm}$ is shown in figure 3, B. Obviously the 253.7 nm line makes a rather small contribution to the photoinduced decomposition process. Using $2 \times 10^{-4} \text{ mol} \cdot \text{dm}^{-3} \text{Cl}_2\text{C=CCl}_2$ and a low pressure Hg-Lamp (184.9 and 253.7 nm) it has been calculated that about 90% of the VUV-light is absorbed by the water. Hence, the primary products of the water photolysis initiate the degradation process. The rest of the absorbed energy is consumed by the substrate, leading to its decomposition (Getoff 1991).

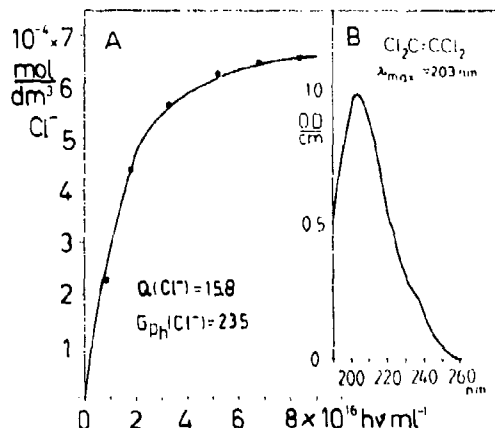


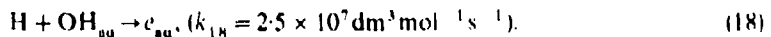
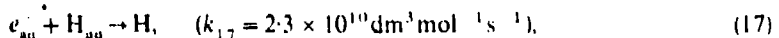
Figure 3. (A) Photoinduced Cl⁻ cleavage of 2×10^{-4} mol dm⁻³ tetrachloroethylene in the presence of air at 30°C ($\text{pH} \sim 6.4$). (B) Absorption spectrum of 10^{-4} mol dm⁻³ $\text{Cl}_2\text{C}=\text{CCl}_2$ in water ($\text{pH} \sim 6.4$); $\epsilon_{203} = 9870 \text{ dm}^3 \text{ mol}^{-1} \text{ cm}^{-1}$.

The formation of the Cl⁻ ions from tetrachloroethylene as a function of the absorbed VUV-dose (184.9 nm) is presented in figure 3A. In this case also, chain reactions are operative, similar to the above described for the CH_2Cl_2 -system, leading to a very high Q - and G_{ph} -yields (see figure 3). As decomposition products, in addition to Cl⁻ ions, small amounts of aldehydes, formic and oxalic acids were detected. However, these substances are also decomposed at higher VUV-doses.

It should be mentioned that the photoinduced degradation of various halogenated substances e.g. of trihalomethanes is investigated by various authors (e.g. Nicole *et al* 1991, and references therein).

2.2 Photoinduced formation of e_{aq}^- as promotor for pollutant degradation

The solvated electrons (e_{aq}^-) represent the basic form of the reducing primary species of water photolysis. In acid solution they can be transformed into H-atoms and vice-versa in alkaline media:



Both, H and e_{aq}^- are strong reducing transients and in the presence of air they are converted into peroxy radicals, (5) to (7). Each of their forms (H , e_{aq}^- , HO_2 , O_2^\cdot) can initiate the degradation of pollutants. The e_{aq}^- can originate by photoexcitation of certain inorganic or organic substances in aqueous solution. Hence, for completeness their photoinduced formation is mentioned very briefly.

2.2a Formation of e_{aq}^- from inorganic ions: Some photoexcited inorganic ions can lead to the formation of e_{aq}^- . It has been found for the first time that Fe^{2+} can be oxidized by illumination to Fe^{3+} by ejection of e_{aq}^- (Getoff *et al* 1960; Getoff 1962). The same observation has been made for halide ions (e.g. Jortner *et al* 1962) and for

Table I. Quantum yield (Q) of photoinduced e_{aq}^- formation from some inorganic and organic compounds in aqueous solution.

Substrate	$\lambda_{\text{exc}} [\text{nm}]$	Energy [eV/hv]	$Q(e_{\text{aq}}^-)$	References
OH ⁻	184.9	6.7	0.11	Dainton and Fowles (1965a)
Br ⁻	184.9	6.7	0.34	
Cl ⁻	184.9	6.7	0.43	
SO ₄ ²⁻	184.9	6.7	0.71	
Fe ²⁺	253.7	4.9	0.07	Airey and Dainton (1966)
Fe(CN) ₆ ⁴⁻	253.7	4.9	0.66	
Fe(CN) ₆ ⁴⁻	214 to 228	5.79 to 5.4	~0.9	Shirom and Stein (1971)
Fe ²⁺	292 to 314	4.2 to 3.9	0.0038	Solar and Getoff (1979)
C ₆ H ₅ OH	253.7	4.9	0.03	Zechner <i>et al</i> (1976)
C ₆ H ₅ OH	228.8	5.4	0.06	
C ₆ H ₅ O	253.8	4.9	0.17	Grabner <i>et al</i> (1977)
C ₆ H ₅ O	228.8	5.4	0.27	Getoff (1989a)
C ₆ H ₅ NH ₂	276.7	4.5	0.06	
C ₆ H ₅ NH ₂	253.7	4.9	0.27	Köhler <i>et al</i> (1977)
C ₆ H ₅ NH ₂	228.8	5.4	0.28	
C ₆ H ₅ NH ₂	213.9	5.8	0.34	Getoff (1989)
C ₆ H ₅ OPO ₃ ²⁻	253.7	4.9	0.028	Getoff and Solar (1974)
C ₆ H ₅ OPO ₃ ²⁻	213.9	5.8	0.23	Köhler and Getoff (1978)

other inorganic ions (Matheson *et al* 1963; Dainton and Fowles 1965b), e.g.:



The quantum yields (Q) of the photoinduced e_{aq}^- resulting from some inorganic ions are given in table I.

2.2b Photoejection of e_{aq}^- from organic compounds: It has been established that photoinduced electron ejection and formation of e_{aq}^- from certain electronically excited organic substances in aqueous solution, having substituents such as $-\text{OH}$, $-\text{O}^-$, $-\text{OCH}_3$, $-\text{OPO}_3\text{H}_2^-$, $-\text{OPO}_3\text{H}^-$, $-\text{COO}^-$, $-\text{NH}_2$, $-\text{NHCH}_3$, $-\text{N}(\text{CH}_3)_2$ etc., can take place (Grossweiner *et al* 1963; Getoff 1989a, and references therein).

The ejection of electrons occurs from the singlet state (S_1 or S_2), where the energy input is much lower than the ionization potential of a given compound in its gas phase. To explain this process, therefore, it is suggested that the dipole-dipole interaction between the polarized excited substrate molecules and the surrounding water molecules as well as the solvation energy of the resulting charged species contribute energetically and enable e_{aq}^- formation (Getoff 1989a).

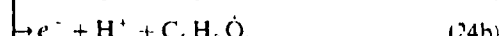
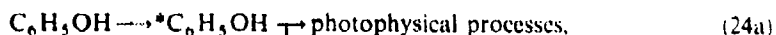
The formation of e_{aq}^- is also observed by illumination of dyes in aqueous solution, e.g. methylene blue (Vonach and Getoff 1983), a number of flavins (Getoff *et al.* 1978), aromatic amines (Köhler *et al.* 1977) etc.

The $Q(e_{aq}^-)$ -value strongly depends on several factors: *excitation energy* (see table 1), the *structure of the substrate molecule* as well as on the *pH* and *temperature of the solution* (Getoff 1989a, and references therein). It has also been established that the formation of e_{aq}^- takes place at the expense of the fluorescence (Köhler and Getoff 1974, 1976; Zechner *et al.* 1976, 1981; Grabner *et al.* 1977, 1980). This proves that the electron photoejection process occurs from the singlet state.

2.3 Photoinduced decomposition of phenol

Phenol is frequently observed as a pollutant in water. Its photoinduced degradation has been investigated in the presence of oxygen and small amounts of ozone (Getoff 1987). The reactivity of ozone with olefinic and aromatic compounds (without irradiation) can be designated as an electrophilic addition to the double-bond of the molecule (e.g. Bühlér *et al.* 1984, Sehested *et al.* 1984, Hoigne 1985, Getoff 1989b, 1992, Gehringer *et al.* 1992, and references therein).

As already mentioned above, the electronically excited aqueous phenol leads to the formation of e_{aq}^- in addition to other processes (Grossweiner *et al.* 1963; Jortner *et al.* 1963; Grabner *et al.* 1977, 1980; Getoff 1989b) e.g.:



The quantum yields (Q) of the primary products (e_{aq}^- , resulting from S_1 - and S_2 -states are given in table 1. As already mentioned, in the presence of air e_{aq}^- is converted

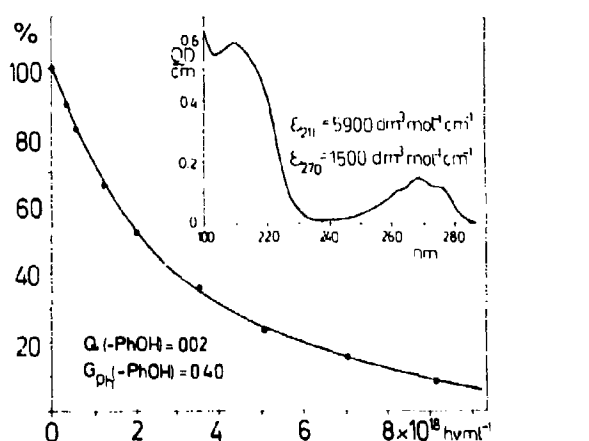
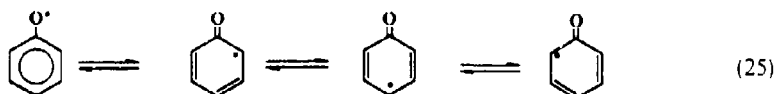


Figure 4. Photoinduced degradation (%) of aqueous $10^{-4} \text{ mol} \cdot \text{dm}^{-3}$ phenol in the presence of $1.25 \times 10^{-3} \text{ mol} \cdot \text{dm}^{-3}$ O_2 and $1.1 \times 10^{-3} \text{ mol} \cdot \text{dm}^{-3}$ O_3 ($\text{pH} = 7.5$) as a function of the absorbed UV-dose ($\lambda = 253.7 \text{ nm}$). Inset: absorption spectrum of $10^{-4} \text{ mol} \cdot \text{dm}^{-3}$ phenol.

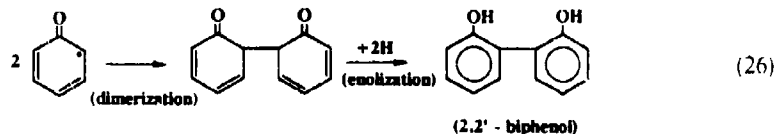
into peroxy radicals (see reactions (5) to (7)), which are subsequently involved in the decomposition process.

The photoinduced degradation of phenol using UV-light (253.7 nm) in the presence of oxygen and small concentrations of ozone in neutral solutions is shown in figure 4. The achieved Q - and G_{ph} -values, as well as the absorption spectrum of phenol are given as inserts in figure 4.

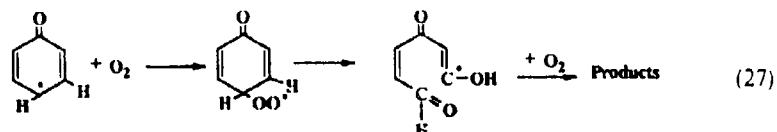
The major reaction steps leading to the decomposition of phenol may start with the formation of phenoxy radicals (reactions (24b) and (24c)), which exist in several resonance structures.



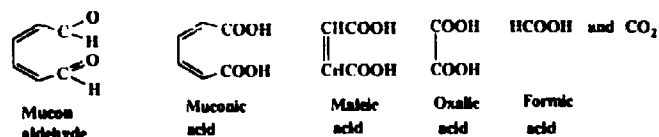
Each of them can result in different final products or add on oxygen as shown below.



Naturally, the above-mentioned peroxy radicals can also attack phenol and initiate its decomposition. In addition to this, each of the resonance structures can be scavenged by O_2 as follows.



In the presence of sufficient oxygen in the solution, the pathway (27) will proceed preferentially, however, the exact reaction mechanism of the photoinduced phenol decomposition is not yet known. The yield and the kind of the products depend on the applied UV-dose, pH and the oxygen concentration. As final products of an incomplete degradation of the substrate, the following compounds were observed (Getoff 1987).



It might be mentioned that in addition to the OH, H and e_{aq}^- resulting in the VUV-water photolysis, the triplet state of the pollutant as well as the singlet oxygen (${}^1\text{O}_2$) can be involved in the photochemical decomposition process in the presence of air.

3. Semiconductor-promoted pollutant degradation using solar energy

3.1 General remarks

Since the discovery by Fujishima and Honda (1971) of water splitting to H₂ and O₂ using solar energy by means of an *n*-TiO₂-photoanode and metal cathode, separated by a membrane, a new pathway for research in photochemistry and photoelectrochemistry was found (Getoff *et al* 1977, Hantala *et al* 1979, etc.). The *n-type semiconductors* (e.g. TiO₂, SrTiO₃, GaAs etc.) have an excess of electrons (e⁻) and, hence, are used as photoanodes or as suspensions (e.g. Izumi *et al* 1980, Vonach and Getoff 1981) or colloids (Hsiao *et al* 1983, Ahmed and Ollis 1984, Ollis 1985, 1990, Matthews 1985, 1988, Okamoto *et al* 1985, Al-Ekabi and Serpone 1988, Grabner *et al* 1991 etc.) for promoting the oxidation reaction. The *p-type semiconductors* (CdTe, GaP etc.) possess positive holes (p⁺) in excess and serve as photocathodes in photoelectrochemical cells or for instance in the form of small particles and act as reduction photocatalysts (Bart 1979, Schiavello 1988, and references therein). Semiconductors can be also coated on glass (Dislich 1984) or on other carrier materials.

The application of semiconductors for photocatalyzed oxidation of aqueous pollutants is very recently discussed in an excellent review by Halmann (1992). Further, it might be mentioned that many papers dealing with TiO₂ photocatalytic purification and treatment of polluted water are presented at the 1st International Conference in London, Canada (Al-Ekabi *et al* 1992).

On illuminating a TiO₂ particle immersed in aqueous media with light of 315 to 450 nm, band-bending takes place and electrons rise from the valence band (E_v) to the conductivity band (E_c) and, hence, a charge separation takes place (see figure 5). Based on this fact, each individual particle represents a redox-system and can promote reduction or oxidation processes depending on the experimental conditions. Each semiconductor has a characteristic band-gap (in eV; 1 eV = 23 kcal/mol), e.g. for TiO₂, E_g = 3 eV. Knowing the wavelength (λ in nm) of the light, one can calculate the energy per quantum: (E in eV/hv) and vice versa.

$$E = [1240/\lambda(\text{nm})](\text{eV}/\text{hv}) \quad (28)$$

The relative energy levels for some semiconductors are shown in figure 6. Silicon has the lowest energy-gap (E_g = 1.1 eV) but is not stable in aqueous solution.

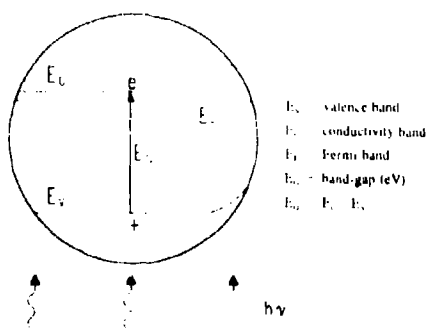


Figure 5. Simplified scheme of the energy levels of an illuminated *n*-type semiconductor particle.

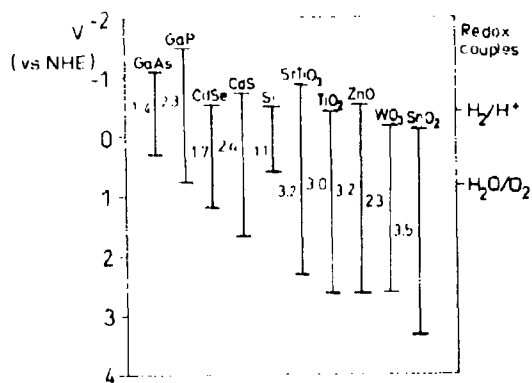


Figure 6. Relative energy levels (E_g in eV) of some semiconductors (after Nozik 1980).

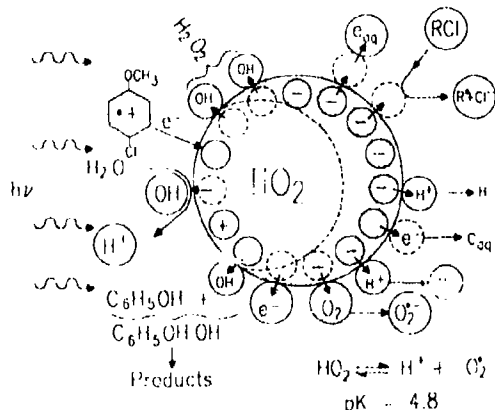


Figure 7. Some possible photoinduced processes on the surface of TiO_2 particles in polluted water.

3.2 Primary processes on semiconductor surfaces

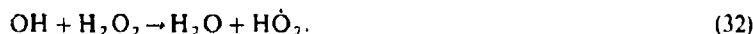
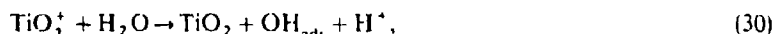
The photoinduced degradation of pollutants on the surface of e.g. TiO_2 is not a simple process. In order to visualize the possible redox-reactions, a simplified scheme is presented in figure 7. The illuminated part of the TiO_2 -particle absorbs the light-energy in 10^{-16} s and the electrons are moved from the E_g to the E_{c} (shadow side of the particle) bands. As a consequence of this charge separation, the illuminated part (positively charged holes, h^+) is able to decompose the adsorbed H_2O molecules to OH radicals and H^+ ions. Also, an e^- can be transferred from a pollutant (having a suitable redox-potential) to h^+ of the TiO_2 particle (see figure 7). On the other hand, the e^- can be also transferred to adsorbed H^+ , O_2 or the chlorinated pollutant initiating various reactions. It cannot be ruled out that some electrons can diffuse away from the TiO_2 surface and become "solvated electrons" (e_{aq}^-) as demonstrated by Walker (1967) on anode surfaces.

3.3 Photocatalytic degradation of pollutants

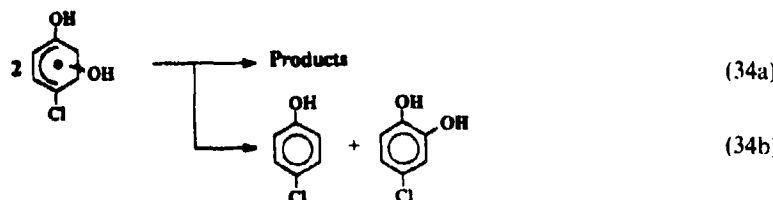
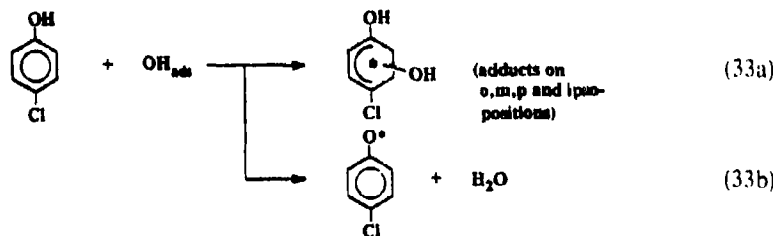
For illustration of photocatalytic degradation, some major reactions taking place on the TiO_2 surface in slightly acidic solution, are presented.



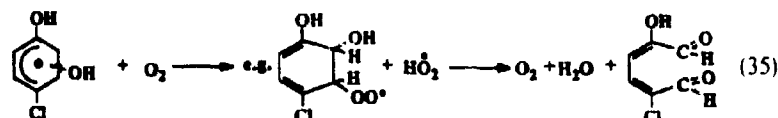
On the illuminated side of TiO_2 particles (figure 7) a number of reactions can take place:



In the presence of a pollutant, e.g. 4-Cl-phenol, similar reactions can take place as studied by pulse radiolysis (Getoff and Solar 1988) as below.

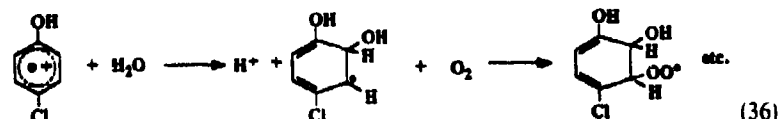


In competition with these processes, O_2 can be scavenged as below resulting in peroxy-radicals.



As a consequence of further OH attack and addition of oxygen, the resulting dialdehyde (35) can be decomposed to CO_2 and H_2O (see also reactions (25) to (27)).

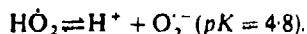
Another pathway for $\text{ClC}_6\text{H}_4\text{OH}$ degradation is the formation of a radical cation on the surface of TiO_2 particles as indicated in figure 7 which can react further.



On the shadow side of the TiO_2 -particles (see figure 7) in slightly acid media some reactions can be initiated by the electrons in the presence of oxygen:



and from (7)



The HO_2 and O_2^- species can attack the water pollutants in the same way as the OH radicals followed by O_2 addition (see reaction (35)).

As mentioned above, a number of papers have been published in recent years in the field of pollutant degradation assisted by semiconductors. Figure 8 shows some data concerning the oxidation rates of some pollutants in water (Matthews 1988). TiO_2 (Degussa, P25 grade) was coated on the inside of a 7-m long 65-turn spiral of borosilicate glass ($\varnothing 6$ mm, 40 ml solution was circulated through the spiral) illuminated with a 20-W lamp.

It has been also found that the TiO_2 -assisted photodecomposition of 4-Cl-phenol is temperature-dependent (Hofstädler *et al* 1992). By studying the kinetics of the laser-induced phenol oxidation, it was observed that the Cl_2^- species essentially contribute to the process (Grabner *et al* 1991; Li *et al* 1991). Further, it should be mentioned that TiO_2 particles or colloids can also mediate the transformation of CO (Park *et al* 1988) as well as CO_2 (Halimann 1978) into simple organic substances. In the absence of oxygen in the solution, the polymerisation of pollutants can also take place on the semiconductor surface.

With respect to photocatalytic water purification, there are still a number of problems to be solved. Although sunlight is free of cost and is readily available in many parts of the world, its intensity is rather low and it has to be collected and concentrated by appropriate means for the purpose of water purification on a technical scale.

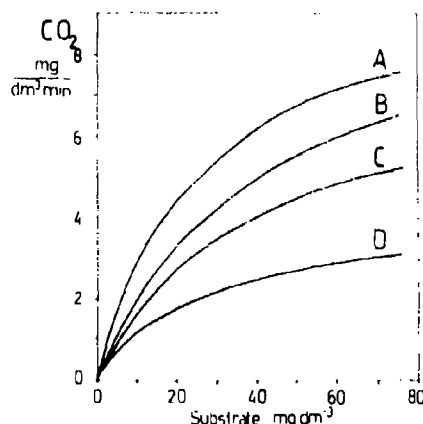


Figure 8. CO_2 rates observed by TiO_2 oxidation of various substrates as a function of their initial concentrations: (A) 4-Cl-phenol, (B) phenol, (C) acetic acid, and (D) 2-propanol (after Matthews 1988).

Further problems which have to be overcome are:

- to increase the low quantum yield of photocatalytic pollutant degradation.
- to improve the corrosion resistance and to reduce inhibition by poisoning of the semiconductor,
- the solvation of peculiar features of semiconductor coating on various support materials,
- lowering of the costs for semiconductor regeneration, water pumping etc.

Therefore, further investigations in this area are needed.

4. Pollutant decomposition by ionizing radiation

4.1 General remarks

In the last two decades, a relatively large number of papers have been published concerning radiolytic degradation of harmful substances in water. Hence, only some characteristic data for comparison with the above discussed photochemical methods will be presented. Gamma-rays as well as high-energy electrons can be used for production of reactive transients from water which can initiate the desired decomposition processes. Preference is given to high-energy electrons for several reasons: no manipulation with radioactive isotopes (e.g. ^{60}Co) or their disposal required, easy regulation of the output power and simple handling in case of repair work as well etc. The modern electron accelerators (EA-machines) provide electrons with variable

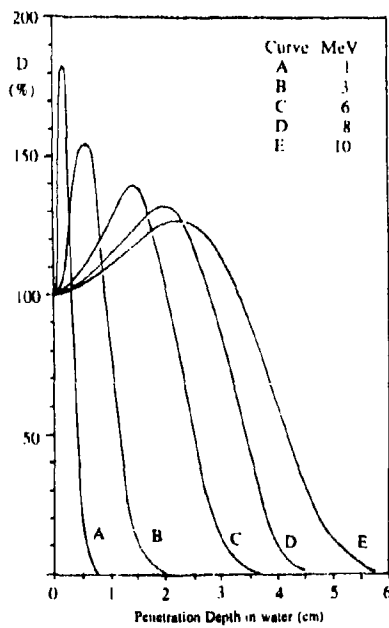


Figure 9. Depth-dose ($D \%$) distribution in water at different electron energies.

energy (e.g. from 0.5 to 2.8 MeV) and a rather high output power (80 to 100 kW) with a conversion factor (η = electron power/electricity power) of about 80%. EA-machines delivering electrons with energies of 4.5–5 (output power > 400 kW) or 10 MeV (25–50 kW) can be also used for water purification. The electron penetration in water depends on their energy. Figure 9 shows the depth dose distribution (D in %) in water for different electron energies (in MeV). The depth dose of the applied electrons and the output power (kW) of the EA-machine are determining factors for the quantity of purified water.

4.2 Water radiolysis

As a consequence of the interaction between the ionizing radiation and water, several transients and molecular products are formed. Their yields (G-values) and major

Table 2. Radiolysis of water and some primary reactions.

<i>Primary reactions:</i>	
$\text{H}_2\text{O} \rightarrow \cdot\text{H}_2\text{O}^* \rightarrow \text{H} + \text{OH}$	
\downarrow	
$\text{H}_2\text{O}^* + e^-$	
<i>Gross reaction of water radiolysis (the G-values* at pH 7 are given in brackets):</i>	
$\text{H}_2\text{O} \rightarrow e_{\text{aq}}^-$, H , OH , H_2 , H_2O_2 , H^+ , OH_{aq}^-	
(2.7)(0.6)(2.8)(0.45) (0.7) (3.2) (0.5)	
<i>Major primary reactions:</i>	
$\text{H} + \text{H} \rightarrow \text{H}_2$	$(k = 1 \times 10^{10} \text{ dm}^3 \text{ mol}^{-1} \text{ s}^{-1})$
$\text{H} + \text{OH} \rightarrow \text{H}_2\text{O}$	$(k = 2.5 \times 10^{10} \text{ dm}^3 \text{ mol}^{-1} \text{ s}^{-1})$
$\text{H} + e_{\text{aq}}^- \rightarrow \text{H}_2 + \text{OH}_{\text{aq}}^-$	$(k = 2 \times 10^{10} \text{ dm}^3 \text{ mol}^{-1} \text{ s}^{-1})$
$\text{OH} + \text{OH} \rightarrow \text{H}_2\text{O}_2$	$(k = 6 \times 10^9 \text{ dm}^3 \text{ mol}^{-1} \text{ s}^{-1})$
$\text{OH} + e_{\text{aq}}^- \rightarrow \text{OH}_{\text{aq}}^-$	$(k = 2.5 \times 10^{10} \text{ dm}^3 \text{ mol}^{-1} \text{ s}^{-1})$
$e_{\text{aq}}^- + e_{\text{aq}}^- \rightarrow \text{H}_2 + 2\text{OH}_{\text{aq}}^-$	$(k = 3 \times 10^8 \text{ dm}^3 \text{ mol}^{-1} \text{ s}^{-1})$
$e_{\text{aq}}^- + \text{H}_{\text{aq}}^+ \rightarrow \text{H}$	$(k = 2.3 \times 10^{10} \text{ dm}^3 \text{ mol}^{-1} \text{ s}^{-1})$
$\text{H} + \text{OH}_{\text{aq}}^- \rightarrow e_{\text{aq}}^-$	$(k = 2.5 \times 10^7 \text{ dm}^3 \text{ mol}^{-1} \text{ s}^{-1})$
$\text{OH} \rightleftharpoons \text{H}_{\text{aq}}^+ + \text{O}_{\text{aq}}^-$	$(pK = 11.9)$
$\text{H}_2\text{O} \rightleftharpoons \text{H}_{\text{aq}}^+ + \text{HO}_{\text{aq}}^-$	$(pK = 11.65)$
<i>Scavenger reactions:</i>	
$\text{N}_2\text{O} + e_{\text{aq}}^- \rightarrow \text{OH} + \text{OH}^- + \text{N}_2$	$(k = 0.9 \times 10^{10} \text{ dm}^3 \text{ mol}^{-1} \text{ s}^{-1})$
$\text{O}_2 + e_{\text{aq}}^- \rightarrow \text{O}_2^-$	$(k = 2 \times 10^{10} \text{ dm}^3 \text{ mol}^{-1} \text{ s}^{-1})$
$\text{O}_2^- + \text{H} \rightarrow \text{HO}_2^-$	$(k = 1.9 \times 10^{10} \text{ dm}^3 \text{ mol}^{-1} \text{ s}^{-1})$
$\text{HO}_2^- \rightleftharpoons \text{H}^+ + \text{O}_2^-$	$(pK = 4.8)$
$\text{i-C}_4\text{H}_9\text{OH} + \text{OH}^- \rightarrow \text{H}_2\text{O} + \text{i-C}_4\text{H}_9\text{OH}$	$(k = 5.5 \times 10^8 \text{ dm}^3 \text{ mol}^{-1} \text{ s}^{-1})$

* G-value = number of changed molecules per 100 eV (1.60×10^{-17} J) absorbed energy. For conversion in SI-units: multiply the G-value by 0.10364 to obtain G(x) in $\mu\text{mol} \cdot \text{J}^{-1}$.

Absorbed dose units:

$$\begin{aligned}1 \text{ rad} &= 100 \text{ erg/g H}_2\text{O}; & 10^6 \text{ rad} &\Rightarrow 1 \text{ Mrad} = 10 \text{ kGy}; \\10^2 \text{ rad} &= 1 \text{ Gray (1 Gy)} = 1 \text{ J/kg H}_2\text{O}; & 10^6 \text{ Gy} &\Rightarrow 1 \text{ MGy} = 1 \text{ kW s/g H}_2\text{O}; \\10^3 \text{ rad} &= 10 \text{ Gy} = 6.24 \times 10^{16} \text{ eV/g H}_2\text{O}.\end{aligned}$$

primary reactions are summarized in table 2. The common units for absorbed radiation dose are also given for convenience.

As shown above, in the presence of air ($0.25 \times 10^{-3} \text{ mol} \cdot \text{dm}^{-3} \text{ O}_2$ at 20°C) both e_{aq} and H atoms are converted into peroxy radicals which, together with the OH species, attack the available pollutants and initiate their degradation.

4.3 Decomposition of chlorinated hydrocarbons

Chlorinated hydrocarbons have been studied extensively by various research groups (e.g. Balkas *et al* 1970, 1971, Köster and Asmus 1971, Neumann-Spallart and Getoff 1979, Pikaev and Shubin 1984, Gehringer *et al* 1985, 1986, 1988, 1990, 1992, Getoff and Lutz 1985, Mönig *et al* 1985, Getoff 1986, 1989–1991, Proksch *et al* 1988, Draper *et al* 1989, etc.). Some data concerning radiation-induced degradation of several chlorinated aliphatic and olefinic hydrocarbons are presented in table 3 (Getoff 1989b). These pollutants frequently appear in drinking water. Obviously, their complete decomposition is achieved at a relatively low dose. In aerated water containing olefins or aromatic pollutants, the presence of ozone strongly enhances the degradation process (Masschelein 1982, Rice and Netzer 1984, Gehringer *et al* 1992, Getoff 1992 etc.).

The following major reaction can explain the ozone effect:

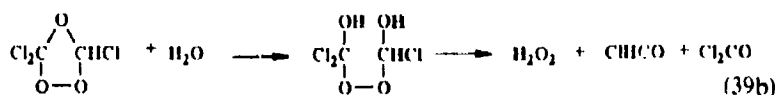
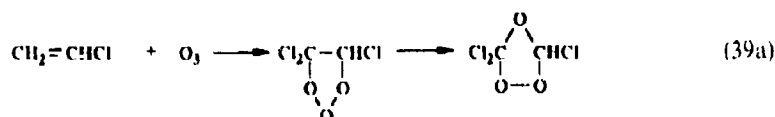


Table 3. Radiation induced decomposition of some chlorinated hydrocarbons in aerated water*. Applied dose: 1.9 kGy.

Sample No.	Treatment†	Pollutants in water/ μdm^{-3}					
		CH_2Cl_2	CHCl_3	CCl_4	$\text{Cl}_3\text{C}-\text{CH}_3$	$\text{Cl}_2\text{C}-\text{CHCl}$	$\text{Cl}_2\text{C}-\text{CCl}_2$
1	U	—	32	—	0.7	—	—
	I	—	nd	—	nd	—	—
2	U	—	—	25	0.2	—	—
	I	—	—	1	nd	—	—
3	U	48	—	—	107	1.1	—
	I	nd	—	—	0.8	nd	—
4	U	23	2.3	1.1	0.2	—	—
	I	nd	nd	0.1	nd	—	—
5	U	—	2.5	0.2	4.5	361	0.2
	I	—	nd	nd	nd	nd	nd

† U-unirradiated; I-irradiated; * the GC-analysis was performed by Dr U Bauer. Traceable limit: $<0.1 \mu\text{g} \cdot \text{dm}^{-3}$

Abbreviations: nd = non-detectable; $\text{Cl}_3\text{C}-\text{CH}_3$ = 1,1,1-trichloroethane; CH_2Cl_2 = dichloromethane; $\text{Cl}_2\text{C}=\text{CHCl}$ = trichloroethylene; CHCl_3 = chloroform; $\text{Cl}_2\text{C}=\text{CCl}_2$ = tetrachloroethylene; CCl_4 = carbon tetrachloride.



These reactions can also occur without irradiation. They take place in the case of aromatic pollutants likewise.

4.4 Decomposition of aromatic substances

Steady state as well as pulse radiolysis studies of various aromatic pollutants in water have been published (e.g. Schuler *et al* 1976, Getoff and Solar 1986, 1988, Draper *et al* 1989, Getoff 1990b, 1992, Nickelsen *et al* 1992 etc.). For comparison with the above discussed photochemical methods, radiation-induced phenol decomposition is discussed in brief. As shown in figure 10, at a dose of about 1.2 kGy in the presence of oxygen the initial phenol is practically decomposed. However, due to competition reactions certain amounts of pyrocatechol, hydroquinone and hydroxyhydroquinone are formed. The initial *G*-values (*G*_i) are given as an insert in figure 10 (Getoff 1986b). At higher doses these compounds and the resulting aldehydes and acids are decomposed to CO₂ and H₂O. The major reactions taking place in this case are given below, (42) to (50). In addition to these, reactions (25) to (27) are also involved.

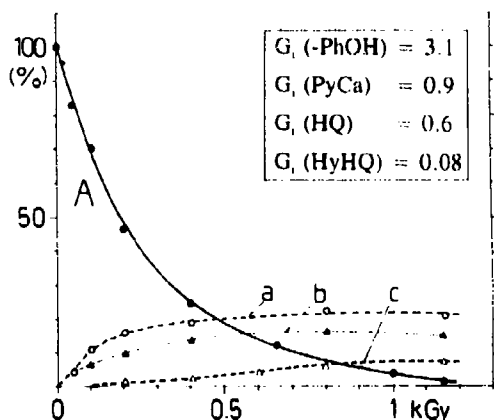
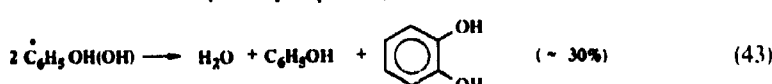
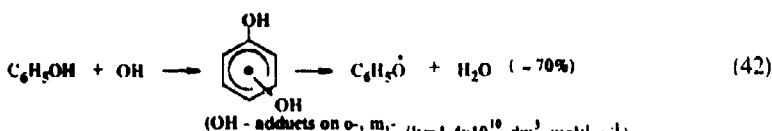
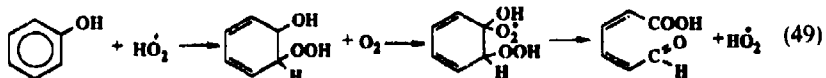
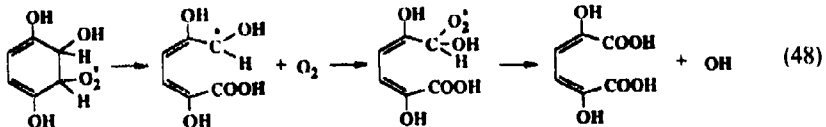
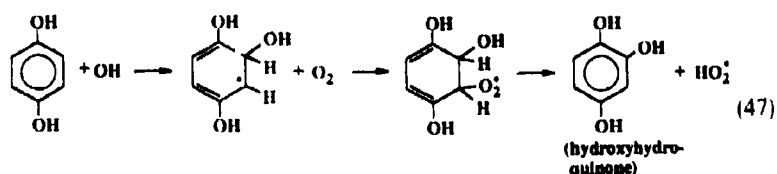
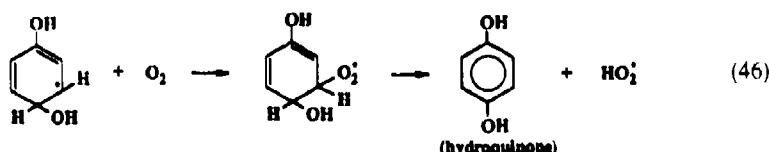
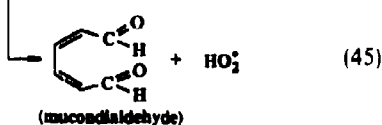
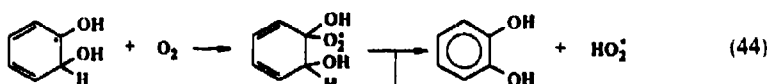


Figure 10. Decomposition of $10^{-4} \text{ mol} \cdot \text{dm}^{-3}$ phenol (A) in the presence of $1.25 \times 10^{-3} \text{ mol} \cdot \text{dm}^{-3}$ O₂, as well as formation of pyrocatechol (a), hydroquinone (b) and hydroxyhydroquinone (c) as a function of the absorbed dose at pH 7; dose rate: 3kGy/h. Insert: Initial *G*-values (*G*_i) of phenol decomposition and of the major products.



Based on the above data, it is now calculated that for a 50% decomposition of 10^{-4} mol dm⁻³ phenol by UV-light ($\lambda = 254$ nm, $E = 4.85$ eV/hv), an energy of 1.56 kGy is needed. Using γ -rays or electrons in order to achieve the same decomposition degree, an energy of 0.2 kGy is necessary. Obviously, the ionizing radiation is much more efficient than the UV-light in this case.

Finally, it should be mentioned that by means of pulse radiolysis of pollutant transients, their absorption spectra and the kinetics of their formation and decay, in addition to their chemical analysis, we can essentially elucidate their reaction mechanisms.

5. Conclusion

An attempt has been made to investigate the photochemical, photocatalytic and radiation-induced decomposition of pollutants in water. Special attention has been made to explain the primary processes initiating their degradation. On the other hand, a relationship is also established between the above-mentioned three pathways.

Although a great deal of research work has been done concerning the degradation of water pollutants, further experiments are needed on a pilot scale in order to gain technical experience for construction of industrial plants for water purification.

Acknowledgements

The author would like to express his thanks to the Austrian Federal Ministry for Science and Research, the Fonds zur Förderung der wissenschaftlichen Forschung, and the Jubiläumsfonds of the Austrian National Bank for their financial support.

References

- Ahmed S and Ollis D F 1984 *Sol. Energy* **32** 597
- Airey P L and Dainton F S 1966 *Proc. R. Soc. London A* **291** 340
- Al-Ekabi H, de Mayo P and Ollis D (eds) 1992 *Abstr. 1st Intern. Conf. on TiO₂ photocatalytic purification and treatment of water and air*, London, Ontario
- Al-Ekabi H and Serpone N 1988 *J. Phys. Chem.* **92** 572b
- Alfassi Z B, Mossery S and Neta P 1987 *J. Phys. Chem.* **91** 3383
- Asmus K-D, Bahnenmann D, Krichler K, Lal M and Möning J 1985 *Life Chem.* **3** 1
- Balkus T, Fendler J H and Schuler R H 1970 *J. Phys. Chem.* **26** 4497
- Balkus T, Fendler J H and Schuler R H 1971 *J. Phys. Chem.* **26** 445
- Bart A J 1979 *Photochemistry* **10** 59
- Bühler R E, Staelin J and Hoigne J 1984 *J. Phys. Chem.* **88** 2560
- Buxton G, Greenstock, Helman W P and Ross A B 1988 *J. Phys. Chem. Reference Data*, **17** 513-886
- Dainton F S and Fowles P 1965a *Proc. R. Chem. Soc. London A* **284** 312
- Dainton F S and Fowles P 1965b *Proc. R. Chem. Soc. London A* **287** 295
- Dislich H 1984 *Glass Sci. Technol.* **2** 173
- Draper R B, Fow M A, Pelizzetti E and Serpone N 1989 *J. Phys. Chem.* **93** 1938
- Fujishima A and Honda K 1971 *Bull. Chem. Soc. Jpn.* **44** 1148
- Gehringer P, Proksch E, Eschweiler H and Sinovatz W 1990 *Radiat. Phys. Chem.* **35** 456
- Gehringer P, Proksch E, Eschweiler H and Sinovatz W 1992 *Appl. Radiat. Isot.* **43** 1107
- Gehringer P, Proksch E and Sinovatz W 1985 *Int. J. Appl. Radiat. Isot.* **4** 313
- Gehringer P, Proksch E, Sinovatz W and Eschweiler H 1986 *Z. Wasser Abwasser Forsch.* **19** 196
- Gehringer P, Proksch E, Sinovatz W and Eschweiler H 1988 *Appl. Radiat. Isot.* **39** 1227
- Getoff N 1962 *Z. Naturforsch.* **17b** 87
- Getoff N 1968a In *Radiation Chemistry and its Applications* (Vienna: IAEA) p. 172
- Getoff N 1968b *Monatsh. Chem.* **99** 136
- Getoff N 1986a *Water Res.* **20** 1261
- Getoff N 1986b *Appl. Radiat. Isot.* **37** 1103
- Getoff N 1987 AECL Accelerator Systems, Report, Deep River, Ontario
- Getoff N 1989a *Radiat. Phys. Chem.* **34** 711
- Getoff N 1989b *Appl. Radiat. Isot.* **40** 585
- Getoff N 1990a (unpublished results)
- Getoff N 1990b *Radiat. Phys. Chem.* **35** 432
- Getoff N 1991 *Radiat. Phys. Chem.* **37** 673
- Getoff N 1992 In *Applications of Isotopes and radiation in conservation of the environment* (Vienna: IAEA) p. 153
- Getoff N, Hartig K J, Kittel G, Pescheck G A and Solar S 1977 *Wasserstoff als Energieträger. Herstellung, Lagerung, Transport* (in German) (Wien, New York: Springer)
- Getoff N and Lutz W 1985 *Radiat. Phys. Chem.* **25** 21
- Getoff N and Prucha M 1983 *Z. Naturforsch.* **A38** 589
- Getoff N and Schenck G O 1968 *Photochem. Photobiol.* **8** 167
- Getoff N, Scholes G and Weiss J J 1960 *Tetrahedron Lett.* **17**
- Getoff N and Solar S 1974 *Monatsh. Chem.* **105** 241

- Getoff N and Solar S 1986 *Radiat. Phys. Chem.* **28** 443
Getoff N and Solar S 1988 *Radiat. Phys. Chem.* **31** 121
Getoff N, Solar S and McCormick 1978 *Science* **201** 616
Grabner G, Köhler G, Zechner J and Getoff N 1977 *Photochem. Photobiol.* **26** 449
Grabner G, Köhler G, Zechner J and Getoff N 1980 *J. Phys. Chem.* **84** 3000
Grabner G, Li G, Quint R M, Quint R and Getoff N 1991 *J. Chem. Soc., Faraday Trans.* **87** 1097
Grossweiner L I, Swenson G W and Zwicker E F 1963 *Science* **141** 805
Halmann M 1978 *Nature (London)* **275** 115
Halmann M 1992 In *Progress in photochemistry and photophysics* (ed.) J F Rabek (Boca Raton, FL: CRC Press) vol. 5
Hantala R R, King R B and Katal C (eds) 1979 *Solar energy - chemical conversion and storage* (Clifton, NJ: Humana)
Hofstädler K, Ruppert G, Bauer R, Heisler G and Novalic S 1992 (to be published)
Holgne J 1985 In *Radiation for a clean environment* (Vienna: IAEA) p. 219
Hsiao G -Y, Lee C, Li and Ollis D F 1983 *J. Catal.* **82** 418
Hutzinger O et al (eds) 1982 *Chlorinated dioxines and related compounds. Impact on the environment* (Oxford: Pergamon)
Izumi I, Dunn W W, Wilbourn K O, Fan F, Ren F and Bard A J 1980 *J. Phys. Chem.* **84** 3207
Jortner J, Ottolenghi M and Stein G 1962 *J. Phys. Chem.* **66** 2037
Jortner J, Ottolenghi M and Stein G 1963 *J. Am. Chem. Soc.* **85** 2712
Köhler G and Getoff N 1974 *Chem. Phys. Lett.* **26** 525
Köhler G and Getoff N 1976 *J. Chem. Soc., Faraday Trans. I* **72** 2101
Köhler G and Getoff N 1978 *J. Chem. Soc., Faraday Trans. I* **74** 1029
Köhler G, Rosicky C and Getoff N 1977 In *Excited states in organic chemistry and biochemistry* (eds) B Pulman and N Goldblum (Dordrecht: D Reidel) pp. 303-311
Köster K and Asmus K-D 1971 *Z. Naturforsch.* **B26** 1108
Li G, Grabner G, Quint R M, Quint R and Getoff N 1991 *Proc. Indian Acad. Sci. (Chem. Sci.)* **103** 505
Masschelein W J ed. 1982 *Ozonization manual for water and wastewater treatment* (Chichester: J Wiley & Son)
Matheson M, Mulac W A and Rabani J 1963 *J. Phys. Chem.* **67** 2613
Matthews R W 1985 *Sun World* **9** 3
Matthews R W 1988 *J. Catal.* **111** 264
Mönig J, Göbel M and Asmus K-D 1985 *J. Chem. Soc., Perkin Trans. 2* 647
Neumann-Spallart M and Getoff N 1979 *Radiat. Phys. Chem.* **13** 101
Nickelsen M G, Cooper W J, Kurucz C N and Walte I D 1992 *Environ. Sci. Technol.* **26** 144
Nicole I, DeLaat J, Dore M, Dugnet J P and Suty H 1991 *Environ. Technol.* **12** 21
Nozik A J 1980 *Annu. Rev. Phys. Chem.* **A29** 453
Okamoto K, Yamamoto Y, Tanaka H, Tanaka M and Itaya A 1985 *Bull. Chem. Soc. (Japan)* **58** 2015
Ollis D F 1985 *Environ. Sci. Technol.* **19** 480
Ollis D F 1990 Solar-assisted photocatalysis for water purification. *Proceeding 8th Int. Solar Energy Conversion Conference*, Palermo, Italy
Packer J E, Willson R L, Bahnemann D and Asmus K -D 1980 *J. Chem. Soc. Perkin Trans. II* 296
Park H -R, Li G and Getoff N 1988 *Z. Naturforsch.* **A43** 1126
Pikaev A K and Shubin V N 1984 *Radiat. Phys. Chem.* **24** 77
Prokush E, Gehring P, Sinovatz W and Eschweiler H 1988 *Appl. Radiat. Isot.* **39** 1227
Rice R G and Netzer A (eds) 1984 *Handbook of ozone technology and application* (Boston: Butterworth)
Rock J N 1974 *Water Treatm. Exam.* **23** 234
Schiavello M (ed) 1988 *Photocatalysis and environment. Trends and applications* (Dordrecht: Kluwer)
Schuler R H, Neta P, Zemet H and Feissenden R W 1976 *J. Am. Chem. Soc.* **98** 3825
Sehested K, Holzman J, Bejergbakke E and Hart E 1984 *J. Phys. Chem.* **88** 4144
Shirom M and Stein G 1971 *J. Chem. Phys.* **55** 3372
Sokolov U and Stein G 1966 *J. Chem. Phys.* **44** 3329
Solar S and Getoff N 1979 *Int. Hydrogen Energy* **4** 403
Vonach T and Getoff N 1983 *J. Photochem.* **23** 233
Vonach W and Getoff N 1981 *Z. Naturforsch.* **A36** 876
Walker D C 1967 *Can. J. Chem.* **45** 807
Watanabe K and Zelikoff M 1953 *J. Opt. Soc. Am.* **43** 753
Zechner J, Köhler G, Getoff N, Tatischeff I and Klein R 1981 *Photochem. Photobiol.* **34** 163
Zechner J, Köhler G, Grabner G and Getoff N 1976 *Chem. Phys. Lett.* **37** 297

Heterogeneous and homogeneous photoassisted wastewater treatment

G RUPPERT^{*1}, K HOFSTADLER¹, R BAUER¹ and G HEISLER²

¹Institute of Physical Chemistry, Technical University of Vienna, Getreidemarkt 9, A-1060 Wien, Austria

²Austrian Energy and Environment, SGP/Waagner-Biro GmbH, Siemensstr. 89, A-1210 Wien, Austria

Abstract. Photochemical degradation of 4-chlorophenol (4-CP) as a model wastewater contaminant with three methods: UV/TiO₂, UV/H₂O₂ and UV/TiO₂/H₂O₂ ($\lambda > 310\text{ nm}$) has been investigated and compared to the dark Fenton reaction and to direct photolysis. A UV-irradiated combination of TiO₂ and H₂O₂ was found to be the most effective degradation method for TOC (total organic carbon). 4-CP was degraded most rapidly by the dark Fenton reaction. In the heterogeneous process on illuminated TiO₂ without H₂O₂, only small amounts of by-products were formed during irradiation in contrast to homogeneous processes where H₂O₂ was involved. During UV/H₂O₂ and Fenton experiments, coloured by-products appeared during irradiation and degradation rates of 4-CP and TOC showed strong differences between homogeneous and heterogeneous processes.

Keywords. Wastewater treatment; photooxidation; hydroxyl radicals; titanium dioxide; Fenton reaction.

1. Introduction

Chemical oxidation of organic contaminants in wastewater is an effective method to remove pollutants without further environmental problems. In contrast to other wastewater treatment methods, e.g. adsorption on activated granular carbon or air stripping, the contaminants are converted to harmless materials such as carbon dioxide and inorganic salts. Various processes suggested for oxidation of organic compounds are UV-photolysis in the presence of H₂O₂ [(1)] or ozone, photolysis on UV-irradiated TiO₂, (3) + (4), and on the system Fe²⁺/H₂O₂ (Fenton reaction, (2)). The active species in all photochemical processes is the hydroxyl radical (Haag and Yao 1992), a strong oxidant with an oxidation potential of 2.8 V. It is generated, e.g., by the following reactions (Carey 1990):

(a) *homogeneous*



or



(b) *heterogeneous*



*For correspondence

In this work, the degradation of 4-chlorophenol (4-CP, 1.01×10^{-3} mol/l = 72.9 ppm TOC) and of TOC (total organic carbon) by photochemical methods with UV/H₂O₂, UV/TiO₂, and UV/TiO₂/H₂O₂, has been studied. The results were compared to the dark Fenton reaction, and to photolysis without additives.

Chlorophenols are widely used in the manufacture of herbicides and fungicides. Their traces were found in ground water but also in drinking water (caused by the disinfection of phenolic waters with chlorine). Because of their low biodegradability, chemical methods for the removal of chlorophenols have been developed. Degradation of chlorophenols (with low substrate concentrations) using UV-photolysis (Yasuhara *et al* 1977), UV-illuminated TiO₂ (Matthews 1987), UV-photolysis with H₂O₂-addition (Moza *et al* 1988) and Fenton's reagent (Barbeni *et al* 1987) was reported elsewhere.

2. Experimental details

4-Chlorophenol (4-CP, reagent grade, Merck), TiO₂ (Degussa P25), H₂O₂ (30%, p.a., Riedel de-Haën) and FeSO₄·7H₂O (p.a., Merck) were used without further purification.

All experiments were performed at an initial pH of 5.8 in a three-necked-2l flask equipped with a plane glass window (Duran, irradiated area 3300 mm²) and thermostatted at 25° C. The initial concentration of 4-CP was 1.01×10^{-3} mol/l (= 72.9 ppm TOC). A 400 W high pressure Hg-lamp (Osram Ultramed) with quartz optics and water filter was used as light source. The solution (2000 ml) was stirred and purged with pure oxygen during the reaction. Concentration of TiO₂-suspension was 2 g/l, molar excess of H₂O₂ was 10:1 or 50:1 in comparison to 4-CP, concentration of Fe²⁺ in the Fenton experiment 2.5×10^{-4} mol/l. 4-CP was analysed by HPLC (column: Spherisorb S5 ODS 50 µm, eluent: methanol:H₂O = 40:60 Vol%, flow: 1 ml/min), TOC was monitored with a TOC analyser (Shimadzu). H₂O₂ was determined by a modified iodometric method (Greenberg *et al* 1985).

3. Results and discussion

The difference between heterogeneous and homogeneous reaction mechanisms can be explained by comparing degradation of 4-CP and TOC (figures 1 & 2). Degradation curves of 4-CP and TOC in the UV/TiO₂ and UV/TiO₂/H₂O₂ experiments show a similar course, in contrast to homogeneous reactions, where the 4-CP concentration decreases more rapidly than TOC-concentration. During the dark Fenton reaction, 4-CP disappears rapidly within a few minutes but TOC removal is only 42% after 24 hours. With photolysis in the presence of a 10:1 excess of H₂O₂, 4-CP is completely degraded after 24 hours with a TOC reduction of only 51%. A very high excess of H₂O₂ reduces the degradation rates of both 4-CP and TOC because of recombination of the hydroxyl radicals (Carey 1990).

In case of UV/TiO₂, the pollutant has to be adsorbed before reaction. This explains the low degradation rate of 4-CP. In solution, there are more free substrate molecules and more OH-radicals for reaction, therefore 4-CP concentration in homogeneous processes decreases very rapidly. Hydroxyl radicals are able to attack the molecules without steric restrictions in contrast to the 4-CP molecule adsorbed on the

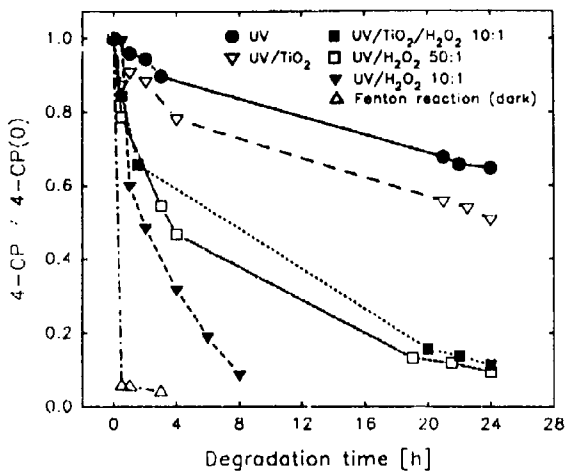


Figure 1. Degradation of 4-chlorophenol ($1\text{-01 mmol/l} \approx 72.9 \text{ ppm TOC}$) with different homogeneous and heterogeneous methods.

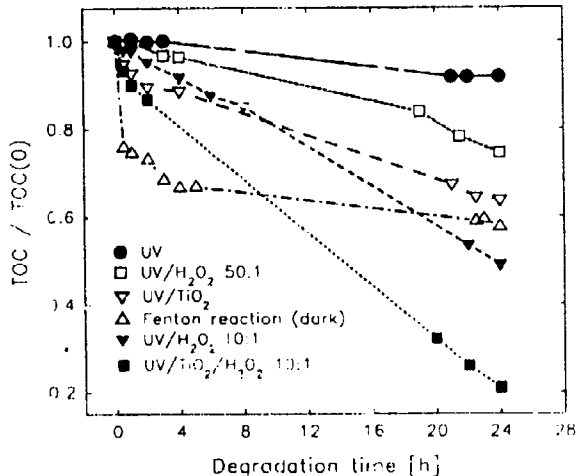


Figure 2. Degradation of TOC ($72.9 \text{ ppm} = 1\text{-01 mmol/l 4-CP}$) with different homogeneous and heterogeneous methods.

TiO₂-surface. In this case, a molecule has to be degraded nearly completely to CO₂ and to desorb before a new molecule can take its place. Therefore, the amount of by-products formed during the heterogeneous process is small compared to Fenton's reagent or UV/H₂O₂. Among the described wastewater treatment methods, the system UV/TiO₂/H₂O₂ combining homogeneous and heterogeneous reactions, was found to be the best degradation method for TOC. TOC degradation was about 80% after 24 hours.

In all processes degradation of H₂O₂ (figure 3) follows the curves of TOC degradation (figure 2). The most rapid decrease of H₂O₂ was observed with Fenton's reagent.

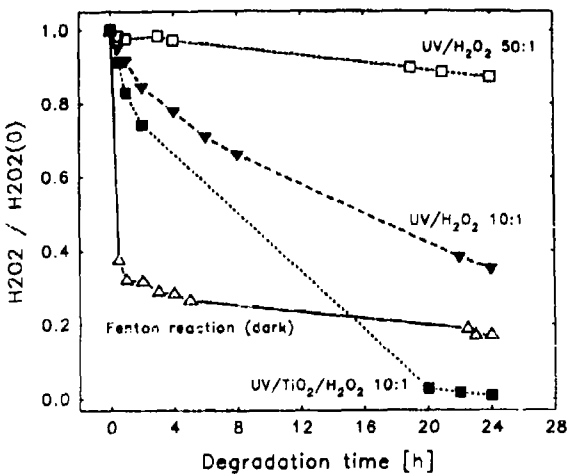


Figure 3. Decrease of H_2O_2 during reaction.

After one hour, the reaction retards because of complete oxidation of Fe^{2+} to Fe^{3+} , (2). Fe^{3+} can be re-reduced during excitation with visible light ($\lambda < 580 \text{ nm}$) (Ruppert and Bauer 1993). The presence of TiO_2 in the $\text{UV}/\text{H}_2\text{O}_2$ process accelerates the degradation of H_2O_2 .

For industrial use, homogeneous processes like $\text{UV}/\text{H}_2\text{O}_2$ (Hager 1990) and UV/ozone (Kearney *et al* 1984) are preferred to heterogeneous processes because of higher degradation rates and no separation problems with the catalyst. In recent years, reactors with immobilized TiO_2 have been developed to avoid this problem (Al-Ekabi and Serpone 1988; Hofstadler 1992; Hofstadler *et al* 1992).

Indeed, photochemical oxidation is an effective way to destroy organic water pollutants although the process has to be optimized and adapted to the contaminant and its concentration.

Acknowledgements

The authors would like to thank the FFF (Forschungsförderungsfonds der Gewerblichen Wirtschaft Österreichs, P 3/8669) for their financial support.

References

- Al-Ekabi H and Serpone N 1988 *J. Phys. Chem.* **92** 5726
- Barbini M, Minero C and Pelizzetti E 1987 *Chemosphere* **16** 2225
- Carey J H 1990 *Proc.-Symp. Adv. Oxid. Processes Treat. Contam. Water Air* (Burlington/Ontario: Water Technol. Center) Paper No. 1
- Greenberg A E, Trussell R R and Clesceri L S (eds) 1985 *Standard methods for the examination of water and wastewater* (Washington: Am. Public Health Assoc.) p. 426
- Haag W R and Yao C C D 1992 *Environ. Sci. Technol.* **26** 1005
- Hager D G 1990 *Innovative Hazard. Wastes Treat. Technol. Ser.* **2** 143

- Hofstädler K 1992 *Development of a photocatalytic reactor with immobilized TiO₂ for wastewater purification*, Doctoral thesis, Technical University, Vienna
- Hofstädler K, Ruppert G, Bauer R, Heisler G and Novalic S 1993 In *Photocatalytic purification and treatment of water and air* (eds) D F Ollis and H Al-Ekabi (Amsterdam: Elsevier) pp. 777–782
- Kearney P C, Zeng Q and Ruth J M 1984 *ACS Symp. Ser.* **259** 195
- Matthews R W 1987 *Sol. Energy* **38** 405
- Moza P N, Fytianos K, Samanidou V and Korte F 1988 *Bull. Environ. Contam. Toxicol.* **41** 678
- Ruppert G and Bauer R 1993 *J. Photochem. Photobiol. A* **73** 75
- Yasuhara A, Otsuki A and Fuwa K 1977 *Chemosphere* **10** 659

Kinetics of sunlight photodegradation of 2,3,4,7,8-pentachlorodibenzofuran in natural water

KEN J FRIESEN* and MYROSIA M FOGA

Department of Chemistry, University of Winnipeg, Winnipeg, Manitoba, Canada R3B 2E9

Abstract. The aquatic photodegradation of the environmental contaminant 2,3,4,7,8-pentachlorodibenzofuran ($P_5\text{CDF}$) was studied under midsummer sunlight conditions at 50°N latitude both in distilled water-acetonitrile solutions and in lake water. The observed net photodegradation rate of $P_5\text{CDF}$ in natural water was 240-fold faster than the rate of direct photolysis in distilled water-acetonitrile solutions. The difference in rates of photodegradation is attributed to the action of sensitizers present in natural waters.

Keywords. Aquatic; photodegradation; polychlorinated dibenzofurans; sunlight.

1. Introduction

Polychlorinated dibenzofurans (PCDFs) are persistent environmental contaminants characterized by low water-solubilities (Friesen *et al* 1990b) and extreme hydrophobicity (Sijm *et al* 1990). 2,3,4,7,8-Pentachlorodibenzofuran is one of the most toxic PCDF isomers, with a toxic equivalency factor (TEF) of 0.5 (Safe 1990) and a single oral dose LD_{50} value of < 10 µg/kg body weight for the guinea pig (Kociba and Cabey 1985).

Although these pollutants tend to resist chemical and microbial degradation, there is some evidence that they undergo aqueous photodegradation. The quantum yields for the direct photolysis of PCDFs in water-acetonitrile mixtures at 313 nm vary from 10^{-2} to 10^{-5} for a series of PCDFs (Choudhry *et al* 1990; Foga 1991). Recent reports (Dung and O'Keefe 1992) indicate that several tetrachlorinated PCDFs are photolyzed in both distilled and natural waters under sunlight conditions, with degradation rates in natural water roughly 2 times faster than in distilled water.

The objective of this study was to determine the rate of sunlight photolysis of 2,3,4,7,8-pentachlorodibenzofuran under environmental conditions, and in particular to ascertain the importance of direct versus indirect photolysis.

2. Experimental

2.1 Chemicals

$^{14}\text{C}_6$ -dichlorophenyl-2,3,4,7,8-pentachlorodibenzofuran ($^{14}\text{C}-\text{P}_5\text{CDF}$) with a specific activity of 1.25×10^{10} Bq/mmol, was purchased from Wellington Laboratories (Guelph,

*For correspondence

ON) and purified (to a radiopurity of 99.9%) by RP-HPLC with 85:15 CH₃OH/H₂O as the mobile phase and redissolved in acetonitrile.

Liquid scintillation fluors, Scintiverse II and Atomlight, were purchased from Fisher Scientific (Winnipeg, MB) and Biotechnical Systems (Boston, MA), respectively.

All solvents used in sample preparation or as HPLC mobile phases were Burdick & Jackson Brand (High Purity) from Baxter Diagnostics Corporation, Canlab, Winnipeg, MB.

2.2 Instrumentation

Quantitative analysis of ¹⁴C-P₅CDF was carried out with a Waters Associates HPLC system equipped with a Model 6000A pump, a Rheodyne Model 7125 injector, and a 25 cm × 3.2 mm μBondapak C₁₈ column (Waters Scientific, Mississauga, ON). Three-minute fractions of HPLC eluent were collected, mixed with 12 ml of Scintiverse II, and analysed for carbon-14 on a Beckman LS 7500 Liquid Scintillation System.

2.3 Kinetics of sunlight photolysis

All glassware was thoroughly cleaned and sterilized at 180°C for 4–5 hours.

Direct aqueous photolysis was studied by preparing solutions of ¹⁴C-2,3,4,7,8-P₅CDF (1.1 ng/ml) in 10:25 (v/v) filter-sterilized CH₃CN/HPLC water (Mill *et al* 1982) and exposing to sunlight in 50 ml Pyrex centrifuge tubes. Indirect aqueous photolysis was monitored under similar conditions but in filter-sterilized lake water obtained from Lake 375 of the Experimental Lakes Area (ELA) near Kenora, ON. Dark controls, in which P₅CDF solutions in lake water were wrapped with aluminium foil to prevent sunlight photolysis, were used to check for biological and chemical degradation. The tubes were placed in a rack near the surface of Lake 375 (ELA), with sunlight exposures carried out over a 3-day period in June 1989.

All solutions were adjusted to pH 9 and extracted with four 5 ml portions of hexane. The extracts were dried by passing through a Na₂SO₄ column and concentrated prior to analysis. Concentrations of parent ¹⁴C-P₅CDF were determined by HPLC-LSC using 85:15 CH₃OH/H₂O as the mobile phase. The extracted aqueous phase was tested for nonextractable ¹⁴C by adding 12 ml of Atomlight to 4 ml of water and counting by LSC. A standard ¹⁴C-P₅CDF was used to establish both the extraction efficiency (105%) and the overall recovery of P₅CDF at the analytical stage (90%).

3. Results and discussion

3.1 Direct photolysis

The absorption spectrum of P₅CDF shows a weak, tailing band above 290 nm (figure 1) producing the potential for direct photolytic degradation of this compound under environmental conditions. However, the aqueous photolysis of P₅CDF was extremely slow in water-acetonitrile solutions (figure 2), with a pseudo-first-order direct photolysis rate constant (k_{DE}) of $0.015 \pm 0.007 \text{ d}^{-1}$ ($t_{1/2} = 46 \text{ d}$). This rate constant has been corrected for tube geometry (Dulin and Mill 1982) to provide a value applicable to surface waters. Quantitative recoveries of P₅CDF from the dark controls

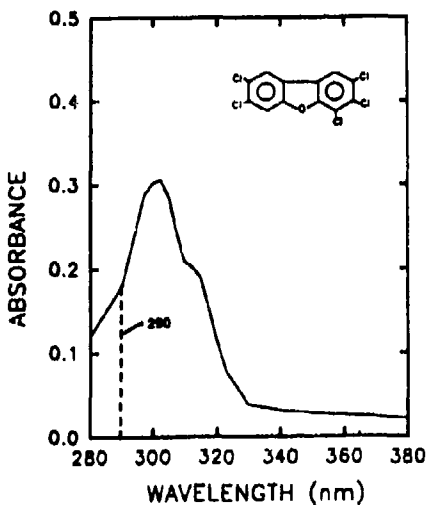


Figure 1. The absorption spectrum of a 1.2×10^{-5} M solution of 2,3,4,7,8-pentachlorodibenzofuran in 1:1 $\text{CH}_3\text{CN}/\text{H}_2\text{O}$ determined with a Hewlett-Packard 8452A diode array spectrophotometer using a quartz cell with a 1 cm pathlength.

sampled over the entire exposure period indicated negligible losses due to biological degradation, volatilization, and/or analytical procedures. Therefore, the observed decreases are attributed to photolytic degradation of this congener under sunlight conditions.

No ^{14}C -labelled intermediates could be detected by HPLC-LSC analysis and no detectable levels of nonextractable ^{14}C appeared throughout the entire experiment. The results are consistent with recent reports which showed that polychlorinated dibenzofurans (Dung and O'Keefe 1992) and polychlorinated dibenzo-*p*-dioxins (Dulin *et al* 1986; Friesen *et al* 1990a) undergo very slow direct aqueous photolysis under environmental conditions.

3.2 Indirect sunlight photolysis

P_5CDF transformation in filter-sterilized lake water was much more rapid with essentially complete degradation after 6 hours of sunlight exposure. Although degradation rates are affected by solar flux and temperature changes, fitting the data to a first-order model (figure 2) and correcting for tube geometry provided a net pseudo-first-order photolytic degradation rate constant (k_{P_5}) of $3.6 \pm 0.3 \text{ d}^{-1}$ ($t_{1/2} = 0.19 \text{ d}$). Dark controls showed no significant changes over the sampling period, hence biological and chemical degradation was again negligible.

The dramatic increase in the rate of photolysis of P_5CDF in lake water relative to distilled water (240-fold) is attributed to the action of photosensitizers present in natural waters. Indirect photolysis of organic contaminants in natural waters is known to be sensitized by dissolved humic material (Zafiriou *et al* 1984; Mill 1989). The dissolved organic carbon (DOC) content of the lake water used in this study ($440 \mu\text{M}$) is believed to contribute to the rapid photolytic destruction of P_5CDF . Photooxidation

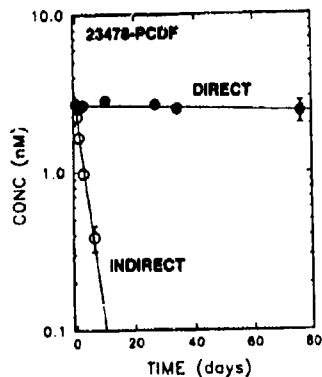


Figure 2. Midsummer sunlight photolysis of 2,3,4,7,8-pentachlorodibenzofuran in lake water (○) and in distilled water-acetonitrile solutions (●) at 50°N latitude.

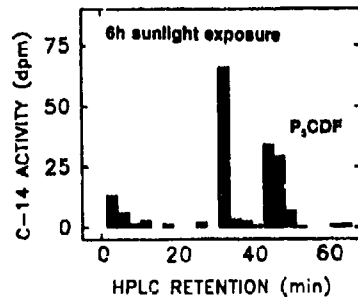


Figure 3. Reconstructed chromatogram for the HPLC-LSC analysis of the hexane extract of a solution of 2,3,4,7,8-pentachlorodibenzofuran exposed to sunlight for 6 h in filter-sterilized lake water. The major bands include unreacted parent P₅CDF ($t_r = 45$ min) and a suspected T₄CDF ($t_r = 33$ min).

by singlet oxygen (Zafiriou *et al.* 1984; Haag and Hoigne 1986), reaction with photochemically generated peroxy and hydroxy radicals (Mill 1989), triplet energy transfers (Zepp *et al.* 1985), and electron transfers (Zafiriou *et al.* 1984) are possible routes of photodegradation of chlorinated dibenzofurans in natural waters.

Only one apparent nonpolar ¹⁴C-labelled degradation product was isolated by HPLC-LSC. This band (figure 3), with a chromatographic retention time corresponding to that of a tetrachlorinated dibenzofuran (T₄CDF) standard ($t_r = 33$ min), reached a maximum concentration after 6 hours of sunlight exposure. However, chromatographic resolution was not adequate to determine the identity of the product or to verify the number of products formed. The disappearance of the product on longer sunlight exposures supported the formation of lower chlorinated dibenzofurans which would then undergo further photolytic degradation. Significant amounts (42%) of ¹⁴C were non-extractable following 52 hours of exposure to sunlight, suggesting formation of polar degradation products. Previous studies have shown similar behaviour for photolysis of several polychlorinated dibenzo-p-dioxins in natural water (Friesen *et al.* 1990a).

Although sunlight emits energy of 35·8–98·6 kcal/mol in the 290–800 nm region (Leiser 1988), sufficient to break typical Ar-O and C-Cl bonds (Lyman *et al* 1982), 2,3,4,7,8-pentachlorodibenzofuran was essentially nonreactive via direct aqueous photolysis. The large enhancement in the rate of photolytic degradation of P₅CDF in natural water relative to distilled water at 50°N latitude in midsummer indicates the important effect that naturally occurring components in lake water have on environmental photodegradation. Further work is underway to identify the degradation products and to determine the role of various sensitizers in the photolytic reaction.

Acknowledgements

Financial support by the Natural Sciences and Engineering Research Council of Canada and by the University of Winnipeg is gratefully acknowledged.

References

- Choudhry G G, Foga M M, Webster G R B, Muir D C G and Friesen K J 1990 *Toxicol. Environ. Chem.* **26** 181
Dulin D, Drossman H and Mill T 1986 *Environ. Sci. Technol.* **20** 72
Dulin D and Mill T 1982 *Environ. Sci. Technol.* **16** 815
Dung M and O'Keefe P W 1992 Organohalogen compounds. *Proceedings of the 12th International Symposium on Dioxins and Related Compounds* (Helsinki: Finnish Institute of Occupational Health) vol. 8
Foga M M 1991 Environmental aquatic photochemistry of 2,3,7,8-tetrachlorodibenzofuran and 2,3,4,7,8-pentachlorodibenzofuran, M Sc thesis, University of Manitoba
Friesen K J, Muir D C G and Webster G R B 1990a *Environ. Sci. Technol.* **24** 1739
Friesen K J, Vilk J and Muir D C G 1990b *Chemosphere* **20** 27
Haag W R and Hoigné J 1986 *Environ. Sci. Technol.* **20** 341
Dulin D, Drossman H and Mill T 1986 *Environ. Sci. Technol.* **20** 72
Leiser A 1988 *The kinetics of environmental aquatic photochemistry - theory and practice* (Washington, DC: Am. Chem. Soc.) pp. 7, 100
Lyman W J, Rechl W F and Rosenblatt D H 1982 *Handbook of chemical property estimation methods: environmental behaviour of organic compounds* (New York: McGraw-Hill)
Mill T 1989 *Environ. Toxicol. Chem.* **8** 31
Mill T, Mabey W R, Bomberger D C, Chou T W, Hendry D G and Smith J H 1982 In Laboratory protocols for evaluating the fate of organic chemicals in air and water, EPA Final Report EPA-600/3-82-022, 50-99
Safe S 1990 *Crit. Rev. Toxicol.* **21** 51
Sijm D T H M, Wever H, de Vries P J and Opperhuizen A 1990 *Chemosphere* **19** 263
Zafiriou O C, Joussot-Dubien J, Zepp R G and Zika R G 1984 *Environ. Sci. Technol.* **18** 358A
Zepp R G, Schlotzhauer P F and Sink R M 1985 *Environ. Sci. Technol.* **19** 74

Applied photochemistry in dental science

LARS-ÅKE LINDÉN

Department of Dental Materials, Karolinska Institute, Royal Institute of Medicine, Box 4064, S-141 04 Huddinge, Stockholm, Sweden

Abstract. This paper presents a short review of the most important problems involved in the photocuring of dental polymer materials, such as a choice of photoinitiating system (mainly based on camphorquinone-amines), kinetics of polymer conversion, depth of curing, shrinkage etc., and also discusses problems with damage of photocured surfaces by chemical, biological, and mechanical degradation.

Keywords. Dental materials; photocuring of polymeric materials; damage to photocured surfaces; photoinitiating system.

During the last two decades, the production of polymers and plastics (composite resins) for dental applications has increased rapidly. These materials are inexpensive, easy to use, and have recently been applied to replace amalgams and other traditional dental materials such as gold, cements, and ceramics. However, they must meet strict demands such as physico-chemical (dimensional stability, strength, craze, and wear resistance), chemical (resistance to hydrolytic and enzymatic degradation), and biological (resistance to biodegradation by microorganisms), toxicological and allergiological demands.

The most common group of dental polymers are polymethacrylates based on mono-, di-, oligomonomers and oligomers. They are used in dentistry for processing denture bases, crown and bridge prosthetics, artificial teeth, orthodontic appliances, and for restorative dentistry (filling materials). For these applications, liquid monomer (modified methyl methacrylates), prepolymerized poly(methyl methacrylates) and cross-linking monomers based on di-, or tri-functional vinyl monomers (e.g ethyleneglycol dimethacrylate or butenediol dimethacrylate) are polymerized by free radical or ionic initiators. More than 100 commercially produced monomers have been used by private companies to prepare dental composites. Some examples are listed in table 1.

Polymerization of dental composites in the oral cavity is restricted by biological demands and should not exceed temperatures of 50°C. This condition eliminates almost all thermally initiated free-radical polymerizations. The soft tissues in the oral cavity are very sensitive to the strong acids formed in some ionic polymerization systems that can be polymerized at room temperature. All of these problems can be overcome by the use of photocuring.

Most common photoinitiators such as analogues of benzoin methyl ethers undergo photofragmentation with the formation of free radicals when exposed to UV irradiation below 400 nm. Use of this type of radiation is restricted in dental applications, because of carcinogenic and photoallergic effects, and the risk of tissue burning

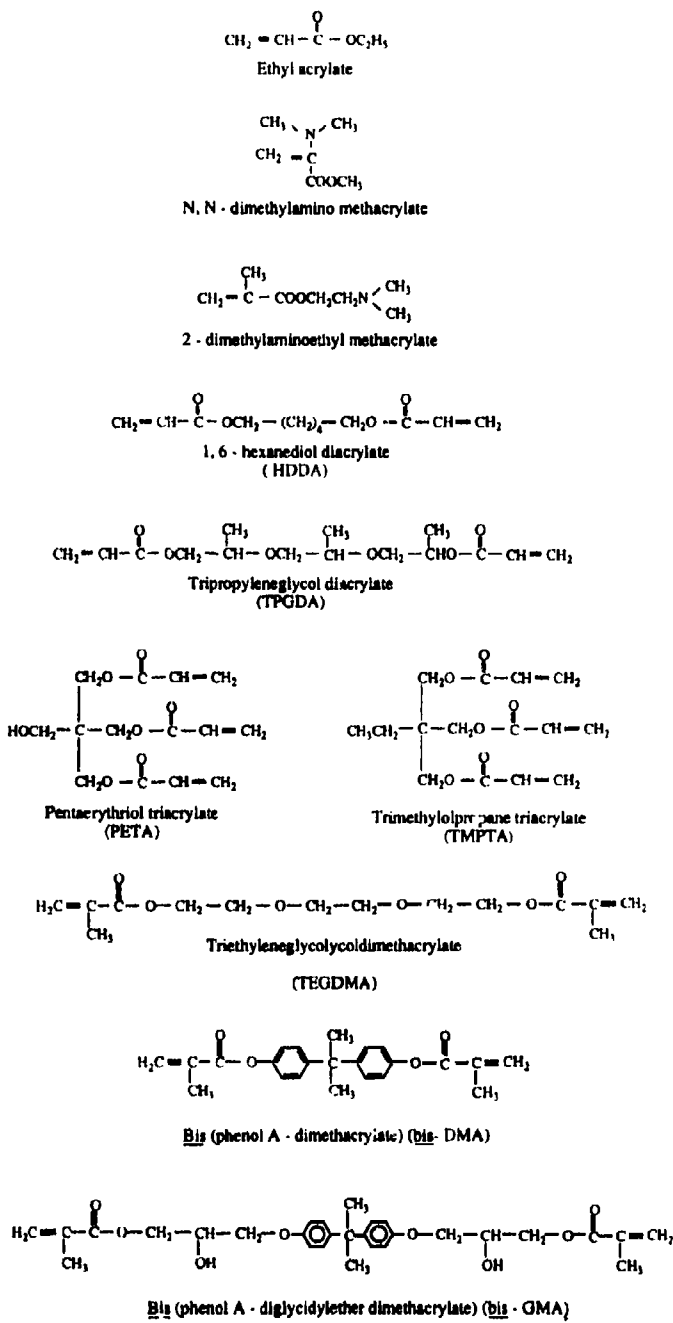
Table 1. Examples of monomers used in photocured resins.

Table 1. (Continued)

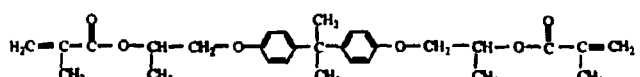
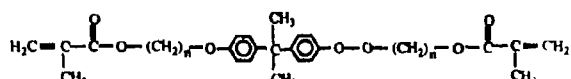
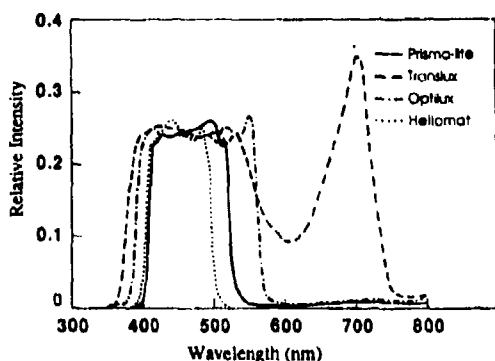
Bis (phenol A - propylether dimethacrylate)Bis (phenol A - n alkylether dimethacrylate)
($n = 2$: bis - EMA, $n = 3$: bis - PMA)

Figure 1. Emission spectra from typical commercial lamps designed for intra-oral photocuring.

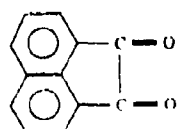
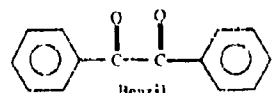
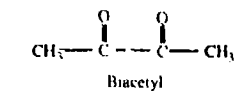
(Birdsell *et al* 1977). The only light irradiation allowed for application in the oral cavity is at wavelengths over 400 nm (Cook 1982).

Most commercially produced irradiation-lamp devices operate with blue light at a maximum of 470 nm (figure 1). This causes a number of problems in finding a photoinitiating system which is effective in this spectral region, that is, which absorbs blue light.

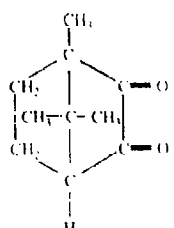
The most common photoinitiating system used in dental applications consists of camphorquinone (which is a diketone, table 2) and different amines (coinitiators) such as N,N-3,5-tetra-methylaniline, N,N-dimethylamino phenethyl alcohol, N,N-dimethylaminoethyl methacrylate (table 3) (Sheela 1991; Cook 1992).

Camphorquinone has a maximum absorption at 468 nm (figure 2), and its excited triplet state reacts with amine to form an exciplex (excited state complex). The exciplex is a short-lived species and it fragments into camphorquinone pinacol radical (A) and amine radical (B) according to reactions 1 and 2 (scheme 1) (Dietliker 1991).

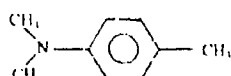
Camphorquinone pinacol radical (A) is deactivated by hydrogen abstraction and/or dimerization reaction and cannot initiate polymerization, whereas the amine radical (B) is responsible for the initiation of polymerization.

Table 2. Examples of di-ketones (photoinitiators) used in photocured resins.

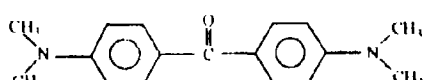
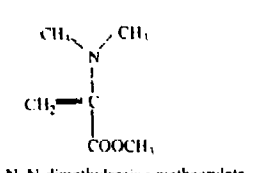
Acenaphthenequinone



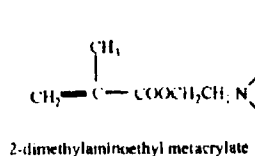
Camphorquinone

Table 3. Examples of amine coinitiators used in photocured resins

N,N-dimethyl-p-toluidine

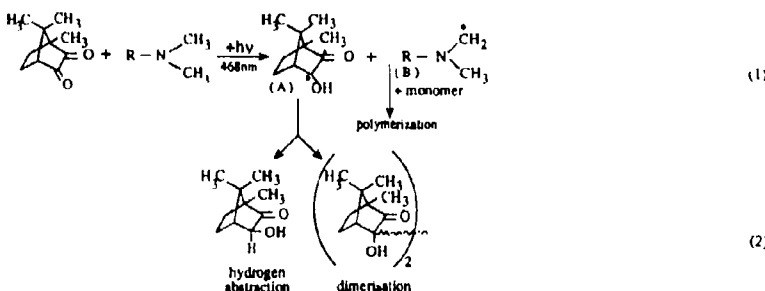
4,4'-bis (N,N-dimethylamino)biphenyl
(Michler's ketone)

N,N-dimethylamino methyl acrylate



2-dimethylaminoethyl methacrylate

Amines which may polymerize,
copolymerize, and/or crosslink
during photoirradiation in
the presence of ketones
(photoinitiators)



Scheme 1. Camphorquinone pinacol radical (A) is deactivated by hydrogen abstraction and/or dimerisation reaction and cannot initiate polymerisation, whereas the amine radical (B) is responsible for the initiation of polymerisation.

Many other diketones (table 2) could be considered as photoinitiators, because of their extended absorption in the region 400–500 nm. Most of them, however, are toxic and mutagenic and are not acceptable for application in dental photocuring.

Camphorquinone irradiated with light at 470 nm does not give free radicals which would initiate polymerization of monomers with unsaturated double bonds (e.g. methacrylates and their analogues). The presence of coinitiators with tertiary amine groups –NR₂ (where R=CH₃, CH₂CH₃) is a condition for the formation of the reactive amino radical NCH₂ in reaction with excited triplet state (*T*) of camphorquinone (reaction 1). The hybrid photoinitiator system camphorquinone-amine e.g. N,N-dimethylaminoethyl methacrylate is very sensitive to light at 470 nm. Changes of spectra of this hybrid photoinitiating system under light irradiation are shown in figure 2.

The reactions (2) are responsible for the decreasing absorption spectra of camphorquinone. One of the most effective hybrid systems is mixture of camphorquinone with Michler's ketone (4,4'-bis(N,N-dimethylamino)benzophenone). The latest one is itself a very active photoinitiator (Rabek 1987). However, it does not absorb light in the visible range > 400 nm. Michlers ketone is, as are many other low molecular amines such as N,N-dimethyl-*p*-toluidine, toxic and mutagenic, and therefore not acceptable for application in intra-oral curing procedures. In spite of this very important toxicological problem, many companies use N,N-dimethyl-*p*-toluidine as a coinitiator.

In our laboratory we are working on hybrid photoinitiating systems, in which coinitiators (amines) are polymerized into homopolymers, or copolymerize with monomers used in composite restorative systems. Polymers with amine groups are almost non-toxic in comparison with low-molecular amines.

One such system is a hybrid formed from camphorquinone and N,N-dimethylaminoethyl methacrylate which after irradiation with light at 480 nm initiates polymerization of other methacrylic mono-, di- and tri-functional monomers, but also causes polymerization of amine methacrylate itself (figure 3). The kinetics of photopolymerization of N,N-dimethylaminoethyl methacrylate in the presence of camphorquinone is shown in figure 4.

This system has a rather long induction period and low conversion efficiency (maximum 75%). The length of the inhibition period depends on the concentration of the inhibitor e.g. *p*-hydroquinone (ca. 0.1%) and initial oxygen concentration. For practical application of this photoinitiator hybrid system in dental composites, the

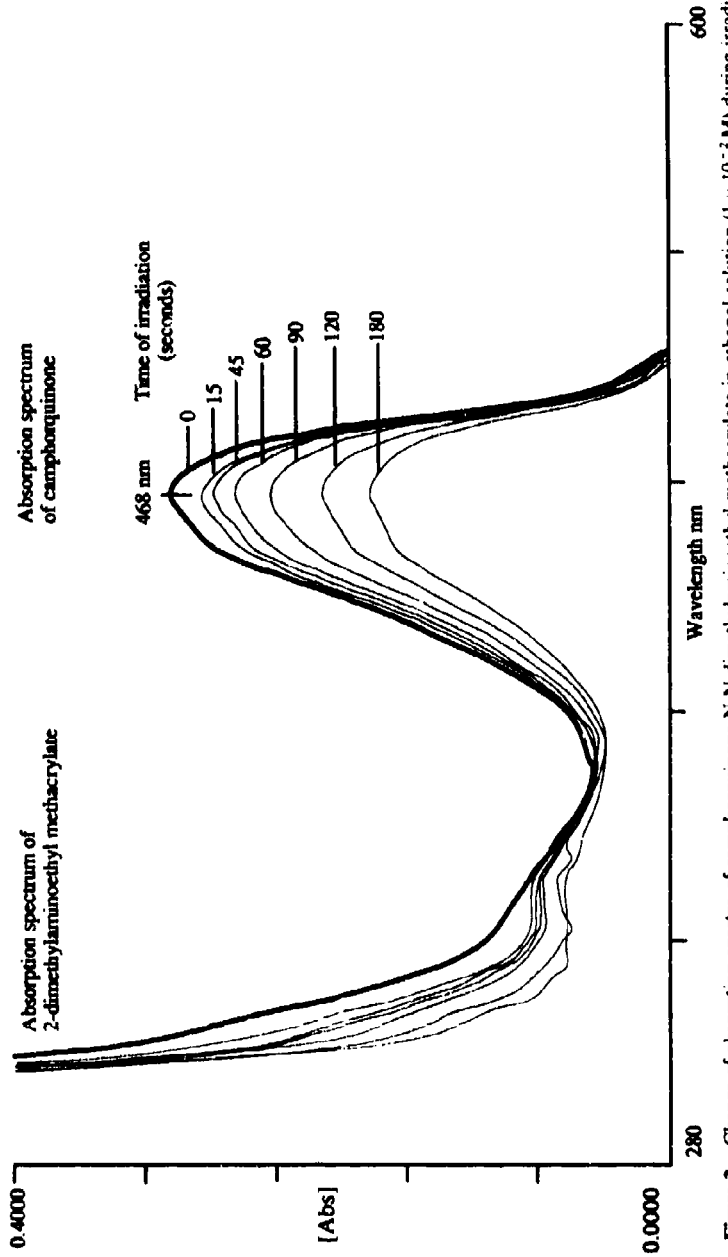


Figure 2. Change of absorption spectra of camphorquinone-N,N-dimethylaminoethyl methacrylate in ethanol solution (1×10^{-2} M) during irradiation with dental photocuring device ($\lambda_{\text{max}} = 480$ nm).



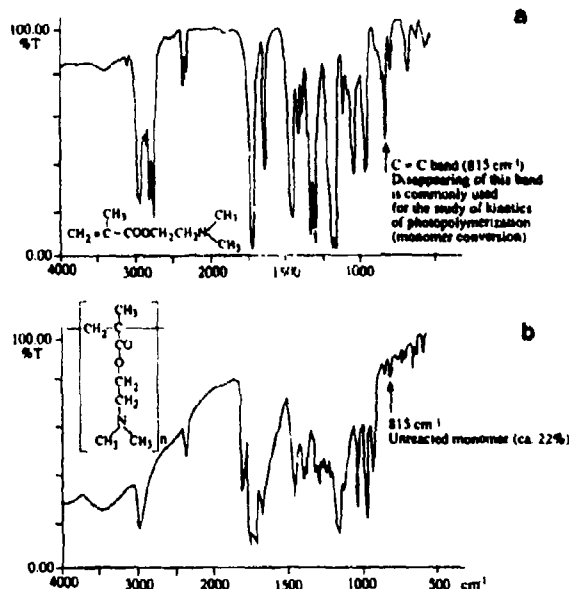


Figure 3. FTIR spectra of (a) pure N,N-dimethylaminoethyl methacrylate and (b) poly(N,N-dimethylaminoethyl methacrylate) obtained after 10 min light irradiation in the presence of camphorquinone.

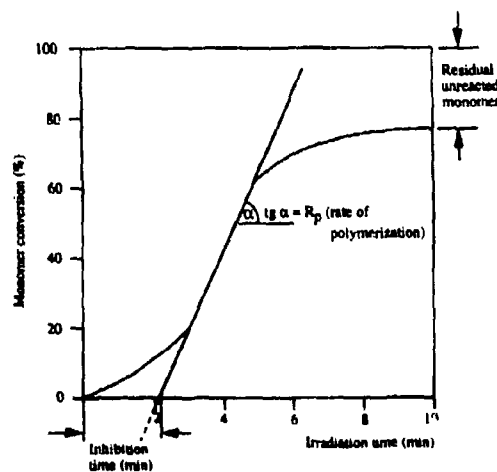


Figure 4. Kinetics of photopolymerization of 2-dimethylaminoethyl methacrylate in the presence of camphorquinone, determined from decreasing absorption of $\text{C}=\text{C}$ band at 815 cm^{-1} (FTIR).

presence of inhibitors is necessary to avoid prepolymerization. During the inhibition period, oxygen is consumed by the amino-radicals that have been formed. However, a very thin surface layer of monomer which is in contact with air remains unpolymerized. The thickness of the unpolymerized layer is dependent on the concentration of

camphorquinone. At a ratio 1:10 of camphorquinone to amine, even the upper surface layer is polymerized. A higher intensity of light also decreases the induction period because the rate of radical formation is much higher.

Photocuring reactions occur, however, in much more complicated systems, depending on the type of dental formulation, which consist of different components

- (i) a mixture of monomers (mono-, di-, tri-functional oligomers), which differ in viscosities, initiation reactivities, propagation and termination reactions.
- (ii) photoinitiator (systems) with different efficiencies of photofragmentations into free radicals or hydrogen transfer reactions producing active free radicals. Free radicals that are formed have differing reactivities with the monomers used in the initiation step, and they also participate in side reactions, e.g. deactivation, dimerisation, hydrogen abstraction, termination of polymerization propagation reactions, reactions with oxygen, and polymerization inhibitors.
- (iii) additives such as prepolymerization inhibitors (used for storage stability), light stabilizers (against colour change of polymerized sample and to protect against its photodegradation).
- (iv) reinforcing phase (fillers) such as silanized quartz, fused borosilicate and aluminosilicate glasses, silicon nitride, calcium silicate, calcium phosphates, aluminium oxide, ceramics, or hybrid fillers (e.g. prepolymerized resins with fumed or pyrogenic silica), which constitute the dispersed phase (50–85%), limits the approach of light to the cured layers.
- (v) coupling agents (as interface on the filler particles) usually 3-methacryloxypropyltrimethoxysilane

Dental pit and fissure sealants, bonding agents, or orthodontic adhesives have similar compositions, except that they are unfilled or lightly filled materials. Dental composites are used as two-component formulations, e.g. powder/liquid, paste/paste or as uniform paste.

Photoinitiated polymerization (photocuring) must often proceed in the oral cavity (e.g. in conservative dentistry when filling cavities in teeth) within 20–40 seconds, but should never exceed one minute. The main problem is the limited depth of polymerization (figure 5) and low conversion efficiency (maximum 75%) (figure 6). The low conversion efficiency can be the result of different causes

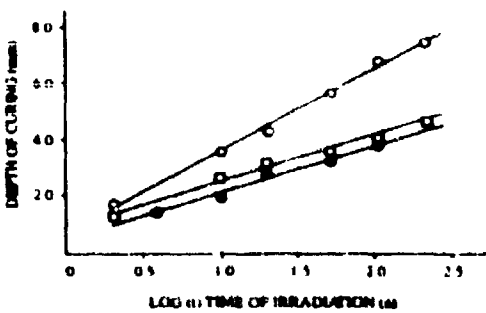


Figure 5. Depth of curing for different polymethylmethacrylic compositions as a function of time of irradiation (Ornat et al. 1990).

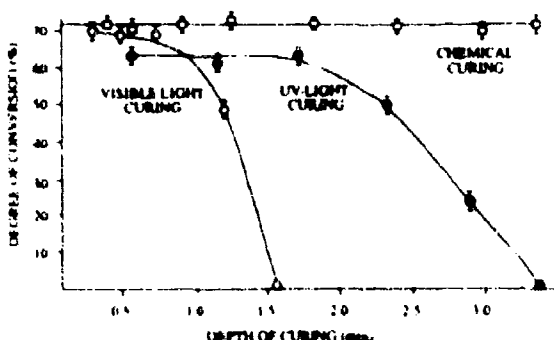


Figure 6. Comparison of degree of conversion at different depths of curing from the surface using different radiation sources with a chemical curing system (Ruyter and Sjovik 1981).

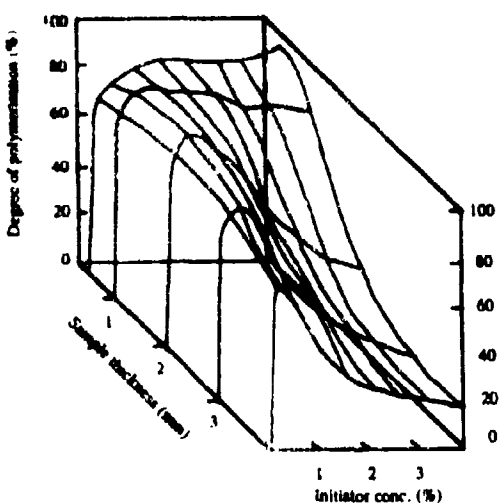


Figure 7. Degree of polymerization (degree of conversion in %) as a function of sample thickness (mm) and initiator concentration (wt %) (Guthrie *et al* 1986).

- (i) Low radical concentration, low radical initiation effectiveness, sample thickness (figure 7) (Guthrie *et al* 1986). For example, increasing the initiator concentration from 1 to 5% can decrease the amount of unreacted monomer molecules from 22 to 8% (Derker and Mousa 1990);
- (ii) increase of viscosity during the propagation and on reaching gel point, which restricts the mobility of propagating radicals;
- (iii) termination reactions.

At low degrees of conversion (about 70% in most dental formulations), the final cured product contains unreacted monomer in addition to low molecular products of photolysis of photoinitiator and other organic additives (inhibitors, stabilizers). All these components are distributed in a polymer cross-linked three-dimensional matrix network.

A severe problem in the application of polymeric materials is the shrinkage of polymerizing formulations, which should not exceed 0·2–2%. Shrinkage, which is a result of volume change, causes a decrease in the dimensions of the final product, i.e. thickness of the sample layer. As a result of shrinkage, a gap is formed between the wall of the cavity and the filling material. This gap is easily accessible to food debris and microorganisms, which can cause secondary caries.

The shrinkage that occurs during polymerization arises from different causes.

- (i) The major factor relates to the fact that monomers are located at Van der Waals' distances from one another, while in the corresponding polymer the (mono)mer units have moved to within a covalent radius which is approximately 1/3 Van der Waals' radius. This causes the shrinkage that is roughly related to the number of mono(mer) units per unit volume that is converted to polymer.
- (ii) The change in entropy and the relative free volumes of monomer and polymer. Free volume is primarily determined by the packing efficiency of the macromolecules. Crystalline (and to some extent semi-crystalline) polymers are, for example, more closely packed than the corresponding amorphous polymers.

Thus crystalline monomers will shrink less than noncrystalline (liquid) monomers. In the case of methacrylate monomers it is impossible to avoid shrinkage (which ranges up to 10%).

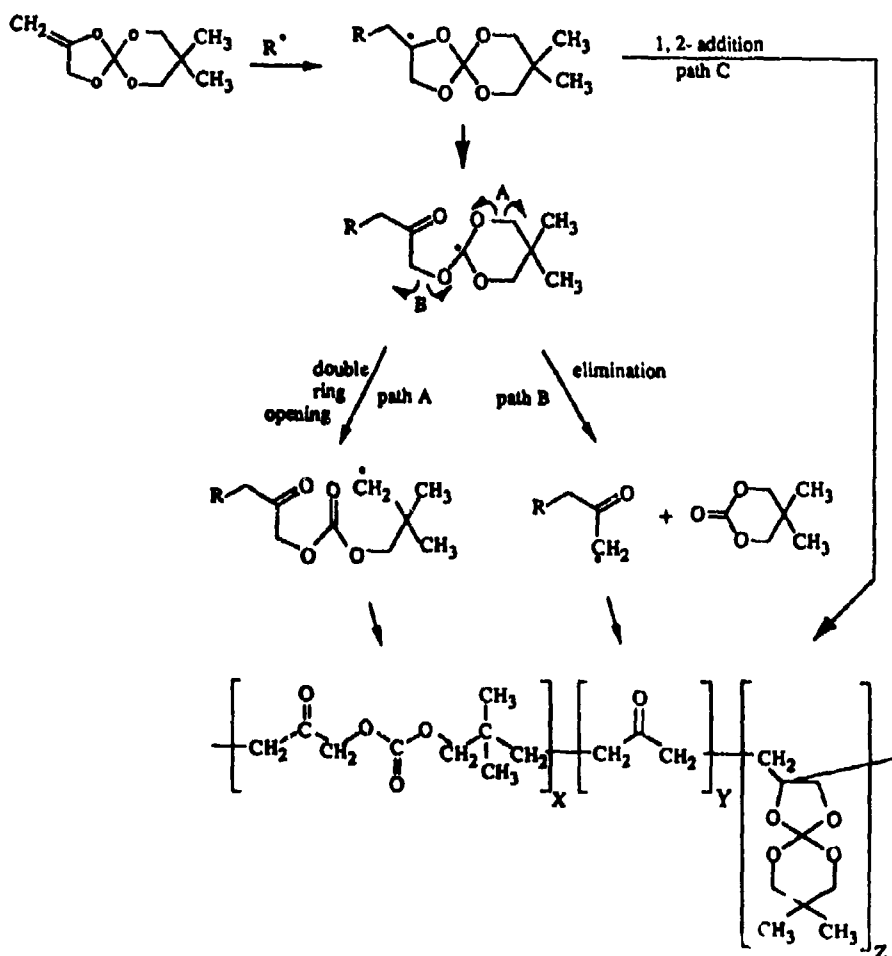
Only polymerization with expansion in volume can solve this problem (Cook 1980). In this type of polymerization, expansion in volume can be achieved through a ring-opening process, wherein two bonds are cleaved for each new bond formed giving a polymer with a volume shrinkage of 1·4–1·7% (Thompson *et al* 1979). The free-radical ring-opening polymerization of a 2-methylene spiro orthocarbonate monomer can be initiated by the hybrid photoinitiator system camphorquinone-(4-N,N-dimethylaminobenzoate) and occurs by the following mechanism (Stansbury 1992) (scheme 2).

The resulting expansion can be applied to counteract the polymerization shrinkage associated with the conventional methacrylate monomers used in dental composites, and thereby provide formulations with drastically reduced shrinkage (Thompson *et al* 1979).

Shrinkage causes not only volumetric and dimensional changes but also builds up large stresses within the material. A variety of material deficiencies has been attributed to the volume contraction associated with the polymerization of dental resins in composites for clinical applications. These deficiencies arise from the generation of stresses which are of sufficient magnitude to cause defects within the resin matrix, and debonding at the surface (Feilzer *et al* 1987, 1990; Zindan *et al* 1987). These complications weaken performance and often restrict those situations for which composites and other related dental resin materials can be considered.

Applications of photocured dental composites in the oral cavity bring several other problems.

- (i) In a photocured polymer formulation there can exist trapped radicals, which have relatively long lifetimes at room temperature. The lifetime of free radicals can exceed five months when certain dimethylacrylates (such as 1,6-hexanediol diacrylate and bis(2-hydroxyethyl acrylate bisphenol-A dimethacrylate) are polymerized (Kloosberer *et al* 1984). The presence of free radicals in a dental



Scheme 2.

composite material in contact with oral soft tissues might cause genetic changes (a problem which has not been investigated yet).

- (ii) Unreacted monomer and other low-molecular (non-polymerized) (Ruyter and Svendsen 1978; Söderholm 1983; Lindén *et al* 1993) components gradually diffuse out of the matrix because they are not compatible with the polymer matrix. They are removed from the surface of filling material by wear or are dissolved and/or transported with saliva to the intestine, where these substances (e.g. poly(acrylic acid)) (Cook 1982) can be absorbed and distributed in the body (Lindén 1991).

Some of these substances can be toxic to pulp and surrounding mucous membranes, and can also cause allergic reactions. It is well known that all methacrylic monomers are toxic (much less than acrylic), whereas amines, together with their high toxicity, are mutagenic and can also cause allergic reactions. Little is known about the toxicity and allergenicity of low molecular products of

fragmentation of photoinitiators (not attached to polymer chains). On the other hand, polymers, especially cross-linked ones, are non-toxic but their allergenic and mutagenic effects are still not well known. It has been observed that many patients and dental personnel show allergic reactions in connection with restorative dentistry using polymeric materials.

- (iii) Chemical and biodegradation of photocured dental composites in the oral cavity. This mode of degradation is caused by rapid changes of pH in the oral cavity (bases and acids present in food), oxidation processes in which oxygen is involved (from air and dissolved in liquids and present in food), and fermentation processes in which acid is produced. These hydrolytic and oxidative degradations cause de-esterification processes, formation of OH/OOH groups, and chain scission and cross-linking processes. Many polyacrylic materials are susceptible to biodegradation and enzymatic hydrolysis (Munksgaard and Freund 1979) caused by microorganisms such as bacteria and fungi.
- (iv) Photocured dental composites are also exposed to often rapid thermal changes (from -70° to +70°C) in the oral cavity. Typical damage due to such forces is the formation of microcracks, cavities, and a rough and corrugated surface. Saliva and fluid foodstuffs may also cause hydrodynamic damage to the surface and participate in the removal of material (figure 8). Such damaged surfaces serve as retentive areas for food debris, bacterial plaque, and discolorations. Finally, polymeric materials become brittle and numerous surface microcracks render them less resistant to mechanical wear, and surface layers are thus removed.

The lifetime for anterior polymeric restorative materials is about 8 years, but for posterior (fillings attaining loads) it is often not longer than 2-4 years (Qvist *et al* 1990). Most polymeric materials used as restoratives must be repaired and polished during this time. Traditional restorative materials for posterior teeth are dental amalgams with very long lifetimes (10-20 years). In the last decade, questions about mercury release from fillings and a growing social concern about metal toxicity has raised serious doubts about using amalgams. This has led to the necessity of replacing amalgams by non-toxic materials, e.g. polymeric composite resins. In comparison with dental amalgam fillings with lifetimes exceeding 10 years, polymeric materials are, however, still inferior.

Another very important group of polymeric dental materials are polyionomer cements based on poly(acrylic) or other polycarboxylic acid analogues and inorganic glass materials (aluminosilicates) (Wilson and McLean 1988). Carboxylic groups present in poly(acrylic acid) form, with aluminosilicate glasses, very strong coordination complexes which are bonded to various substrates such as dentin, enamel, and several metallic materials.

Despite the many advantages of polyionomers used for dental applications (high biocompatibility, good adhesion to enamel, dentin and metallic restorations), they are easily hydrolysed by acids. In order to improve the hydrolytic degradation properties of polyionomer cements, blends with difunctional monomers and/or its copolymers with monomers having functional double bonds (remaining after copolymerization) are used instead of pure poly(acrylic acid). These polyionomers are further photocured in the presence of aluminosilicate glasses. Such cross-linked polymeric networks (figure 9) protect coordination bonds against acids that cause their hydrolytic decomposition and improve their dimensional tensile strength.

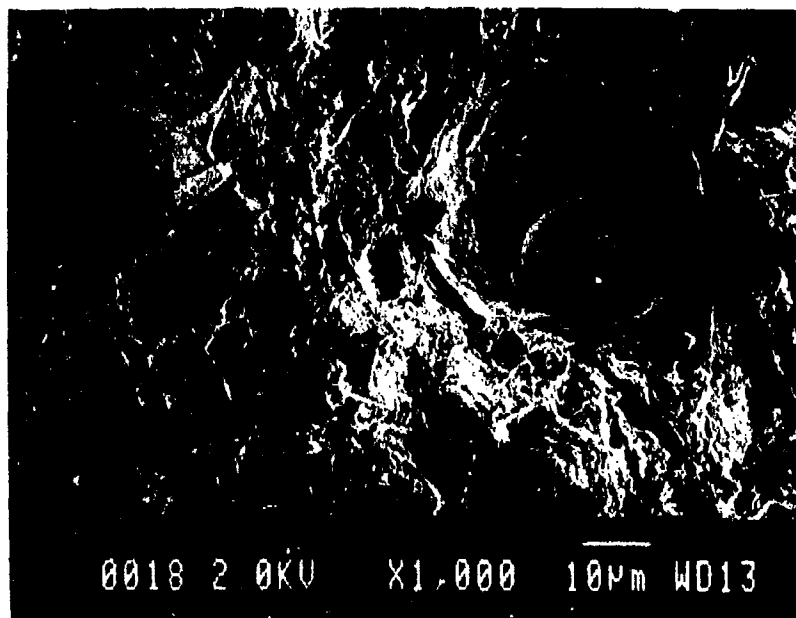


Figure 8. SEM micrograph of surface of photocured dental glass-inomer cement after exposure in an oral environment for 120 days (Lindén *et al* 1993).

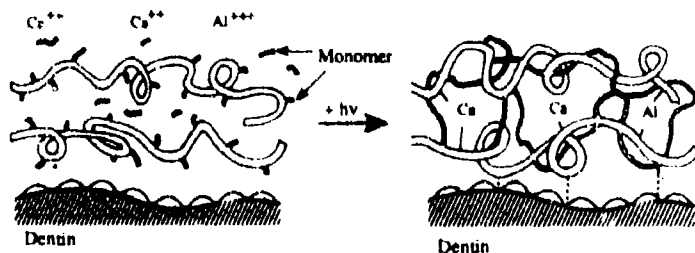
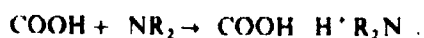


Figure 9. Photopolymerization and formation of coordination complexes in glass ionomers.

Poly(acrylic acid) also forms ionic complexes with a number of metallic salts e.g. FeCl_3 , giving a hydrogel (Lindén and Rabek 1993), which was used for tightening micro-channels in human dentine (figure 10) in order to block transportation of toxins and bacteria to the underlying pulp tissue.

In order to decrease hydrolytic degradation of these ionic complexes, it is possible to photocross-link them with mono- and difunctional monomers, e.g. N,N-dimethylaminoethyl methacrylate in the presence of camphorquinone. Free carboxylic groups (COOH) that do not participate directly in formation of ionic complexes with FeCl_3 , can react with amine groups (NR_2):



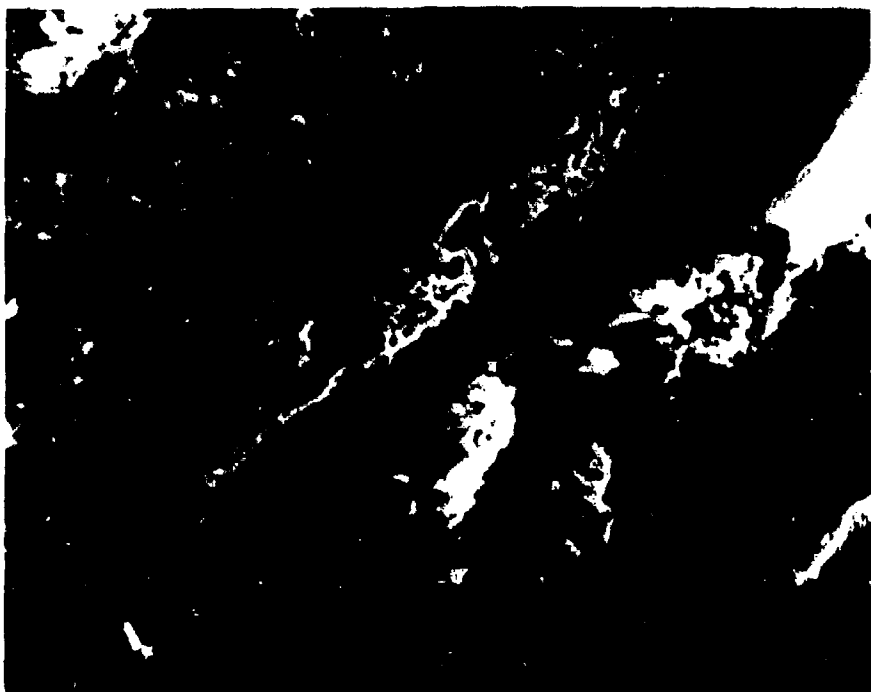


Figure 10. SEM micrograph of human dentin with tubule (micro-channel) blocked by a complex formed between polycarboxylic acid and FeCl₃, (Lindén and Rubek 1993).

In this way a three-dimensional cross-linked network is formed that consists of both covalent (from photocuring) and ionic bonds, and is resistant against hydrolytic degradation.

In conclusion, there are no "ideal" polymeric dental materials yet available that could replace the unique properties of the "old" amalgam-filling materials. It is necessary to search for new monomers with a high degree of conversion, which can give a polymer with very low shrinkage, and which could be resistant to all types of degradation processes that occur in the oral cavity. It is also important to synthesize fluoromonomers, which during degradation processes could release fluoride to decrease the risk of secondary caries.

However, synthetization of monomers and production of new materials for dental applications should be accompanied by careful testing of their ageing in an oral environment and for release of substances that may have toxicological and allergiological implications in their use. Our institute is currently engaged in researching these problems.

References

- Birdsell D C, Bannon P J and Webb R B 1977 *J. Am. Dent. Assoc.* **94** 311
Cook W D 1980 *J. Dent. Res.* **59** 800

- Cook W D 1982 *J. Dent. Res.* **61** 1436
Cook W D 1992 *Polymer* **33** 600
Decker C and Mousa K 1990 *Makromol. Chem.* **191** 963
Dietliker K 1991 In *Chemistry and technology of UV and EB formulation for coatings, inks and paints* (ed.) P K T Oldring (London: SITA Technology) p. 267
Feilzer A J, De Gee A J and Davidson C L 1987 *J. Dent. Res.* **66** 1636
Feilzer A J, De Gee A J and Davidson C L 1990 *Dent. Mater.* **6** 167
Guthrie J, Jegannathan M B, Otterbrun M S and Woods J 1986 *Polym. Bull.* **15** 51
Kloosbergen E, Van der Heij M M, Gossinkad R G and Dortant M C G 1984 *Polym. Commun.* **25** 322
Lindén L Å, Morge S and Adameczak E 1993 *Swed. Dent. J.* (in press)
Lindén L Å and Rabek J F 1993 *J. Appl. Polym. Sci.* (in press)
Munksgaard E C and Freund M 1979 *Scand. J. Dent. Res.* **98** 261
Qvist V, Qvist J and Mjör I A 1990 *Acta Odontol. Scand.* **48** 305
Rabek J F 1987 *Mechanisms of photophysical processes and photochemical reactions in polymers* (Chichester Wiley) p. 297
Ruyter I E and Sjövik I J 1981 *Acta Odontol. Scand.* **39** 133
Ruyter I E and Svendsen S A 1978 *Acta Odontol. Scand.* **36** 75
Sheela M S, Selvy K T, Krishan V K and Paul S N 1991 *J. Appl. Polym. Sci.* **42** 561
Söderholm K J 1983 *J. Dent. Res.* **62** 126
Stansbury J W 1992 *J. Dent. Res.* **71** 1408
Thompson V, Williams E F and Bailey W J 1979 *J. Dent. Res.* **58** 1522
Wilson A D and McLean J W 1988 *Glass ionomer cement* (Chicago: Quintessence Book)
Zindan O, Gomez-Martin O and Tsuchiya T 1987 *J. Dent. Res.* **66** 716

Supramolecular photochemistry. Luminescent and redox active dendritic polynuclear metal complexes

VINCENZO BALZANI,^{a,*} GIANFRANCO DENTI,^b
SCOLASTICA SERRONI,^b SEBASTIANO CAMPAGNA,^c
VITTORIO RICEVUTO^c and ALBERTO JURIS^a

^aDipartimento di Chimica "G. Ciamician" dell'Università, 40126 Bologna, Italy

^bLaboratorio di Chimica Inorganica, Istituto di Chimica Agraria dell'Università, 56124 Pisa, Italy

^cDipartimento di Chimica Inorganica e Struttura Molecolare dell'Università, 98166 Vill. S. Agata, Messina, Italy

Abstract. The synthetic strategies used to prepare di-, tri-, tetra-, hexa-, hepta-, deca-, trideca- and docosanuclear Ru(II) and/or Os(II) polyipyridine-type complexes containing the 2,3-dpp and/or 2,5-dpp bridging ligands and the bpy and/or biq terminal ligands are described (dpp = bis(2-pyridyl)pyrazine; bpy = 2,2'-bipyridine; biq = 2,2'-biquinoline). The light absorption, luminescence, and redox properties of these polynuclear compounds can be varied by changing (i) the nuclearity, (ii) the nature of metal ions, bridging ligands and/or terminal ligands, and (iii) the position of the various components in the supramolecular structure. Because of their strong absorption in the visible spectral region and the possibility of predetermining the direction of energy migration, these compounds can be used as photochemical molecular devices (e.g., as antennas for harvesting solar energy). Because of the presence of several interacting and/or noninteracting redox centres, they are good candidates to play the role of multielectron-transfer catalysts.

Keywords. Photochemistry; photophysics; supermolecules; molecular devices.

1. Introduction

Supramolecular chemistry has shown that molecular components can be assembled to give species of nanometric dimensions (Lehn 1990; Balzani and Scandola 1991; Schneider and Durt 1991; Vögtle 1991; Whitesides *et al* 1991; Anelli *et al* 1992; Balzani and DeCola 1992). Of particular interest are tree-like structures that incorporate in their building blocks specific pieces of information, such as electronic excited states and redox levels at accessible energy values. To pursue this aim, we have designed a synthetic strategy to build up dendritic species based on luminescent and redox-active transition metal complexes, where desired metals and ligands can be placed in specific sites of the supramolecular structure. Species made of 2, 3, 4, 6, 7, 10, 13 and 22 metal-based units have already been prepared and larger species can in principle be obtained. This strategy opens the way to the synthesis of species of nanometric dimension capable of harvesting visible light and exhibiting made-to-order patterns for energy and electron migration.

* For correspondence

2. Building blocks and bridging ligands

In the last 20 years extensive investigations carried out on the photochemical and electrochemical properties of transition metal compounds have shown that Ru(II) and Os(II) complexes of aromatic diimines, e.g. $\text{Ru}(\text{bpy})_3^{2+}$ and $\text{Os}(\text{bpy})_3^{2+}$ ($\text{bpy} = 2,2'$ -bipyridine), exhibit a unique combination of chemical stability, redox properties, excited state reactivity, luminescence, and excited state lifetimes (Juris *et al* 1988; Balzani *et al* 1990; Kalyanasundaram 1991). Furthermore, their properties can be tuned within rather broad ranges by changing ligands or ligand substituents. Several hundreds of these complexes have been synthesized and characterized, and some of them have been used as sensitizers for the interconversion of light and chemical energy as well as for other purposes. Such complexes are ideal building blocks (components) to obtain supramolecular species capable of exhibiting light-induced functions.

In order to assemble such metal-containing building blocks in a supramolecular array, a variety of bridging ligands can be employed. We have concentrated our efforts on the use of the 2,3- and 2,5-bis(2-pyridyl)pyrazine (2,3- and 2,5-dpp) bridging ligands (BL) shown in figure 1.

Some important properties of the $M(\text{BL})_{3-n}(\text{L})_n^{2+}$ compounds can be summarized as follows (Braunstein *et al* 1984; Brewer *et al* 1986; Campagna *et al* 1989a; Denti *et al* 1990a): (1) there are intense ligand-centred (LC) absorption bands in the UV region and moderately intense ($\epsilon_{\text{max}} \sim 1 \times 10^4 \text{ M}^{-1} \text{ cm}^{-1}$) metal-to-ligand charge transfer (MLCT) bands in the visible region; (2) a relatively long-lived luminescence (10^{-7} – 10^{-8} s time scale at room temperature) is present in the red spectral region; (3) reversible one-electron oxidation of the metal ion takes place in the potential window +0.8/+1.7 V (vs SCE); (4) reversible one-electron reduction of each ligand takes place in the potential window –0.6/-1.1 V. Important differences relevant to our discussion are as follows: (i) Os(II) complexes are oxidized at potentials considerably less positive than Ru(II) complexes; (ii) the MLCT absorption and luminescence bands lie at lower energies for the Os(II) complexes than for the Ru(II) ones; (iii) the energy of the LUMO of the (mono-coordinated) ligands decreases in the series bpy > 2,3-dpp > 2,5-dpp > biq; as a consequence, the lowest (luminescent) ${}^3\text{MLCT}$ level involves the lowest ligand of the above series which is present in the complex; (iv) the electron donor power decreases in the ligand series bpy > biq \geq 2,3-dpp \sim 2,5-dpp.

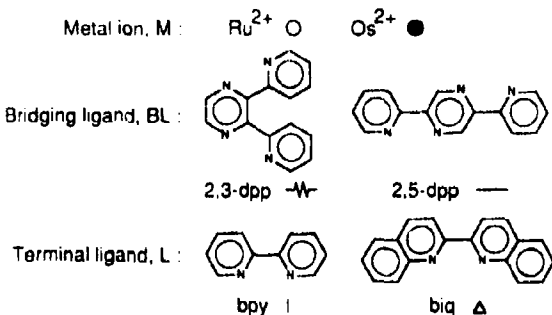


Figure 1. Components of the polynuclear complexes and symbols used.

3. Synthetic strategies

Mononuclear transition metal complexes are synthesized by combining metal ion (M) and free ligands (L), as shown below:

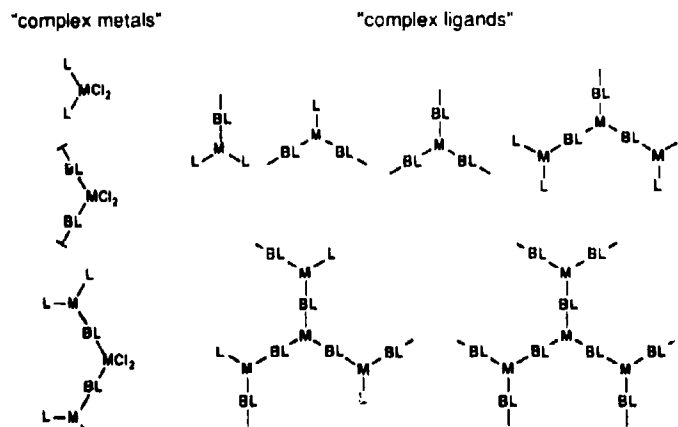


In the last few years we have been developing a procedure to synthesize oligonuclear metal complexes of desired nuclearity and chemical structure (Campagna *et al* 1989b, 1991, 1992; Denti *et al* 1990–1993; Serroni *et al* 1991–1992). Such a procedure is based on the use of *complexes* (building blocks) in the place of the metal (M) and/or ligands (L) in the synthetic reaction (1). The place of M can be taken by mono- or oligonuclear complexes that possess easily replaceable ligands, and the place of L can be taken by mono- or oligonuclear complexes which contain free chelating sites ("complexes as metals" and "complexes as ligands" strategy).

Some of the building blocks used in our syntheses are sketched in scheme 1. The synthetic routes followed to obtain complexes of nuclearity from 10 to 22 are illustrated in table 1. In each equation, the first reactant plays the role of a metal and the second one plays the role of a ligand. A list of the complexes prepared in our laboratory is also reported in the same table. More details on the synthetic procedures (and on the characterization of the compounds) can be found in the original papers. The final step to obtain the docosanuclear compound is shown in scheme 2.

Schematic views of the decanuclear and tridecanuclear complexes containing 2,3-dpp as a bridging ligand are shown in figures 2 and 3.

As shown in table 1, the synthetic strategy used is versatile and selective, since the sites occupied by different metals and ligands in the structure of the polynuclear compounds can be synthetically predetermined by the appropriate choice of the building blocks. Recently we have also elaborated a strategy to grow oligonuclear metal complexes in an arborol-like structure according to a divergent approach (scheme 3) (Serroni *et al* 1992).



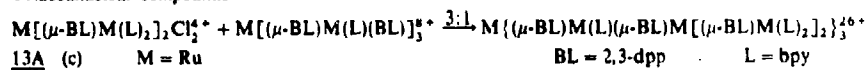
Scheme 1.

Table 1. Synthetic routes used for the synthesis of deca-, trideca-, and docosanuclear complexes. Original references a, b etc are given in parentheses.

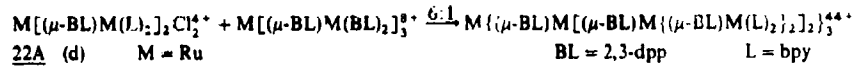
Decanuclear compounds

$M_a[(\mu\text{-BL})M_b(L)_2]_2Cl_4^{4+} + M_c(BL)_3^{8+} \xrightarrow{3:1} M_a\{(\mu\text{-BL})M_b(L)_2\}_2\}^{10+}$		
<u>10A</u> (a, b) $M_a = M_b = M_c = Ru$	BL = 2,3-dpp	L = bpy
<u>10B</u> (a) $M_a = M_b = M_c = Ru$	BL = 2,3-dpp	L = biq
<u>10C</u> (a) $M_a = M_b = Ru, M_c = Os$	3L = 2,3-dpp	L = bpy
<u>10D</u> (a) $M_a = M_b = Ru, M_c = Os$	BL = 2,3-dpp	L = biq
<u>10E</u> (a) $M_a = Ru, M_b = M_c = Os$	BL = 2,3-dpp	L = bpy
<u>10F</u> (a) $M_a = M_c = Ru, M_b = Os$	BL = 2,3-dpp	L = bpy

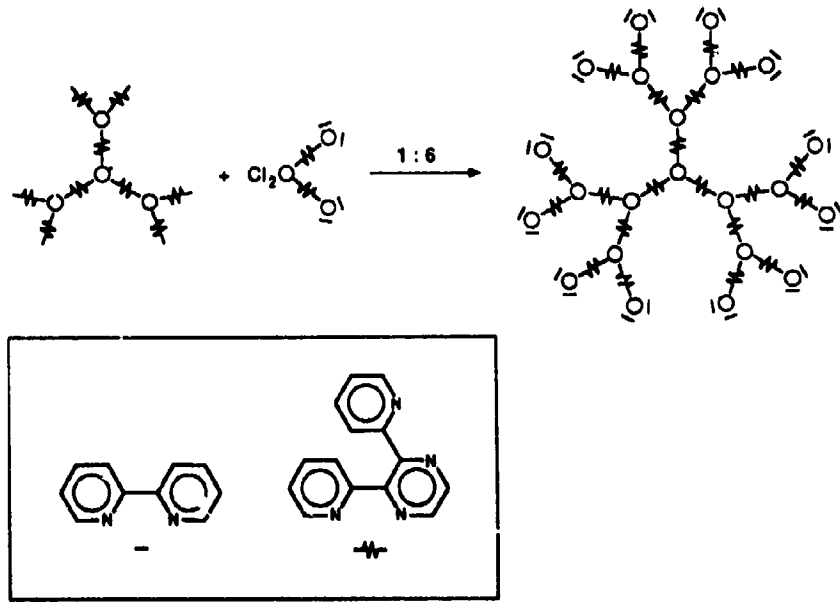
Tridecanuclear compounds



Docosanuclear compounds



References: (a) - Denti *et al* (1992a); (b) - Serroni *et al* (1991); (c) Campagna *et al* (1992); (d) - Serroni *et al* (1992).



Scheme 2.

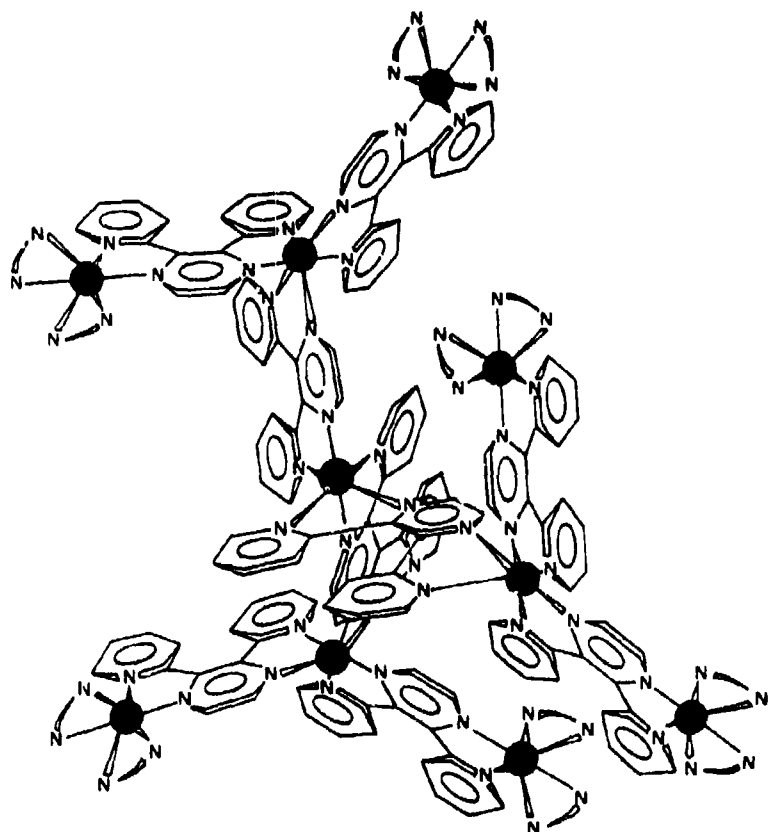


Figure 2. Schematic view of a decanuclear complex.

4. General properties

The compounds described in this paper are well-characterized supramolecular species made of a well-defined number of metal-containing components. They carry an overall positive charge that is twice the number of the metal atoms. Neglecting the PF_6^- counter ions, the docosanuclear compound 22A (6 in scheme 2) is made of 1090 atoms, has a molecular weight of 10890 daltons, and an estimated size of about 5 nm. Besides the 22 metal atoms, it contains 24 terminal bpy ligands and 21, 2,3-dpp bridging ligands (Serroni *et al* 1992). Differences arising from the possible presence of isomeric species are not expected to be sizeable in the electrochemical and spectroscopic properties discussed below.

As one can understand from the schematic views shown in figures 2 and 3, species with high nuclearity exhibit a three-dimensional branching structure of the type shown by otherwise completely different compounds based on polyamidoamines or other organic components (for some recent papers see Shahrai and Hart 1990, Gopidas *et al* 1991, Hawker *et al* 1991, Newkome *et al* 1991 and Nagasaki *et al* 1992; see

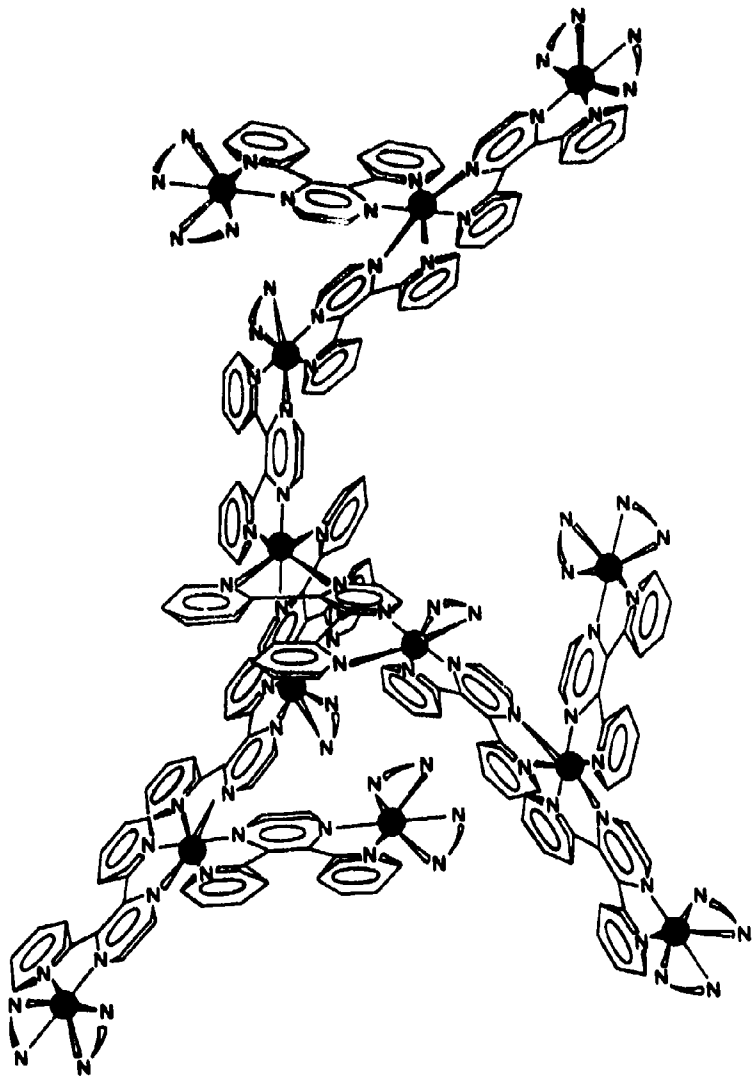
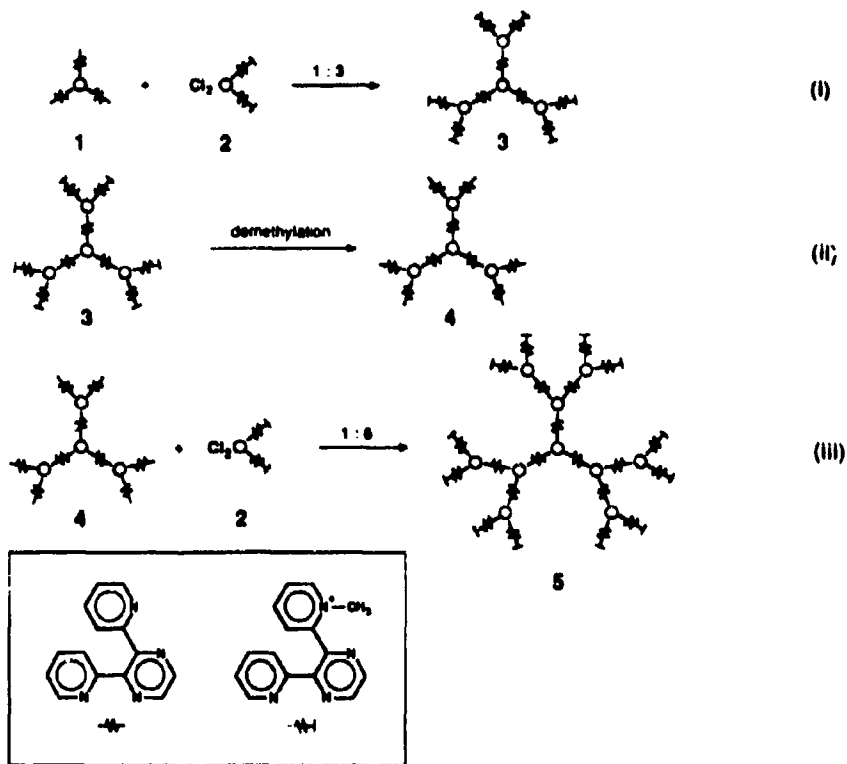


Figure 3. Schematic view of a tridecanuclear complex.

Tomalia *et al* 1990, for a comprehensive review). Therefore endo- and exoreceptor properties can be expected, which will be the object of future investigations.

We would like to stress that our complexes differ from most of the organic-type arborols or dendrimers prepared so far owing to two fundamental reasons: (i) each component exhibits valuable intrinsic properties such as absorption of visible (solar) radiation, luminescence, and redox levels at accessible potentials; (ii) by a suitable choice of the building blocks, different components can be placed in specific sites of the supramolecular array, as one can understand from figure 4 where the syntheses of 6 different decanuclear complexes, using different precursors, are schematized. In



Scheme 3.

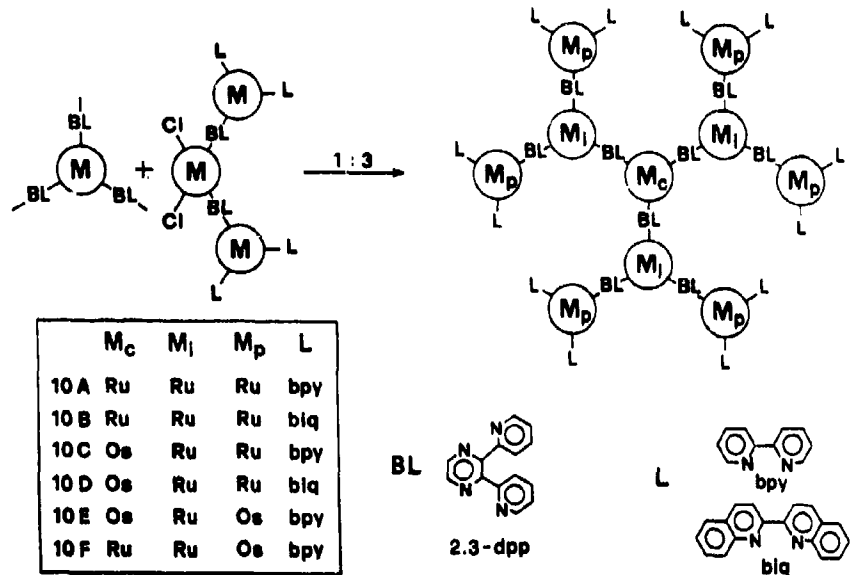


Figure 4. Scheme showing the synthetic control of the composition of decanuclear compounds.

Table 2. Spectroscopic and electrochemical properties of selected polynuclear compounds.^a

Compounds		Absorption		Emission		Electrochemistry
		$\lambda_{\text{max}}^{\text{a}}$ (nm)	ϵ (M ⁻¹ cm ⁻¹)	$\lambda_{\text{max}}^{\text{b}}$ (nm)	τ (ns)	
<u>10A</u>	Ru{(μ -2,3-dpp)Ru{(μ -2,3-dpp) Ru(bpy) ₃] ₂ } ²⁰⁺	541	125000	809	55	+1.46 [6]
<u>10B</u>	Ru{(μ -2,3-dpp)Ru{(μ -2,3-dpp) Ru(biq) ₃] ₂ } ²⁰⁺	555	109000	789	130	+1.62 [6]
<u>10C</u>	Os{(μ -2,3-dpp)Ru{(μ -2,3-dpp) Ru(bpy) ₃] ₂ } ²⁰⁺	550	117000	808	65	+1.17 [1]
				860	d	+1.50 [6]
<u>10E</u>	O{(μ -2,3-dpp)Ru{(μ -2,3-dpp) Os(bpy) ₃] ₂ } ²⁰⁺	563	140500	900 ^c	d	+1.05 [6] +1.39 [1]
<u>13A</u>	Ru{(μ -2,3-dpp)Ru(bpy)(μ -2,3-dpp) Ru{(μ -2,3-dpp)Ru(bpy) ₂] ₂ } ²⁶⁺	544	133000	800	62	+1.50 [9] ^f
<u>22A</u>	Ru{(μ -2,3-dpp)Ru{(μ -2,3-dpp) Ru{(μ -2,3-dpp)Ru(bpy) ₂] ₂ } ⁴⁴⁺	542	202400	802	d	+1.52 [12]

(a) Experiments in acetonitrile solution at room temperature, unless otherwise noted. Luminescence lifetimes are aerated values, unless otherwise stated. (b) Lowest energy 'MLCT' band. (c) The numbers within brackets indicate the number of electrons exchanged. (d) Not measured. (e) At 90 K in MeOH/EtOH 4:1 (v/v) glassy matrix. (f) This wave exhibits a large separation between cathodic and anodic peaks ($\Delta E = 180$ mV). This suggests that there is a superposition of two closely spaced oxidation processes; the first one has been attributed to one-electron oxidation of six independent redox sites, and the second one to one-electron oxidation of three independent redox sites.

other words, our arborols are species with a high "information" content and can therefore be exploited to perform valuable functions (*vide infra*).

The absorption, emission, and redox properties of some selected compounds are shown in table 2.

5. Absorption spectra

Since the interaction between the various metal-containing units is weak (*vide infra*) the absorption spectra of the oligonuclear complexes are, as one can expect, a combination of the absorption spectra of the single metal-containing components. When many components are present, the absorption spectra show very intense bands all over the UV and visible spectral region. For example, the spectra of the decanuclear compounds 10B and 10C (figure 5) (Denti *et al.* 1992a) show absorption bands with ϵ up to 600,000 M⁻¹cm⁻¹ in the UV region and up to 140,000 M⁻¹cm⁻¹ in the visible region. The bands with maxima at 262 and 380 nm can be assigned to $\pi \rightarrow \pi^*$ transitions of the biq ligands, the band at 282 nm to $\pi \rightarrow \pi^*$ transitions of the bpy ligands, and the broad absorption in the 300–350 nm region to $\pi \rightarrow \pi^*$ transitions of the biq and 2,3-dpp ligands. The broad bands observed in the visible region receive contributions from several types of metal-to-ligand charge-transfer (MLCT) transitions. The energies of these transitions depend on the nature of the donor metal ion, the acceptor ligand and the ancillary ligands.

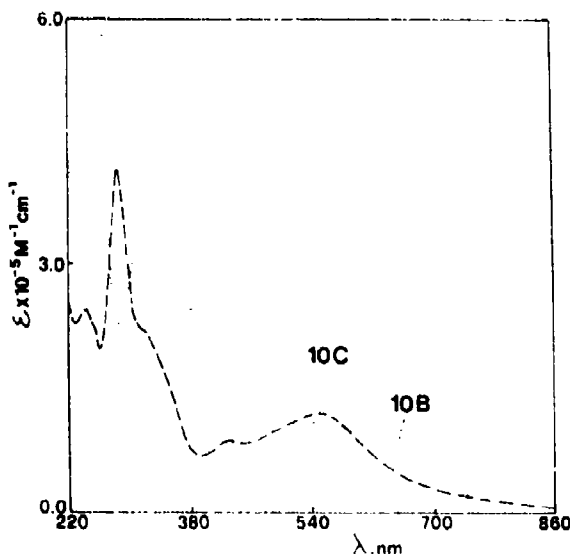


Figure 5. Absorption spectra of the decanuclear compounds 10B and 10C in acetonitrile solution at room temperature.

6. Electrochemical properties

The mononuclear compounds of the $M(BL)_3$, $_{n}(L)_n^{2+}$ series exhibit reversible redox-processes. On reduction, each L ligand is reduced twice and each BL ligand is reduced four times in the potential window $-0.5 \text{--} 3.1 \text{ V}$ (Rossia *et al* 1993). The reduction potential of each ligand depends on its electronic properties and, to a smaller extent, on the nature of the metal and of the other ligands coordinated to the metal. It follows that on reduction of a polynuclear complex which contains several ligands (e.g., 21 ligands are present in the decanuclear complexes), an extremely complicated pattern with many overlapping peaks is observed. On oxidation of mononuclear complexes in the potential window $< +1.6 \text{ V}$, only one peak is observed in the differential pulse voltammograms, which concerns the metal ion. The oxidation potential depends strongly on the nature of the metal ion (Os(II) is oxidized at less positive potentials compared to Ru(II)) and, less dramatically, on the nature of the coordinated ligands. Because of the electronic properties of the isolated components (and of the stabilization of the LUMO of 2,3-dpp and 2,5-dpp on coordination to a second metal centre), it can be expected that for the metal-containing building blocks which are present in the synthesized polynuclear compounds the oxidation potential of the metal (and the energy of the lowest (luminescent) excited state) increases in the series $\text{Os}(\text{bpy})_2(\mu\text{-}2,5\text{-dpp})^{2+} < \text{Os}(\text{bpy})_2(\mu\text{-}2,3\text{-dpp})^{2+} < \text{Os}(\text{biq})_2(\mu\text{-}2,5\text{-dpp})^{2+} < \text{Os}(\text{biq})_2(\mu\text{-}2,3\text{-dpp})^{2+} < \text{Os}(\mu\text{-}2,5\text{-dpp})^{2+} < \text{Os}(\mu\text{-}2,3\text{-dpp})_3^{2+} < \text{Ru}(\text{bpy})_2(\mu\text{-}2,5\text{-dpp})^{2+} < \text{Ru}(\text{bpy})_2(\mu\text{-}2,3\text{-dpp})^{2+} < \text{Ru}(\text{bpy})(\mu\text{-}2,5\text{-dpp})_2^{2+} < \text{Ru}(\text{bpy})(\mu\text{-}2,3\text{-dpp})_2^{2+} < \text{Ru}(\mu\text{-}2,3\text{-dpp})_3^{2+}$.

It can also be expected (and it is confirmed by the experimental data, table 2) that in the polynuclear complexes the metal-metal interaction is non-negligible for metals coordinated to the same bridging ligand, whereas it is very weak for metals that do not share the same bridging ligand. Thus, equivalent units that are not directly

connected are oxidized at the same potential. This allows us to control the number of electrons lost at certain potentials by placing in the supramolecular species the desired number of suitable, equivalent, and noninteracting units. For example, in compound 10C (figure 4), the differential pulse voltammogram (figure 6) shows an oxidation peak at +1.17 V, which is assigned to one-electron oxidation of the central Os³⁺ metal ion, and another peak at +1.50 V, which has the same bandwidth but six times higher intensity, that can be assigned to the independent one-electron oxidation of the six peripheral noninteracting Ru²⁺ ions. Oxidation of the three intermediate Ru²⁺ ions is further shifted towards more positive potentials and cannot be observed in the potential window examined. For 10E, oxidation involves first the six peripheral Os³⁺ ions (which contain the stronger electron donor bpy ligand in their coordination sphere), and then the central one (figure 6).

In conclusion, the electrochemical data offer a fingerprint of the chemical and topological structure of the oligonuclear compounds. Furthermore, made-to-order synthetic control of the number of electrons exchanged at a certain potential can be achieved.

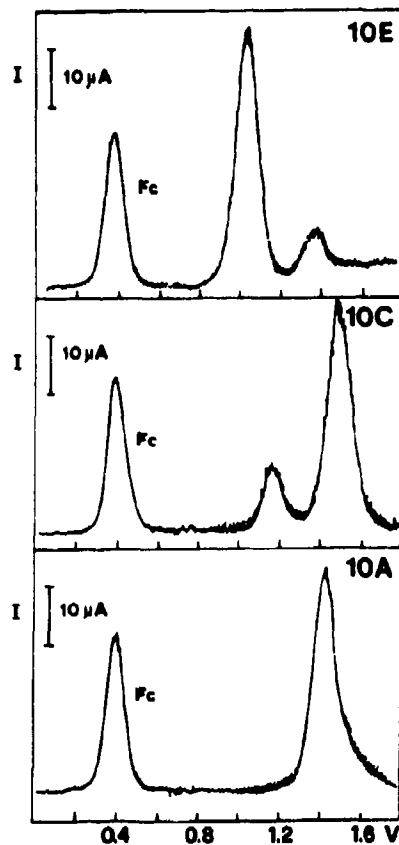


Figure 6. Oxidation patterns for some decanuclear complexes. Fc indicates the oxidation peak of ferrocene, used as an internal standard.

7. Luminescence

Light excitation in the visible absorption bands populates $^1\text{MLCT}$ excited states in the various components. Investigations carried out on $\text{Ru}(\text{bpy})_3^{2+}$ with fast techniques indicate that the originally populated $^1\text{MLCT}$ excited states undergo relaxation to the lowest energy $^3\text{MLCT}$ level in the subpicosecond time scale (Carrol and Bruss 1987; Bradley *et al* 1989; Yabe *et al* 1989; Cooley *et al* 1990). If this behaviour, as it seems likely, is of general validity for the various components of the polynuclear compounds, the actual result of light excitation is the population with unitary efficiency of the lowest energy $^3\text{MLCT}$ level of the component where light absorption has taken place. If each component were isolated, as it happens in mononuclear complexes, competition between radiative (luminescence) and radiationless decay to the ground state would account for the deactivation of the $^3\text{MLCT}$ level, with an overall rate constant, measured from the luminescence decay, in the range $10^6\text{--}10^8\text{ s}^{-1}$. All the members of the mononuclear $\text{M}(\text{BL})_{3-n}(\text{L})_n^{2+}$ family, in fact, display a characteristic luminescence both in rigid matrix at 77 K and in fluid solution at room temperature. When the components are linked together in a supramolecular array, electronic energy can be transferred from an excited component to an unexcited one even if the electronic interaction is weak. In most of the polynuclear compounds examined, only a luminescence band corresponding to the lowest energy $^3\text{MLCT}$ level is observed (table 2), indicating that energy transfer from upper-lying to lower-lying levels does occur (*vide infra*).

8. Antenna effect

The natural photosynthetic systems show that for solar energy conversion purposes supramolecular arrays are needed which absorb as much visible light as possible and are capable of channelling the resulting excitation energy towards a specific site of the array (*antenna devices*). The polynuclear metal complexes described in this paper are excellent light absorbers in the entire visible region. Furthermore, efficient energy transfer can take place between their components, as shown by the presence of only one luminescence band for compounds which contain more than one type of chromophoric units. The occurrence of energy transfer can be established by the quenching of the luminescence of the donor unit and the sensitization of the luminescence of the acceptor unit, and its efficiency can be estimated by comparing the absorption and excitation spectra. The energy levels involved in energy transfer are the lowest $^3\text{MLCT}$ excited state of each component. Because of these properties of the components and of the stabilization of the LUMO of 2,3-dpp and 2,5-dpp on coordination to a second metal centre, it can be expected that for the metal-containing building blocks which are present in the polynuclear compounds the energy of the lowest (luminescent) excited state increases (as does the oxidation potential, *vide supra*) in the series $\text{Os}(\text{bpy})_2(\mu\text{-2,5-dpp})^{2+} \leq \text{Os}(\text{bpy})_2(\mu\text{-2,3-dpp})^{2+} < \text{Os}(\text{biq})_2(\mu\text{-2,5-dpp})^{2+} \leq \text{Os}(\text{biq})_2(\mu\text{-2,3-dpp})^{2+} < \text{Os}(\mu\text{-2,5-dpp})_3^{2+} < \text{Os}(\mu\text{-2,3-dpp})_3^{2+} < \text{Ru}(\text{bpy})_2(\mu\text{-2,5-dpp})^{2+} \leq \text{Ru}(\text{bpy})_2(\mu\text{-2,3-dpp})^{2+} < \text{Ru}(\text{biq})_2(\mu\text{-2,5-dpp})^{2+} \leq \text{Ru}(\text{biq})_2(\mu\text{-2,3-dpp})^{2+} < \text{Ru}(\text{bpy})(\mu\text{-2,5-dpp})_2^{2+} \leq \text{Ru}(\text{bpy})(\mu\text{-2,3-dpp})_2^{2+} < \text{Ru}(\mu\text{-2,3-dpp})_3^{2+}$.

By using the above guidelines, it is possible to design polynuclear complexes where the component(s) with the lowest energy excited state(s) is (are) located in the desired

position(s) of the supramolecular structure. This allows a synthetic control of the direction(s) of energy migration after light absorption.

For the decanuclear compounds 10A–10F, the directions along which energy transfer processes are exoergic are schematically indicated by arrows in figure 7 (Denti *et al* 1992a). 10A displays a luminescence band at 809 nm that can be assigned straightforwardly to the peripheral $(\text{bpy})_2\text{Ru} \rightarrow \text{BL}$ excited states. The lack of luminescence at shorter wavelengths and the constancy of the luminescence quantum yield on changing the excitation wavelength indicate that the chromophoric groups based on the central and intermediate Ru^{2+} ions undergo an efficient deactivation to the peripheral Ru-based units as expected because energy transfer is exoergic in the direction from centre to periphery. 10B exhibits exactly the same behaviour as 10A. For compounds 10C and 10D, a broad luminescence band is observed at room temperature, with a shoulder on its low energy tail. The maxima of the luminescence bands almost coincide with those of the bands exhibited by 10A and 10B, respectively. The predominant emission can thus be assigned to the peripheral units. Subtraction (after normalization) of the luminescence band of 10A from that of 10C and of the band of 10B from that of 10D yields a band with maximum at ~ 860 nm, as expected for the luminescence of a central Os unit. We conclude that, at room temperature, 10C and 10D emit from both the central and the peripheral units. Such behaviour is consistent with the fact that in 10C and 10D the lowest excited state of the intermediate Ru-based units lies at higher energy ($\sim 2000\text{ cm}^{-1}$) than the lowest excited state of the peripheral units. Thus for 10C and 10D the two-step energy-transfer process from the peripheral units to the central one (where the lowest energy excited state of the supramolecular array is located) must be very slow since its first step is endoergic by $\sim 2000\text{ cm}^{-1}$. Direct (through space) energy transfer from the peripheral to the central units is exoergic but should be slow because of the large separating distance. A quantitative evaluation of the energy transfer efficiency from the peripheral to the central unit is difficult to make from luminescence quantum yield data because of the strong overlap between the absorption bands of the various units.

For 10E and 10F the lowest excited states are localized on the peripheral $(\text{bpy})_2\text{Os} \rightarrow \text{BL}$ units which are expected to emit around 900 nm. With infrared-sensitive equipment (Juris *et al* 1993) luminescence bands at 900 and 892 nm can in fact be observed for 10E and 10F, respectively. The lack of any Ru-based luminescence for 10F indicates a 100% efficient centre-to-periphery channelling of the excitation energy, as expected because of the energy gradient (figure 7). For 10E, deactivation of the central Os-based unit by the peripheral ones should not occur because the first step of this process is endoergic. The lack of observable luminescence from such a central unit may simply be due to the fact that most of the light, at any excitation wavelength, is absorbed by the much more numerous peripheral and intermediate units.

9. Conclusion

A synthetic strategy has been developed to obtain supramolecular dendritic structures of nanometric dimensions made of metal complex units capable of a high information content (light absorption, luminescence, redox activity). Specific metal and/or ligands

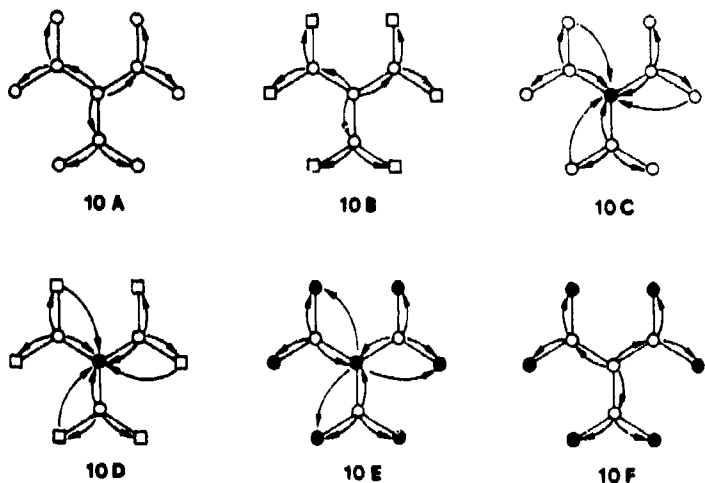


Figure 7. Energy migration patterns for some decanuclear compounds. Empty and full circles indicate Ru^{2+} and Os^{2+} , respectively. In the peripheral positions, circles and squares indicate $\text{M}(\text{bpy})_3$ and $\text{M}(\text{biq})_3$ components, respectively. The arrows indicate the exoergic transfer steps.

can be placed in predetermined sites of the supramolecular array by an appropriate choice of the building blocks. It is thus possible to design species where several important functions can be synthetically controlled. In particular, made-to-order control of the number of electrons lost at a certain potential and of the direction of electronic energy transfer can be achieved.

Because of their strong absorption in the visible spectral region and the possibility of predetermining the direction of energy migration, these compounds can be used as photochemical molecular devices (e.g., as antennas for harvesting solar energy) (Balzani *et al* 1987; Balzani and DeCola 1992, chap. 7). Because of the presence of several interacting and/or noninteracting redox centres, they are good candidates to play the role of multielectron-transfer catalysts.

Acknowledgements

We wish to thank V Cacciari, G Gubellini, L Minghetti and F Stillitani for technical assistance. This work was supported by the Ministero dell'Università e della Ricerca Scientifica e Tecnologica.

References

- Anelli P L, Ashton P R, Ballardini R, Balzani V, Delgado M, Gandolfi M T, Goodnow T T, Kaiser A E, Philp D, Pietraskiewicz M, Prodi L, Reddington M V, Slawin A M Z, Spencer N, Stoddart J F, Vincent C and Williams D J 1992 *J. Am. Chem. Soc.* **114** 193
- Balzani V, Barigelletti F and De Cola L 1990 *Topics Curr. Chem.* **150** 31
- Balzani V and De Cola L (eds) 1992 *Supramolecular chemistry* (Dordrecht: Kluwer)

- Balzani V, Moggi L and Scandola F 1987 In *Supramolecular photochemistry* (ed.) V Balzani (Dordrecht: Reidel)
- Balzani V and Scandola F 1991 *Supramolecular photochemistry* (Chichester: Horwood)
- Bradley P C, Kreas N, Hornberger B A, Dallinger R F and Woodruff W H 1989 *J. Am. Chem. Soc.* **103** 7441
- Braunstein C H, Baker A D, Strekas T C and Gafney H D 1984 *Inorg. Chem.* **23** 857
- Brewer K J, Murphy W R, Spurin S R and Petersen J D 1986 *Inorg. Chem.* **25** 882
- Campagna S, Denti G, Sabetino L, Serroni S, Ciano M and Balzani V 1989a *J. Chem. Soc., Chem. Commun.* 1500
- Campagna S, Denti G, Sabatino L, Serroni S, Ciano M and Balzani V 1989b *Gazz. Chim. Ital.* **119** 415
- Campagna S, Denti G, Serroni S, Ciano M and Balzani V 1991 *Inorg. Chem.* **30** 3728
- Campagna S, Denti G, Serroni S, Ciano M, Juris A and Balzani V 1992 *Inorg. Chem.* **31** 2982
- Carroll P J and Bruss L E 1987 *J. Am. Chem. Soc.* **109** 7613
- Cooley L F, Bergquist P and Kelley D F 1990 *J. Am. Chem. Soc.* **112** 2612
- Denti G, Campagna S, Sabatino L, Serroni S, Ciano M and Balzani V 1990a *Inorg. Chem.* **29** 4750
- Denti G, Campagna S, Sabatino L, Serroni S, Ciano M and Balzani V 1990b *Inorg. Chim. Acta* **176** 175
- Denti G, Campagna S, Sabatino L, Serroni S, Ciano M and Balzani V 1991a In *Photochemical conversion and storage of solar energy* (eds) E Pellizzetti and M Schiavello (Dordrecht: Kluwer) p. 27
- Denti G, Serroni S, Campagna S, Ciano M and Balzani V 1992a *J. Am. Chem. Soc.* **114** 2944
- Denti G, Serroni S, Campagna S, Juris A and Balzani V 1993 *Mol. Cryst. Liquid. Cryst.* (in press)
- Denti G, Serroni S, Campagna S, Juris A, Ciano M and Balzani V 1992b In *Perspectives in coordination chemistry* (eds) A F Williams, C Floriani and A Merbach (Basel: VCH) p. 153
- Denti G, Serroni S, Campagna S, Ricevuto V and Balzani V 1991b *Inorg. Chim. Acta* **182** 127
- Denti G, Serroni S, Campagna S, Ricevuto V and Balzani V 1991c *Coord. Chem. Rev.* **111** 227
- Denti G, Serroni S, Campagna S, Ricevuto V, Juris A, Ciano M and Balzani V 1992c *Inorg. Chim. Acta* **198-200** 507
- Gopidas K R, Leheny A R, Caminati G, Turro N J and Tomalia D A 1991 *J. Am. Chem. Soc.* **113** 7335
- Hawker C J, Lee R and Fréchet J M J 1991 *J. Am. Chem. Soc.* **113** 4583
- Juris A, Balzani V, Barigelli F, Campagna S, Belser P and von Zelewsky A 1988 *Coord. Chem. Rev.* **84** 85
- Juris A, Balzani V, Campagna S, Denti G, Serroni S, Frei G and Güdel H U 1993 *Inorg. Chem.* (in press)
- Kalyanasundaram K 1991 *Photochemistry of polypyridine and porphyrin complexes* (London: Academic Press)
- Lehn J -M 1990 *Angew. Chem., Int. Ed. Engl.* **29** 1304
- Nagasaki T, Ukon M, Arimori S and Shinkai S 1992 *J. Chem. Soc., Chem. Commun.* 608
- Newkome G R, Moorefield C N, Baker G R, Saunders M J and Grossman S H 1991 *Angew. Chem., Int. Ed. Engl.* **30** 1178
- Roffia S, Marcoccio M, Paradisi C, Paolucci F, Balzani V, Denti G, Serroni S and Campagna S 1993 *Inorg. Chem.* **32** 3003
- Schneider H J and Durr H (eds) 1991 *Frontiers in supramolecular organic chemistry and photochemistry* (Weinheim: VCH)
- Serroni S, Denti G, Campagna S, Ciano M and Balzani V 1991 *J. Chem. Soc., Chem. Commun.* 944
- Serroni S, Denti G, Campagna S, Juris A, Ciano M and Balzani V 1992 *Angew. Chem., Int. Ed. Engl.* **31** 1493
- Shahjai K and Hart H 1990 *J. Am. Chem. Soc.* **112** 3687
- Tomalia D A, Naylor A M and Goddard W A III 1990 *Angew. Chem., Int. Ed. Engl.* **29** 138
- Vögtle F 1991 *Supramolecular chemistry* (Chichester: John Wiley)
- Whitesides G M, Mathias J P and Seto C T 1991 *Science* **254** 1312
- Yabe T, Anderson D R, Orman L K, Chang Y J and Hopkins J B 1989 *J. Phys. Chem.* **93** 2302

Light-induced electron transfer in simple and supramolecular Ru-polypyridine complexes

HEINZ DÜRR*, STEFAN BOßMANN, GISELA HEPPE,
RALPH SCHWARZ, URS THIERY and
HANS-PETER TRIERWEILER

FB 11 Organische Chemie, Universität des Saarlandes, D-6614 Saarbrücken, Im Stadtwald,
Germany

Abstract. In artificial photosynthesis the chief research goal is to duplicate the function of the photosynthetic unit in nature but not its structural subunits. In this paper, light-induced electron-transfer processes of Ru-polypyridines as energy-storing systems, in the presence of suitable acceptors and catalysts, are described. New highly photostable photosensitizers are presented. A new approach using supramolecular (non-covalently) connected assemblies in addition to covalently linked systems for energy-storing processes is demonstrated. The use of classical and new Ru-complex assemblies in oxygen or hydrogen generation from water is dealt with. The efficiency of the new systems in the reduction of CO₂ to methane is presented.

Keywords. Electron transfer; supramolecular photochemistry; supramolecular Ru-polypyridine complexes.

1. Introduction

The photosynthetic unit has been characterized in *Rhodopseudomonas viridis* by Deisenhofer *et al* (1984, 1985) and Mathis (1990). This work has stimulated intensive photoinduced electron-transfer studies (Juris *et al* 1988). In the recent past, this field has developed extremely fast and is defined today as artificial photosynthesis. Researchers aim to duplicate nature's functions but not its molecular design (Creutz and Sutin 1975; Balzani *et al* 1978; Kiwi *et al* 1982; Seddon and Seddon 1984). The complicated connections and interrelations of the different components of such systems have led to the birth of a new field, supramolecular photochemistry (Balzani 1987; Balzani and Scandola 1990; Dürr and Schneider 1991). Natural as well as artificial photosyntheses possess, as primordial characteristics, efficient light harvesting units for the conversion of solar energy. The basic reaction to be realized is light-induced charge separation leading to the cleavage of water. In artificial photosynthesis this is achieved by sensitizers absorbing in the visible region of the solar spectrum by electron relays functioning as short-time reservoirs of chemical energy and redox active components that can be used for energy storage (Juris *et al* 1988). Catalysts play an important role in these processes concerned in lowering

*For correspondence

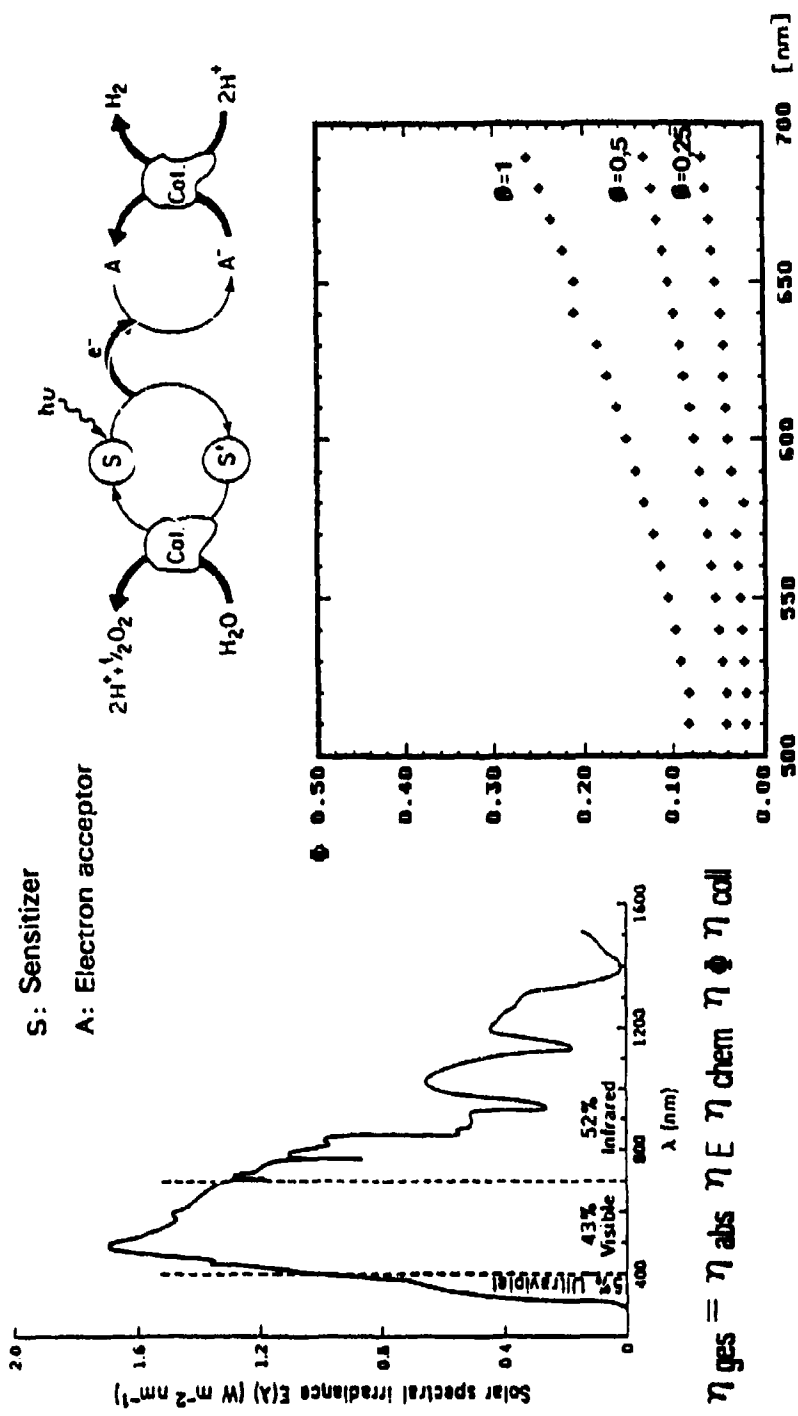
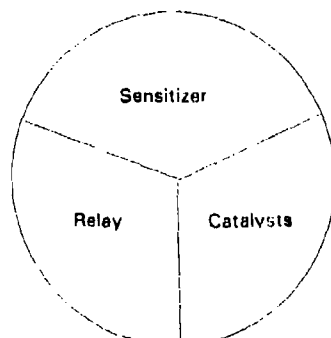


Figure 1. Artificial photosynthetic unit.

kinetic barriers of the dark reactions induced by the photochemical primary processes. The typical components for such an artificial photosynthetic unit are shown in figure 1. The energy to be stored in a photoelectron-transfer reaction is shown in figure 2. Following excitation an ($S^* - R$) pair is generated. Electron transfer then produces ($S^+ + R^-$). This pair can undergo a reaction on a catalyst to afford H_2 and O_2 from water or a competition reaction $S^+ + R^-$ to SR occurs, the so-called back reaction. This leads to annihilation of the stored energy or, in other words, to waste of energy. In order to avoid this problem a fast electron transfer (bimolecular) is necessary. Looking for the optimal system thus means that both unimolecular and bimolecular light-induced processes should have high values. The main task of modern research in the field of artificial photosynthesis is to find a cyclic system for water cleavage. It should possess:

- (1) a fast forward reaction of the radical pair ($S^+ R^-$) with a negligible back reaction.
- (2) an efficient system to allow the one-electron sensitizers to carry out multielectron redox processes as nature does.

Until today no reproducible cyclic system for artificial photosynthesis has been found (not regarding semiconductors however, Serpone *et al* 1985). Therefore, studies of sacrificial systems are good models for photoredox processes to generate oxygen (Henglein 1984; Harriman *et al* 1988; Mills *et al* 1988; Heppe 1994), hydrogen (Creutz and Sutin 1975; Balzani *et al* 1978; Kiwi *et al* 1982; Dürre *et al* 1983, 1985; Seddon and Seddon 1984; Kalyanasundaram 1992) or methane (Willner *et al* 1987) from water or carbon dioxide. Typical parameters to be optimized in such systems are collected in scheme 1.



Scheme 1. Tailor made compounds.

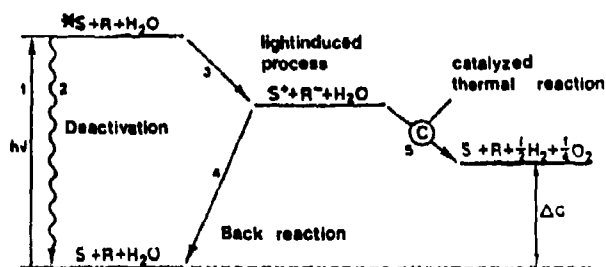
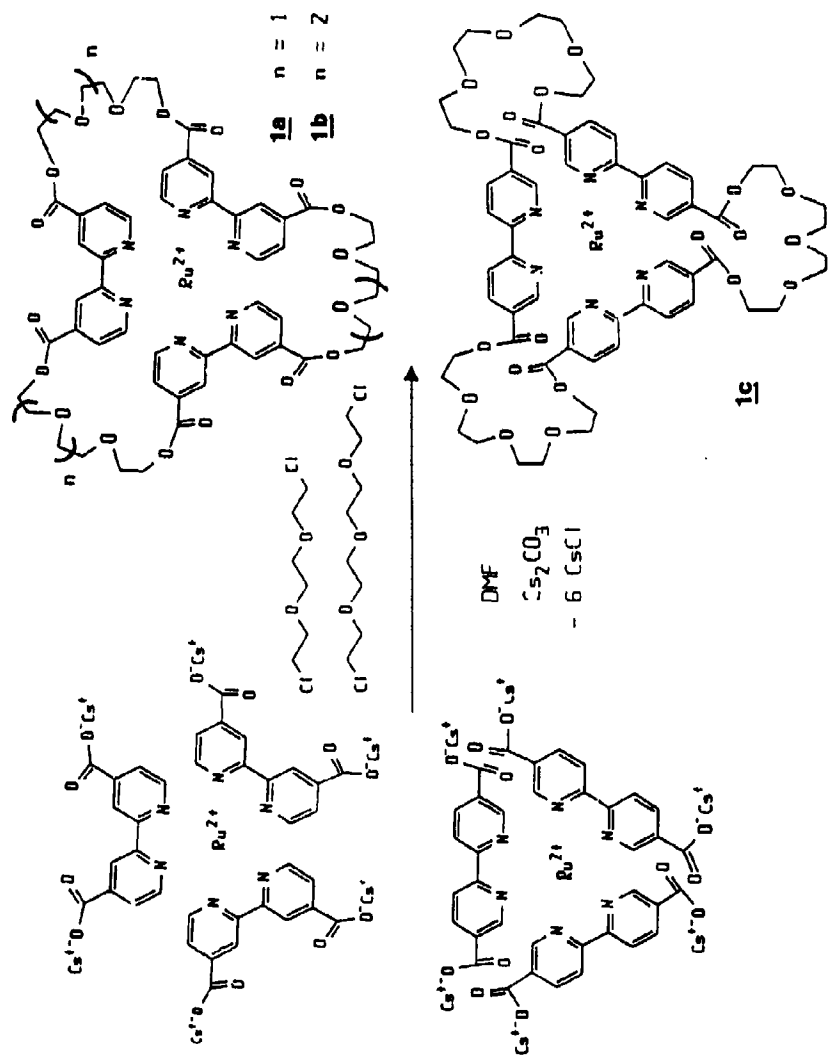


Figure 2. Reaction scheme for the photochemical water cleavage.



Scheme 2. Synthesis of Ru(II)-coronates using the cesiumcarbonate method.

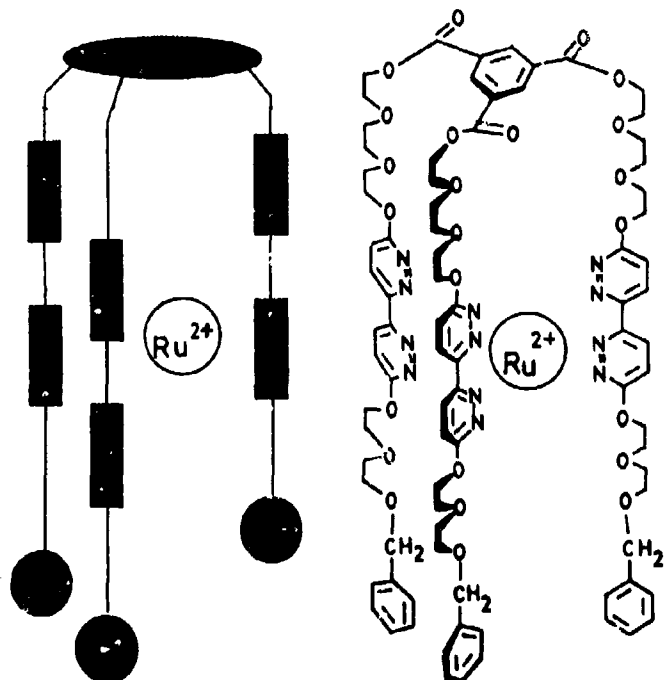
1.1 Sensitizers

From the different possible sensitizers, we have mainly focussed our interest on Ru-polypyridine complexes (Dürr *et al* 1983, 1985). Good results in this field have been obtained by various groups (Creutz and Sutin 1975; Balzani *et al* 1978; Kiwi *et al* 1982; Seddon and Seddon 1984; Balzani 1987; Balzani and Scandola 1990; Dürr and Schneider 1991) as well as by us (Dürr *et al* 1983, 1985) regarding the parameters mentioned in scheme 1.

One value however – high photostability – is still a major challenge.

A very efficient way of stabilization is the change of the MLCT versus the MC-levels in Ru-polypyridine complexes (Balzani 1987; Balzani and Scandola 1990). Another approach is linking the different bipyridine units in such complexes by intramolecular bridges. This concept was advanced for the first time by Sargeson (1984). We have used this approach to generate two types of new molecules, the Ru-coronates 1 (Boßmann and Dürr 1992) and the Ru-podates (Dürr and Schwarz 1993) 2. The synthetic scheme for 1 and the formula for 2 is shown in schemes 2 and 3. These two classes of bridged Ru-polypyridine complexes possess the photophysical properties as shown in tables 1 and 2. All parameters of this new class of molecules are suitable for artificial photosynthetic systems. One parameter, is however, especially remarkable, i.e. photostability or the inverse, called photoanation of the bridged Ru complexes.

Table 3 shows that Ru-coronates 1 are among the most photostable Ru-polypyridines. Ru-podate 2f seems to exceed even this photostability and is amongst



Scheme 3. Ru-podate (Pod) 2.

Table 1. Photophysical properties of Ru-(bpdz)₃-polyethers and Ru-podate.

Complex	λ_{on} (nm)	λ_{em} (nm)	ϕ_p
<u>2a</u>	421	457	0.045
<u>2b</u>	420	458	0.048
<u>2c</u>	420	459	0.055
<u>2d</u>	422	469	0.13

Table 2. Photophysical data of Ru(bpdz)₃-polyethers 2a-2d and Ru-podate 2f.

Complex	$\tau_L(\text{H}_2\text{O})$ [ns]	$\tau_L(\text{MeOH})$ [ns]	$\tau_L(\text{CH}_3\text{CN})$
<u>2a</u>	1463 + 54	2295 + 87	3154
<u>2b</u>	1571 + 64	2275 + 86	3136
<u>2c</u>	1943 + 87	2480 + 114	
<u>2d</u>	3345 + 95	3246 + 97	3448
<u>2f</u>	1986 + 309		

Table 3. Photoanation quantum yields and rates of Ru-coronates 1c and -podates 2. Photoanation of Ryl_3^{+} -compounds (at 298 K).

	τ [ns]	$\phi \times 10^3$	ϕ_p
Ru(coronate) <u>1</u>	3.45 ^b	6.0	< 10 ^{-6a}
Ru(podate) <u>2f</u>	1986 ^c	5.3	<< 10 ^{-6a}

^aNo change after 10 d irradiation; ^bpropio-/butyronitrile; ^c H_2O

the best Ru-polypyridines (Rodriguez-Ubis *et al* 1984; Grammenudi and Vögtle 1986; Alpha *et al* 1987; Dürr *et al* 1988, 1991) with respect to photoanation.

3. Covalently and non-covalently linked sensitizer-relay-assemblies—Supramolecular effects

Balzani (Balzani 1987; Balzani and Scandola 1990) has shown that nature employs, in principle, a molecular photochemical device which is used for vectorial transport of electric charge. Thus light is converted to chemical or electrical energy (figure 3).

In principle two approaches to realize nature's functions are possible. The components of an artificial photosynthetic unit can be based on a supramolecular

Function Photoinduced vectorial transport of electric charge
Utilization Conversion of light into chemical or electrical energy

Molecular photochemical device

Role of light Thermodynamic

Necessary functions Light absorption; electron transfer

Components:

Interface towards light Pel

Interface towards use Pel and/or Rel

Other components C, (Rel)

Supramolecular structure Appropriate sequential assembly of the components; one-dimensional (rigid) structure

Requirements Those of Pel, Rel, C. thermodynamic and kinetic requirements of the electron transfer acts to make the charge separation efficient

Example Artificial photosynthesis

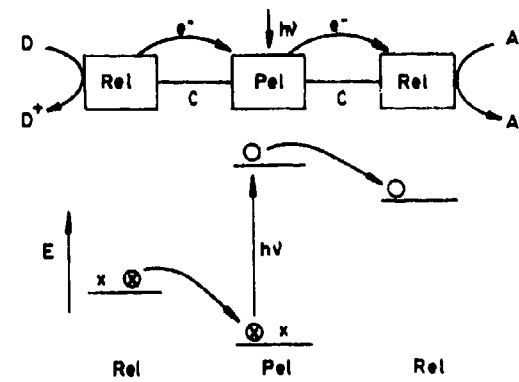


Figure 3. Supramolecular photochemistry – photoinduced vectorial transport of electrical charge (adapted from Balzani 1987).

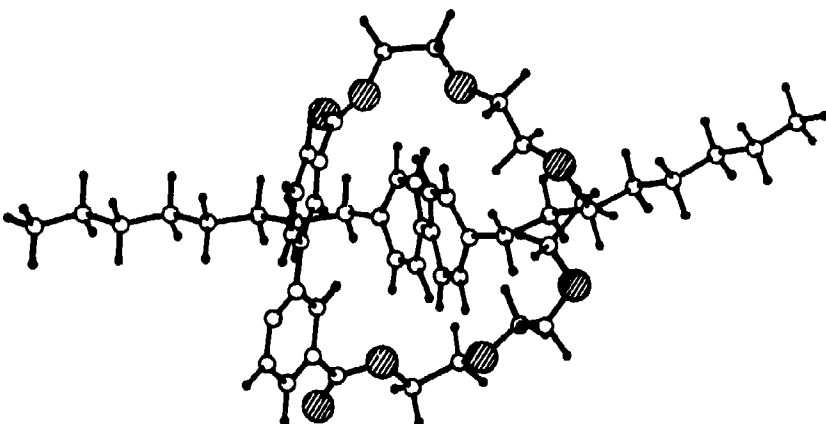
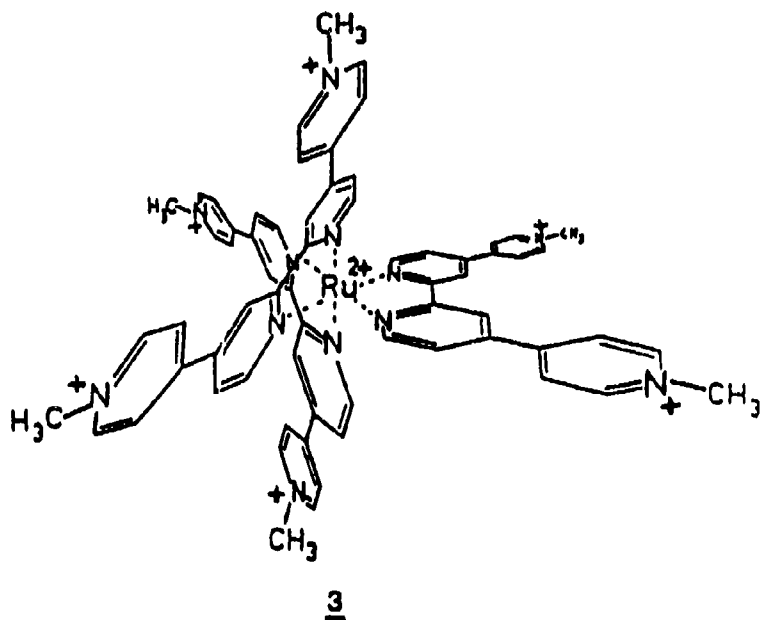
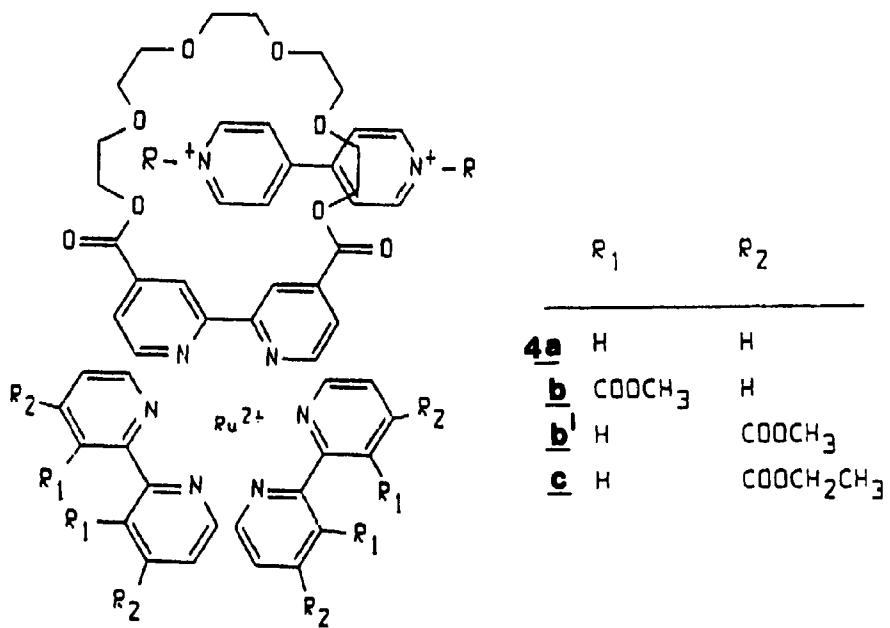


Figure 4. Model (charmm calculation) of octylviologen/bpy-crown interaction.



Scheme 4.



Scheme 5.

assembly which is linked: (a) by strong (covalent) bonds, or (b) by weaker (non-covalent) bonds.

In these supramolecular structures energy dissipation should be fast and back transfer -- the energy wasting step -- should be negligible. Triads paralleling the natural photosynthetic unit were studied by Maruyama (Osuka *et al* 1988, 1990), Wasilewski (1992) and others. Lehn and coworkers (Rodriguez-Ubis *et al* 1984; Grammenudi and Vögtle 1986; Alpha *et al* 1987; Dürr *et al* 1988, 1991) published an absorption-energy transmission diad.

Meyer (1990) prepared with his group the first Ru-polypyridine-containing triad. A similar one was made by Sauvage *et al* (1989).

(a) We synthesized a Ru-polypyridine diad (Dürr *et al* 1989) 3. This diad contains the sensitizer and the relay in the same molecule (scheme 4).

(b) A second approach was tested in our group by including crown-ether units at suitable positions in the Ru-polypyridine complex 4 (Dürr and Schneider 1991). The structure of these complexes is shown in scheme 5 and figure 4 (showing the interaction of ligand and OV^{2+}). These molecules were studied by typical Stern-Volmer techniques. MV^{2+} and the more lipophilic octylviologen were employed as quenchers. As figure 5 demonstrates typical nonlinear Stern-Volmer plots for quenching are obtained. The kinetic scheme 6 shows that a complex situation prevails. MV^{2+} and OV^{2+} may act in the quenching modes shown in scheme 6 (Boßmann *et al* 1992).

4. Oxidation of water to oxygen

The cleavage of water as has been demonstrated (*vide supra*) needs good light harvesting molecules having suitable parameters in the excited state. However, to

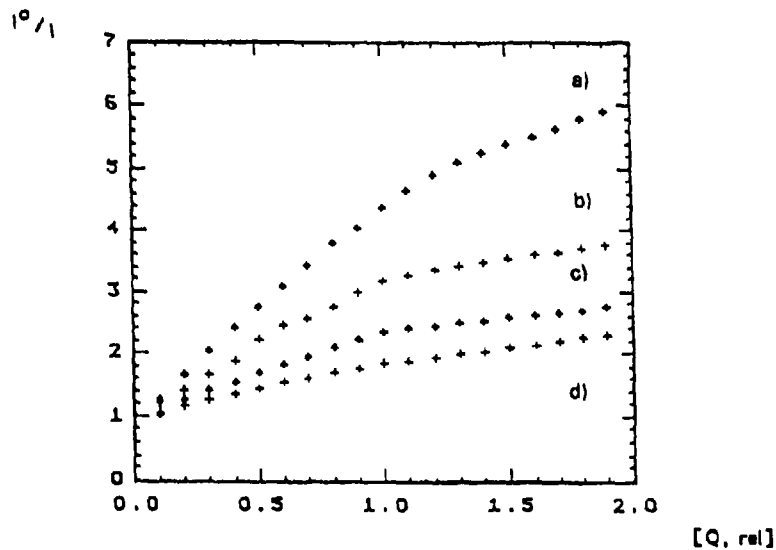
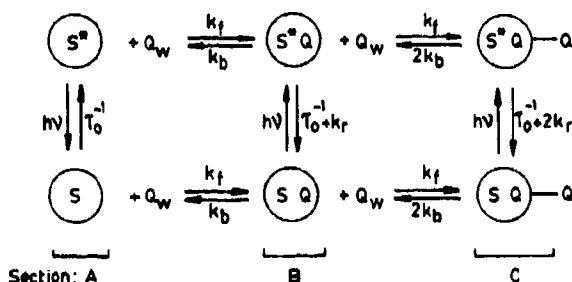


Figure 5. Stern-Volmer plot of statical quenching of Ru-crown ether 4 with relay (MV^{2+} and OV^{2+}) (a) and (b) $\underline{4b}/\text{MV}^{2+}$ or $\underline{4b}/\text{OV}^{2+}$; (c) and (d) $\underline{4c}/\text{MV}^{2+}$ or $\underline{4c}/\text{OV}^{2+}$.



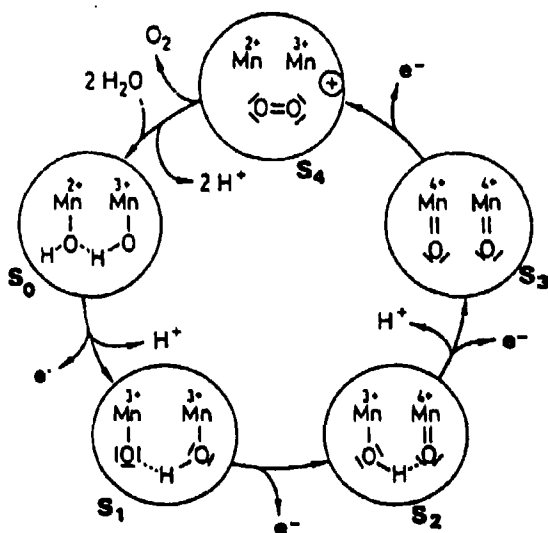
Scheme 6. Kinetic scheme for quenching of sensitizers 1–4 with viologens (MV^{2+} , OV^{2+}). S = sensitizers 4; Q = boundquencher in the crown ether unit (MV^{2+} , OV^{2+}); τ_0 = luminescence lifetime in the absence of Q ; k_f and k_b = forward and backward rate of binding of Q , respectively; k_r = unimolecular reactive rate constant of quenching in the crown ether unit; Q_w = water solubilized quencher (MV^{2+} , OV^{2+}).

reduce or oxidize water the excited state species must also have the appropriate redox potentials.

Table 4 summarizes the redox potentials required for water cleavage. The redox potentials for CO_2 reduction (*vide infra*) are included as well. To study the different reactions involved separately, many groups have investigated so called sacrificial systems to simplify the very complex processes.

For oxygen generation nature uses the catalytic system shown in scheme 7. We have worked with a sacrificial system for oxygen generation represented in scheme 8.

The main problem here is to exclude atmospheric oxygen rigorously, a task many groups have struggled with (Harriman *et al* 1988; Mills *et al* 1988; Heppe 1994).



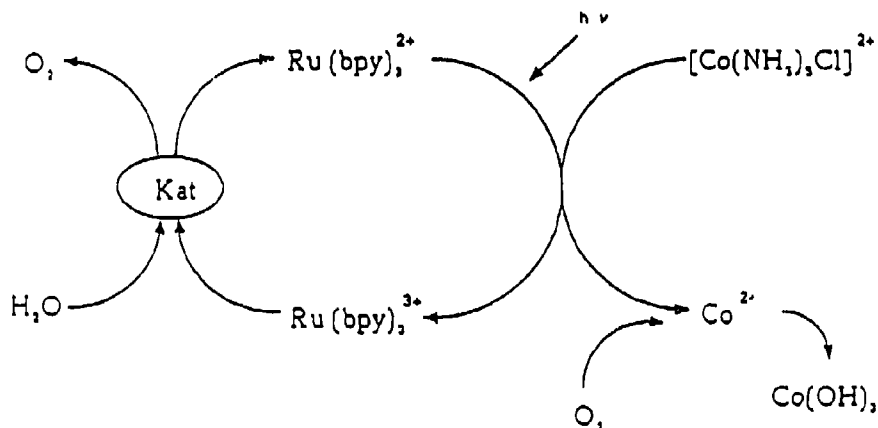
Scheme 7. Hypothetical scheme for water oxidation.

Table 4. Redox potentials for H_2O and CO_2 reduction and H_2O oxidation.

Reaction	Potential, $E^\circ(\text{V})$
$2\text{H}^+ + 2e^- \rightarrow \text{H}_2$	-0.41
$\text{CO}_2 + 2\text{H}^+ + 2e^- \rightarrow \text{CO} + \text{H}_2\text{O}$	-0.52
$\text{CO}_2 + 2\text{H}^+ + 2e^- \rightarrow \text{HCOOH}$	-0.62
$\text{CO}_2 + 6\text{H}^+ + 6e^- \rightarrow \text{CH}_3\text{OH} + \text{H}_2\text{O}$	-0.38
$\text{CO}_2 + 8\text{H}^+ + 8e^- \rightarrow \text{CH}_4 + 2\text{H}_2\text{O}$	-0.24
$\text{O}_2 + 2\text{H}^+ + 4e^- \rightarrow 2\text{OH}^- - 2e^-$	+0.82

---> $\text{Co}(\text{NH}_3)_5\text{Cl}_3$ $E^\circ = 0.54 \text{ V}$ (NHE)

---> NaS_2O_8 $E^\circ = 2.1 \text{ V}$ (NHE)



Scheme 8. Photoinduced sacrificial water oxidation.

Table 5. O_2 -production in the sacrificial system Ru-polypyridine/
 $\text{Co}(\text{NH}_3)_5\text{Cl}_3/\text{RuO}_2$.
 Acceptor: $\text{Co}(\text{NH}_3)_5\text{Cl}_3\text{ClCl}_2$ in acetate buffer ($\text{pH } 4.75$)
 Catalyst: RuO_2 -suspension

Sensitizers (S)	Maximal O_2 yield [μl]	Slope ($\mu\text{l}/\text{min}$)
$\text{Ru}(\text{bpy})_3(3',5'-\text{dmbpy})\text{Cl}_3$	13.0	0.60
$\text{Ru}(\text{bpy})_3(4,4'-\text{dmbpy})\text{Cl}_3$	12.0	0.38
$\text{Ru}(\text{bpy})_3(3,6-\text{dmphen})\text{Cl}_3$	10.5	0.49
$\text{Ru}(4,4'-\text{dmbpy})_3\text{Cl}_3$	10.3	0.27
$\text{Ru}(4,4'-\text{dmbpy})_2(\text{bpy})\text{Cl}_3$	10.2	0.44
$\text{Ru}(3,5'-\text{dmbpy})_3\text{Cl}_3$	9.0	0.36
$\text{Ru}(\text{bpy})_3\text{Cl}_3$	6.9	0.33
$\text{Ru}(\text{phen})_3(4,4'-\text{dmbpy})\text{Cl}_3$	6.6	0.22
$\text{Ru}(\text{bpy})_3(\text{Bp}4\text{COOTEK})\text{Cl}_3$	6.0	0.21
$\text{Ru}(3,6-\text{dmphen})_3\text{Cl}_3$	4.2	0.19

We were using a set up developed by Memming, Meissner and coworkers (Memming et al 1992).

In the sacrificial system referred to above we have generated O_2 as is shown in table 5. The standard system being based on $Ru(bpy)_3^{2+}$ is exceeded in its O_2 -producing ability by modified Ru-polypyridines. Donating groups in the bipyridine moiety of $Ru(L_3)^{2+}$ have proved to be most efficient.

5. Reduction of water and carbon dioxide

The reduction of water employing Ru-polypyridines has been studied for quite a while by many groups (Kalyanasundaram et al 1969; Creutz and Sutin 1975; Balzani et al 1978; Kiwi et al 1982; Seddon and Seddon 1984; Kalyanasundaram 1992). The essential problem is to use efficient and selective catalysts. A series of Pt-metals has been employed in these investigations. As typical examples $Ru(bpy)_3^{2+}$ -and $Ru(phen)_3^{2+}$ -derivatives are selected (figure 6) (Dürr et al 1985; Trierweiler 1989; Kraus

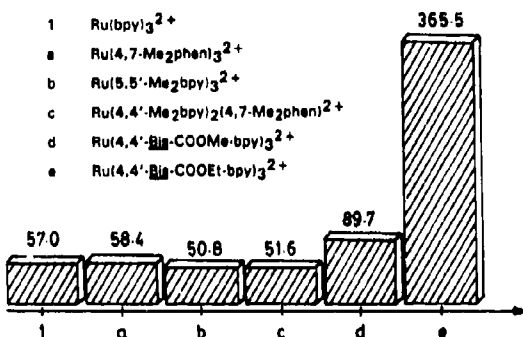


Figure 6. Hydrogen production depending on sensitizer (sensitizer $Ru(L_3)^{2+}$; relay: MPVS®, catalyst: Ru-Sol, donor: TEOA).

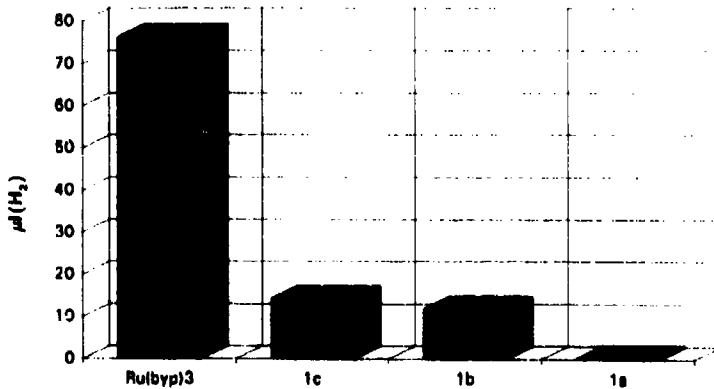


Figure 7. H_2 -generation rates with the coronate sensitizers 1a, 1b and 1c.

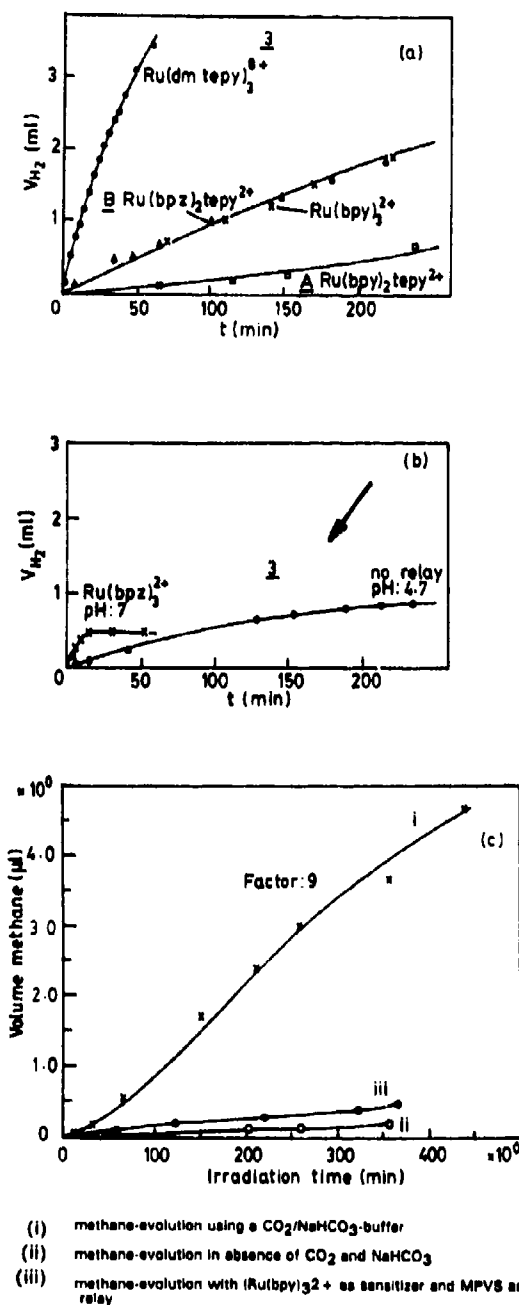


Figure 8. (a, b) Hydrogen evolution in the sacrificial system containing A (□), B (▲) or 3 (●) as sensitizer and 2-TMV²⁺ as relay at pH = 7 and 4.7. (c) CH_4 -evolution using the sensitizer-relay-assembly 3, TEOA as donor and Ru as catalyst.

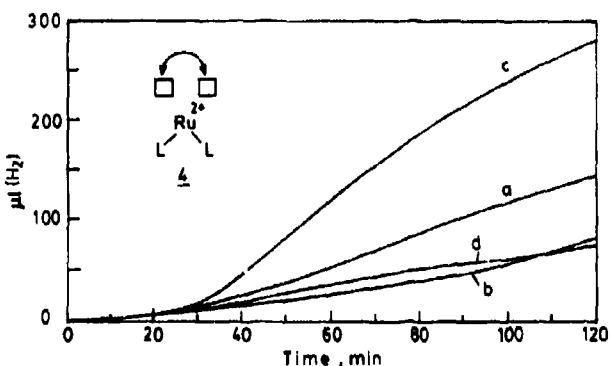


Figure 9. H_2 -generation with sensitizer-relay-assembly 4a/MV²⁺, 4b/MV²⁺ and 4c/MV²⁺, triethanolamine as donor, methylviologen/propylviologen-sulfonate as electron relay and a microheterogeneous TiO₂-Pt-catalyst compared to Ru(bpy)₃²⁺. (a) Ru(bpy)₃²⁺; PEC(4a); (b) Ru(bp4CO₂Me)₂bp4 (pentaethylenecrown) 4b; (c) Ru(bp4CO₂Et)₂bp4 (pentaethylenecrown) 4c; (d) Ru(bpy)₃.

1991). Using Ru and Os catalysts instead of Pt-metals extends the scope of this reaction considerably. In addition to H_2 from H_2O , CH_4 may also be generated by reduction of CO_2 (Rodriguez-Ubis *et al* 1984; Alpha *et al* 1987; Willner *et al* 1987; Dürr *et al* 1988, 1991).

This is an interesting process which – if optimized and used on a large scale – would contribute to the solution of the greenhouse effect.

It has been found by Willner (Willner *et al* 1987), in collaboration with our group, that Ru(bpy)₃²⁺ yields H_2 and CH_4 . Employing Ru(bpz)₃²⁺ as sensitizer gives rise to a selective production of CH_4 (Willner *et al* 1987).

In model studies for our supramolecular systems we examined a series of Ru-bipyridine and phenanthroline complexes. One of the best complexes in hydrogen generation is the diester (Ru-4,4'-bis-CO₂Et-bpy)₃²⁺) (Willner *et al* 1990) (figure 6). This is also one of the most efficient complexes producing CH_4 from CO_2 . Ru-coronates 1 have been shown to produce H_2 despite the large sterical demand of the sensitizers involved. However, the sterically very large Ru-complexes give about 1/6 of the hydrogen yield compared to Ru(bpy)₃²⁺ (Boßmann and Dürr 1990) (figure 7). The sensitizer-relay assembly 3 has been employed for H_2 and methane generation. It is much more efficient than the standard system as shown in figures 8a–c. Hydrogen evolution from the supramolecular Ru(bpy)₂ PEK²⁺ (4)/MV²⁺ assembly is clearly superior to the standard Ru(bpy)₃²⁺ (see figure 9). In figure 10 a schematic representation of the mechanism of this system is given.

6. Conclusions

It has been shown that Ru-polypyridine complexes can

- (i) be stabilized with respect to photoanation by intramolecular links as in coronates 1 or podates 2;

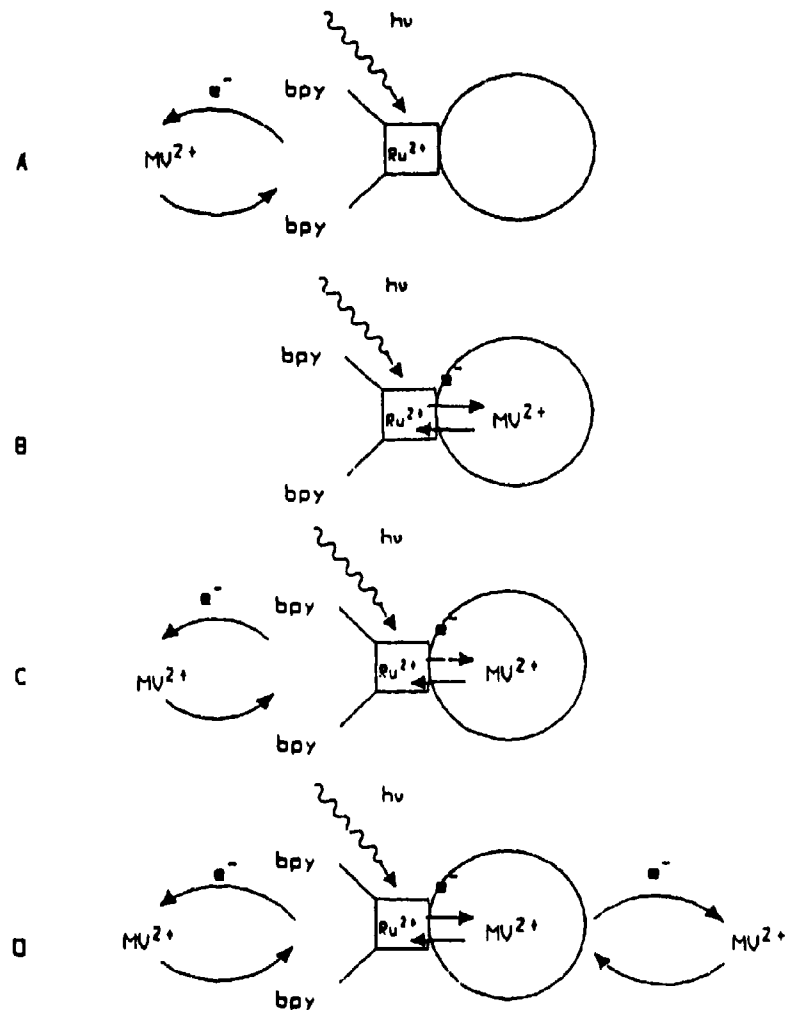


Figure 10. Quenching model of the bis-heteroleptic-crown ether-ruthenium sensitizers 4. (A) The quenching mechanism is diffusion controlled; the binding of MV²⁺ in the crown ether receptor is not observed because of its low concentration ([Q] rel = 0–0.2). (B) The binding MV²⁺ in the crown ether unit is the dominant process; the quenching constants are higher than the diffusion-controlled rate of diffusion ([Q] rel = 0.2–0.8). (C) The quenching constants decrease; further quenching is diffusion controlled. (D) At relatively high total concentrations electron transfer from the bound MV²⁺ to the free MV²⁺ occurs, leading to a rapid increase in the quenching constants.

- (ii) undergo efficient bimolecular electron transfer in covalently or non-covalently (supramolecular) linked sensitizer-relay-aggregates, such as 3 and 4;
- (iii) be used efficiently in oxygen formation involving electron-donating groups;
- (iv) be employed in hydrogen generation in classical and supramolecular systems;
- (v) efficiently produce CH₄ from CO₂.

Acknowledgements

This work has been supported by the BMFT (project: 0329 111A) and the financial help is greatly appreciated.

References

- Alpha B, Lehn J M and Mathis G 1987 *Angew. Chem.* **59** 256
 Balzani V 1987 *Supramolecular photochemistry* (Dordrecht: Reidel Verlag)
 Balzani V, Boletta L, Gandolfi M and Maezu M 1978 *Top. Curr. Chem.* **75** 247
 Balzani V and Scandola F (eds) 1990 *Supramolecular photochemistry* (Chichester: Horwood)
 Boßmann S and Dürr H 1990 *Synthesis* 733
 Boßmann S and Dürr H 1992 *New J. Chem.* **16** 769
 Boßmann S, Seiler M and Dürr H 1992 *J. Phys. Org. Chem.* **5** 63
 Creutz C and Sutin N 1975 *Proc. Natl. Acad. Sci.* **72** 2858
 Diesenhofer J, Epp O, Miki K, Huber R and Michel H 1984 *J. Mol. Biol.* **180** 385
 Diesenhofer J, Epp O, Miki K, Huber R and Michel H 1985 *Nature (London)* **318** 618
 Dürr H, Boßmann S, Kilburg H, Trierweiler H P and Schwarz R 1991 *Frontiers in supramolecular organic chemistry and photochemistry* (eds) H Dürr and H J Schneider (Weinheim: VCH)
 Dürr H, Dürr G and Braun A 1983 *Helv. Chim. Acta* **66** 2653
 Dürr H, Dürr G, Mayer E and Zengerle K 1985a *Nouv. J. Chim.* **9** 717
 Dürr H and Schneider H J 1991 *Frontiers in organic chemistry and photochemistry* (Weinheim: VCH)
 Dürr H and Schwarz R 1993 *J. Am. Chem. Soc.* (in press)
 Dürr H, Zengerle K, Mayer E, Curchod J and Braun A M 1985b *Nouv. J. Chim.* **9** 717
 Dürr H, Zengerle K and Trierweiler H P 1988 *Z. Naturforsch.* **B43** 361
 Grammenudi S and Vögtle F 1986 *Angew. Chem.* **98** 1119
 Harriman A, Pickering I J and Thomas J M 1988 *J. Chem. Soc., Faraday Trans. 1* **84** 2795
 Henglein A 1984 *Pure Appl. Chem.* **56** 1215
 Heppe G 1994 O_2 generation, Ph D thesis, University Saarbrücken, (in preparation)
 Juris A, Barigeletti F, Campagna S, Balzani V, Belser P and Zelewsky A v 1988 *Coord. Chem. Rev.* **84** 85
 Kalyanasundaram K 1992 *Photochemistry of polypyridine and complexes* (London: Academic Press)
 Kalyanasundaram K, Kiwi J and Grätzel M 1969 *Helv. Chim. Acta* **61** 1345
 Kiwi J, Kalyanasundaram K and Grätzel M 1982 *Struct. Bonding* **49**
 Kraus H 1991 *Sensitizer-relay assemblies for photochemical water reduction*, Ph D thesis, University Saarbrücken
 Mathis P 1990 *Pure Appl. Chem.* **62** 1521
 Memming R, Meissner D and Deppe J 1992 Institute for Solarenergieforschung, diploma thesis
 Meyer T J 1990 *Pure Appl. Chem.* **62** 1003
 Mills A, Dodsworth E and Willis G 1988 *Inorg. Chim. Acta* **150** 101
 Osuka A, Maruyama K, Yamazaki I and Tamai N 1990 *Chem. Phys. Lett.* **165** 396
 Osuka A, Tomita H and Maruyama K 1988 *Chem. Lett.* 1205
 Rodriguez-Ubis J, Alpha B, Plancherel D and Lehn J M 1984 *Helv. Chim. Acta* **67** 2264
 Sargeant A M 1984 *Pure Appl. Chem.* **56** 1603
 Sauvage J P, Collin J P and Guillerez S 1989 *J. Chem. Soc., Chem. Commun.* 776
 Seddon E and Seddon K 1984 *Top. Inorg. Org. Chem.* **19**
 Serpone N, Pelizzetti E and Grätzel M 1985 *Coord. Chem. Rev.* **64** 225
 Trierweiler H P 1989 CO_2 -reduction with Ru-polypyridines, Ph D thesis University Saarbrücken
 Wasilewski M R 1992 *Chem. Rev.* **92** 435
 Willner I, Maidan R, Mandler D, Dürr H, Dürr G and Zengerle K 1987a *J. Am. Chem. Soc.* **109** 6680
 Willner I, Maidan R, Dürr H, Trierweiler H P 1990 *New J. Chem.* **14** 317
 Willner I, Mandler D and Steinberger B 1987b *New J. Chem.* **11** 109

Photophysics of pyrene substituted oligosilanes

D DECLERCQ¹, E HERMANS¹, F C DE SCHRYVER^{1*} and R D MILLER²

¹K U Leuven, Department of Chemistry, Laboratory of Molecular Dynamics and Spectroscopy, Celestijnlaan 200F, B-3001 Heverlee, Belgium

²IBM Research Division, 650 Harry Road, San Jose, CA 95120-6099, USA

Abstract. The absorption and fluorescence properties of 1-pyrenyl substituted permethyl-oligosilanes are reported. The charge transfer in 1-pyrenyltridecamethylhexasilane is explained by electron transfer from the Si-Si σ orbitals to pyrene in the excited state. Evidence is found for ground state interactions in 1,3-di(1-pyrenyl)hexamethyltrisilane, based on absorption and $^1\text{H-NMR}$ measurements. The fluorescence properties of 1-(1-pyrenyl)-3-(*p*-N,N-dimethylanilino)hexamethyltrisilane are compared with its carbon analogue 1-(1-pyrenyl)-3-(*p*-N,N-dimethylanilino)propane. Ground state interactions are found for the silicon-bridged donor-acceptor compound.

Keywords. Pyrene substituted oligosilanes; ground state interactions; silicon-bridged compounds; exciplex; electron transfer.

1. Introduction

Polysilanes or polysilylenes are polymers which contain only silicon atoms in the backbone. Recently, polysilanes attracted a lot of scientific interest, mainly due to the unexpected chemical and spectroscopic properties of the completely sigma-bonded silicon backbone (Miller and Michl 1989). The first electronic transition of oligosilanes and polysilanes ($\text{Si}_n\text{R}_{2n+2}$) occurs at surprisingly low energies as compared to their carbon analogues. This transition shifts to higher wavelengths with increasing silicon-chain length and reaches a constant value for n between 40 and 50. The transition has been assigned as a $\sigma(\text{Si}-\text{Si}) \rightarrow \sigma^*(\text{Si}-\text{Si})$ in which the sigma electrons are delocalised along the silicon backbone. The electronic structure and spectral properties of oligo- and polysilanes more closely resemble those of conjugated π -systems such as polyacetylenes than those of the related carbon-based systems such as polyethylene. It has been proposed that the conjugation through *gauche* SiSiSiSi is smaller than that of conjugation through *trans* SiSiSiSi (Klingensmith *et al* 1986). Recently, Plitt and Michl (1992) demonstrated that *trans*- $\text{Si}_4\text{Me}_{10}$ shows the expected red shift relative to Si_3Me_8 , but *gauche*- $\text{Si}_4\text{Me}_{10}$ does not, which is experimental evidence for the better conjugation in a *trans* than in a *gauche* chain.

Charge transfer fluorescence has been observed for several pentamethyldisilanyl-substituted aromatic compounds. This charge transfer was not observed for the

*For correspondence

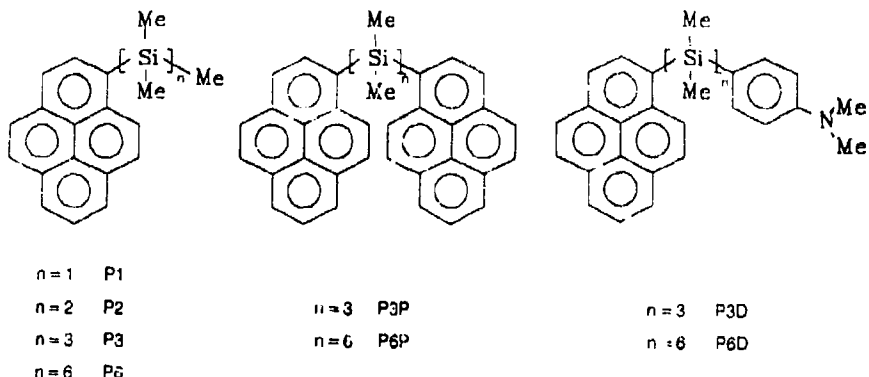


Figure 1. Structures and abbreviations of the compounds studied.

trimethylsilyl substituted aromatic compounds. Shizuka assigned the charge transfer fluorescence to a state produced by electron transfer from the aromatic ring to the $3d\pi$ orbitals of the disilane (Shizuka *et al* 1981, 1985). However, Sakurai *et al* (1990) proposed electron transfer from the Si-Si sigma bond to the aromatic moiety in the excited state. Orthogonal intramolecular charge transfer was suggested in which the Si-Si sigma bond lies in the plane of the aromatic ring and thus orthogonal to the π orbitals. We reported already that P6 (see figure 1) showed charge transfer fluorescence although P1, P2 and P3 showed only fluorescence from the locally excited state (Declercq *et al* 1991). We concluded that electron transfer in P6 occurred from the hexasilane chain to pyrene in the excited state, which supports the mechanism proposed by Sakurai *et al* (1990). In this paper, the charge transfer of P6 is studied in greater detail and additional evidence on the proposed mechanism is given. P3P and P6P (figure 1) were synthesised in order to study the excimer formation between two pyrene groups linked by a silane chain. P3D and P6D (figure 1) were synthesised in order to study the possibility of through bond interaction, mediated by a silicon chain, between a donor (N,N-dimethylaniline) and an acceptor (pyrene).

2. 1-Pyrenylsubstituted oligosilanes: P1, P2, P3 and P6

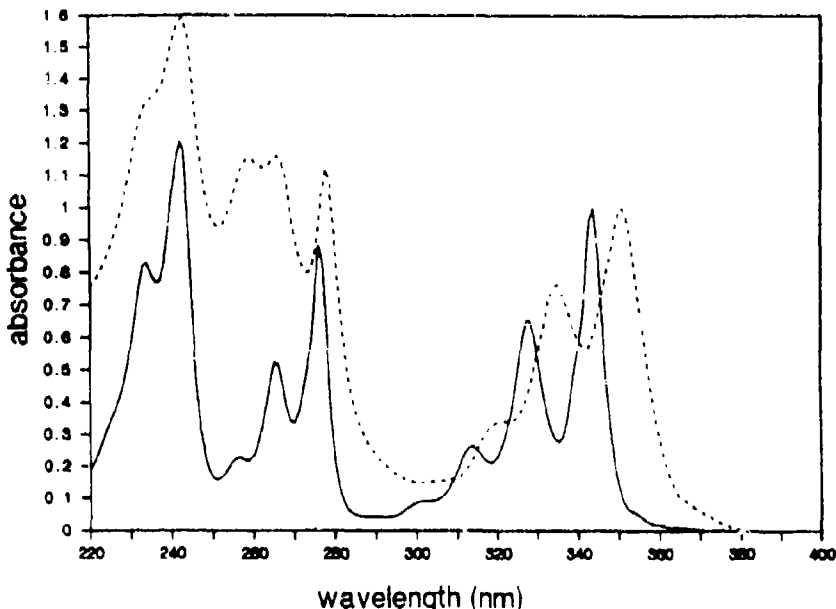
2.1 Absorption properties

The absorption spectrum of P1, is comparable to that of 1-methylpyrene. The maximum of the ${}^1\text{La}$ -transition is situated at 344 nm. Introduction of a disilanyl group (P2) results in a bathochromic shift towards 349 nm. The higher homologues P3 and P6 show a maximum at 350 and 351 nm respectively. Going from P1 towards P6, a gradual decrease of the absorption vibrational fine structure and the molar extinction coefficient at the maximum is observed (see table 1 and figure 2).

The weak ${}^1\text{Lb}$ transition ($\epsilon < 1000$), detected at 375 nm for P1 and P2 could not be observed for P3 and P6, due to overlap of the ${}^1\text{La}$ transition. The increased absorbance around 250–270 nm for P6 as compared to P1, is due to the absorbance of the hexasilane chain, tetradecamethylhexasilane has an absorption maximum around 260 nm (Gilman *et al* 1964). The effect of the silicon chain on the absorption spectra

Table 1. Absorption properties of pyrene, P1, P2, P3 and P6 in iso-octane.

Compound	$\lambda_{\max}^{\text{1La}}(\text{nm})$	$\epsilon^{\text{1La}}(\text{L mol}^{-1} \text{cm}^{-1})$
Pyrene	334	54,300
P1	344	50,600
P2	349	43,500
P3	350	38,600
P6	351	27,170

**Figure 2.** Absorption spectra of P1 (—) and P6 (···) in iso-octane at room temperature.

of pyrene is remarkable if we compare this with the carbon analogues of the compounds mentioned above: 1-methylpyrene and 1-ethylpyrene have an absorption maximum of the ${}^1\text{La}$ transition at 342.4 and 342.6 nm, respectively (Reynders 1988). It can be concluded that although the electronic transition is still recognizable as perturbed pyrene $\pi \rightarrow \pi^*$ transition, there is an interaction in the ground state between a saturated silicon system and pyrene.

2.2 Fluorescence properties

The fluorescence maxima of P1, P2 and P3 are situated around 390 nm, and they are not dependent on solvent polarity. The fluorescence decay, recorded by means of the 'single photon timing' technique, could be analysed as monoexponential decay. This fluorescence can be attributed to a $\pi^* \rightarrow \pi$ pyrene fluorescence. The respective fluorescence quantum yields, Φ_f , together with their fluorescence decay times, are given in table 2.

Table 2. Quantum yields and fluorescence decay times in iso-octane at 25°C.

Compound	Φ_f	τ (ns)	$k_f(10^6 \text{ s}^{-1})$	Φ_{isc}
Pyrene			2.2	
P1	0.80	324	2.5	0.19
P2	0.75	282	2.7	0.25
P3	0.74	230	3.2	0.26
P6	0.47	76.4	6.1	—

The fluorescence rate constants can be calculated using the fluorescence quantum yield and the fluorescence decay time. k_f increases on going from pyrene towards P3. The fluorescence of pyrene occurs from the ${}^1\text{L}_\text{b}$ state. The increase of k_f could be due to a contribution of the ${}^1\text{L}_\text{a}$ state in the lowest excited state, which increases the transition probability. It has already been suggested that Φ_{isc} is very small for planar polycyclic aromatic compounds such as pyrene (Wilkinson 1975), so that Φ_{isc} can be calculated using $(1 - \Phi_f)$. Going from P1 towards P2 results in an increase of Φ_{isc} by a factor 1.5, probably due to the introduction of a second heavy silicon atom. However, introduction of a third silicon atom in the silane chain does not affect Φ_{isc} that much. The same value of Φ_{isc} within experimental error was obtained using Laser Induced Photoacoustic Spectroscopy (LIOAS) (Van Haver *et al* 1992).

In contrast with P1, P2 and P3, the fluorescence of P6 is dependent on the solvent polarity (Declercq *et al* 1991). A change from iso-octane to ethylacetate as solvent results in a bathochromic shift of the fluorescence maximum from 390 to 476 nm and a decrease of the fluorescence quantum yield from 0.47 to 0.05 (figure 3). The fluorescence decay in iso-octane could be analysed as a monoexponential function, which indicates that the charge transfer state is produced very rapidly. The fluorescence rate constant k_f of P6 in iso-octane is much larger than the k_f of P1, P2 and P3 (table 2), which indicates that the fluorescence from the charge transfer state is faster than from the locally excited state. Using the Lippert-Mataga formalism (Von Lippert 1957; Beens *et al* 1967), the dipole moment of the excited state can be calculated as 21D, assuming 6 Å for the solvent cavity radius ρ . This indicates that in the excited state, a very polar species is produced, in which the charges are separated over more than 4 Å. This polar species is attributed to a charge transfer state, which is produced by electron transfer from the hexasilane chain towards pyrene in the excited state. The fact that no electron transfer is observed for P1, P2 and P3 can be explained based on the change of free energy for electron transfer. The $\Delta G_{\text{et}}^\circ$ values can be calculated using the redox potentials of the respective permethylated silane chain and of pyrene, the excitation energy and the Coulombic stabilisation energy. If the redox potentials are measured in acetonitrile, the Coulombic attraction energy can be neglected. If it is assumed that the oligosilane chain acts as a donor, $E_{(A/A-)}^\circ + h\nu_{0,0}$ equals 1.18 eV, and $E_{(D+/D)}^\circ$ of Si_2Me_6 , Si_3Me_8 and $\text{Si}_6\text{Me}_{14}$ equals 1.880, 1.520 and 1.075 eV, respectively (Boberski and Allred 1975). It can then be worked out that $\Delta G_{\text{et}}^\circ$ will be negative for P6 and positive for P1, P2 and P3. Thus, electron transfer is possible from the hexasilane chain towards pyrene in the excited state due to the lower redox potential of the hexasilane chain.

$$\Delta G_{\text{et}}^\circ = E_{(D+/D)}^\circ - E_{(A/A-)}^\circ - h\nu_{0,0} - e^2/(4\pi\epsilon_0\epsilon_r r).$$

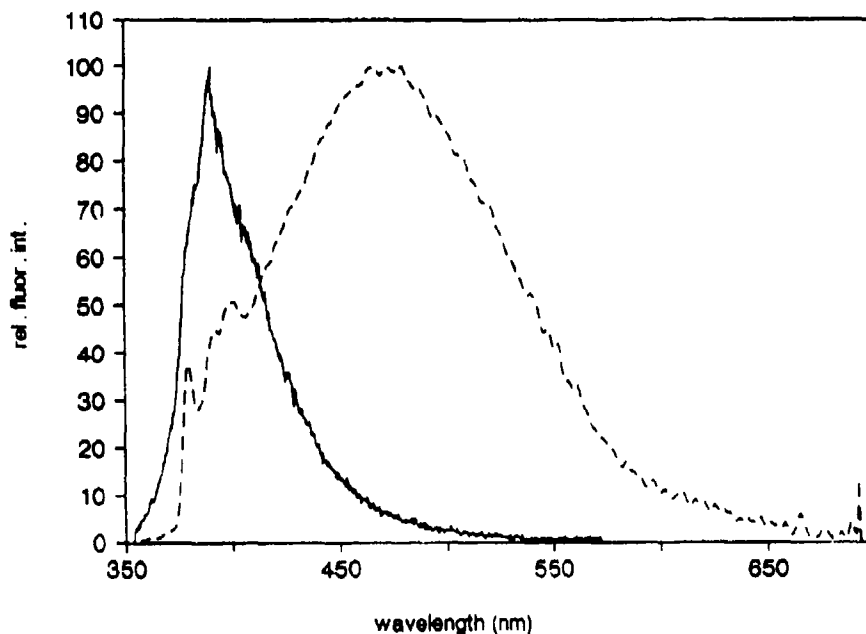


Figure 3. Fluorescence spectra of P6 in *iso*-octane (—) and ethylacetate (···)

The fluorescence spectrum in benzene does not change upon cooling the solution from 10°C to a rigid matrix at -33°C, beneath the melting point of benzene. This suggests that no rotation is necessary to have intramolecular charge transfer in P6, which has been proposed by Sakurai (Sakurai *et al.* 1990) for the phenyldisilanes.

3. Bipyrenyl-substituted oligosilanes: P3P and P6P

The absorption spectrum in *iso*-octane of P3P clearly differs from that of its reference compound P3, which is an indication that the two pyrene groups interact in the ground state. However, almost no differences in the absorption spectra of P6 and P6P can be observed (figure 4).

The ¹H-NMR spectra of P3P and P6P were analysed and compared with those of their reference compounds. A strong shielding is observed for the aromatic signals of P3P, compared with P3, which indicates that the two pyrene groups exert ring current effects in the ground state (figure 5). These effects are much smaller for P6P compared with P6, suggesting that the average distance between the two pyrene groups is larger in the latter bichromophore.

The large shielding effects in P3P were not observed for the related carbon compound 1,3-(di-1-pyrenyl)-propane, which is an indication that the two pyrene groups in the silicon system have a much larger tendency to come together in the ground state than in the carbon-based system. It should be emphasized that the Si-Si bond length is 2.35 Å, a value much larger than the CH₂-CH₂ bond, so that the methyl groups on the silicon atoms do not hinder the rotation of the silicon chain.

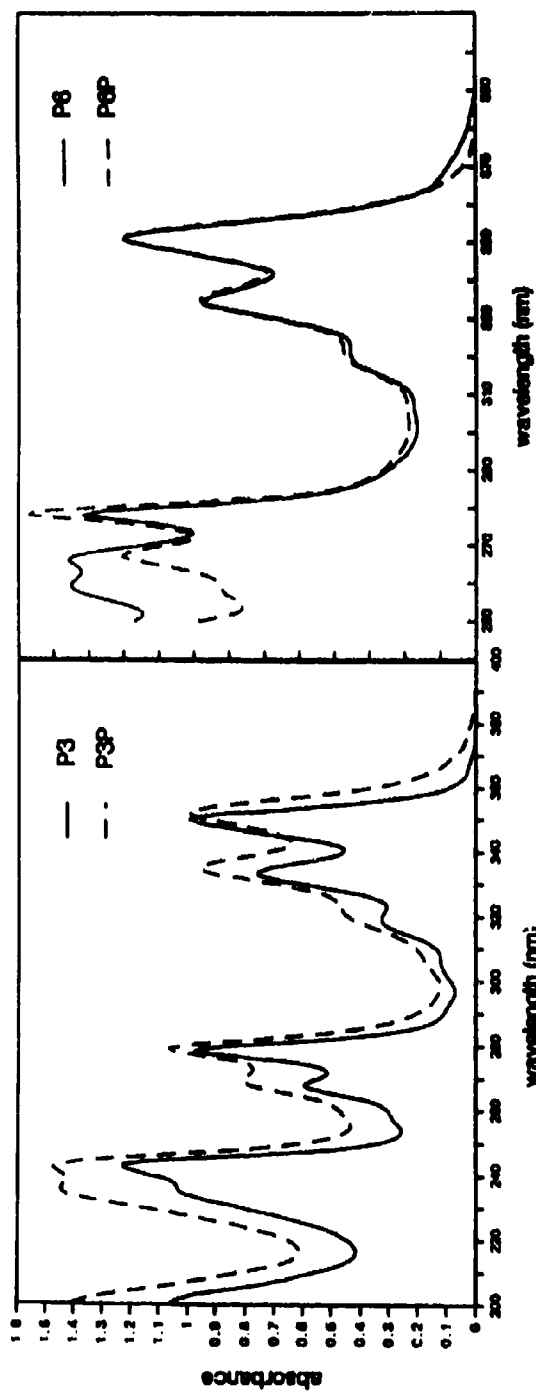


Figure 4. Absorption spectra of P3P, P3, P6P and P6 in iso-octane.

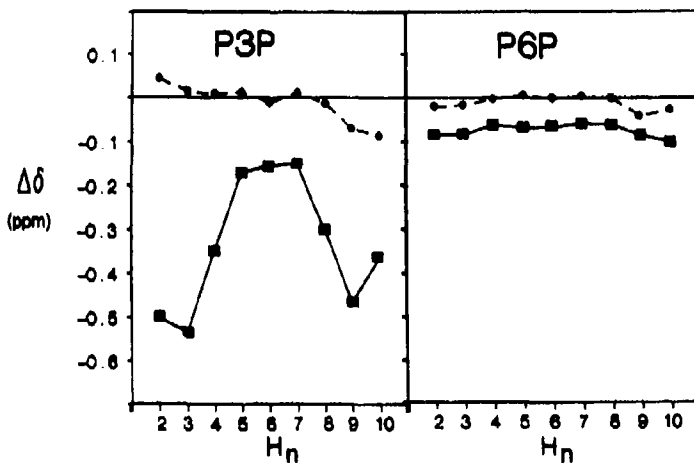


Figure 5. $\Delta\delta = \delta(\text{P3P}) - \delta(\text{P}6)$ and $\Delta\delta = \delta(\text{P}6\text{P}) - \delta(\text{P}6)$ for the pyrene protons of the silicon compounds (■) and for the related carbon compounds (●) in CDCl_3 .

One can conclude that the hexamethyltrisilane chain is more flexible than the propane chain. Welsh and Johnson (1990) calculated the energy barrier for the rotation of a Si-Si bond in all-trans poly(dimethylsilane). The maximum energy barrier was located at the *cis* conformation, $2.75 \text{ kcal.mol}^{-1}$ higher in energy than the *trans*, which is indeed in sharp contrast with the relatively high barriers ($> 6 \text{ kcal.mol}^{-1}$) in the case of *n*-alkanes.

The emission spectrum of P3P is dominated by a broad, solvent-independent fluorescence band, which can be assigned to excimer fluorescence (Declercq *et al.* 1991). However, the fluorescence of P6P is dependent on the solvent polarity, and can consequently not be described as an excimer fluorescence. The fluorescence maximum depends on the solvent polarity, in the same way as for P6, so that the excited state of P6P can also be explained as a $\sigma(\text{Si-Si}) \rightarrow \pi^*$ charge transfer state.

4. Donor-acceptor substituted oligosilanes: P3D and P6D

The differences in the absorption spectra of P3D and its reference compound P3 in *iso*-octane indicate interactions in the ground state. P6D and P6, however, show similar absorption spectra (figure 6). The fluorescence of P6D is dependent on the solvent polarity. The dependence of the fluorescence maximum on the solvent polarity term $f - 1/2f = (\epsilon - 1)/(2\epsilon - 1) - (n^2 - 1)/2(2n^2 + 1)$ is the same as for P6, so that the dipole moment of the excited state of P6D should be approximately the same as for P6 (figure 7). However, the Stokes shifts of P6D are systematically larger than those of P6, suggesting an additional interaction of the N,N-dimethylaniline group with the $\sigma(\text{Si-Si}) \rightarrow \pi^*$ charge transfer state. N,N-dimethylaniline is a better donor than tridecamethylhexasilane, so that electron transfer could occur from N,N-dimethylaniline towards pyrene by mediation of the hexasilane chain.

P3D also shows a solvent-dependent fluorescence spectrum. Using the Lippert-Mataga formalism (Von Lippert 1957; Beens *et al.* 1967), the dipole moment of the

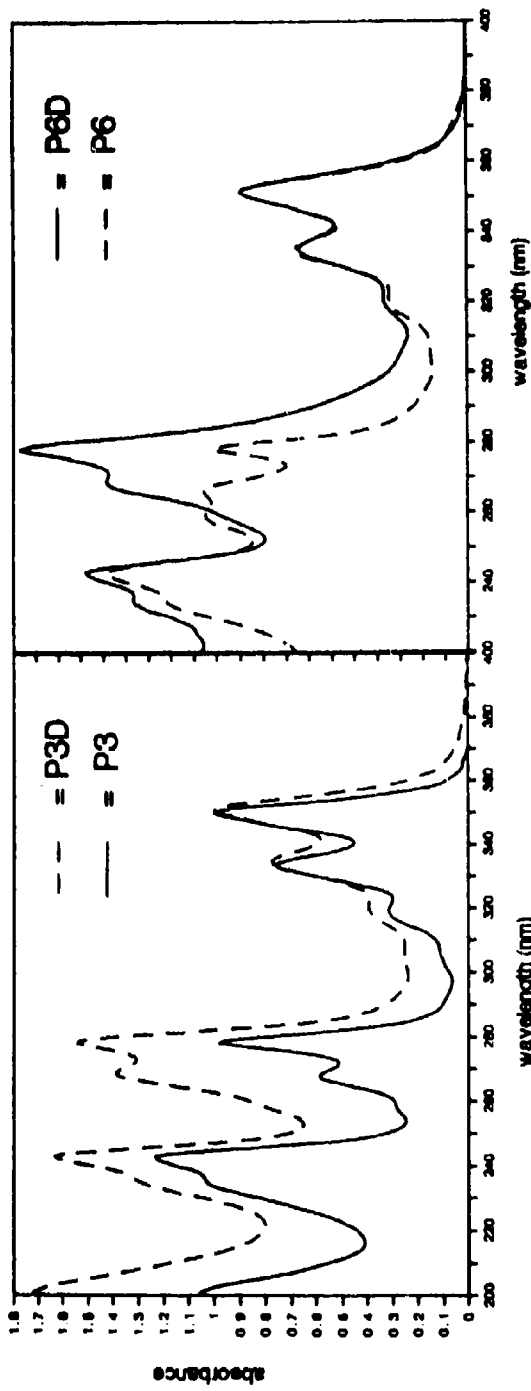


Figure 6. Absorption spectra of P3D, P3, P6 and P6 in iso-octane.

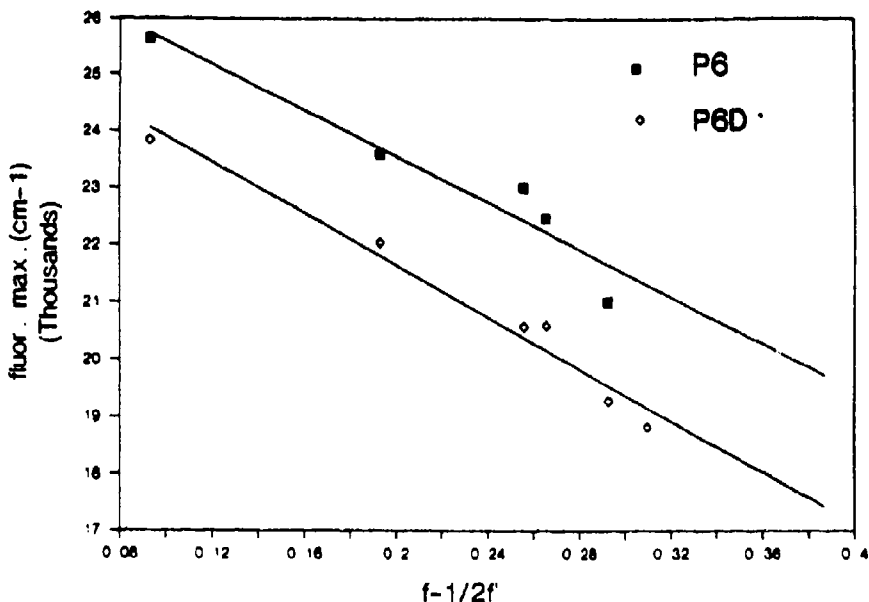


Figure 7. Fluorescence maxima of P6D, P6 and P3D in function of the solvent polarity term $f - \frac{1}{2}f'$.

Table 3. Comparison of the absorption and fluorescence properties of P3D and P3'D.

	P3D	P3'D
¹ La absorption maximum	351 nm	342 nm
Maximum exciplex fluorescence	467 nm	477 nm
$\mu_{exciplex}$	14.3D	12.2D
Φ_f	0.012	0.247
τ_1	0.57 ns	3.73 ns
τ_2	3.12 ns	88.1 ns
A_1/A_2 (exciplex region)	-0.64	-1

excited state of P3D is 14.3D, a value which is comparable with 12.2D of the related carbon compound 1-(1-pyrenyl, 3-(*p*-N,N-dimethylanilinopropyl)) (P3'D) (Imabayashi *et al* 1988). The photophysical properties of P3D and its carbon analogue P3'D are compared in table 3.

It is immediately clear that the fluorescence quantum yield is much smaller for P3D than for its carbon analogue. The fluorescence decay in the exciplex region could be fitted to a difference of two exponentials, with two decay times which are much smaller than the ones of the carbon system. This could suggest that exciplex formation in P3D is much faster than in P3'D. In contrast with P3'D, the ratio of the negative pre-exponential factor to the positive pre-exponential factor (A_1/A_2 in table 3) deviates from -1, which suggests that the Birks kinetic scheme is not applicable to exciplex formation in P3D (Reynders *et al* 1990) and that there is

interaction in the ground state between the donor and the acceptor. Further, the differences in the absorption spectra of P3D and P3 and the differences in the excitation spectra of P3D, measured in the locally excited state wavelength region and in the exciplex region, give additional evidence for the interaction between the donor and the acceptor. It is important to note that the fluorescence spectrum of P3D in benzene does not change upon cooling from room temperature to -3.3°C , below the melting point of benzene. Further, X-ray analysis showed that the trisilane chain is not folded but in an extended conformation so that the pyrene and N,N-dimethylaniline can not interact through space. The fact that the fluorescence is the same in solution as in a rigid matrix indicates that the trisilane chain does not need to rotate to ensure exciplex emission, which suggests that through-bond effects might be important in the interaction between pyrene and N,N-dimethylaniline.

5. Conclusions

Delocalised sigma systems can act as donors in the fluorescence quenching of aromatic compounds, provided that the ionisation potential of the sigma system is low enough: electron transfer is observed from the hexasilane chain towards pyrene in the excited state in P6. However, no electron transfer occurs in P3, due to the higher ionisation potential of the trisilane chain, a shorter delocalised system than the hexasilane chain. It has been shown that the two pyrene groups in P3P tend to come together in the ground state, which is not observed in the carbon analogue where the dimethylsilane groups are replaced by CH_2 groups. This suggests that a hexamethyltrisilane chain is more flexible than a carbon chain. The fluorescence of P3P is characterised as excimer fluorescence and P6P shows a $\sigma(\text{Si}-\text{Si}) \rightarrow \pi^*$ charge transfer, such as with P6. P3D shows exciplex fluorescence and it is proposed that the observed interactions between pyrene and N,N-dimethylaniline could be mediated through the trisilane chain.

Acknowledgements

DD is an 'Aspirant Onderzoeker' of the Belgian 'Nationale Fonds voor het Wetenschappelijk Onderzoek (NFWO)'. The FKFO, and the Ministry of 'Wetenschapsprogrammatie' of Belgium (through IUAP-16 and IUAP-040) are greatly thanked for their support to the laboratory.

References

- Beens H, Knibbe M and Weller J 1967 *J. Chem. Phys.* **47** 1183
- Boberski W G and Allred A L 1975 *J. Organomet. Chem.* **88** 65
- Declercq D, De Schryver F and Miller R D 1991 *Chem. Phys. Lett.* **186** 467
- Gilman H, Atwell W H and Schwebke G L 1964 *J. Organomet. Chem.* **2** 369
- Imbayashi S, Kitamura N and Tazuke S 1988 *Chem. Phys. Lett.* **153** 23
- Klingensmith K A, Downing J W, Miller R D and Michl J 1986 *J. Am. Chem. Soc.* **108** 7438
- Miller R D and Michl J 1989 *J. Chem. Rev.* **89** 1359
- Plitt H S and Michl J 1992 *Chem. Phys. Lett.* **198** 400

- Reynders P 1988 *Spektroskopische Untersuchungen zur Intramolekularen Excimer bildung.* Ph.D thesis,
University of Göttingen
- Reynders P, Kühnle W and Zachariasse K A 1990 *J. Am. Chem. Soc.* **112** 3929
- Sakurai H, Sugiyama H and Kira M 1990 *J. Phys. Chem.* **94** 1837
- Shizuka H, Obuchi H, Ishikawa M and Kumada J 1981 *J. Chem. Soc., Chem. Commun.* 405
- Shizuka H, Okazaki K, Tanaka M, Ishikawa M, Sumatani M and Yoshihara K 1985 *Chem. Phys. Lett.*
113 89
- Van Haver P, Van der Auweraer M, Viaene L, De Schryver F C, Verhoeven J W and van Ramesdonk H J
1992 *Chem. Phys. Lett.* **198** 361
- Von Lippt E 1957 *Z. Electrochem.* **61** 962
- Welsh W J and Johnson W D 1990 *Macromolecules* **23** 1881
- Wilkinson F 1975 In *Organic molecular photophysics* (ed.) J B Birks (New York: Wiley)

Kinetics of charge transfer reactions in photoelectrochemical cells

R MEMMING

FB Physik der Carl-von-Ossietzki-Universität Oldenburg und Institut für Solarenergieforschung (ISFH), Sokelantstraße 5, D-3000 Hannover 1, Germany

Abstract. In the present paper, fundamental aspects of charge transfer processes at semiconductor particles and extended electrodes are analyzed and compared. Although, in principle, the same reactions occur at particles and electrodes, different factors, such as light intensity, particle size, adsorption of electron donors or acceptors and formation of space charges, influence the reaction rates and sometimes even the reaction route. It is shown that rate constants are preferably determined from measurements at extended electrodes. Various mechanisms are discussed in detail.

Keywords. Semiconductor-electrodes; semiconductor-particles; kinetics.

1. Introduction

For almost 20 years many research groups have been studying and developing solid state devices, photoelectrochemical and photochemical systems with respect to conversion of solar energy. From this research it has become quite clear that high conversion efficiencies can only be obtained with heterogeneous systems. From this point of view, systems containing solid-solid and solid-liquid interfaces are of particular interest. Solid-solid systems, such as for instance *pn*-junctions, are adequate for conversion of solar energy into electricity, whereas semiconductor-liquid systems can, in principle, be used for the production of electricity as well as of storable chemical fuel.

During the last decade, many reactions in semiconductor suspensions and colloidal solutions besides processes at extended electrodes have been extensively studied. Various aspects of this research have been summarized in review articles. Restricting ourselves to the last decade, review articles have been published on photoelectrochemical conversion by Gerischer (1979), Tributsch (1982, 1988), Lewis (1984), Hodes (1985), Memming (1988, 1990, 1991), on charge transfer reactions at semiconductor electrodes by Pleskov and Gurevick (1986), Morrison (1980), Jaegermann and Tributsch (1988), Memming (1983, 1993) and Gomes and Cardon (1982) and on semiconductor particles by Henglein (1988, 1989) and Bahnemann (1991). In the present paper, the kinetics of reactions at semiconductor electrodes and particles will be compared with the main emphasis on the question of which factors determine the reaction rates in both cases.

2. Reactions at semiconductor particles

Since a semiconductor crystal or particle is a multi-atom or a multi-electron system, the electron energy levels are usually degenerated into energy bands. The distance

between the conduction and valence bands can be determined by absorption measurements, from which an absorption edge can be determined. The energy position of the conduction and valence band is usually entirely determined by the liquid contacting the semiconductor electrode or particle. This result is due to the strong interaction between the semiconductor surface and the electrolyte, such as for instance water, as proved experimentally by capacity measurements, which can be performed only with electrodes and not with particles (see also § 3). Accordingly, the positions of the conduction and valence bands at the surface of a semiconductor do not change upon addition of an electron donor or acceptor, such as a redox system, to the electrolyte. The absorption of the colloidal particles changes, however, if their dimensions become smaller than about 5 nm. On decreasing the size, at first a larger gap is observed, the finally – at very small diameter – exciton bands occur in the absorption spectra. Since the long range interaction disappears, quantization of the energy bands occurs. The exciton formation in small particles is due to a stronger coulomb interaction within the limited space in small particles. The energy levels in a particle have been calculated by using a simple quantum mechanical model for a particle in a 3-dimensional box (see e.g. Weller *et al* (1984), Rosetti *et al* (1985)). An exact position of the energy levels of the extremely small particles cannot be determined. One can only estimate it by studying electron transfer reactions from the conduction band of the particle to an electron acceptor during light excitation. One example is the reduction of protons at 5 nm PbSe- and HgSe-colloids, which has only been observed with small and not with big particles (Nedeljkovic *et al* 1986; Micic *et al* 1992). Accordingly, the conduction band of big particles occurs at energies below the H^+/H_2 -redox potential and above it in the case of quantization.

Concerning photo-induced charge-transfer reactions at small or big semiconductor particles, such processes are only possible if both oxidation by hole transfer and reduction by electron transfer occur simultaneously, as illustrated in figure 1b. Accordingly, the slowest reaction step determines the overall rate, as expected in the case of excited aromatic molecules also. On the other hand, if no electron acceptor

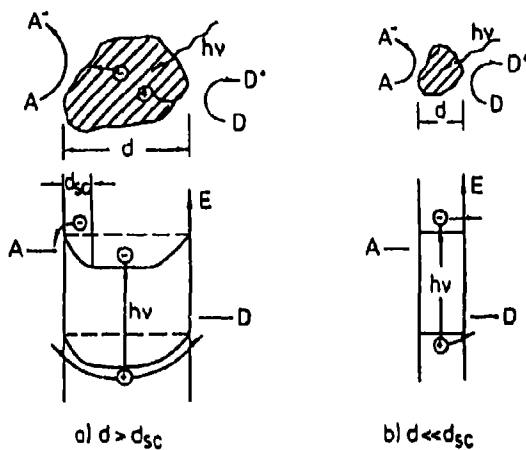


Figure 1. Electron- and hole transfer at large (a) and small (b) semiconductor particles to an electron acceptor A and donor D.

is present in the solution, then the photoexcited electrons may be trapped at surface sites, as found with colloidal TiO_2 (Bahnemann *et al* 1984). These electrons exhibit a characteristic transient absorption spectrum, which can be easily measured by laser flash spectroscopy because of the large surface area of the TiO_2 colloidal solution. Also the trapping of holes has been observed when electrons are efficiently scavenged. Corresponding transient spectra of trapped holes have been found with TiO_2 (Bahnemann *et al* 1984) and CdS-particles (Baral *et al* 1986).

As discussed above, electrons and holes produced by light excitation in a small semiconductor particle can be easily transferred to an electron-acceptor and -donor, respectively, provided that the energetic requirements are fulfilled. The quantum efficiency of the reaction depends on the transfer rate at the interface, on the recombination rate within the particle and on the transit time, the latter being given by (Grätzel and Frank 1982),

$$\tau = R^2/\pi^2 D, \quad (1)$$

where R is the radius of the particle and D the diffusion coefficient of the excited charge carriers. Taking a typical value of $D \approx 0.1 \text{ cm}^2 \text{ s}^{-1}$ and a radius of 10 nm, the average transit time is only about 1 ps. This value is much smaller than that for recombination, which is usually greater than several nanoseconds. Accordingly, the kinetics of a reaction is mainly determined by the surface properties of a particle. Besides surface effects, particles behave like excited organic molecules.

Mostly, oxidation and reduction of organic molecules have been studied in semiconductor suspensions and colloidal solutions. This implies that two charges per molecule have to be transferred before a stable state is reached. Taking the oxidation of ethanol as an example, the transfer of two electrons to a particle leads to the formation of aldehyde. This reaction has been studied at different semiconductor particles such as TiO_2 , CdS and ZnS by using H_2O or O_2 as an electron acceptor. In the case of TiO_2 , SnO_2 and CdS, only acetaldehyde is formed, whereas with small ZnS-particles butanediol was also formed as an oxidation product (Müller *et al* 1993). The latter result can be explained by a single-hole transfer from an excited ZnS-particle to ethanol, leading to the formation of a hydroxyethyl radical which diffuses into the solution. There it undergoes dimerization and disproportionation by reacting with another radical, as illustrated in figure 2 (Müller *et al* 1993). A similar mechanism has been proposed by Henglein *et al* (1984), who observed the formation of pinacol at nm-particles of ZnS in the presence of 2-propanol, using CO_2 as an electron acceptor. Cross-reaction products have also been reported. For instance, Yanagida (1991 – private communication) has observed the formation of pinacol at small CdS-colloids with an excess of 10 mol % of S^{2-} when using methanol as an electron donor and benzophenone as an acceptor. It should be mentioned that some published experimental data on reaction products at ZnS- and CdS-colloids are controversial. This is due to very complex surface chemistry, as studied in detail by Müller *et al* (1993). Already the synthesis of the particles plays an important role, for instance, whether the ZnS-particles are prepared in a solution with an excess of S^{2-} - or Zn^{2+} -ions. A discussion of the influence of the surface chemistry on the kinetics, however, would be beyond the scope of the present paper.

It is interesting to note that acetaldehyde but no butanediol is formed at excited TiO_2 , SnO_2 and CdS-particles. Here also a hole is transferred to ethanol, leading to

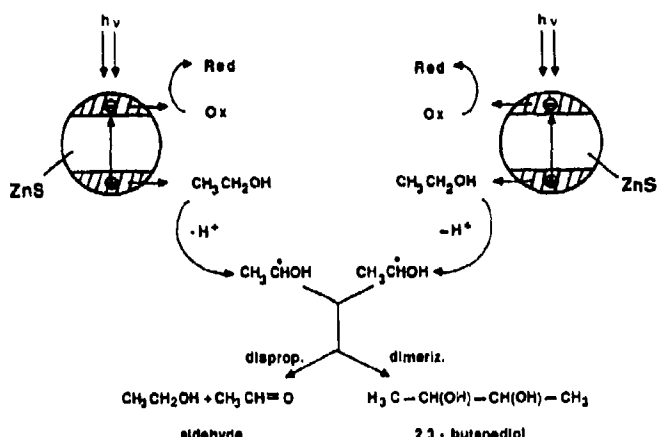


Figure 3. Two-step oxidation of ethanol at small TiO₂-particles ("current doubling effect") during illumination

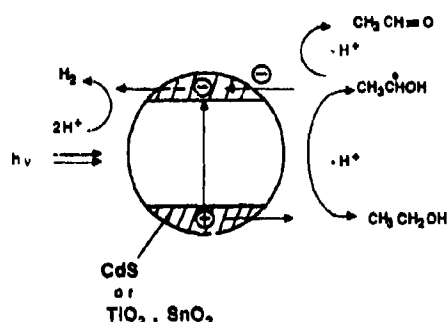


Figure 3. Two-step oxidation of ethanol at small TiO_2 -particles ("current doubling effect") during illumination.

the formation of a radical. Since, however, the energy bands occur at much lower energies, an electron can be injected into the conduction band of these materials (figure 3), i.e. aldehyde is formed immediately at the same particle. Here, a second electron is created in the conduction band besides the other one produced by light excitation. This is possible because in a semiconductor-particle the density of energy states is high. In this aspect, even a small particle differs considerably from an excited aromatic molecule. The different behaviour of ZnS as compared to the other semiconductors becomes clear by comparing the position of the energy bands with respect to the redox potentials of the ethanol/radical- and of the radical/aldehyde-couples, the latter being determined by Lilie *et al* (1971) (see figure 4). The phenomenon that both energy bands are involved in the oxidation of organic molecules is well known from investigations with semiconductor electrodes ("current-doubling-effect"). For details see e.g. Memming (1983).

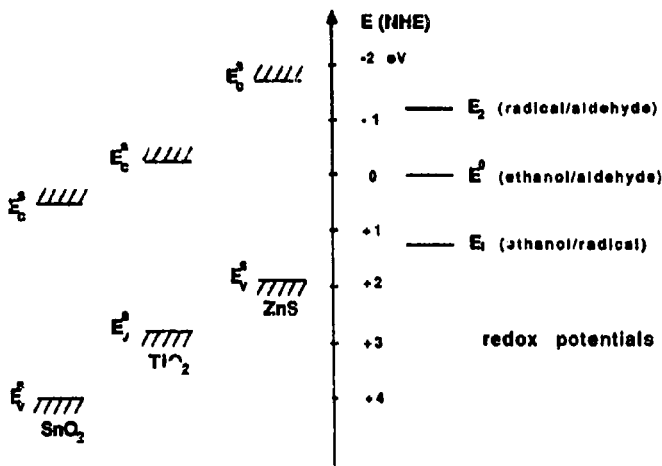


Figure 4. Energy scheme of various semiconductors (left) and redox potentials of the ethanol/aldehyde system (right).

Returning to the oxidation of C_2H_5OH to the radical by a single hole transfer at an excited ZnS-particle, the question arises as to why this radical is not immediately further oxidized to the aldehyde by a second hole transfer, which is energetically feasible. Concerning this problem, it has to be realized that this second hole has also to be generated by light excitation, and that it may take a considerable time until a second photon is absorbed by the same particle. This time interval can be estimated as follows.

Taking a 3-nm ZnS-particle as an example, its absorption cross-section σ can be calculated from the Mie-theory (Ribarsky 1985). We thus obtained $\sigma = 5.4 \times 10^{-16} \text{ cm}^{-2}$ at a wavelength of 320 nm. Using light intensity of $3 \times 10^{16} \text{ photons cm}^{-2} \text{ s}^{-1}$, the time interval between two absorption incidents is, on the average, about 60 ms. Within this period, a radical formed by hole transfer can certainly diffuse away from the particle, which explains the formation of butanediol in the solution (figure 2). Since the absorption cross-section increases with the diameter of the particle, the time interval between two absorption incidents in an individual particle decreases. For instance, in the case of a 4- μm -particle $\sigma = 1.3 \times 10^{-7} \text{ cm}^{-2}$, and the time interval is of the order of 100 ps for the same photon flux, i.e. it is shorter than for 3-nm-particles by 8 orders of magnitude. According to this estimate, it was predicted several years ago that the reaction mechanism may change due to this particle size effect (Memming 1988). Recently, we succeeded in proving this effect also by studying the oxidation of ethanol at small (3 nm) and big (4 μm) ZnS-particles. As shown in figure 5, butanediol is only formed at the 3 nm-particles, whereas aldehyde was formed with 4 μm -particles (Müller *et al* 1993).

Electrochemical investigations with semiconductor electrodes have shown that a space charge layer exists below the surface, i.e. energy bands are bent. This occurs of course also in a particle, as already illustrated in figure 1a. The thickness of the space charge layer depends on the doping, i.e. it is large for a low doping density and small for a large doping. Typical values of the thickness are of the order of

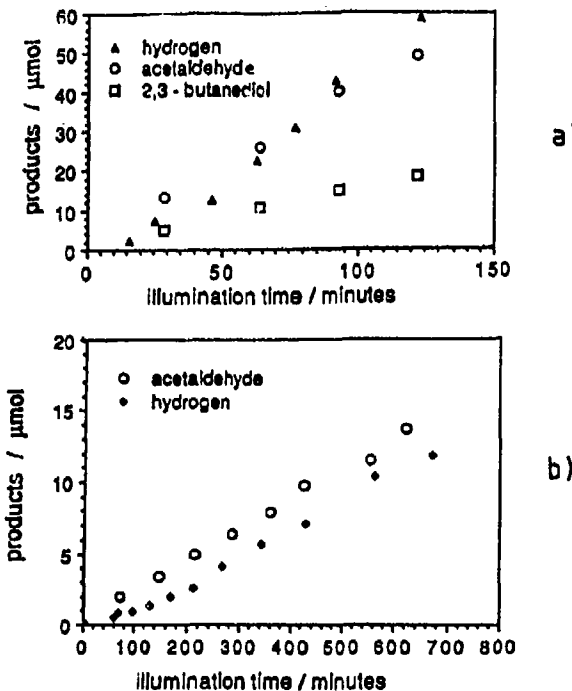
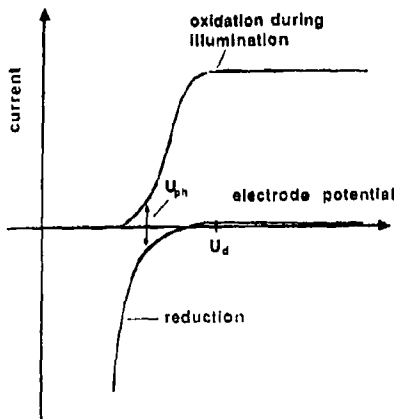


Figure 5. Formation of products upon illumination of ZnS-particles (17 mol % SH^- -excess) in $\text{EtOH}/\text{H}_2\text{O}$ (ratio 1:5) at pH 10: (a) 3 nm ZnS-particles; (b) 4 μm ZnS-particles. From Müller *et al* (1993).

$d_{\text{sc}} \approx 10^{-5} \text{ cm}$ for a density of 10^{17} cm^{-3} . Since there is an energy barrier for electrons (figure 1a), the question arises whether this barrier influences the kinetics and therefore the transfer rate of reactions at particles of a size $d \gg d_{\text{sc}}$. Since the electron density at the surface can be rather small, the rate of the electron transfer to an acceptor and consequently the rate of the overall reaction will be small. In such a case, the recombination rate will increase. On the other hand, the holes created by light excitation are driven towards the surface because of the electrical field across the space charge layer. This leads to a negative charging of the particle, causing a flattening of bands, so that electrons are more easily transferred (see dashed line in figure 1a). The actual rates of the two processes, i.e. electron and hole transfer, finally depend on the rate constants.

3. Reactions at extended electrodes

Frequently it is difficult to get an insight into the mechanism of reactions at particles because the two processes, reduction of the electron-acceptor and oxidation of the donor, always take place at the same time. In many cases, it is easier to study reactions at semiconductor electrodes because one of two processes can be avoided by polarizing

Figure 6. Schematic current-voltage characteristic for an *n*-type semiconductor electrode.

the electrode. The charge transfer process can be analyzed in terms of partial currents in the dark and under illumination, as schematically illustrated for an *n*-type semiconductor electrode in figure 6. The cathodic current corresponds to the reduction of an electron acceptor and the anodic current to the oxidation of a donor. Since the latter current is increased by illumination, the corresponding process requires holes. Under open circuit conditions ($j = 0$), the electrode potential occurs at U_d . Under illumination the open circuit potential is shifted to U_{ph} , i.e. to a potential at which anodic photo current and cathodic dark current are equal. This shift to the open circuit potential is the same as that already discussed for the big particles in § 2 (see also § 3.2). It means a decrease of band bending. Assuming again that the cathodic reaction is a conduction band process, the current is given by

$$j^- = -k_{c,red} c_{ox} n_s \quad (2)$$

in which c_{ox} is the concentration of the electron acceptor in a number of molecules or ions per cubic centimeter, n_s the electron density (cm^{-3}) and $k_{c,red}$ a second-order rate constant ($\text{cm}^4 \text{s}^{-1}$). Using the theories of Marcus (1964) and of Gerischer (1960, 1961), the rate constant is given by

$$k_{c,red} = k_{c,red}^{\max} \exp[-(E_c - E_{F,redox}^0 + \lambda)^2 / 4kT\lambda], \quad (3)$$

in which E_c is the lower edge of the conduction band, $E_{F,redox}^0$ the standard energy potential of the redox system (electron acceptor) and λ the reorientation energy. $k_{c,red}^{\max}$ is the maximum rate constant for $(E_c - E_{F,redox}^0 + \lambda) = 0$. The electron density at the surface n_s is related to the bulk density n_0 by

$$n_s = n_0 \exp(-e\phi_{sc}/kT), \quad (4)$$

in which ϕ_{sc} is the potential across the space charge layer, as shown in figure 7b. Inserting (4) into (2), one has:

$$j^- = e k_{c,red} c_{ox} n_0 \exp(-e\phi_{sc}/kT). \quad (5)$$

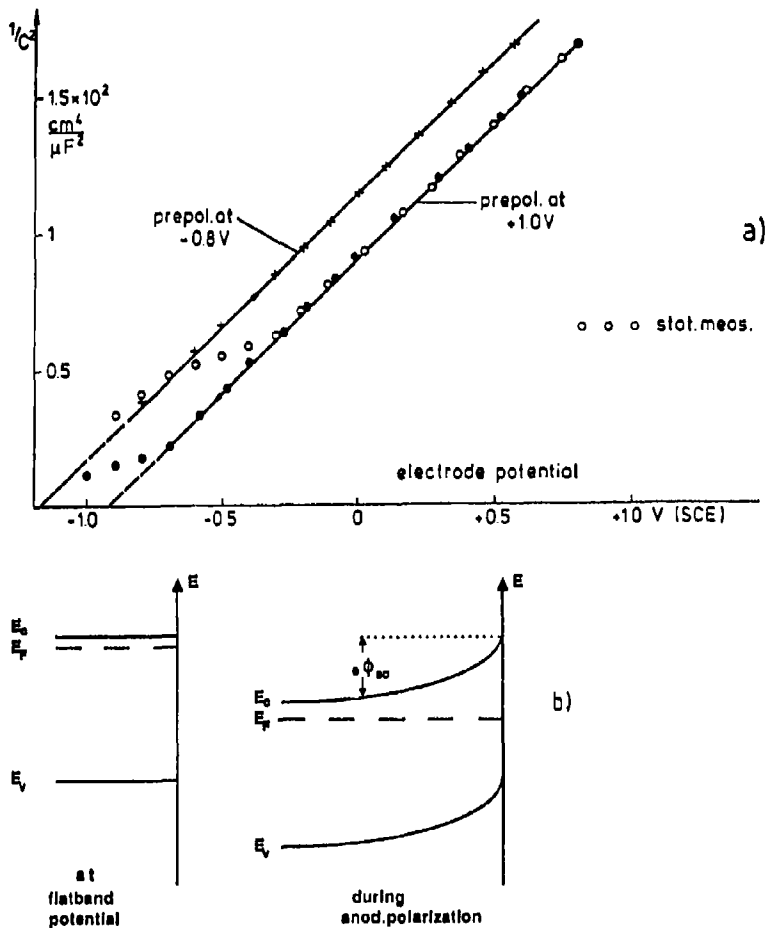


Figure 7. (a) Mott-Schottky plot of the space charge capacity of *n*-GaAs in 0.1 M H_2SO_4 after anodic (+1 V) and cathodic (-0.8 V) prepolarization. (b) Energy bands at flatband potential and at an anodic potential. From Schröder and Memming (1985).

According, the cathodic dark current increases exponentially with the potential across the space-charge layer. The latter can be determined by measurements of the space-charge capacity, which is given by the Mott-Schottky equation (Memming 1983),

$$\frac{1}{C_s^2} = \left(\frac{2L_{D,\text{eff}}}{\epsilon\epsilon_0} \right)^2 \left(\frac{e\phi_{sc}}{kT} - 1 \right), \quad (6)$$

in which ϵ is the dielectric constant of the semiconductor, ϵ_0 the permittivity of the free space and $L_{D,\text{eff}}$ the effective Debye length given by

$$L_{D,\text{eff}} = [(e\epsilon_0 kT / 2n_0 e^2)]^{1/2}. \quad (7)$$

Corresponding measurements have been performed with many semiconductor electrodes, one example (*n*-GaAs) is given in figure 7a. Since $1/C_s^2$ is plotted versus the electrode

potential U_E , an extrapolation of the curve to $1/C_{sc} \rightarrow 0$ yields the so-called flatband potential ($U_E = U_{fb}$). Accordingly we have

$$U_{sc} = U_E - U_{fb}. \quad (8)$$

Using this question, one should predict from (5) that a plot of $\log j^-$ vs. ϕ_{sc} or U_E should yield a straight line with a slope of 60 mV/decade. The rate constant can be obtained by extrapolating such a curve to the equilibrium or redox potential and determining it by using (5). The potential across the space charge layer ϕ_{sc}^0 for the equilibrium case can also be taken from the capacity measurement.

Unfortunately, not many current-potential curves have been evaluated according to this model. There is one example (*n*-ZnO) given in the literature where the cathodic current really increases at 60 mV/decade, as required according to (5). Morrison (1969) has investigated the current-potential behavior of ZnO in aqueous electrolytes using various redox systems (electron acceptors). Evaluating these results in terms of rate constants, one obtains values of $k_{c,red} \leq 10^{-18} \text{ cm}^4 \text{s}^{-1}$, depending on the electron acceptor (Memming 1993). These data are in accordance with theoretical values obtained by using Marcus (1964) or Gerischer's (1970) theories. Recently, Lewis (1991) has estimated from these theories a maximum rate constant of $k_{c,red}^{\max} = 10^{-17}$ to $10^{-16} \text{ cm}^4 \text{s}^{-1}$ (compare also with (3)). Rate constants of $k_{c,red} \leq 10^{-18} \text{ cm}^4 \text{s}^{-1}$ determined experimentally are reasonable if one inserts values of the reorientation energy of $\lambda = 0.5$ to 1.0 eV into (3).

However, there are several other current-potential curves published in the literature where these curves exhibit a slope considerably larger than 60 mV/decade. The origin is not clear yet. In some cases it may be due to a change of the potential across the Helmholtz layer because of a change of the surface coverage. For instance, the Mott-Schottky curve may be different for anodic and cathodic prepolarization, as shown for *n*-GaAs in figure 7a. Obviously, here a hydroxyl surface being formed during anodic prepolarization, is changed into a hydride surface after cathodic prepolarization (Schröder and Memming 1985). This leads to a shift of the energy bands at the surface. Since such a shift also changes the energy distance between conduction band (E_c) and the standard redox potential ($E_{F,redox}^0$) in the exponent in (3), the rate constant is also changed. Recently, the kinetics of hydrogen evolution at *n*-GaAs electrodes has been studied in more detail by performing impedance spectroscopic and current-potential measurements simultaneously. However, protons act here as electron acceptors (pH 3.5). From impedance spectroscopy analysis the space charge capacity C_{sc} was determined (Uhendorf 1993). Since there is a fixed relation between C_{sc} and ϕ_{sc} (6), the potential across the space charge capacity could be determined for all currents. The result, i.e. j^- vs. ϕ_{sc} , is given by the solid line in figure 8. Here, the slope of $\log j^-$ vs. ϕ_{sc} corresponds to 60 mV/decade, as required by (5). This result is of special interest because the rate constant derived from this curve is of the order of $k_{c,red} = 10^{-12} \text{ cm}^4 \text{s}^{-1}$, i.e. it is 4 to 5 orders of magnitude higher than the maximum value of $k_{c,red}^{\max} = 10^{-16}$ to $10^{-17} \text{ cm}^4 \text{s}^{-1}$ estimated theoretically. On the other hand, an excellent fit can be obtained by comparing the experimental curve with a theoretical $j_c^- - \phi_{sc}$ -curve derived from the thermionic emission model, the latter being given by Memming (1987):

$$j_c^- = AT^2 \left(\frac{m^*}{m_e} \right)^{-1/2} \frac{n_0}{N_c} \exp \left(-\frac{e\phi_{sc}}{kT} \right). \quad (9)$$

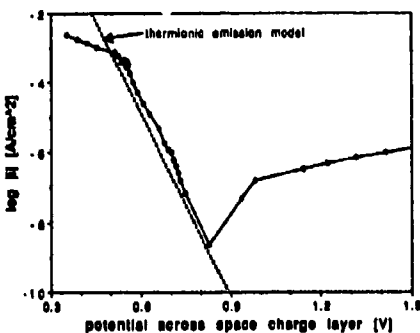


Figure 8. Current vs. potential across the space charge layer at *n*-GaAs in H_2SO_4 (pH 3); solid line – experimental data; dashed line – theoretical curve calculated from the thermionic emission model. (From Uhendorf *et al.* 1993).

in which m^* is the effective electron mass and m_e that in free space, N_c the density of energy states at the lower edge of the conduction band, and A is a constant = 120 $\text{A cm}^{-2}\text{K}^{-2}$. This equation has been derived originally for semiconductor-metal junctions on the basis that all electrons reaching the surface are transferred with a probability of unity, i.e. the current is actually determined by the electron transport from the bulk to the surface of the semiconductor (see e.g. Sze 1981).

The question arises as to how to explain such a high rate constant. In connection with this problem it should be mentioned that the analysis of the impedance spectroscopy measurements is based on a model in which hydrogen atoms are bonded or adsorbed on the electrode surface (Butler–Vollmer or Heyrovsky mechanism), which cannot be derived here. Accordingly, an electron transfer between the semiconductor and an adsorbed electron acceptor is involved, and obviously this is extremely fast, so that the electron transport in the semiconductor is a limiting step. There are a few other current–potential curves published in the literature which also indicate an extremely high rate constant. Examples are the reduction of H_2O_2 at *n*-GaAs (Minks *et al.* 1989) and of ferrocene at *p*-GaAs (Rosenwaks *et al.* 1992). In the latter case (reduction of ferrocene), the rate constant has been determined by fluorescence decay measurements. Also these large rate constants can only be interpreted assuming adsorption of the electron acceptor as also assumed by Nozik (1993).

So far we have discussed only the determination of rate constants for an electron transfer from the conduction band of an *n*-type semiconductor to an electron acceptor in the dark. As illustrated in figure 6, an anodic photocurrent occurs under illumination. This current is due to a hole transfer from the valence band to an electron donor or due to anodic decomposition. In this case, the anodic current is given by

$$j_v^+ = ek_{v,ox} C_{red} p_s, \quad (10)$$

with

$$p_s = p_L \exp(e\phi_{sc}/kT), \quad (11)$$

where p_L is the hole density at the inner edge of the space charge. Since holes are minority carriers in the *n*-type electrode, p_L differs from p_0 , and during light excitation $p_L \gg p_0$. In addition, the photocurrent is entirely determined by the light intensity,

so that p_L or p_i are not known. In order to evaluate a rate constant, the anodic process has to be measured with a *p*-type electrode of the same material, in which holes are majority carriers. Since the position of energy bands is usually identical for *n*- and *p*-type electrodes, the same rate constant should be valid for the *n*-type electrode. A quantitative evaluation is possible by using the quasi-Fermi level concept, as described by Reineke and Memming (1992).

Finally it should be mentioned that the slope of 60 mV/decade of a current-potential curve, as required according to (5), is also obtained when the reaction is diffusion-controlled (reversible reaction). In this case, the origin of this slope is due to the Nernst law with respect to concentrations of the components of the redox system at the surface (Reineke and Memming 1992). Accordingly, the current-voltage behavior has to be measured and analyzed by using a rotating disc electrode, in order to distinguish between kinetic and diffusion-controlled reactions (Meissner and Memming 1992).

4. Conclusions

In the present paper it is shown that, in principle, the same reactions occur at particles and at extended electrodes, but different factors, such as absorption of light, particle size effect, adsorption of the electron donor or -acceptor and formation of a space charge influence the reaction rate. The best way of determining the rate constant is by the analysis of current-voltage curves.

References

- Bahnemann D W 1991 In *Photochemical conversion and storage of solar energy* (eds) E Pelizzetti and M Schiavello (Amsterdam: Kluwer) p. 251
Bahnemann D W, Henglein A and Spanhel L 1984 *Faraday Discuss. Chem. Soc.* **78** 151
Baral S, Fojtik A, Weller H and Henglein A 1986 *J. Am. Chem. Soc.* **108** 375
Gerischer H 1960 *Z. Phys. Chem. N.F.* **26** 223, 325
Gerischer H 1961 *Z. Phys. Chem.* **27** 48
Gerischer H 1970 In *Physical chemistry* (eds) M Eyring, W Jost and D Henderson (New York: Academic Press) p. 463, vol. 4A
Gerischer H 1979 In *Topics in applied physics* (ed.) B O Seraphin (Berlin: Springer Verlag) p. 115
Gomes W P and Cardon F 1982 *Prog. Surf. Sci.* **12** 155
Grätzel M and Frank A I 1982 *J. Phys. Chem.* **86** 2964
Henglein A 1988 *Top. Curr. Chem.* **143** 113
Henglein A 1989 *Chem. Rev.* **89** 1861
Henglein A, Gutiérrez M and Fischer C H 1984 *Ber. Bunsenges. Phys. Chem.* **88** 170
Hodes G 1985 In *Energy resources through photochemistry and catalysis* (ed.) M Grätzel (New York: Academic Press) p. 521
Jaegermann W and Tributsch H 1988 *Prog. Surf. Sci.* **29** 1
Lewis N S 1984 *Annu. Rev. Mater. Sci.* **14** 95
Lewis N S 1991 *Annu. Rev. Phys. Chem.* **42** 543
Lille I, Beck G and Henglein A 1971 *Ber. Bunsenges. Phys. Chem.* **75** 458
Marcus R A 1964 *Annu. Rev. Phys. Chem.* **15** 155
Meissner D and Memming R 1992 *Electrochim. Acta* **37** 799
Memming R 1983 In *Comprehensive treatise of electrochemistry* (eds) B E Conway, J O M Bockris and E Yeager (New York: Plenum) vol. 7, p. 529
Memming R 1987 *Ber. Bunsenges. Phys. Chem.* **91** 353

- Memming R 1988 *Top. Curr. Chem.* **143** 79
- Memming R 1990 In *Photochemistry and photophysics* (ed.) I F Rabek (Boca Raton, FL: CRC Press) vol. 2, p. 143
- Memming R 1991 In *Photochemical conversion and storage of solar energy*, (eds) E Pelizzetti and M Schiavello (Amsterdam: Kluwer) p. 193
- Memming R 1993 *Top. Curr. Chem.* (in press)
- Micic O I, Rajh T and Comor M V 1992 In *Electrochemistry in colloids and dispersions* (eds) R A Mackay and J Texter (New York: VCH) p. 457
- Minks B P, Oskam G, Vanmaekelbergh D and Kelly J J 1989 *J. Electroanal. Chem.* **273** 119
- Morrison S R 1969 *Surf. Sci.* **15** 363
- Morrison S R 1980 *Electrochemistry at semiconductor and oxidized metal electrodes* (New York: Plenum)
- Müller B, Majoni S and Meissner D 1993 (MS in preparation)
- Nedeljkovic I M, Nenadovic M T, Micic O I and Nozik A I 1986 *J. Phys. Chem.* **90** 12
- Nozik A I 1993 2nd Int. Conf. Solar Energy Storage and Appl. Photochemistry, Cairo
- Pleskov Yu V and Gurevick Y U 1986 *Semiconductor photoelectrochemistry* (New York: Consultant Bureau)
- Reineke R and Memming R 1992 *J. Phys. Chem.* **96** 1310, 1317
- Ribarsky M W 1985 In *Handbook of optical constants of solids* (New York: Academic Press) p. 795
- Rosenwaks Y, Thacker B R, Ahrenkiel R K and Nozik A J 1992 *J. Phys. Chem.* **96** 10096
- Rosetti R, Hall R, Gibson J M and Bruylants L E 1985 *J. Chem. Phys.* **82** 552
- Schröder K and Memming R 1985 *Ber. Bunsenges. Phys. Chem.* **89** 385
- Sze S 1981 *Physics of semiconductor devices* 2nd edn (New York: John Wiley & Sons)
- Tributsch H 1982 In *Solar energy materials. Structure and Bonding Series. Vol. 49*. (eds) M J Clarke et al (Berlin: Springer Verlag) p. 127
- Tributsch H 1988 In *New trends and applications of photocatalysis and photochemistry for environmental problems* (ed.) M Schiavello (Dordrecht: D Reidel) p. 297
- Uhendorf I 1993 Ph D thesis, Hamburg
- Weller H, Koch U, Gutiérrez M and Henglein A 1984 *Ber. Bunsenges. Phys. Chem.* **88** 694

Cis-trans photoisomerization of 1,2-diarylethylenes: Effect of charge transfer interactions

U MAZZUCATO*, G G ALOISI and F ELISEI

Dipartimento di Chimica, Università di Perugia, I-06123 Perugia, Italy

Abstract. This paper describes the results of an extensive study of *trans*- \rightarrow *cis* photoisomerization of various 1,2-diarylethylenes (DAE). The structure effect on the competitive radiative and reactive deactivations and on the isomerization mechanism (singlet/triplet, diabatic/adiabatic) is discussed. The effect of charge-transfer (CT) interactions of DAE with electron donors and acceptors are then presented. Triplet-induced isomerization is generally the common effect in non-polar solvents, and is particularly efficient when a heavy atom is involved. Typical examples of CT-induced triplet photoisomerization of DAE by electron donors and acceptors are illustrated. New results on some fluorescent *cis* compounds are also reported. Prevalent radical ion formation in polar solvents is shown to generally quench isomerization from *trans* to *cis* but to induce isomerization from *cis* to the more stable *trans* radical ion.

Keywords. Photoisomerization; diarylethylenes; charge-transfer; triplet induction; radical ions.

1. Introduction

Stilbene analogues, the 1,2-diarylethylenes (DAE), have been the object of deep investigations during the last decade. Sustained interest in such molecules lies in the fact that they are simple models for the study of *cis*-*trans* photoisomerization around the ethylenic bond (Saltiel and Charlton 1980; Saltiel and Sun 1990) and of *s-cis*-*s-trans* (photo)isomerization around the quasi-single bond between the aryl and the ethylenic bridge (Mazzucato and Momicchioli 1991) as well as in the inherent importance of these processes for applicative research (photography, photochromism, processes of biological interest such as vision etc.).

Recent studies on photoisomerism of DAE have shown that the excited-state properties depend to a large extent on the size and nature of the aryl groups linked to the ethylenic bridge (Bartocci *et al* 1992; Mazzucato 1982, 1987).

Greater attention has been paid to the *trans* isomers, where fluorescence, isomerization to *cis* in S_1 (singlet mechanism) and intersystem crossing (ISC) (eventually followed by isomerization in T_1 , triplet mechanism) are the competitive deactivation channels of the S_1 state. In the parent molecule, stilbene (S), the avoided crossing between the $S_1(B_u)$ energy curve as a function of the twist angle around the central double bond (with the energy increasing by twisting towards 90°, at the *perp*

*For correspondence

configuration) and the upper (doubly excited?) $S_n(A_g)$ curve (with an "ethylenic" minimum in the *perp* configuration) leads to the well known and widely accepted diabatic isomerization mechanism in S_1 . From the *trans* side, this pathway involves an activated ${}^1\text{trans}^* \rightarrow {}^1\text{perp}^*$ twisting towards the energy minimum, followed by internal conversion to the ground state configuration, ${}^0\text{perp}$, and almost 50:50 partitioning to the stable *trans* and *cis* isomers (Saltiel and Charlton 1980; Saltiel and Sun 1990). When a phenyl group (P) of stilbene is replaced by larger polycyclic aryl groups of gradually decreasing S_1 and T_1 energy, such as naphthyl (N), phenanthryl (Ph), chrysanyl (C), pyrenyl (Py) and anthryl (An) groups, the S_1 curve shifts towards lower energies (more in the *trans* and *cis* than in the *perp* geometry) while the S_n curve is less affected by the aryl substitution. Therefore, the $S_1 - S_n$ crossing is no longer possible and a maximum, instead of a minimum, is present at 90° in the S_1 energy curve. The activation energy to twisting in S_1 does gradually increase (Mazzucato 1982, 1987), thus leading to a decrease in the isomerization quantum yield in S_1 , ${}^1\phi_{t-c}$, and can become insuperable at room temperature. The competitive processes of fluorescence (possibly accompanied by some internal conversion) and ISC are then much more favoured, their relative amounts being determined by the nature of the aryl groups (Bartocci *et al* 1992). When ISC is substantial, the triplet mechanism can maintain an overall high isomerization yield, unless high barriers to ${}^3\text{trans}^* \rightarrow {}^3\text{perp}^*$ twisting completely inhibit the *trans* to *cis* isomerization, as in the case of the anthryl derivatives ("one-way" isomerization, only from *cis* to *trans*) (Sandros and Becker 1987; Arai *et al* 1988; Tokumaru and Arai 1992). A suitable choice of the aryl groups linked to the central ethylenic bridge allows the gradual tuning of the *cis-trans* photoisomerization from a singlet to a triplet pathway and finally the inhibition of the reaction in the *trans* \rightarrow *cis* way.

From the *cis* side, the torsional barriers are always lower compared with those from the *trans* side. Therefore, when a maximum instead of a funnel is present at the *perp* configuration, a direct adiabatic mechanism (${}^1\text{cis}^* \rightarrow {}^1\text{trans}^*$) can become operative in both the singlet (Spalletti *et al* 1991; Mazzucato *et al* 1993) and triplet (Arai *et al* 1988; Tokumaru and Arai 1992) manifolds.

The fluorescence of *trans*-DAE is quenched by charge transfer (CT) interactions with electron donors (e.g., amines) or acceptors (e.g., cyano-aromatics) and exciplex formation, as evidenced by their typical emission bands, is observed in non-polar solvents (Aloisi *et al* 1980, 1988; Aloisi and Elisei 1990; Elisei *et al* 1992). Singlet-induced CT interactions may result in enhanced formation of DAE triplets in non-polar solvents (Elisei *et al* 1990; Aloisi *et al* 1992; Görner *et al* 1992) and DAE radical ions in polar solvents (Aloisi *et al* 1991, 1992; Görner *et al* 1992). The extent of the quenching, which depends on the nature of the two partners and the solvent, may then affect both the yield and the mechanism of photoisomerization (Aloisi *et al* 1980; Aloisi and Elisei 1990; Aloisi *et al* 1988, 1991; Elisei *et al* 1992).

On the basis of published data obtained from the spectroscopic and photochemical study of a large series of DAE as well as of some new results recently obtained in our laboratory, the main features of the structure effect on photoisomerism of DAE are reported here. The CT interactions of the fluorescent *trans* isomers and some *cis* analogues with electron donors and acceptors will then be discussed to evidence their effects on the excited state behaviour of DAE.

2. Experimental

All compounds were synthesized by standard procedures as per previous work. Fluorimetric, photochemical and flash photolytic measurements were made as described in previous papers (see Bartocci *et al* 1987 and Aloisi *et al* 1992, and papers cited therein). Benzene, *n*-hexane, methylcyclohexane (MCH), chlorobenzene (CB), ethylacetate (EtAc) and acetonitrile (MeCN) from Carlo Erba (RPE grade) were used as solvents, tributylamine (TBA), diethylaniline (DEA), 4-bromo-N,N-dimethylaniline (BrDMA) from Fluka AG and potassium iodide from Carlo Erba as electron donors, and chloranil (Chl) from Fluka AG and dicyanobenzene (DCNB) from EGA-Chemie as electron acceptors.

3. Results and discussion

3.1 Photoisomerization

Figure 1 shows a qualitative sketch (a), based on theoretical and experimental data, of the torsional potential energy of the S_1 state of three typical DAE together with a scheme (b) of the energy levels of the lowest singlet excited state of the DAE and of their arene (1L_a , 1L_b) and ethylene (1B_u) chromophores (Bartocci *et al* 1992). Perturbation coupling of the excited state localized on the largest arene chromophore

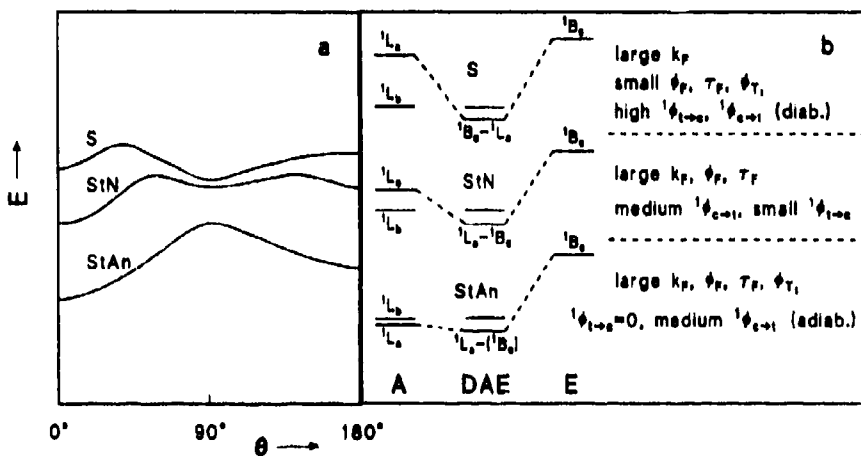


Figure 1. (a) Sketch of the torsional energy barrier for the S_1 state of stilbene (S: singlet mechanism), styrylnaphthalenes (StN: prevalent singlet mechanism at room temperature, mixed singlet + triplet mechanism at lower temperatures) and styrylanthravenes (StAn: no *trans* \rightarrow *cis* isomerization); (b) sketch of the interactions between the lowest excited states L_a and L_b of the polycyclic aryl chromophore (A) and the B_u state of ethylene (E) to give the resulting S_1 state of the *trans*-DAE (the effect of the relative positions of the energy levels on the fluorescence rate parameter, quantum yield and lifetime and on the photoisomerization quantum yields are also indicated).

(particularly of 1L_a , which has a higher transition moment) with the 1B_u state of ethylene gives rise to lowest excited states of different character for the DAE molecules.

When the energy of the arene 1L_a state is high, not much lower than that of the lowest excited state 1B_u of ethylenic character, the interaction is strong leading to a mixing of local states with a large contribution of the ethylenic π, π^* state to the S_1 state of the DAE. A high $^1\phi_{t-c}$ and low ϕ_f is expected in this case, as found for *trans*-S.

When the energy of 1L_a decreases markedly (naphthyl, phenanthryl derivatives), the DAE excitation energy is largely localized in the aryl (prevalent L_a character) and a high torsional barrier in S_1 leads to a small $^1\phi_{t-c}$. However, in some cases, particularly when the lowest excited state is the aryllic 1L_b state (weak $S_0 \rightarrow S_1$ transition and low extinction coefficients), ISC can become substantial opening the triplet pathway to isomerization.

A limiting situation is reached when 1L_a (lying in such cases below 1L_b) is so far apart from 1B_u that the mixing is very weak (S_1 of aromatic character, as in anthryl derivatives). The barriers to twisting are high in both S_1 and T_1 and no isomerization occurs from *trans* to *cis* but only from *cis* to *trans* ("one-way" isomerization, Arai *et al* 1988; Tokumaru and Arai 1992). The presence of a maximum, instead of a minimum, at the $^1\text{perp}^*$ configuration for the pyrene and anthracene derivatives causes the activated twisting of $^1\text{cis}^*$ to directly produce $^1\text{trans}^*$, thus favouring an adiabatic photoisomerization mechanism, as reported for the triplet state (Arai *et al* 1988; Tokumaru and Arai 1992), particularly in polar solvents where the activation energy in S_1 is lowered because of the stabilization of the zwitterionic twisted configuration (Spallati *et al* 1991; Mazzucato *et al* 1993).

Figure 2 shows the increase in the fluorescence quantum yield (ϕ_f) and the decrease in the $\text{trans} \rightarrow \text{cis}$ photoisomerization quantum yield (ϕ_{t-c}) of some styryl-arenes on increasing the size of the arene and the aromatic character of the S_1 state of the DAE. Table 1 shows how the nature of the largest arene affects the photoisomerization mechanism (singlet/triplet, diabatic/adiabatic). Stilbene isomerizes with high yield via a singlet diabatic mechanism (Saltiel and Charlton 1980; Saltiel and Sun 1990). The

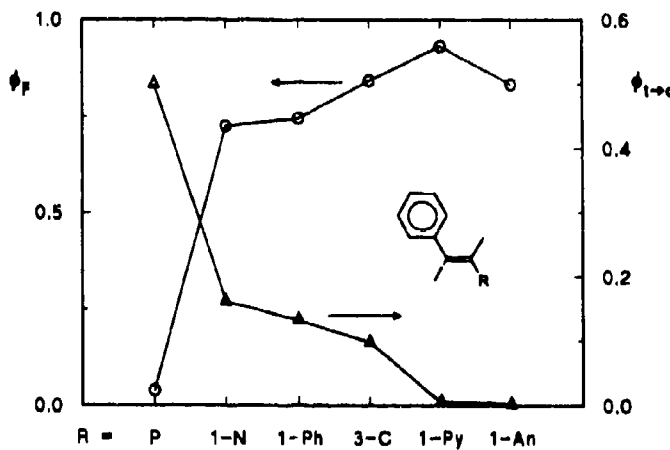


Figure 2. Effect of the nature and size of the aryl substituent of styrene on the fluorescence (○) and $\text{trans} \rightarrow \text{cis}$ photoisomerization (Δ) quantum yields of some DAE.

Table I. Fluorescence, triplet and isomerization quantum yields and prevalent isomerization mechanism for some typical *trans*-DAE in non-polar solvents at room temperature.

Compound	ϕ_f	ϕ_T	ϕ_{cis}	Prevalent mechanism
S ^a	0.04	<0.01	0.50	Singlet, diabatic
1-StN ^b	0.72	0.04	0.16	Singlet, diabatic
1-StPh ^c	0.61	0.18	0.14	Triplet, diabatic
2-StPh ^c	0.35	<0.01	0.24	Upper triplet, diabatic
9-StPh ^c	0.67	0.32	0.13	Mixed, diabatic
1-StPy ^d	0.94	<0.03	<0.02	Only <i>cis</i> → <i>trans</i> : singlet, adiabatic
9-StAn ^d	0.44	0.32	—	Only <i>cis</i> → <i>trans</i> : mixed, adiabatic

References: ^a Saltiel and Charlton (1980); ^b Elisei *et al* (1989); ^c Aloisi and Elisei (1990); Elisei *et al* (1990); ^d Bartocci *et al* (1992).

n-styrylnaphthalenes (*n*-StNs) (Bartocci *et al* 1984; Elisei *et al* 1989) have a prevalent radiative deactivation of S_1 : they isomerize by the same mechanism as *S* above room temperature but follow a prevalent triplet pathway below 270 K (or at slightly lower temperatures in polar solvents). The *n*-styrylphenanthrenes (*n*-StPhs) (Bartocci *et al* 1987) follow a mixed singlet/triplet mechanism already at room temperature due to higher torsional barriers in S_1 and larger triplet yields. In some cases (e.g., in 2-StPh), upper S_n or T_n states of ethylenic character may play a role in the isomerization favouring a fast twisting which by-passes the lowest excited states (Elisei *et al* 1990, Aloisi *et al* 1991a). In fact, 2-StPh has a high torsional barrier in S_1 and a ϕ_{cis} value as large as 0.24 which would indicate that at least ~50% of the excited molecules deactivate through a *trans* → *perp* twisting in the triplet manifold. However, T_1 cannot be an intermediate since its yield is smaller than 0.01. Therefore, one could think of an isomerizable upper T_n state, almost isoenergetic with S_1 . In fact, at low temperatures, when twisting in T_n is slowed down by the viscosity barrier, the population of T_1 increases substantially by $T_n \rightarrow T_1$ internal conversion and the lowest excited triplet state becomes readily detectable. A similar mechanism was hypothesized for the isomerization of 4-halogenated stilbenes (Görner and Schulte-Frohlinde 1979). In any case, the presence of a shallow minimum in the ^{1,3}*perp** configuration of StPhs still seems to favour the diabatic mechanism. Practically, the 1-styrylpyprene (StPy) and *n*-styrylanthracenes (StAns) do not isomerize from *trans* to *cis* because of very high torsional barriers in both S_1 and T_1 . They follow a mixed (singlet/triplet) mechanism from *cis* to *trans* with a prevalent adiabatic character.

In conclusion, the singlet mechanism is favoured at high temperatures and in polar solvents; the adiabatic mechanism is favoured in the presence of a maximum at the ^{1,3}*perp** configurations, particularly in polar solvents where the activation energy is smaller.

3.2 Effect of CT interactions on *trans* → *cis* photoisomerization

The *trans* → *cis* isomerization quantum yield (ϕ_{cis}) in the presence of the fluorescence quencher Q is the sum of two contributions, by the monomer (non-complexed) molecules (ϕ_{CM}) and by those which react through the exciplex (ϕ_{CE}). When $[Q] \rightarrow \infty$,

the fluorescence and photoisomerization quantum yields of the exciplex reach their limiting values, $\phi_{\text{FE}}^{\text{lim}}$ and $\phi_{\text{CE}}^{\text{lim}}$, respectively.

Often, the overall photoisomerization is less quenched than fluorescence or even enhanced by addition of electron donors or acceptors since CT-induced ISC can lead to isomerization in the triplet manifold. In fact, since both S_1 and T_1 are potentially reactive states (the actual reactivity depending on their torsional barriers), the expected effect is generally modest. Since the quenching efficiency of the singlet-excited *trans*-DAE by electron donors or acceptors depends on the redox potential of the two partners, a suitable choice of the additive is required for an efficient CT-induced photoisomerization, based on the following criteria: high quenching rate constant k_Q , low yields of both the radiative decay (ϕ_{FE}) and the internal conversion to the ground state (ϕ_{GE}) and high ISC yield (ϕ_{TE}) of the exciplex so as to induce a substantial population of the reactive triplet state of the olefin.

Figure 3 shows, as an example, the decreasing of fluorescence intensity of 9-StPh together with the parallel increase of the triplet and isomerization yields in the case of the interaction with DEA as donor in *n*-hexane. Table 2 shows some typical cases

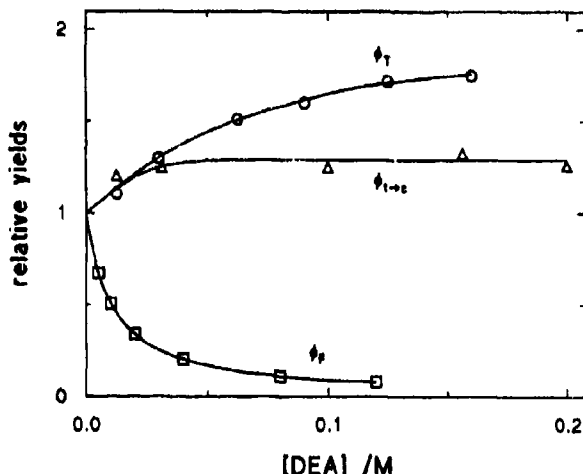


Figure 3. Effect of DEA concentration on the quantum yields of fluorescence (squares), photoisomerization (triangles) and triplet (circles) for *trans*-9-StPh/DEA in *n*-hexane.

Table 2. Limiting ($[Q] \rightarrow \infty$) fluorescence and *trans* \rightarrow *cis* photoisomerization quantum yields of some typical DAE in the presence of three amines as donors in *n*-hexane and DCNB as acceptor in benzene.

DAE	ϕ_F	ϕ_{TE}	$\phi_{\text{FE}}^{\text{lim}}$			$\phi_{\text{CE}}^{\text{lim}}$			
			TBA	DEA	BrDMA	TBA	DEA	BrDMA	
2-StN	0.65 ^a	0.12 ^a	0.17 ^a	0.72 ^b		0.17 ^c	0.10 ^a	0.12 ^b	0.26 ^c
1-StPh ^d	0.61	0.14	0.19	0.36	~0.01		0.10	0.20	0.44
9-StPh	0.67 ^d	0.13 ^d	0.17 ^d	0.57 ^d	<0.01 ^d	0.37 ^c	0.11 ^d	0.10 ^d	0.28 ^d
2,3'-NPE	0.67 ^e	0.15 ^b	0.03 ^e			0.24 ^e	0.09 ^e		0.34 ^e

References: ^a Aloisi *et al* (1980); ^b Aloisi *et al* (1977); ^c Aloisi *et al* (1991b); ^d Aloisi and Elisei (1990).

of the limiting ($[Q] \rightarrow \infty$) quantum yields of radiative and reactive deactivation of the exciplexes with three amine donors and one acceptor in non-polar solvents. Chromatographic control showed that the formation of photoproducts different from the *cis* isomers, as observed for the S/amine systems (Lewis 1979; Lewis and Simpson 1979; Lewis *et al.* 1992), is generally negligible in our experimental conditions. Perusal of table 2 shows that substantial isomerization is induced by DCNB in benzene where higher triplet yields were measured even if accompanied by substantial yields of radiative decay of the exciplex. On the other hand, radiative decay is the prevalent deactivation pathway of the exciplex with DEA and internal conversion is the prevalent one with the less efficient TBA quencher. For the exciplex of 9-StPh, quenching rate constants, k_Q , of 9.2 and 3.4 ($10^9 \text{ M}^{-1} \text{s}^{-1}$) were obtained with DEA and TBA, respectively. As expected, larger induction was obtained with BrDMA. Inclusion of a heavy atom in the solvent or, even better, in one of the two partners increases the isomerization yield because the spin-orbit coupling controlled by the exciplex produces the isomerizable T_1 state. In this case ϕ_{FE} is very low (smaller than 0.01) but enough to demonstrate the existence of the complex and then of a CT-assisted spin-orbit coupling effect.

The data above allow some conclusions to be drawn about the CT effect on the photoisomerization of *trans*-DAE in non-polar solvents. When both the lowest excited states of the olefin can be effectively reactive (as in S and many other DAE) or non-reactive (as in n-StAns), the effect of the CT interaction is expected to be zero or very small (both positive and negative), the quenching of S_1 being generally more or less compensated by a recovery of quanta in T_1 . A typical case is offered by DAE with small ϕ_{ISc} and ϕ_{I-IC} and high ϕ_F values (as for n-StNs); the quenching can be accompanied here by a gain of reactivity in T_1 , as observed in table 2 for the effect of DCNB on the two DAE bearing a naphthyl group. When, as in the pyrenyl derivative, only T_1 is reactive (because of a high torsional barrier in S_1) but the triplet yield is very small (because of the competitive fluorescence), the addition of Q can again enhance the ϕ_{I-IC} values through induced ISC.

In polar solvents, such as MeCN, non-emitting CT complexes are formed (Aloisi *et al.* 1991a, 1992; Görner *et al.* 1992). They induce little ISC since the concomitant formation of *trans* radical ions (generally non-isomerizable) prevails. A parallel increase was generally found both in the absorbance change of the radical ion and the conductivity signal (Aloisi *et al.* 1991a). The photoreaction yield increases slightly in some cases (e.g. with DCNB as acceptor) probably because the radical recombination can lead, at least in part, to formation of the isomerizable triplet state. In any case, the fluorescence quenching by amines was always accompanied by a decrease in the isomerization yield. For example, in the case of 1-StPh/DEA, the $\phi_{CE^{1/2}}$ value was halved (0.07); however, no triplet transient was observed, since T_1 produced by charge recombination is shorter-lived compared with the radical anion. In some experiments, the radical cations of the olefin were sensitized by irradiation of chloranil, a well-known electron acceptor in the triplet state. Figure 4 refers to the system 1-StPy/Chl in MeCN after irradiation of the acceptor at 308 nm. It shows the spectra of the triplet state of the acceptor ($\lambda_{\max} = 510 \text{ nm}$) and its radical anion (450 nm) and of the DAE radical cation (590 nm) together with the decay kinetics of the first and last transients. The triplet state of Chl was formed within the laser pulse while the DAE radical reached its maximum ΔA after 0.6 μs and decayed with a lifetime of 2.5 μs .

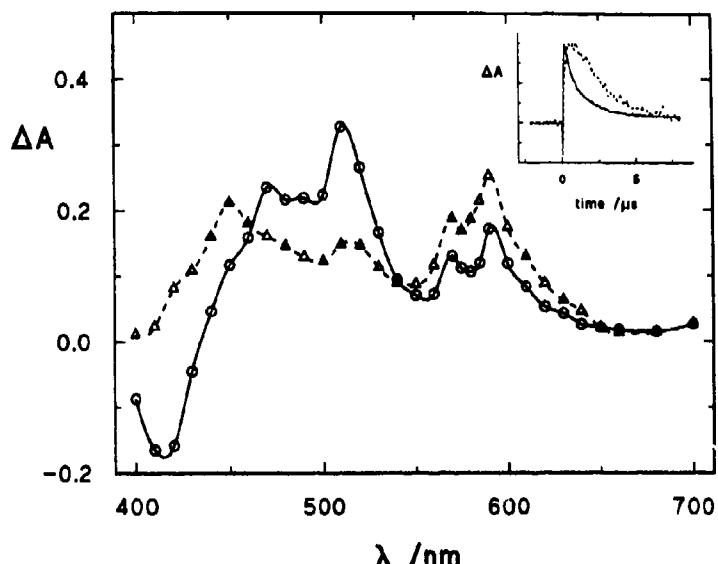


Figure 4. Time-resolved absorption spectra of the *trans*-1-StPy/Chl system in MeCN recorded 0.2(—) and 1(-----) μ s after the laser pulse ($\lambda_{\text{exc}} = 308$ nm). Inset: decay kinetics at 510(—) and 590(-----) nm.

An interesting case is presented by azastilbenes, and particularly by 1-(*n*-pyridyl), 2-(*n'*-pyridyl)ethylenes (*n*, *n'*-DPE), where the photoreaction is inhibited by the high efficiency of the $S_1 \rightarrow S_0$ internal conversion to the ground state induced by the low-lying n, π^* states introduced by the heteroatom. Here, the quenching effect is expected to reduce the internal conversion in favour of reactive deactivation pathways through the complex. However, preliminary experiments indicate that the situation is complicated by formation of by-products. In any case, the S_1 lifetime of DPE is very short, so that high concentrations are needed in order to induce complexation and then isomerization.

An important heavy atom effect was found on using halide anions as quenchers of some DAE and their aza-analogues, the latter in both neutral and protonated forms. Some typical examples showing an important induction of isomerization are reported in table 3. Particularly interesting is the huge increase in reactivity for the two last protonated substrates. Nanosecond laser flash photolysis measurements were carried out to investigate the transients formed by the interaction of iodide anions with some singlet excited *n*-StPhs. No sign of radical anions of the DAE was found but only a substantial production of their T_1 states. Figure 5 shows the $T_1 \rightarrow T_1$ spectrum of 1-StPh ($\lambda_{\text{max}} = 460$ nm) obtained in the presence of KI ~ 0.2 M in MeCN/H₂O (1/1, v/v) together with the enhancement of the triplet population by increasing the KI concentration (inset). The question of the relative importance of the CT and heavy atom effects on the quenching by halide anions has never received a convincing answer (Watkins 1973, 1974). The heavy atom effect probably operates in conjunction with association phenomena, particularly in the case of the charged olefins. In agreement with what was reported for the quaternary salts of DPE (Gutierrez and Whitten 1976), we believe that the actual quenching is controlled by

Table 3. Limiting *trans* \rightarrow *cis* photoisomerization quantum yields of some DAE, their neutral and protonated aza-analogues induced by iodide anions in polar solvents, compared with the intrinsic values in the absence of additives.

Compound	$\phi_{\text{t} \rightarrow \text{c}}$	$\phi_{\text{c}\text{H}}^{\text{lim}}$
2-StN ^a	0.19	0.48
3-StPh ^b	0.13	0.43
9-StPh ^b	0.29	0.40
3-StP ^a	0.44	0.52
2,3'-NPE ^a	0.14	0.38
3-StPH ^{++c}	0.27	0.25
4'-OCH ₃ -3-StPH ^{++c}	0.0006	0.36
3,3'-DPEH ₂ ^{++d}	0.045	0.50 ^d

^a In water-acetonitrile 60:40, (Mazzucato *et al* 1982); ^b in water-acetonitrile 50:50, this work; ^c in water-ethanol 90:10 (Bartocci *et al* 1976/77); ^d quencher: bromine anion.

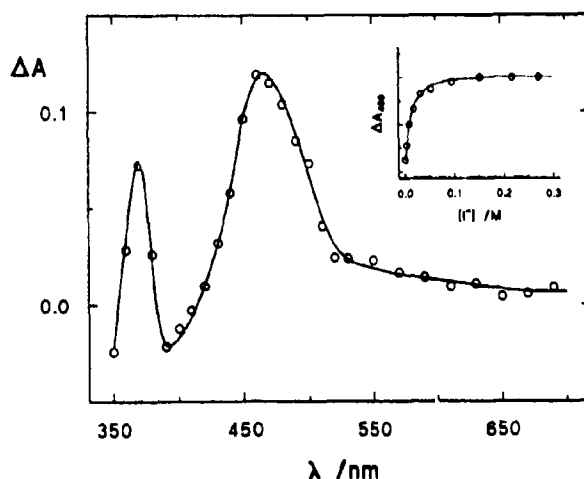


Figure 5. Triplet-triplet absorption spectrum of *trans*-1-StPh in MeCN/H₂O (1/1, v/v) in the presence of 0.5 M KI recorded 60 ns after the laser pulse ($\lambda_{\text{osc}} = 308$ nm). Inset: effect of iodide concentration on the absorbance change at 460 nm.

the electron donor-acceptor interaction while the heavy atom makes the triplet formation of the olefin fast enough to dominate all other paths of exciplex decay.

3.3 Effect of CT interactions on *cis* \rightarrow *trans* photoisomerization

The quenching of the *cis*-DAE by donor-acceptor interactions has been little investigated thus far since these isomers are generally non-fluorescent due to their fast (small barriers) isomerization to *trans* or to polycyclic compounds (dihydrophenan-

threne in the case of S) and the consequent very short S_1 lifetime. Since photocyclization is a competitive singlet reaction, CT-induced formation of the triplet state can favour the $cis \rightarrow trans$ isomerization (particularly for the naphthyl and phenanthryl derivatives which are characterized by substantial cyclization yields). When a maximum is present in ${}^1perp^*$, the ${}^1cis^*$ lifetime increases; as mentioned earlier, the twisting becomes more or less activated and leads directly to ${}^1trans^*$ by an adiabatic mechanism (Sandros and Becker 1987; Spalletti *et al* 1991; Mazzucato *et al* 1993). In such cases, e.g. for the *cis* isomer of 9-StAn, the CT-induced fluorescence quenching can be measured thus obtaining more quantitative information about the CT interactions. Figure 6 shows the fluorescence spectra of *cis*-9-StAn quenched by DEA with a Stern-Volmer constant ($K_Q = k_Q \tau_F$) of 3.2 and 8 M^{-1} in MCH (a) and CB (b), respectively. The increase of the fluorescence band of the exciplex is clearly observable in both solvents, particularly in the more polar CB where the emission is weaker but redshifted.

The CT interactions of the *cis*-DAE in polar solvents open a new way to isomerization since their radical ions can thermally convert to the more stable *trans*

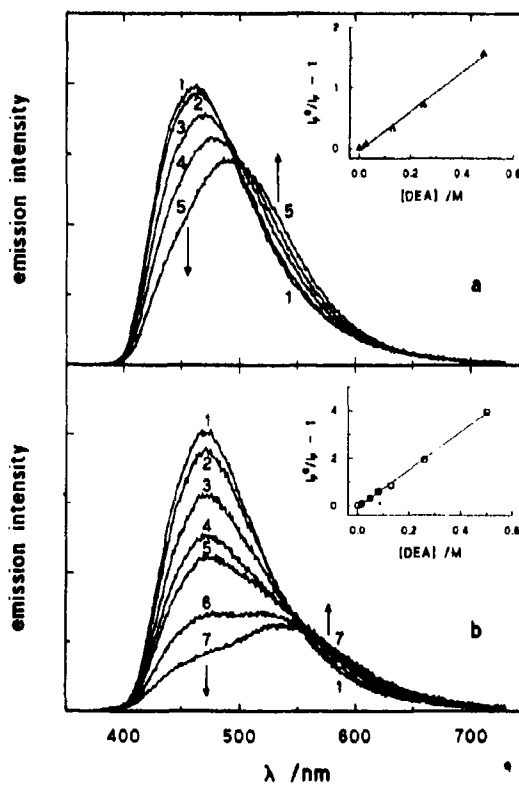


Figure 6. Fluorescence spectra of the *cis*-9-StAn/DEA system (a) in MCH without (1) and in the presence of 0.026 (2), 0.13 (3), 0.25 (4) and 0.48 (5) M DEA ($\lambda_{exc} = 370\text{ nm}$) [inset: Stern-Volmer plot obtained from the fluorescence intensities recorded at 420 nm] and (b) in CB without (1) and in the presence of 0.0164 (2), 0.0492 (3), 0.082 (4), 0.13 (5), 0.26 (6) and 0.50 (7) M DEA ($\lambda_{exc} = 370\text{ nm}$) [inset: Stern-Volmer plot obtained from the fluorescence intensities recorded at 470 nm].

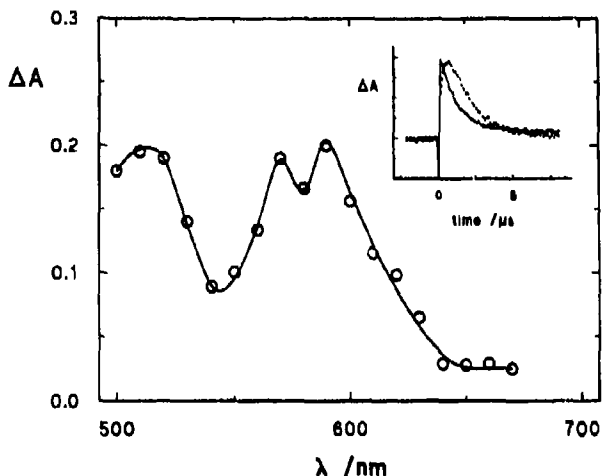


Figure 7. Transient absorption spectrum of the *cis*-1-StPy/Chl system in MeCN recorded 0.6 μ s after the laser pulse ($\lambda_{exc} = 308$ nm). Inset: decay kinetics at 510(—) and 580(-----) nm.

radical ions, thus contributing to the overall photoreaction quantum yield. For the *cis* isomers investigated here (1-StPh, 9-StPh and 1-StPy), laser irradiation of *cis*-DAE/Chl produced the radical cation in the *trans* configuration (as indicated by comparison with the transients obtained after direct sensitization of the *trans* isomers and by its mono-exponential decay) due to the fast *cis*⁺ \rightarrow *trans*⁺ twisting. Such behaviour is different from that found for *cis*-stilbene in the presence of Chl and reported with different acceptors by other authors (Lewis *et al* 1985; Tokumaru *et al* 1991; Kuriyama *et al* 1992), which showed biexponential decay assigned to the *cis*⁺ (shorter-lived) and *trans*⁺ (longer-lived) contributions. This difference can be due to a smaller barrier to twisting for the radical cations of the present compounds. A study of the temperature effect is in progress to confirm such hypothesis. Figure 7 shows an example for the system *cis*-1-StPy/Chl in MeCN. The transient spectrum at room temperature was assigned to the radical cation in the *trans* configuration (see figure 4) formed after ³Chl* sensitization of the *cis* cation. The *trans*⁺ absorption was found to increase by addition of LiClO₄ and by increasing the *cis* concentration (chain mechanism) as reported for *cis*-stilbene (Lewis *et al* 1985). Such effects indicate that the alkali metal cation protects the olefin radical cation from recombination with the acceptor radical anion (back transfer) (Lewis *et al* 1985) or with the superoxide anion (formed by Chl⁻ + O₂) (Kuriyama *et al* 1992; Tokumaru *et al* 1991).

Acknowledgement

Financial support by the Italian Consiglio Nazionale delle Ricerche (Progetto Finalizzato Chimica Fine e Secondaria II) and Ministero per l'Università e la Ricerca Scientifica e Tecnologica (Rome) is gratefully acknowledged.

References

- Aloisi G G, Bartocci G, Fuvaro G and Mazzucato U 1980 *J. Phys. Chem.* **84** 2020
 Aloisi G G and Elisei F 1990 *J. Phys. Chem.* **94** 5813
 Aloisi G G, Elisei F and Görner H 1991a *J. Phys. Chem.* **95** 4225
 Aloisi G G, Elisei F and Latterini L 1992 *J. Chem. Soc., Faraday Trans.* **88** 2139
 Aloisi G G, Elisei F, Mazzucato U and Prats M 1991b *J. Photochem. Photobiol.* **A62** 217
 Aloisi G G, Masetti F, Elisei F and Mazzucato U 1988 *J. Phys. Chem.* **92** 3394
 Aloisi G G, Mazzucato U, Birks J B and Minuti L 1977 *J. Am. Chem. Soc.* **99** 6340
 Arai T, Karatsu T, Misawa H, Kuriyama Y, Okamoto H, Hiresaki T, Furuuchi H, Zeng H, Sakuragi H and Tokumaru K 1988 *Pure Appl. Chem.* **60** 989
 Bartocci G, Masetti F, Mazzucato U and Marconi G 1984 *J. Chem. Soc., Faraday Trans.* **2**, **80** 1093
 Bartocci G, Masetti F, Mazzucato U, Spalletti A, Baraldi I and Momicchioli F 1987 *J. Phys. Chem.* **91** 4733
 Bartocci G, Mazzucato U and Bortolus P 1976/77 *J. Photochem.* **6** 309
 Bartocci G, Mazzucato U, Spalletti A, Orlandi G and Poggi G 1992 *J. Chem. Soc., Faraday Trans.* **88** 3139
 Elisei F, Aloisi G G and Masetti F 1992 *J. Chem. Soc., Faraday Trans.* **88** 2155
 Elisei F, Aloisi G G and Mazzucato U 1990 *J. Phys. Chem.* **94** 5818
 Elisei F, Mazzucato U and Görner H 1989 *J. Chem. Soc., Faraday Trans.* **1** **85** 1469
 Görner H, Elisei F and Aloisi G G 1992 *J. Chem. Soc., Faraday Trans.* **88** 29
 Görner H and Schulte-Frohlinde D 1979 *J. Phys. Chem.* **83** 3107
 Gutierrez A R and Whitten D G 1976 *J. Am. Chem. Soc.* **98** 6233
 Kuriyama Y, Arai T, Sakuragi H and Tokumaru K 1992 *Chem. Lett.* 879
 Lewis F D 1979 *Acc. Chem. Res.* **12** 152
 Lewis F D, Petacci J R, Oxnian J D and Nepras M J 1985 *J. Am. Chem. Soc.* **107** 203
 Lewis F D, Reddy G D and Bassani D 1992 *J. Photochem. Photobiol.* **A65** 205 and references therein
 Lewis F D and Simpson J T 1979 *J. Phys. Chem.* **83** 2015
 Mazzucato U 1982 *Pure Appl. Chem.* **54** 1705
 Mazzucato U 1987 *Gazz. Chim. Ital.* **117** 661
 Mazzucato U, Aloisi G G and Masetti F 1982 *J. Photochem.* **18** 211
 Mazzucato U and Momicchioli F 1991 *Chem. Rev.* **91** 1679
 Mazzucato U, Spalletti A, Bartocci G and Galluzzo G 1993 *Coord. Chem. Rev.* **125** 251
 Saltiel J and Charlton J L 1980 *Rearrangements in ground and excited states* (ed.) P de Mayo (New York: Academic Press) vol. 3, p. 25
 Saltiel J and Sun Y -P 1990 *Photochromism: Molecules and systems* (eds) H Dürr and H Bouas-Laurent (Amsterdam: Elsevier) p. 64
 Sundros K and Becker H -D 1987 *J. Photochem.* **39** 301
 Spalletti A, Bartocci G, Mazzucato U and Galluzzo G 1991 *Chem. Phys. Lett.* **186** 29
 Tokumaru K and Arai T 1992 *J. Photochem. Photobiol.* **A65** 1
 Tokumaru K, Kuriyama Y, Arai T, Lednev I K, Akaba R and Sakuragi H 1991 *Photocromatic processes in organized molecular systems* (ed.) K Onda (Amsterdam: Elsevier) p. 199
 Watkins A R 1973 *J. Phys. Chem.* **77** 1207
 Watkins A R 1974 *J. Phys. Chem.* **78** 1885, 2555

Photo-induced charge separation by ruthenium(II) photosensitizers

HAI SUN and MORTON Z HOFFMAN*

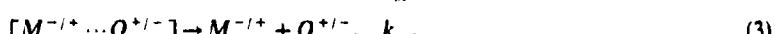
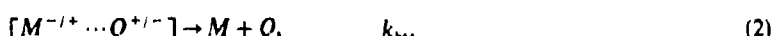
Department of Chemistry, Boston University, Boston, MA 02215, USA

Abstract. The values of the cage escape yields of redox products (η_{ce}) were determined for the reductive quenching of the excited states of homo- and heteroleptic complexes of Ru(II) and 2,2'-bipyridine (bpy), 2,2'-bipyrimidine (bpm), and 2,2'-bipyrazine (bpz) by triethanolamine (TEOA) as a sacrificial reductive quencher in aqueous, acetonitrile, and propylene carbonate solutions. In aqueous solution, η_{ce} varies with the standard reduction potential (E^0) of the complex, describing a weak dependence. The values of η_{ce} are independent of E^0 in propylene carbonate, but exhibit an inverted dependence in acetonitrile; the values of η_{ce} in acetonitrile are generally higher than those in aqueous and propylene carbonate solutions, due to the higher diffusional rate constant for cage escape of the redox geminate pair in acetonitrile. The variable dependencies of η_{ce} in the different solvents on the driving force of back electron transfer require that the conventional model be modified to account for the reorientation of the geminate pair within the solvent cage.

Keywords. Charge separation; photochemistry; ruthenium(II) complexes; photosensitizers; electron transfer.

1. Introduction

The yield of redox products (η_{ce}) released into bulk solution upon electron-transfer quenching is the critical parameter governing the efficacy of a redox photosensitizer; Ru(II) complexes are among the most popular and effective photosensitizers. In the simplest model (1)–(3) below, the quenching reaction can be visualized as occurring via the formation of a geminate redox pair within a solvent cage as a result of the transfer of one electron, with η_{ce} a measure of the competition between back electron transfer (k_{bt}) and diffusional escape of the redox products (k_{ce}) (Balzani and Scandola 1983). According to this model, the experimental determination of η_{ce} , the calculation of k_{ce} from (4) and (5) below, and the application of the equations that describe the diffusion of species in fluid solution permit the dependence of energetics and solution medium on k_{bt} to be evaluated. If, in a series of photosensitizer-quencher pairs, k_{ce} and the parameters that affect k_{bt} , except ΔG_{bt}^0 , can be kept constant, the variation of η_{ce} would be dependent only on the variation of the exoergicity of the back electron transfer reaction.



*For correspondence

$$\eta_{ce} = \frac{k_{ce}}{k_{ce} + k_{bi}}, \quad (4)$$

$$\frac{k_{bi}}{k_{ce}} = \frac{1}{\eta_{ce}} - 1. \quad (5)$$

The back electron-transfer reaction of the geminate redox pair within the solvent cage is a subset of the general phenomenon of intramolecular electron transfer, for which many examples of well-defined dependencies of k_{ce} on the reaction driving force in accord with Marcus' theory are now in the literature. Recently, Yonemoto *et al* (1992) reported on the values of k_{ce} for the forward electron transfer between the MLCT excited state of Ru(II) and covalently bound viologen acceptors, and the back electron transfer between the Ru(III) center and the reduced viologen radical; the dependence on ΔG^0 of the reactions traversed the "normal" and "inverted" Marcus regions. However, when the viologens are uncoupled from the complex and act as bimolecular quenchers, the plot of $\ln(\eta_{ce}^{-1} - 1)$ vs ΔG^0 is very scattered and does not show any evident correlation. A very weak (or no) correlation of $\ln(\eta_{ce}^{-1} - 1)$ vs ΔG_{bi}^0 was also obtained for the oxidative quenching of the excited states of nine Ru(II) complexes by methylviologen (4,4'-dimethylpyridinium dication; MV²⁺) (Ohno *et al* 1991) as well as no evident dependency for the reductive quenching of a derivative of *Ru(bpy)₃²⁺ (bpy = 2,2'-bipyridine) by aromatic amines (Ohno *et al* 1993). On the other hand, Ohno *et al* (1986, 1987, 1989, 1990) obtained very dramatic "bell-shaped" curves for the quenching of the excited states of Ru(II) complexes by aromatic amines and methoxybenzenes. These conflicting results suggest the need to investigate further the validity of the simple model.

In this work, values of η_{ce} for the reductive quenching of the excited states of a series of Ru(II) complexes that contain bpy, bpm (2,2'-bipyrimidine) and bpz (2,2'-bipyrazine) ligands by TEOA (triethanolamine) were determined in aqueous, acetonitrile and propylene carbonate solution. In this way, a common quencher is used and the complexes all have the same size, shape, and charge: the use of the different solvents permits a variation in viscosity and dielectric constant, which will affect the value of k_{ce} in a systematic way.

2. Experimental

The Ru(II) complexes (RuL²⁺) were from our laboratory supply; their structures and abbreviations are shown in figure 1, and their photophysical and electrochemical properties are given in table 1. Methylviologen dichloride (Aldrich) was converted to the PF₆⁻ salt and was recrystallized three times from water. TEOA (Fluka) and propylene carbonate (Fluka) were fractionally distilled thrice. Acetonitrile (Aldrich Optima) was used without further purification. Distilled water was further purified by passage through a Millipore purification train. All quencher solutions were freshly prepared prior to use. The pH values of the solutions were set at 10·0 with the use of 1–3 mM borax buffer.

Solutions contained 50 μM Ru(II), 2–7 mM MV²⁺, and up to 0·6 M TEOA. The excitation wavelength for the continuous photolysis was chosen as the absorption maximum of the 400-nm charge transfer band for each complex under examination.

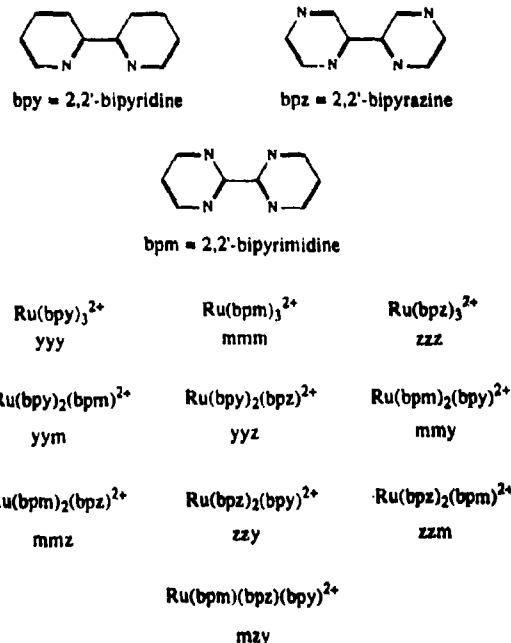


Figure 1. Structures of and notations for the Ru(II) photosensitizers used in this study.

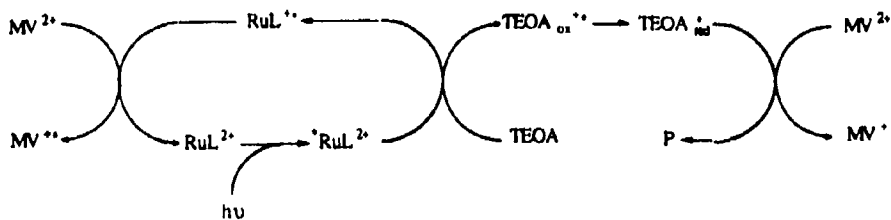
The concentration of the reduced methylviologen radical cation ($MV^{+ \cdot}$) was evaluated from its absorbance at 605 nm by taking $\epsilon_{605} = 1.37 \times 10^4 M^{-1} cm^{-1}$ (Watanabe and Honda 1982).

The continuous photolysis experiments were performed using a Bausch & Lomb high-intensity monochromator in conjunction with a 100 W quartz-halogen lamp; the light intensity was monitored by an associated photon counter that was calibrated by potassium ferrioxalate actinometry. In a typical experiment, 4 ml of Ar-purged

Table 1. Photophysical and electrochemical properties of Ru(II) photosensitizers in aqueous solution.

Complex	λ_{em} (nm)	t_0 (μs)	$E^\circ(2+/+)$ (V)*	$E^\circ(*2+/+)$ (V)*
zzz	602	0.94	-0.50	1.68
zzm	613	0.71	-0.55	1.63
mmz	634	0.52	-0.61	1.43
zzy	640	0.40	-0.63	1.44
mzy	666	0.22	-0.67	1.33
zyy	695	0.092	-0.77	1.16
mmm	622	0.077	-0.73	1.34
mmy	660	0.044	-0.77	1.28
myy	680	0.014	-0.83	1.15
yyy	610	0.060	-1.22	0.93

*D'Angelantonio *et al* (1991)

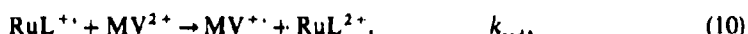
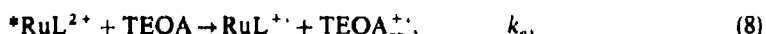
Figure 2. Reaction scheme for the $\text{RuL}^{2+}/\text{TEOA}/\text{MV}^{2+}$ system.

and magnetically stirred solution was contained in a sealed 1×1 cm spectrofluorimeter cuvette.

3. Results and discussion

3.1 Cage escape yields

The mechanism for the quenching of ${}^*\text{RuL}^{2+}$ by TEOA in the presence of MV^{2+} can be expressed by (6)–(11) below, where $\text{TEOA}_{\text{ox}}^{+*}$ is the cation radical produced as a result of the one-electron oxidation of TEOA, and $\text{TEOA}_{\text{red}}^{+}$ is the reducing radical derived from the irreversible transformation of $\text{TEOA}_{\text{ox}}^{+*}$.



The generation of the lowest energy luminescent excited state with an efficiency of ~ 1 via (6) is followed by quenching (8), in competition with the natural decay of ${}^*\text{RuL}^{2+}$ (7), forming RuL^{+} and $\text{TEOA}_{\text{ox}}^{+*}$ in bulk solution. $\text{TEOA}_{\text{ox}}^{+*}$ undergoes transformation (9) ($k_{tr} = 3.3 \times 10^6 \text{ M}^{-1} \text{ s}^{-1}$) (Chan *et al.* 1981), converting the oxidative species to a reductive one ($\text{TEOA}_{\text{red}}^{+}$). Both RuL^{+} and $\text{TEOA}_{\text{red}}^{+}$ reduce MV^{2+} to MV^{+} (10) and (11) with rate constants in the order of $10^8\text{--}10^9 \text{ M}^{-1} \text{ s}^{-1}$ (D'Angelantonio *et al.* 1991). The reaction scheme is given in figure 2.

The efficiency of the quenching reaction, η_q , is the result of the competition between the natural decay (7) and the electron transfer quenching (8) of the excited states, and can be expressed as (12) below. The efficiency of (8) with regard to the escape of the redox pair from the solvent cage, in which they were generated by the quenching interaction, into the bulk solution is given by (4). The quantum yield of MV^{+} formation for the system upon continuous photolysis is given in (13) below.

$$\eta_q = \frac{k_q[D]}{k_0 + k_q[D]}, \quad (12)$$

$$\Phi(\text{MV}^{+}) = 2\eta_{ce}\eta_q. \quad (13)$$

The excited states of six complexes (zzz, mmz, zzy, zzm, mzy, mmm) in aqueous solution and all but Ru(bpy)₃²⁺ in acetonitrile and propylene carbonate were quenched by TEOA; the values of $\Phi(MV^{+})$ were determined in all three solvents. As predicted by (13), plots of $\Phi(MV^{+})$ vs η_{ϵ} were, indeed, all linear, and the values of η_{ϵ} were obtained from such plots; examples of the plots are given in figure 3. Taking $E^0(TEOA_{ox}^{+}/TEOA) = 0.84$ V (Sun and Hoffman 1993), the standard free energy change for the back electron-transfer between RuL^{2+} and $TEOA_{ox}^{+}$ (ΔG_{bi}^0) can be

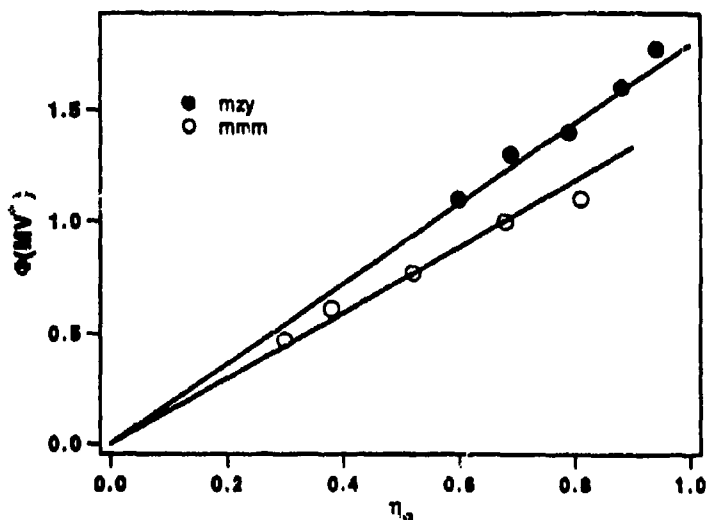


Figure 3. Plots of $\Phi(MV^{+})$ vs η_{ϵ} for $RuL^{2+}/TEOA/MV^{+}$ systems in acetonitrile.

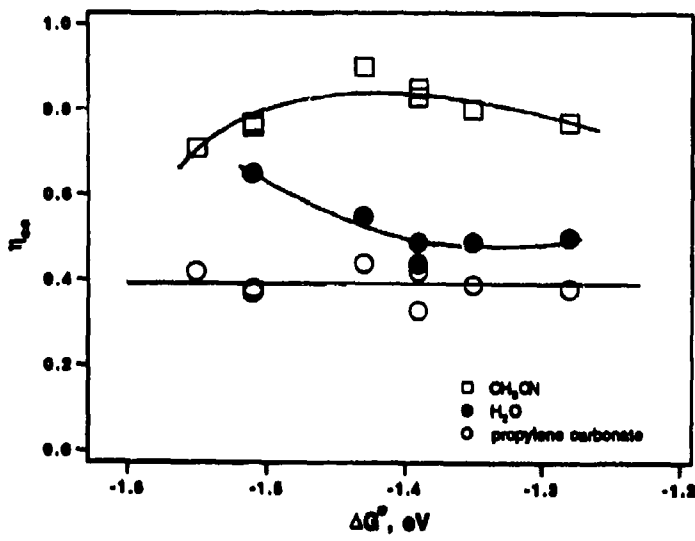


Figure 4. Plots of η_{ϵ} vs ΔG_{bi}^0 for aqueous, acetonitrile, and propylene carbonate solutions.

estimated from the excited state reduction potentials (table 1) (D'Angelantonio *et al.* 1991). Plots of η_{ce} vs ΔG_{hi}^0 are given in figure 4. The data in propylene carbonate show no dependence of η_{ce} on ΔG_{hi}^0 . In aqueous solution, η_{ce} increases as ΔG_{hi}^0 becomes more negative, suggesting that k_{hi} decreases as the reaction driving force is increased, which is "inverted" Marcus behavior. However, the data in acetonitrile show the opposite dependence of η_{ce} on ΔG_{hi}^0 to that obtained in aqueous solution, although the variation of η_{ce} is smaller. Overall, the dependencies of η_{ce} on ΔG_{hi}^0 are rather weak, especially for propylene carbonate and acetonitrile solutions; the values of η_{ce} in the different solvents reflect the variation of solution medium parameters, especially the viscosity.

The weak dependencies of η_{ce} on ΔG_{hi}^0 observed in this work (and in other studies) are in sharp contrast to the predicted bell-shaped curves, and those reported earlier, suggesting that the kinetic events within the solvent cage may be very different from that of the simple model for those systems.

3.2 Solvent cage models

The observation of unpredicted dependencies of η_{ce} on ΔG_{hi}^0 indicates that the cage events may be more complicated than those described by (1)-(3). Before modifications are made to the model, it should be noted that in the reductive quenching of the MLCT excited state of Ru(II) complexes, which can be described as possessing a one-electron reduced ligand coordinated to a Ru(III) center ($[\text{Ru}^{\text{III}}\text{L}^{\cdot-}]^{2+}$), different orbitals in the complex are involved in the quenching reaction and back electron-transfer reaction within the cage. The electron-rich quencher might approach the excited complex at a side opposite to the reduced ligand, and transfer its electron into the t_{2g} orbital of the metal center. However, back electron-transfer occurs between the reduced ligand and the oxidized quencher, they are well separated, and are in a sterically unfavorable position for rapid transfer unless the geminate pair undergoes reorientation to permit the establishment of overlap (or coupling) between the donating and accepting orbitals (figure 5). Similarly, for the oxidative quenching of the MLCT

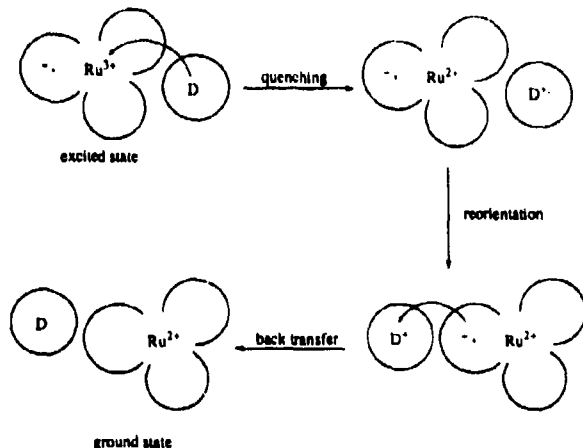


Figure 5. Schematic diagram of the reductive quenching of ${}^*\text{Ru}(\text{II})$ complexes by an electron donor and the subsequent reorientation and back electron-transfer reactions.

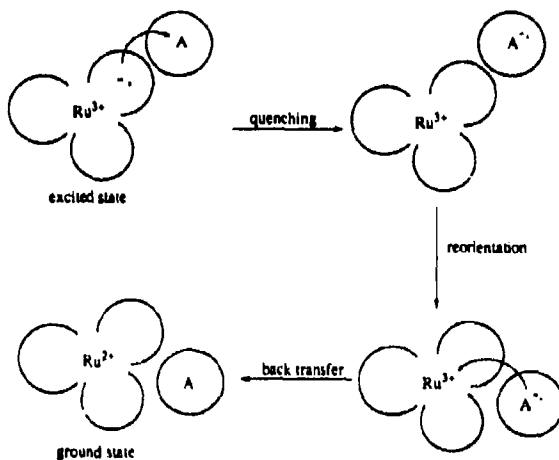
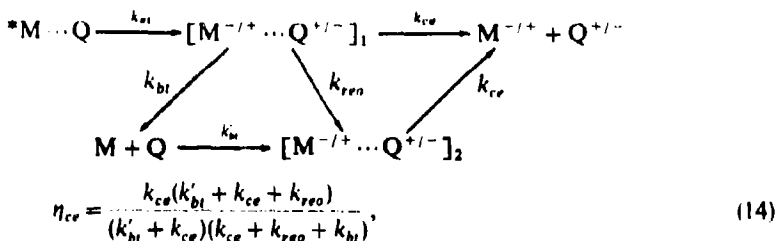


Figure 6. Schematic diagram of the oxidative quenching of ${}^*\text{Ru}(\text{II})$ complexes by an electron acceptor and the subsequent reorientation and back electron-transfer reactions.

excited state of Ru(II) complexes, the quencher might approach the electron-rich reduced ligand of the excited state and accept the electron from its π^* orbital in the quenching act, and then donate the electron to the metal center d orbital in the back transfer process. A reorientation process may be needed to reposition the redox pair and allow the establishment of the orbital overlapping (or coupling) between the two donating and accepting orbitals (figure 6).

We wish to propose a modification to the cage model in order to account for the increasing body of evidence that values of η_{ce} in bimolecular quenching reactions involving Ru(II) sensitizers are weakly dependent, if at all, on ΔG_m^0 . In this new model, $[\text{M}^{-/+} \dots \text{Q}^{+/-}]_1$ and $[\text{M}^{-/+} \dots \text{Q}^{+/-}]_2$ represent the solvent cage before and after the reorientation processes, respectively, k_{rea} is the rate constant for reorientation, and k'_{bt} is the back electron-transfer rate constant after the reorientation has occurred. By applying the steady-state approximation to $[\text{M}^{-/+} \dots \text{Q}^{+/-}]_2$, (14) and (15) are obtained.



$$\frac{1}{\eta_{ce}} - 1 = \frac{k_{bt}k'_{bt} + k_{bt}k_{ce} + k'_{bt}k_{rea}}{k_{ce}(k'_{bt} + k_{ce} + k_{rea})}. \quad (15)$$

There are two limiting cases for which (14) and (15) can be simplified. If $k_{rea} \ll k_{bt}$ and $k_{rea} \ll k_{ce}$, (15) reduces to (5); the previous model can be viewed as a limiting case in which the reorientation process is very slow compared to back electron-transfer

and cage escape. If, on the other hand, the back transfer in $[M^{-/+} \cdots Q^{+/-}]_1$ is very slow due to an unfavorable orientation of the reacting species ($k_{bi} \ll k_{reo}$ and $k_{bi} \ll k_{ce}$), and the back transfer in $[M^{-/+} \cdots Q^{+/-}]_2$ is faster than cage escape ($k_{bi} \gg k_{ce}$), (15) is reduced to (16) below; η_{ce} becomes a measure of the competition between the cage escape and reorientation processes. Thus, the observed weak or negligible dependencies of η_{ce} on ΔG_{bi}^0 can be viewed as representing this limiting case, since k_{reo} is not expected to be dependent on the driving force of the back electron-transfer reaction.

$$(1/\eta_{ce}) - 1 = k_{reo}/k_{ce}. \quad (16)$$

For intermediate cases, (14) and (15) would be operative, resulting in a range of observed dependencies of η_{ce} on ΔG_{bi}^0 that are functions of the magnitudes of the rate constants of the mechanistic steps. Of course, the reorientation process, like cage escape and back electron-transfer, will be dependent on the solvent and the counter ions within the cage. The various rate constants are likely to have different activation parameters, resulting in further changes in the functional relationships between η_{ce} and ΔG_{bi}^0 with changes in temperature. The challenge for the future is to discover the molecular features that control the values of the rate constants in order to be capable of fine-tuning the efficiency of photoinduced charge separation in excited state quenching reactions.

Acknowledgements

This research was supported by the Office of Basic Energy Sciences, US Department of Energy.

References

- Balzani V and Scandola F 1983 *Energy resources through photochemistry and catalysis* (ed.) M Grätzel (New York: Academic Press) pp. 1–48
- Chan S F, Chou M, Creutz C, Matsubara T and Sutin N 1981 *J. Am. Chem. Soc.* **103** 369
- D'Angelantonio M, Mulazzani Q G, Venturi M, Ciano M and Hoffman M Z 1991 *J. Phys. Chem.* **95** 5121
- Ohno T, Yoshimura A and Mataga N 1986 *J. Phys. Chem.* **90** 3295
- Ohno T, Yoshimura A and Mataga N 1990 *J. Phys. Chem.* **94** 4971
- Ohno T, Yoshimura A, Mataga N, Tazuke S, Kawanishi Y and Kitamura N 1989 *J. Phys. Chem.* **93** 3546
- Ohno T, Yoshimura A, Prasad D R and Hoffman M Z 1991 *J. Phys. Chem.* **95** 4723
- Ohno T, Yoshimura A, Prasad D R and Hoffman M Z 1993 (in preparation)
- Ohno T, Yoshimura A, Shioyama H and Mataga N 1987 *J. Phys. Chem.* **91** 4365
- Sun H and Hoffman M Z 1993 (in preparation)
- Watunabe T and Honda K 1982 *J. Phys. Chem.* **86** 2617
- Yonemoto E H, Riley R L, Kim Y I, Atherton S J, Schmehl R H and Mallouk T E 1992 *J. Am. Chem. Soc.* **114** 8081

Photoinduced ET and back-ET in bimetallic compounds of Ru(II)–Rh(III) and Ru(II)–Co(III)

K NOZAKI, A YOSHIMURA and T OHNO*

Chemistry Department, College of General Education, Osaka University, Toyonaka, Osaka 560, Japan

Abstract. Intramolecular electron transfer processes in bimetallic donor-acceptor compounds have been investigated by means of laser photolysis kinetic spectroscopy. An excited Ru(II)-moiety of donor-acceptor compounds undergoes intramolecular electron-transfer to either a rhodium(III) ion or a cobalt(III) ion, followed by back-electron transfer. An Arrhenius plot of the electron-transfer-rate gave a straight line of intercept (frequency factor) and slope (activation energy) for the photoinduced electron transfers and the back electron transfers. A common and large frequency factor observed for Ru(II)–Rh(III) compounds is accounted for in terms of solvent-relaxation dynamics. The activation energy observed consists ofoutersphere rearrangement energy depending on the metal ion-metal ion distance. For the photoinduced electron transfers and subsequent back-electron transfers in the Ru(II)–Co(III) compounds, the electron-transfer-rates are reduced because of weak electronic coupling, large rearrangement energy and negative entropy change.

Keywords. Donor-acceptor linked compound; electron transfer; nuclear tunnelling; temperature-dependence of ET rate; rearrangement energy.

1. Introduction

Electron transfer (ET) is one of the chemical reactions that have been most intensively investigated. The reaction rate of ET is given in (1) below for nonadiabatic ET by assuming no change of force constants between the initial and final states (Kestner *et al.* 1974; Ulstrup and Jortner 1975). Equation (1) indicates that the rate depends on many factors, electronic coupling (H_{rp}), energy gap between the reactant and the product (ΔG°), rearrangement energy involved in ET (λ), vibronic coupling strength (S), and angular vibrational frequency of the product (ω).

$$k = \frac{2\pi|H_{rp}|^2}{\hbar(4\pi k_B T \lambda)^{1/2}} \sum_n \frac{(e^{-S} S^n)}{n!} \exp\left(-\frac{(\Delta G + \lambda + n\hbar\omega)^2}{4\lambda k_B T}\right), \quad (1)$$

$$k = \frac{2\pi|H_{rp}|^2}{\hbar(4\pi k_B T)^{1/2}} \exp\left(-\frac{(\Delta G + \lambda)^2}{4\lambda k_B T}\right), \quad (2)$$

$$\ln k T^{1/2} = \ln A - (E_a/k_B T), \quad (3a)$$

$$A = [2\pi|H_{rp}|^2]/[\hbar(4\pi k_B \lambda)^{1/2}], \quad (3b)$$

$$E_a \approx (\Delta G^\circ + \lambda)^2/(4\lambda k_B T). \quad (3c)$$

*For correspondence

When the energy gap is much smaller than the rearrangement energy, nuclear tunnelling followed by vibrational excitation of the product can be neglected and the rate formula is close to (2) presented by Marcus earlier (1956, 1965), which is recast to a more simple form (3). A is the frequency factor which depends on nuclear frequency and electronic coupling. E_a is the apparent activation energy depending on energy gap and rearrangement energy. This paper is devoted to the understanding of both A and E_a , which could be obtained from the temperature-dependence of rates of intramolecular ET in donor-acceptor linked compounds.

When the energy gap between initial and final states is so small that no vibrational excitation of the product occurs, decrease in temperature reduces the rate of ET to a large extent. The temperature-dependence of the ET rate allows us to estimate the frequency factor and the activation energy separately.

However, if the force constants of the final state differ from those of the initial state, rearrangement of the inner-coordination shell of the final state gives rise to rearrangement energy and entropy change. The entropy change accompanied by a change of vibrational state density enhances or reduces the frequency factor depending on a positive or negative value of the entropy change, because a term of $\exp[\Delta S^*/k_B]$ appears as a factor in A . It may make the frequency factor hard to interpret without estimation of ΔS^* .

When a high frequency vibrational mode of the product is coupled with ET, the ET rate is weakly dependent on both temperature and energy gap in a high energy-gap region (Liang *et al* 1990; Bixon and Jortner 1991). Only when nuclear tunnelling followed by vibrational excitation in a highly exergonic ET does not occur because of no vibrational overlap between the reactant and the product, the rate of ET might be dependent on temperature.

2. Estimation of rearrangement energy and bridging ligand mediated electronic coupling

(Ohno *et al* 1992) Samples studied in this research on photoinduced ET are donor-acceptor linker compounds. Two kinds of metal ions as donors and acceptors are linked by a bridging ligand containing a biphenyl moiety, benzene moiety, or

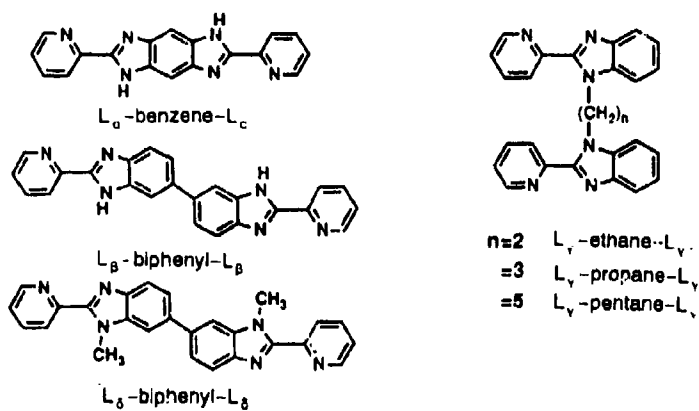


Figure 1. Bridging ligands and abbreviations.

methylene chain as a spacer. The general formula of the sample compounds is $[(\text{bpy})_2\text{Ru}(\text{L}-\text{spacer}-\text{L})\text{M}(\text{bpy})_2]^{5+}$ shown in figure 1, where bpy denotes 2,2'-bipyridine, L denotes a bidentate coordinating group of 2-(2'-pyridyl)imidazole, M denotes ruthenium, rhodium or cobalt. Intramolecular bonds and size of a spacer controls electronic coupling (Larsson 1981, 1984) and rearrangement energy (Brunschwig *et al.* 1984; Isied *et al.* 1988).

Photoexcitation of a Ru(II)-Rh(III) compound produces either an excited Ru(II) or an excited Rh(III) which undergoes ET to generate a charge-shifted state of Ru(III)-Rh(II) in which a back-ET from Rh(II) to Ru(III) subsequently takes place. It is known that redox processes of both ruthenium and rhodium compounds take place with small changes of the metal-ligand bond and intra-ligand bonds (Creutz *et al.* 1982; Sutin and Creutz 1983). In other words, innersphere-rearrangement energy is negligibly small for ET processes of ruthenium and rhodium compounds.

An intramolecular ET within an M(II)-M(III) compound accompanies reorientation of solvent molecules to a charge-shifted state of M(III)-M(II). Charge-transfer photoexcitation of an Ru(II)-moiety causes a small amount of solvent reorientation around the excited Ru(II)-Rh(III) compound. An electron transfer from the Ru(II)-moiety to the Rh(III)-moiety is followed by rearrangement of solvent molecules surrounding the Ru(II)-Rh(III). Otherwise, the electron on the Rh-moiety goes back to the Ru-moiety so that the charge transfer excited state of the Ru-moiety suffers no quenching.

In the optical charge transfer transition of a mixed-valence symmetric Ru(II)-Ru(III) compound, an electron-jump from the left Ru(II) to the right Ru(III) generating a charge-shifted state of Ru(III)-Ru(II) is followed by rearrangement of solvent molecules to generate a newly solvated state of the Ru(III)-Ru(II) compound. Provided that the energy of a charge-shift state (Ru(III)-Ru(II)) is the same as that of original state (Ru(II)-Ru(III)), the transition energy of optical charge transfer is assumed to be the same as the nonvertical rearrangement energy of solvent molecules surrounding a charge-shift state of Ru(III)-Ru(II) (Creutz 1983). The nonvertical rearrangement energy increases with center-center distance between the metal ions because of more solvent molecules reorientating to the Ru(III)-Ru(II) compound.

The extent of bridging ligand-mediated electronic coupling between Ru(II) and Ru(III) can be estimated from an integrated intensity of the optical charge transfer transition (Hush 1967). The electronic coupling strength between the metal ions only depends on the intramolecular bonds and size of a spacer, since coordination bonds

Table 1. Electronic coupling (H_{rp}) andoutersphere rearrangement energy (λ) estimated from the intensity and the energy of optical charge transfer transition of $[(\text{bpy})_2\text{Ru}^{\text{II}}(\text{L}-\text{spacer}-\text{L})\text{Ru}^{\text{III}}(\text{bpy})_2]^{5+}$ in acetonitrile at 298 K.

Bridging ligand	Metal-metal distance* (nm)	λ (eV)	H_{rp} (meV)
L ₂ -benzene-L ₂	0.8	0.76	58
L ₂ -biphenyl-L ₂	1.2-1.5	0.91	7.5 ~ 10
L ₂ -biphenyl-L ₂	1.3	0.96	22
L ₂ -ethane-L ₂	1.1	0.96	8.7

*Estimated by using a molecular model

of 2-(2'-pyridyl)imidazole moieties to metal ions are kept constant among the bridging ligands used here. When the ET process is nonadiabatic, the observed extent of the electronic coupling between metal ions must be reflected on the ET rates.

Broad absorption bands of the Ru(II)-benzene-Ru(III), the Ru(II)-biphenyl-Ru(III), and the Ru(II)-ethane-Ru(III) compounds observed in the near infrared region are assigned to a charge transfer band (Ohno *et al* 1992). Values of rearrangement energy and electronic coupling are estimated from the energy and intensity of the Ru(II)-to-Ru(III) charge-transfer transition (table 1). The extent of electronic coupling between the metal ions decreases with the spacers in the following order, benzene > biphenyl > ethane. The smallest rearrangement energy is obtained for the Ru(II)-benzene-Ru(III) with the shortest metal-metal distance.

3. ET on the excitation of Ru(II)-moiety in Ru(II)-Rh(III) compounds

(Nozaki *et al* 1992) A second harmonic pulse of the nano-second YAG laser excites the Ru-moiety of the Ru(II)-Rh(III) compound into the charge transfer state, which exhibits at a lower temperature a transient absorption spectrum similar to the metal-to-ligand charge transfer excited state of the Ru(II)-Ru(II) compound. The decay of the transient absorption in a mixture of propionitrile and butyronitrile becomes faster as temperature increases.

A nicely linear Arrhenius plot of the decay rate of the excited Ru(II)-moiety was obtained (figure 2). The Ru(II)-benzene-Rh(III) compound displays the fastest decay

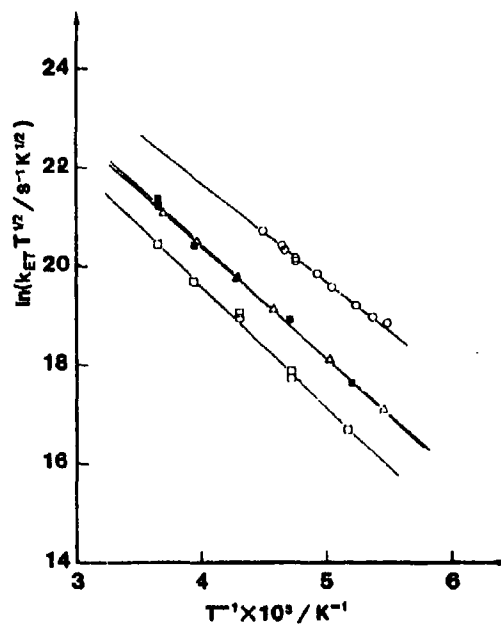


Figure 2. Arrhenius plots of photoinduced ET in $[(\text{bpy})_2\text{Ru}(\text{L-spacer-L}')\text{Rh}(\text{bpy})_2]^{5+}$. ○; $\text{L}_\text{b}-\text{benzene}-\text{L}'$, □; $\text{L}_\text{b}-\text{biphenyl}-\text{L}'$, ■; $\text{L}_\text{b}-\text{biphenyl}-\text{L}'$, Δ; $\text{L}_\text{b}-\text{ethane}-\text{L}'$.

Table 2. Photoinduced electron transfer of $[(\text{bpy})_2\text{Ru}(\text{L-spacer-L})\text{Rh}(\text{bpy})_2]^{n+}$ in mixed solvent (butyronitrile + propionitrile). Observed and calculated values of energy gap (ΔG°), Arrhenius frequency factor (A), and activation energy (E_a).

Bridging ligand	ΔG° (eV)	A (10^{11} s^{-1})	A^{cal} (10^{11} s^{-1})	E_a (eV)	E_a^{cal} (eV)
L _x -benzene-L _y	~0.02	4.1	5.7	0.166	0.17-0.18
L _x -biphenyl-L _y	~0.13	2.3	4.6	0.200	0.15-0.16
L _x -biphenyl-L _y	~0.08	3.2	4.5	0.190	0.185-0.195
L-ethane-L _y	~0.04	3.2	4.5	0.190	0.205-0.215
L-ethane-L _y	~0.04	0.6*	1.1-1.6*	0.172*	0.17-0.18*

*In benzonitrile

rate at a given temperature and the smallest slope of the linear plot among the Ru(II)-Rh(III) compounds. Table 2 shows a nearly constant frequency factor (A) of $2 \times 10^{11} \text{ s}^{-1}$ for the Ru(II)-Rh(III) compounds in the mixed solvent, which is in contrast to the variation in the extent of bridging ligand-mediated electronic coupling estimated from the optical charge-transfer transition intensities, and implies that the rate of ET is independent of the spacer.

Replacing the mixed solvent with benzonitrile reduced the frequency factor to 1/5. A slow longitudinal relaxation (5 ps) of benzonitrile compared with butyronitrile (0.5 ps) (Simon 1988) demonstrates that the solvent relaxation dynamics following ET is the rate-determining step. Therefore, the frequency factor is regarded as the nuclear frequency for the adiabatic ET studied.

$$k = v^\circ \exp(-E_m/RT) \exp(-\Delta G^\circ/RT), \quad (4a)$$

$$\Delta G^\circ = [(\Delta G^\circ + \lambda)^2/4\lambda] - |H_{rp}|. \quad (4b)$$

The nuclear frequency of ET processes can be estimated to be $3.9 \times 10^{11} \text{ s}^{-1}$ in butyronitrile and $0.85 \times 10^{11} \text{ s}^{-1}$ in benzonitrile at 298 K from the rotational and longitudinal relaxation times of the solvent molecules as per Calef and Wolynes (1983). If the temperature-dependence of Debye dielectric relaxation for benzonitrile is similar to that of butyronitrile ($E_m = 45 \text{ meV}$), the nuclear frequency at the infinitely high temperature (v°) can be calculated as $\sim 5 \times 10^{11} \text{ s}^{-1}$ for benzonitrile and $\sim 2.3 \times 10^{11} \text{ s}^{-1}$ for butyronitrile.

For an adiabatic ET controlled by solvent relaxation dynamics, the ET rate can be expressed as in (4), where ΔG° is given by energy gap (ΔG°), rearrangement energy (λ), and electronic coupling (H_{rp}). Let us assume that ΔG° is similar to ΔH° in magnitude and λ is close to theoutersphere rearrangement energy.

$$\ln A = \ln v^\circ + \frac{\alpha}{2k_B n^3} \frac{dn}{dT}, \quad (5a)$$

$$E_a = \frac{\Delta H^\circ}{2} + \frac{\alpha}{4n^2} \left(1 + \frac{2T}{n} \frac{dn}{dT} \right) - |H_{rp}| + E_m. \quad (5b)$$

The value ofoutersphere rearrangement energy is estimated from the optical charge transfer transition energy mentioned above. Finally, we obtained (5) for frequency

factor and activation energy for weakly exergonic ET, where α is structural constant depending on sizes of metal ions and metal–metal distance. The second terms of (5) come from the temperature dependence of refractive index ' n ', which theoutersphere-rearrangement energy is a function of. The values of A and E_a are calculated to be in the order of $2 \times 10^{11} \text{ s}^{-1}$ and $\sim 0.2 \text{ eV}$, respectively, by using (5a) and (5b), which are in agreement with the observed ones except for the Ru-biphenyl-Rh(III) compound, as table 2 shows.

4. ET and back ET on the excitation of Rh-moiety in Ru(II)-Rh(III) compounds

(Nozaki *et al* 1993) When the Rh-moiety of a Ru(II)-spacer-Rh(III) compound is excited by 317 nm picosecond pulse, ET from Ru to Rh is expected to occur rapidly because the energy gap of 0.6 eV is much larger than the energy gap of ET ($< 0.1 \text{ eV}$) on the excitation of Ru-moiety. The subsequent back-ET could be distinguished from the rapid ET.

Time evolution of transient absorption showed the fast decay of excited rhodium-moiety with a rate constant of $\sim 10^{10} \text{ s}^{-1}$ and the subsequent recovery of the Ru(II)-moiety with a rate constant of $1.2 \times 10^9 \text{ s}^{-1}$ for the Ru(II)-pentane-Rh(III) compound. The Ru(II)-propane-Rh(III) exhibited only a faster recovery of the Ru(II)-moiety with a rate constant of $4.7 \times 10^9 \text{ s}^{-1}$. The decay of the excited Rh-moiety of Ru(II)-propane-Rh(III) was hardly observed because of such a fast process. The back-ET of the Ru(II)-biphenyl-Rh(III) compound is a little faster (of the order of 10^{10} s^{-1}) at ambient temperature. Meanwhile, the ET rate estimated by putting the energy gap and the rearrangement energy into the classical Marcus equation of (3) is smaller than 10^8 s^{-1} because the energy gap is much larger ($\sim 2 \text{ eV}$) than the rearrangement energy. Nuclear tunnelling followed by the vibrational excitation is

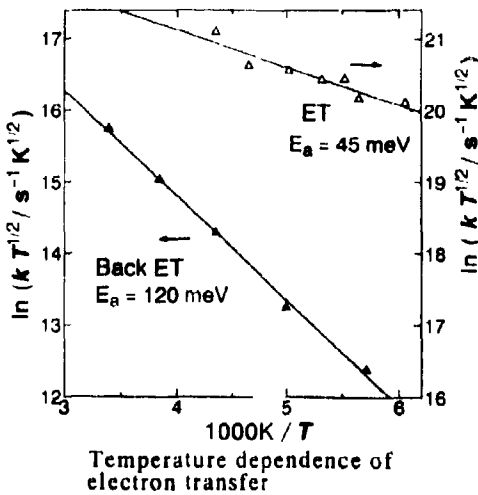


Figure 3. Arrhenius plots of photoinduced ET and subsequent back-ET in $[(\text{bpy})_2\text{Ru}(\text{L}-\text{pentane}-\text{L}')\text{Co}(\text{bpy})_2]^{3+}$; Δ : photoinduced ET, \blacktriangle : back-ET.

the only explanation for the much faster back-ET compared to the rate estimated by using the classical Marcus equation (3). The decreasing order of the rates in the Ru(II)-spacer-Rh(III) compounds (benzene > biphenyl > ethane > propane > pentane) is suggestive of non-adiabaticity of the back-ET processes in the spacer compounds.

5. ET and back ET on the excitation of the Ru(II)-moiety in Ru(II)-Co(III) compounds

(Yoshimura *et al* 1993) The second samples of donor-acceptor linked compounds studied consist of a ruthenium (II) ion and a cobalt (III) ion. The energy gap of the back-ET, which follows ET from an excited Ru(II)-moiety to a cobalt(III)-moiety, is changed from 880 meV at 200 K to 750 meV at 300 K. The standard entropy change (ΔS°) of -1.3 meV/K is responsible for the energy-gap change with temperature. An activation entropy (ΔS^*) is suspected to be involved in the activation process, because the transition state may have an intermediate amount of entropy between the entropy values of the reactant and the product (Hupp and Weaver 1984; Marcus and Sutin 1986). Provided that the activation entropy due to the rearrangement of the inner-coordination shell around a cobalt ion is as negligibly small as that around a ruthenium ion, (3) can be recast by using a temperature-dependent ΔG° into (6). The entropy change (ΔS^*) even in this case reduces apparent values of A and E_a , from which the frequency factor and the activation energy are obtained as shown in (6).

$$k = \frac{2\pi}{h} \frac{|H_{rp}|^2}{(4\pi k_B T \lambda)^{1/2}} \exp\left(\frac{(\Delta G^\circ + \lambda)\Delta S^*}{2\lambda k_B}\right) \exp\left(-\frac{(\Delta H^\circ + \lambda)^2 - (T\Delta S^\circ)^2}{4\lambda k_B T}\right) \quad (6)$$

A nicely linear plot between the natural logarithms of rate constant and the reciprocal of temperature gives values of an intercept and a slope (figure 3), from which the frequency factor and activation energy are obtained after the correction of entropy term as are shown in table 3. The extent of electronic coupling decreases from the Ru(II)-benzene-Co(III) to the Ru(II)-pentane-Co(III) compound. Since a similar trend in the extent of electronic coupling between an Ru(II) and an Ru(III) of the Ru(II)-Ru(III) compound, was obtained as mentioned above, the back-ET from Co(II) to Ru(III) can be regarded as a nonadiabatic process.

The rearrangement energy of ~ 2 eV observed can be decomposed to an innersphere-rearrangement energy of 1 eV and anoutersphere-rearrangement energy of ~ 1 eV. The large innersphere rearrangement energy is consistent with the longer bond-

Table 3. Back electron transfer in $[(bpy)_3Ru(L\text{-spacer}\text{-}L')Co(bpy)_3]^{3+}$ in acetonitrile: Energy gap (ΔG°), entropy change (ΔS°), Arrhenius frequency factor (A), activation energy (E_a), rearrangement energy (λ) and electronic coupling (H_{rp}).

Bridging ligand	ΔG° (eV)	ΔS° (meV/K)	A (10^9 s $^{-1}$)	E_a (meV)	λ (eV)	H_{rp} (meV)
L _x -benzene-L _y	-0.65	-1.3	300	77	1.8	5
L _x -biphenyl-L _y	-0.75	-1.3	40	87	2.05	2
L _x -pentane-L _y	-0.70	-1.3	1.5	120	2.2	0.4

distances of the Co(II)-ligand bonds than with those of the Co(III)-ligand bonds, which are seen for many cobalt compounds (Buhks *et al.* 1979; Endicott *et al.* 1981; Newton 1991). This may call into question the application of (6) to the Co(II)-to-Ru(III) electron-transfer. While the estimation of rearrangement energy might yield more error, the estimated values of $\sim 1\text{ eV}$ are not so strange.

Photoinduced ET of Ru(II)-moiety-to-Co(III) was also observed for Ru(II)-biphenyl-Co(III) and Ru(II)-pentane-Co(III) compounds. The rate of the forward-ET with the exergonicity of 0.6 eV is the following $\sim 1 \times 10^8\text{ s}^{-1}$ for the Ru(II)-pentane-Co(III) compound, $6 \times 10^9\text{ s}^{-1}$ for the Ru(II)-biphenyl-Co(III) compound and $> 5 \times 10^{10}\text{ s}^{-1}$ for the Ru(II)-benzene-Co(III) compound at ambient temperature. This trend suggests the nonadiabaticity of the forward-ET, though the frequency factors are not determined by extrapolating an Arrhenius plot of the ET rate constants. A very small activation energy of 0.045 eV for Ru(II)-pentane-Co(III) implies the formation of the doublet excited state of the Co(II)-moiety without change in entropy, which is followed by a rapid relaxation to the quartet ground state of the Co(II)-moiety.

6. Conclusions

Both rearrangement energy and extent of ligand-mediated electronic coupling between metal ions, which are estimated from transition energy and intensity of intramolecular CT transition band of Ru(II)-Ru(III) bimettallated compound, are dependent on the intramolecular bonds and the size of the spacer.

Meanwhile, the extent of electronic coupling and rearrangement energy involved in ET processes with a small exergonicity are evaluated from the temperature-dependence of ET rate.

Frequency factors for ET from an excited ruthenium-moiety to a rhodium-moiety with a small exergonicity is determined by solvent relaxation dynamics. Outersphere rearrangement energy estimated from the activation energy are dependent on the size of spacers of bridging ligands. Back-ET occurring via nuclear tunnelling from Rh(II) to Ru(III) with a high exergonicity is nonadiabatic.

ET from an excited ruthenium(II)-moiety to a cobalt-moiety with an intermediate exergonicity is nonadiabatic. Frequency factors for back-ET from a cobalt(II)-moiety to a ruthenium(II)-moiety is reduced by weak electronic coupling between the metal ions, and reduction in entropy. Activation energy for the back-ET of the Ru(III)-spacer-Co(II) compounds are also reduced by a negative entropy change and by an innersphere rearrangement energy in addition to the outersphere one.

References

- Bixon M and Jortner J 1991 *J. Phys. Chem.* **95** 1941
- Brunschwig B S, Ehrenson S and Sutin N 1984 *J. Am. Chem. Soc.* **106** 6858
- Buhks E, Bixon M, Jortner J and Navon G 1979 *Inorg. Chem.* **18** 2014
- Calef D F and Wolynes P G 1983 *J. Phys. Chem.* **87** 3387
- Creutz C 1983 *Prog. Inorg. Chem.* **30** 1
- Creutz C, Deller A D, Sutin N and Zipp A P 1982 *J. Am. Chem. Soc.* **104** 3618

- Endicott J F, Durham B, Glick M D, Anderson T J, Kuszaj J M, Schmonsees W G and Balakrishnan K P 1981 *J. Am. Chem. Soc.* **103** 1431
Hupp J T and Weaver M J 1984 *Inorg. Chem.* **23** 256
Hush N S 1967 *Prog. Inorg. Chem.* **8** 391
Isied S S, Vassilian A, Wishart J F, Creutz C, Schwartz H A and Sutin N 1988 *J. Am. Chem. Soc.* **110** 635
Kestner N R, Logan J and Jortner J 1974 *J. Chem. Phys.* **78** 2148
Larsson S 1981 *J. Am. Chem. Soc.* **103** 4034
Larsson S 1984 *J. Phys. Chem.* **88** 1321
Liang N, Miller J R and Closs G L 1990 *J. Am. Chem. Soc.* **112** 5353
Marcus R A 1956 *J. Phys. Chem.* **24** 966
Marcus R A 1965 *J. Phys. Chem.* **43** 679
Marcus R and Sutin N 1986 *Comment Inorg. Chem.* **119**
Newton M D 1991 *J. Phys. Chem.* **95** 30
Nozaki K, Ohno T and Haga M 1992 *J. Phys. Chem.* **96** 10880
Nozaki K, Ohno T, Hirata Y and Okada T 1993 *Photoinduced electron transfer and back electron transfer within bimetallic compounds of Ru(II) and Rh(III)* (to be published)
Ohno T, Nozaki K and Haga M 1992a *Inorg. Chem.* **31** 548
Ohno T, Nozaki K and Haga M 1992b *Inorg. Chem.* **31** 4256
Simon J D 1988 *Acc. Chem. Res.* **21** 128
Sutin N and Creutz C 1983 *J. Chem. Educ.* **60** 809
Ulstrup J and Jortner J 1975 *J. Chem. Phys.* **63** 4358
Yoshimura A, Nozaki K, Ikeda N and Ohno T 1993 *J. Am. Chem. Soc.* **115** 752

Photoinduced charge transfer processes in ultrasmall semiconductor clusters. Photophysical properties of CdS clusters in Nafion membrane

K R GOPIDAS[†] and PRASHANT V KAMAT*

Radiation Laboratory, University of Notre Dame, Notre Dame, Indiana 46556, USA

* Present address: Regional Research Laboratory, Trivandrum 695019, India

Abstract. The photophysical properties of quantized CdS clusters in a perfluorosulfonate polymer (Nafion) film have been investigated by time-resolved emission spectroscopy. The ultrasmall CdS clusters were prepared by exposing Cd²⁺-exchanged polymer film to H₂S. Size-dependent absorption and emission properties were observed during the growth of these clusters. The emission decay is multiexponential with lifetimes ranging from 0.85 to 480 ns.

Keywords. Semiconductor clusters; CdS; size quantization effect; Nafion; emission lifetimes

1. Introduction

Considerable attention has been given in recent years to the application of semiconductor colloids, powders and films for conversion of solar energy into electricity and chemical energy (Bard 1982; Kalyanasundaran *et al* 1986; Henglein 1988, 1989; Memming 1988; Grätzel 1989; Kamat and Dimitrijevic 1990; Kamat 1991, 1993). Of particular interest are the quantized semiconductor colloids which exhibit hybrid molecular solid state properties (Brus 1986; Henglein 1988, 1989; Bawendi *et al* 1990; Steigerwald and Brus 1990; Wang and Herron 1991; Kamat and Meisel 1993). These ultrasmall colloidal particles contain a high density of defect sites, usually at the semiconductor surface, and the nature of these defect sites depends strongly on the method of chemical synthesis. Upon optical excitation, the free carriers are rapidly trapped at the defect sites and these trapped charge carriers further undergo radiative and nonradiative recombination.

The mechanistic and kinetic details of the charge transfer processes in metal oxide (TiO₂, ZnO) and metal chalcogenides (CdS, CdSe) have been presented in our earlier studies (see, for example, Kamat and Dimitrijevic 1990, Kamat 1991, 1993, for detailed reviews on this topic). Both transient absorption and emission spectroscopy techniques have been employed to characterize the primary photophysical and photochemical events that occur in the picosecond millisecond time domain.

Efforts have also been made to prepare ultrasmall semiconductor particles in various heterogeneous environments (Fendler 1985, 1987; Wilner and Wilner 1988; Fox 1991). Microencapsulation of semiconductor particles in an organized medium controls not only the morphology but also the photocatalytic properties of the semiconductors. For example, metal chalcogenide clusters can easily be synthesized

* For correspondence

in a polymer film (Meisner *et al* 1983; Kuczynski *et al* 1984; Wang and Mahler 1987; Mahler 1988; Honda *et al* 1988; Nosaka *et al* 1989; Dalas *et al* 1990; Gopidas and Kamat 1990; Miyoshi *et al* 1990; Smotkin *et al* 1990; Misawa *et al* 1991; Yoneyama 1991). Such preparations provide isolated small semiconductor particles which are stabilized in an organized medium. In most of these studies, CdS has been the popular choice since it can be prepared easily by chemical precipitation and characterized readily by absorption and emission spectra. The photophysical properties of CdS clusters prepared in Nafion membrane are presented in this paper.

2. Experimental section

2.1 Materials

Nafion 117 in H⁺ form was obtained from Aldrich and H₂S gas was obtained from Matheson Gas Products. All other chemicals were analytical reagents and were used as supplied.

2.2 Sample preparation

The Nafion film was extracted with methanol for 4·5 h and was dried in an oven at 60°C for 24 h. The sodium-exchanged form of the Nafion was prepared by soaking the film in an aqueous solution of 1 M NaOH for 24 h and then washing thoroughly with deionized water. The film was then dried in the oven for 24 h. The optically transparent Nafion film was then cut into 0·5 × 4 cm pieces so that the film could conveniently be introduced into a 2 mm thick optical cell.

Cd²⁺ ions in the Nafion film were exchanged by immersing Na⁺-Nafion in a CdI₂ solution (100 ml of 10⁻⁵–10⁻³ M) for 30 min to 3 h. The film was then thoroughly washed with deionized water and dried in an oven at 60°C for 24 h. A single piece (0·5 × 4 cm) of Cd²⁺-exchanged Nafion film was introduced in an optical cell (2 mm thick). The cell was closed with a rubber septum and flushed with a stream of argon for 30 min to remove adsorbed O₂ from the film. About 10 ml of H₂S gas was then injected into the cell for initiating CdS formation. The reaction could be arrested at any stage by quick degassing. The yellow coloration of the film confirmed the formation of CdS particles. Care was taken to exclude O₂ from the cell. As a precautionary measure all the Nafion films containing CdS were stored in an argon atmosphere.

2.3 Optical measurements

The absorption spectra were recorded with a Perkin Elmer 3840 diode-array spectrophotometer. The emission spectra were recorded with an SLM S-8000 photon-counting spectrofluorometer in a front-face configuration. Emission lifetime measurements were performed by the time-correlated single-photon counting technique using an apparatus that has been described elsewhere (Federici *et al* 1985). The excitation source was a mode-locked, Q-switched Quantronix 416 Nd:YAG laser which provided 80 ps pulses of 355 nm light with a frequency of 5 kHz and an integrated power of 10 mW.

Time-resolved emission spectra were recorded from laser flash photolysis experiments using 337 nm laser pulses from a PRA LN1000 nitrogen laser system

(pulse width 0.5 ns). The details of the experimental arrangement can be found elsewhere (Nagarajan and Fessenden 1985). All the experiments were done at room temperature (23 °C).

3. Results and discussion

3.1 Formation of CdS clusters in the Nafion film and size quantization effects

The CdS clusters within the polymer matrix could be synthesized by exposing the Cd²⁺-doped Nafion films to an atmosphere of H₂S. The absorption spectra recorded following the exposure of Cd²⁺/Nafion to H₂S are shown in figure 1. The color of the film slowly changed from colorless to yellow as the H₂S exposure time was increased. This is clearly evident from the increased absorption in the spectra recorded at longer times (figure 1). In the bulk form, CdS is deep yellow in color ($E_g = 2.4$ eV) with an onset absorption around 520 nm. However, in smaller diameter particles (< 50 Å), the absorption shifts to the blue as the effective bandgap increases. The morphology of the Nafion polymer is such that it controls the clustering of CdS molecules (D_p 15–150 Å) within the hydrocarbon network.

Semiconductor particles which exhibit size-dependent optical and electronic properties are termed quantized (or Q-) particles or nanoclusters (Meisner *et al* 1983; Kuczynski *et al* 1984; Wang and Mahler 1987; Honda *et al* 1988; Mahler 1988; Nosaka *et al* 1989; Dalas *et al* 1990; Gopidas and Kamat 1990; Miyoshi *et al* 1990; Smotkin *et al* 1990; Misawa *et al* 1991; Yoneyama 1991). These ultrasmall semiconductor particles are molecular clusters in which complete electron delocalization has not yet occurred. Quantization in these ultrafine semiconductor particles arises from the confinements of charge carriers with potential wells of small dimensions (less than the DeBroglie wavelength of the electrons and holes). Under these conditions the energy levels available for electrons and holes in the conduction and valence bands become discrete. The absorption spectra recorded in figure 1 show the transition from small molecular clusters to bulk aggregates. In addition to its very large effect

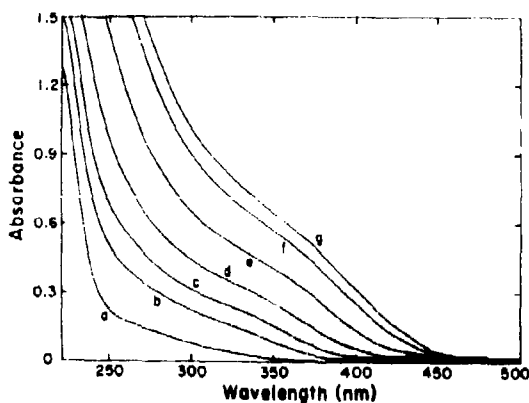


Figure 1. Absorption spectra of CdS clusters in Nafion film. The spectra were recorded at various time intervals following the exposure of the Cd²⁺-doped (1 mmole) Nafion film to H₂S for 0 (a), 5 (b), 10 (c), 20 (d), 45 (e), 90 (f), and 120 min (g).

on optical properties, size quantization also leads to enhanced redox activity of the photogenerated charge carriers.

The slow rate of CdS formation in dry Nafion film facilitates control of particle size by limiting the time of H₂S exposure. For example, it was possible to stop the growth of CdS clusters by quickly degassing the sample cell and storing the film in an inert (N₂ or Ar) atmosphere. Similar control of particle size has also been reported for CdS (Nosaka *et al* 1989; Smotkin *et al* 1990; Misawa *et al* 1991), PbS (Mahler 1988) and CdSe (Gopidas and Kamat 1990; Yoneyama 1991) in polymer films. Another approach to control the particle size is to decrease the concentration of Cd²⁺ in the polymer film. By decreasing the concentration of Cd²⁺ from 10⁻⁴ moles to 10⁻⁶ moles, it is possible to grow Q-size CdS clusters with long time H₂S exposure. By diluting Cd²⁺ concentration in Nafion with inert cations such as Ca²⁺, it is also possible to control the size of CdS and CdSe clusters (Smotkin *et al* 1990).

3.2 Emission spectra of CdS clusters in Nafion

Emission spectra recorded during the growth of CdS crystallites are shown in figure 2. The blank film (spectrum *a*, recorded before the H₂S exposure) exhibits relatively small emission below 400 nm. This emission, which arises as a result of some organic impurities imbedded in the Nafion film, does not interfere with the measurement of CdS emission. Once the Cd²⁺ doped Nafion film is exposed to H₂S a new emission band arises as CdS clusters are formed within the polymer matrix. As shown earlier, this emission mainly arises from the sulfur vacancies at the CdS crystallites. With increasing H₂S exposure time an increase in the CdS emission is seen. In the initial stages (spectra *a* in figure 2), the growth in CdS clusters leads to an increased

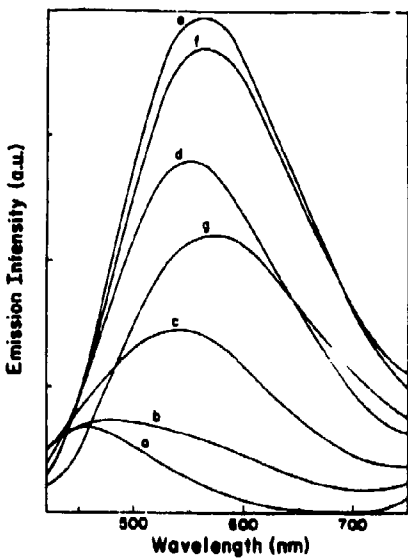


Figure 2. Emission spectra of CdS clusters in Nafion film. The spectra were recorded at various time intervals following the exposure of the Cd²⁺ doped (1 mmole) Nafion film to H₂S for 0 (*a*), 8 (*b*), 15 (*c*), 22 (*d*), 60 (*e*), 90 (*f*), and 180 min (*g*).

absorption at the excitation wavelength, which in turn leads to the enhancement of the emission yield. However, at longer times (spectra *f* and *g* in figure 2) a decrease in the emission yield is observed. This shows that once the CdS clusters are fully grown the efficiency of radiative recombination process decreases. Decreased surface area and saturation of sulfur vacancies in larger crystallites is likely to affect the radiative recombination in the larger clusters.

Another interesting feature is the shift in the emission maximum of the CdS clusters in the Nafion film. When the crystallites are small, the emission maximum is centered around 480 nm. But as the CdS cluster grows, the emission band shifts to the red. In a fully grown cluster, the emission maximum is observed at 580 nm. The blue shift in the emission maximum of smaller CdS clusters is parallel to the shift observed in the absorption edge (figure 1) and attributed to the size quantization effects. Thus, one can utilize the emission properties to probe the size quantization of CdS clusters in the polymer films.

3.3 Emission lifetimes

It has been shown earlier that the emission decay of semiconductor clusters provides important information regarding kinetic and mechanistic details of charge carrier recombination. A typical decay profile of CdS emission at 470 nm is shown in figure 3. Such a nonexponential decay is attributed to the distribution of excited states at various trapping sites that emit with different lifetimes. This multiexponential decay was fit by a nonlinear least squares procedure to the three component decay law as given by (James *et al* 1985),

$$F(t) = a_1 \exp(-t/\tau_1) + a_2 \exp(-t/\tau_2) + a_3 \exp(-t/\tau_3). \quad (1)$$

The lifetimes analyzed from its decay kinetics are summarized in table 1. These range from 0.85 to 480 μ s. The shorter-lived states were found to emit at higher energies.

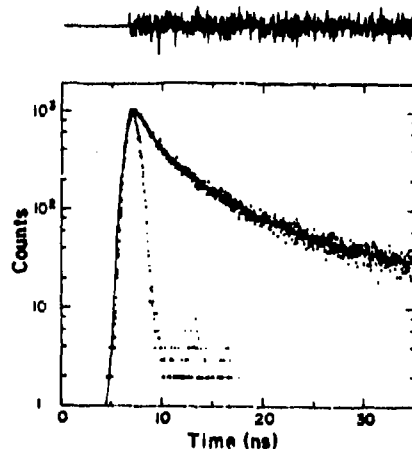


Figure 3. Emission decay profile of CdS clusters in Nafion monitored at 470 nm. The analysis was carried out by fitting it to the three exponential decay kinetics, (1), using the parameters: $a_1 = 0.037$, $\tau_1 = 1.03$ ns, $a_2 = 0.019$, $\tau_2 = 4.29$ ns, $a_3 = 0.0029$ and $\tau_3 = 23.73$ ns. The profile of the laser pulse is also shown for comparison.

Table 1. Emission lifetimes of CdS clusters in Nafion.

Emission wavelength (nm)	Emission lifetimes ^a (ns)			
	τ_1	τ_2	τ_3	$\langle \tau \rangle^b$
400	0.85	3.32	14.73	5.61
470	1.03	4.29	23.73	10.75
580	14.80	111.51	379.75	179.10
680	18.77	124.31	480.00	283.70

^aLifetimes were analyzed by fitting the decay to three exponential decay kinetics

^bThe average lifetime $\langle \tau \rangle$ was calculated based on the expression of James *et al* (1985): $\langle \tau \rangle = \sum a_i \tau_i^2 / \sum a_i \tau_i$

Similar wavelength-dependent emission lifetimes have been observed for ZnO, ZnS, CdS and CdSe colloids (see, for example, Kamat and Dimitrijević 1980, Kamat 1991, 1993). The wavelength dependence of the emission lifetime arises from the contribution of the Coulombic energy of interaction of the electron-hole pair to the total energy of the emitted photon. A more detailed analysis of these lifetimes in CdS clusters has been carried out by Chestnoy (Chestnoy *et al* 1986).

3.4 Time-resolved emission spectra

The contribution of various emitting centers which exhibit different emission lifetimes was further probed by recording time-resolved emission spectra. The CdS-doped Nafion film was excited with 337 nm laser pulses from an N₂ laser (pulse width 0.5 ns) and the emission spectra were recorded at different time intervals (figure 4). These spectra were normalized for the photomultiplier response. A decrease in the emission yield as well as a red-shift in the maximum was seen with increasing time. The spectrum recorded immediately after the pulse shows a maximum around 440 nm, while the spectrum recorded 52 ns after the laser pulse has an emission maximum at 480 nm. Similarity in the shape of the emission band in all these spectra suggests that the same surface vacancy (sulfur vacancy) is responsible for all the emission spectra recorded in figure 4. The steady state emission spectrum at 77 K is also shown for comparison. This steady state emission band is considerably red-shifted and exhibits very little emission at higher energy (below 420 nm). This further supports the earlier proposal (Chestnoy *et al* 1986) that close pairs with small separating distances emit faster and at higher energy than distant pairs for a fixed particle diameter.

3.5 Possible applications of CdS films in solar energy conversion

It has been shown earlier that CdS clusters imbedded in the polymer film are an excellent choice for the photoelectrolysis of water (Krishnan *et al* 1983; Meissner *et al* 1983; Finlayson *et al* 1983). Relatively large quantities of H₂ generation were produced in the presence of an electron donor such as S²⁻. It should also be possible to utilize such thin semiconductor particulate films in photoelectrochemical cells for directly converting light energy into electricity. Significantly higher photocurrents have been reported for larger size CdS particles precipitated from solution in Nafion films

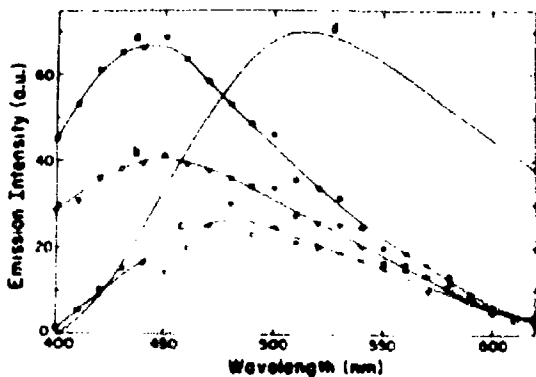


Figure 4. Time resolved emission spectra of CdS clusters in Nafion film. The spectra were recorded following the excitation of the CdS doped Nafion film with 337 nm laser pulses at 1.2 ns (a), 16 ns (b) and 100 ns (c). The spectrum (d) is the steady state emission spectra at 77 K shown for comparison. (The intensity scale of spectrum (d) is not normalized with the scale for the spectra (a)-(c)).

(Honda *et al.* 1988). We also checked this effect for quantized CdS particles by casting the film on a conducting glass electrode using Nafion solution (5% in alcohol, Aldrich). The Nafion modified electrode was then doped with Cd²⁺ and exposed to an H₂S atmosphere. Unfortunately, the quantized CdS clusters prepared in this Nafion membrane exhibited very small photocurrents (< 100 nA). Since these small clusters are isolated, it is not possible to observe the collective photoelectrochemical effect as seen in particulate films directly cast on conducting glass plates (Hotchandani and Kamat 1992).

The quantized CdS clusters have potential applications in developing materials for nonlinear optics. CdS and CdSe clusters exhibit transient bleaching in the subnanosecond time domain (see, for example, Hilenski *et al.* 1988, Kamat *et al.* 1989, Giopidas and Kamat 1990). This transient bleaching, arising as a result of a photoduced blue-shift in the absorption edge of the semiconductor, has been attributed to the decrease in the oscillator strength of the excitonic transitions in quantized clusters (Hilenski *et al.* 1988) and dynamic Purcell-Moss effect in larger clusters (Kamat *et al.* 1989). Time resolved study of the transient bleaching of CdSe clusters in Nafion film has been reported in our earlier study (Giopidas and Kamat 1990).

4. Conclusions

CdS clusters which exhibit size quantization effect are prepared in Nafion film. The photophysical properties of these nanoclusters can be varied by controlling the growth of CdS in the polymer matrix. These semiconductor clusters are fluorescent with lifetimes ranging from 0.05–400 ns. The photoduced charge transfer processes have been probed by time resolved emission spectroscopy. A better understanding of these photoduced processes is essential before one could use these systems for solar energy conversion.

Acknowledgements

The work described herein was supported by the Office of Basic Energy Sciences of the US Department of Energy. This is Contribution No. NDRL-3555 from the Notre Dame Radiation Laboratory.

References

- Card A J 1982 *J. Phys. Chem.* **86** 172
 Bewendi M G, Steigerwald M L and Brus L E 1990 *Annu. Rev. Phys. Chem.* **41** 427
 Brus L E 1986 *J. Phys. Chem.* **90** 2555
 Chevrel N, Harris T D and Brus L E 1986 *J. Phys. Chem.* **90** 1391
 Dolai F, Sakkoula S, Kalitza J, Vratoras F and Koutsopoulos P G 1990 *Zangmu* **6** 1346
 Fedenco J, Holman W P, Hug G L, Kane C and Patterson L K 1985 *Comput. Chem.* **9** 171
 Fendler J H 1985 *J. Phys. Chem.* **89** 2730
 Fendler J H 1987 *Chem. Rev.* **87** 877
 Finlayson M F, Park K H, Kakuta N, Bard A J, Campion A, Fox M A, Webber S F and White J M 1988 *J. Luminesc.* **39** 205
 Fox M A 1991 *Rev. Chem. Intermed.* **15** 153
 Gopidas K R and Kamat P V 1990 *Mater. Lett.* **9** 372
 Gratzel M 1989 *Heterogeneous photochemical electron transfer* (Boca Raton, FL: CRC Press) chap. 3
 Honglun A 1988 *Top. Cur. Chem.* **143** 113
 Honglun A 1990 *Chem. Rev.* **89** 1861
 Hileski E F, Lucas P A and Wang Y 1988 *J. Phys. Chem.* **92** 3435
 Honda K, Kawano A, Chiba K, Iikawa A and Miyama H 1988 *Chem. Lett.* 195
 Hochandau S and Kamat P V 1992 *J. Phys. Chem.* **96** 6834
 James D R, Liu Y-S, De Mayo P and Ware W R 1985 *Chem. Phys. Lett.* **120** 460
 Kalyanasundaram K, Gratzel M and Pelizzetti E 1986 *Coord. Chem. Rev.* **69** 57
 Kamat P V 1991 *Kinetics and catalysis in microheterogeneous systems* (eds) M Gratzel and K Kalyanasundaram (New York: Marcel Dekker) pp. 375-436
 Kamat P V 1993 *Chem. Rev.* (in press)
 Kamat P V and Dimitrijevic N M 1990 *Solar Energy* **44** 83
 Kamat P V, Dimitrijevic N M and Nozik A J 1989 *J. Phys. Chem.* **93** 2873
 Kamat P V and Meiss D (eds) 1993 *Int. J. Chem.* A special issue on *Quantum Size Particles*.
 Krishnan M, White J R, Fox M A and Bard A J 1983 *J. Am. Chem. Soc.* **105** 7002
 Kuczynski B H, Milosevic B H and Thomas J K 1984 *J. Phys. Chem.* **88** 980
 Mahler W 1988 *Inorg. Chem.* **27** 436
 Messner D, Memming R and Kastening 1983 *Chem. Phys. Lett.* **96** 34
 Memming R 1988 *Top. Cur. Chem.* **143** 79
 Minowa K, Yao H, Hayashi T and Kobayashi T 1991 *Chem. Phys. Lett.* **172** 113
 Miyoshi H, Tanaka K, Uchida H, Yoneyama H, Mori H and Sakata T 1990a *J. Electroanal. Chem.* **295** 71
 Miyoshi H, Yamachika M, Yoneyama H and Mori H 1990b *J. Chem. Soc., Faraday Trans.* **86** 815
 Nagarajan V and Fessenden R W 1985 *J. Phys. Chem.* **89** 2330
 Nonaka Y, Yamaguchi K, Yokoyama H and Miyama H 1989 *MRS International Meeting on Adv. Mater.* (Pittsburgh: Materials Research Society) **12** 155
 Smotkin E S, Brown R M, Rabenberg L K, Salmon K, Bard A J, Campion A, Fox M A, Mallouk T E, Webber S E and White J M 1990 *J. Phys. Chem.* **94** 7543
 Steigerwald M L and Brus L E 1990 *Acc. Chem. Res.* **23** 183
 Wang Y and Herron N 1991 *J. Phys. Chem.* **95** 525
 Wang Y and Mahler W 1987 *Opt. Commun.* **61** 233
 Wilner I and Wilner B S 1988 *Int. J. Hydrogen Energy* **13** 593
 Yoneyama H 1991 *Rev. Chem. Intermed.* **15** 101

Photosensitizing properties of squaraine dyes

SURESH DAS¹, K GEORGE THOMAS¹, PRASHANT V KAMAT²
and M V GEORGE^{1,2*}

¹Photochemistry Research Unit, Regional Research Laboratory (CSIR), Trivandrum
695019, India

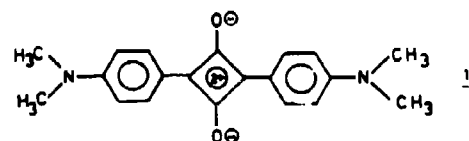
²Radiation Laboratory, University of Notre Dame, Notre Dame, IN 46556, USA

Abstract. The present report summarizes our results on the photophysical and photochemical investigations of a series of squaraine dyes which exhibit intense and sharp absorption bands in the visible and near infrared regions. The intramolecular charge-transfer transitions arising from the "donor-acceptor-donor" arrangements of these dyes have an interesting effect on their excited state properties. The major nonradiative decay process of squaraines is by rotation about the C-C bonds between the central cyclobutane unit and its neighbouring phenyl groups. Microencaging of one of the dyes by β -cyclodextrin or poly(4-vinylpyridine) was found to restrict this motion, bringing about up to 90-fold enhancement in its fluorescence yield. These aspects as well as the dynamics of charge transfer from the excited singlet state of some of the squaraine dyes to TiO_2 and the recombination of the injected charge with the dye radical cation are discussed.

Keywords. Photochemistry of squaraine dyes, β -cyclodextrin complexes, poly(4-vinylpyridine) complexes, TiO_2 -photosensitization

1. Introduction

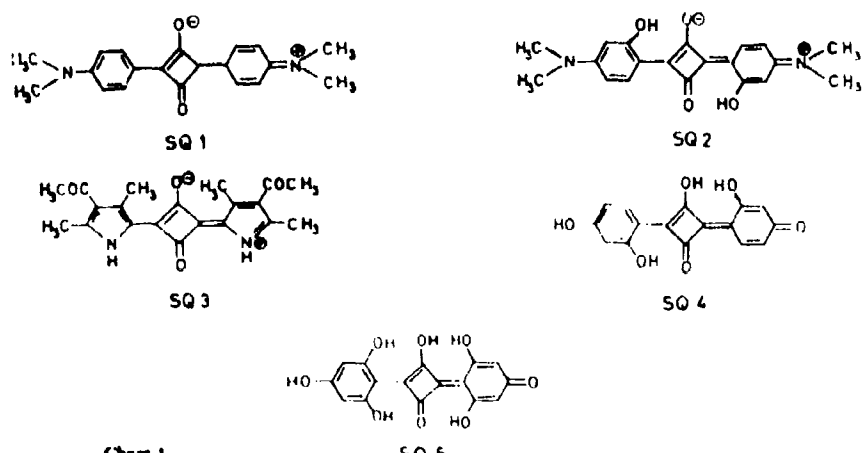
Squaric acid is known to undergo condensation reactions with a variety of nucleophiles to form 1,3-disubstituted derivatives (squaraines), which have very strong absorption in the visible and near infrared regions (Sprenger and Ziegenbein 1966; Schmidt 1980). The chemistry of squaric acid and other oxocarbons (Seitz and Imming 1992) and near-infrared dyes (Fabian *et al* 1992) have been reviewed recently. Although the technological applications of squaraine dyes in organic solar cells (Morel *et al* 1984; Piechowski *et al* 1984), xerographic photoreceptors (Tam 1980; Law 1993) and optical recording media (Emmelius *et al* 1989) have been extensively investigated, reports on the photophysical properties of squaraine dyes have been limited (Loutfy *et al* 1983; Law 1987, 1989, 1990; Vieira *et al* 1991). MNDO and CNDO calculations on the ground and excited states of *bis*[(4-dimethylamino)phenyl]squaraine (1)



*For correspondence

have shown that the molecule is highly polarized with the amino moiety being an electron donor (D) and the central cyclobutane unit being an electron acceptor (A) (Bigelow and Freund 1986).

These calculations also indicate that the $S_0 \rightarrow S_1$ electronic excitation is accompanied by a charge transfer (CT), which is primarily confined to the central C_6O_2 unit, with a small degree of CT from the aniline moiety. However, the calculations indicate that both the S_0 and S_1 states are highly polarized intramolecular D-A-D CT states. The charge-transfer nature of these dyes also brings about interesting effects in their solid state chemistry. Extensive intermolecular charge transfer interactions in the solid state cause a red-shift accompanied by a broadening of their absorption bands. These intermolecular interactions also make these dyes highly photoconductive in the solid state. Highly conducting polymeric forms of such oxocarbon dyes have also been recently reported by Havinga and Wynberg (Emsley, 1992).



Chap. I.

Multiple emission bands have been observed for SQ1 (chart 1) and its derivatives in solution. In a detailed study involving the effects of solvent and temperature on the emission spectra of these dyes, three emission bands have been observed which have been assigned to emission from the free dye (α), dye-solvent complex (β) and a twisted excited state resulting from the C-C bond rotation (γ) (Law and Bailey 1987).

Here, our work on the spectral characterization of the excited singlet, triplet and redox states of the squaraine dyes SQ1–SQ5 (chart 1), the hydrophobic interactions of SQ5 with β -cyclodextrin and poly(4-vinylpyridine), as well as the dye sensitization of a large band gap semiconductor, TiO_2 , are discussed.

2. Experimental

The squaraine dyes SQ1-SQ5 were synthesised by reacting squaric acid with the appropriate nucleophiles, by reported procedures (Sprenger and Ziegenbein 1966, 1968; Schmidt 1980). All solvents were of spectroscopic grade. Colloidal suspensions of TiO₂ were prepared by a method described earlier (Kamat 1989). The details of

quantum yield measurements, as well as the experimental set-up used for flash-photolysis and pulse-radiolysis have been described earlier (Das *et al* 1992a; Kamat *et al* 1992).

3. Results and discussion

3.1 Excited singlet, triplet and redox states

3.1a Bis[4-(dimethylamino)phenyl]squaraine derivatives: The spectroscopic characteristics of the squaraine dyes SQ1-SQ_n, as well as their excited and redox states are summarised in table 1 (Kamat *et al* 1992; Patrick *et al* 1992).

Both SQ1 and SQ2 have sharp absorption bands with absorption maxima at 628 and 636 nm, respectively. The fluorescence quantum yield and fluorescence lifetime of SQ2 are about twice that of SQ1. It has been suggested that the substituent OH groups in SQ2 facilitate hydrogen bonding between these groups and the CO-group in the cyclobutane ring, which can restrict the rotational relaxation process of the excited state (Law 1987). The excited singlets of SQ1 and SQ2 in methylene chloride were generated by direct excitation with 532 nm pulse. The transient absorption spectra recorded at different time intervals, following laser pulse (18 ps) excitation of SQ1 is shown in figure 1. As discussed in an earlier section, the excited singlet state

Table 1. Excited state properties of squaraine dyes

Dye	Absorp- tion max (nm)	Emis- sion max (nm)	Absorp- tion max (nm)	τ_f (ns)	Absorp- tion max (nm)	F^*D/D vs SCF	Radical anion λ_{maximum} (nm)	Radical cation λ_{maximum} (nm)		
SQ1	628	654	0.45	400	1.5	$> 10^3$	540	0.305	400	550
SQ2	636	658	0.84	475	3.0	$> 10^3$	565	0.365	445	545
SQ3	568	587	0.08	442	0.22	0.007	420	0.976	415	505

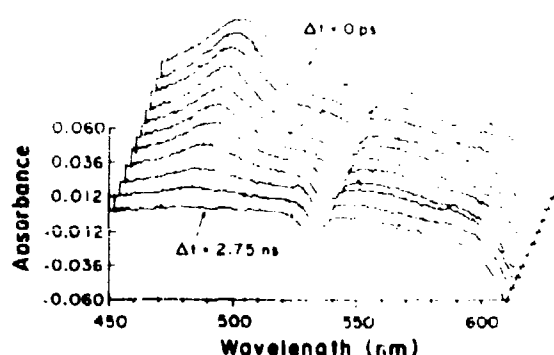


Figure 1. Transient absorption spectra of singlet-excited SQ1 in methylene chloride. The spectra were recorded, following 532 nm laser pulse excitation of 10 μM SQ1 in methylene chloride, at time intervals of 0, 0.05, 0.1, 0.15, 0.2, 0.25, 0.35, 0.5, 0.75, 1.75 and 2.75 ns. (Reprinted with permission from Kamat *et al* 1992 (© 1992, Am. Chem. Soc.)

can also exist in the solute-solvent complex and twisted-excited state forms. An attempt was made to probe these states in transient absorption studies. Only a single absorption peak was observed in the wavelength region 400–600 nm. Our studies so far on the excited singlet states, viz. emission lifetimes and transient absorption measurements, have failed to gather supportive evidence for the existence of multiple singlet excited states.

To study the triplet excited states of the dyes by laser flash photolysis, a triplet-triplet energy transfer method using 9,10-dibromoanthracene (DBA) ($E_T = 167.4 \text{ kJ mol}^{-1}$) as triplet sensitizer was employed, since direct excitation of the dyes led to very low yields of the dye triplets ($\phi_T = 0.01$). Time-resolved transient absorption spectra recorded after 355 nm pulse excitation of DBA in methylene chloride solution containing SQ1 is shown in figure 2. The transient absorption spectrum recorded immediately after laser pulse excitation ($\lambda_{\text{max}}: 425 \text{ nm}$) corresponds to the sensitizer triplet. The absorption spectra recorded at time intervals greater than $10 \mu\text{s}$ correspond to the SQ1 triplet. The extinction coefficients were determined for the triplets of SQ1 and SQ2 by a method described earlier (Carmichael and Hug 1986). The triplet lifetimes of these dyes were $3.5 \times 10^3 \mu\text{s}$, indicating that the triplet excited states, unlike the singlet excited states, are insensitive to the presence of the OH group on the phenyl ring.

The dye radical cation spectra were recorded by generating these cations by pulse radiolysis of the dyes in methylene chloride solutions. Radiolysis of methylene chloride produces highly oxidising radicals such as RCl^\cdot (Ford *et al.* 1989). The oxidation potential of the squaraine dye is very low (0.35 and 0.41 V vs Ag/AgCl for SQ1 and

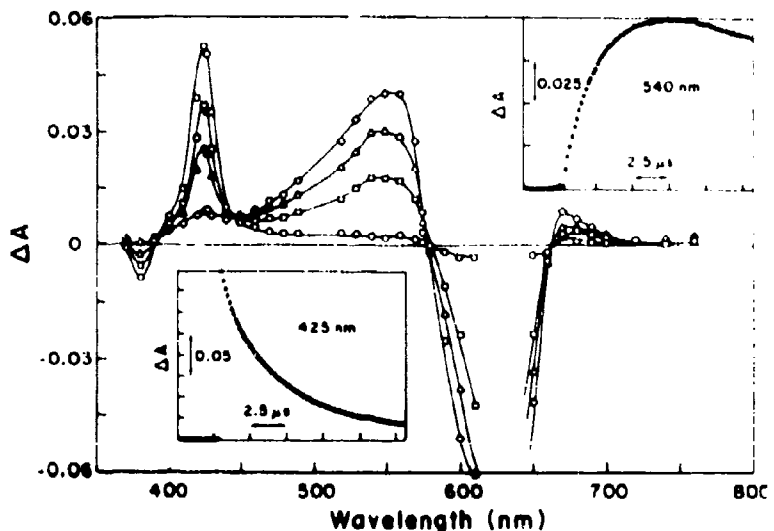


Figure 2. Energy transfer from triplet-excited 9,10-dibromoanthracene to SQ1 in methylene chloride. Transient absorption spectra were recorded, following 355 nm laser pulse excitation of a solution containing 0.1 mM 9,10-dibromoanthracene and 10 μM SQ1 at time intervals 0, 1, 1.3, 1, 3.0 (Δ) and 8.0 (···) μs . The absorption time profiles in the insets show the decay of the 9,10-dibromoanthracene triplet at 425 nm and the formation of ${}^3\text{SQ1}$ at 540 nm. [Reprinted with permission from Kamat *et al.* 1992 (© 1992, Am. Chem. Soc.).]

SQ2, respectively) and, hence, they can be oxidised by RCI'. The spectra of the dye radical cations obtained by pulse radiolysis are shown in figure 3. A strong overlap of SQ1 absorption with the ground state absorption of SQ1 was evident from the small bleaching of the S_0 - S_1 band of SQ1.

Direct excitation of SQ1 at high laser doses also gave rise to transient spectra similar to those observed in the above pulse radiolysis experiments (figure 4) indicating the formation of dye radical cations under these conditions. The formation of the radical cation spectra at high laser doses, and the linear dependence of the transient absorbance on the square of the laser dose as shown in the inset of figure 5, indicate

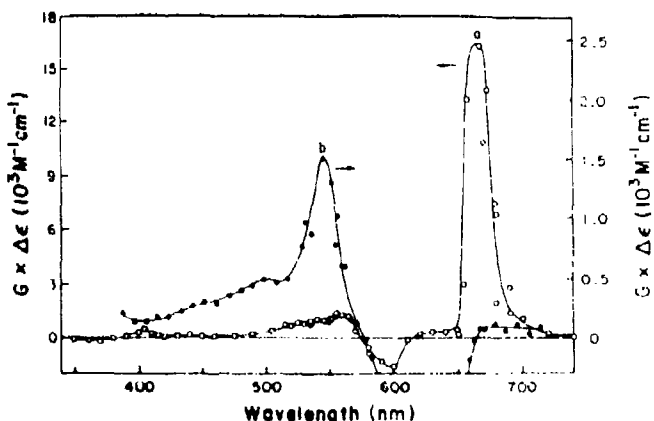


Figure 3. Transient absorption spectra of pulse radiolytically generated cation radical of (a) SQ1 and (b) SQ2 in methylene chloride. The difference absorption spectra were recorded, following the pulse radiolysis of O_2 , saturated CH_2Cl_2 solutions containing 10–20 μM of (a) SQ1 ($\Delta t = 25 \mu s$) and (b) SQ2 ($\Delta t = 60 \mu s$). [Reprinted with permission from Kamat *et al.* 1992 (© 1992, Am. Chem. Soc.)]

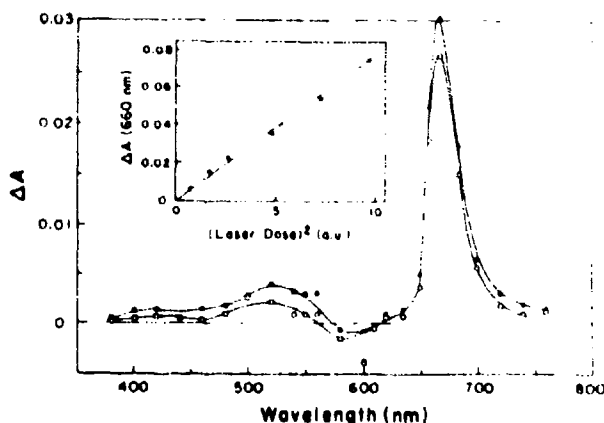


Figure 4. Photoionization of SQ1 in CH_2Cl_2 . The different absorption spectra recorded (●) 0 μs and (○) 150 μs after 532 nm excitation of 10 μM SQ1 in CH_2Cl_2 . The inset shows the dependence of SQ1⁺ yield (ΔA at 660 nm) on the square of laser intensity. [Reprinted with permission from Kamat *et al.* 1992 (© 1992, Am. Chem. Soc.)]

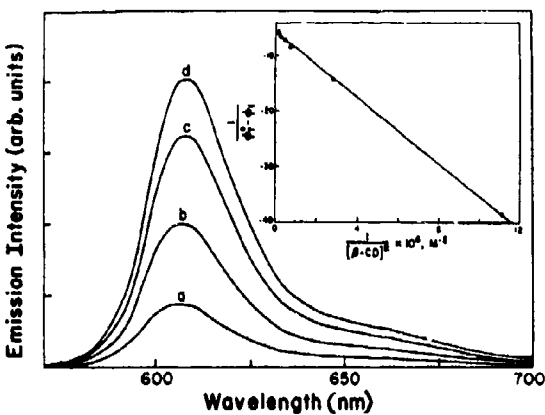


Figure 5. Influence of β -cyclodextrin concentration, $[\beta\text{-CD}]$ on the emission spectrum of 3.5×10^{-5} M SQ5 in aqueous solution at $\text{pH} = 8.6$; ($\beta\text{-CD}$) (a) 0.06; (b) 0.3; (c) 1.2; (d) 2.4 mM. Excitation wavelength, 560 nm; inset shows plot of $1/(\phi_f^0 - \phi_f)$ vs $1/[\beta\text{-CD}]^2$ for the fluorescence yield enhancement of SQ5^- , on addition of $\beta\text{-CD}$. [Reprinted with permission from Das *et al* 1992b (© 1992, R. Soc. Chem.)]

a biphotonic photoionization process as shown below



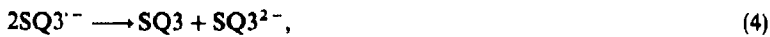
The spectrum of the radical anion of SQ1 was recorded by carrying out pulse-radiolysis studies in nitrogen-saturated ethanolic solutions. A transient formed with absorption maximum around 405 nm was assigned to the SQ1 radical anion on the basis of the known reducing nature of irradiated ethanol solutions (Butler and Henglein 1980; Ford *et al* 1989). The formation of SQ1^{1-} , has a half-life of $285 \mu\text{s}$ and this is attributed to the reaction of SQ1 with the solvated electron formed in the above system. No decay of the transient absorption was observed for up to 1 ms.

3.1b Bis(3-acetyl-2,4-dimethylpyrrole)squarene (SQ3): The spectral characteristics of the ground and excited states of SQ3, as well as the oxidised and reduced radical ions are shown in table 1. Unlike SQ1 and SQ2, the pyrrole derivative (SQ3) was relatively non-fluorescent ($\phi_f = 0.08$) with an extremely short-lived singlet excited state ($\tau_s = 222 \text{ ps}$). The intersystem crossing efficiency was also very low ($\phi_T = 0.02$), although relatively higher than for SQ1 and SQ2. The spectra of the triplet state as well as the radical cation were generated and characterized as discussed earlier for SQ1 and SQ2 (Patrick *et al* 1992).

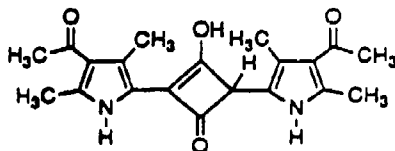
Photoelectrochemical reduction of SQ3 in colloidal semiconductor was carried with 308 nm laser pulse excitation. At this wavelength the absorbance of SQ3 is very low and the TiO_2 colloid can be selectively excited. Since the reduction potential of SQ3 was estimated as -0.43 V , which is below the conduction band of the TiO_2 semiconductor ($E_{CB} = -0.5 \text{ V}$), reduction of the dye can be carried out as below (Kamat 1985):



The absorption characteristics of the radical anion formed within the laser-flash duration is given in table 1. Steady state irradiation at 325 nm of degassed colloidal solutions of TiO_2 in acetonitrile containing SQ3 leads to a bleaching of the dye. On bubbling oxygen through this solution, the original colour is partially recovered. The bleaching of the dye may be attributed to the following disproportionation reactions of the radical anion.



The structure of the reduced product SQ3H_2 is tentatively suggested as



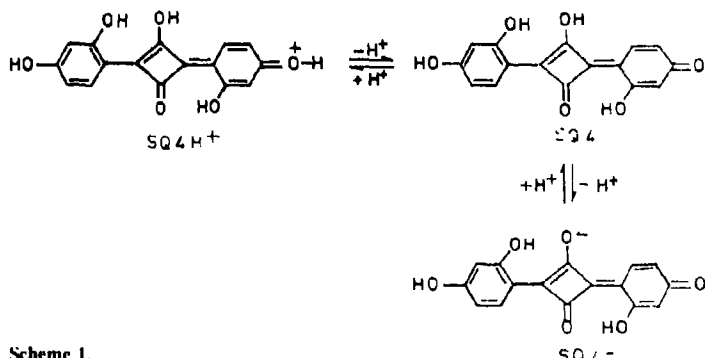
An analogous product has been observed in the case of a bis(methoxyphenyl)squarene dye. This compound could be oxidised to the corresponding dye using strong oxidising agents such as bromine (Farnum *et al* 1968).

3.1c Bis(2,4-dihydroxyphenyl)squarene (SQ4) and bis(2,4,6-trihydroxyphenyl)squarene (SQ5): These dyes exist as several distinct ionic species in protonation equilibria with each other and the spectral properties of the different species are summarised in table 2. The difference in spectral details can be attributed to protonation equilibria as described in scheme 1. In the case of SQ5, four distinct forms were observed (table 2). The emission spectra indicate that the singly deprotonated species ($\text{SQ4}^{\cdot-}/\text{SQ5}^{\cdot-}$) are the most fluorescent forms for both dyes. However, the much higher quantum yield of SQ4 as compared to SQ5, suggests that the additional hydroxy groups in the 6- and 6'-positions of SQ5 might distort the planarity of the molecules due to steric

Table 2. Absorption and emission characteristics of various ionic forms of bis(2,4-dihydroxyphenyl)squarene^a (SQ4) and bis(2,4,6-trihydroxyphenyl)squarene^b (SQ5).

Dye	Ionic form (pH)	Absorption	Emission	Absorption		
		max (nm)	max (nm)	ϕ_f	t_i (ps)	max ($S_1 - S_n$)(nm) $10^4 \text{ M}^{-1} \text{ cm}^{-1}$
SQ4	$\text{SQ4H}^+ (1)$	563	583	0.010	≤ 100	c
	$\text{SQ4}(5)$	530	582	0.037	130	449 3.9 ^d
	$\text{SQ4}^{\cdot-} (9)$	588	607	0.092	740	453 11.0 ^d
SQ5	$\text{SQ5H}^+ (2)$	561	--	< 0.001	--	457 2.1 ^d
	$\text{SQ5}(5)$	508	--	< 0.001	30 ^e	--
	$\text{SQ5}^{\cdot-} (8.2)$	588	601	0.01	240 ^e	--
	$\text{SQ5}^{2-} (11)$	543	--	< 0.001	230 ^e	--

^a In 10% v/v acetonitrile/water solution; ^b in 30% v/v methanol/water solution; ^c signal is too weak to analyse precisely; ^d determined from ground state bleaching (it was assumed that the singlet state has no significant absorption at $S_0 - S_1$ maximum); ^e in 50% v/v acetonitrile water solution



Scheme 1.

strain. The absorption characteristics of the excited singlet state formed by direct processes, as well as the triplet state formed through the DBA-sensitized processes, are summarised in table 2.

3.2 Fluorescence enhancement of bis(2,4,6-trihydroxyphenyl)squaraine (SQ5) by β -cyclodextrin and poly(4-vinylpyridine) microencapsulation

As discussed above, the anionic form of SQ5 has a fluorescence yield of 0.01 in methanol. The other ionic forms of SQ5 are relatively non-fluorescent. In aqueous medium, SQ5⁻ is relatively non-fluorescent ($\phi_f = 0.001$) and also very sensitive to air oxidation. Addition of β -cyclodextrin (β -CD) to an aqueous solution of SQ5

Table 3. Absorption and emission characteristics of bis(2,4,6-trihydroxyphenyl) squaraine (SQ5) in the presence and absence of (a) β -cyclodextrin [β -CD] in water ($pH = 8.6$) and poly(4-vinylpyridine) [P4VP] in methanol.

Solvent	$[\beta\text{-CD}] \text{ mM}$	$\lambda_{\text{max}} (\text{nm})$		ϕ_f	t_{r} (ps)	Absorption max ($S_1 - S_\infty$) (nm)
		Absorption	Emission			
$[\beta\text{-CD}] \text{ mM}$						
Water	0	584	595	0.002	85	
Water	2.4	598	608	0.16	1200	
Methanol:water (30% v/v)	0	588	598	0.01		
Methanol:water (30% v/v)	1.5	591	601	0.01		
$[P4VP] \text{ M}$						
Methanol	0	510	597	< 0.001	≤ 30	414
Methanol	0.1	510, 602	610	0.02	~ 100	a
Methanol containing 3 mM KOH	0	588	601	0.02	185	420, 490
Methanol containing 3 mM KOH	0.1	602	615	0.2	2000	425, 495

* Signal is too weak to be analysed precisely

brings about a significant enhancement (nearly 90-fold) in the fluorescence yield of the anion (figure 5), which is accompanied by a shift of about 13–14 nm in the absorption and emission bands (table 3). Complexation of the dye by β -CD also significantly enhances the chemical stability. The Benesi–Hildebrand analysis of the emission data as a function of β -CD concentration (inset, figure 5) suggests a 2:1 host-guest complex formation, i.e. two β -CD molecules complex with one anion molecule. β -CD encapsulation can bring about a decrease in the rotational freedom of the phenyl groups, leading to an increase in the fluorescence yield. For the uncomplexed dye anion, hydrogen bonding with solvent molecules is an additional factor influencing the non-radiative decay route. Encapsulation of the dye anion by two β -CD molecules is likely to exclude the intermolecular hydrogen bonding between the anion and water molecules. In the absence of such intermolecular hydrogen bonding, the central oxygen atoms of the cyclobutane ring would preferentially form hydrogen bonds with the OH groups in the adjacent phenyl groups, bringing about a rigidization of the molecule. Such intramolecular hydrogen bonding was shown to enhance fluorescence yield for the dimethylanilino derivatives (Kamat *et al.* 1992). The fluorescence lifetime ($\tau_f = 1.23$ ns) of the complexed dye anion is much higher than that of the uncomplexed anion (85 ps). Intersystem crossing efficiency is a minor pathway for decay of the excited singlet states of both the uncomplexed and complexed dye anions, as evidenced by the low triplet yields.

In basic methanolic solutions of SQ5, addition of P4VP brings about a clear red shift in the absorption band of the dye anion. The red shift in the absorption band is accompanied by a significant enhancement of the fluorescence quantum yield (figure 6; table 3). In neutral methanolic solution, the dye is predominantly in the neutral form, with minor amounts of the anion being present. Addition of P4VP to neutral methanolic solutions brings about a selective complexation of the ionic form, accompanied by a slight enhancement in fluorescence yields (Das *et al.* 1992).

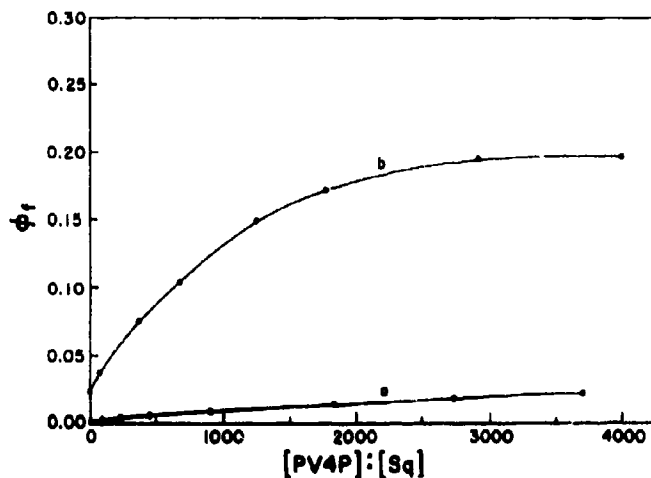


Figure 6. Dependence of fluorescence quantum yield of SQ5 on the concentration of P4VP: (a) neutral methanol, (b) basic methanol ($[KOH] = 30 \times 10^{-3}$ M). The excitation wavelength was 540 nm and the absorption at this wavelength was adjusted to 0.1. [Reprinted with permission from Das *et al.* 1992a (© 1992, Am. Chem. Soc.)]

Hydrophobic interactions between the dye anion and P4VP may be attributed to the selective complexation of the anion. At the low concentrations of P4VP employed, the macroviscosity will not affect the fluorescence yields very significantly. Interestingly, addition of poly(2-vinylpyridine) does not bring about any fluorescence enhancement, thus ruling out macroviscosity effects due to the addition of polymer. Hydrogen bonding between the nitrogen atom of P4VP and the anion seems to be the major factor in bringing about complex formation. In P2VP, the nitrogen atom may be too sterically hindered for this purpose.

3.3 Interaction of squaraines with TiO_2

The bis[(4-dimethylamino-2-hydroxy)phenyl]squaraine (SQ2) dye strongly interacts with colloidal TiO_2 , as indicated by the changes in the absorption spectrum (figure 7). The presence of an isobestic point at 650 nm in these absorptions shows the existence of the dye in the equilibrium between absorbed and unabsorbed states. The apparent association constant, as determined by the Benesi-Hildebrand method, was 2667 M^{-1} , indicating strong interaction between the dye and TiO_2 (Kamat et al 1991).



The fluorescence of the dye is strongly quenched by TiO_2 . This could be the result of charge injection from the excited state to the conduction band of TiO_2 . The oxidation potential of SQ1 is 1.5 V vs NHE (Law 1990), which is favourable for such charge injection. Picosecond laser flash photolysis of solutions of the dye with and without TiO_2 give the transient spectra shown in figure 8. In the absence of TiO_2 , the spectrum characteristic of the excited singlet state of SQ1 is obtained. However, in the presence of colloidal TiO_2 , an additional absorption peak appears at 580 nm. The absorption band at 580 nm closely matches the absorption characteristics of the

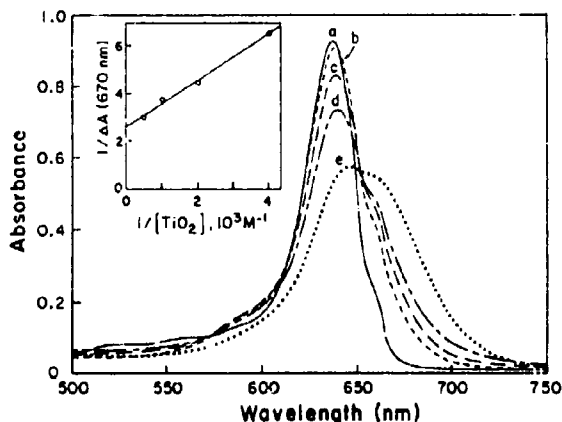


Figure 7. Absorption spectra of SQ1 (3 mM) in 40% v/v methylene chloride and 60% v/v acetonitrile containing (a) 0, (b) 0.25, (c) 0.5, (d) 1 and (e) 2 μM of colloidal TiO_2 . The insert shows the fitting of the 670 nm absorption to the Benesi-Hildebrand plot. [Reprinted with permission from Kamat et al 1991 (© 1991, Elsevier Science Publishers, BV.)]

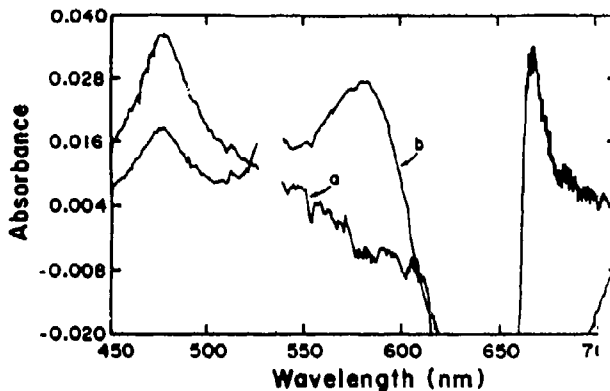
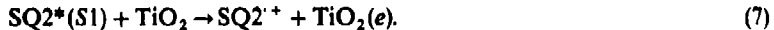


Figure 8. Transient absorption spectra recorded immediately after 532 nm laser pulse excitation ($\Delta t = 0$ ps) of SQ1 in 50% v/v dichloromethane and 50% v/v acetonitrile, without (a) and with (b) colloidal TiO_2 ($2.5 \mu\text{M}$). (The absorption around 532 nm is masked because of the interference from the excitation pulse scatter.) [Reprinted with permission from Kamat *et al* 1991 (© 1991, Elsevier Science Publishers, BV.).]

dye radical cation, observed in the pulse radiolysis studies (table 1). The difference in the medium and adsorption on TiO_2 surface may be responsible for the small red shift observed (20 nm). The charge injection may be represented as



The decay of the transient was analysed to give a lifetime of 270 ps for the dye radical cation ($k = 2.7 \times 10^{-10} \text{ s}^{-1}$).

The photosensitization of TiO_2 particulate films by the squaraine dye, SQ4, has also been investigated (Kamat *et al* 1993). The sensitizing behaviour was probed by adsorbing the dye on TiO_2 colloid-coated OTE(OTE/TiO_2) electrode. The photoresponse of the dye-modified OTE/ TiO_2 electrode is shown in figure 9. Upon illumination of this electrode with visible light (500 nm), a rise in photovoltage is seen. The open circuit voltage remained steady as long as the irradiation was continued. When the lamp was turned off the voltage quickly dropped to the dark value. The photoelectrochemical effect at the OTE/ TiO_2 /dye was reproducible over several cycles of irradiation. The photocurrent action spectrum closely matches that of the dye anion. The maximum photon-to-photocurrent efficiency obtained was only 0.05%, which is considerably lower than the fluorescence quantum efficiency of 3–9%. This shows that the reverse electron transfer is still a major factor in limiting the photosensitization. By suitable modification of the dye or by using a suitable redox coupled semiconductor system it should be possible to improve the performance of such photoelectrochemical cells.

4. Conclusions

The strong absorption and emission bands of the squaraine dyes in the visible and near infrared regions, along with their ability to undergo reversible oxidative and

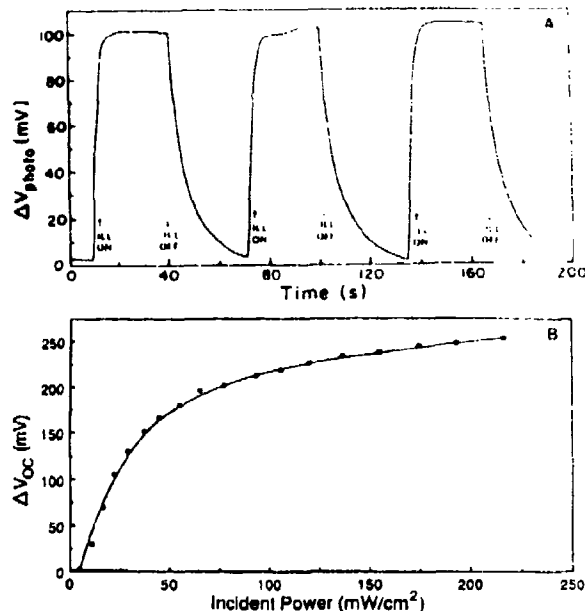


Figure 9. (A) The photovoltage (open-circuit) response of a squaraine dye (SQ4-) modified electrode (OTE/TiO₂/SQ4⁻) to illumination at 500 nm in a photoelectrochemical cell containing Pt foil as counter electrode and aqueous 1.5 M KCl as electrolyte. (B) The dependence of maximum open-circuit photovoltage of OTE/TiO₂/SQ4⁻ on the incident light intensity. [Reprinted with permission from Kamat et al 1991 (© 1991, R. Soc. Chem.)]

reductive photoelectron transfer processes, make these dyes highly suitable for photosensitization purposes. These dyes are capable of sensitizing semiconductors such as TiO₂. The extreme sensitivity of the absorption and emission properties to the solvent media can be utilised for probing hydrophobic and hydrophilic environments.

Acknowledgements

We (SD, KGT and MVG) thank the Council of Scientific and Industrial Research, Government of India, Regional Research Laboratory, Trivandrum, (MVG) Jawaharlal Nehru Centre for Advanced Scientific Research and (PVK and MVG) the Office of Basic Energy Sciences of the US Department of Energy for financial support of this work. This is Contribution No. RRLT-PRU-30 from RRL, Trivandrum and NDRL-3601 from the Notre Dame Radiation Laboratory.

References

- Bigelow R W and Freund H J 1986 *J. Chem. Phys.* **107** 159
Butler J and Henglein A 1980 *Radiat. Phys. Chem.* **15** 603

- Carmichael I and Hug G L 1986 *J. Phys. Chem. Ref. Data* **15** 76
- Das S, Kamat P V, De la Barre B, Thomas K G, Apayaghosh A and George M V 1992a *J. Phys. Chem.* **96** 10327
- Das S, Thomas K G, George M V and Kamat P V 1992b *J. Chem. Soc., Faraday Trans. 2* **88** 3419
- Emmelius M, Pawłowski G and Vollmann H W 1989 *Angew. Chem. Int. Ed. Engl.* **28** 1445
- Emaley J 1992 *New Sci.* **138** 16
- Fabian J, Nakazumi H and Matsushita M 1992 *J. Am. Chem. Soc.* **92** 1197
- Farnum D G, Webster B and Wolf A D 1988 *Tetrahedron Lett.* 5003
- Ford W E, Hiratsuka H and Kamat P V 1989 *J. Phys. Chem.* **93** 6692
- Kamat P V 1985a *J. Photochem.* **28** 513
- Kamat P V 1985b *J. Chem. Soc., Faraday Trans. 1* **81** 909
- Kamat P V 1989 *J. Phys. Chem.* **93** 2873
- Kamat P V, Das S, Thomas K G and George M V 1991 *Chem. Phys. Lett.* **188** 671
- Kamat P V, Das S, Thomas K G and George M V 1992 *J. Phys. Chem.* **96** 195
- Kamat P V, Hotchandani S, De Lind M, Thomas K G, Das S and George M V 1993 *J. Chem. Soc., Faraday Trans. 2* **89** 2397
- Law K Y 1987 *J. Phys. Chem.* **91** 5184
- Law K Y 1989 *J. Phys. Chem.* **93** 5925
- Law K Y 1990 *J. Imaging Sci.* **34** 31
- Law K Y 1993 *Chem. Rev.* 449
- Law K Y and Bailey F C 1987 *J. Imaging Sci.* **31** 192
- Loutfy R O, Hsiao C K and Kazmaier P M 1983 *Photogr. Sci. Eng.* **27** 5
- Morel D L, Stogryn E L, Ghosh A K, Feng T, Purwin P E, Shaw R E, Fishman C, Bird G R and Piechowski A P 1984 *J. Phys. Chem.* **88** 923
- Patrick B, George M V, Kamat P V, Das S and Thomas K G 1992 *J. Chem. Soc., Faraday Trans. 2* **88** 671
- Piechowski A, Bird G R, Morel D L and Stogryn E L 1984 *J. Phys. Chem.* **88** 933
- Schmidt A H 1980 *Synthesis* 961
- Seitz G and Imming P 1992 *Chem. Rev.* **92** 1227
- Sprenger H E and Ziegenbein 1966 *Angew. Chem. Int. Ed. Engl.* **5** 894
- Sprenger H E and Ziegenbein 1968 *Angew. Chem. Int. Ed. Engl.* **7** 530
- Tan A C 1980 *Appl. Phys. Lett.* **37** 978
- Vieira F L V, Costa S M B and Pereira E 1991 *J. Photochem. Photobiol. A* **55** 361

Photoinduced electron transfer reactions of *trans*-stilbene surfactants in Langmuir-Blodgett assemblies and phospholipid bilayers

DAVID G WHITTEN*, INNA FURMAN, CRISTINA GEIGER,
WANDA RICHARD and SUSAN P SPOONER
Department of Chemistry, University of Rochester, Rochester, New York 14627, USA

Abstract. The photochemistry and photophysics of a series of stilbene-functionalized fatty acids (SFA) have been examined in homogeneous solutions, supported Langmuir-Blodgett assemblies, and as guests in phospholipid bilayers and micellar dispersions. The spectroscopic characteristics of stilbene-functionalized derivatives of phosphatidyl choline (SFA-PC) have also been examined in organic solvents, aqueous dispersions and aqueous solution containing an excess of dipalmitoyl choline (DPPC), as well as in aqueous-methanol solutions containing γ -cyclodextrin. Langmuir-Blodgett assemblies of individual SFAs, as well as mixtures of various SFAs, exhibit spectroscopic properties (blue-shifted absorbance and red-shifted fluorescence relative to those observed in organic solvents) consistent with the formation of an "H" aggregate. The same effect is observed for SFA-PCs in aqueous dispersions and in aqueous-methanol solutions containing γ -cyclodextrin. The "H" aggregate is found to be the preferred geometric orientation of the stilbene chromophores which may correspond to an energy minimum for the systems investigated. Preliminary studies with SFA-PC in methanol-water solutions containing γ -cyclodextrin suggest that an association of only two stilbene chromophores is required to form the "H" aggregate.

Keywords. Photoinduced electron transfer; stilbene surfactants; Langmuir-Blodgett assemblies; phospholipid bilayers.

1. Introduction

The stilbene chromophore is one of the most widely investigated conjugated organic systems, due both to its characteristic and rich photochemistry and its spectroscopic accessibility (Hammond *et al* 1964; Saltiel *et al* 1975; Saltiel and Charlton 1980; Itoh and Kohler 1987; Allen and Whitten 1989; Saltiel 1992). In recent years, we and others have focused considerable attention towards the photophysics and photochemistry of substituted stilbenes and related molecules incorporated as guests in a variety of microheterogeneous media (Geiger and Turro 1977; Russell *et al* 1980, 1981; Brown *et al* 1985; Suddaby *et al* 1985). The sensitivity of the stilbene chromophore towards viscosity and local order results in its serving as a fairly sensitive probe to the local environment provided by these media; dramatic effects have been observed on both the thermal and photoinduced reactions of the stilbene chromophore in these media in a number of different investigations (Brown *et al* 1985; Mizutani and Whitten 1985; Takagi *et al* 1986). Incorporation of the *trans*-stilbene chromophore into a saturated fatty acid results in an amphiphile which is expected to form assemblies "anchoring"

*For correspondence

the stilbene chromophore in a relatively hydrophobic and ordered site, especially in Langmuir-Blodgett and various bilayer assemblies in aqueous media. In fact, we have found that the "stilbene fatty acids" (SFAs) are excellent surfactants which have film-forming properties very similar to the corresponding saturated fatty acids having the same overall lengths (Mooney 1983; Mooney *et al* 1984). In examining the compression, for example, of SFA films at the air-water interface, the behavior and limiting dimensions are found to be almost indistinguishable from corresponding saturated fatty acids when either pure SFA or SFA fatty acid mixtures are examined. However, our earliest investigations of these films revealed that both in compressed films at the air-water interface and in assemblies supported on rigid optically transparent supports (formed via sequential transfer of films from the air-water interface) the stilbene chromophore shows evidence of aggregation which sharply modifies the absorption and photophysics of the parent chromophore (Mooney 1983; Mooney *et al* 1984; Mooney and Whitten 1986). In the present manuscript, we discuss the behavior of these SFAs in several media with emphasis on their reactivities in transferred supported multilayers.

2. Results and discussion

2.1 General properties of the SFAs

Chart 1 illustrates the structures of several of the SFAs used in this study and shows the codes used in representing them. These stilbene derivatives can all be incorporated into fluid solutions of microheterogeneous media such as detergent micelles or phospholipid bilayers. Incorporation into sodium dodecylsulfate micelles results in reactivity very similar to that observed in homogeneous organic solvents. Absorption and fluorescence spectra characteristic of the stilbene monomer are observed and the fluorescence and isomerization efficiencies are comparable to those observed in nonviscous homogeneous solutions (Brown *et al* 1985). In contrast, several of the SFAs shown in chart 1 exhibit pronounced changes compared to homogeneous solutions when incorporated as "guests" into phospholipid bilayer solutions with strong increases in the monomer fluorescence efficiency and lifetime, particularly in the more rigid low temperature or gel phase (Suddaby *et al* 1985). For the intrachain SFAs, $\text{}_4\text{S}_{6A}$ and $\text{}_6\text{S}_{4A}$, the fluorescence efficiencies approach unity and isomerization is virtually eliminated. As indicated above, the SFAs exhibit quite different behavior when incorporated into supported Langmuir-Blodgett multilayers. Typically the SFAs can form pure monolayer films or they can be used in mixtures with saturated fatty acids of similar overall indicated length for the fully extended molecules. Figure 1 compares the solution and LB multilayer assembly fluorescence and absorption for $\text{}_6\text{S}_{4A}$. The red shift in fluorescence and concurrent blue shift in absorption can be readily ascribed to the formation of an "H" aggregate which would be predicted for a closely packed array of SFA molecules enforced by film compression (Mooney *et al* 1984). The types of aggregates that might be anticipated for chromophores such as the SFAs are demonstrated in figure 2. We originally suspected that "H" aggregate formation should be observed for very concentrated LB films and supported multilayers formed from a single SFA as a consequence of a packing phenomenon, rather than due to any preferential association phenomenon (Mooney *et al* 1984). Nonetheless we found that aggregate formation is very general for all the SFAs studied

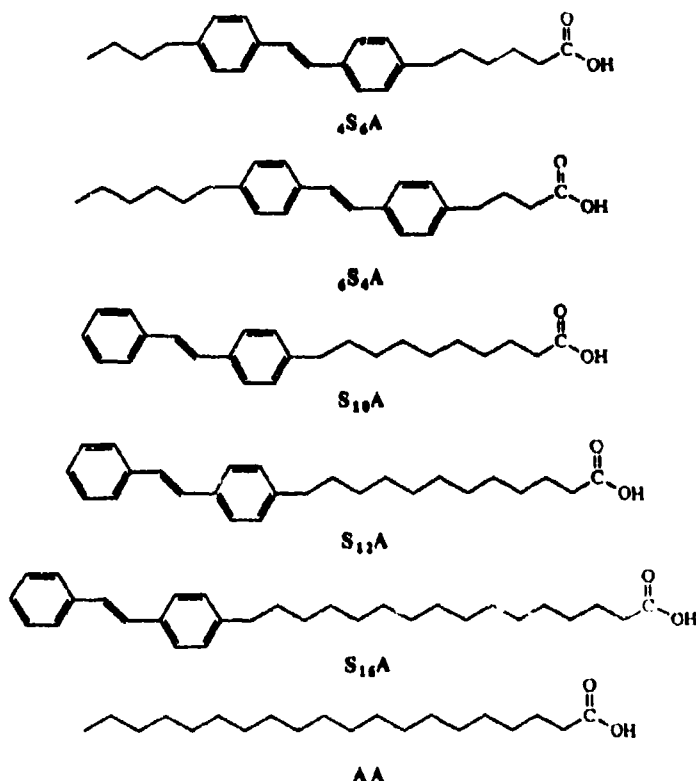


Chart I.

to date and persists for these compounds to the lowest dilutions (1:20 SFA:fatty acid "host") with little change in the appearance of the aggregate fluorescence or absorption (Spooner *et al.*, unpublished results).

Studies of the aggregate photophysics in assemblies containing potential quenchers which might serve as energy or electron acceptors from the SFAs indicate that the aggregates function as good donors in both cases but are very inefficient in transferring energy between adjacent layers of SFA (Mooney and Whitten 1986). For example, in an earlier study with layers of S_4A , it was found that while energy transfer (half-quenching distance of 70 Å) occurs even when the SFA and cyanine quencher are separated by more than one layer, there is no enhancement of the quenching when multilayers of the SFA are placed in contact with a single layer of the cyanine (Mooney and Whitten 1986). This indicates quite clearly that the SFA aggregates are very inefficient at "relaying" energy by degenerate transfer of singlet excitation across adjacent layers and result in no "antenna effect" such as might be anticipated were degenerate energy transfer to occur with reasonable efficiency. This observation is probably reasonable in view of the low oscillator strength of the low energy (long wavelength) transition associated with the H aggregate and the large "Stokes shift" between fluorescence and absorption.

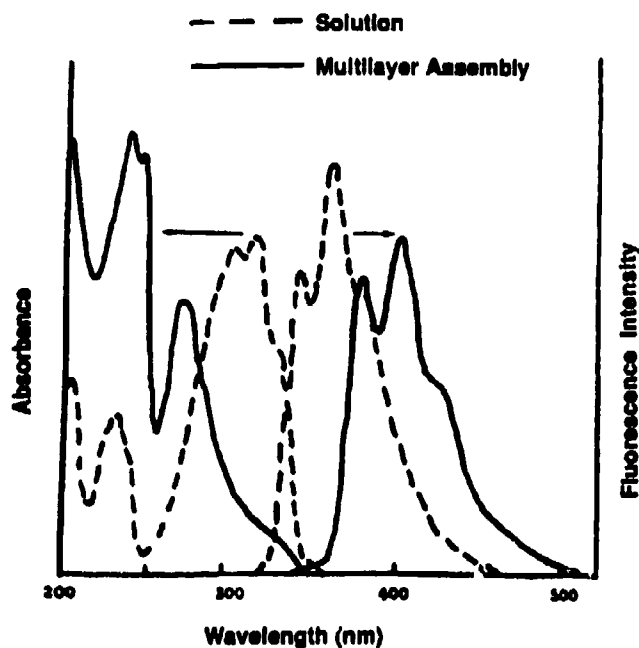


Figure 1. Comparison of solution and multilayer assembly spectra of $4S_{6A}$.

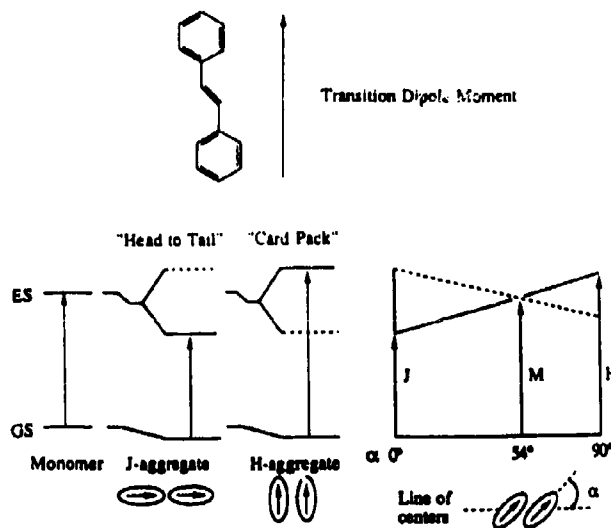


Figure 2. Geometrical arrangement of chromophores leading to the formation of H and J aggregates.

2.2 Experiments with mixtures of stilbene fatty acids

The diagram shown in figure 2 suggests that different SFAs might associate to form aggregates having different photophysical properties. Most notable is the prospect that two or more SFAs in an array leading to a large "offset" of the stilbene chromophore might result in an aggregate having "J" character which could lead to a high oscillator strength and fast fluorescence from the low energy transition with a resultant highly efficient degenerate energy transfer or "antenna effect". Towards this end, we have examined Langmuir-Blodgett assemblies formed from mixtures of three or five SFAs with a saturated fatty acid host. In one case we used a 1:1:1:1:1:5 mixture of $_{4}S_{6A}$, $_{6}S_{4A}$, S_{10A} , S_{12A} , S_{16A} and arachidic acid; more extensive investigations have been carried out with a 1:1:1:3 mixture of $_{4}S_{6A}$, $_{6}S_{4A}$, S_{12A} and arachidic acid. In both cases, relatively similar behavior has been observed (Spooner and Whitten 1991). The absorption spectrum is very similar to that shown for a single SFA in figure 1 and the fluorescence is rather similar (figure 3) and dominated by a relatively long-lived component suggesting a forbidden lowest energy transition similar to the "H" aggregate observed with a single stilbene. However, a number of studies with assemblies of different compositions have shown that the SFA mixture gives very different photophysical behavior compared to assemblies of similar composition but with only a single SFA. Fluorescence from a single layer or bilayer of the SFA mixture is readily quenched when a quencher (electron acceptor such as a surfactant viologen or cobalt complex) is incorporated into the same or adjacent layer with hydrophilic-hydrophilic contact. Moreover, quenching by a single layer of quencher can be effective for assemblies containing several sequentially deposited layers as illustrated in figure 4. Thus, for the SFA mixture we observe results consistent with the effective migration or delocalization of excitation over several multilayers but overall spectroscopic characteristics associated with the "H" aggregate. This raises several questions which we have attempted to address in recent investigations.

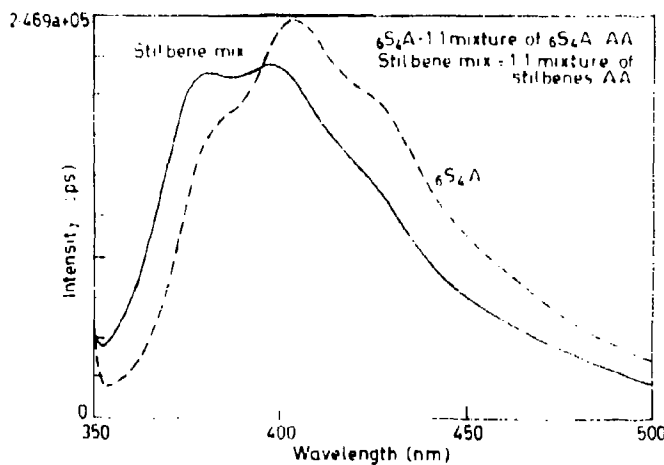


Figure 3. Fluorescence quenching of 5 layers of the stilbene mixtures vs 5 layers of a single type of stilbene.

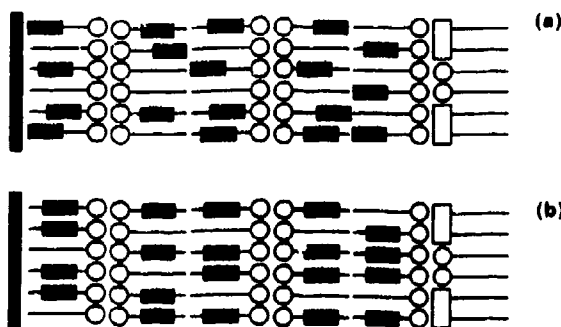


Figure 4. Fluorescence spectra of α S_{4A} and the stilbene mixtures - as compared to a slide containing five layers of the stilbene mixture, the addition of a layer of V₂₁₈ (as shown above) results in 41% (a) and 5% (b) reduction in the fluorescence intensity.

2.3 Questions concerning the "H" aggregate

The finding that mixtures containing several SFAs give absorption spectra similar to those for a single SFA or SFA-arachidate mixture and dominated by the relatively sharp "blue-shifted" transition near 270 nm suggests that the "H" aggregate may represent a selective association of the stilbene chromophore and not simply an association "forced" by packing of the amphiphiles as the films are compressed. Although the SFA mixture films exhibit limiting areas/molecules and high compressibility similar to those of either arachidate or single SFA-arachidate mixtures, the "lift off" (initial rise in surface pressure as the film is compressed) occurs for the mixed films at somewhat larger areas/molecules than for those of simpler composition (Spooner *et al.*, unpublished results). This might be taken as evidence that some association of the SFAs occurs before the films are completely compressed. While various theoretical models of the "H" aggregate suggest a range of sizes from fairly small limiting numbers/aggregate to relatively large numbers of monomers, the persistence of similar aggregate spectra and photophysical properties over a wide dilution range for a single SFA-arachidate mixture suggests that the limiting aggregate probably consists of a relatively small number of monomer units. We shall address the important question of limiting size of the aggregate a little later.

One of the interesting features of the "H" aggregate formed from the SFAs is that it is a rather general process for a series of amphiphiles containing conjugated systems similar to the stilbene chromophore (Spooner *et al.*, unpublished results). Moreover, the absorption spectra of a series of aggregates from different amphiphiles are remarkably similar even in cases where significant substitution occurs that results in rather large differences in the solution monomer spectra. Chart 2 shows the structures of several surfactants we have found exhibiting similar behavior with regard to aggregate formation either in pure films and supported layers or in mixtures with saturated fatty acids of corresponding chain length. Figure 5 compares absorption spectra of several of these aggregates in quartz-supported Langmuir-Blodgett assemblies. While the aggregate absorption spectra are all quite similar, the aggregate fluorescence differs substantially, depending upon the individual chromophores and these differences

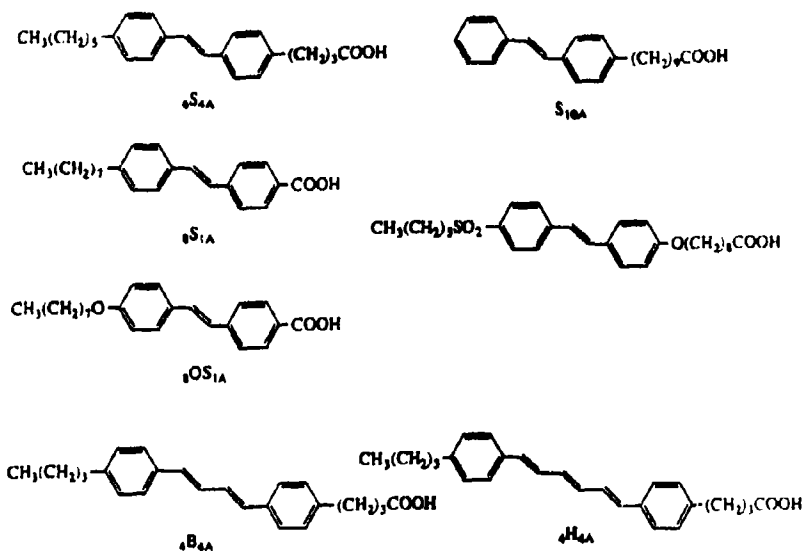


Chart 2.

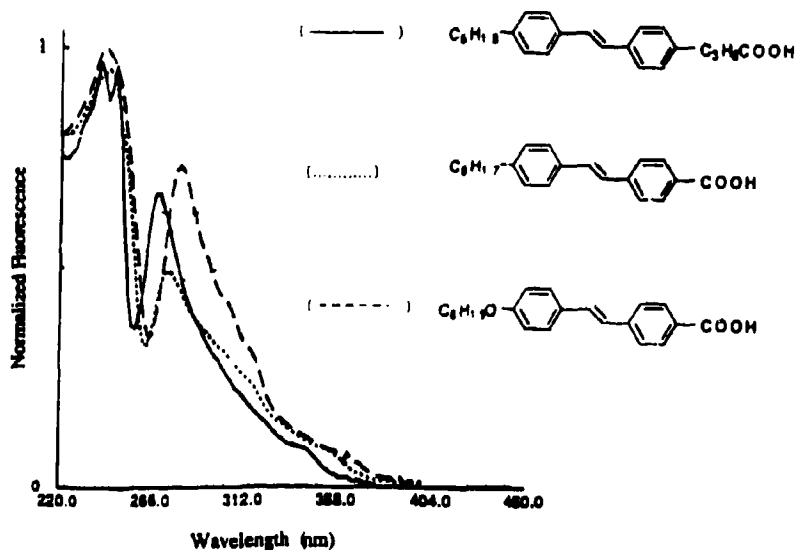


Figure 5. Multilayer absorption of 1:1 mixtures of substituted surfactant stilbenes and arachidic acid.

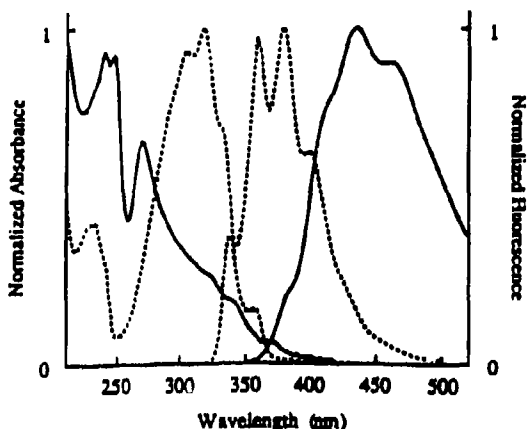


Figure 6. Comparison of solution and multilayer assembly spectra of $_{\text{4}}\text{B}_{\text{4A}}$.

have not yet been systematically studied. Interestingly, the strength of the aggregate seems to be quite variable and generally decreases with extension of the α, ω -diphenyl-polyene chain. Thus $_{\text{4}}\text{H}_{\text{4A}}$ and $_{\text{4}}\text{B}_{\text{4A}}$ can be rather readily diluted from "aggregate" to monomer by dilution with arachidate (see figure 6 for $_{\text{4}}\text{B}_{\text{4A}}$) in contrast to the SFAs. Furthermore, addition of a small amount of functionalized surfactant with a lower energy fluorescence than that from the SFA aggregates results in a fluorescence spectrum dominated by the "guest" indicating that energy transfer within a single LB film layer is very efficient.

While the presence of the "pure" "H" aggregate is easy to assess in the many cases discussed thus far, either with a single conjugated surfactant or a mixture, the question of different or "mixed" aggregates remains somewhat unresolved. It is tempting to associate the small differences in fluorescence spectra for the SFA mixture shown in figure 3 with a small amount of mixed aggregate (fluorescence occurs at wavelengths longer than pure monomer fluorescence in solution but at wavelengths shorter than those associated with the "H" aggregate). The presence of such a species could also account for the efficient "delocalization" of excitation discussed above in connection with the SFA mixture in LB multilayers. Spectral subtraction of the single SFA aggregate from the mixture provides what might be the spectrum of a "mixed aggregate" (figure 7).

2.4 Stilbene fatty acid phospholipids

A different approach, which we have recently initiated, to the study of aggregate formation with the SFA derivatives involves the synthesis and study of stilbene fatty acid esters of phosphatidyl choline (Furman *et al*, unpublished results). Synthesis of bis-SFA-phosphatidyl choline derivatives is reasonably straightforward; selective enzymatic hydrolysis to the mono-SFA-phosphatidyl choline and esterification with a second SFA afford phosphatidyl choline derivatives containing two different SFAs (Furman *et al*, unpublished results). Chart 3 shows the structures of the three SFA-phosphatidyl choline derivatives that we have initially studied. To date, we have

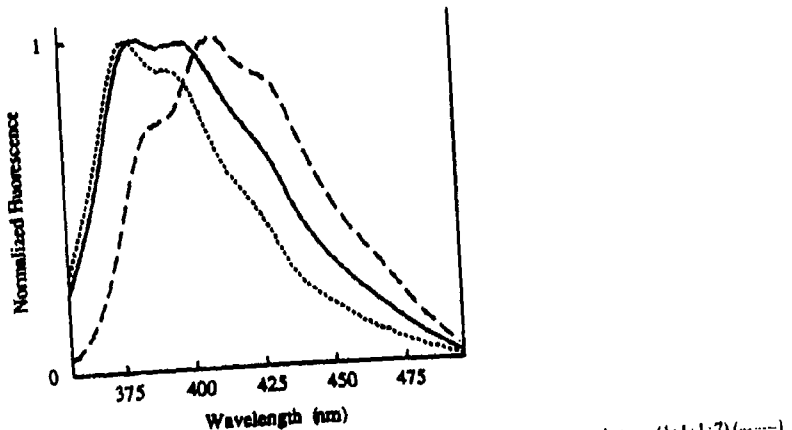
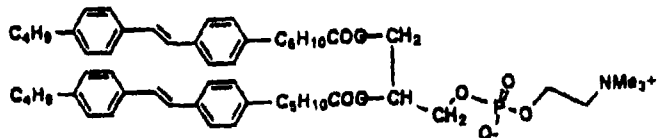
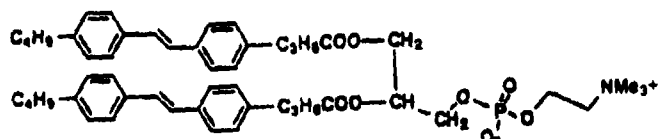


Figure 7. Normalized fluorescence spectra of four component SFA mixture (1:1:1:7) (—), S_{AA} :AA (3:7) (---), and "H" dimer spectrum resulting from the subtraction of S_{AA} and AA from SFA mixture (···).

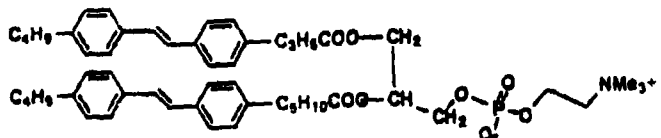
SFA Phospholipids



Bis 4S₆E PC



Bis 1S_{1/2}PC



1S₄-4S₆E-PC

Chart 3.

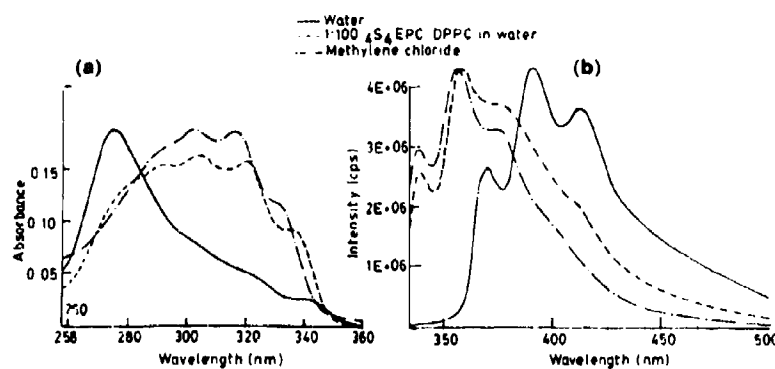


Figure 8. Absorbance (a) and fluorescence spectra (b) for *bis*(₄S₄E)PC in water (—), methylene chloride (---) and 1:100 ₄S₄E PC:DPPC in water (···).

examined the behavior of these three SFA-PC derivatives in dilute organic solvents, in water and in water-containing excess of dipalmitoyl phosphatidyl choline (DPPC). We have also examined the behavior of the SFC-PC's in aqueous and aqueous methanol solutions with γ -cyclodextrin. All three SFC-PC's show essentially identical behavior in dilute methylene chloride solution. The absorption and fluorescence spectra are nearly identical to those of the monomeric stilbene fatty acid (e.g. ₆S_{4A}) in the same solvent; the fluorescence quantum yield and lifetime are also similar for the SFC-PC's in methylene chloride to that of the SFA monomer. This clearly indicates that in a non-polar or moderately polar aprotic solvent there is little tendency for the *trans*-stilbene chromophores of the SFC-PC's to associate with one another, even though the "local concentration" is extremely high. The three SFC-PC's all show rather similar behavior on dispersal in pure water; both the absorption and fluorescence spectra are clearly those of the "H" aggregate and nearly identical to those obtained in LB assemblies of the SFA's. Some preliminary studies indicate that the organized assemblies formed from pure SFA-PC - presumably bilayer vesicles or multilamellar vesicles - are much larger than those formed by similar treatment of DPPC. The spectral behavior of the SFA-PC's in dispersions 1:100 with DPPC in water is slightly different for each PC but in general different from either monomer or "H" aggregate (figure 8). The absorption spectra show rather broad bands extending from the range of the "H" aggregate on the blue to slightly beyond the monomer to the red. The fluorescence is predominantly monomer but has at least some contribution from a longer wavelength component.

More illuminating results are obtained from studies of the SFA-PCs in aqueous methanol solutions containing γ -cyclodextrin (Furman *et al*, unpublished results). Although pure aqueous solutions give only an "H" aggregate spectrum, addition of methanol results in conversion to a monomer absorption and fluorescence, indicating that the bilayer aggregates are being dispersed and solubilized into dissolved monomer. However addition of γ -cyclodextrin results in a change in both absorption and fluorescence as shown in figure 9. The changes are most pronounced for the *bis*(₄S_{4E}) PC for which both the absorption and fluorescence are clearly that of the "H" aggregate. For *bis*(₆S_{4E}) PC and (₄S_{6E},₄S_{4E}) PC, the spectra resemble those of the same PC's in diluted aqueous solutions with DPPC as the "host." The results with the *bis*(₄S_{6E})

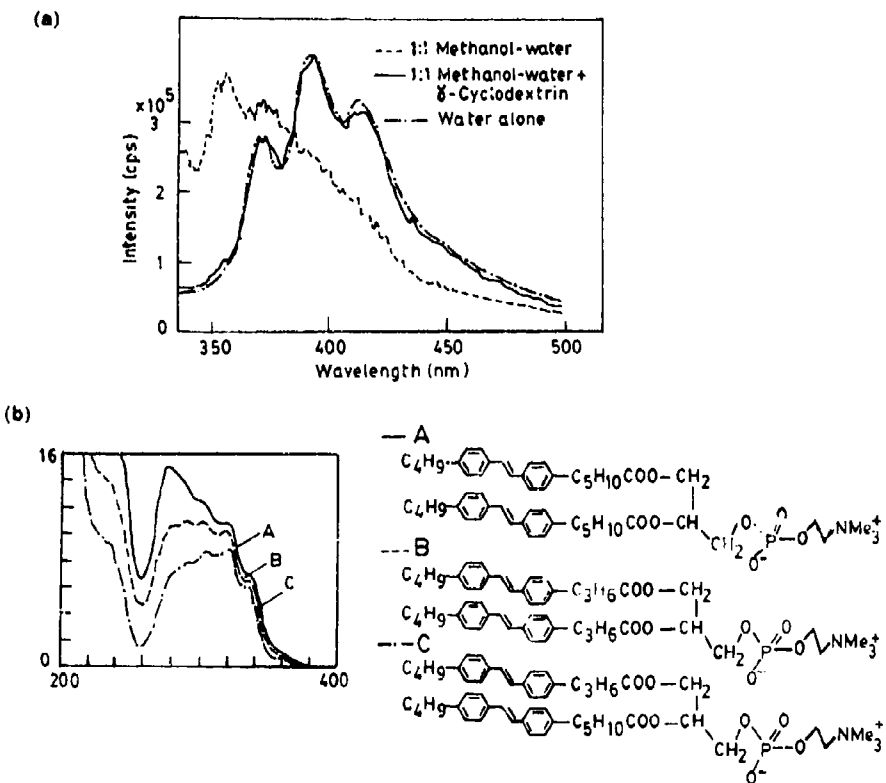


Figure 9. (a) Fluorescence spectra of $bis\ \Delta_{6E}$ PC in water, 1:1 methanol-water and 1:1 methanol-water + γ -cyclodextrin. (b) Absorbance spectra of Δ_5 EFC, Δ_{4E} PC and Δ_{4E} , Δ_{4E} PC diluted 1:100 with DPPC in water.

PC suggest that the minimum "H" aggregate is a dimer (since models suggest it is impossible to force more than two *trans*-stilbene units into the cyclodextrin cavity). The difference between this PC and the other two examined thus far is ascribed to the distance of the stilbene chromophore from the phosphatidyl choline head group and glycerol backbone. For the two PC's containing shorter chains it appears reasonable that there is insufficient flexibility for the two stilbenes to form the "ideal" "H" dimer and so forced association leads to an aggregate having different spectroscopic properties. In the case of the longer chain separation, ideal "H" aggregate geometry can be attained and the spectroscopic properties are almost identical to those in the extended bilayer or multilayer assemblies.

3. Conclusions

While we are still examining many aspects of the controlled formation of aggregates in LB assemblies and phospholipid bilayers, the results obtained thus far suggest that the limiting spectral shifts for the aggregate can be attained with an "H" dimer and that this species does indeed represent an energy minimum. The association to form

the "H" aggregate or dimer is evidently closely related to apolar association of other aromatic chromophores in aqueous media (Dewey *et al* 1978; Diederich 1990; Smithrud *et al* 1990) and may exert important control over the type of assembly formed by these aromatic-functionalized amphiphiles. While the "H" aggregate clearly represents an energy minimum or at least a favored aggregate, our studies with the phospholipids, and to some extent the LB assemblies, suggest that packing forces can in some cases lead to the formation of different aggregates having quite different photophysical properties which may be of interest in tuning the behavior of extended arrays of these chromophores. While these arrays of organic chromophores may be thought of as "supramolecular" species having a commonality with inorganic quantum species such as clusters or semiconductor colloids (Lehn 1988; Kortan *et al* 1990), the stereochemical complexity of the organic chromophores makes their behavior potentially much more complex and possibly quite versatile.

Acknowledgements

We are grateful to the US National Science Foundation (grant number CHE 9211586) for support of this research.

References

- Allen M T and Whitten D G 1989 *Chem. Rev.* **89** 1691
- Brown P E, Mizutani T, Russell J C, Suddaby B R and Whitten D G 1985 *ACS Symp. Ser.* **278** 171
- Dewey T G, Wilson P S and Turner D H 1978 *J. Am. Chem. Soc.* **100** 4550
- Diederich F 1990 *J. Chem. Edu.* **67** 813
- Furman I, Geiger H C, Richard W and Whitten D G (unpublished results)
- Geiger M W and Turro N 1977 *J. Photochem. Photobiol.* **26** 221
- Hammond G S *et al* 1964 *J. Am. Chem. Soc.* **86** 3197
- Itoh T and Kohler B E 1987 *J. Phys. Chem.* **91** 1760
- Kortan A R, Hull R, Opila R L, Bawendi M G, Steigerwald M L, Carroll P J and Brus L E 1990 *J. Am. Chem. Soc.* **112** 1327
- Lehn J-M 1988 *Angew. Chem. Int. Ed. Engl.* **27** 90
- Mizutani T and Whitten D G 1985 *J. Am. Chem. Soc.* **107** 3621
- Mooney W F III 1983 *Energy and electron transfer in multilayer assemblies of surfactant stilbene derivatives* Ph D dissertation, University of North Carolina, Chapel Hill
- Mooney W F III, Brown P E, Russell J C, Costa S B, Pedersen L G and Whitten D G 1984 *J. Am. Chem. Soc.* **106** 5659
- Mooney W F and Whitten D G 1986 *J. Am. Chem. Soc.* **108** 5712
- Russell J C, Costa S B, Seiders R P and Whitten D G 1980 *J. Am. Chem. Soc.* **102** 5678
- Russell J C, Whitten D G and Braun A M 1981 *J. Am. Chem. Soc.* **103** 3219
- Saltiel J 1992 *J. Photochem. Photobiol.* **65** 29
- Saltiel J, Chang D W L, Megarity E D, Rousseau A D, Shannon P T, Thomas B and Uriarte A K 1975 *Pure Appl. Chem.* **41** 559
- Saltiel J and Charlton J L 1980 In *Rearrangements in ground and excited states* (ed.) P deMayo (New York: Academic Press)
- Smithrud D B, Sanford E M, Chao I, Ferguson S B, Carcanague D R, Evanseck J D, Houk K N and Diederich F 1990 *Pure Appl. Chem.* **12** 2227
- Spooner S P, Furman I, Geiger H C and Whitten D G (unpublished results)
- Spooner S P and Whitten D G 1991 *Proc. Soc. Photo-Opt. Instrum. Eng.* **82** 1436
- Suddaby B R, Brown P E, Russell J C and Whitten D G 1985 *J. Am. Chem. Soc.* **107** 5609
- Takagi K, Suddaby B R, Vadas S L, Backer C A and Whitten D G 1986 *J. Am. Chem. Soc.* **108** 7865

Electron transfer through vesicle membranes: Mechanistic ambiguities

LEIF HAMMARSTRÖM* and MATS ALMGREN

Department of Physical Chemistry, University of Uppsala, Box 532, S-751, 21 Uppsala,
Sweden

Abstract. We have studied transmembrane electron transfer mediated by an amphiphilic viologen ($C_{16,1}V^{2+}$) in lecithin vesicles. There is no long-range electron transfer between viologens bound to opposite interfaces of the vesicle membrane, as is often proposed. Instead we proposed a mechanism where the rate-determining step is the disproportionation of two viologen radical cations ($2C_{16,1}V^+ \leftrightarrow C_{16,1}V^{2+} + C_{16,1}V^0$) forming a doubly reduced, uncharged viologen that transfers electrons by rapid transmembrane diffusion and subsequent reduction of electron acceptors. Studies on other redox mediators provided further information. A brief background to the field is given, including comments on work done by others in relevant systems.

Keywords. Electron transfer; membrane; viologen; disproportionation mechanism.

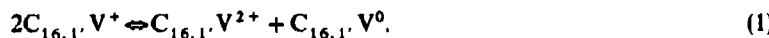
1. Introduction

The separation of electron transfer products is the primary step in both natural and artificial photosynthesis. There are basically two approaches to separation of the initially produced "electron/hole" -pair: one is by using microheterogeneous media (micelles, vesicles etc.) and the other is by using a sequence of electron transfer steps between species in a relatively ordered array, as for example in covalently linked donor-acceptor systems (CLDA) (Balzani and Scandola 1991). There are only few examples of artificial systems combining both approaches (see e.g. Matsuo 1985, Moore *et al* 1987, Krueger *et al* 1988, Nango *et al* 1988, Momenteau *et al* 1989, Kobuke *et al* 1991, Kugimura *et al* 1991), as natural photosystems do. Using, for example, a CLDA in a vesicle is an attractive extension of the artificial systems. However, it is necessary to control and understand the simple vesicular systems better before trying to incorporate more complicated molecules. Despite the great number of articles describing transmembrane electron transfer in vesicles (for recent reviews, see Hurst 1990, Robinson and Cole-Hamilton 1991, Lymar *et al* 1991), the general understanding of these systems is still very limited, especially concerning the mechanism of transmembrane electron transfer.

We have studied a system where an amphiphilic viologen ($C_{16,1}V$) acts as redox mediator in vesicles of egg lecithin. We have found that there is no long-range electron transfer through the vesicle membrane between viologens bound to opposite interfaces,

* For correspondence

as is often proposed. Instead, we propose a mechanism where two singly reduced viologen radical cations exchange an electron in a disproportionation reaction, (1).



The doubly reduced, uncharged species thus formed diffuses rapidly through the membrane and reduces a secondary acceptor. By comparing with similar redox mediators we have been able to examine detailed reaction steps and draw further conclusions.

This article will summarize our results (Hammarström *et al* 1992, 1993) and comment briefly on the results of others in similar or otherwise relevant systems.

2. Transmembrane electron transfer in vesicular systems

2.1 Vesicle characteristics

A very common type of vesicle is that composed of phosphatidylcholine lipids. Some of its properties are summarized in figure 1. The zwitterionic head-group is rather large and the two acyl chains usually contain 16 or 18 carbons. Natural lecithin is

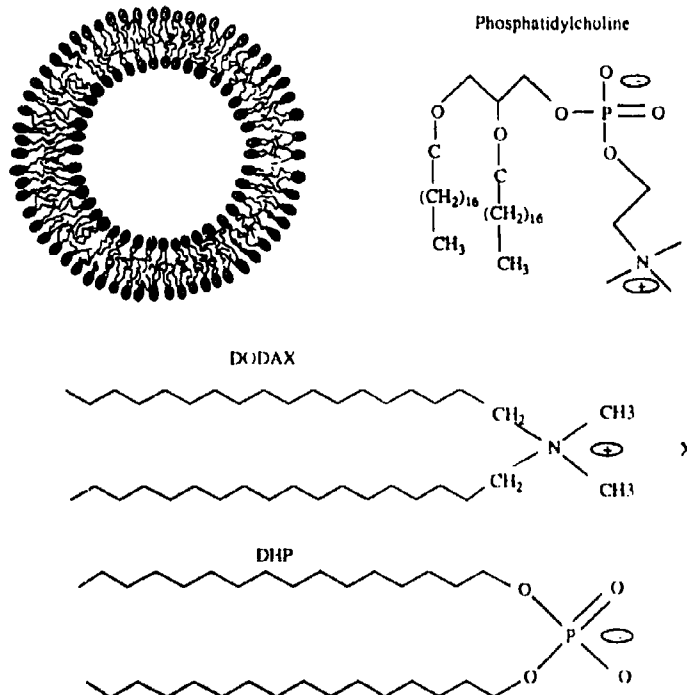


Figure 1. A schematic cross-section of a small, unilamellar vesicle of lecithin. There are typically ≈ 3000 monomers; the diameter is $200\text{--}300\text{ \AA}$ and the thickness of the membrane bilayer is $\approx 40\text{ \AA}$. Also shown are the structures of a typical phosphatidylcholine lipid, a monomer of DHP, and of DODAX (see text).

a mixture with many mono-(or poly-) unsaturated chains. Because of the mixture and presence of unsaturated chains the lecithin vesicles are in a liquid state instead of a gel state at room temperature. Lateral diffusion is thus rapid, but exchange of monomers between the different monolayers in the same vesicle or between different vesicles is extremely slow (of the order of one day).

The most important types of synthetic vesicles are composed of dihexadecylphosphate (DHP) or dioctadecyldimethylammoniumhalide (DODAX, figure 1). They are, of course, highly charged and the effective size of the monomer head group is strongly dependent on the counter-ions present. They are therefore more sensitive to perturbations from di- or multivalent ions – and also from complex-forming additives – than lecithin vesicles and are thus known to fuse or to be destroyed upon addition of several species (Carmona-Ribeiro 1992; Hurst *et al* 1983; Robinson *et al* 1990). Vesicles of DHP and DODAX are larger than the small, unilamellar vesicles of egg lecithin, but the thickness of the bilayer is about the same ($\approx 40 \text{ \AA}$). As for vesicles of non-mixed saturated phosphatidyl choline (e.g. pure DPPC), they are in a gel-state at room temperature.

It is possible to trap water-soluble species in the internal water phase of the vesicles since the membrane allows only very slow diffusion of most ions, and the same species can be removed from the bulk (external) water phase by gel exclusion chromatography resulting in an asymmetric arrangement. It is also possible to dissolve hydrophobic species in the hydrocarbon core of the vesicle and to bind amphiphilic molecules to the interfaces. Thus, vesicular systems allow manifold arrangements of redox-active species.

2.2 Mechanistic principles

There are two types of mechanisms possible for electron transfer through vesicle membranes mediated by water soluble or interfacially bound species (figure 2). One is diffusive, where the redox-mediator is reduced on one side and oxidized on the other, and at least one redox form diffuses through the membrane. More than one electron can be carried by each mediator and protonation/deprotonation can also be involved. The diffusion can be facilitated by a carrier, for example, and the reduction/

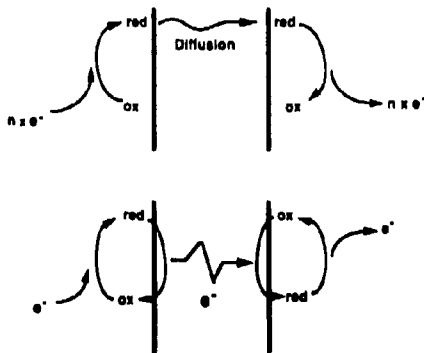


Figure 2. Schematic picture of the two types of mechanistic principles for transmembrane electron transfer discussed in the text: diffusional mechanism (top) and self-exchange mechanism (bottom).

oxidation steps of the mediator can be very complicated. The important feature is that the diffusive mechanism does not involve long-range electron transfer but requires transmembrane molecular motion, reversible or not.

The other type of mechanism is self-exchange between a reduced mediator on one side of the vesicle and an oxidized mediator on the other (figure 2). In the self-exchange reaction, the electron is supposed to be transferred via tunnelling, perhaps in several steps if there are mediators distributed at different depths in the membrane. A super-exchange mechanism where the hydrocarbon chains of the vesicle surfactants would facilitate electron transfer has also been suggested. Direct self-exchange between interfacially bound mediators, i.e. over a distance of at least 30 Å, is not possible. Simple calculations on both barrier penetration and super-exchange result in predicted rates that are several orders of magnitude slower than the observed ones. Sometimes it is argued that the actual transfer distance is diminished by simultaneous, momentary and partial penetration of the membrane by two mediators on opposite interfaces prior to their self-exchange reaction, thus depending on a sequence of coincident events. The ideas of self-exchange mechanisms over long distances has of course been inspired by the increasing awareness of the importance of long-range electron transfer in biological systems (Johnson *et al.* 1990) and of the successful work on artificial covalently linked donor-acceptor systems (CLDA; Balzani and Scandola 1991). The term "long-range" in those systems usually refers to 15 Å or less, while the thickness of the hydrophobic part of a vesicle membrane is ≥ 30 Å. Furthermore, in the vesicular systems the donors and acceptors are (usually) not linked either to each other or to the surfactants of the vesicle, and the hydrocarbon chains of the latter are flexible and not linked across the bilayer. Thus there are substantial differences between the systems that make long-range electron transfer via tunnelling or super-exchange across the entire membrane of the vesicles much less plausible.

The self-exchange type of mechanism is electrogenic, i.e. if there is no charge compensating ionic flow a transmembrane electric potential will rapidly build up, thus terminating the electron transfer reaction. The diffusive type of mechanism is also electrogenic if the diffusing species is charged. This complicates interpretation further since the charge compensating ions are often not identified. These could be H^+ / OH^- , one of the redox-active species themselves or any other ions present. Usually the rates of transmembrane diffusion of those species are not known. Thus it is often possible to explain unexpected results by suggesting that there are different rate-limiting steps under different circumstances. Very rapid (in the order of 1 ms) rates of proton transfer through lecithin vesicle membranes have been reported by several workers (Cevc and Marsh 1987, and references therein). If this is correct, the charge compensation is usually not a problem since the observed rates are much slower in most cases.

2.3 Systems with biological redox mediators

This section contains a few examples of systems relevant to the question of the mechanism of transmembrane electron transfer. For a more complete list the reader is referred to the reviews on this topic (*vide supra*).

Many biological redox mediators are large compared to the membrane thickness, and are also, at least partially, hydrophobic. For example in a system studied by Tabushi and coworkers (Tabushi and Nishiya 1981) cytochrome-c3 was bound to both

interfaces of lecithin vesicles. Due to their large size ($\approx 30 \text{ \AA}$) and partial penetration of the membrane by cytochromes on different sides of the membrane, they could form an aggregate acting as an electron channel through the membrane allowing for electron transfer between the cytochromes.

There is evidence (Ford and Tolin 1982) that chlorophyll-*a*(chl-*a*) binds in a heterogeneous manner to lecithin vesicles so that there are chl-*a* bound interfacially as well as in the hydrophobic part of the membrane. The rapid transmembrane electron transfer observed in this system ($k_{obs} \geq 10^4 \text{ s}^{-1}$) can be explained by a sequence of electron transfer steps between chl-*a* molecules distributed at different depths in the membrane. The distance in each step can then be small or of moderate size (a few Ångströms).

Transmembrane electron transfer between hydrophobic Mg-porphyrins linked by spacers of different lengths to hydrophilic "anchors" on different interfaces of the membrane has been studied (Dannhauser *et al* 1986). No electron transfer was observed until the edge-to-edge distance between the porphyrins was 4 Å or less.

There are several systems with porphyrins that exhibit transmembrane electron transfer. For photoinduced reactions in many systems, it has been observed that the transmembrane electron transfer is a two-photon process. This has sometimes been taken as evidence for a long-range self-exchange reaction between a photo-oxidized porphyrin on one side of the membrane and a photo-excited or photo-reduced porphyrin on the other (Katagi *et al* 1981, 1982; Lymar *et al* 1991). However, in other systems there was a carrier for the electron acting as a mediator via diffusion between the porphyrins (Matsuo *et al* 1980). A two-photon ionization of a porphyrin dimer on one side of the membrane has also been proposed as the initial reaction step, explaining the quadratic dependence on the number of photons (Jusupov *et al* 1985). It seems possible that the relatively hydrophobic porphyrins could be distributed in the membrane in the same way as the chl-*a* (*vide supra*) allowing for short-range, multi-step electron transfer, even if some results indicate that most porphyrins are located closer to the interface of the membrane than to the middle (Lymar *et al* 1991). In the latter case the observed two-photon dependence could be explained by the dimer-process according to Jusupov *et al* (1985).

2.4 Systems with viologens as mediators

Violagens constitute a very important class of redox mediators (Bird and Kuhn 1981). Usually the substituents on the nitrogens of the bipyridine rings are simple alkyl groups (figure 3), but several compounds with, for example, charged substituents have been synthesized (Summers 1991). The alkyl substituted violagens are in the following abbreviated $C_{n,n'}V$ where n and n' are the number of carbons in the substituents. The air-stable form is a dication which can be reduced to the radical cation, which under certain circumstances can be further reduced to the electro-neutral, doubly reduced form. The redox steps are reversible and an equilibrium constant, K_d , for disproportionation, (1), can be defined as below:

$$K_d = ([C_{n,n'}V^{2+}][C_{n,n'}V^0])/[C_{n,n'}V^+]^2. \quad (2)$$

This equilibrium has been studied in several homogenous media (Bird and Kuhn 1981; Mohammad *et al* 1981). Violagens are also known to form dimers; in particular the radical dimer has been studied, but mixed dimers are also known to exist (Bird

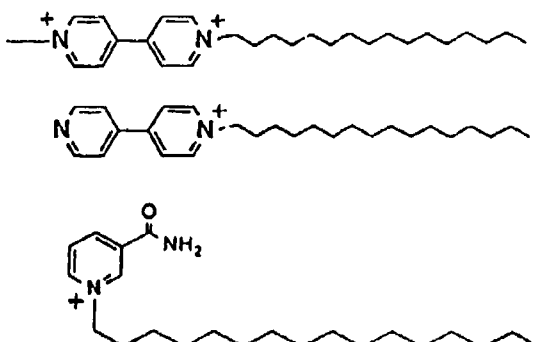


Figure 3. The redox mediators used (from top): $C_{16,1}V^{2+}$, $C_{16}B^+$, $C_{16}NA^+$.

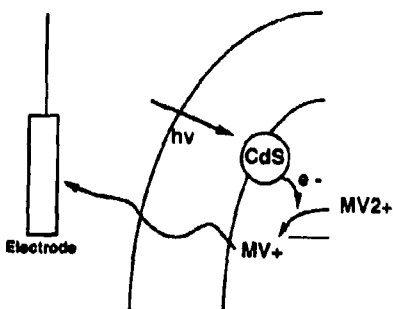


Figure 4. The system of Tricot and coworkers. Shown is the configuration where both CdS and MV^{2+} are in the interior of the DHP vesicles. The curved lines represent the interfaces of the membrane where the exterior is to the left and the interior to the right of the lines.

et al 1981). The different redox forms are spectroscopically distinct and can thus be detected by absorption spectroscopy.

Tricot and coworkers (Tricot and Manassen 1988; Tricot *et al* 1991) have used colloidal particles of CdS adsorbed to DHP-vesicles as photoexcited electron donors with water soluble methylviologen (MV^{2+}) as acceptor (figure 4). By combining absorption spectroscopy and electrochemical detection they were able to distinguish between viologen radicals in the internal water phase of the vesicles and those in the bulk phase. They concluded that there was no photostimulated diffusion of oxidized MV^{2+} through the membrane, but upon reduction of internal viologen the radical (MV^+) diffused through the membrane. Since no viologen was initially present outside the vesicles this excludes the possibility of the self-exchange type of mechanism (*vide supra*). Note that it is not possible to conclude from these experiments alone in what form the reduced viologen is diffusing, e.g. if it is MV^+ or MV^0 that is actually transversing the membrane. Electron transfer in this system also occurred between CdS on the outside and MV^{2+} on the inside of the vesicles, but only at high loadings of CdS on the vesicle and at high light-intensities. It might be suspected that under those conditions there is some critical perturbation of the vesicle that induces transmembrane diffusion and/or partial penetration of the membrane by species

otherwise membrane impermeable/impenetrable. Especially in steady-state illuminated systems, photostimulated diffusion has proved to be a problem as pointed out by the authors (Tricot and Manassen 1988). Tricot and coworkers found that the CdS particles penetrate the membrane to some extent and this must perturb the membrane locally due to the large size of the CdS particles.

A diffusional model for transmembrane electron transfer with a conjugation of inward flux of $C_{n,n}V^+$ and outward flux of $C_{n,n}V^{2+}$ for alkylviologens in lecithin vesicles has been developed (Tabushi and Kugimiya 1984, 1985). The authors divided the reaction in steps of entrance of viologen radicals into the membrane and exit to the opposite water phase. They claimed that, in stopped-flow experiments, a steady-state was obtained where the viologen fluxes and the rates of reduction by external dithionite and oxidation by an internal electron acceptor were the same. It has been shown that the oxidized $C_{n,n}V^{2+}$ does not permeate the membrane of a lecithin vesicle (Zamaraev *et al* 1988; Hammarström *et al* 1992). Also, the kinetic trace shown (Tabushi and Kugimiya 1985) for the fastest mediator used, $C_{4,4}V^{2+}$, exhibits almost no change in concentration of viologen radical between 20 and 30 s (taken as evidence for steady-state kinetics) which is not consistent with later results (Zamaraev *et al* 1988) where the observed rate in an identical experiment with $C_{16}V^{2+}$ was of the order of one second. According to the figure caption (Tabushi and Kugimiya 1985), the amount of internal, secondary acceptor was too small to be able to re-oxidize all viologen since two equivalents are needed (*vide infra*), which explains the long-time stability of the viologen radical. Considering the discrepancies with the results of other groups as indicated above, this model of flux conjugation can be rejected.

$Ru(bpy)_3^{2+}$ -sensitized transmembrane electron transfer mediated by alkylviologen in phosphatidylcholine vesicles was studied by flash-photolysis (Khannanov *et al* 1987). The authors found no dependence of the observed rate on the ratio of viologen to lipid, which is an argument against self-exchange mechanisms since they depend on the probability of two viologens diffusing to adjacent positions on opposite sides of the membrane. Note that the increase in viologen/lipid ratio does not necessarily result in more viologen radical produced by each laser flash if there is already an efficient quenching of the excited $Ru(bpy)_3^{2+}$. Thus, it was not shown how the observed rate varies with the surface concentration of viologen radical. The authors suggested that diffusion of viologen radical was responsible for transmembrane electron transfer, and their interpretation of the temperature-dependence supported this suggestion. However, they unexpectedly found that the observed rate was independent of the length of the alkyl chains of the viologens, contrary to what was found in stopped-flow experiments by others (Thompson *et al* 1987; Zamaraev *et al* 1988).

A combination of self-exchange and viologen radical diffusion was proposed by Zamaraev and co-workers in a system where $C_{16,16}V^{2+}$ mediated electron transfer from dithionite (stopped-flow) or excited $Ru(bpy)_3^{2+}$ (flash-photolysis) on one side of lecithin vesicle membranes to $Fe(CN)_6^{3-}$ or $C_{n,n}V^{2+}$ on the other (figures 5 and 6, Lymar *et al* 1991, and references therein). If, in the stopped-flow experiments, $Fe(CN)_6^{3-}$ was absent the observed rate was proportional to the viologen/lipid ratio and electron tunnelling between viologens on different interfaces of the membrane was proposed to be rate-determining. If $Fe(CN)_6^{3-}$ was present the observed rate was somewhat slower and independent of the viologen/lipid ratio, in which case it was proposed that a charge-compensating transmembrane diffusion of viologen

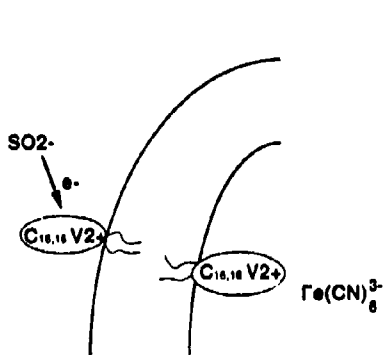


Figure 5. The system of Zamarayev and coworkers. Shown is the configuration where dithionite is used as reductant (SO_2^-) reduced the viologen after the equilibrium $\text{SO}_2\text{O}_4^{2-} \leftrightarrow 2\text{SO}_2^-$). When excited $\text{Ru}(\text{bpy})_3^{2+}$ is used as a reductant it is dissolved in the vesicle interior and $\text{Fe}(\text{CN})_6^{3-}$ is in the exterior.

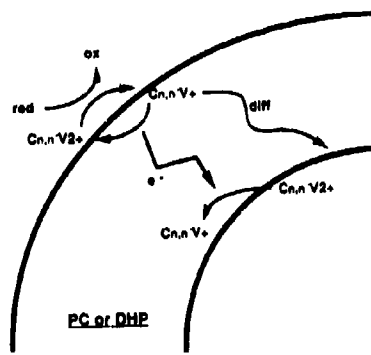


Figure 6. The mechanism for viologen-mediated transmembrane electron transfer proposed by Zamarayev and coworkers and by Hurst and coworkers.

radical was rate limiting. The independence of the rate on the lipid/viologen ratio is a surprising observation which is not consistent with the proposed mechanism. Any charge-compensating transmembrane diffusion of ions in the case without $\text{Fe}(\text{CN})_6^{3-}$ would be active in the case with $\text{Fe}(\text{CN})_6^{3-}$ and would give the same observed rate and rate-dependences. A proportional dependence of the observed rate on the viologen/lipid-ratio was later observed in identical experiments with $\text{C}_{16,18}\text{V}^{2+}$ and internal $\text{Fe}(\text{CN})_6^{3-}$ (Hammarström *et al* 1992).

An important finding was that, with an excess of both external (membrane impermeable) dithionite and internal $\text{Fe}(\text{CN})_6^{3-}$, all viologen on the vesicle exterior migrated to the interior and was trapped there as the membrane impermeable dication (Zamarayev *et al* 1988). This was explained by transmembrane diffusion of the viologen radical and its subsequent reoxidation by internal $\text{Fe}(\text{CN})_6^{3-}$. In flash-photolysis, the observed kinetic trace deviated from a single exponential and could be accounted for by a model where the created transmembrane electric potential following tunnelling of one electron slows down the tunnelling of the next (Lymar *et al* 1991). This model assumed that the rate of the charge-compensating ionic flow was slower than the electron tunnelling. The observed rate at large number (> 8) of transferred electrons per vesicle agreed with the observed rate in the stopped-flow experiments. In this case the rate of electron tunnelling was supposed to be retarded so that it was equal to the rate of charge-compensating diffusion of ions. However, the observed rate constant in stopped-flow experiments varied between 1 and 6 s^{-1} when the viologen/lipid ratio was varied (Khramov *et al* 1987), while charge-compensating diffusion would not be dependent upon that ratio. Note also that second-order kinetics, as is predicted by our mechanism (*vide infra*), result in qualitatively the same behaviour, i.e. the kinetic trace can be divided in parts, each of which can be fitted to one single exponential with a rate constant that is somewhat different from the others. Unfortunately, no value was given for the observed rate constant when less than eight viologen radicals were produced per vesicle. In case of second-order kinetics the rate would be slower when the surface concentration of viologen radical is lower, as observed

in pulse-radiolysis (*vide infra*), while the model of Zamaraev and co-workers predicts that the rates would be the same so long as an equal number of electrons has been transferred per vesicle. It is very difficult to discriminate between different kinetic models by the shape of the kinetic traces, especially considering the low signal-to-noise ratio usually obtained in flash-photolysis experiments in vesicular systems.

Transmembrane electron transfer mediated by viologens with alkyl chains of different lengths has been extensively studied in DHP vesicles (Hurst 1990 and references therein; Lymar and Hurst 1992). The authors proposed basically the same mechanism as Zamaraev and co-workers (figure 6), based on several experimental indications. The major experimental support comes from the kinetics and stoichiometry of the redistribution of viologen between the outside and the inside of the vesicle upon reduction by external dithionite. Interesting differences in behaviour between $C_{n,1}V^{2+}$ with $n \geq 12$ and $n \leq 10$ was observed in several types of experiments, indicating that there are at least two binding sites available at the external interface of the vesicle for viologens with $n \leq 12$. For $n \leq 10$, all viologen reduced by dithionite on the outside migrated to the inside of the vesicle if there was an excess of $C_{n,1}V^{2+}$ acting as electron acceptor in the vesicle interior. When $n \geq 12$ not all external viologen moved to the interior (Hurst 1990; Lymar and Hurst 1992). The authors explained this by proposing that some of the viologens with longer chains were bound to the outer interface of the vesicle in a way that they could not diffuse through the membrane as radical cations ($C_{n,1}V^+$). The proposed electron tunneling pathway should therefore be blocked due to lack of charge-compensating ion flow. As a consequence, addition of lipophilic cations, allowing for charge compensation, would increase the amount of reduced acceptor (internal $C_{n,1}V^{2+}$) in the vesicle interior, as was indeed observed. The same effect of lipophilic cations was observed when the external viologen had extra charged groups attached (Patterson and Hurst 1990). However, N-methyl-4,4'-bipyridine (MB^+) was used as lipophilic cation, and the authors have later shown that the oxidized form (MB^+) does not permeate the membrane of vesicles composed of DHP (Lymar and Hurst 1992). Reduced N-cetyl-4,4'-bipyridine ($C_{16}B^0$, figure 3) has been shown to rapidly permeate lecithin vesicles (Hammarström *et al* 1993, *vide infra*). It seems probable that the dithionite in the system of Hurst and coworkers was able to partially reduce MB^+ to MB^0 which rapidly diffused across the membrane and reduced viologen in the vesicle interior, in which case it was not a question of charge-compensation. Note also that the same redistribution stoichiometry is expected from the mechanism of Zamaraev and others and Hurst and others and the disproportionation mechanism proposed by Hammarström and coworkers (*vide infra*).

3. Results and discussion

We have studied transmembrane electron transfer mediated by cetyltrimethylviologen ($C_{16,1}V^{2+}$) in lecithin vesicles, mainly by pulse radiolysis and stopped-flow techniques (Hammarström *et al* 1992, 1993). The advantage of these methods is the rapid reduction of viologen to a great extent compared to photoinduced methods. This allowed us to study the kinetic dependence on various parameters. In photoinduced experiments the slow rate and/or small extent of reaction may allow background processes to be significant and photostimulated diffusion might occur.

3.1 Kinetic studies

We have used different arrangements of the system as described in figure 7. In vesicles of type I the amphiphilic viologen was bound to both interfaces of the vesicles, while in type II it was bound only to the outside. In vesicles of type III and IV, $\text{Fe}(\text{CN})_6^{3-}$ was present in the internal water phase as an acceptor. The kinetic traces from dithionite-induced reduction in stopped-flow are shown in figure 8. In all types of vesicles a fast reduction of external viologen by dithionite was observed, which obeyed pseudo-first order kinetics since dithionite was in excess. In vesicles of type II (figure 8b) the absorption signal from the viologen radical was quite stable after that, while in type I (figure 8a) a slower reduction step was observed. In vesicles of types III and IV, identical kinetic traces were observed (figure 8c) where the initial fast reduction was followed by a slower reoxidation of viologen by the internal $\text{Fe}(\text{CN})_6^{3-}$. Figure 8d shows the trace of the absorbance at 420 nm where the extinction coefficients for $\text{C}_{16,16}\text{V}^+$ and $\text{Fe}(\text{CN})_6^{3-}$ are 2600 and $1000 \text{ M}^{-1} \text{ cm}^{-1}$, respectively. It can be seen that the initial, rapidly produced signal from the viologen radical decayed simultaneously with bleaching of $\text{Fe}(\text{CN})_6^{3-}$, and from the amplitudes of the phases it can be shown that two $\text{Fe}(\text{CN})_6^{3-}$ were reduced for each viologen initially reduced on the outside of the membrane. Even though dithionite was in excess, all viologen was in oxidized form at the end of the reaction. The stoichiometry and the complete migration of reduced viologen to the vesicle interior was also confirmed by careful measurements in a spectrophotometer, and is consistent with the earlier observations for $\text{C}_{16,16}\text{V}^{2+}$ (Lymar *et al* 1991; *vide supra*). The kinetics and observed rates for

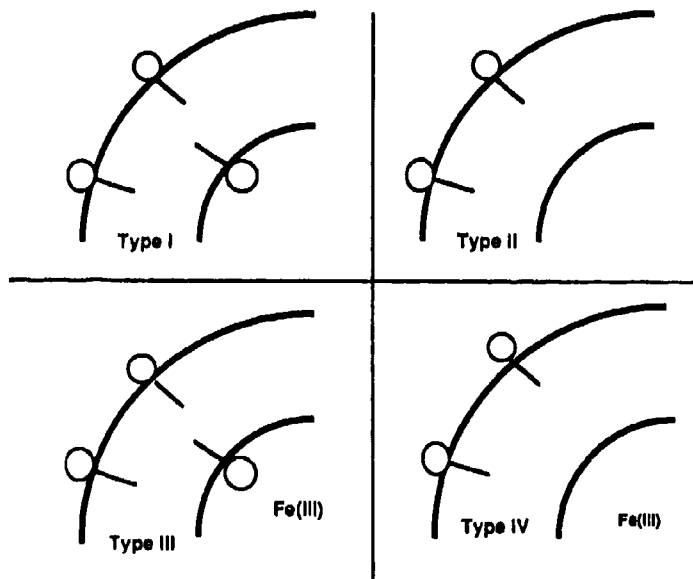


Figure 7. The types of vesicle configurations used by Hammarström and coworkers. The curved lines represent the interfaces of the membrane and the "ball-and-stick"-structures represent the amphiphilic viologen. The figure shows viologen distributed on both interfaces (types I and III) or only on the outer (types II and IV). In types III and IV, $\text{Fe}(\text{CN})_6^{3-}$ is present in the interior. The buffer used was 50 mM phosphate ($\text{pH} = 8$).

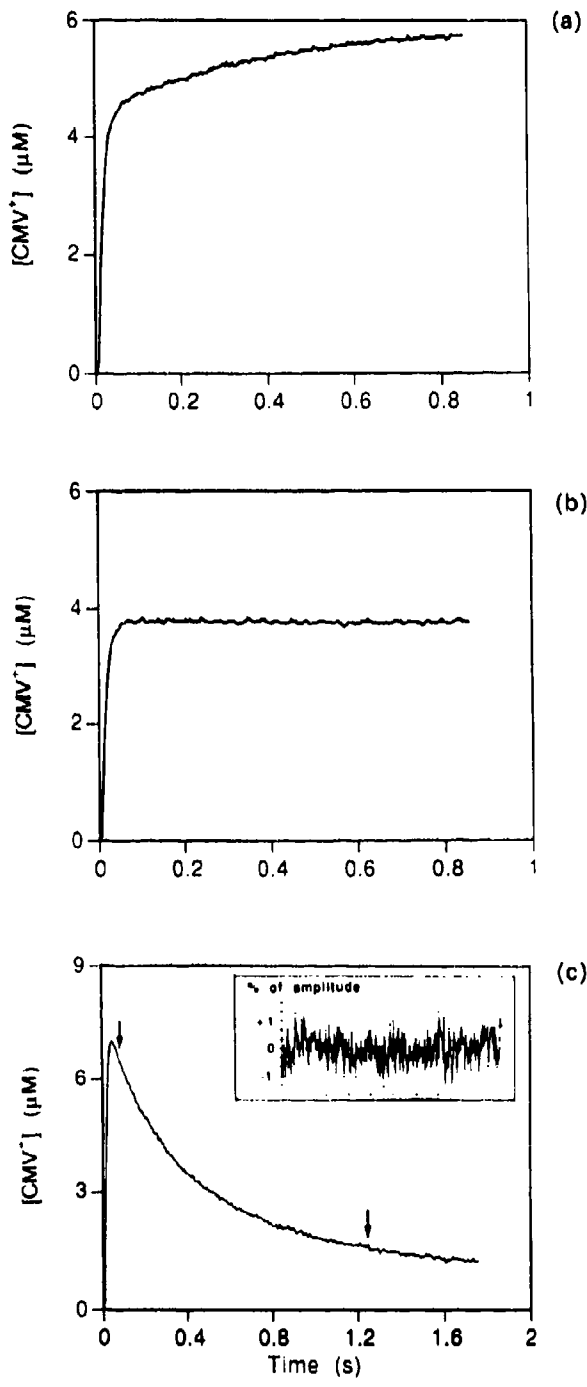


Figure 8. (a-c) (Caption on next page.)

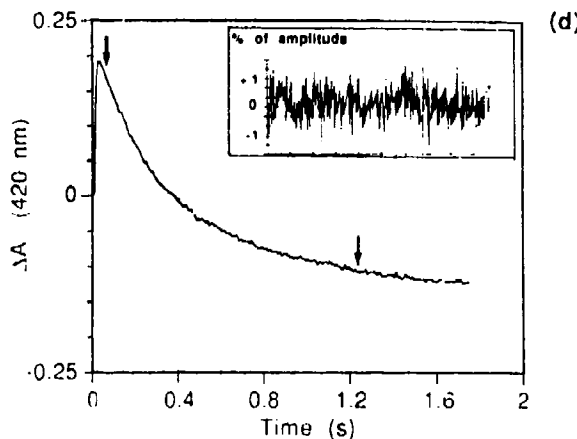


Figure 8. Kinetic traces from stopped-flow reduction of vesicles. The absorbance at 602 nm was followed: (a) type I, (b) II, (c) III and IV; (d) the absorbance followed at 420 for the same solution as in 8c. In c and d the residuals from a second-order fit for the part of the curve between the arrows are shown. Note that in 8a–b solutions were less concentrated than in 8c–d, but the violagen/lipid ratio was higher. (Reprinted with permission from Hammarström *et al* 1992, © 1992, Am. Chem. Soc.)

the fast reduction step were the same for all types of solutions if the concentration of dithionite was the same. The slower step could in all cases be fitted to a second-order kinetic model, and the rate was the same for types III and IV (figure 8c, decaying signal) and also for type I (figure 8a, growing signal) if the violagen/lipid ratio was the same. This is the transmembrane electron transfer step where external violagen mediates reduction to internal violagen (type I) or $\text{Fe}(\text{CN})_6^{3-}$ (types III and IV). The identical behaviour of vesicles of types III and IV shows that transmembrane electron transfer proceeds in the same way irrespective of the presence or absence of violagen on the internal interface of the membrane, an observation excluding self-exchange types of mechanisms.

For vesicles of type IV the violagen/lipid ratio was varied in stopped-flow experiments and the observed rate was found to be proportional to this ratio (figure 9). This shows that the transmembrane electron transfer is second-order in violagen radical on the outer interface of the vesicle ($[\text{C}_{16,1}\text{V}^+]'_{\text{out}}$). Such a dependence was earlier found in vesicles equivalent to type I, i.e. with $\text{C}_{16,16}\text{V}^{2+}$ present on both interfaces and no $\text{Fe}(\text{CN})_6^{3-}$, but was interpreted as a first-order dependence on both $[\text{C}_{16,16}\text{V}^+]_{\text{out}}$ and $[\text{C}_{16,16}\text{V}^{2+}]_{\text{in}}$ (Khramov *et al* 1987).

We also varied the extent of reduction of violagen on the outer interface of vesicles of type IV by pulse radiolysis (figure 10). The rate was found to be proportional to the surface concentration of violagen radical produced by the radiation pulse. If the line fitted to the data is extrapolated to 100% reduction of violagen ($= 24 \mu\text{M}$) the observed rate is $\approx 5 \text{ s}^{-1}$, which is in excellent agreement with the rate obtained in the stopped-flow experiments (100% reduction by dithionite in excess) for the same violagen/lipid ratio (1:100). Together this shows that the rate of transmembrane electron transfer is second-order in $[\text{C}_{16,1}\text{V}^+]_{\text{out}}$ and independent of $[\text{C}_{16,1}\text{V}^{2+}]_{\text{out}}$.

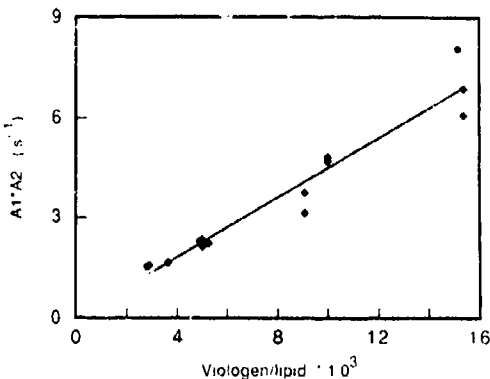


Figure 9. The rate (inverse half-life) versus the viologen/lipid:1 ratio for stopped-flow reduction of vesicles of type IV (100% reduction). Each point is an average of 4-8 individual determinations for the same vesicle preparation. The standard deviation (not shown) was less than the size of the points. The line is a least-squares fit to the data. (Reprinted with permission from Hammarström *et al.* 1992, © 1992, Am. Chem. Soc.)

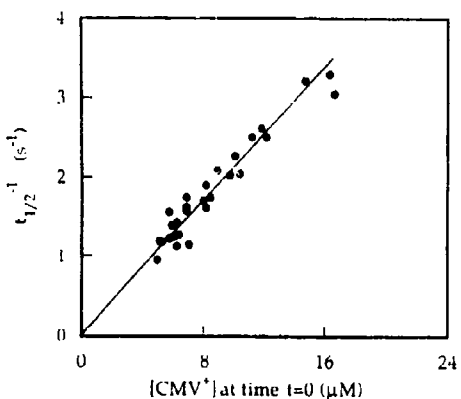


Figure 10. The rate (inverse half-life) versus the concentration of external viologen radical immediately after the pulse for pulse radiolytic reduction of vesicles of type IV (partial reduction). All data are individual determinations for the same vesicle preparation. The line is a least-squares fit through the origin.

and $[C_{16,1}V^{2+}]_{in}$. This excludes both self exchange types of mechanisms and simple diffusions of viologen radicals.

3.2 Mechanism

The mechanism we propose for the transmembrane electron transfer mediated by viologen is shown schematically in figure 11. The rate-determining step is the disproportionation, (1), of two viologen radicals forming one oxidized $C_{16,1}V^{2+}$ and one doubly reduced $C_{16,1}V^0$. This uncharged viologen diffuses rapidly through the membrane and is re-oxidized by $Fe(CN)_6^{3-}$ in two steps. There is never any detectable

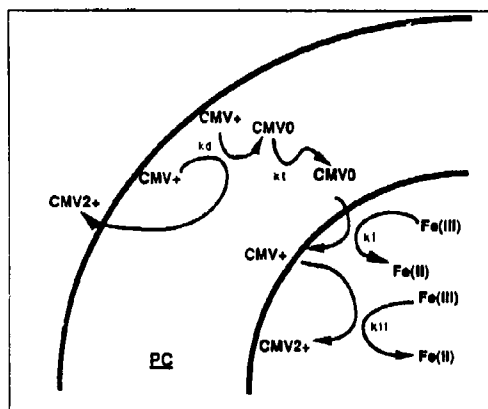


Figure 11. Reduction scheme for the mechanism proposed by Hammarström and coworkers. The scheme depicts the situation in pulse radiolysis where there is no external reductant after the first 100 μ s. The viologen used ($C_{16,1}V^{2+}$) is denoted CMV^{2+} . The individual steps are marked by their rate constants: k_d , k_t , k_i and k_{II} for the disproportionation, transmembrane diffusion and for the two steps of re-oxidation by $Fe(CN)_6^{3-}$, respectively.

amount of $C_{16,1}V^0$ present. The rate of conproportionation, i.e. the reverse of (1), is slower than the transmembrane diffusion and re-oxidation of $C_{16,1}V^0$. This explains the observed independence on $[C_{16,1}V^{2+}]_{out}$, while second-order dependence on $[C_{16,1}V^+]_{out}$ is explained by the rate-determining bimolecular disproportionation. We have found no other mechanism explaining the same rate-dependencies and stoichiometry. Formation of radical dimers ($C_{16,1}V^+$)₂ is a bimolecular reaction between viologen radicals, but the dimers are larger and more highly charged than the radical monomers, so there is no reason why transmembrane diffusion of the former would be faster than that of the latter. Also, diffusion of radical dimers is not consistent with the stoichiometry in the re-oxidation by $Fe(CN)_6^{3-}$. Note that, since the external reductants produced in pulse radiolysis (alcohol radicals) recombine within 100 μ s, disproportionation is the only possibility of forming significant amounts of doubly reduced $C_{16,1}V^0$.

Under the experimental conditions, it was not possible to directly produce measurable amounts of $C_{16,1}V^0$, hence N-cetyl-4,4'-bipyridine ($C_{16}B^+$, figure 3) was used as a model compound for the viologen. The singly reduced form ($C_{16}B^0$) is structurally very similar to the doubly reduced $C_{16,1}V^0$ and both species are uncharged. Thus, the rates of transmembrane diffusion for the two species is expected to be very similar. By pulse radiolysis we were able to study transmembrane electron transfer mediated by $C_{16}B^+$ in vesicles equivalent to type IV (Hammarström *et al* 1993). The observed rate (1.5×10^3 s $^{-1}$) was independent of the extent of reduction of $C_{16}B^+$. The mechanism for the reaction was simple reduction of $C_{16}B^+$ to $C_{16}B^0$ by the radiation pulse. The uncharged form diffused through the membrane and was re-oxidized by $Fe(CN)_6^{3-}$ in the vesicle interior. Assuming that the rate of transmembrane diffusion of $C_{16,1}V^0$ is the same as for $C_{16}B^0$, this observed rate is probably large enough, as compared to the conproportionation, to explain the negligible influence of the latter on the overall mechanism (*vide infra*).

N-cetyl-nicotinamide ($C_{16}NA^+$, figure 3) was shown to mediate transmembrane electron transfer by the same simple mechanism as $C_{16}B^+$, i.e. by diffusion of the singly reduced $C_{16}NA^0$, but the observed rate was much lower (3 s^{-1}), probably due to the relatively high polarity of the amide group (Hammarström *et al* 1993). This shows the sensitivity of the transmembrane diffusion to differences in structure and polarity.

3.3 Disproportionation equilibrium

The equilibrium constant of disproportionation can be calculated according to (3), since both redox steps are reversible;

$$\log_{10} K_d = (E^0_2 - E^0_1)/0.060. \quad (3)$$

In homogeneous media it is rather low. For methylviologen in water the first and second reduction potentials are reported as -0.45 V and $-0.8 \pm 0.1\text{ V}$ vs NHE, respectively (Bird and Kuhn 1981) yielding a value of $K_d = 10^{-5}-10^{-8}$. The low solubility of the doubly reduced MV^0 in water is the cause of the large scatter in the data for the second reduction step. Heterogeneous media, e.g. vesicles, will increase the solubility of all redox forms of $C_{n,n}V$ due to the variety of environments prevalent. As a consequence, the disproportionation must be much more favourable in such systems. Attempts to measure the redox potentials of amphiphilic viologens in membranes have been made by several authors and the potentials reported for $C_{16,1}V$ in lecithin vesicles are -0.38 V and -0.66 V vs NHE respectively, i.e. $\Delta E^0 = 280\text{ mV}$ (Lei and Hurst 1991). This yields a value of $K_d = 2 \times 10^{-3}$. However, the measured redox potentials for a microheterogeneous system must be corrected for the different distributions of all redox forms over all phases present, and the different responses at the tool of measurement (the electrode, redox dye etc.) from species in different phases must be considered. In principle, this situation could be handled if all relevant distribution constants and relative measurement responses were known. However, in practice this is not the case, especially since there are a variety of interfacial equilibrium sites for the different redox forms. If the "true" ΔE^0 i.e. the kinetically relevant ΔE^0 in (3) equals -180 mV a rate of transmembrane diffusion of $[C_{16,1}V^0] \approx 1.5 \times 10^3\text{ s}^{-1}$ (*vide supra*) is sufficient to explain the negligible effects of conproportionation (Hammarström *et al* 1993).

4. Conclusion

A common feature of the mechanism of transmembrane electron transfer in the systems we have studied is that the transfer step is the diffusion of an uncharged form of the redox mediator. For $C_{16}B^+$ and $C_{16}NA^+$ there is a simple one-step reduction preceding the transmembrane step, but for $C_{16,1}V^{2+}$ the formation of $C_{16,1}V^0$ proceeds through a rate-determining disproportionation. We have shown that there is no long-range self-exchange (electron tunnelling) between viologens as is often supposed. A disproportionation mechanism has been proposed earlier in water-in-oil microemulsions (Goren and Willner 1983) and we suggest that it might be general for viologen in microheterogenous media.

Acknowledgements

The authors wish to acknowledge the fruitful collaboration with Thomas Norrby and Björn Åkermark, Department of Organic Chemistry, and with Johan Lind and Gabor Merényi, Department of Nuclear Chemistry, all at The Royal Institute of Technology, Stockholm, Sweden. This work was supported by the Swedish Natural Science Research Council and by NUTEK (formerly the National Energy Administration).

References

- Balzani V and Scandola F 1991 *Supramolecular photochemistry* (Chichester: Ellis Horwood)
- Bird C L and Kuhn A T 1981 *Chem. Soc. Rev.* **10** 49
- Carmon-Ribeiro A M 1992 *Chem. Soc. Rev.* **209**
- Cevc G J and Marsh D 1987 *Phospholipid bilayers* (New York: Wiley) pp. 190–193
- Dannhauser T J, Nango M, Oku N, Anzai K and Loach P A 1986 *J. Am. Chem. Soc.* **108** 5865
- Ford W E and Tollin G 1982 *Photochem. Photobiol.* **35** 809
- Goren Z and Willner I 1983 *J. Am. Chem. Soc.* **105** 7764
- Hammarström L, Almgren M, Lind J, Merényi G, Norrby T and Åkermark B 1993 *J. Phys. Chem.* **97** 10083
- Hammarström L, Almgren M and Norrby T 1992 *J. Phys. Chem.* **96** 5017
- Hurst J K 1990 *In Kinetics and catalysis in microheterogeneous systems: Surfactant science series* (eds M Grätzel and K Kalyanasundaram) (New York: Marcel Dekker)
- Hurst J K, Lee L Y C and Grätzel M 1983 *J. Am. Chem. Soc.* **105** 7048
- Johnson M K, King R B, Kurtz D M Jr, Kutil C, Norton M L and Scott R A (eds) 1990 *Electron transfer in biology and the solid state; Adv. Chem. Ser.* (Washington, DC: Am. Chem. Soc.) vol. 226
- Jusupov P G, Asanov A N and Khairdinov R F 1985 *Izv. Akad. Nauk. SSSR. Ser. Khim.* **227**
- Katagi T, Yamamura T, Saito T and Sasaki V 1981 *Chem. Lett.* 1451
- Katagi T, Yamamura T, Saito T and Sasaki V 1982 *Chem. Lett.* 417
- Khannanov N K, Kuzmin V A, Levin P P, Shafirovich V Y and Yablonskaya E E 1987 *New J. Chem.* **11** 687
- Khramov M I, Lyman S V, Parmon V N and Zamaraev K I 1987 *Dokl. Phys. Chem. (Eng. Transl.)* **289** 598
- Kobuke Y, Yamanishi M, Hamachi I, Kagawa H and Ogoshi H 1991 *J. Chem. Soc., Chem. Commun.* 895
- Krueger J S, Mayer J E and Mallouk T E 1988 *J. Am. Chem. Soc.* **110** 8232
- Kugimiya S, Lazark T, Blanchard-Desce M and Lehn J M 1991 *J. Chem. Soc., Chem. Commun.* 1179
- Lei Y and Hurst J K 1991 *J. Phys. Chem.* **95** 7918
- Lymar S V and Hurst J K 1992 *J. Am. Chem. Soc.* **114** 9498
- Lymar S V, Parmon V N and Zamaraev K I 1991 *Top. Curr. Chem.* **159** 1
- Matsuo T 1985 *J. Photochem.* **29** 41
- Matsuo T, Itoh K, Takuma K, Hashimoto K and Nagamura T 1980 *Chem. Lett.* 1009
- Momenteau M, Loock B, Seta P, Bienvenue E and d'Epenoux B 1989 *Tetrahedron* **45** 4893
- Moore T A, Gust D, Moore A L, Bensasson R V, Seta P and Bienvenue E 1987 *In Supramolecular photochemistry*, (ed) V Balzani (Dordrecht: D Reidel)
- Mohammad M, Iqbal R, Khan A Y, Bhatti M, Zahir K and Jahan R 1981 *J. Phys. Chem.* **85** 2816
- Nango M, Kryu H and Loach P A 1988 *J. Chem. Soc., Chem. Commun.* 697
- Patterson B C and Hurst J K 1990 *J. Chem. Soc., Chem. Comm.* 1137
- Robinson J N and Cole-Hamilton D J 1991 *Chem. Soc., Rev.* **20** 49
- Robinson J N, Cole-Hamilton D J, Whittlesey M K and Camilleri P 1990 *J. Chem. Soc., Faraday Trans.* **86** 2897
- Summers L A 1991 *J. Heterocyclic Chem.* **28** 827
- Tabushi I and Kugimiya S I 1984 *Tetrahedron Lett.* **25** 3723
- Tabushi I and Kugimiya S I 1985 *J. Am. Chem. Soc.* **107** 1859
- Tabushi I and Nishiya M 1981 *Tetrahedron Lett.* **22** 4989
- Thompson D H P, Barrette W C Jr and Hurst J K 1987 *J. Am. Chem. Soc.* **109** 2003
- Tricot Y M and Manassen J 1988 *J. Phys. Chem.* **92** 5239
- Tricot Y M, Porat Z and Manassen J 1991 *J. Phys. Chem.* **95** 3242
- Zamaraev K I, Lymar S V, Khramov M I and Parmon V N 1988 *Pure Appl. Chem.* **60** 1039

Sunlight-initiated cycloaddition reactions of the benzene ring

S Y AL-QARADAWI,^a D C BLAKEMORE^b and A GILBERT^{*b}

^aChemistry Department, Qatar University, P O Box 110003, Doha, Qatar

^bChemistry Department, The University of Reading, Whiteknights, P O Box 224, Reading, Berkshire, RG6 2AD, UK

Abstract. Both 1,2-(ortho) and 1,3-(meta) cycloaddition of ethenes to the benzene ring can be accomplished using sunlight-initiated chemistry. The process is most effective for arenes which have both electron-donor and electron-acceptor substituents and occurs both inter- and intramolecularly giving an inexpensive and convenient access to complex molecular skeletons from readily available starting materials.

Keywords. Sunlight; photocycloaddition; benzocyclobutene; triquinane.

1. Introduction and brief historical perspective of sunlight-initiated chemistry

There are many examples, dating back several thousand years, of the importance of sunlight in middle-eastern cultures (Morsi and Abdel-Mottaleb 1991). The study of photochemistry as a science, however, is widely regarded as having its origins during the late 19th and early 20th centuries. During this period, numerous reports appeared describing the sunlight-initiated reactions of organic compounds (Singer 1986; Carassiti 1988; Roth 1988; Morsi and Abdel-Mottaleb 1991). For example, Sestini (1866) had published the first paper on the solution photochemistry of santonin and Fritzsche (1867) had observed the photodimerisation of anthracene but referred to the product as a "para body". Liebermann (1877) and Breuer and Zincke (1878) noted the bleaching of the yellow crystals of thymoquinone and 2-phenylnaphtho-1,4-quinone respectively in sunlight, and these photoreactions were later shown to be the first observed examples of $(2\pi + 2\pi)$ cycloadditions of ethenes. By 1902 the cyclobutane nature of the products of the photodimers of ethenes had been established by Riiber (1902), and *cis-trans* isomerisation of cinnamic acid in sunlight had been reported by Perkin (1881) and by Liebermann (1890). The photoreduction of 1,4-quinones and their light-induced reactions with aldehydes attracted much attention at this time. Such interest in these reactions caused Heinrich Klinger (Klinger and Slandke 1891), one of the principal investigators of these processes, to refer to them as *Synthesen durch Sonnenlicht*.

It was during this period that Ciamician and Silber at the University of Bologna were carrying out their extensive and thorough investigations into the sunlight-initiated chemistry of organic compounds (Carassiti 1988). Indeed so great was their contribution at that time that Ciamician was later described as "the father of

*For correspondence

photochemistry" (Turro 1965), and 1900 as the year which "marks the basic date in the history of photochemistry" (Nasini 1929).

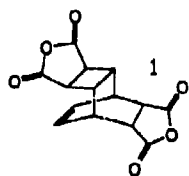
Ciamician and Silber were, however, far from being alone in recognising that sunlight could induce such remarkable changes in the molecular structure of organic compounds. One of their more notable fellow pioneers of the time was the Italian chemist Paterno. His major contribution arose from the observation that exposure of solutions of benzaldehyde and 2-methylbut-2-ene to sunlight produced an oxetane (Paterno and Chieffi 1909). The importance of this work was not fully appreciated until much later when Buchi and coworkers greatly extended the scope of the process (Buchi *et al* 1954) and this reaction is now fittingly known as the "Paterno-Buchi" reaction.

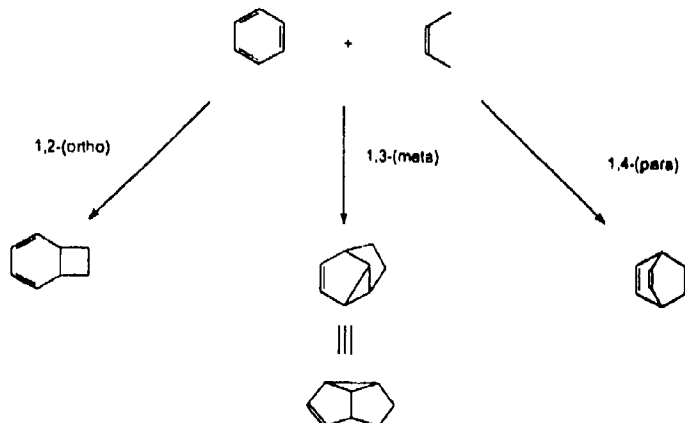
The appointment in 1937 of Alexander Schonberg to the Chair of Chemistry and as Director of the Chemistry Department at the University of Cairo increased interest in the study of sunlight-initiated processes in Egypt. From this time until his return to Berlin in 1958, Schonberg, in collaboration with Mustafa, produced a considerable number of publications describing the outstanding achievements of the Egyptian research group (Singer 1986).

Interest in sunlight-initiated processes during the past 35 years has, however, almost exclusively concentrated on the conversion of solar energy into more versatile energy sources but, at the same time, photochemistry has been shown to be a viable and useful synthetic technique (Horspool 1984; Coyle 1986). As noted recently, however, the photon may be a clean and convenient reagent but it can also be expensive to generate from artificial sources (Hulsdunker *et al* 1992); hence the growing interest in "solar chemistry" and a desire for *Synthesen durch Sonnenlicht*.

2. Results and discussion

With few exceptions, early studies on sunlight-initiated processes of organic compounds have been concerned with the reactions of ethenes, carbonyl compounds, and diazo and diazonium compounds. In contrast, our interest is in inducing reactions of the benzene ring using sunlight. These studies originate from our investigations in the early 1960's on the photochemistry of ground-state charge-transfer complexes between dienophiles and benzenoid compounds. The complex between maleic anhydride and benzene absorbs at longer wavelengths than either of the components and "tails" well beyond 290 nm (Andrews and Keefer 1964). Excitation within this charge-transfer absorption band results in the formation of the 2:1 cycloadduct 1 (Angus and Bryce-Smith 1959). The process can be sensitised by aromatic ketones of triplet energy greater than 275 kJ mol⁻¹ (Schenck and Steinmetz 1960) and both sensitised and unsensitised reactions occur on exposure of the solutions to (Reading)





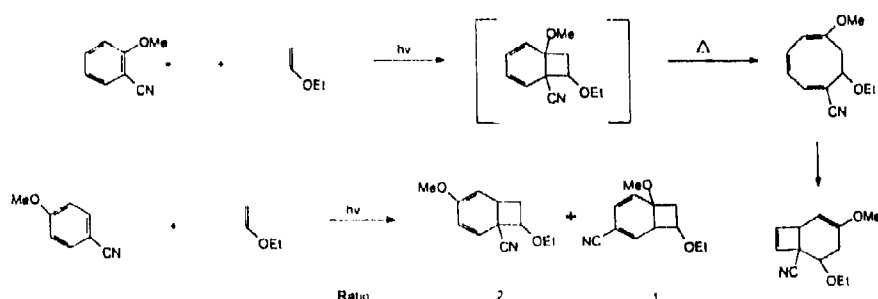
Scheme 1. Modes of photocycloaddition of ethenes to the benzene ring.

sunlight (Bryce-Smith *et al* 1962). The 2:1 adduct has attracted considerable interest not only because it was the first photoaddition product of the benzene ring reported but also because of its potential to yield condensation polymers of high thermal stability with diamines and because the diimide derivative shows appreciable cytotoxic activity (Lomax and Narayanan 1984).

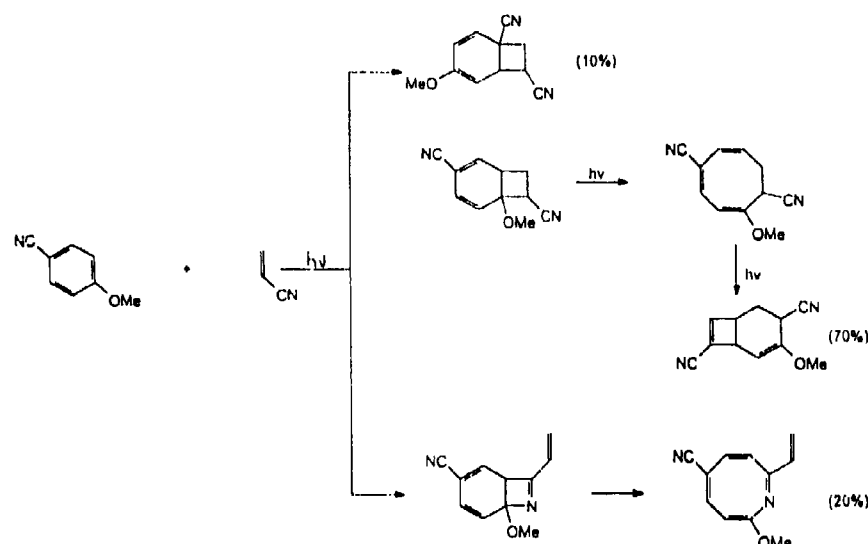
However, the process is remarkably limited and despite the ready formation of derivatives of 1 from 313 nm radiation of solutions of maleic anhydride in alkyl benzenes (but not alkoxybenzenes), only the parent compound can be obtained using sunlight initiation: from the other systems maleic anhydride-based polymers are obtained (Bryce-Smith *et al* 1962). It has now long been recognised that excitation within charge-transfer bands is not a prerequisite for photocycloaddition to the benzene ring, and numerous products derived from 1,2-(ortho), 1,3-(meta), and 1,4-(para) cycloadditions (scheme 1) of ethenes have been reported. The majority of the arenes in these reactions require 254 nm radiation for excitation and, of course, their reactions are not initiated by sunlight. Recently, we have recognised that a combination of both electron donors and electron acceptors as substituents on the benzene ring not only provides functionalisation of the carbon skeletons of the cycloadducts, but also, and importantly, leads to a red-shift in the arene absorption beyond 300 nm while maintaining the lowest π, π^* excited state. These arenes can be directly excited using the shorter wavelength components of sunlight and by employing this simple and inexpensive methodology, functionalised complex carbon skeletons can be readily and conveniently accessed. The following cycloadditions to the benzene ring can all be induced by exposure of solutions of the reactants to sunlight.

2.1 1,2-(Ortho)-photocycloaddition

There is a correlation between the preferred mode of cycloaddition (ortho versus meta) of an ethene to the benzene ring and the relative electron donor-electron acceptor characteristics of the addends. This donor-acceptor relationship has been estimated by ionisation potential differences (Bryce-Smith and Gilbert 1977) and more rigorously by the magnitude of the free energy change ΔG° of electron transfer between



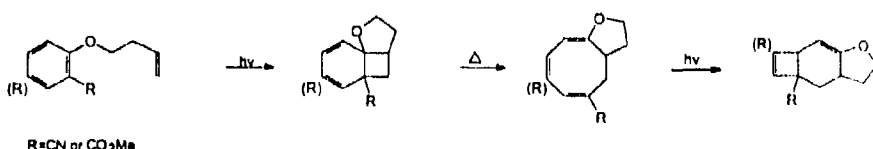
Scheme 2. Cycloaddition of ethyl vinyl ether to 2- and 4-cyanounisoles.



Scheme 3. Cycloaddition of acrylonitrile to 4-cyanoanisole.

the addends (Mattay 1985). Thus the ortho cycloaddition is favoured for addend pairs which have an electron donor-electron acceptor relationship whereas the meta process predominates or is the sole reaction for systems in which this feature is not evident. For example, enol ethers undergo cycloaddition at the 1,2-positions of benzonitrile, whereas cycloalkenes add at the 2,6-positions of toluene. When both electron donor and acceptor substituents (e.g. cyano and methoxy groups) are present on the benzene ring, then arene absorption allows sunlight excitation. Furthermore when the substituents are in conjugative positions (i.e. 1,2- or 1,4-substitution), the sites of ortho addition of electron donor and electron acceptor ethenes reflect the donor/acceptor natures of the arene substituents: this regiochemical feature is illustrated by the ortho cycloaddition products of acrylonitrile and ethyl vinyl ether with 2- and 4-cyanoanisoles shown in schemes 2 and 3 (Al-Jalal *et al* 1988). The formation of azacyclo-octatetraenes by the novel addition of the ethene cyano group to the benzene ring has been well-documented by Al-Jalal (1990).

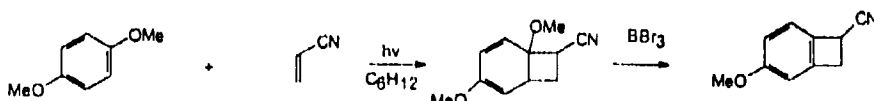
The primary cycloadduct from such 1,2-disubstituted benzene is thermally labile since the common sigma bond in the bicyclic skeleton is weakened by the electron-donor and electron-acceptor groups. Disrotatory ring opening gives the cyclo-octatriene which absorbs in the 320 nm region and hence in sunlight undergoes disrotatory ring closure to yield the bicyclo[4.2.0]octa-2,7-diene as the sole product. This type of reaction also occurs intramolecularly with 4-phenoxybut-1-enes substituted with electron acceptor groups in the 2'- or 4'-positions (Cosstick *et al* 1987; Wagner and Nahm 1987). For example, 4-(2'-cyanophenoxy)but-1-ene undergoes an essentially



Scheme 4. Intramolecular photocycloaddition of 4-phenoxybut-1-enes.

quantitative conversion to the 4-oxatricyclo[7.2.0.0^{3,7}]undeca-2,10-diene in sunlight (scheme 4). We have demonstrated that the formation of the triene can be quenched by common triplet quenchers but that the subsequent closure to the tricyclic system is not influenced by the presence of 1,3-dienes. The primary process is thus deduced to be a rare example of cycloaddition to the triplet state of the benzene ring, whereas the secondary photoreaction arises from the triene singlet state.

When both substituents of the benzene ring are electron donors or electron acceptors, excitation of the $\pi\pi^*$ transition of the arene is possible in sunlight. In such cases, if the ethene is a powerful electron acceptor or electron donor, respectively, substantially complete electron transfer can occur. For example, irradiation of methanol solutions of the 1,4-dimethoxybenzene-acrylonitrile system leads to substitution of the benzene ring by initial formation of the radical ion pair (Ohashi *et al* 1976, 1977). We have, however, adapted this system, as shown in scheme 5, to yield the benzocyc-

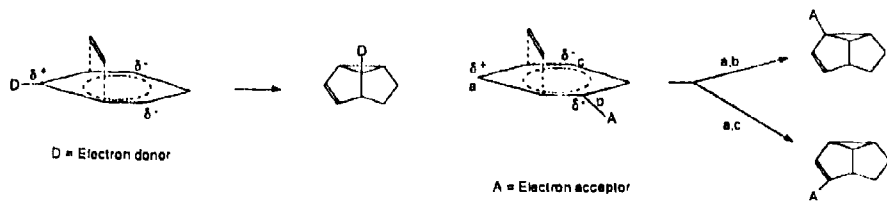


Scheme 5. Photocycloaddition of acrylonitrile to 1,4-dimethoxybenzene in non-polar solvents.

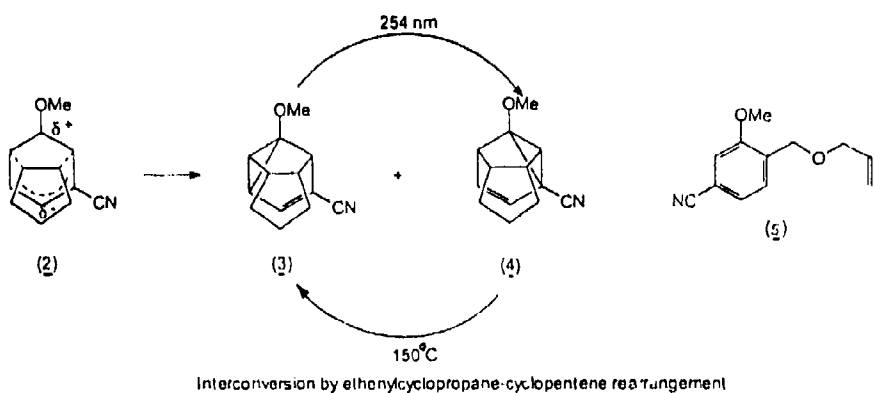
lobutene which has been used as a synthon in alkaloid and steroid synthesis (Kametani 1979, 1981) by the simple expedient of mediating the electron transfer by using a nonpolar solvent. In this case, the reaction can be run to complete consumption of the arene, and decanting the reaction solution from the immiscible ethene photodimers (Al-Jalal and Gilbert 1983) allows an almost quantitative yield of the ortho cycloadduct to be obtained.

2.2 1,3-(Meta) photocycloaddition

The formation of meta photocycloadducts results in the greatest increase of "molecular complexity" (as defined by Bertz 1981) of any general reaction. The importance of



Scheme 6. Regiochemistry of meta cycloaddition of ethenes to substituted benzenes.



this process in synthetic organic chemistry has been elegantly demonstrated by Wender and co-workers by its use in a number of sequences to complex target molecules. As Wender notes "the value of the arene–alkene meta photocycloaddition (to synthetic organic chemistry) can be seen to arise from its capacity to produce a cycloadduct with three new rings and up to six new stereocentres, an impressive feat even when compared with the highly regarded Diels–Alder cycloaddition." (Wender 1990).

The basic feature of the widely accepted mechanism of meta photocycloaddition involves development of charge in the S_1 arene on approach of the S_0 ethene. The addends orient with respect to each other in order that the stabilisation of the developing charge centres in the C_6 ring by the substituents is maximised: this accounts for the observed regiochemistry of the reaction (scheme 6). In 1,3-disubstituted benzenoid compounds such as 3-cyanoanisole, the charge stabilisation and hence the directing effects of the electron-withdrawing and electron-donating groups reinforce one another to give the orientation of the addends shown in 2. Delocalisation of the developing allylanion system by the cyano group promotes the intramolecular cyclisation giving the cyclopropane ring to favour formation of the 1-methoxy-4-cyano- rather than the 1-methoxy-2-cyano-dihydrosemibullvalene. Exposure of the 3-cyanoanisole–cyclo-octene to sunlight yields the two isomers 3 and 4 in the respective ratio of 1:1.5 initially. This ratio changes with time reflecting the interconversion of the adducts photochemically and thermally by an enethiacyclopropane–cyclopentene rearrangement. Indeed 3 or 4 may be obtained essentially free from the other isomer by the respective use of 254 nm radiation and heating at 150°C. The formation of these meta photocycloadducts comprise the first reported example of sunlight-initiated

meta photocycloaddition of an ethene to the benzene ring, but the process appears to be general for alkene additions to arenes 1,3-disubstituted with electron-donor and electron-acceptor groups and is currently being extended to the non-conjugated bichromophoric systems of type 5.

3. Experimental

All sunlight-induced reactions were carried out in a double-walled Pyrex apparatus. Solutions of the reactant(s) in cyclohexane or methanol under air were placed in the inner vessel and cooled water circulated through the outer jacket by convection. Product formation was monitored by GC and the photoadducts were isolated and identified as described previously for the reactions initiated by 254 nm radiation (see, for example, Al-Qaradawi *et al* 1992).

Acknowledgements

Finance from the University of Qatar (to SYA-Q) and a Postgraduate Studentship from the University of Reading (to DCB) is gratefully acknowledged.

References

- Al-Jalal N 1990 *J. Photochem. Photobiol. A* **54** 99
Al-Jalal N and Gilbert A 1983 *J. Chem. Res.* 266
Al-Jalal N, Gilbert A and Heath P 1988 *Tetrahedron* **44** 1449
Al-Qaradawi S Y, Cosstick K B and Gilbert A 1992 *J. Chem. Soc., Perkin Trans. I* 1145
Andrews L J and Keefer R M 1964 *Molecular complexes in organic chemistry* (San Francisco: Holden-Day)
Angus H and Bryce-Smith D 1959 *Proc. Chem. Soc.* 326
Bertz S H 1981 *J. Am. Chem. Soc.* **103** 3599
Breuer A and Zincke Th 1878 *Berichte* **11** 1403
Bryce-Smith D and Gilbert A 1977 *Tetrahedron* **33** 2459
Bryce-Smith D, Gilbert A and Vickery B 1962 *Chem. Ind.* 2060
Buchi G, Inman C G and Lipinsky E S 1954 *J. Am. Chem. Soc.* **76** 4327
Carassiti V 1988 *EPA Newslett.* (no. 33) 11
Cosstick K B, Drew M G B and Gilbert A 1987 *J. Chem. Soc., Chem. Commun.* 1867
Coyle J D (ed.) 1986 *Photachemistry in organic synthesis: Special Publication No. 57* (London: The Royal Society of Chemistry)
Fritzsche J 1867 *J. Prakt. Chem.* **101** 333
Horspool W M (ed.) 1984 *Synthetic organic photochemistry* (New York: Plenum)
Hulsdunker A, Ritter A and Demuth M 1992 *EPA Newslett.* (no. 45) 23
Kametani T 1979 *Pure Appl. Chem.* **51** 747
Kametani T 1981 *Tetrahedron* **37** 3
Klinger H and Siedeke O 1891 *Berichte* **24** 1340
Liebermann C 1877 *Berichte* **10** 2177
Liebermann C 1890 *Berichte* **23** 2510
Lomax N R and Narayanan V L 1984 *Chemical structures of interest to the Division of Cancer Treatment* (Bethesda, MD: National Cancer Institute)
Mattay J 1985 *Tetrahedron* **41** 2393
Morsi S E and Abdel-Mottaleb M S A 1991 *EPA Newslett.* (no. 43) 11
Nasini R 1929 *J. Chem. Soc.* 996

- Ohashi M, Tanaka T and Yamada S 1976 *J. Chem. Soc., Chem. Commun.* 800
Ohashi M, Tanaka T and Yamada S 1977 *Tetrahedron Lett.* 3629
Paterno E and Chieffi G 1909 *Gazz. Chim. Ital.* **39** 341
Perkin W H 1881 *J. Chem. Soc.* **39** 409
Riiber C N 1902 *Berichte* **35** 2908
Roth H D 1988 *EPA Newslett.* (no. 32) 1
Schenck G O and Steinmetz R 1960 *Tetrahedron Lett.* **83** 1705
Sestini F 1866 *Bull. Soc. Chim.* **5** 202
Singer E 1986 *EPA Newslett.* (no. 26) 1
Turro N J 1965 *Molecular photochemistry* (New York: Benjamin)
Wagner P J and Nahm K 1987 *J. Am. Chem. Soc.* **109** 4404, 6528
Wender P A 1990 *Pure Appl. Chem.* **62** 1597

Synthetic chemistry via radicals generated by photoinduced electron transfer

A ALBINI^a, E FASANI^b, M MELLA^b and M FRECCERO^b

^aInst. Organic Chemistry, University of Torino, via Giuria 7, I-10125 Torino, Italy

^bDepartment of Organic Chemistry, University of Pavia, via Taramelli 10, I-27100 Pavia, Italy

Abstract. Radical cations generated by photoinduced electron transfer often undergo a fragmentation fast enough to compete with back electron transfer. In this way, radicals are generated. Examples of the chemistry of benzyl and alkyl radicals under these conditions are given.

Keywords. Radicals, electron transfer, photochemistry.

1. Introduction

Oxidations are a well-established method for the generation of radicals for non-chain reactions.



High-valency metal compounds or anodic oxidations are used for this purpose (Curran 1991). This method suffers from some shortcomings, e.g. limitation in the choice of solvent due to the properties of the salt used as oxidizer or as supporting electrolyte, and competition from other oxidative processes, such as two-electron oxidation to yield a non-radical dication or oxidation of the generated radical to the corresponding cation.

Photosensitization offers an alternative access to radical cations, and hence to radicals (Albini *et al* 1982), due to the strong oxidizing properties of excited states (Fox and Chanon 1988).



Under these conditions substrates which could not be practically oxidized otherwise yield the corresponding radical cations and, if fragmentation is fast enough to compete with back electron transfer to the radical anion, these cleave to the expected radicals. This process involves only organic species and thus solubility problems are minimized. Furthermore, since the oxidizer is a short-lived species generated photochemically, problems of over-oxidation are avoided.

*For correspondence

An evaluation of the single bond energy of the radical cation (fragmentation according to (2)) is generally possible (Wayner *et al* 1986, 1988; Dinnocenzo *et al* 1989; Sulpizio *et al* 1989; Popielartz and Arnold 1990) and often shows a remarkable weakening of the bond, leading to the expectation that monomolecular or nucleophile-assisted fragmentation is fast and, indeed, this is borne out by the experiments.

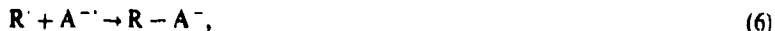
Both resonance-stabilized (allyl, benzyl, α -amino, α -oxy) radicals and non-stabilized aliphatic radicals can be prepared by this method from the appropriate precursor.

The follow-up reactions include:

(1) reduction of the radical by the acceptor radical anion, usually followed by protonation,



(2) addition of the radical to the radical anion, when $E_{red}(A) < E_{red}(R^{\cdot})$,



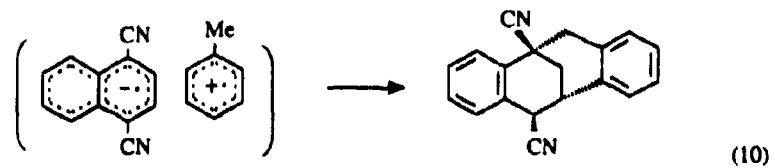
(3) addition of the radical to an added radicophile

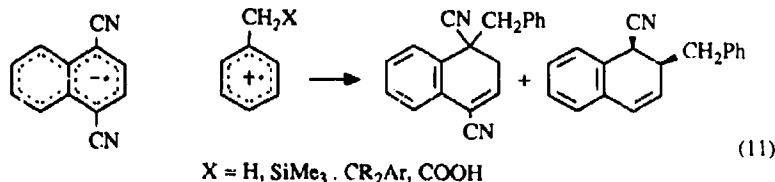


Some examples of these reactions are discussed below.

2. Reaction of resonance-stabilized radicals

A typical reaction pertaining to this class involves benzylic radicals generated by deprotonation of the corresponding radical cation. Such species are extremely strong acids (e.g. calculated pK_a of the toluene radical cation = -12, Nicholas and Arnold 1982). However, kinetic factors may limit the importance of the process, which depends on the proton acceptor present. With toluene as the donor and 1,4-dicyanonaphthalene, DCN, as the acceptor in acetonitrile, proton transfer occurs in the cage, and is followed by rapid combination of the radicals to yield a tetracyclic derivative as the main product, (10) (Albini 1982; Sulpizio *et al* 1989). However, when deprotonation occurs out of the cage (e.g. when the reaction is carried out in methanol, and the solvent is the proton acceptor), or when the radical is formed by splitting a cation different from the proton, e.g. a carbocation or an organometallic cation, a different addition leads to benzyldihydroronaphthalenes, (11).



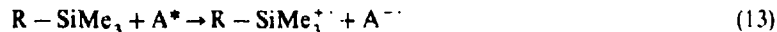


On the contrary, when the acceptor used is less easily reduced, e.g. 1,4-dicyanobenzene, DCB, rather than DCN, the radical is in most cases reduced; thus Popielartz and Arnold (1990) have shown that cleavage of bibenzyls occurs through this path



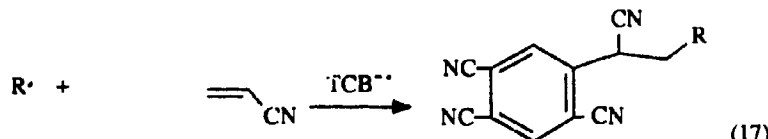
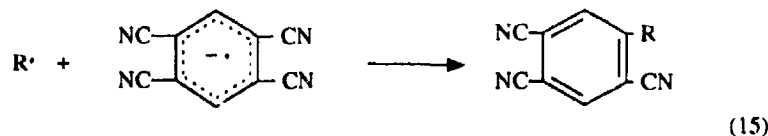
3. Non-stabilized alkyl radicals

Non-stabilized alkyl radicals can be generated via the radical cations by using strong photochemical oxidizers such as DCB or 1,2,4,5-tetracyanobenzene, TCB, and substrates such as silanes (Kyushin *et al* 1990), acetals (Mella *et al* 1992) and carboxylic acids (Tsujimoto *et al* 1992), as in the following example.



Reduction of such radicals is generally not possible, and the other reactions occur efficiently.

Typical examples are alkylation of the aromatic used as electron acceptor (15), alkylation of electron-poor alkenes (16), termolecular addition (17), and reduction (18). The competition between the different processes depends on the redox properties of the species involved.



4. Conclusions

The examples above show some of the potentialities of this new method for the generation of radicals. It is expected that much more synthetic chemistry can be developed following these lines.

References

- Albini A, Fasani E and Oberti R 1982 *Tetrahedron* **38** 1034
Curran D P 1991 In *Comprehensive organic synthesis* (eds) B M Trost and I Fleming (Oxford: Pergamon) p. 714
Dinnocenzo J P, Farid S, Goodman J L, Gould I R, Todd W P and Mattes S L 1989 *J. Am. Chem. Soc.* **111** 8973
Fox M A and Chanon M (eds) 1988 *Photoinduced electron transfer* (Amsterdam: Elsevier)
Kyushin S, Masuda Y, Matsushita K, Nadaira Y and Ohashi M 1990 *Tetrahedron Lett.* **63** 95
Mella M, Fasani E and Albini A 1992 *J. Org. Chem.* **57** 3051
Nicholas A M P and Arnold D R 1982 *Can. J. Chem.* **60** 2165
Popielartz R and Arnold D R 1990 *J. Am. Chem. Soc.* **112** 3068
Sulpizio A, Albini A, d'Alessandro N, Fasani E and Pietra S 1989 *J. Am. Chem. Soc.* **111** 5773
Tsujimoto K, Nakao N and Ohashi M 1992 *J. Chem. Soc., Chem. Commun.* 366
Wayner D D M, Dannenberg J J and Griller D 1986 *Chem. Phys. Lett.* **131** 189
Wayner D D M, McPhee D J and Griller D 1988 *J. Am. Chem. Soc.* **110** 132

Amine-assisted photochemical dehalogenation of haloanthracenes (9-halo and 9,10-dihalo compounds) and their triplet formation

TOSHIHIRO NAKAYAMA, KAZUYASU IBUKI and KUMAO HAMANOUE*

Department of Chemistry, Kyoto Institute of Technology, Matsugasaki, Sakyo-ku, Kyoto 606,
Japan

Abstract. Steady-state photolysis of haloanthracenes (XA; 9,10-dichloro, 9,10-dibromo, 9-chloro and 9-bromo compounds) in acetonitrile-amine (triethylamine or N,N-dimethylaniline) causes the consecutive reactions: 9,10-dihalo compounds → 9-halo compounds → anthracene. Although both the lowest excited singlet [$^1\text{XA}(\text{S}_1)$] and triplet [$^3\text{XA}(\text{T}_1)$] states of XA are quenched by amine, the appearance of absorption spectra due to the haloanthracene radical anions ($\text{XA}^{\cdot-}$) within the duration of nanosecond pulse excitation indicates that the intermediates for dehalogenation of XA are $\text{XA}^{\cdot-}$ produced by a diffusion-controlled reaction of $^1\text{XA}(\text{S}_1)$ with the ground-state amine yielding the singlet exciplexes [$(\text{XA-amine})^*$] which decompose rapidly into $\text{XA}^{\cdot-}$ and the amine radical cations. Moreover, an amine-assisted formation of $^3\text{XA}(\text{T}_1)$ has been attributed to the intersystem crossing from $(\text{XA-amine})^*$ to the triplet exciplexes [$(^3(\text{XA-amine})^*)$] followed by decomposition into $^3\text{XA}(\text{T}_1)$ and ground-state amine.

Keywords. Photochemical dehalogenation of haloanthracenes by amines; amine-assisted triplet formation of haloanthracenes; haloanthracene radical anions; 9,10-dihalo and 9-halo anthracenes.

I. Introduction

The photoinduced dehalogenation of aromatic halocompounds by amine is well known and the generally accepted mechanism is that the radical anions produced via the exciplexes of singlet halocompounds with ground-state amines are the reaction intermediates which decompose into the aryl radicals and the halogen anions (Ohashi *et al* 1973; Tsujimoto *et al* 1975; Bunce *et al* 1976, 1978; Chittin *et al* 1978; Davidson and Goodwin 1981; Fulara and Latowski 1990; Saeva 1990). Upon investigation of the photochemical debromination of *meso*-substituted bromanthracenes (9,10-dibromo and 9-bromo compounds) by amine [triethylamine (TEA) or N,N-dimethylaniline (DMA)] in acetonitrile, we have also concluded that the reaction intermediates are the bromanthracene radical anions produced by a diffusion-controlled reaction of the lowest excited singlet states of bromanthracenes with the ground-state amines yielding singlet exciplexes followed by decomposition into bromanthracene radical anions and amine radical cations (Hamanoue *et al* 1984b). Meanwhile, Soloveichik *et al* (1989) have found that the photochemical dechlorination of 9,10-dichloroanthracene by DMA in acetonitrile is strongly retarded upon addition of azulene (or

* For correspondence

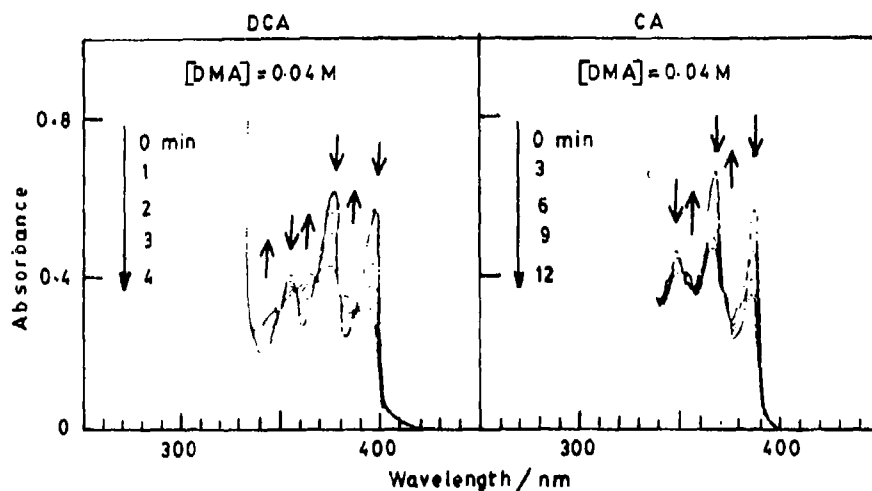


Figure 1. Dechlorination of DCA and CA upon steady-state photolysis in $\text{CH}_3\text{CN}/\text{DMA}$ (0.04 M) at room temperature.

ferrocene) and that the increment of triplet decay rate constant with increasing DMA concentration is not linear. Based on these results, they have concluded that the haloanthracene radical anions produced via the exciplexes of singlet haloanthracenes with ground-state amine do not participate in the dehalogenation but the exciplexes of triplet haloanthracenes with ground-state amine are the reaction intermediates. In order to contest this conclusion, the present review deals with our recent results obtained by steady-state photolysis and nanosecond laser photolysis of haloanthracenes (9,10-dichloro, 9,10-dibromo, 9-chloro and 9-bromo compounds) by amine (TEA or DMA) in acetonitrile at room temperature (Nagamura *et al* 1991, 1992; Hamanoue *et al* 1992, 1993).

2. Photochemical reaction of haloanthracenes and their triplet formation in acetonitrile/amine

Figure 1 shows the absorption spectral change caused upon steady-state photolysis of 9,10-dichloro (DCA) and 9-chloro (CA) compounds in acetonitrile (CH_3CN) containing 0.04 M DMA at room temperature. Since similar results are also obtained not only in $\text{CH}_3\text{CN}/\text{TEA}$ (0.04 M) but also for 9,10-dibromo (DBA) and 9-bromo (BA) compounds in $\text{CH}_3\text{CN}/\text{amine}$ (0.04 M DMA or TEA), and since the photo-products from 9,10-dihalo compounds and 9-halo compounds have been identified to be 9-halo compounds and anthracene, respectively, it can safely be concluded that the dehalogenation of 9,10-dihalo compounds by amine proceeds by the consecutive reactions: 9,10-dihalo compounds \rightarrow 9-halo compounds \rightarrow anthracene. Although Soloveichik *et al* (1989) have reported that the quantum yield for dechlorination of DCA by DMA decreases remarkably upon addition of azulene or ferrocene, we have confirmed that addition of these additives (1×10^{-4} M) does not affect the decrement

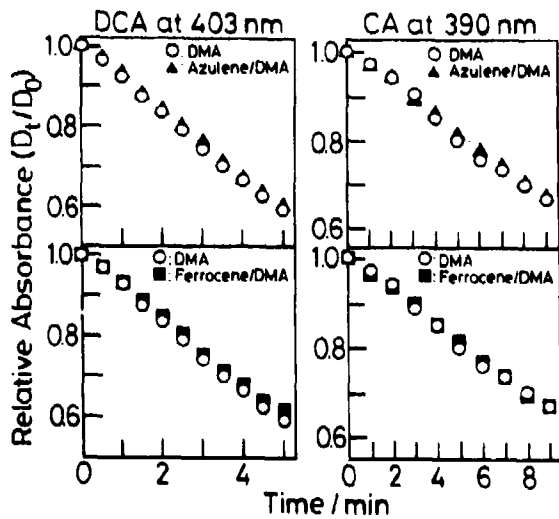


Figure 2. Decrement in the relative absorbances (D_t/D_0) of DCA and CA during steady-state photolysis at room temperature in $\text{CH}_3\text{CN}/\text{DMA}$ (0.04 M) without (○) and with 1×10^{-4} M azulene (▲) [or ferrocene (■)].

in the relative reactant absorbances (D_t/D_0) during steady-state photolysis of haloanthracenes (XA) in $\text{CH}_3\text{CN}/\text{amine}$ (0.04 M); typical examples obtained for chloro compounds in $\text{CH}_3\text{CN}/\text{DMA}$ (0.04 M) are shown in figure 2, where D_t and D_0 are the absorbances measured at photolysis time of t and 0 min, respectively.

We have found that the intensity of triplet-triplet ($T' \leftarrow T_1$) absorption spectra due to the lowest excited triplet states [${}^3\text{XA}(T_1)$] of XA decreases with increasing amine concentration, but a normalization of the $T' \leftarrow T_1$ absorption spectrum in the presence of amine to those in the absence of amine reveals no change in the spectral profile. Since all the $T' \leftarrow T_1$ absorption spectra are recorded at a decay time of 70 ns and a gate time of 20 ns and since the $T' \leftarrow T_1$ absorptions are found to decay in the microsecond time regime even in the presence of amine, the intensity decrease of $T' \leftarrow T_1$ absorption spectra caused upon addition of amine can be ascribed to the decrement in the yields of the lowest excited singlet states [${}^1\text{XA}(S_1)$] of XA. Calculating the intensities of $T' \leftarrow T_1$ absorption spectra in the absence (I_0^T) and presence (I_A^T) of amine, the ratios of I_0^T/I_A^T are plotted against amine concentration as shown by open circles in figures 3 and 4. If ${}^3\text{XA}(T_1)$ are produced only via the indirect ${}^1\text{XA}(S_1) \rightarrow {}^3\text{XA}(T_n) \rightarrow {}^3\text{XA}(T_1)$ intersystem crossing through an adjacent higher excited triplet (T_n) state (Hamanoue *et al.* 1983; Tanaka *et al.* 1983), the ratio of I_0^T/I_A^T can be given by

$$I_0^T/I_A^T = 1 + k_q \tau [\text{amine}], \quad (1)$$

where τ is the fluorescence lifetime of ${}^1\text{XA}(S_1)$ in the absence of amine and k_q is the fluorescence quenching rate constant by amine. Hence, the value of k_q obtained from I_0^T/I_A^T should be equal to that obtained by the Stern-Volmer plot of I_0^F/I_A^F against amine concentration; I_0^F and I_A^F are the fluorescence intensities in the absence and presence of amine, respectively. In contrast, as shown in figures 3 and 4, the values

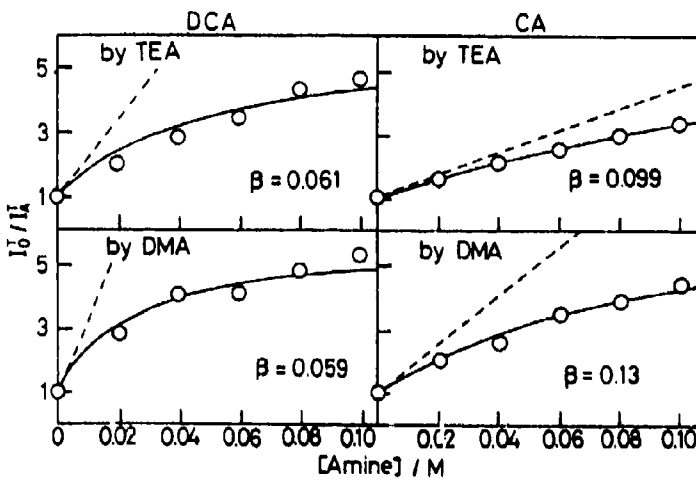
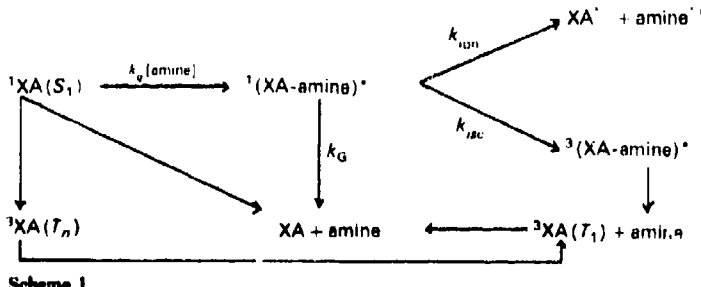


Figure 3. Plots of I_0^T/I_A^T against amine concentration obtained for DCA and CA in CH_3CN at room temperature. The dashed lines correspond to the Stern-Volmer plots of fluorescence intensities against amine concentration, and the full lines are simulated by (1) using the values of k_q obtained from the fluorescence quenching by amine: $k_q = 1.4 \times 10^{10}$ (by TEA) and 2.7×10^{10} (by DMA) $\text{M}^{-1}\text{s}^{-1}$ for DCA, and $k_q = 1.1 \times 10^{10}$ (by TEA) and 2.4×10^{10} (by DMA) $\text{M}^{-1}\text{s}^{-1}$ for CA.

of I_0^T/I_A^T (open circles) deviate from the dashed lines obtained from I_0^F/I_A^F giving k_q of the order for that of a diffusion-controlled reaction. The smaller values of I_0^T/I_A^T than those of I_0^F/I_A^F may reflect an additional formation of ${}^3\text{XA}(T_1)$ by amine.

Probably, the additional formation of ${}^3\text{XA}(T_1)$ in the presence of amine may be interpreted in terms of the intersystem crossing from ${}^1(\text{XA-amine})^*$ to the triplet exciplexes $[{}^3(\text{XA-amine})^*]$ followed by decomposition into ${}^3\text{XA}(T_1)$ and ground-state amine as shown by scheme 1.



Scheme 1.

Hence, I_0^T/I_A^T should be given by:

$$\frac{I_0^T}{I_A^T} = \frac{1 + k_q \tau [\text{amine}]}{1 + \alpha [\text{amine}]} \quad (4)$$

$$\alpha = \beta k_q / k_{ic}, \quad (5)$$

$$\beta = k'_{ic} / (k_G + k_{ion} + k'_{ic}). \quad (6)$$

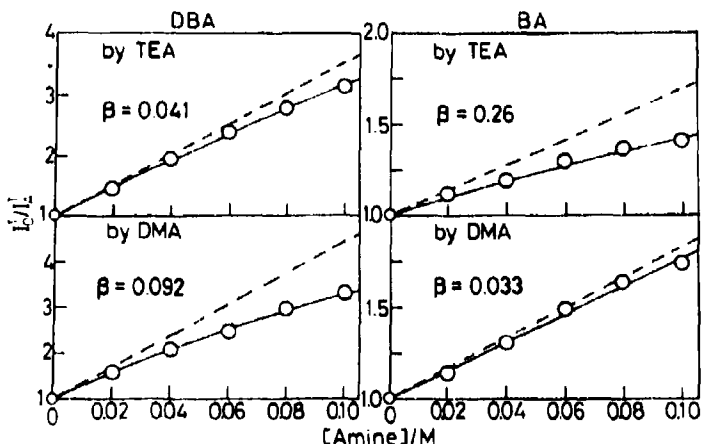


Figure 4. Plots of I_0^T/I_A^T against amine concentration obtained for DBA and BA in CH_3CN at room temperature. The dashed lines correspond to the Stern-Volmer plots of fluorescence intensities against amine concentration, and the full lines are simulated by (1) using the values of k_q obtained from the fluorescence quenching by amine: $k_q = 2.0 \times 10^{10}$ (by TEA) and 2.7×10^{10} (by DMA) $\text{M}^{-1}\text{s}^{-1}$ for DBA, and $k_q = 4.3 \times 10^{10}$ (by TEA) and 5.2×10^{10} (by DMA) $\text{M}^{-1}\text{s}^{-1}$ for BA.

By a best-fit of the calculated values $\{(1 + k_q \tau [\text{amine}])/(1 + \alpha[\text{amine}])\}$ to the experimental values, the change of I_0^T/I_A^T with amine concentration can well be reproduced as shown by the full curves in figures 3 and 4. Since the fluorescence quantum yield (Φ_F) in CH_3CN without amine are found to be 0.64 (DCA), 0.02 (CA), 0.09 (DBA) and 0.04 (BA), the rate constants (k_{lsc}) for the ${}^1\text{XA}(S_1) \rightarrow {}^3\text{XA}(T_1)$ intersystem crossing are calculated to be 4.2×10^7 (DCA), 3.0×10^8 (CA), 7.1×10^8 (DBA) and 6.0×10^9 (BA) s^{-1} . Using the best-fit values of α , the values of β are calculated as indicated in figures 3 and 4, and the greater values of $k_q[\text{amine}]$ in $\text{CH}_3\text{CN}/\text{amine}$ (1 M), i.e., $1.4 - 2.7 \times 10^{10}$ (DCA), $1.1 - 2.4 \times 10^{10}$ (CA), $2.0 - 2.7 \times 10^{10}$ (DBA) and $4.3 - 5.2 \times 10^{10}$ (BA) s^{-1} , compared with those of k_{lsc} indicate that ${}^1(\text{XA-amine})^*$ are produced with efficiencies of ~ 1.0 (DCA, CA), 0.97 (DBA) and 0.88 - 0.90 (BA), and that almost all ${}^3\text{XA}(T_1)$ are produced via the indirect ${}^1(\text{XA-amine})^* \rightarrow {}^3(\text{XA-amine})^* \rightarrow {}^3\text{XA}(T_1)$ process shown in scheme 1.

3. Formation of the haloanthracene radical anions via the singlet exciplexes of ${}^1\text{XA}(S_1)$ with ground-state amine

Figure 5 shows the transient absorption spectra obtained by nanosecond laser photolysis of DCA and CA in $\text{CH}_3\text{CN}/\text{amine}$ (1 M) at room temperature; the spectra are recorded at a delay time of 0 ns and a gate time of 50 ns. Similar transients are also obtained for DBA and BA. In the absence of amine, however, only the $T' \leftarrow T_1$ absorptions (bands C and D) of ${}^3\text{XA}(T_1)$ can be seen. We have assigned bands F, G and H to absorptions of the haloanthracene radical anions ($\text{XA}^{\cdot-}$) based on the following facts: (1) The spectra with bands F - H are identical with those of $\text{XA}^{\cdot-}$ which are produced by pulse radiolysis of XA at room temperature in CH_3CN

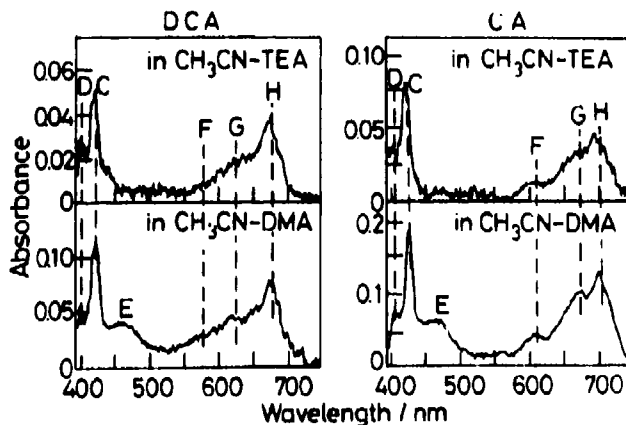


Figure 5. Transient absorption spectra obtained by nanosecond laser photolysis of DCA and CA in CH_3CN /amine (1 M) at room temperature.

without amine (Hamanoue *et al.* 1984a) or γ -radiolysis of XA at 77 K in 2-methyltetrahydrofuran without amine. (2) Band E observed in the presence of DMA is very similar to that of the published absorption spectrum due to $\text{DMA}^{\cdot+}$ (Hamil 1968; Shida 1988; Iwamura and Eaton 1991); no clear observation of the absorption band due to $\text{TEA}^{\cdot+}$ may be ascribed to its weak absorption (Shida 1988).

We propose that $\text{XA}^{\cdot-}$ are produced by a diffusion-controlled reaction of ${}^1\text{XA}(S_1)$ with ground-state amine yielding ${}^1(\text{XA-amine})^*$ followed by decomposition into $\text{XA}^{\cdot-}$ and the amine radical cations (amine $^{\cdot+}$): Because, (1) ${}^3\text{XA}(T_1)$ in CH_3CN decay following a single-exponential function irrespective of absence and presence of amine, and the decay rate constants thus obtained increase linearly with increasing amine concentration; (2) the quenching rate constants ($k'_q \approx 10^4 - 10^5 \text{ M}^{-1} \text{s}^{-1}$) of ${}^3\text{XA}(T_1)$ by amine, however, are much smaller than those ($k_q \approx 10^{10} \text{ M}^{-1} \text{s}^{-1}$) obtained for the quenching of ${}^1\text{XA}(S_1)$ by amine, indicating that the spectra observed at 0-ns delay (shown in figure 5) cannot be attributed to $\text{XA}^{\cdot+}$ produced by a reaction of ${}^3\text{XA}(T_1)$ with amine.

The absorptions of $\text{XA}^{\cdot-}$ in CH_3CN /amine(1 M) decay with time following a single-exponential function and the decay rate constants ($k_{\text{XA}^{\cdot-}}$) obtained are of the order of $10^4 - 10^5 \text{ s}^{-1}$; typical decay curves obtained for DCA and CA in $\text{CH}_3\text{CN}/\text{DMA}$ (1 M) are shown in figure 6. If ${}^3(\text{XA-amine})^*$ produced by a reaction of ${}^3\text{XA}(T_1)$ with ground-state amine as proposed by Soloveichik *et al.* (1989) give rise to the formation of $\text{XA}^{\cdot-}$, the values of $k_{\text{XA}^{\cdot-}}$ shown in figure 6 indicate that one cannot confirm the formation of $\text{XA}^{\cdot-}$ in $\text{CH}_3\text{CN}/\text{DMA}$ (1 M) owing to the larger values of $k_{\text{XA}^{\cdot-}} = 3.5 \times 10^5 (\text{DCA}) - 9.5 \times 10^5 (\text{CA}) \text{ s}^{-1}$ compared with those of $k'_q[\text{DMA}] = 5.0 \times 10^4 (\text{DCA}) - 2.2 \times 10^5 (\text{CA}) \text{ s}^{-1}$. In $\text{CH}_3\text{CN}/\text{TEA}$ (1 M), however, the rise and decay of absorptions due to $\text{XA}^{\cdot-}$ should be detectable in the microsecond time regime, because $k_{\text{XA}^{\cdot-}} = 2.8 \times 10^4 (\text{DCA}) - 9.7 \times 10^4 (\text{CA}) \text{ s}^{-1}$ are smaller than $k'_q[\text{TEA}] = 1.8 \times 10^3 (\text{DCA}) - 2.3 \times 10^3 (\text{CA}) \text{ s}^{-1}$. In contrast, no such evidence has been obtained. Even if the dehalogenation does occur in ${}^3(\text{XA-amine})^*$ produced by a reaction of ${}^3\text{XA}(T_1)$ with ground-state amine and no $\text{XA}^{\cdot-}$ are produced, the following results cannot support the triplet exciplex mechanism: (1) The decay rate constants of

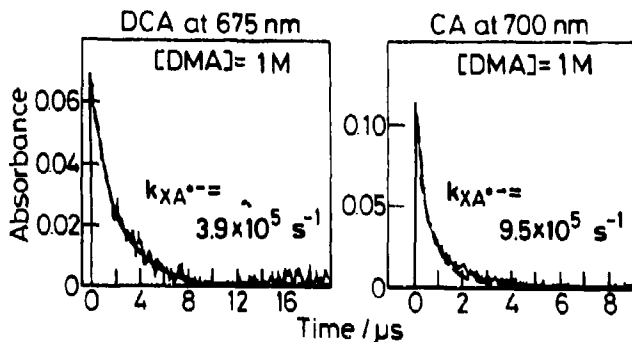


Figure 6. Decays of absorptions (full lines) due to $\text{DCA}^{\cdot-}$ and $\text{CA}^{\cdot-}$ in $\text{CH}_3\text{CN}/\text{DMA}$ (1 M) at room temperature. The dashed lines are simulated single-exponential functions with decay rate constants ($k_{\text{X}^{\cdot-}}$) indicated in the figure.

${}^3\text{XA}(T_1)$ in $\text{CH}_3\text{CN}/\text{amine}$ increase linearly with increasing amine concentration, showing no existence of such an equilibrium between ${}^3\text{XA}(T_1)$ + amine and ${}^3(\text{XA-amine})^*$ as proposed by Soloveichik *et al* (1989); during decrement of the $T' \leftarrow T_1$ absorption spectra of ${}^3\text{XA}(T_1)$ with time in $\text{CH}_3\text{CN}/\text{amine}$ (0.04 M), moreover, no change in the spectral profile can be seen. (2) Addition of azulene or ferrocene in CH_3CN accelerates the decay of ${}^3\text{XA}(T_1)$ with quenching rate constants of the order of $10^8 - 10^9 \text{ M}^{-1} \text{ s}^{-1}$, while figure 2 reveals no effects of these additives on the decrement of reactant absorptions during steady-state photolysis in $\text{CH}_3\text{CN}/\text{DMA}$ (0.04 M); similar results are also obtained in $\text{CH}_3\text{CN}/\text{TEA}$ (0.04 M). (3) The quantum yields (Φ_R) for the dechlorination of DCA yielding CA in $\text{CH}_3\text{CN}/\text{amine}$ (0.08 M) are found to be greater than those in $\text{CH}_3\text{CN}/\text{amine}$ (0.04 M), while the quantum yields (Φ_T) for the formation of ${}^3\text{XA}(T_1)$ decrease with increasing amine concentration; in the presence of 0.08 M DMA, moreover, $\Phi_R = 0.117$ is greater than $\Phi_T = 0.073$.

4. Conclusion

All the results obtained so far are consistent with those reported in our previous paper (Hamanoue *et al* 1984b). Thus, again we conclude that the intermediates for the photochemical dehalogenation of haloanthracenes (XA) are really their radical anions ($\text{XA}^{\cdot-}$) produced by a diffusion-controlled reaction of ${}^1\text{XA}(S_1)$ with ground-state amine yielding the singlet exciplexes [${}^1(\text{XA-amine})^*$] followed by decomposition into $\text{XA}^{\cdot-}$ and amine $^+$ (cf. scheme 1).

The absorption spectra with bands D-F shown in figure 5 might be ascribed to the absorptions of ${}^1(\text{XA-amine})^*$. Although no exciplex emissions can be seen in $\text{CH}_3\text{CN}/\text{TEA}$, an exciplex emission with $\lambda_{\max} \approx 550 \text{ nm}$ can be seen for DBA in cyclohexane (CH)/TEA (2 M) and picosecond laser photolysis of DBA in CH/TEA (1 M) gives rise to the appearance of not only an absorption band due to ${}^1\text{DBA}(S_1)$, i.e., a singlet-singlet ($S' \leftarrow S_1$) absorption band with $\lambda_{\max} \approx 620 \text{ nm}$, but also an exciplex absorption band due to ${}^1(\text{DBA-TEA})^*$ with $\lambda_{\max} \approx 680 \text{ nm}$ (Nakayama *et al* 1993). Since the $S' \leftarrow S_1$ absorption decays following a bi-exponential function with lifetimes of $\alpha_1 = 75 \text{ ps}$ and $\alpha_2 = 260 \text{ ps}$, and since the exciplex absorption increases at first with

a rise time of $\alpha_1 = 75$ ps and then decreases with a lifetime of $\alpha_2 = 260$ ps, one can conclude that $^1(\text{DBA-TEA})^*$ is really produced in CH/TEA (1 M). On the other hand, no exciplex absorption can be seen for DBA in $\text{CH}_3\text{CN}/\text{TEA}$ (1 M) and the $S' \leftarrow S_1$ absorption decays following a single exponential function with a lifetime of 50 ps which is equal to the fluorescence quenching time by 1 M TEA. For DBA in CH/TEA (1 M), moreover, nanosecond laser photolysis reveals no formation of $\text{DBA}^{\cdot-}$ and steady-state photolysis reveals that the rate of debromination is extremely slow compared with that in $\text{CH}_3\text{CN}/\text{TEA}$. Hence, we have concluded that the spectra with bands D-F shown in figure 5 are really a result of the absorptions of λ, λ' and that $^1(\text{DBA-TEA})^*$ produced in CH/TEA decomposes very slightly into $\text{DBA}^{\cdot-}$ and $\text{TEA}^{\cdot+}$, i.e., the formation of haloanthracene radical anions is essential for the photochemical dehalogenation of haloanthracenes by amine.

References

- Bunce N J, Kumar Y, Ravanal L and Safe S 1978 *J. Chem. Soc., Perkin Trans. 2* 880
 Bunce N J, Pilon P, Ruzo L O and Sturch D J 1976 *J. Org. Chem.* **41** 3023
 Chittin B, Safe S, Bunce N, Ruzo L, Oli K and Hutzinger O 1978 *Can. J. Chem.* **56** 1253
 Davidson R S and Goodwin J W 1981 *Tetrahedron Lett.* **22** 163
 Fulara J and Latowski T 1990 *Pol. J. Chem.* **64** 369
 Hamanoue K, Hidaka T, Nakayama T, Teranishi H, Sumitani M and Yoshihara K 1983 *Bull. Chem. Soc. Jpn.* **56** 1851
 Hamanoue K, Kimoto M, Nakayama T, Teranishi H, Tagawa S and Tabata Y 1984a *Radiat. Phys. Chem.* **24** 445
 Hamanoue K, Nakayama T, Ikenaga K and Ibuki K 1992 *J. Phys. Chem.* **96** 10297
 Hamanoue K, Nakayama T, Ikenaga K, Ibuki K and Otani A 1993 *J. Photochem. Photobiol. A* **69** 305
 Hamanoue K, Tai S, Hidaka T, Nakayama T, Kimoto M and Teranishi H 1984b *J. Phys. Chem.* **88** 4380
 Hamil W H 1986 *Radical ions* (eds E T Kaiser and L Kevan) (New York: Wiley) chap. 9
 Iwamura H and Eaton D F 1991 *Pure Appl. Chem.* **63** 1003
 Nagamura T, Nakayama T and Hamanoue K 1991 *Chem. Lett.* 2051
 Nagamura T, Nakayama T and Hamanoue K 1992 *Chem. Phys. Lett.* **193** 30
 Nakayama T, Hanada T, Ibuki K and Hamanoue K 1993 *Chem. Phys. Lett.* **209** 367
 Ohashi M, Tsujimoto K and Seki K 1973 *J. Chem. Soc., Chem. Commun.* 384
 Saeva F D 1990 *Top. Curr. Chem.* **156** 61
 Shida T 1988 *Electronic absorption spectra of radical ions* (Amsterdam: Elsevier)
 Soloveichik O M, Ivanov V L and Kuz'min M G 1989 *High Energy Chem. (Engl. Transl.)* **23** 281
 Tanaka M, Tanaka I, Tai S, Hamanoue K, Sumitani M and Yoshihara K 1983 *J. Phys. Chem.* **87** 813
 Tsujimoto K, Tasaka S and Ohashi M 1975 *J. Chem. Soc., Chem. Commun.* 758

Preparation of some organic precursors via photolytic demetallation of their iron complexes

ALAA S ABD-EL-AZIZ*, CHRISTINE R DE DENUS and
KRYSTYNA LEZYNSKA

Department of Chemistry, University of Winnipeg, Winnipeg, Manitoba, R3B 2E9, Canada

Abstract. Nucleophilic aromatic substitution (S_NAr) of chloroarenes complexed to the cyclopentadienyl iron moiety with ethyl cyanoacetate or phenylsulfonylacetonitrile in the presence of potassium carbonate in DMF resulted in the formation of arylated ethyl cyanoacetate or phenylsulfonylacetonitrile complexes. Photolytic demetallation of these complexes led to the liberation of the substituted arene ligands in high yield. This synthetic route is more advantageous than those previously reported and is a practical way to synthesize heterocycles and alcanoic acid precursors.

Keywords. S_NAr ; photolysis; ethyl arylcyanoacetate; aryl phenylsulfonylacetonitrile.

1. Introduction

There has been considerable interest in the development of new and efficient routes to the synthesis of arylated ethyl cyanoacetates and phenylsulfonylacetonitriles (Shen 1972; Suzuki *et al* 1987; Sakamoto *et al* 1990). These materials are known to be versatile intermediates in the synthesis of heterocyclic compounds (e.g. azetinones, pyrimidines, and oxazaphosphorinane derivatives) and alcanoic acids, which are used for medicinal purposes (Matsui and Motoi 1973; Giordano *et al* 1984; Shih and Wang 1984). One of the well-recognized alcanoic acids is 2-(4-isobutylphenyl)propanoic acid, known as Ibuprofen. This acid is an anti-inflammatory analgesic, finding use in the treatment of patients with rheumatoid arthritis and in relieving general muscle pain and stiffness (Adams *et al* 1969; Chalmers 1969; Shen 1979). The synthesis of ethyl arylcyanoacetates and arylated phenylsulfonylacetonitriles cannot be achieved directly through nucleophilic substitution reactions of ethyl cyanoacetate or phenylsulfonylacetonitrile anions with arylhalides. The routes to these compounds involve the use of certain organometallic reagents or catalysts to promote nucleophilic substitution on the aromatic ring (Kaiser *et al* 1971; Osuka *et al* 1983; Uno *et al* 1985; Sakamoto *et al* 1988; Kozyrod *et al* 1991). In these synthetic routes, the most problematic step is the nucleophilic aromatic substitution.

Activation of normally unreactive chloroarenes towards nucleophilic aromatic substitution reactions (S_NAr) by complexation to a metal moiety such as chromium tricarbonyl, manganese tricarbonyl or cyclopentadienyliron ($CpFe$) have been

* For correspondence

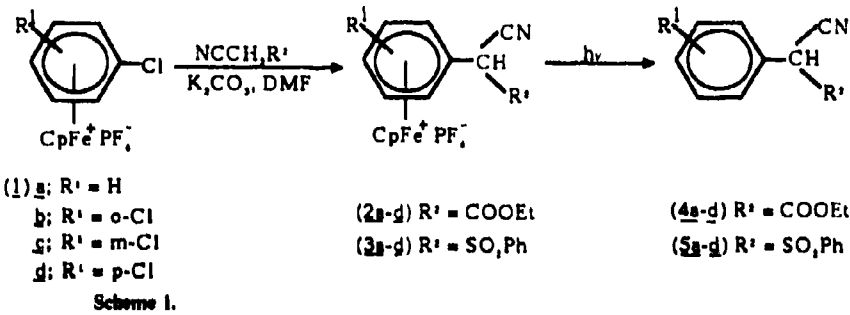
reported (Semmelhack 1976; Pearson *et al* 1986; Kerber 1991). Nesmeyanov *et al* (1967) were the first to establish the efficient displacement of the chlorine atom in η^6 -chlorobenzene- η^3 -cyclopentadienyliron complex cations by some oxygen, sulfur and nitrogen nucleophiles. We have been very active in utilizing this methodology in the synthesis of various functionalized aromatic compounds (Abd-El-Aziz *et al* 1988, 1993; Abd-El-Aziz and de Denus 1992, 1993).

Nesmeyanov *et al* (1970) examined the effect of irradiation of arene complexes. They found that the photolytic degradation of these complexes in acetonitrile solution resulted in liberation of the arene ligands with ferrocene and iron(II) salt. This photolytic degradation was proven to be greatly dependent on the nature of the solvent, with σ -donor ligands resulting in the greatest yields. Gill and Mann (1980, 1981, 1983) have also given detailed descriptions of the photoinduced replacement of the arene by one 6-electron or three 2-electron ligands.

In this article, we describe our approach to the arylation of ethyl cyanoacetate and phenylsulfonylacetonitrile via S_NAr followed by photolytic demetallation.

2. Results and discussion

η^6 -Chloroarene- η^3 -cyclopentadienyliron hexafluorophosphates (**1a-d**) were prepared via ligand exchange reactions involving ferrocene and chlorobenzene, *o*-, *m*- or *p*-dichlorobenzene according to the method reported by Khand *et al* (1968). Reactions of the product complexes (**1a-d**) with phenylsulfonylacetonitrile or ethyl cyanoacetate in the presence of potassium carbonate in N,N-dimethylformamide, led to the formation of complexed arylated ethyl cyanoacetates (**2a-d**) and phenylsulfonyl-acetonitriles (**3a-d**) as shown in scheme 1. These complexes were isolated as yellow solids or yellow-brown oils in very good yields (71–94%). Ortho substituents on the complexed aromatic ring did not cause any sterically induced inhibition of the reaction. 1H and ^{13}C NMR and IR were used to characterize the prepared complexes (**2a-d**, **3a-d**). In the 1H NMR spectra of these complexes, a very distinctive singlet appeared around 5.31–5.47 ppm which is characteristic of the cyclopentadienyl (Cp) ring. For complexes (**3a-d**), in many cases the methine proton appeared at 6–7 ppm overlapping with the arene protons. The assignment of some of these methine protons was based on the integration of the peaks in the region between 6–7 ppm relative to other proton peaks in the spectra. The ^{13}C NMR was also in agreement with expectations, as is outlined in § 3.



Liberation of the arylated ethyl cyanoacetates and phenylsulfonylacetonitriles from their iron complexes is one of the most important steps in this synthetic strategy. Since photolysis is known to be an efficient method for the decomplexation of some (arene)cyclopentadienyliron complexes, we successfully applied this technique to liberate the free organic ligands. The complexes were dissolved in a mixture of acetonitrile/dichloromethane and irradiated under a nitrogen atmosphere for 2 h, using a Xenon lamp as the source of radiation. Purification of the products by column chromatography resulted in isolation of the free aromatic ligands (4a-d, 5a-d) in yields ranging from 70–84%.

The identities of all photolysed products were confirmed by ¹H and ¹³C NMR, IR, and MS. The major differences in the ¹H and ¹³C NMR of these compounds from the complexes are the absence of the cyclopentadienyl peak, the shift of the arene peaks downfield, and a shift of the methine peak to a higher field. Compounds (4a-d) are some of the heterocyclic precursors, and compounds (5a-d) are the desired precursors for some alkanoic acid synthesis. Our synthetic methodology is extremely versatile and efficient in the preparation of such precursors.

In conclusion, we would like to point out that photolysis is an important and efficient step in the synthetic strategy and the *S_NAr* route to the synthesis of arylated ethyl cyanoacetates and phenylsulfonylacetonitriles is very useful owing to its ease and the use of mild reagents.

3. Experimental

Ethyl cyanoacetate, phenylsulfonylacetonitrile, potassium carbonate and N,N-dimethylformamide (DMF) are commercially available and were used without further purification.

¹H and ¹³C NMR were recorded on a Gemini 200 NMR spectrometer, with chemical shifts calculated from the solvent signals. MS spectra were recorded on a HP 5970 Series Mass Selective Detector in *m/z* units. IR spectra were recorded using a Perkin-Elmer 781 spectrophotometer.

3.1 Nucleophilic substitution reactions

(a) *Reactions with ethyl cyanoacetate:* A mixture of 1 mmol of starting cation (1a-d), 2.5 mmol potassium carbonate, and 1.05 mmol of ethyl cyanoacetate in 10 ml of DMF was stirred at 50–60°C, under a nitrogen atmosphere for 3 h. The resulting dark red reaction mixture was filtered into 10 ml of 10% hydrochloric acid. A concentrated aqueous solution of ammonium hexafluorophosphate was added to the reaction mixture, and the product extracted with dichloromethane (3 × 50 ml). The combined extract was washed with water (4 × 40 ml), dried over magnesium sulphate, and the solvent was evaporated off under reduced pressure at 25°C. The residual yellow-brown oil was washed with diethyl ether (3 × 20 ml). Thus the following compounds were prepared.

(b) (η^5 -Cyclopentadienyl) [η^6 -ethyl 2-phenyl cyanoacetate]-iron(II) hexafluorophosphate (2a): (0.362 g, 80%) ν_{max} (cm⁻¹) (neat) 2260 (CN), 1755 (CO); δ_H (CD₃COCD₃) 1.24 (3H, *t*, *J* = 7.1, CH₃), 4.24 (2H, *q*, *J* = 6.7, CH₂), 5.31 (5H, *s*, Cp), (5.72 (1H, *s*, CH), 6.63 (5H, *br*, *s*, ArH); δ_C (CD₃COCD₃) 13.86 (CH₃), 43.11 (CH), 64.55 (CH₂),

78·83 (5C, Cp), 86·98, 89·09, 89·19, 89·37, 90·21 (5C, ArC), 96·93 (quaternary ArC), 115·33 (CN), 163·70 (CO).

(c) (η^5 -Cyclopentadienyl) [η^6 -ethyl-(*o*-chlorophenyl) cyanoacetate]-iron(II) hexafluorophosphate (2b): (0·346 g, 71%) ν_{max} (cm⁻¹) (neat) 2305 (CN), 1755 (CO); δ_{H} (CD₃COCD₃) 1·25 (3H, *t*, *J* = 7·2, CH₃), 4·30 (2H, *q*, *J* = 6·8, CH₂), 5·47 (5H, *s*, Cp), 6·26 (1H, *s*, CH), 6·71 (1H, *t*, *J* = 6·1, ArH), 6·85 (2H, *m*, ArH), 7·05 (1H, *d*, *J* = 7·3, ArH); δ_{C} (CD₃COCD₃) 13·76 (CH₃), 41·56 (CH), 64·67 (CH), 80·87 (5C, Cp), 87·12, 88·53, 89·71, 89·90 (4C, ArC), 95·30, 108·56 (quaternary ArC), 114·85 (CN), 162·48 (CO).

(d) (η^5 -Cyclopentadienyl) [η^6 -ethyl-(*m*-chlorophenyl) cyanoacetate]-iron(II) hexafluorophosphate (2c): (0·365 g, 74%) ν_{max} (cm⁻¹) (neat) 2200 (CN), 1760 (CO); δ_{H} (CD₃COCD₃) 1·26 (3H, *t*, *J* = 7·1, CH₃), 4·31 (2H, *q*, *J* = 7·1, CH₂), 5·46 (5H, *s*, Cp), 5·83 (1H, *s*, CH), 6·65, 7·05 (4H, *t*, *J* = 6·1, ArH); δ_{C} (CD₃COCD₃) 13·02 (CH₃), 41·74 (CH), 63·93 (CH₂), 80·28 (5C, Cp), 86·41, 87·98, 88·96, 89·82 (4C, ArC), 96·04, 107·08 (quaternary ArC), 115·26 (CN), 162·45 (CO).

(e) (η^5 -Cyclopentadienyl) [η^6 -ethyl-(*p*-chlorophenyl) cyanoacetate]-iron(II) hexafluorophosphate (2d): (0·396 g, 81%) ν_{max} (cm⁻¹) (neat) 2310 (CN), 1760 (CO); δ_{H} (CD₃COCD₃) 1·25 (3H, *t*, *J* = 7·0, CH₃), 4·25 (2H, *q*, *J* = 7·1, CH₂), 5·42 (5H, *s*, Cp), 5·72 (1H, *s*, CH), 6·74 (2H, *d*, *J* = 5·1, ArH), 6·97 (2H, *d*, *J* = 6·5, ArH); δ_{C} (CD₃COCD₃) 13·07 (CH₃), 41·67 (CH), 63·91 (CH₂), 80·41 (5C, Cp), 86·11, 88·52, 88·55, 88·64 (4C, ArC), 95·34, 107·48, (quaternary ArC), 115·30 (CN), 162·54 (CO).

3.2 Reactions with phenylsulfonylacetonitrile

A mixture of 1 mmol of starting cation (1a-d), 2·5 mmol of potassium carbonate, 1·05 mmol phenylsulfonylacetonitrile, and 10 ml of DMF was stirred at room temperature under a nitrogen atmosphere for \approx 7 h. The resulting red reaction mixture was rapidly filtered into 10% hydrochloric acid (10 ml). The reaction flask was then washed with ethanol and the washing added to the filtrate. The ethanol was removed under reduced pressure at 25°C using a rotary evaporator (Buchi RE-111). A concentrated aqueous solution of ammonium hexafluorophosphate was added to the reaction mixture. The solution was then stirred for 10 min and the resulting yellow product was collected by filtration. Thus the following were prepared.

(a) (η^5 -Cyclopentadienyl) [η^6 -phenyl phenylsulphonylacetonitrile]-iron(II) hexafluorophosphate (3a): (0·414 g, 79%) ν_{max} (cm⁻¹) (neat) 2320 (CN), 1335, 1165 (SO); δ_{H} (CD₃COCD₃) 5·32 (5H, *s*, Cp), 6·46–6·70 (6H, *m*, complexed ArH and CH), 7·71–7·80 (2H, *m*, SO₂PhH), 7·85–7·99 (3H, *m*, SO₂PhH); δ_{C} (CD₃COCD₃) 61·96 (CH), 79·41 (5C, Cp), 87·68, 89·78, 89·82, 90·31, 91·47 (5C, ArC), 92·20 (quaternary ArC), 113·13 (CN), 130·81 (2C, SO₂PhC), 130·91 (2C, SO₂PhC), 137·29 (quaternary SO₂PhC).

(b) (η^5 -Cyclopentadienyl) [η^6 -(*o*-chlorophenyl)-phenylsulphonyl-acetonitrile]-iron(II) hexafluorophosphate (3b): (0·527 g, 94%) ν_{max} (cm⁻¹) (neat) 2300 (CN), 1338, 1163 (SO); δ_{H} (CD₃COCD₃) 5·46 (5H, *s*, Cp), 6·71–7·08 (5H, *s*, complexed ArH and CH), 7·76–7·83 (2H, *m*, SO₂PhH), 7·93–8·02 (3H, *m*, SO₂PhH); δ_{C} (CD₃COCD₃) 60·25 (CH), 81·86 (5C, Cp), 89·40 (quaternary ArC), 88·10, 89·61, 90·96, 91·09 (4C, ArC), 109·50 (quaternary ArC), 113·41 (CN), 130·93 (2C, SO₂PhC), 131·23 (2C, SO₂PhC), 135·41 (quaternary SO₂PhC), and 137·63 (SO₂PhC).

(c) (η^5 -Cyclopentadienyl) [η^6 -(*m*-chlorophenyl)-phenylsulphonyl-acetonitrile]-iron(II) hexafluorophosphate (3c): (0·451 g, 81%) ν_{max} (cm⁻¹) (neat) 2280 (CN), 1345, 1162

(SO); δ_H (CD₃COCD₃) 5.47 (5H, s, Cp), 6.40–7.06 (5H, m, complexed ArH and CH), 7.75–7.85 (2H, m, SO₂PhH), 7.90–8.05 (3H, m, SO₂PhH); δ_C (CD₃COCD₃) 61.38 (CH), 81.77 (5C, Cp), 86.57, 87.24, 89.61, 90.85 (4C, ArC), 92.95 (quaternary ArC), 108.44 (quaternary ArC), 112.71 (CN), 130.93 (4C, SO₂PhC), 135.17 (quaternary SO₂PhC), 137.40 (SO₂PhC).

(d) (η^5 -Cyclopentadienyl)-[η^6 -(*p*-chlorophenyl)-phenylsulphonyl-acetonitrile]-iron(II) hexafluorophosphate (3d): (0.428 g, 77%) v_{max} (cm⁻¹) (neat) 2305 (CN), 1348, 1142 (SO); δ_H (CD₃COCD₃) 5.44 (5H, s, Cp), 6.55–6.77 (3H, m, complexed ArH and CH), 7.02 (2H, d, J = 6.2, complexed ArH), 7.72–7.81 (2H, m, SO₂PhH), 7.89–7.98 (3H, m, SO₂PhH); δ_C (CD₃COCD₃) 61.12 (CH), 81.73 (5C, Cp), 87.40, 90.04, 90.07, 91.15 (4C, ArC), 91.51 (quaternary ArC), 109.09 (quaternary ArC), 112.93 (CN), 130.80 (2C, SO₂PhC), 130.91 (2C, SO₂PhC), 134.70 (quaternary SO₂PhC), and 137.32 (SO₂PhC).

4. Photolysis

1.0 mmol of complexes 2a-d, 3a-d were dissolved in a mixture of CH₂Cl₂/CH₃CN (30 ml: 10 ml) in a pyrex tube. The solution was deoxygenated by bubbling nitrogen through it and the reaction tube was fitted into a photochemical apparatus equipped with a xenon lamp (lower limit = 290 nm), and irradiated at room temperature for 2 h. The solvent was concentrated to a volume of 1–2 ml using rotary evaporation, and introduced into a column of silica gel, prepared in hexane. The residue was washed with hexane, and the product eluted with chloroform; by passage through a short column. Removal of the solvent from the eluate gave the expected liberated arene, with the following yields and spectral data.

- (a) *Ethyl 2-phenyl cyanoacetate* (4a): Yellowish crystals (0.151 g, 80%). v_{max} (cm⁻¹) (neat) 2220 (CN), 1750 (CO); δ_H (CDCl₃): 1.26 (3H, t, J = 7.1, CH₃), 4.23 (2H, q, J = 7.2, CH₂), 4.70 (1H, s, CH), 7.38–7.46 (5H, br s, ArH). δ_C (CDCl₃): 13.87 (CH₃), 43.76 (CH), 63.29 (CH₂), 115.60 (CN), 123.05 (quaternary ArC), 127.89, 129.20, 129.32 (5C, ArC) and 164.50 (CO). m/z 189 (M^+ , 3%), 145 (5), 117 (100), 89 (24).
- (b) *Ethyl-(o-chlorophenyl) cyanoacetate* (4b): (0.183 g, 82%), yellowish oil. v_{max} (cm⁻¹) (neat) 2220 (CN), 1750 (CO); δ_H (CDCl₃): 1.26 (3H, t, J = 7.1, CH₃), 4.23 (2H, q, J = 7.2, CH₂), 4.70 (1H, s, CH), 7.38–7.46 (5H, br s, ArH). δ_C (CDCl₃): 13.87 (CH₃), 43.76 (CH), 63.29 (CH₂), 115.60 (CN), 123.05 (quaternary ArC), 127.89, 129.20, 129.32 (5C, ArC), and 164.50 (CO). m/z 225 [³⁷Cl], 2], 223 [³⁵Cl], 5], 151 (100), 116 (20).
- (c) *Ethyl-(m-chlorophenyl) cyanoacetate* (4c): (0.187 g, 84%), yellowish oil. v_{max} (cm⁻¹) (neat) 2260 (CN), 1755 (CO); δ_H (CDCl₃): 1.27 (3H, t, J = 7.0, CH₃), 4.25 (2H, q, J = 7.1, CH₂), 4.67 (1H, s, CH), 7.35 (4H, br s, ArH). δ_C (CDCl₃): 13.82 (CH₃), 43.20 (CH), 63.56 (CH₂), 115.23 (CN), 126.08, 128.09, 129.48, 130.51 (4C, ArC), 131.59, 135.15 (quaternary ArC) and 164.34 (CO). m/z 225 [³⁷Cl], 4], 223 [³⁵Cl], 11], 151 (100), 116 (32).
- (d) *Ethyl-(p-chlorophenyl) cyanoacetate* (4d): (0.176 g, 79%), yellowish oil. v_{max} (cm⁻¹) (neat) 2300 (CN), 1750 (CO); δ_H (CDCl₃): 1.26 (3H, t, J = 7.1, CH₃), 4.23 (2H, q, J = 7.1, CH₂), 4.68 (1H, s, CH), 7.39 (4H, br s, ArH). δ_C (CDCl₃): 13.82 (CH₃), 43.05 (CH), 63.49 (CH₂), 115.22 (CN), 128.37 (quaternary ArC), 129.25, 129.49 (4C, ArC), 135.40 (quaternary ArC) and 164.52 (CO). m/z 225 [³⁷Cl], 3], 223 [³⁵Cl], 10], 151 (97), 116 (15).
- (e) *Phenyl phenylsulphonylacetonitrile* (5a): Yellowish solid (0.206 g, 80%). v_{max} (cm⁻¹) (neat) 2310 (CN), 1370, 1160 (SO). δ_H (CDCl₃): 5.15 (1H, s, CH), and 7.25–7.74 (10H,

m, 2 Ph). δ_c (CDCl₃): 63·00 (CH), 113·37 (CN), 125·34 (quaternary ArC), 128·98 (2C, SO₂PhC), 129·14 (2C, SO₂PhC), 129·68 (2C, ArC), 130·01 (2C, ArC), 130·45 (1C, ArC), 134·29 (quaternary SO₂PhC), and 135·19 (SO₂PhC). *m/z* 257 (*M*⁺, 15%), 141 (16), 116 (100), 77 (26).

(f) (*o*-Chlorophenyl)phenylsulphonylacetonitrile (*5b*): White solid (0·215 g, 74%). ν_{max} (cm⁻¹) (neat) 2305 (CN), 1340, 1165 (SO). δ_H (CDCl₃): 5·81 (1H, s, CH), 7·34–7·63 (4H, *m*, ArH), 7·74–7·85 (2H, *m*, SO₂PhH), 7·84–7·89 (3H, *m*, SO₂PhH). δ_c (CDCl₃): 58·94 (CH), 113·26 (CN), 124·08 (quaternary ArC), 127·70 (ArC), 129·50 (2C, SO₂PhC), 130·00 (2C, SO₂PhC), 130·19, 131·26, and 132·04 (3C, ArC), 135·30 (quaternary SO₂PhC), 135·45 (SO₂PhC), 135·60 (quaternary ArC). *m/z* 293 [(³⁷Cl), 8], 291 [(³⁵Cl), 20], 150 (100), 77 (74).

(g) (*m*-Chlorophenyl)phenylsulphonylacetonitrile (*5c*): Yellowish oil (0·204 g, 70%). ν_{max} (cm⁻¹) (neat) 2305 (CN) and 1340, 1162 (SO). δ_H (CDCl₃): 5·12 (1H, s, CH) and 7·18–7·46 (4H, *m*, ArH), 7·52–7·62 (2H, *m*, SO₂PhH), 7·72–7·80 (3H, *m*, SO₂PhH). δ_c (CDCl₃): 62·16 (CH), 112·90 (CN), 127·09 (quaternary ArC), 127·82 (ArC), 129·22 (2C, SO₂PhC), 129·62 (ArC), 129·87 (2C, SO₂PhC), 130·14, 130·60 (2C, ArC), 133·99 (quaternary SO₂PhC), 134·84 (quaternary ArC), and 135·40 (SO₂PhC). *m/z* 293 [(³⁷Cl), 4], 291 [(³⁵Cl), 14], 141 (91), 77 (100).

(h) (*p*-Chlorophenyl)phenylsulphonylacetonitrile (*5d*): Yellowish oil (0·218 g, 75%). ν_{max} (cm⁻¹) (neat) 2305 (CN) and 1338, 1160 (SO). δ_H (CDCl₃): 5·12 (1H, s, CH), and 7·21 (2H, *d*, *J* = 8·4, ArH), 7·34 (2H, *d*, *J* = 8·4, ArH), 7·51–7·65 (2H, *m*, SO₂PhH), 7·75–7·81 (3H, *m*, SO₂PhH). δ_c (CDCl₃): 60·08 (CH), 113·07 (CN), 123·82 (quaternary ArC), 129·25 (4C, SO₂PhC), 129·91, 130·94 (4C, ArC), 134·13 (quaternary SO₂PhC), 135·35 (SO₂PhC), and 136·90 (quaternary ArC). *m/z* 293 [(³⁷Cl), 3], 291 [(³⁵Cl), 7], 150 (100), 141 (11), 77 (28).

Acknowledgement

Financial support by the University of Winnipeg is gratefully acknowledged.

References

- Abd-El-Aziz A S and de Denus C R 1992 *Synth. Commun.* **22** 581
- Abd-El-Aziz A S and de Denus C R 1993 *J. Chem. Soc., Perkin Trans. (accepted)*
- Abd-El-Aziz A S, Lee C C, Piorko A and Sutherland R G 1988a *Synth. Commun.* **18** 291
- Abd-El-Aziz A S, Lee C C, Piorko A and Sutherland R G 1988b *J. Organomet. Chem.* **348** 95
- Abd-El-Aziz A S, Tesfalidet S, de Denus C R and Lezynska K 1993 *Synth. Commun. (accepted)*
- Adams S S, McCullough K F and Nicholson J S 1969 *Arch. Int. Pharmacodyn.* **178** 115
- Chalmers T M 1969 *Ann. Rheum. Dis.* **28** 513
- Gill T P and Mann K R 1980 *Inorg. Chem.* **19** 3007
- Gill T P and Mann K R 1981 *J. Organomet. Chem.* **22** 1986
- Gill T P and Mann K R 1983 *Inorg. Chem.* **22** 1986
- Giordano C, Castaldi G and Uggeri F 1984 *Angew. Chem., Int. Ed. Engl.* **23** 413
- Kaiser E M, Solter L E, Schwarz R A, Beard R D and Hauser C R 1971 *J. Am. Chem. Soc.* **93** 4237
- Kerber R C 1991 *J. Organomet. Chem.* **404** 107
- Khand I U, Pauson P L and Watts W F 1968 *J. Chem. Soc. (C)* 2261
- Kozyrod R P, Morgan J and Pinhey J T 1991 *Aust. J. Chem.* **44** 369
- Matsui K and Motoi M 1973 *Bull. Chem. Soc. Jpn.* **46** 1755
- Nesmeyanov A N, Vol'kenau N A and Bolesova I N 1967 *Dokl. Akad. Nauk. SSSR* **175** 606

- Nesmeyanov A N, Vol'kenau N A and Shilovtseva L S 1970 *Dokl. Nauk. Akad. SSSR* **190** 857
Osuka A, Kobayashi T and Suzuki H 1983 *Synthesis* 67
Pearson A J, Bruhn P R and Hsu G-Y 1986 *J. Org. Chem.* **51** 2137
Sakamoto T, Katoh E, Kondo Y and Yamanka H 1988 *Chem. Pharm. Bull.* **36** 1664
Sakamoto T, Katoh E, Kondo Y and Yamanka H 1990 *Chem. Pharm. Bull.* **38** 1513
Semmelhack M F 1976 *J. Organomet. Chem. Libr.* **1** 361
Shen T Y 1972 *Angew. Chem., Int. Ed. Engl.* **11** 6
Shen T Y 1979 Prostaglandin synthetase inhibitors I. In *Handbook of experimental pharmacology* (Berlin Heidelberg, New York: Springer-Verlag) vol. 50/II, pp. 305-347
Shih Y and Wang J 1984 *Heterocycles* **22** 2799
Suzuki H, Yi Q, Inoue J, Kusume K and Ogawa T 1987 *Chem. Lett.* 887
Uno M, Seto K, Ueda W, Masuda M and Takahashi S 1985 *Synthesis* 506

Light induced cycloadditions of captodative alkenes

D DÖPP*, J BREDEHORN, A W ERIAN[†], A JUNG,
H LANFERMANN, H R MEMARIAN[‡], B MÜHLBACHER
and M PIES

Fachgebiet Organische Chemie, Universität GH-Duisburg, D-47048 Duisburg, Germany

[†]Present address: Department of Chemistry, Cairo University, Giza, Cairo, Egypt

[‡]Present address: Department of Chemistry, University of Esfahan, Esfahan 81744, Iran

Abstract. Triplet excited 1-acynaphthalenes add captodative alkenes, especially 2-aminoacrylonitriles, in a formal [4 + 2] mode to form 1,4-dihydro-1,4-ethanonaphthalenes. This reaction is in some cases preceded by an independent and ultimately less efficient photoreversible 1,2-addition yielding cyclobutanaphthalene derivatives. There is no indication of a common intermediate partitioning into both types of products. Both additions occur with remarkable regio- and stereoselectivity. The chirally labelled alkene *S* or *R*-2-(2-methoxymethyl-1-pyrrolidinyl)acrylonitrile is added in the [4 + 2] mode with over 99% diastereoselectivity leading to practically enantiomerically pure 1,4-adducts. Sensitized cyclodimerizations of 2-morpholinocrylonitrile are also discussed briefly.

Keywords. Photoadditions; triplet excited state; 1,4-dihydro-1,4-ethanonaphthalenes; tetrahydrocyclobuta[n]naphthalenes; asymmetric induction.

1. Introduction

Photocycloadditions of alkenes to aromatic nuclei continue to be of considerable interest (McCullough 1987). In recent years, numerous novel [4 + 2] cycloadditions of so called captodative (Viehe *et al* 1985) alkenes to carbon atoms 1 and 4 of 1-acynaphthalenes have been observed (Döpp *et al* 1985, 1989; Döpp and Memarian 1986, 1990; Memarian 1986; Pies 1989; Mühlbacher 1991). Most recently, novel 1,8-photoadditions of alkenes in a formal [3 + 2] mode to naphthalene 1,4-dicarboxylates and 1,4-dicarbonitriles have been reported (Kubo *et al* 1992).

The 1,4-additions to acynaphthalenes observed by us are of marked regio-, stereo- and diastereoselectivities and are occasionally preceded and/or accompanied by 1,2-additions. Our findings, including hitherto unpublished work, will be summarized and interpreted in the following sections.

2. Results

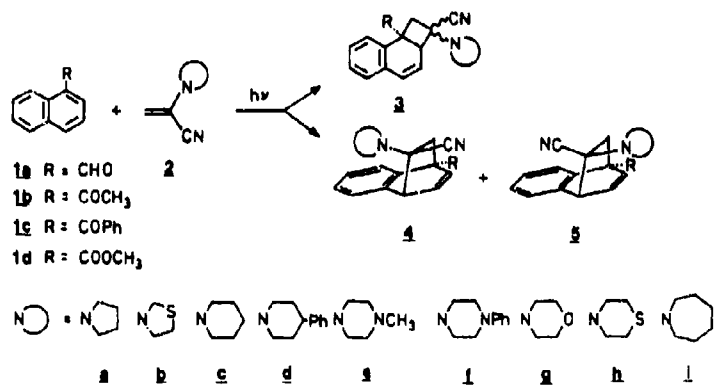
2.1 1,4-Ethanonaphthalenes and tetrahydrocyclo-but[a]naphthalenes from 1-naphthyl carbonyl compounds

Triplet-excited 1-acetonaphthonone (**1b**) as well as photoexcited 1-naphthaldehyde (**1a**) and 1-naphthophenone (**1c**) form 1,4-photoadducts of type **4** with various

*For correspondence

2-aminoacrylonitriles (**2**) in a highly regio- and stereoselective manner (Döpp *et al* 1985; Pies 1989; Döpp and Memarian 1990; Mühlbacher 1991). Without exception, only the benzenoid ring bearing the acyl group is affected. Most investigations have been carried out using 1-acetonaphthone (**1b**) as substrate. Rate constants for quenching of triplet-**1b** by various type **2** alkenes range from 3×10^8 to 3×10^9 M $^{-1}$ s $^{-1}$ in methanol or acetonitrile and are thus smaller than the diffusion controlled limit (Döpp *et al* 1990).

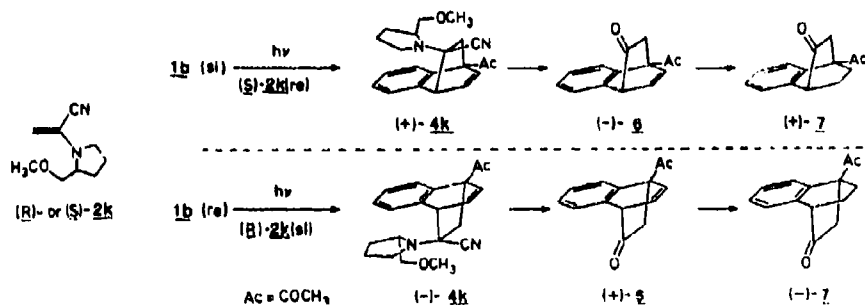
When we repeated our earlier preparative runs, we found that besides the donor-*syn* products **4a-i** (R = COCH₃ in most cases), minor amounts of the donor-*anti* adducts **5a-h** are formed, the *syn/anti* ratio varying between 95:5 and 89:11 (Mühlbacher 1991).



The same trend is observed when methyl-1-naphthoate (**1d**) is photoexcited in the presence of type **2** olefins (*syn/anti* varying from 95:5 to 88:12). Thus, the aromatic ester **1d** exhibits photochemical behaviour parallel to that of the aromatic ketone **1b** (Mühlbacher 1991).

Such regio- and stereoselective 1,4-additions to acylnaphthalenes are not restricted to 2-aminoacrylonitriles. Very similar results are obtained with 2-(*tert*-butylthio) acrylonitrile (Döpp *et al* 1989). A remarkably high (>99%) double diastereofacial differentiation leading to practically enantiomerically pure adducts (+)- or (-)-**4k** can be demonstrated in the [4 + 2]-photoaddition of either (*S*)- or (*R*)-(2-methoxy-methyl-pyrrolidin-1-yl)acrylonitrile (**2k**) to 1-acetonaphthone (**1b**) (Döpp and Pies 1987). The absolute configuration of (+)-**4k** and (-)-**4k** (as shown) has been derived from a comparison of ¹H-NMR-chemical shifts of (+)-**4k** with those of analogous 1,4-adducts, in which the donor-*syn* geometry had clearly been demonstrated by either X-ray structural analysis (Döpp *et al* 1985, 1989) and/or NOE intensity difference determinations (Mühlbacher 1991), together with the determination of the circular dichroism in the hydrogenated ketone (+)-**7** (Pies 1989). From the positive sign for the Cotton-effect in its n,π^* -absorption the absolute arrangement of the benzenoid ring (formally representing a double bond) and the oxo-group at C-9 (Legrand and Rougier 1977) as depicted is clearly established. Since both the ketones (-)-**6** and (+)-**6** had been demonstrated to be practically free of the respective enantiomers by HPLC using a chiral stationary phase (Döpp and Pies

1987), (*S*) -- 2k is added solely with its *re*-face to the *si*-face of 1b, and (*R*) -- 2k solely with its *si*-face to *re*-1b.

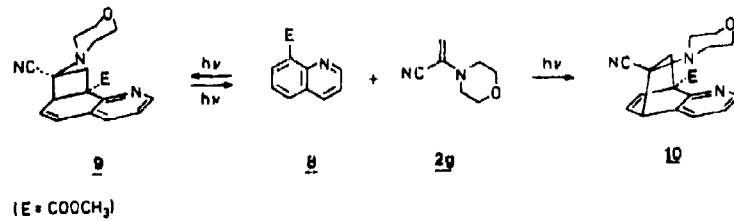


The origin of the high differentiation observed with 2k must be sought in the properties of the donor auxiliary and its capabilities for complexation either within a pre-oriented complex of the reactants or within a preferred conformation of a favourable precursor diradical collapsing to 4k.

Although temperature-dependency studies, which could cast some light on the relative importance of the precursors mentioned, have not been made yet (and probably will be difficult due to the thermal lability of products of type 4), two levels of selection may be envisaged as outlined in recent pioneering work on the temperature-dependence of asymmetric induction in the Paterno-Büchi reaction (Buschmann *et al* 1989).

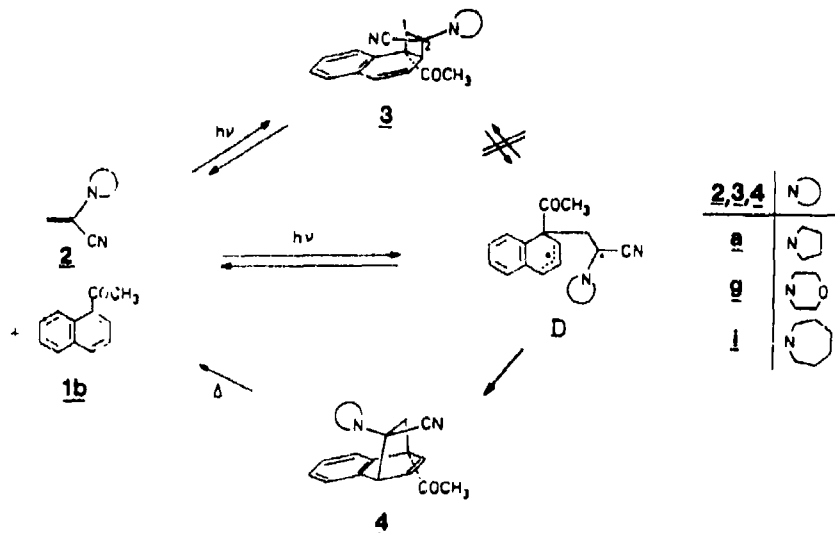
It had been observed earlier (Menarian 1986; Pies 1989), that 2a and 2g also give rise to minor amounts of type 3 adducts of hitherto not clarified configuration at C-2. It could be shown unambiguously that 2i definitely adds to photoexcited 1b to form 3i prior to the appearance of 4i in the photolysis mixture. Upon prolonged irradiation, however, 3i is degraded again due to its styrene-like and therefore (compared to 4i) conjugated chromophore into starting materials, from which relatively photostable 4i is finally formed. Further, since by X-ray single-crystal structure determination the configuration of 3i has recently been established to be *rel*-(*S*, *2aS*), that is with the hexamethyleneimino group *anti* to the dihydronaphthalene moiety, a direct interconversion of 3i into 4i with least motion of the groups involved is not possible but would require a 180° torsion around the former cyclobutanaphthalene C-1/C-2 bond.

1,2-and 1,4-Additions selectively to the benzenoid nucleus are observed when common solutions of 2g and methyl 8-quinoline carboxylate (8) are irradiated



(> 280 nm) in benzene or acetonitrile solution (Döpp and Jung 1992). Again, it can be demonstrated that products 9 and 10 emanate from parallel reactions, and that after long irradiation times, 10 is favoured at the expense of 9.

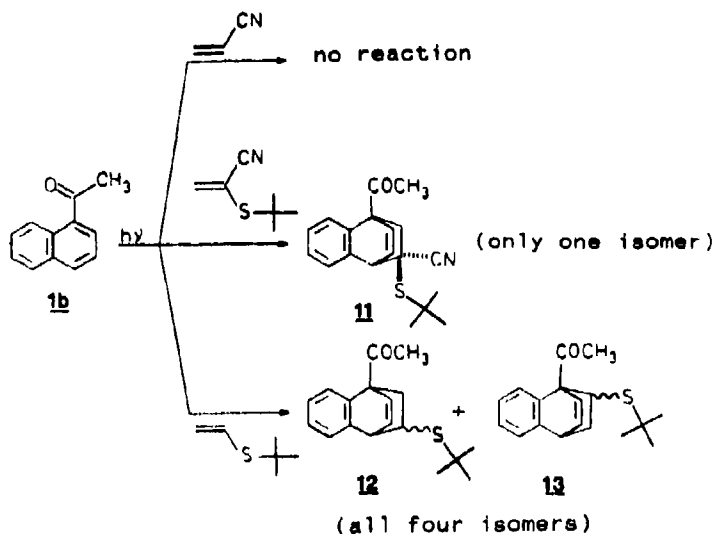
From this, and the aforementioned case, it may be ruled out that a common intermediate, e.g. the diradical D, connects type 3 and type 4 products. On the other hand, a diradical like D is an attractive and also logical intermediate in the 1,4-addition, since from spectroscopic (Döpp et al 1990) and quenching studies (Döpp et al 1985; Pies 1989; Mühlbacher 1991), the lowest (π, π^*) excited triplet state is envisaged as the reactive state in the 1,4-cycloadditions observed. Most logically, this state is followed by a triplet diradical obtained from addition of one molecule of olefin.



Quantum yields of product formation do not exceed 0.02, this may reflect low rates of diradical formation and/or efficient fragmentation of unfavourable (extended) conformation of diradicals like D into starting materials (Buschmann et al 1989). It should be stressed, however, that complex-forming orientation of the reactants prior to or after excitation cannot be ruled out at this stage. Neither a ground-state interaction nor an exciplex following the triplet have been detected experimentally, though.

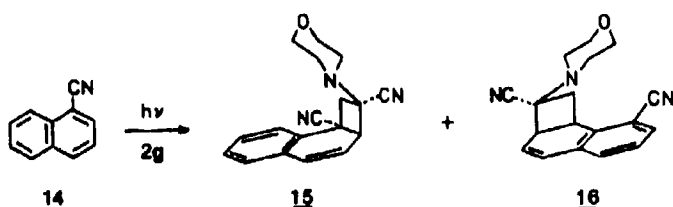
The unique substitution pattern of captodative (Viehe et al 1985) alkenes (one donor and one acceptor group at the same terminus of the double bond) does indeed manifest special features in light-induced cycloadditions. This may also be demonstrated by the comparison of the reactivity of excited 1-acetonaphthonone (1b) towards acrylonitrile, 2-(*tert*-butylthio)acrylonitrile and *tert*-butyl vinyl sulphide.

Acrylonitrile is not added at all, and, in contrast to the very regio- and stereoselective addition of 2-(*tert*-butylthio)acrylonitrile giving rise solely to product 11, *tert*-butyl vinyl sulphide is added with complete lack of regio- and stereoselectivity to form a mixture of all four *a priori* possible regio- and stereoisomeric 1,4-dihydro-1,4-ethanonaphthalenes (12, 13) (Döpp and Memarian 1986; Lanfermann



1990). Vinyl ethers, on the other hand, prefer 1,2-addition to **1b,d** (Döpp and Lanfermann 1992), and conventional enamines could not be added in any way to acylnaphthalenes.

It had been tempting to compare the reactivity of excited 1-naphthonitrile (**14**) with that of the acylnaphthalenes **1a-d** towards a representative captodative alkene. Electronically excited **14**, probably via its first excited singlet state (McCullough 1987), adds **2g** with the same direction of addition as observed with **1a-d** to yield 1,2-adducts **15** and **16**. In the main product **15**, the *syn*-orientation of the morpholino group and 1,2-dihydronaphthalene moiety is again derived from an X-ray single crystal structure determination and from NOE intensity difference studies (Döpp *et al* 1993). Solely NOE results support the *syn* orientation in by-product **16**.

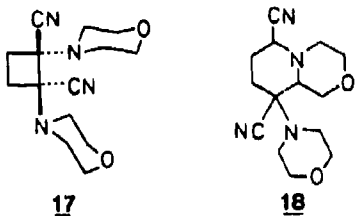


2.2 Morpholinoacrylonitrile cyclodimerizations

Whereas 2-alkylthioacrylonitriles tend to dimerize spontaneously (Gundermann and Röhrl 1974), such behaviour is unknown for 2-aminoacrylonitriles.

2-Acetonaphthone and naphthalene-1,8-dicarboxylic acid N-methylimide were found to sensitize, albeit in low yield, the [2 + 2] head-to-head dimerization of

2-morpholinoacrylonitrile (**2g**) (Memarian 1986; Döpp and Bredehorn 1993). The *trans* structure of the dimer **17** has been confirmed by single-crystal X-ray structural analysis. The role of the sensitizers is still not quite clear, since the photodimerization of **2g** cannot be driven to yields larger than 12%, whereas the [2 + 2] dimerization of 2-aminoacrylonitrile, sensitized by benzophenone, has been reported to provide a 75% yield of both diastereomeric head-to-head dimers (Ksander et al 1987).



In addition, both benzophenone and 2-acetonaphthone cause the formation of another cyclodimer from **2g**, to which structure **18** has been assigned on the basis of its 300 MHz ^1H -NMR-spectrum (Döpp and Bredehorn 1993).

3. Conclusion

The highly regio- and stereoselective photoadditions to the naphthalene skeleton, as described here, had not been expected. They add cycloadditions originating from a triplet-excited state to the already rich cycloaddition photochemistry of aromatic compounds starting from excited singlets. Selectivities observed must be attributed at least partly to the unique substitution pattern of captodative alkenes. Since the aminonitrile function at carbon atoms 9 in products of type **4** and **5** and at carbon 2 in **3** may be hydrolysed to give way to an oxo-group, the photoadditions described practically make novel 1,4-dicarbonyl compounds accessible. Thus captodative alkenes function as ketene equivalents in cycloadditions.

Acknowledgements

The authors are very much indebted to G Henkel, University of Duisburg, for recent unpublished single-crystal X-ray structural determinations and to the late G Snatzke, University of Bochum, for a Cotton-effect determination. Thanks are due to the Deutsche Forschungsgemeinschaft for a fellowship granted to H -R Memarian and to the A V Humboldt-Foundation for a fellowship awarded to A W Erian. Generous financial support of this work by the Ministerium für Wissenschaft und Forschung des Landes Nordrhein-Westfalen, by Deutsche Forschungsgemeinschaft and by Fonds der Chemischen Industrie, is gratefully acknowledged.

References

- Buschmann H, Scharf H -D, Hoffmann N, Plath M W and Runsink J 1989 *J. Am. Chem. Soc.* **111** 5367
 Döpp D and Bredehorn J 1993 (unpublished) (Part of planned doctoral thesis by J Bredehorn, University of Duisburg)

- Döpp D, Erian A W and Henkel G 1993 *Chem. Ber.* **126** 239
- Döpp D and Jung A 1992 (unpublished) (Part of planned doctoral thesis by A Jung, University of Duisburg)
- Döpp D, Krüger C, Memarian H -R and Tsay Y -H 1985 *Angew. Chem., Int. Ed. Engl.* **24** 1048
- Döpp D and Lanfermann H 1992 (unpublished) (Part of planned doctoral thesis by H Lanfermann, University of Duisburg)
- Döpp D and Memarian H -R 1986 *Substituent effects in radical chemistry* (eds) H G Viehe, Z Janousek and R Merényi (NATO ASI Series, C 189) (Dordrecht: Reidel) p. 383
- Döpp D and Memarian H -R 1990 *Chem. Ber.* **123** 315
- Döpp D, Memarian H -R, Krüger C and Raabe E 1989 *Chem. Ber.* **122** 585
- Döpp D, Memarian H -R, van Eijk A M J and Varma C A G O 1990 *J. Photochem. Photobiol. A* **53** 59
- Döpp D and Pies M 1987 *J. Chem. Soc., Chem. Commun.* 1734
- Gundermann K -D and Röhrl E 1974 *Lieb. Ann. Chem.* 1661
- Ksander G, Bold G, Lattmann R, Lehmann C, Früh T, Xiang Y -B, Inomata K, Buser H P, Schreiber J, Zass E and Eschenmoser A 1987 *Helv. Chim. Acta* **70** 1115
- Kubo Y, Inoue T and Sakai H 1992a *J. Am. Chem. Soc.* **114** 7660
- Kubo Y, Noguchi T and Inoue T 1992b *Chem. Lett.* 2027
- Lanfermann H 1990 *Photocycloaddition of tert-butyl vinylsulfide to 1-acetonaphthone*, diploma thesis, University of Duisburg
- Legrand L M and Rougier M J 1977 *Stereochemistry Fundamentals and methods. Vol. 2. Determination of configuration by dipole moments CD or ORD* (ed.) H B Kagan (Stuttgart: Thieme) p.33
- McCullough J J 1987 *Chem. Rev.* **87** 811, and references cited therein
- Memarian H -R 1986 *Photoadditions of captodative olefins to acylnaphthalenes*, doctoral thesis, University of Duisburg.
- Mühlbacher B 1991 *Photocycloaddition of captodative olefins to 1-acetonaphthone and methyl 1-naphthoate*, doctoral thesis, University of Duisburg
- Pies M 1989 *Regio-, diastereo- and enantioselectivity in a photo-Diels-Alder-addition*, doctoral thesis, University of Duisburg
- Viehe H -G, Janousek Z, Merényi R and Stella L 1985 *Acc. Chem. Res.* **18** 148, and references cited therein

Applied photochemistry for free radical organic synthesis by means of distannane reagents

W P NEUMANN[†], M HARENDA, J JUNGGEBAUER*,
K LESSMANN and H TEWS

Department of Chemistry, University of Dortmund, Otto-Hahn-Str. 6, D-4600 Dortmund
50; Germany

Abstract. With optimized triplet sensitizers and longwave UV light (300–350 nm), distannanes $R_3Sn-SnR_3$, R being Bu by preference, are used as advantageous sources of stanny radicals R_3Sn^{\cdot} that are versatile reagents for initiating organic free radical syntheses of many kinds. Elusive examples are presented. Thus, desired but slow radical steps like cyclizations, intermolecular additions or dimerization of the intermediate radicals can be preferentially carried out by using mild, adjusted, or no H-donors for terminating the radical reactions. In the second part, the development of a polystyrene-supported distannane is reported, where both tin atoms are covalently and firmly bound to the polymer. This reactive polymer is insoluble in common solvents. Its porous beads can be separated from the mixture after the reaction quantitatively and simply by filtration and regenerated for multiple use. The application of this new-type of photochemical source of stanny radicals is demonstrated by typical examples. Its application offers both economical and ecological advantages of easier processing and of avoidance of organotin waste products, thus contributing to environmental protection.

Keywords. Free radical syntheses; stanny radicals, distannanes, reactive polymers; polystyrene-supported distannane.

1. Introduction

In recent years, great interest in organic synthesis has been directed toward free radical reactions. Complicated molecular structures including biomolecules and products of pharmaceutical interest can be synthesized in very high yields by this method, often in multistep, one-pot reactions, which are called tandem or cascade reactions. Stanny radicals play a major role as reagents in these syntheses that are very often of high or complete chemo-, regio-, stereo-, and enantioselectivity (Hoffmann 1992). A few additional, important statements should be cited:

"Within the last 15 years, an authentic explosion of synthetic applications of free radical reactions occurred; they have gained a remarkable position among the selective methods of synthesis." (Minisci 1989.)

The dramatic advances in the application of free radical reactions to problems in organic synthesis can be attributed in good measure to the versatility of trialkyltin hydride reagents." (Curran 1989.)

*For correspondence; [†]deceased

"The reduction of organic functional groups by organotin hydrides ... has become the most commonly used method for the synthetic application of free radical carbon-carbon bond formation." (Curran 1988.)

For example, organotin hydrides, mostly Bu_3SnH (Neumann 1987) are used for highly selective defunctionalizations of complicated, often multifunctional molecules (figure 1).

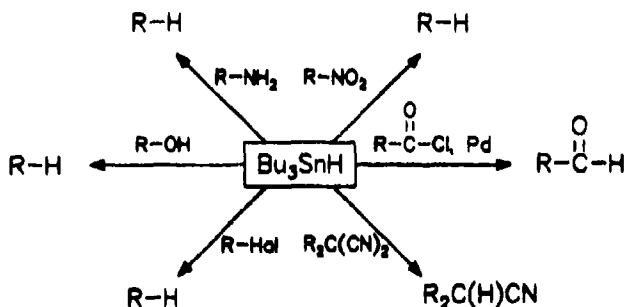
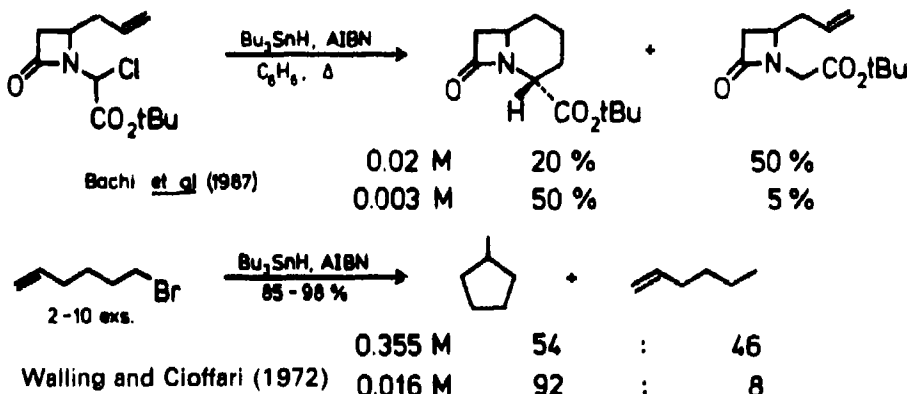


Figure 1. The versatility of trialkyltin hydrides in organic synthesis.

But, in all these cases, the generation of the reagent $\text{R}_3\text{Sn}^\bullet$ is inherently coupled with the presence of R_3SnH which is a very strong radical scavenger. This can be, in multistep reactions, a limiting drawback, since the desired, but relatively slow intermediate radical transformations like cyclizations cannot take place, or only proceed to an unsatisfactory extent, as explained by a few examples (scheme 1), selected out of the many described in the literature. In several cases, a syringe technique, i.e. very slow mechanical pumping (e.g. within 4 h) of the R_3SnH solution into the reaction mixture provided some improvement (Curran 1988).



Scheme 1. Examples of intermediate radical transformations.

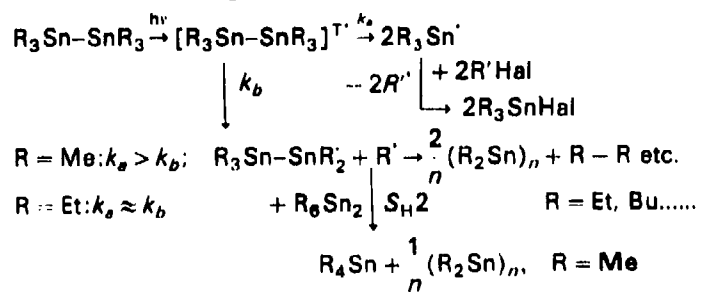
Nevertheless, in most of these cases, a decoupling of the generation of stannyl radicals $\text{R}_3\text{Sn}^\bullet$ from the presence of the very strong radical scavenger R_3SnH is desirable. Other sources of stannyl radicals are therefore to be sought for.

2. Distannanes $R_3Sn-SnR_3$ as sources for stannyl radicals

Based on our experience with organotin compounds (Neumann 1970), we regarded distannanes as promising objects in our search for new R_3Sn sources. With normal residues like $R = Bu$, they are thermally very stable, generally up to 200°C. Therefore, a photochemical splitting of their Sn-Sn bond had to be envisaged.

2.1 Direct photolysis of distannanes

Direct photolysis needs shortwave UV light and gives, besides the desired Sn-Sn splitting, an unpleasant multitude of side and consecutive reactions, ending up with yellow or red polystannanes causing unwanted longwave absorptions, and also R_4Sn , elemental Sn, and so on (Lehnig *et al.* 1978).



Scheme 2. Photoreactions of $R_3Sn-SnR_3$.

This older finding is of new importance now: the λ_{max} of 236 nm corresponds to an energy taken up by the molecule of about 500 kJ, what exceeds largely the dissociation energy of the Sn-Sn bond, the excess energy allowing unselective splitting of any bond in the molecule (figure 2). Even the use of the longer wavelength tailing occurring at higher concentrations, which are normal for preparative purposes, brought about very little progress in photochemical experiments.

2.2 Triplet-sensitized photolysis of distannanes

Therefore, a sensitized photolysis had to be envisaged. Since the degradation of $Bu_3Sn-SnBu_3$ (hopefully the splitting of the Sn-Sn bond) followed from a triplet state, as found by CIDNP experiments (Lehnig *et al* 1978), we tried empirically a number of triplet sensitizers (Harendza 1991; Tews 1991). A selection of these is given in table 1. Whereas benzene and toluene had no or nearly no effect, diphenyl ether, acetone and *p*-methoxy acetophenone gave high yields of R_3Sn^+ , as stated from the percentage of R_3SnBr obtained, after admixing of alkyl halide scavengers for R_3Sn^+ like octyl bromide, by GLC analysis. Thus, an estimate of about 300 kJ/mol for E_7 of Bu_6Sn_2 can be assumed, and benzene or toluene, e.g., can be used as photoinert solvents.

These sensitizers also protect, by their long wavelength absorption, the organic starting materials from direct photoactivation. This prevents undesired side reactions like photopolymerization of olefins. The usefulness of this new photochemical system should be checked now by a number of typical examples.

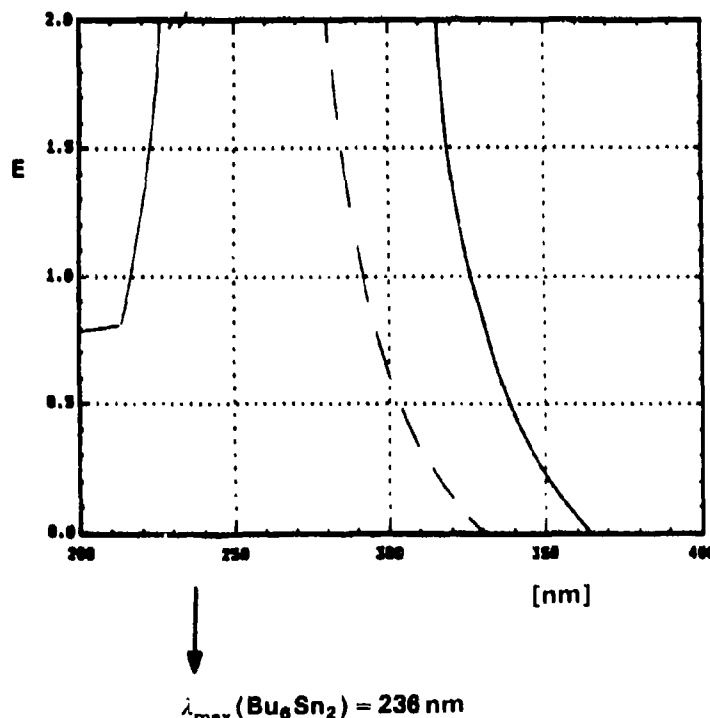


Figure 2. Photochemical application of the distannane $\text{Bu}_6\text{Sn}-\text{SnBu}_3$ (Leßmann 1991). UV-Spectra of Bu_6Sn_2 (0.05 M). THF:tailing up to 352 nm; ---- Me_2CHOH :tailing up to 330 nm. $\lambda_{\max}(\text{Bu}_6\text{Sn}_2) = 236 \text{ nm}$; $E(S_0 \rightarrow S_1) = 507 \text{ kJ/mol}$.

Table I. Triplet energy and triplet lifetime of the used sensitizers.

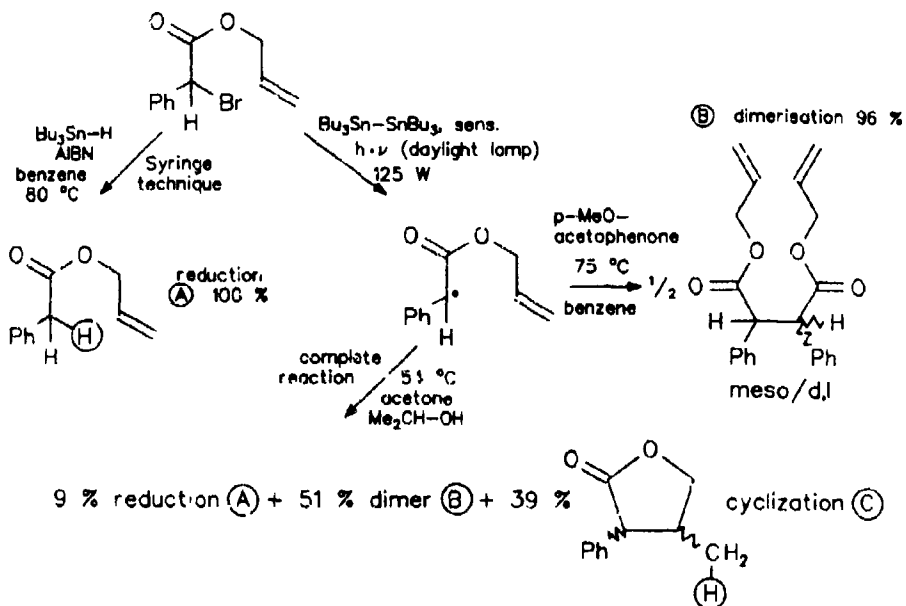
Sensitizer	Triplet energy $E_T[\text{kJ/mol}]^a$	Triplet lifetime $\tau_T[\mu\text{s}] (\text{RT})^a$
Acetone	300	6.3
Diphenyl ether	339 ^b	~1 ^b
p-MeO-acetophenone	301	0.03
Benzene	352	8.0
Toluene	346	7.7

Energy transfer: ${}^3S^* + {}^1Q \rightarrow {}^3Q^* + {}^1S$;
(Rule of thumb^c: $E_T(S) - E_T(Q)$, 12 – 40 kJ/mol);

$E_T(\text{Bu}_6\text{Sn}_2)$, 290 – 310 kJ/mol;

^aScialano (1991); ^bEngel and Monroe (1980); ^cBecker (1984)

2.2a "Clean" generation of R_3Sn^+ and its consequences: With R_3SnH , the α -bromo-phenylacetic acid allyl ester gave, even under application of the syringe technique mentioned above, nothing other than the reduction product A (scheme 3) (Junggebauer 1992), unwanted in this case. This means, that even under these extreme conditions

Scheme 3. Distannane for "clean" generation of stanny radicals ($R_3Sn\cdot$).

the intermediate radical, highly stabilized both by the phenyl and the carbonyl group, is scavenged very rapidly before anything else can happen.

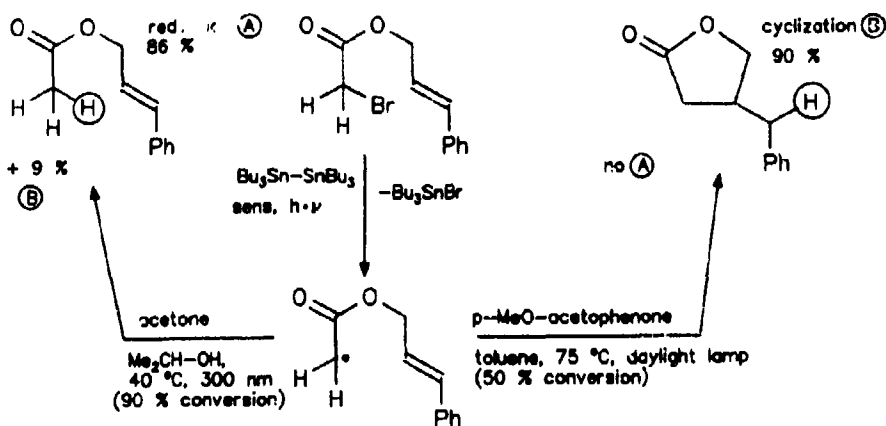
But when we used our new triplet-sensitized distannane system and a 125 W daylight lamp, we obtained, surprisingly and exclusively, the dimer B (meso/d,l mixture) of the intermediate radical. B is new, and may be of interest as a synthon because of its different functionalities.

With acetone and the H-donor of intermediate strength (propanol-2) some A and B, as well as a new product C were identified. It indicates clearly an intermediate cyclization i.e. addition to the isolated olefinic bond (which has to be a reversible one: an observation of importance for the fundamentals of free radical chemistry, whose discussion would exceed the scope of the present topic).

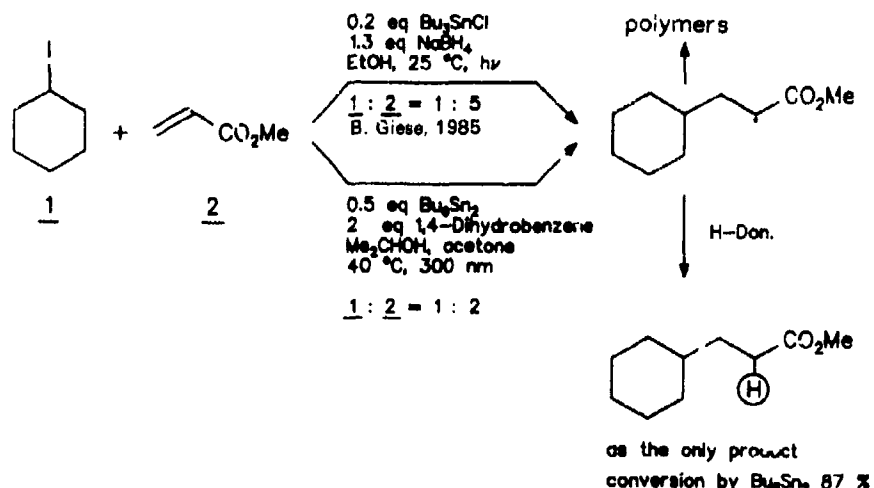
2.2b Further evidence for the governing role of the strength of the H-donor for product formation: The α -bromoacetic acid styrylmethyl ester gives with $Bu_3Sn\cdot$ a radical, stabilized only by a carbonyl group. This is scavenged at 40 °C, before having time to react with anything else even the medium H-donor propanol-2, giving the reduction product B. But at 75 °C, where the horseshoe-shaped conformation of the radical, enabling a cyclization, is more favoured, 90% scavenging of the cyclized radical-forming B is found, when the weaker H-donor toluene is applied (scheme 4).

The two latter examples demonstrate that a new degree of kinetic independence is gained by our system of decoupling the generation of $R_3Sn\cdot$ from any consecutive reactions.

2.2c Intermolecular radical additions: The addition of alkyl radicals to olefins such as acrylic derivatives (Giese 1985) is a kinetically tricky reaction. We selected it



Scheme 4. H-donor strength governs product formation.



Scheme 5. Synthetic application of intermolecular addition.

as a further check for the synthetic application of our tin-mediated radical system (scheme 5). We could lower the excess of the acrylic compound, compared with that in the literature, from 5 to 2 mol per mol alkyl halide, thus also avoiding oligomer or polymer byproducts. With dihydrobenzene as H-donor, we obtained the desired adduct as the only product.

3. A polymer-supported distannane as photochemical source of stannyl radicals

The advantages of stannyl radicals R₃Sn[·] in organic syntheses have clearly been demonstrated in the literature, and in the new results reported above. On the other hand, however, a problem caused by their use has also to be envisaged. In all cases,

an equimolar amount of an organotin consecutive product R_3SnX arises, whatever X may be, and has to be cleanly separated from the desired reaction product.

"The drawback consists in the separation of these mostly toxic compounds and their consecutive products from the desired reaction products, which is mostly a difficult, and rarely a quantitative one. It might be, therefore, a meritorious research project to find new methods using such forms of organotin compounds which are easily to be separated." (Scheffold 1988.)

So we decided to engage ourselves with the synthesis of a polymer-supported distannane whose two tin atoms are both bound firmly to a polymer in a chemically stable position (figure 3). However, severe diffusion problems can arise by inherent motion of the excited sensitizer into the pores of the polymer, raising the question of sufficient lifetime of the triplet state.

We used our experience with polystyrene-supported organotin hydrides (Gericke *et al* 1990; Neumann and Peterseim 1993), and started with the polystyrene-supported butyl tin chloride (scheme 6).

After several other attempts, Bogdanovic's magnesium (Bogdanovic *et al* 1984) was proved to be best suited for the distannane formation (Leßmann 1991). The capacity (1.3 mmol Sn as Sn-Sn per gram resin) is quite satisfying, some pending Sn-Cl groups (0.3 mmol Sn per gram resin) do not disturb the application. Their origin presumably is due to a lack of other Sn-Cl groups in the vicinity within the same pore.

Of course, diffusion is a rate-limiting factor. Thus, we found, for example, in the central parts of larger beads of our macroporous polystyrene support, still high contents of unreacted Sn-Cl groups, whereas in the outer parts the formation of Sn-Sn groups by the Mg reagent is complete. This could be seen by Sn and Cl linescans through the surface of halved beads, using the electron microscope and the EXAFS method (Leßmann 1991).

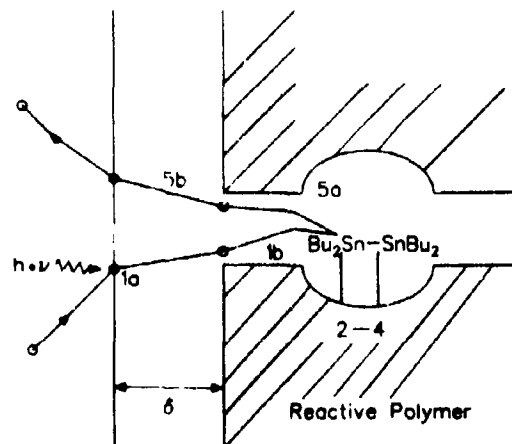
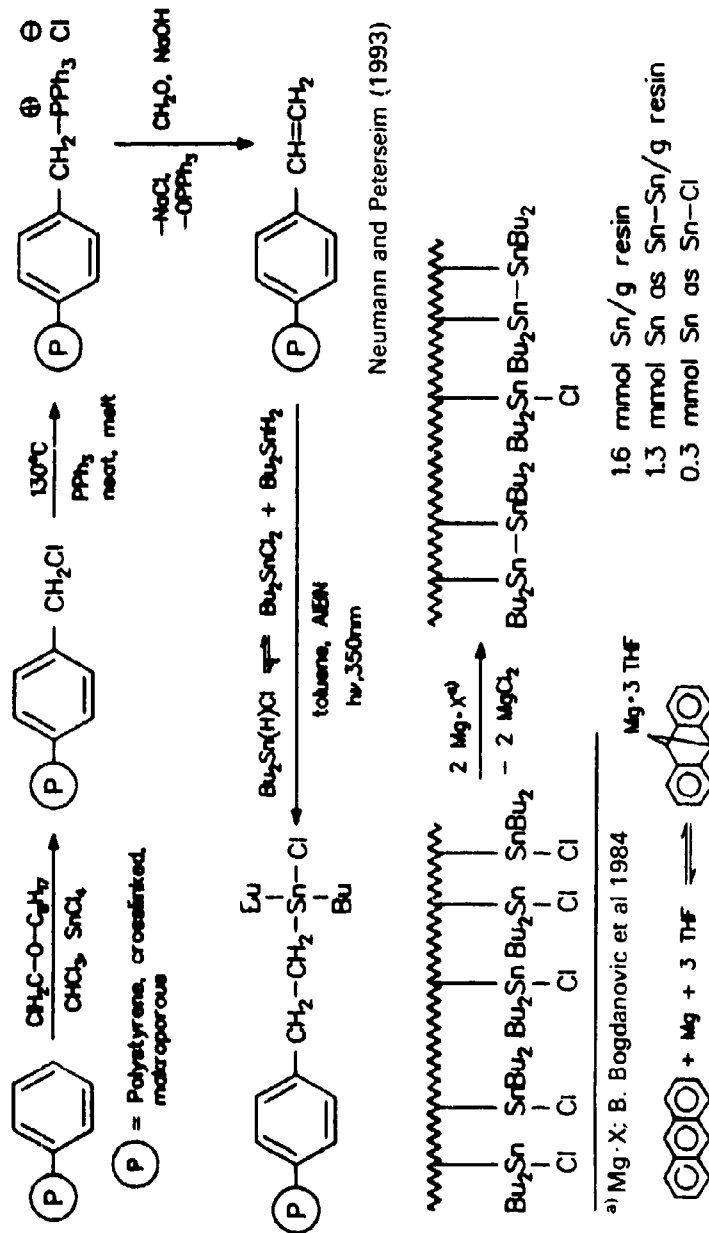
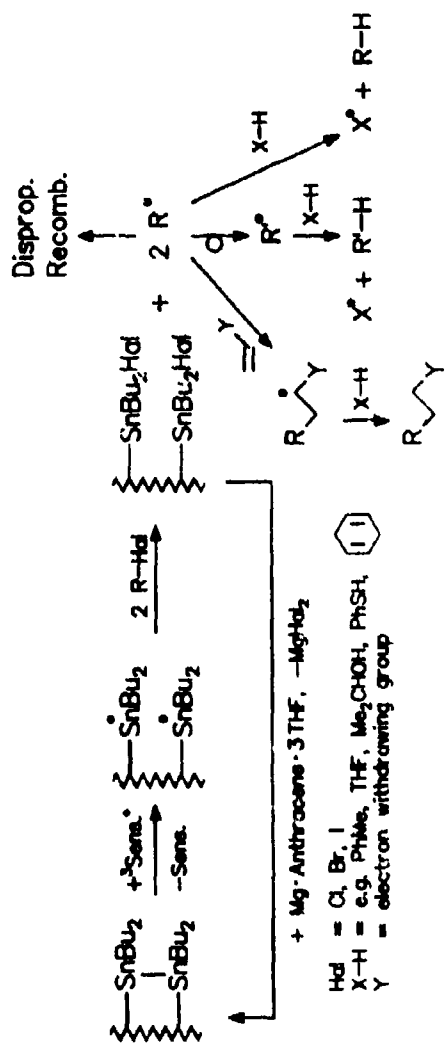


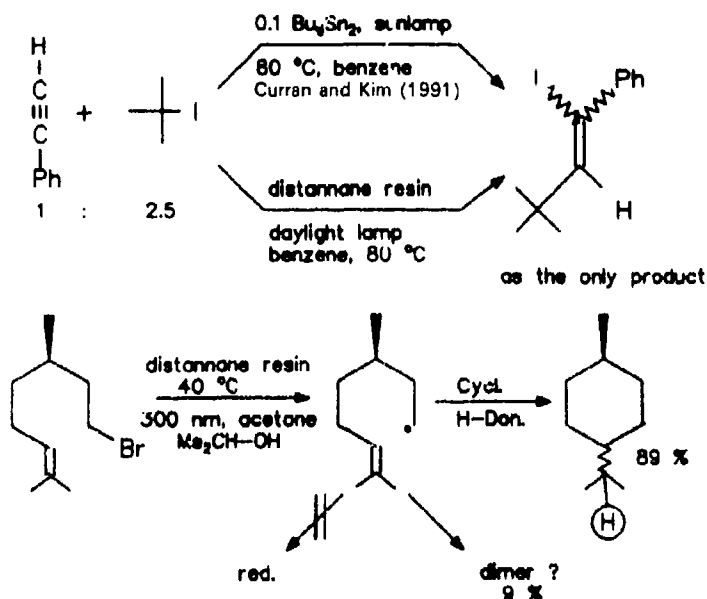
Figure 3. Principle of a Diffusion-Controlled Reaction at a Polymer-Supported Reagent (Simplified). 1a diffusion through the interface; 1b diffusion in the pore; 2 adsorption; 3 reaction at the surface; 4 desorption; 5a diffusion in the pore; 5b diffusion through the interface. Likewise, movements (two-dimensional ?), concentration of the other reactants and products.



Scheme 6. Preparation of the polymer-supported distannane.



Scheme 7. The polymer-supported distannane as radical source for multiple use.



Scheme 8. Synthetic applications of the distannane resin.

Lastly, having gone through different exhausting series of experiments, the breakthrough has been achieved. The new reactive polymer can be used for the basic entrance reactions into free radical synthesis (scheme 7).

It works better than expected from theoretical points of view: rapid diffusion processes, perhaps of two-dimensional kinds in the pores, and a long-lived triplet-state of the immobilized distannane may be anticipated. Manifestation of the kinetics and the theoretical background needs further investigation.

Separation by filtering off, and regeneration of the reagent for multiple use, as shown above, is achieved without any problem.

Finally, two sophisticated examples should demonstrate the synthetic application of the new polystyrene-supported distannane (scheme 8).

4. Conclusion

This new, photochemical generation of stannyl radicals from distannanes opens up a broad variety of possibilities for interesting free-radical reactions useful in organic syntheses, hopefully also for molecules of biological, pharmaceutical or other importance. And, one day, our "daylight lamp", maybe, will be replaced by real daylight of the same wavelength (perhaps by means of a collector), i.e., by the source of daylight, the sun itself.

Acknowledgements

The work has been supported by the Volkswagen Foundation, the Fonds der Chemischen Industrie, and the Bayer AG.

References

- Bachi M D, DeMesmaeker A and Stevenart-DeMesmaeker N 1987 *Tetrahedron Lett.* **28** 2637
Becker H G O 1984 *Eine Einführung in die Photochemie* (Stuttgart: Thieme Verlag)
Bogdanović B, Liao S, Mynott R, Schlichte K and Westeppe U 1984 *Chem. Ber.* **117** 1178
Curran D P 1988 *Synthesis* 417
Curran D P 1989 in *Free radicals in synthesis and biology* (ed.) F Minisci (London: Kluwer) p. 37
Curran D P and Kim D 1991 *Tetrahedron* **32** 6171
Engel P S and Monroe B M 1980 *Advances in photochemistry* (eds) W A Noyes, G S Hammond and J N Pitts (New York: Interscience) vol. 4
Gerigk U, Gerlach M, Neumann W P, Vieler R and Weinritt V 1990 *Synthesis* 448
Giese B 1985 *Angew. Chem., Int. Ed. Engl.* **24** 553
Harendza M 1991 *Photochemical generation of stannyl radicals*, diploma thesis, University of Dortmund
Hoffmann H M R 1992a *Angew. Chem.* **104** 1361
Hoffmann H M R 1992b *Angew. Chem., Int. Ed. Engl.* **31** 910, and references therein
Junggebauer J 1992 *Photochemical syntheses with distannane*, Dr. rer. nat. Thesis, University of Dortmund, (in preparation)
Lehnig M, Neumann W P and Seifert P 1978 *J. Organomet. Chem.* **162** 145
Leßmann K 1991 *New sources of stannyl radicals*, Dr. rer. nat. Thesis, University of Dortmund
Minisci F (ed.) 1989 *Free radicals in synthesis and biology* (London: Kluwer) p. xi
Neumann W P 1987 *Synthesis* 665
Neumann W P 1970 *The organic chemistry of tin* (New York: Wiley)
Neumann W P and Peterseim M 1993 *Reactive polymers* (submitted)
Scalano J C (ed.) *CRC handbook of organic photochemistry* (Boca Raton, FL: CRC-Press)
Scheffold R 1988 *Nachr. Chem. Tech. Lab.* **36** 261
Tews H 1991 *Triplet-sensitized photolysis of distannanes*, Diploma thesis, University of Dortmund
Walling Ch and Cioffari A 1972 *J. Am. Chem. Soc.* **94** 6059

Photocyclization of arylethylenes: Mechanism and scope of the reactions

R LAPOUYADE

Photophysique et Photochimie Moléculaire, UA du CNRS N° 348, Université Bordeaux I,
33405 Talence, France

Abstract. The photocyclization of three structural types of arylethylenes is systematically investigated in order to provide new pathways to regiospecifically substituted and/or partially hydrogenated polycyclic aromatic hydrocarbons. The scope of the photoformation of acenaphthenes from α -arylolefins, in amine solutions, is discussed: when the double bond is acyclic, only the naphthyl and the pyrenyl derivatives are photoreactive, but when the double bond is in a cycle, all the compounds which lead to the *trans* double bond photocyclize. The amine-mediated 1,3-H-shift, discovered with the preceding series, also occurs with 4a,4b-dihydrophenanthrene, formed by irradiation of 1,2-diarylethylenes, and leads to dihydrophenanthrenes. The photocyclization of 2-vinylbiphenyls is stereoselective from the singlet excited state but not from the triplet, where a fast equilibrium between *E* and *Z* configurations precedes the adiabatic cyclization. The radical cation of 2-vinylbiphenyls cyclizes to a phenanthrene radical cation which initiates a protic catalysis to the related fluorenes or, in presence of 2,6-di-*t*-butypyridine or water, leads stoichiometrically to phenanthrenes.

Keywords. Arylethylenes; photocyclization; amine-mediated proton shift; polycyclic aromatic hydrocarbons.

1. Introduction

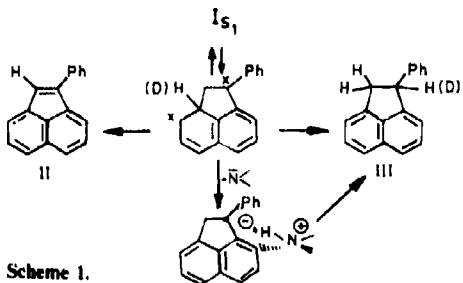
Photocyclization of arylethylenes is the preferred method for synthesis of many different polycyclic aromatic hydrocarbons (PAH). There is an overwhelming amount of literature, recently surveyed (Laarhoven 1983; Mallory and Mallory 1984; Liu *et al* 1991), on the photocyclodehydrogenation of 1,2-diarylethylenes (stilbene-like) into angularly fused PAH (phenanthrene-like). We discovered the photocyclization of α -arylolefins, made chemically efficient by amine-induced proton tautomerism in the primary photoproduct (Lapouyade *et al* 1977), and extended this base-mediated 1,3-H-shift to the photocyclization of 1,2-diarylethylenes, leading to dihydro PAH (Lapouyade *et al* 1982b). We also investigated the cyclization of the 2-vinylbiphenyls (VB) from the singlet and the triplet excited states and from the radical cations (Lapouyade *et al* 1975, 1985, 1987; Fournier de Violet *et al* 1982).

In order to enlarge the field of PAH accessible by photocyclization of arylolefins, we present the main results of a systematic study on the mechanism of cyclization of these three structural types of arylolefins from the singlet and the triplet excited states and from the radical cations.

2. Photocyclization of α -arylolefins

2.1 1,1-Diarylethylenes

1-(α -Styryl)naphthalene (I) yields 1-phenyl acenaphthylene (II) by irradiation in the presence of iodine and oxygen (Lapouyade *et al* 1975). This cyclization is not triplet sensitized (nor quenched by oxygen) and is therefore ascribed to the singlet excited state. When amines are added to a degassed cyclohexane solution of I, the reaction is accelerated and 1-phenylacenaphthene (III) is the almost exclusive product. The catalytic capacity of the amines appears to correlate with their basicity and not with their ionization potential. The labelling experiments, as the fact that all the compounds which do not cyclize in the absence of amine, do not cyclize when it is present, argue in favour of a reversible cyclization which, in the absence of amine, very inefficiently gives II and III while amine generates an ion-pair which collapses into III (Lapouyade *et al* 1977) (scheme 1). Of the several 1-(α -styryl) arenes irradiated, only the naphthyl and the pyrenyl derivatives cyclized while, for example, the fluoranthenyl and the chrysene derivatives were photostable. This contrasting behaviour can be correlated with the fluorescence characteristics (figure 1); while the emission of the unreactive



Scheme 1.

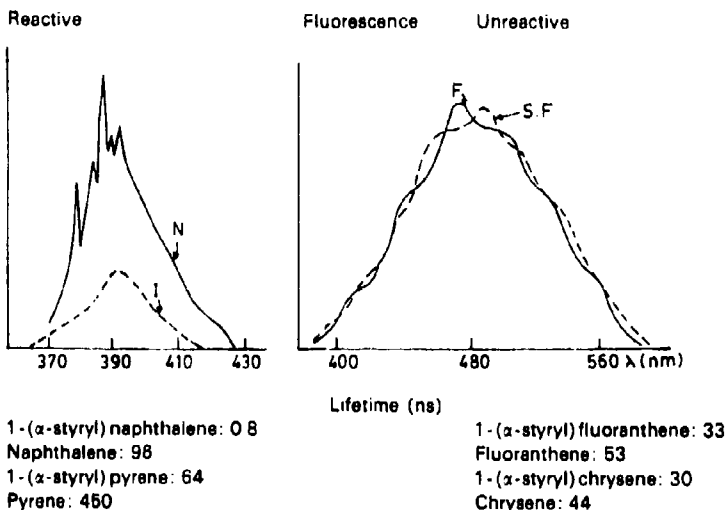
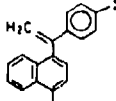
Figure 1. Fluorescence and singlet excited state lifetime of 1-(α -aryl)olefins.

Table 1. Quantum yield* of photocyclization of 1-(α -styryl)naphthalenes.

Σ'	H	CN	OMe	NMe ₂	
H	I	II	III	IV	
CN			V	VI	

Solvent	Compounds					
	I	II	III	IV	V	VI
C ₆ H ₁₂	0.31	0.12	10 ⁻²	<10 ⁻³	<10 ⁻³	<10 ⁻³
CH ₃ CN	0.40	0.16	1.5 × 10 ⁻²	"	"	"

*Irradiation at 373 nm of a 5×10^{-3} M solution of I-VI with 0.22 M of 1,3-diaminopropane

compounds, illustrated by the α -styryl fluoranthene is similar to that of the parent arene (fluoranthene), the reactive compounds have a fluorescence spectra which has lost the vibrational structure of the parent arene, as illustrated by I, and their lifetime is very much shortened as expected for a singlet excited state with an additional non-radiative deactivation path. In other words, the unreactive compounds can be classified as the parent arenes with a substituent perturbation and the reactive ones as new chromophores including all the π electrons.

The simplest reactive system (I) has been substituted to reveal the electronic requirement for the reaction: the unsubstituted compound (I) cyclizes more efficiently and the derivatives which have a large charge transfer character in the excited state ($\mu_{IV}^* = 16.5_D$, Eckert *et al* 1988) do not photocyclize (table 1).

2.2 1-(α -Aryl)cycloalkenes

While the scope of the photocyclization of α -arylolefins with an acyclic double bond was rather narrow, two results led us to explore the photoreactivity of α -arylcycloalkenes: in a preceding work we showed that when the triplet energy of the aryl group is high enough a perpendicular triplet state is formed and a *trans* double bond in the ground state ensues (Lazare *et al* 1984), and some years earlier (Dauben *et al* 1979), the high dienophile reactivity of a *trans* cyclohexene had been evidenced by an intramolecular Diels-Alder addition to 1-phenylcyclohexene.

With the cyclohexenyl derivatives, only the triplet energy of benzene is high enough to induce the formation of a perpendicular triplet (Lazare *et al* 1984) but naphthalene leads to the isomerization of the double bond of a cycloheptene or a cyclooctene cycle and cyclization follows (figure 2).

In the series 1-(α -aryl)olefins we have discovered two new types of photocyclization with very different structural restrictions: while fluoranthene and phenanthrene derivatives are not reactive in the singlet excited state, they cyclize by sensitization of the cycloheptenyl derivatives from the *trans* double bond (Lapouyade and Nourmamode 1984).

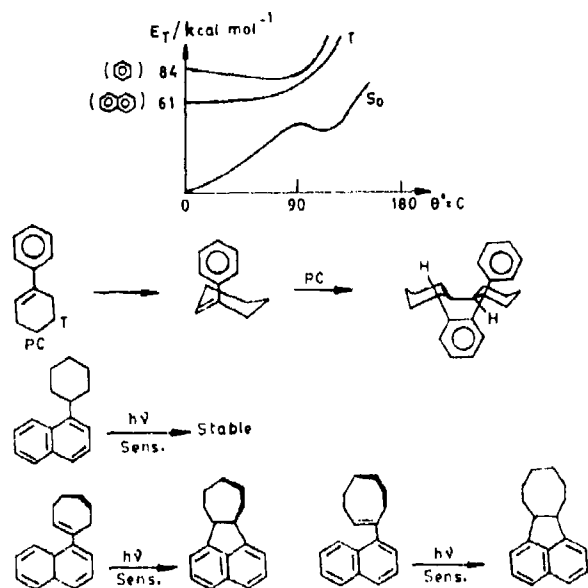


Figure 2. Reactivity and potential energy curves of 1-(α -aryl)cycloalkenes.

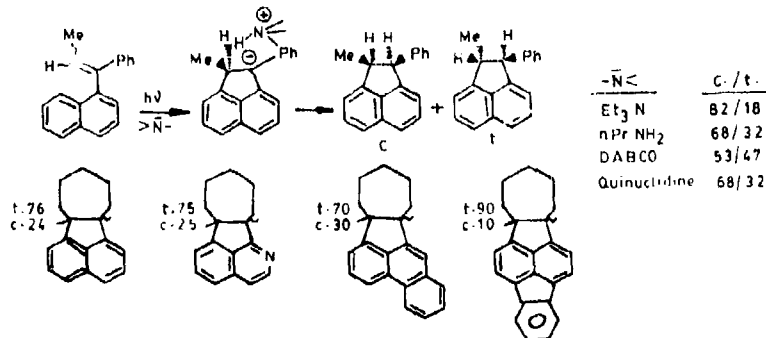


Figure 3. Stereochemistry of photocyclization of 1-(α -aryl)ethylenes.

The stereochemistry of these amine-mediated cyclizations is the result of the protonation of the benzylic anion from the less hindered side i.e. that of the vicinal hydrogen and consequently leads predominantly to the *cis* isomer particularly with the more hindered amines (figure 3).

3. Photocyclization of 1,2-diarylethylenes in primary amines

The amine-mediated 1,3-H-shift discovered with the photocyclization of 1-(α -styryl)naphthalene has been extended to the photochemical syntheses of dihydro PAH from

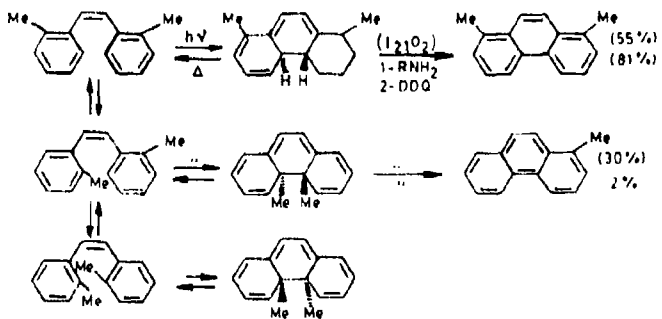


Figure 4. Comparative products of the photocyclization of orthomethylstilbenes under (a) oxidative conditions ($O_2 + I_2$), (b) non-oxidative conditions (RNH_2) followed by DDQ oxidation.

1,2-diarylethylenes (Lapouyade *et al* 1982b). From stilbene the predominant product is 1,4-dihydrophenanthrene (Couture *et al* 1975) while larger diarylethylenes give only compounds analogous to 9,10-dihydrophenanthrene. The mechanism of amine-promoted prototropy, in the intermediate dihydrophenanthrenes has been elucidated (Woning *et al* 1990). Beyond the access to dihydro PAH, amine prototropy reduces the loss of orthoalkyl groups during the photocyclization of orthoalkyl stilbenes (figure 4).

Unfortunately the regioselectivity of cyclization of metaalkyl stilbenes is not markedly changed by substituting iodine by amine and 2-alkyl and 4-alkyl phenanthrenes are formed unselectively.

If we consider 1-(α -naphthyl)1,2-diphenylethylene, the photocyclization could take place from the rotamers of two isomers (*E* and *Z*) to lead to three products. Whatever the trapping agent of the primary product of the photocyclization (iodine or amine) the relative yields of the three photoproducts are very close (figure 5), which is certainly due to a complete trapping of the photocyclized intermediates.

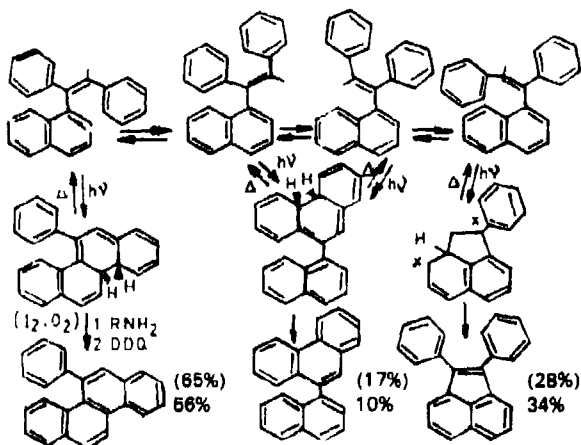


Figure 5. Photocyclization of 1-(α -naphthyl)1,2-diphenylethylene.

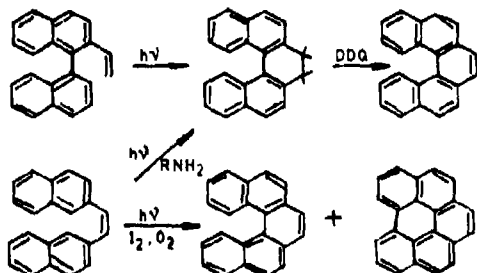


Figure 6. Photochemical synthesis of pentahelicene.

4. Cyclization of 2-vinylbiphenyls

While 4-methylphenanthrene is not regioselectively formed from the photocyclization of meta methylstilbene, irradiation of 2-vinyl-2'-methyl biphenyl leads to 4-methylphenanthrene only, certainly because the bay-interaction between the vinyl and methyl groups inhibits the formation of the corresponding rotamer.

We have earlier shown that a conrotatory cyclization followed by a 1,5-hydrogen shift accounts for the complete stereoselectivity of the singlet cyclization of 2-vinylbiphenyls (Lapouyade *et al* 1980). The sensitized reaction is often more efficient but is not stereoselective unless the double bond is part of a cyclopentene or a cyclohexene ring. When a 90° twist of the vinylic double bond is allowed, the resulting perpendicular triplet gives a non-stereospecific cyclization (Lapouyade *et al* 1985). A laser-flash photolysis study shows that the triplet cyclization is an adiabatic reaction giving a polyene in the triplet state (Lazare *et al* 1985; Bonneau 1986).

From the synthetic point of view the photocyclization of 2-vinylbiphenyls provides the route to a large number of monofluoroPAH (Lapouyade *et al* 1982a) and improves access to pentahelicene where the classical oxidative photocyclization of 1,2-di(β-naphthyl) ethylene inevitably leads to a mixture of pentahelicene and benzo-perylene (figure 6).

5. Reactivity of the arylethylene radical cations

Catalysis of the Diels-Alder reaction by single-electron acceptors has been shown to provide a powerful and highly selective route for the cycloaddition of neutral or electron-rich dienophiles to conjugated dienes (Belleville *et al* 1981). Owing to the bichromophoric character of several of the arylethylenes, one could expect that the radical cation of one part of the molecule could add electrophilically to the unsaturated, electron-rich other part. As ground-state oxidizers, we have used *tris*-(4-bromophenyl) aminium hexachloroantimonate, and as photochemical oxidizers, cyano-arenes in the singlet excited state and quinones in the triplet excited state.

5.1 1,2-Diarylethylene radical cations

Whatever the oxidant, 1,2-diarylethylenes lead only to *cis* ↔ *trans* isomerization, and when only the *cis* isomer exists, as in 1,2-diphenylcyclopentene, the starting compound is recovered.

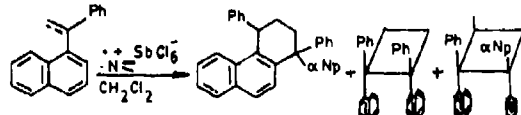
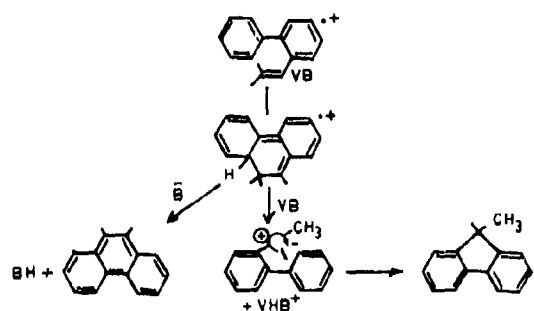
Figure 7. Reactivity of 1-(α -styryl)naphthalene radical cation.

Figure 8. Reactivity of 2-vinylbiphenyl radical cations.

5.2 1,1-Diarylethylene radical cations

1,1-diarylethylenes with a vacant *peri* position, where a cyclization could be expected to occur, do not lead to any intramolecular reaction, but instead to [2 + 2] and [2 + 4] cycloadditions, as has been observed with 1,1-diphenylethylene (Matthes and Farid 1986).

We have observed this chemistry, illustrated with I (figure 7), with several 1-(α -styryl) arenes. When the oxidant is an excited cyanoarene, we also separate a dehydrogenated [4 + 2] cycloaddition product and the reduced sensitizer.

5.3 2-Vinylbiphenyl radical cations

With 10% of *tris*-(4-bromophenyl)aminium hexachloroantimonate in methylene chloride, 2-vinylbiphenyls lead to the radical cation of the electrocyclization product which initiates a protic catalysis to the related fluorenes or, in presence of 2,6-di-*t*-butylpyridine or water, stoichiometrically gives phenanthrene derivatives. With photochemical oxidants, only phenanthrenes or 9,10-dihydrophenanthrenes are obtained (Lapouyade *et al* 1987) (figure 8).

6. Conclusion

We have discovered the photocyclization of α -aryl olefins mediated by primary amines and delineated its scope according to whether the double bond is acyclic or is part of a cycloalkene. In the 1,2-diarylethylene series, irradiation in presence of amine leads to dihydro PAH and protects the alkyl group in the ortho-position against

elimination after cyclization. With 2-vinylbiphenyl compounds the stereochemistry of the cyclization is a function of the excited state multiplicity and from the radical cation, electrocyclization can be pursued by a protic catalysis.

Three structural types of arylolefins have been evaluated as precursors for the photochemical formation of PAH.

References

- Belleville D S, Wirth D W and Bauld N L 1981 *J. Am. Chem. Soc.* **103** 718
Bonneau R 1986 *New J. Chem.* **10** 425
Couture A, Lablache-Combier A and Olsenberg H 1975 *Tetrahedron* **31** 7021
Dauben W G, Van Riel H C H A, Hauw C, Leroy F, Jousset-Dubien J and Bonneau R 1979 *J. Am. Chem. Soc.* **101** 1901
Eckert C, Heisel F, Miche J A, Lapouyade R and Ducasse L 1988 *Chem. Phys. Lett.* **157**
Fournier de Violet P, Lapouyade R and Rayez J C 1982 *J. Photochem.* **19** 253
Laarhoven W H 1983 *Rec. Trav. Chim., Pays-Bas* **102** 185
Lapouyade R, Hanafi N and Morand J -P 1982a *Angew. Chem., Int. Ed. Engl.* **21** 766
Lapouyade R, Koussini R and Bouas-Laurent H 1977 *J. Am. Chem. Soc.* **99** 7374
Lapouyade R, Koussini R, Nourmamode A and Courseille C 1980 *J. Chem. Soc., Chem. Commun.* 740
Lapouyade R, Koussini R and Rayez J-C 1975 *J. Chem. Soc., Chem. Commun.* 676
Lapouyade R, Manigand C and Nourmamode A 1985 *Can. J. Chem.* **63** 2192
Lapouyade R and Nourmamode A 1984 *Synthesis* 161
Lapouyade R, Veyres A, Hanafi N, Couture A and Lablache-Combier A 1982b *J. Org. Chem.* **47** 1361
Lapouyade R, Villenave P, Nourmamode A and Morand J -P 1987 *J. Chem. Soc., Chem. Commun.* 776
Lazare S, Bonneau R and Lapouyade R 1984 *J. Phys. Chem.* **88** 18
Lazare S, Lapouyade R and Bonneau R 1985 *J. Am. Chem. Soc.* **107** 6604
Liu L, Yang B, Katz T J and Poindexter K 1991 *J. Org. Chem.* **56** 3769
Mallory F B and Mallory C W 1984 *Org. Synth.* **30** 1
Matte S L and Farid S 1986 *J. Am. Chem. Soc.* **108** 7356
Woning J, Weisenborn P C M, Varma C A G O and Laarhoven W H 1990 *J. Photochem. Photobiol.* **A55** 169

Spectroscopic and magnetic studies of mixed-ligand complexes of zinc(II)

S YAMAMOTO¹, S IKEDA¹, T AZUMI^{1*} and G A CROSBY²*

¹Department of Chemistry, Faculty of Science, Tohoku University, Sendai 980 Japan

²Department of Chemistry, Washington State University, Pullman, WA 99164-4610 USA

Abstract. Zero-field splittings and the kinetic parameters associated with the triplet spin sublevels of both the triplet $\pi\pi^*$ and the triplet ligand-ligand charge-transfer states were measured by the optically-detected magnetic-resonance method for a series of complexes with a d^{10} closed-shell metal ion of the type, $Zn(X-PhS)_2(\text{phen})$, where $X = \text{F}, \text{Cl}, \text{H}, 4-\text{CH}_3, \text{or } 4-\text{CH}_3\text{O}$. Both the zero-field splittings and the kinetic decay parameters are satisfactorily interpreted in terms of mixing between the lowest phen-localized $\pi\pi^*$ and ligand-ligand charge-transfer states.

Keywords. Zero-field splittings; zinc(II) mixed-ligand complexes; ligand-ligand charge transfer state; optically-detected magnetic resonance method; closed-shell metal ion phosphorescence

1. Introduction

Complexes of closed-shell metal ions, such as zinc(II) and cadmium(II), are usually colorless. This is easily understood in view of their d^{10} closed-shell structures. First of all, no ligand-field $d-d$ transitions exist. Further, since the energy required to remove an electron from the d^{10} configuration is quite high (for example, the ionization energy of a free Zn^{2+} ion is ~ 40 eV), the contribution of metal-to-ligand charge-transfer (MLCT) states to the low-lying excited manifolds in complexes should be very small. Nonetheless some zinc complexes are deeply colored (Crosby *et al.* 1985). These colored materials are of the type, $Zn(NN)(SS)$, where NN represents an aromatic diimine ligand, such as 1,10-phenanthroline or 2,2'-bipyridine and SS represents either a dithiol or two monothiol ligands. Previous studies (Highland *et al.* 1986; Yamamoto *et al.* 1990) have assigned the lowest energy excited states responsible for the color to those involving charge transfer from the SS to the NN ligand. These types of excited states are commonly designated as ligand-to-ligand charge-transfer (LLCT) states.

In order to quantify the nature of these low-lying (LLCT) excited states in the present paper, we examine the phosphorescence spectra of a series of complexes of the general formula, $Zn(X-PhS)_2(\text{phen})$, where $X = \text{F}, \text{Cl}, \text{H}, 4-\text{CH}_3, 4-\text{CH}_3\text{O}$. PhS = thiophenol; phen = 1,10-phenanthroline. With the single exception of $Zn(4-\text{CH}_3\text{O}-\text{PhS})_2(\text{phen})$, all these complexes display phosphorescence in both the phen-localized $\pi\pi^*$ and LLCT excited states. In the current investigation we report

* For correspondence

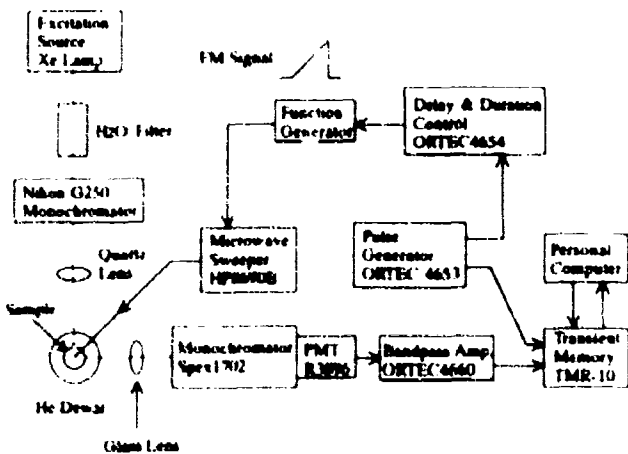


Figure 1. Schematic diagram for measurement of ODMR spectra. Spectra were measured with a Spex 1702 monochromator equipped with a Hamamatsu R3896 photomultiplier. Excitation source was a 500-W Xe lamp combined with a Nikos G250 monochromator and water filter. Microwave power was supplied from a HP8690B sweep oscillator with an appropriate plug-in module. Its frequency was swept in an external FM mode. The signal from the photomultiplier, amplified by an ORTEC 4660 bandpass amplifier, was fed into a Kawasaki Electronics TMR-10 transient memory.

data on the zero-field levels of the phen-localized $^3\pi\pi^*$ excited states as obtained from the optically-detected magnetic-resonance (ODMR) method.

2. Experimental

The spectroscopic properties reported in this paper are (a) phosphorescence spectra, (b) magnitudes of the zero-field splittings, (c) total decay-rate constants associated with the individual spin sublevels of the phen-localized $^3\pi\pi^*$ state, and (d) relative radiative decay-rate constants (at the 0,0-band of the phenlocalized $^3\pi\pi^*$ phosphorescence) of the spin sublevels.

The experimental apparatus for the ODMR measurements is schematically shown in figure 1. The microcrystalline sample was cooled to 1.3 K and irradiated by light from a 500-W xenon lamp. The phosphorescence was dispersed by a Spex 1702 monochromator and detected by a Hamamatsu R 3896 photomultiplier tube coupled to an appropriate amplifier and a transient digitizer. Microwaves were applied from a HP 8690B sweep oscillator operated in the FM mode, and the resultant signal was fed to a computer for accumulation and further data processing.

3. Results and discussion

3.1 Phosphorescence spectra

As a typical example of the luminescence displayed by these complexes, the phosphorescence spectrum of $\text{Zn}(4\text{-Cl-PhS})_2(\text{phen})$ is shown in figure 2. The spectrum

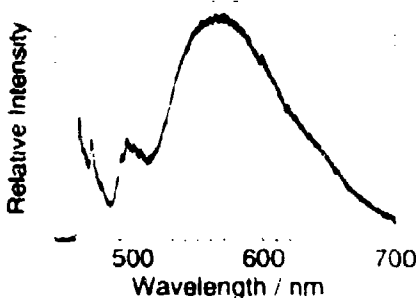


Figure 2. Phosphorescence spectrum observed from a microcrystalline sample of $\text{Zn}(4\text{-Cl-PhS})_2(\text{phen})$ at 4.2 K.

consists of two components. The short-wavelength part is structured, and the spectrum almost coincides with that of the uncoordinated phen, therefore, this component has been assigned to emission from the $^3\pi\pi^*$ level of the phen ligand. The long-wavelength component, which is observed only from mixed-ligand complexes, is broad and structureless and was originally assigned to emission from the $^3\text{LLCT}$ state because of its millisecond lifetime at 77 K. This $^3\text{LLCT}$ assignment was corroborated later by the ODMR action spectrum (Nozaki *et al.* 1992).

3.2 Zero-field splittings of the phen-localized $^3\pi\pi^*$ level

Zero-field energies can easily be obtained from the frequencies of the observed microwave transitions. Direct comparison of these zero-field energies from various complexes is meaningless, however, because the directions of the spin axes may not be identical. Therefore, we discuss the zero-field splittings in terms of the spin-axis-independent quantity, D^* , which is defined as follows (McGlynn *et al.* 1969)

$$D^* = [(3/2)(X^2 + Y^2 + Z^2)]^{1/2}, \quad (1)$$

where X , Y , and Z are the energies of the triplet sublevels measured from the center of gravity, i.e., $X + Y + Z = 0$. The D^* values obtained are summarized in table 1. For comparison, we also include the data from $\text{ZnCl}_2(\text{phen})$, which has no LLCT low-lying triplet state.

As table 1 reveals, the D^* value of the phen-localized $^3\pi\pi^*$ level varies as the X substituent on the thiol ligand changes. This experimental evidence clearly indicates

Table 1. Zero-field splitting parameter D^* , and the $^3\pi\pi^*$ - $^3\text{LLCT}$ mixing coefficients.

	D^* (GHz)	$\cos^2 z$	$\sin^2 z$
$\text{ZnCl}_2(\text{phen})$	3.92	1.00	0
$\text{Zn}(\text{F}_3\text{-PhS})_2(\text{phen})$	3.88	0.99	0.01
$\text{Zn}(4\text{-Cl-PhS})_2(\text{phen})$	3.83	0.98	0.02
$\text{Zn}(4\text{-CH}_3\text{-PhS})_2(\text{phen})$	3.76	0.96	0.04

that the excitation energy of the so-called "phen-localized" state is really delocalized over the whole complex and that the degree of delocalization depends on the X substituent on the thiol ligand. In table 1 the complexes are listed in increasing order of the electron-donating ability of the X substituent. The data show that the D^* value decreases as the electron-donating ability of the substituent increases. We interpret this to mean that the degree of delocalization in the excited state also increases in the same way.

It is convenient to describe the delocalization of excitation in terms of a valence-bond-type mixing of a pure $^3\text{LLCT}$ state with a pure $^3\pi\pi^*$ state. In this framework the wavefunction Ψ for the low-lying (emitting) state is expressed as follows:

$$\Psi = \cos \alpha \psi(^3\pi\pi^*) + \sin \alpha \psi(^3\text{LLCT}). \quad (2)$$

Thus, D^* associated with the emitting state can be expressed as

$$D^* = \cos^2 \alpha D^*(^3\pi\pi^*) + \sin^2 \alpha D^*(^3\text{LLCT}), \quad (3)$$

where $D^*(^3\pi\pi^*)$ is the D^* value of a pure $^3\pi\pi^*$ state and can be approximated from the experimental value for $\text{ZnCl}_2(\text{phen})$, which is 3.92 GHz (see table 1). Further, $D^*(^3\text{LLCT})$ is the D^* value of a pure $^3\text{LLCT}$ state. The D^* value for the charge-transfer state should be extremely small since the electrons are spread over two different ligands. The required D^* value for a pure $^3\text{LLCT}$ state is, however, not available because any experimentally accessible $^3\text{LLCT}$ state has considerable contribution from a nearby $^3\pi\pi^*$ state. Therefore, as a first approximation, we set the value $D^*(^3\text{LLCT})$ to zero. The mixing coefficients in (2) calculated in this manner are also tabulated in table 1. The calculation shows that the degree of mixing of the $^3\text{LLCT}$ state with the $^3\pi\pi^*$ level increases as the electron-donating ability of the substituent X increases.

3.3 Kinetic parameters for triplet sublevels of the $^3\pi\pi^*$ term

The total decay rate constants, $k_u(u = x, y, z)$, and the relative radiative rate constants $k'_v(\text{rel})$ were determined for the $^3\pi\pi^*$ sublevels. The results are summarized in table 2.

First, we consider the total decay-rate constant (that is, the sum of the radiative and radiationless decay-rate constants) for the individual sublevels. A detailed treatment of the data for the individual levels will be presented elsewhere (Yamamoto *et al* 1993). Here we discuss the general behavior in terms of the average rate constant,

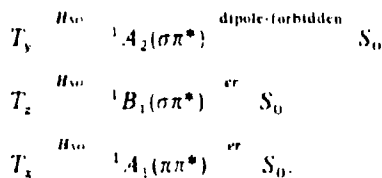
Table 2. Total decay rate constants, $k_u(u = x, y, z)$, and the relative radiative decay rate constants, $k'_v(\text{rel})$ ($u = x, y, z$) associated with the individual spin sublevels.

	$k_u(\text{s}^{-1})$				$k'_v(\text{rel})$		
	x	y	z	Average	x	y	z
Phen	1.36	0.49	1.31	1.12	0.09	0.06	1.00
$\text{Zn}(\text{F}, \text{PhS})_2(\text{phen})$	0.68	3.87	4.87	3.15	0.44	1.00	0.03
$\text{Zn}(\text{4-Cl PhS})_2(\text{phen})$	7.62	3.52	1.48	4.21	0.24	1.00	0.05
$\text{Zn}(\text{PhS})_2(\text{phen})$	8.62	4.07	1.59	4.76	0.36	1.00	0.14

k [$k = (k_x + k_y + k_z)/3$]. Table 2 shows that the average decay-rate constant of the $^3\pi\pi^*$ level of uncoordinated phen generally increases with complexation. This experimental evidence is again interpretable in terms of (2). The decay-rate constant for a pure $^3\text{LLCT}$ is $\approx 50 \text{ s}^{-1}$, significantly larger than that of the pure $^3\pi\pi^*$ state. Thus, the finding that as the electron-donating ability of the substituent X on the thiol ligand increases the decay rate also increases is well accounted for in terms of the mixing of the pure $^3\text{LLCT}$ state with the pure $^3\pi\pi^*$ state (Nozaki *et al* 1992).

We next focus attention on the relative radiative rate constants of individual sublevels. As table 2 indicates, for uncoordinated phen the z-sublevel is the most effective for the radiative transition to the ground state. On the other hand, for all the $\text{Zn}(\text{X-PhS})_2(\text{phen})$ complexes we have studied to date, the y-sublevel is by far the most active in the radiative transition.

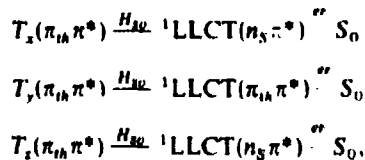
Mechanisms for radiative transitions from the triplet spin states of the $^3B_2(\pi\pi^*)$ level of uncoordinated phen are schematically expressed in the conventional way (Yamauchi and Azumi 1978) as follows:



The spin-orbit-coupling matrix elements associated with the T_y and the T_z sublevels are one-center type. However, the dipole transition associated with the radiative transition from the T_y sublevel is group-theoretically forbidden. Thus, the T_y sublevel is expected to be the most radiative. This theoretical expectation is indeed confirmed experimentally (Ikeda *et al* 1992).

In complexes the situation is different. These complexes do not have C_{2h} symmetry. Therefore, the forbiddenness of the radiative transition from the T_y sublevel is formally lifted; that is, none of the sublevels in the complex is group-theoretically forbidden. Thus, to rationalize the experimental results we must examine the coupling mechanisms a little more quantitatively.

The geometrical structure determined by X-ray analysis for the $\text{Zn}(4\text{-Cl-PhS})_2(\text{phen})$ complex is schematically shown in figure 3 (Gamble G R and Crosby G A, unpublished work). As seen from the figure, one of the thiol ligands is located directly over the phen ligand. Therefore the LLCT state can be ascribed essentially to charge transfer from this adjacent thiol moiety to the phen ligand with a substantial contribution from the coordinated sulfur of the distant ligand. This supposition is supported by our extended Hückel calculation. We further note that the in-plane short axis of this thiol molecule is almost parallel to the y axis (as seen in figure 3, the phen is almost in the yz plane). In view of this geometrical structure, mechanisms for radiative transitions from the $^3\text{LLCT}$ sublevels can be schematically expressed as



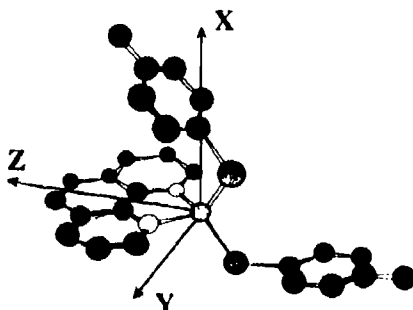


Figure 3. Geometrical structure of $\text{Zn}(\text{4-Cl-PhS})_2(\text{phen})$ and principal spin axes. Spin axes (that is, axes that diagonalize the spin-spin coupling tensor) were determined by an extended Huckel calculation. In this axis system the molecular plane of the phen molecule is almost in the xz plane. Note that the in-plane short axis of one of the benzenethiol molecules is nearly parallel to the y axis.

where π_{ik} is the π orbital on the benzenethiol ligand, π^* refers to an orbital on the phen ligand, and n_S is the non-bonding orbital centered on the S-atom of the thiol.

In the above scheme, spin-orbit coupling between the ${}^1\text{LLCT}$ and ${}^3\text{LLCT}$ states contains a one-center spin-orbit term on the S atom and should have a significant value. Closer examination of the spin-orbit-coupling terms reveals, however, that there is little difference among the three routes described above; that is, from a consideration of the spin-orbit coupling alone, any sublevel selectivity observed experimentally cannot be understood. Therefore we must examine the magnitudes of the dipole-transition moments.

For the transition between the ${}^1\text{LLCT}$ state and the ground state, theoretical evaluation of the transition dipole moment is difficult because no one-center term exists. We, therefore, appeal to a simple approximation. We assume that the transition dipole moment is proportional to the overlap between the component orbitals of the combining states. As can be seen from the geometrical structure in figure 3, the overlap between the π_{ik} and π^* orbitals is much larger than the overlap between the n_S and π^* orbitals. Hence we predict that the y -sublevel should be more radiative than the other two sublevels. This is indeed what we observed experimentally for all the complexes.

4. Conclusions

The zero-field splitting parameter, D^* , of $\text{Zn}(\text{X-PhS})_2(\text{phen})$ complexes decreases as the electron-donating ability of the X substituent on the benzene thiol ligand increases. This trend is satisfactorily interpreted in terms of a valence-bond type mixing of the ${}^1\text{LLCT}$ state with the phen-localized ${}^3\pi\pi^*$ state. The radiative properties of the phen-localized ${}^3\pi\pi^*$ state were also determined for the individual sublevels. For uncoordinated phen the z -sublevel is the most active, whereas for all the complexes the y -sublevel dominates. This experimental observation is rationalized in terms of the magnitudes of the dipole transition moments between the mixing ${}^1\text{LLCT}$ state and the ground state.

Acknowledgements

This research was supported in part by a Grant-in-Aid for International Scientific Research No. 02044011 from the Ministry of Education in Japan, a Grant-in-Aid for Scientific Research on Priority Areas, "Molecular Based Magnetism" (Area No. 228), No. 04242101 from the Ministry of Education in Japan, and the US Department of Energy under Grant No. DEFD-87ER13809.

References

- Crosby G A, Highland R G and Truesdell K A 1985 *Coord. Chem. Rev.* **64** 41
Highland R G, Brummer J G and Crosby G A 1986 *J. Phys. Chem.* **90** 1593
Ikeda S, Yamamoto S, Azumi T and Crosby G A 1992 *J. Phys. Chem.* **96** 6593
McGlynn S P, Azumi T and Kinoshita M 1969 *Molecular spectroscopy of the triplet state* (Englewood Cliffs, NJ: Prentice Hall)
Nozaki K, Ikeda S, Yamamoto S, Ikeyama T, Azumi T, Burt J A and Crosby G A 1992 *Proc. Ind. Acad. Sci. (Chem. Sci.)* **104** 241
Yamamoto S, Ikeda S, Ikeyama T, Azumi T and Crosby G A 1990 *Chem. Phys. Lett.* **174** 176
Yamamoto S, Ikeda S and Azumi T 1993 (to be published)
Yamauchi S and Azumi T 1978 *J. Chem. Phys.* **68** 4138

Studies of photochemical reaction by CIDNP-detected ESR spectrum

Q MENG, Y YAMAKAGE, T AIZAWA, K MAEDA and T AZUMI*

Department of Chemistry, Faculty of Science, Tohoku University, Sendai 980, Japan

Abstract. CIDNP-detected ESR spectroscopy was applied to the study of photochemical reaction. In the CIDNP-detected ESR spectroscopy, the spectrum due to intermediate radical pairs and the spectrum due to free (escaped) radicals can be separately observed. The spectrum due to radical pairs is called stimulated nuclear polarization (SNP), and the spectrum due to free radicals is called dynamic nuclear polarization (DNP). The method was applied to the study of photochemical reaction of 2,6-dichlorobenzoquinone and the isomerization of quadricyclane assisted by photoinduced electron transfer, and the chemical species of the intermediate radical pair and of the radical were clarified.

Keywords. CIDNP-detected ESR; dynamic nuclear polarization; dichlorobenzoquinone; quadricyclane.

1. Introduction

CIDNP-detected ESR spectroscopy is a device to detect ESR spectra of transient free radicals and radical pairs by monitoring the effect of microwaves on the CIDNP spectra of reaction products. The novel aspect of this method is that the ESR spectra of radical pairs and of free radicals can be separately measured (Bagryanskaya *et al* 1986). The nuclear polarization created by the ESR transitions of *radical pairs* is called stimulated nuclear polarization (SNP), and nuclear polarization created by the ESR transition of *free radicals* is called dynamic nuclear polarization (DNP).

The mechanism of SNP is schematically illustrated in figure 1 for a radical pair having two electrons (from radical A and radical B) and one proton. We assume that only radical A has a proton. The figure illustrates the case where the exchange integral J equals zero. The allowed microwave transitions are indicated by vertical lines in the figure. If we could record the ESR spectrum of such a short-lived radical pair, the spectrum would look like the one shown in the right upper corner of the figure. That is, the spectrum consists of two hyperfine lines for radical A and one line for radical B. However, it is absolutely impossible, at this stage, to record the ESR of such short-lived species. In the CIDNP-detected ESR spectroscopy, we monitor the CIDNP of either the cage product or the escaped product. In the case of the negative hyperfine coupling constant and the triplet precursor, as is shown in figure 1, the microwave-induced change of the NMR would be E/A (emission in lower field and absorption in higher field) for a cage product and A/E (absorption in lower field and emission in higher field) for an escaped product. The case of singlet precursor is illustrated in figure 2. In this case the SNP spectrum should be A/E for a cage product

*For correspondence

$A < 0$ T-precursor $J=0$

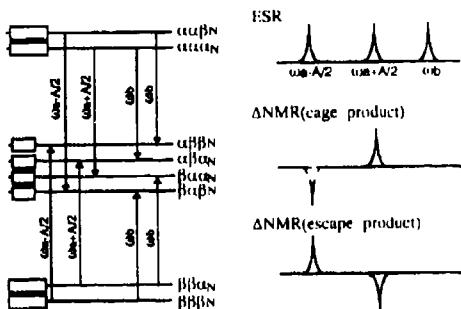


Figure 1. Schematic illustration of the mechanism of stimulated nuclear polarization for the negative hyperfine coupling constant and the triplet precursor.

$A < 0$ S-precursor $J=0$

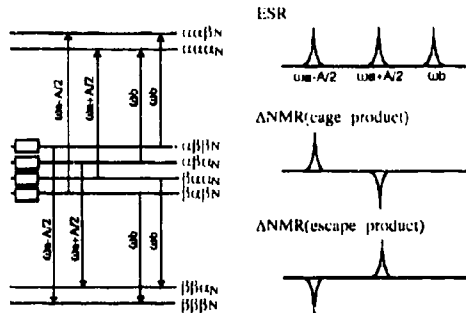


Figure 2. Schematic illustration of the mechanism of stimulated nuclear polarization for the negative hyperfine coupling constant and the singlet precursor.

and E/A for an escaped product. As is understood from these figures, the characteristics of SNP may be summarized as follows.

- (1) SNP corresponds to the ESR spectrum of radical pairs.
- (2) Sign of polarization differs among hyperfine lines. Thus in the one-proton case shown in figures 1 and 2, the SNP spectrum is either E/A or A/E . Thus, the SNP spectrum is symmetric with respect to the center of inversion.
- (3) The polarization pattern (E/A or A/E) is determined by (i) precursor spin state, (ii) reaction product that is monitored, and (iii) microwave power.

The mechanism of DNP is schematically illustrated in figure 3 for a free radical having one electron and one proton. The figure illustrates the cases for both positive and negative hyperfine coupling constants. As is understood from the figure, by the cross relaxation in which total spin quantum number is preserved (i.e. $\Delta m = 0$) the population transfers from the β_N nuclear spin state to the α_N nuclear spin state in the intermediate radical, thus leading to the enhanced absorption in the NMR of the product (that is, absorptive DNP). By the cross relaxation in which total spin quantum number differs by 2 ($\Delta m = 2$), on the other hand, the population transfers from the

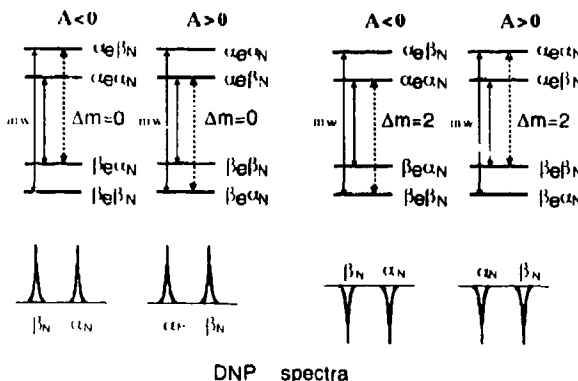


Figure 3. Schematic illustration of the mechanism of dynamic nuclear polarization.

α_N nuclear spin state to the β_N nuclear spin state leading to the emissive DNP. The characteristics of DNP are summarized as follows.

- (1) DNP corresponds to the ESR spectrum of free radicals.
- (2) Signs of polarization are the same for all hyperfine lines. For a specific case of one-proton radicals shown in the figure, polarization pattern is either E/E or A/A . Thus the DNP spectrum has mirror symmetry.
- (3) The polarization pattern (absorption or emission) is determined only by the mechanism of cross relaxation (whether $\Delta m = 0$ or $\Delta m = 2$). It is important to note that the polarization pattern is independent of the sign of the hyperfine coupling constant, contrary to the polarization pattern of CIDNP or of SNP.

As is discussed above, the observed CIDNP-detected ESR spectrum is composed of SNP and DNP. Because of the difference in symmetry (inversion symmetry of SNP and mirror symmetry of DNP) we can easily decompose the observed spectrum into the two components by simulation. (For example, any contribution in the center of the magnetic field should be due to DNP).

We have utilized the technique of SNP and DNP in analyzing various photophysical and photochemical processes. In this paper, however, we discuss only the following two subjects. The first is concerned with the hydrogen abstraction of dichlorobenzoquinone, and the second is related to the isomerization of quadricyclane assisted by photoinduced electron transfer.

2. Experimental apparatus

The apparatus for the measurements of CIDNP-detected ESR is schematically shown in figure 4. This apparatus is essentially identical to that reported previously (Meng *et al* 1990). The sample solution was circulated by a home-made flow system through a sample reservoir, an ESR cavity, and an NMR probe. The sample was irradiated by a 500 W mercury lamp at the ESR cavity. The products of the chemical reaction were rapidly transferred to the NMR spectrometer, where CIDNP was measured. The transfer rate should be faster than the nuclear relaxation time, which is of the

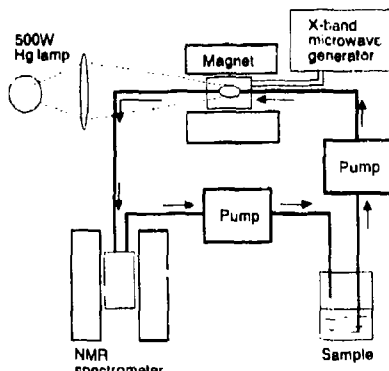


Figure 4. Experimental apparatus for the measurement of CIDNP-detected ESR spectra.

order of a second in the present case. Microwaves amplified to 2 W by a TWT amplifier were applied at the ESR cavity. The plot of microwave-induced intensity change of CIDNP as a function of the external magnetic field constitutes the CIDNP-detected ESR spectrum.

3. Hydrogen abstraction reaction of 2,6-dichlorobenzoquinone

The mechanism of hydrogen abstraction of dichlorobenzoquinone (abbreviated as Q) is schematically shown in figure 5. The mechanism is essentially identical to that of benzoquinone (Pedersen *et al* 1975; Elliot and Wan 1978). Photoexcited triplet state of Q abstracts hydrogen from a hydrogen donor and the triplet radical pair is produced. The triplet radical pair may dissociate either to semiquinone free radicals or by intersystem crosses to the singlet radical pair. The singlet radical pair may recombine to produce nuclear-polarized Q (denoted by Q^* in figure 5). The escaped radicals may undergo further reactions. We note, in the case of dichlorobenzoquinone, that two types of semiquinone radicals, as shown in figure 5, may be visualized.

This is more specifically illustrated in figure 6. The hydrogen from the hydrogen donor may attack either the oxygen that is close to the chlorine or the one that is far from chlorine. Let us denote the former path as path 1 and the latter path as path 2. We denote the radical pairs created by paths 1 and 2, respectively, as radical pairs 1 and 2. The radicals created by the dissociation of these two types of radical pairs are similarly denoted by radicals 1 and 2. As is discussed above, the two types of radical pairs may be detected by SNP, and the two types of free radicals by DNP. For this purpose we have measured the CIDNP-detected ESR spectrum.

How we construct the CIDNP-detected ESR spectrum from experimental data is illustrated in figure 7. The spectrum (a) is the ordinary NMR spectrum of the ring proton of Q. Upon irradiation by light, the NMR spectrum becomes like (b); that is, we have absorptive CIDNP. Now, if we further apply microwaves the intensity of the CIDNP is changed. If the external magnetic field is 323.67 mT the CIDNP intensity becomes small as is shown in (c). Thus we have emissive CIDNP-detected ESR signals. If the external magnetic field is shifted to 324.75 mT, then the CIDNP

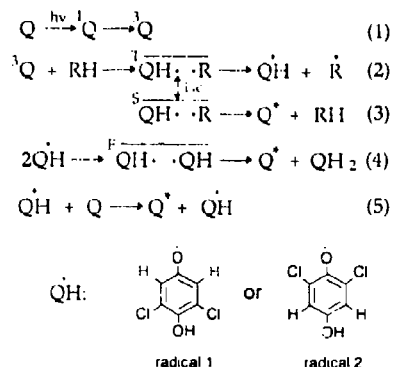


Figure 5. Mechanism of hydrogen abstraction reaction of dichlorobenzoquinone.

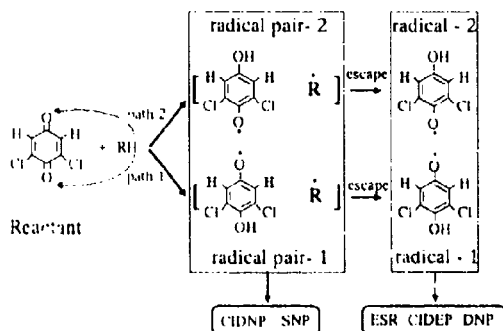


Figure 6. Chemical species that may be present in the hydrogen abstraction reaction of dichlorobenzoquinone.

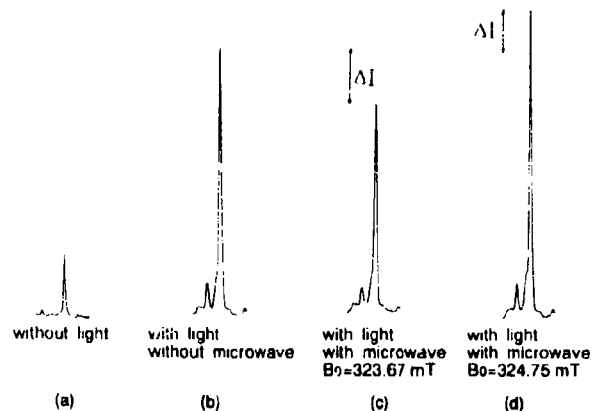


Figure 7. The NMR spectral data that constitute the CIDNP-detected ESR spectra.

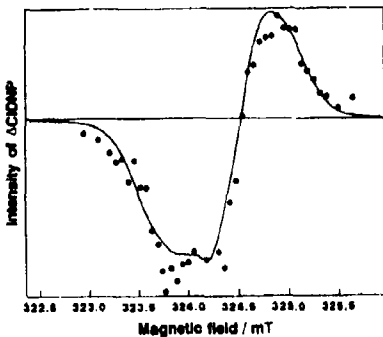


Figure 8. CIDNP-detected ESR spectrum observed during the photolysis of dichlorobenzoquinone.

intensity increases; that is, we have absorptive signals. The CIDNP-detected ESR spectrum is obtained by plotting the microwave-induced NMR intensity change with respect to the external magnetic field.

The observed CIDNP-detected ESR spectrum is shown in figure 8. The dots are the experimental points and the solid curve is the theoretical spectrum calculated in a manner to be discussed below. The spectrum should be composed of four components: SNP of radical pair 1, SNP of radical pair 2, DNP of radical 1, and DNP of radical 2. In order to determine the contributions from the individual components, we try to obtain the theoretical spectra calculated from the stochastic Liouville equation (Koptyug *et al.* 1990).

The stochastic Liouville equation that we are going to solve is as follows:

$$d\rho(t)/dt = -iL\rho(t) + R\rho(t) + W\rho(t) + K\rho(t),$$

where L is the Liouvillian expressed as

$$L\rho(t) = H\rho(t) - \rho(t)H,$$

The spin Hamiltonian is as follows

$$H = H_0 + H_1,$$

where

$$H_0 = \mu_B \hbar^{-1} B_0 (g_a S_{ax} + g_b S_{bx}) - g_a \mu_N \hbar^{-1} B_0 I_{az} + \sum_i I_j S_a \\ + \sum_j I_j S_b - J(r) (\frac{1}{2} + 2S_a S_b)$$

and

$$H_1 = \mu_B \hbar^{-1} B_1 [(g_a S_{ax} + g_b S_{bx}) \cos(\omega t) + (g_a S_{ay} + g_b S_{by}) \sin(\omega t)].$$

The stochastic Liouville equation was solved by a two-site model, which is schematically shown in figure 9. In this model, site 1 represents a radical pair of large J value that may recombine to a recombination product with a rate constant K_r .

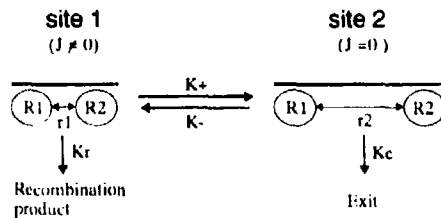


Figure 9. Illustration of the two-site model in the stochastic Liouville equation.

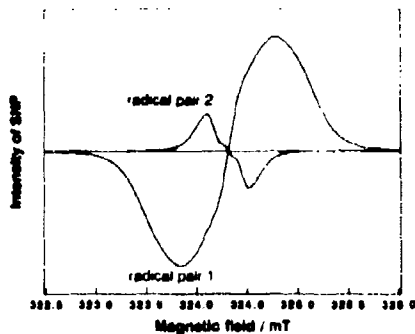


Figure 10. Theoretical SNP spectra for the two types of radical pairs.

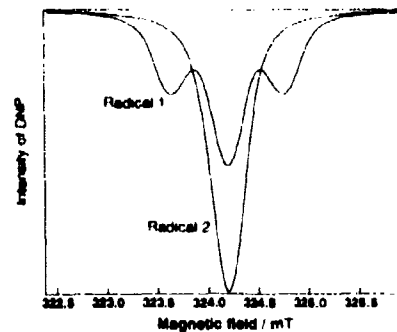


Figure 11. Theoretical DNP spectra for the two types of free radicals.

Site 2 represents the radical pair of $J = 0$ and may exit to free radicals with a rate constant K_e . The transition rate constants between sites 1 and 2 are denoted by K_+ and K_- . The parameters that were determined so as to reproduce the structured SNP spectrum of duroquinone are as follows: recombination rate constant $K_r = 5.0 \times 10^7 \text{ s}^{-1}$, exit rate constant $K_e = 3.0 \times 10^7 \text{ s}^{-1}$, transition rate constants $K_+ = 3.0 \times 10^6 \text{ s}^{-1}$, and $K_- = 1.0 \times 10^5 \text{ s}^{-1}$, exchange integral $J = -5.0 \times 10^9 \text{ rad s}^{-1}$. Even though hyperfine coupling constants of radicals 1 and 2 have not been reported, they are determined from the magnetic parameters of *o*-hydroxy-2,3,5,6-tetrachlorophenoxy radical and *p*-hydroxyphenoxyl radical (Land et al., 1979).

The theoretical SNP spectra thus obtained for radical pairs 1 and 2 are shown in figure 10. We note that the polarization patterns for these two species are different: E/A for radical pair 1 and A/E for radical pair 2. This is due to the difference in the sign of the proton hyperfine coupling constants. Also, the bandwidth of radical pair 1 is much larger reflecting the larger hyperfine coupling constant. Theoretical DNP spectra for radicals 1 and 2 are shown in figure 11. These spectra were obtained from simple stick spectra calculated from estimated hyperfine coupling constants for semiquinone radicals multiplied by a Lorentzian line shape.

We try to simulate the observed spectrum in terms of the theoretical spectra of the four species. The results of simulation show that the observed spectrum is well reproduced by the sum of the SNP of the radical pair 1 and the DNP of the radical 2. The contribution from the radical pair 2 and the radical 1 was negligibly small.

The experimental finding discussed above appears to be interpreted only by the mechanism shown schematically in figure 12. That is, the hydrogen from the solvent attacks only the oxygen that is close to the chlorine, producing only radical pair 1. Immediately after radical pair 1 dissociates into radical 1, the hydrogen (or proton) transfer takes place and only radical 2 is present as free radical. If this mechanism is correct, the ESR and CIDEP spectra should indicate the presence of only radical 2. The steady state ESR and CIDEP spectra (observed at $2.5 \mu\text{s}$ after the laser excitation) are shown in figure 13. As is evident from the comparison between the calculated ESR line spectra of the two radicals, the observed spectra are both due to radical 2 which has smaller hyperfine coupling constants. Thus all the experimental evidence appears to support the mechanism outlined above.

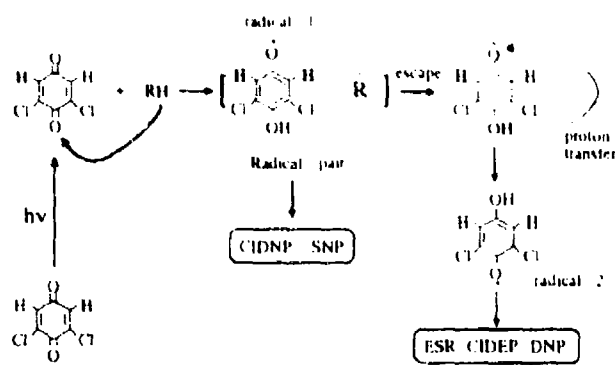


Figure 12. Proposed reaction mechanism of the hydrogen abstraction reaction of dichlorobenzoquinone.

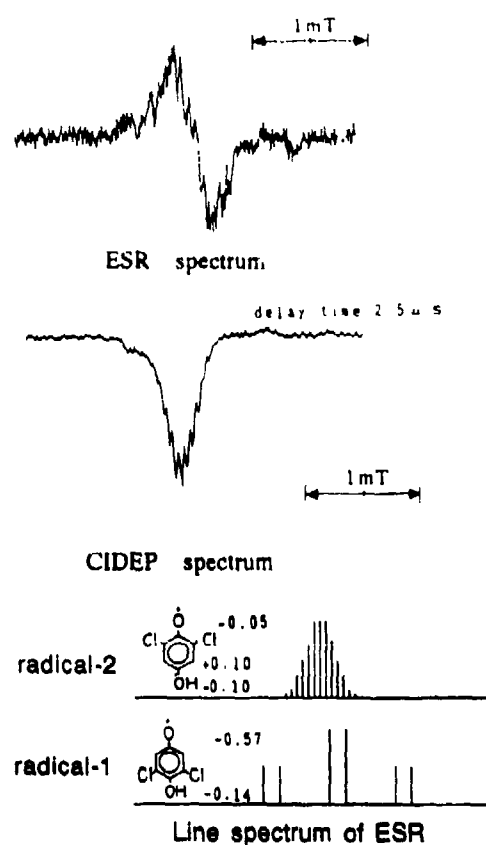


Figure 13. The steady state ESR and the transient CIDEP spectra of radicals produced in the photolysis of dichlorobenzoquinone.

4. Photoinduced-electron transfer reaction of quadricyclane

Quadricyclane is known to isomerize to norbornadiene in the presence of chloranil after photo-induced electron transfer. The reaction is shown in figure 14. A question has arisen as to the species of the intermediate radical pair; is it the cation like I or that like II?



This was the question raised by Roth and coworkers sometime ago (Roth and Schilling 1981; Roth *et al* 1981). They investigated the problem from the viewpoint of the CIDNP spectra and concluded that the intermediate radical pair is composed of the cation I. We try to solve this problem from the viewpoint of the CIDNP-detected ESR spectrum.

The observed CIDNP-detected ESR spectrum in the *L*-band region is shown in figure 15. The signal-to-noise ratio was not necessarily satisfactory; nevertheless, the spectrum clarifies a number of important features. First of all, the spectrum is of the *A/E* type and the observed CIDNP-detected ESR spectrum is entirely due to SNP.

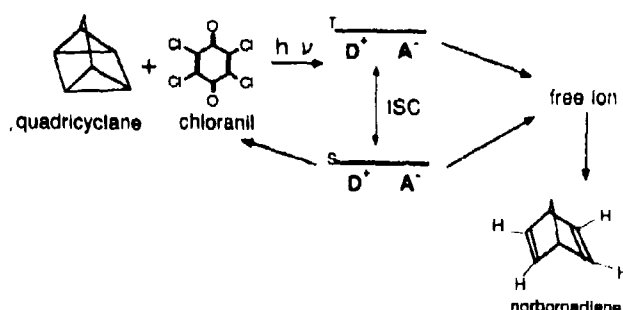


Figure 14. Isomerization of quadricyclane to norbornadiene assisted by photoinduced electron transfer.

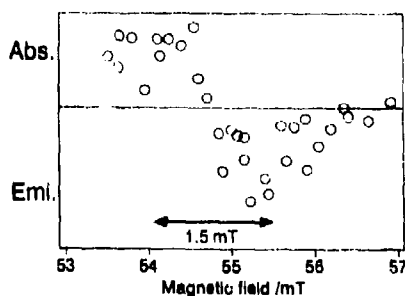


Figure 15. CIDNP-detected ESR spectrum observed during the photolysis of quadricyclane.

Further, the observed spectrum shows that the whole bandwidth of the SNP is around 1.5 mT.

That the A/E pattern was obtained in the case of the triplet precursor, indicates that the hyperfine coupling constant is negative. It is quite important that by SNP the sign of the hyperfine coupling constant can be determined without the knowledge of Δg value.

It is interesting to compare our SNP spectrum with the ESR spectrum of the cation radical that was produced by the X-ray irradiation of norbornadiene and quadricyclane. Toriyama and coworkers analyzed the observed ESR spectrum in terms of 4 protons of 0.8 mT and 2 protons of 0.33 mT, and they denoted the observed species cation II (Toriyama *et al* 1983; Nunome *et al* 1986). The width of 1.5 mT of our observed SNP spectrum is much smaller than the hyperfine coupling constants determined for species II. Thus we conclude that the intermediate radical pair is composed of cation radicals of type I. This conclusion is identical with the conclusion of Roth and coworkers. Even though the conclusion is identical, it is worth pointing out that the species that constitute radical pairs can be determined from the SNP spectrum.

Acknowledgements

The present research was supported by a Grant-in-Aid for Scientific Research No. 03554013 and a Grant-in-Aid for Scientific Research on Priority Areas "Molecular Based Magnetism" No. 04242102 from the Japanese Ministry of Education, Science and Culture.

References

- Bagryanskaya E G, Grishin Y A, Sagdeev R Z and Mohn Y N 1986 *Chem. Phys. Lett.* **128** 162
- Elliot A J and Wan J K S 1978 *J. Phys. Chem.* **82** 444
- Koptyug I V, Lukzen N N, Bagryanskaya E G and Doctorov A F 1990 *Chem. Phys. Lett.* **175** 467
- Landolt-Börnstein 1979 *New series, Group II* (Berlin: Springer) vol. 9, part C2
- Meng Q, Suzuki K, Terazima M and Azumi T 1990 *Chem. Phys. Lett.* **175** 364
- Nunome K, Toriyama K and Iwasaki M 1986 *Tetrahedron* **42** 6315
- Pedersen J B, Parbo C F M and Muus L T 1975 *J. Chem. Phys.* **63** 2398
- Roth H D and Schilling M L M 1981 *J. Am. Chem. Soc.* **103** 7210
- Roth H D, Schilling M L M and Jones G H 1981 *J. Am. Chem. Soc.* **103** 1246
- Toriyama K, Nunome K and Iwasaki M 1983 *J. Chem. Soc., Chem. Commun.* 1346

Electron-nuclear cross-relaxation effect on the photochemical reaction of benzaldehyde as studied by CIDNP and DNP

YUZURU YAMAKAGE, QING-XIANG MENG,
SAMEH SAAD ALI, KIMINORI MAEDA and TOHRU AZUMI*

Department of Chemistry, Faculty of Science, Tohoku University, Sendai 980, Japan

Abstract. The magnetic field dependence of CIDNP was measured for the photolysis of benzaldehyde. At high and low fields, respectively, the CIDNP behavior is satisfactorily interpreted by the $S\cdot I_a$ and $S\cdot T$ mixing of radical pair mechanism (RPM). At around 325 mT the CIDNP of the aldehyde proton is emissive, which cannot be interpreted by RPM. In order to understand this anomalous behavior, we observe the dynamic nuclear polarization.

The DNP sign shows that the cross-relaxation mechanism of the intermediate free radical is $\Delta m = 2$. With this result, the emissive CIDNP at 325 mT is interpreted by the triplet mechanism (TM) with cross-relaxation-induced polarization transfer from electron spin to nuclear spin.

Further, the time-resolved DNP is observed with laser excitation and switching of microwaves. With pulse excitation, the features of CIDNP and DNP are different from that with continuous light excitation. This is interpreted as due to the associated increase of the initial concentration of the ketyl radical. From the time dependence of the DNP intensity, the lifetime of the ketyl radical is estimated to be of the order of hundreds of nanoseconds.

Keywords. CIDNP, CIDNP-detected ESR, DNP, cross-relaxation

1. Introduction

The hydrogen abstraction reaction of benzaldehyde is one of the most interesting systems from the viewpoint of the CIDNP generation mechanism. A number of scientists (Closs and Paulson 1970; Cocivera and Trozzolo 1970; Atkins *et al* 1973; Frith and McLauchlan 1975) have studied the CIDNP with continuous light at high magnetic field, and the reaction scheme and the generation mechanism of the nuclear polarization have been thoroughly discussed. The time-resolved CIDNP has also been studied with laser excitation by Tsentalovich *et al* (1989) and the time-dependent feature of the free radical has been discussed. The CIDNP behavior reported so far is explained satisfactorily by RPM. Although the generation of CIDNP at higher fields in NMR is obvious, the CIDNP process at lower magnetic fields is not necessarily well understood.

As is discussed below, the CIDNP signal at a magnetic field of about 325 mT is anomalously polarized. A plausible pathway for this anomaly appears to be the triplet mechanism (TM) (Adrian *et al* 1976; Meng *et al* 1993), in which polarization transfers from electron spin to nuclear spin via cross relaxation. In order to examine the

*For correspondence

validity of the triplet mechanism in CIDNP, it is necessary to determine the mechanism of the cross-relaxation process ($\Delta m = 0$ or $\Delta m = 2$). The DNP technique is suitable for this because the sign of DNP directly reflects the type of cross-relaxation process as reported in the system of benzoquinone (Meng *et al* 1993). The DNP spectrum is a component of CIDNP-detected ESR, which is obtained by monitoring the microwave-induced nuclear polarization of the reaction product with different external magnetic fields. The effect of the microwave irradiation on the intermediate radicals should include two kinds of components: dynamic nuclear polarization (DNP) and stimulated nuclear polarization (SNP) (Bagryanskaya *et al* 1986). DNP is a microwave effect on free radicals. The saturation of electron-spin transition of free radicals generates nuclear polarization via cross relaxation. Therefore, generation of DNP is a competition between cross-relaxation time and free-radical lifetime. The sign of DNP is independent of hyperfine lines, and directly reflects the cross-relaxation mechanism ($\Delta m = 0$ or $\Delta m = 2$). The SNP is an effect of the microwave transition on radical pairs. Here the sign of SNP depends on hyperfine lines and the shape of SNP should be either E/A (emission at lower magnetic field and absorption at higher magnetic field) or A/E . We try to observe the CIDNP-detected ESR spectrum at around 325 mT to determine the sign of DNP; i.e. cross-relaxation process.

The dynamics of free radicals is closely related to generation of CIDNP by spin-polarization transfer which competes with the quenching of free radicals. DNP phenomena directly reflect the dynamics of free radicals and cross relaxation. Therefore we observed the time-resolved DNP with the switching microwave technique in order to discuss the time scale of dynamics of free-radical and spin-polarization transfer processes.

2. Experimental

The experimental set-up for DNP measurement is shown in figure 1. We used the flow system in order to carry out photoreaction in a variable JEOL RE-IX magnet, and the NMR spectrum was measured at high field in a JEOL JNM-FX100 NMR spectrometer. The sample was irradiated by a 500 W Hg-Xe arc lamp with a UV-D33S glass filter (which filters out $\lambda < 330$ nm) in the X-band ESR cavity. The X-band microwave is amplified with a 20 W continuous wave TWTA. The sample was transferred to the NMR magnet within two seconds. The DNP intensity is recorded as

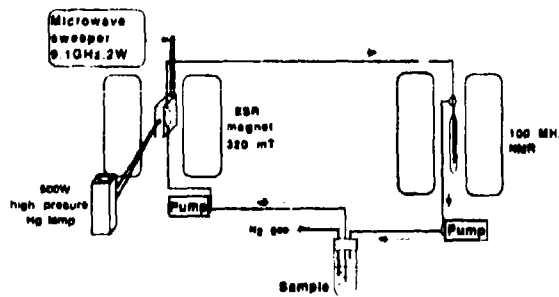


Figure 1. Block diagram of experimental set-up for DNP measurement.

the difference of NMR integral with and without microwave irradiation. The microwave power used in the experiment was two watts.

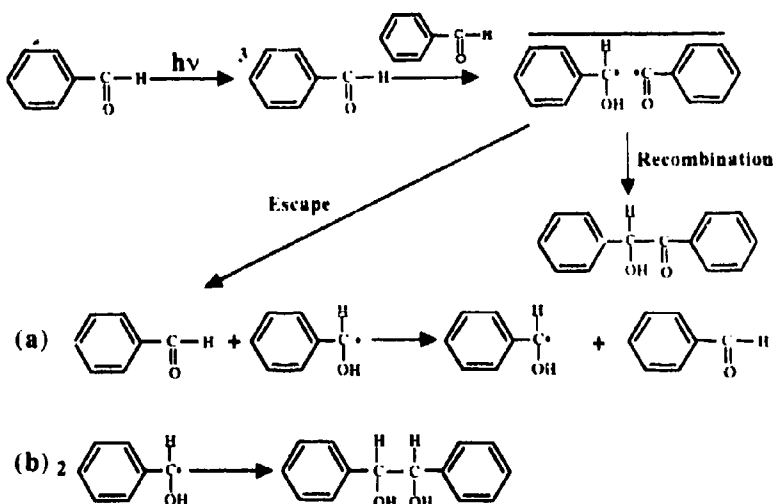
The time-resolved DNP experiment was performed by the switching microwave technique using a PIN diode switch and laser excitation with a Lumonics EX-400 (XeCl, $\lambda = 308$ nm) excimer laser. Microwave-pulse duration was 1 ms which covered the lifetime of the free radical. The solution was deoxygenated by the nitrogen-bubbling method. The solvent was a mixture of deuterated chloroform and carbon tetrachloride (volume ratio 1:1), and the concentration of benzaldehyde was ≈ 0.04 M.

3. Results and discussion

3.1 CIDNP and DNP effect with continuous excitation

In scheme 1, the hydrogen-abstraction reaction of benzaldehyde is outlined. The high field CIDNP spectrum was observed by a number of scientists (Closs and Paulson 1970; Cocivera and Trozzolo 1970; Atkins *et al* 1973; Frith and McLauchlan 1975) and the time-resolved CIDNP was observed by Tsentalovich *et al* (1989). The spectrum was completely explained by Kaptein's theory (Kaptein 1972) in terms of RPM with $S-T_0$ mixing. We observed the CIDNP spectrum (figure 2) at 325 mT with variable magnet and flow system. The aldehyde proton of benzaldehyde exhibits emissive nuclear polarization. At such a high field as 325 mT, $S-T_1$ and $S-T_2$ mixings can be ignored. Therefore this emissive nuclear polarization of the aldehyde proton is anomalous from the viewpoint of RPM. This brings the effect of cross relaxation into our attention.

In order to determine the cross-relaxation mechanism, we need to observe the DNP effect. Since DNP appears as a component of the CIDNP-detected ESR spectrum, we have measured the CIDNP-detected ESR spectrum. The observed spectrum is shown in figure 3. The observation that the CIDNP-detected ESR spectrum is totally



Scheme 1. Reaction scheme of photolysis of benzaldehydes in poor hydrogen donor solvents

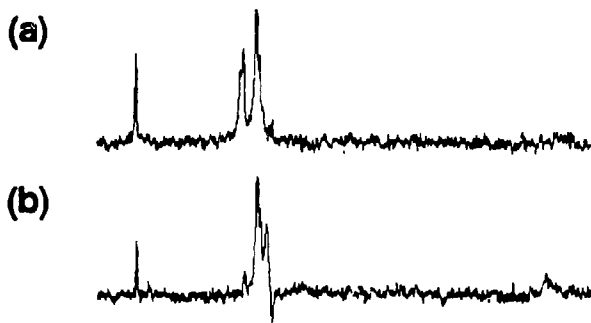


Figure 2. NMR spectra of benzaldehyde. (a) Before irradiation (b) CIDNP at 325 mT

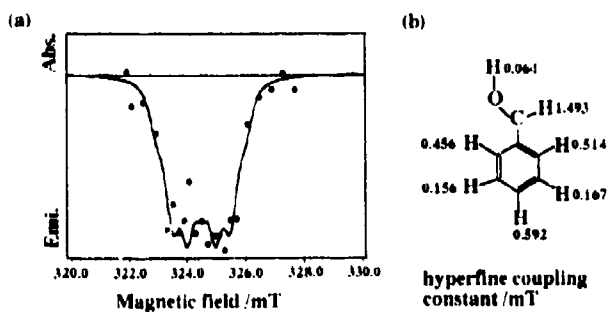


Figure 3. (a) CIDNP-detected ESR spectrum: Dots are experimental data, and solid line is simulated DNP spectrum using hyperfine coupling constants shown in (b).

emissive indicates that the SNP component is negligible, and we can therefore assign the observed spectrum as totally DNP. The solid line is the simulation using the hyperfine coupling constants reported by Wilson (1968). From the agreement between the observation and simulation, we conclude that the observed DNP spectrum is ascribed to the intermediate ketyl radical (α -hydroxybenzyl radical). This DNP spectrum is essentially the same as that reported by Grishin *et al* (1980).

The generation mechanism of DNP is shown in figure 4. The $\Delta m = 2$ cross-relaxation process generates emissive DNP, and the $\Delta m = 0$ generates absorptive DNP. Since the observed DNP is emissive, the cross-relaxation mechanism of the proton of ketyl radical which corresponds to the aldehyde proton of the reaction product (benzaldehyde) should be $\Delta m = 2$. With the cross-relaxation process of $\Delta m = 2$, we will discuss the generation mechanism of anomalous CIDNP signal at 325 mT. The ketyl radical is known to exhibit emissive CIDNP (Yamauchi and Hirota 1984), that is α -electron spin states are populated predominantly. This electron-spin polarization can be transferred to nuclear polarization by cross relaxation. The same mechanism has been observed in the hydrogen-abstraction reaction of benzoquinone and some of its derivatives (Adrian *et al* 1976; Meng *et al* 1993), and has been referred to the triplet mechanism of CIDNP, which is shown in figure 5. The α -electron spin states are initially more populated by the triplet mechanism. The $\Delta m = 2$ cross relaxation

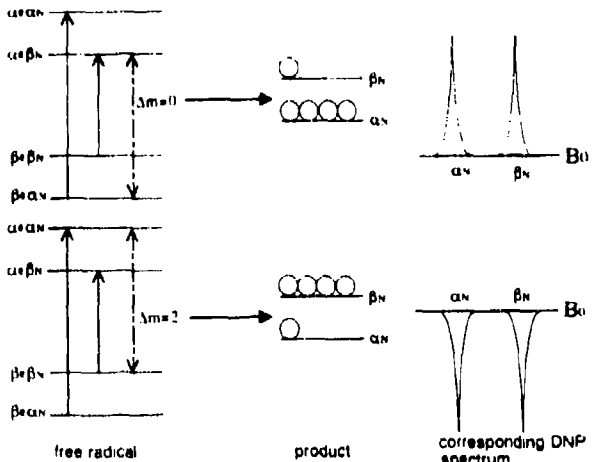


Figure 4. Schematic illustration of relationship between sign of DNP and cross-relaxation processes ($\Delta m = 0$ and $\Delta m = 2$).

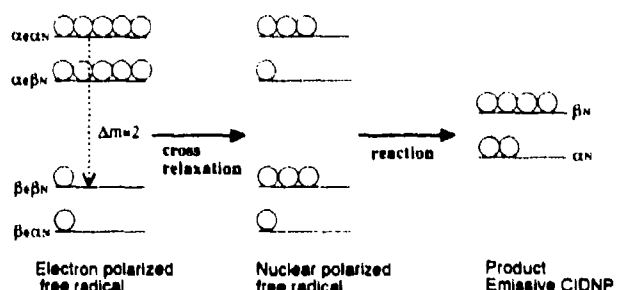


Figure 5. Generation mechanism of TM-induced CIDNP by $\Delta m = 2$ cross-relaxation in the case of emissive CIDEP.

($\alpha_e \alpha_N$ to $\beta_e \beta_N$) transfers the emissive electron polarization to the nuclear polarization. The termination of the nuclear spin-polarized free radicals generates the emissive nuclear-polarized diamagnetic products, which is observed as anomalous CIDNP at 325 mT.

3.2 Results of DNP measurements with laser excitation and time-resolved DNP measurements

NMR spectra with laser excitation are shown in figure 6. The feature of CIDNP at 325 mT is dramatically changed in comparison with the spectrum of continuous light excitation. As shown in figure 6b the CIDNP of the aldehyde proton is weakly absorptive which is explained in terms of RPM. Additionally, the NMR signal of this proton is not affected by microwave irradiation (figure 6c). In contrast, we observe the microwave-induced emissive nuclear polarization at the aromatic protons.

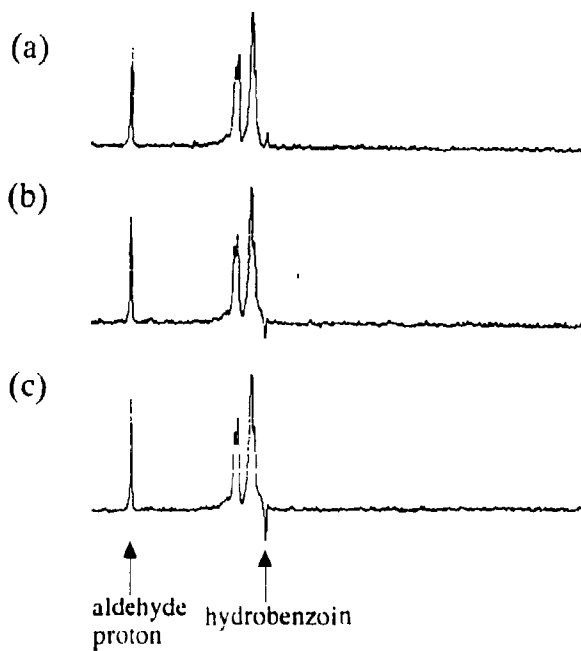


Figure 6. NMR spectra with laser excitation at 325 mT. (a) Before irradiation. (b) Irradiated by laser pulse (repetition rate is 15 Hz). (c) With laser and pulsed microwave irradiation (microwave delay time is ~ 300 ns).

This emissive nuclear polarization by microwave is DNP, not SNP, as is understood from the CIDNP-detected ESR spectrum, and the product which exhibits DNP is assigned as hydrobenzoin. The CIDNP signal of these protons was reported by Tsentalovich *et al* (1989) with time-resolved CIDNP technique at high magnetic field. In their experiment they also used an excimer laser whose pulse energy is about 40 mJ. We should consider that much higher initial concentrations of ketyl radical caused by strong laser power affect the features of CIDNP and DNP. The decay of ketyl radicals is determined by the competition between the recombination of two ketyl radicals which generates hydrobenzoin (reaction (b) in scheme 1) and hydrogen transfer from the ketyl radical to benzaldehyde which generates nuclear-polarized benzaldehyde (reaction (a) in scheme 1). Using very simplified kinetic treatment we calculated the yield of two kinds of products, nuclear-polarized hydrobenzoin and benzaldehyde. We used reaction rate constants reported at time-resolved CIDNP study by Tsentalovich *et al* (1989). The initial radical-concentration dependence of the yields of two products is shown in figure 7. The calculation shows that the hydrobenzoin should be dominant in case of very high initial concentration of ketyl radicals. Although it is difficult to estimate the initial concentration of the free radical exactly, the result of the calculation supports our experimental results qualitatively.

In order to estimate the lifetime of ketyl radicals with laser excitation, we measured the time-resolved DNP with switching microwave as shown in figure 8. The time

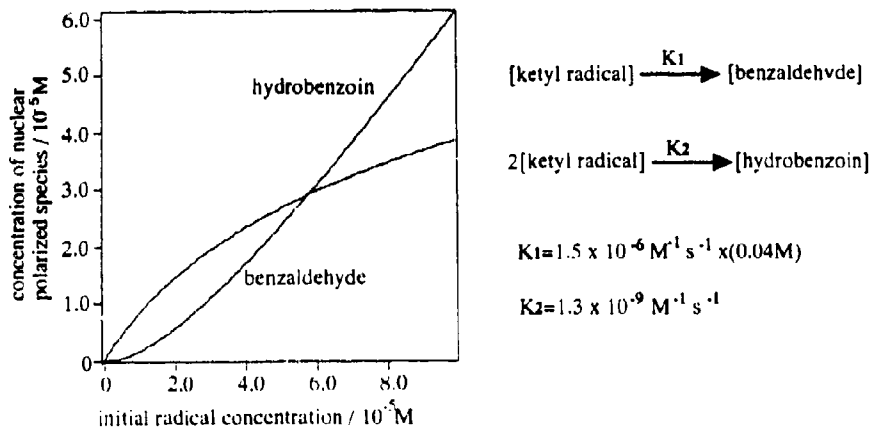


Figure 7. Results of simple reaction kinetics equation. Nuclear-polarized product concentrations are modulated by initial radical concentration.

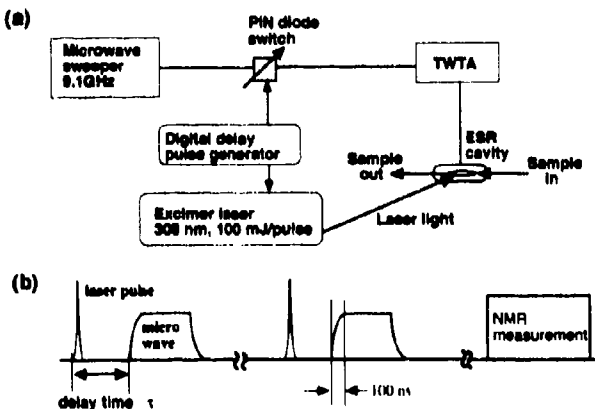


Figure 8. (a) Experimental set-up of time-resolved DNP. (b) Time sequence of excitation laser pulse and microwave pulse.

resolution of the time-resolved DNP measurement is determined by the response time of the microwave cavity, and is about 100 ns in our measurement. The delay-time dependence of DNP intensity (time-resolved DNP) with monitoring the aromatic protons of hydrobenzoin is shown in figure 9. The decay of the time-resolved DNP signal is about 250 ns, and we conclude that the ketyl radical disappeared within 250 to 350 ns after laser excitation by taking the response time of the microwave cavity into account. Although the lifetime of ketyl radicals is less than 350 ns, we could observe the DNP signal of the free radicals. This fact suggests a very fast polarization transfer of the aromatic protons of ketyl radicals from electron spin to nuclear spin. The time resolution of the time-resolved DNP is not enough to discuss the relation between reaction kinetics and dynamics of cross relaxation anymore. We are now developing a cavity with faster response time.

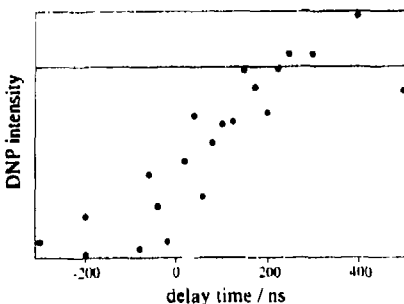


Figure 9. Delay-time dependence of DNP intensity monitoring aromatic protons of hydrobenzoin. Definition of delay time is shown in figure 8b.

4. Conclusion

The triplet mechanism-induced CIDNP should be taken into account for the analysis of the mechanism of CIDNP effect in addition to the radical pair mechanism. The sign of triplet mechanism-induced CIDNP is determined by the initial net electron polarization and the mechanism of cross relaxation ($\Delta m = 0$ or $\Delta m = 2$). The former factor can be determined by time-resolved ESR, and the latter one can be directly determined by the DNP sign. The time-resolved DNP method can give information about the time dependence of intermediate radicals and the cross-relaxation processes.

Acknowledgements

The present research was supported by a Grant-in-Aid for Scientific Research No. 03554013, No. 0474027 and a Grant-in-Aid for Scientific Research on Priority Areas "Molecular Based Magnetism" No. 04242102 from Japanese Ministry of Education, Science and Culture.

References

- Adrian F J, Vyas H M and Wan J K S 1976 *J. Chem. Phys.* **65** 1454
- Atkins P W, Frimston J M, Frith P G, Gurd R G and McLauchlan K A 1973 *J. Chem. Soc., Faraday II* **69** 1543
- Bagryanskaya E G, Tsentalovich Yu P, Avdievitch N I, Sagdeev R Z and Molin Yu N 1986 *Chem. Phys. Lett.* **12**
- Closs G L and Paulson D R 1970 *J. Am. Chem. Soc.* **92** 7229
- Cocivera M and Trozzolo A M 1970 *J. Am. Chem. Soc.* **92** 1772
- Frith P G and McLauchlan K A 1975 *J. Chem. Soc., Faraday II* **71** 1984
- Grishin Yu A, Gogolev A Z, Bagryanskaya E G, Dukushkin A V, Sagdeev R Z and Molin Yu N 1980 *Dokl. Akad. Nauk. SSSR* **255** 1160
- Kaptein R 1972 *J. Am. Chem. Soc.* **94** 6251
- Meng Q X, Suzuki K, Maeda K, Terazima M and Azumi T 1993 *J. Phys. Chem.* **97** 1265
- Tsentalovich Yu, Obnochny A A and Sagdeev R Z 1989 *Chem. Phys. Lett.* **139** 301
- Wilson R 1968 *J. Chem. Soc.* **B84** 1581
- Yamauchi S and Hirota N 1984 *J. Phys. Chem.* **88** 4631

Exciplex mechanism of fluorescence quenching in polar media

MICHAEL G KUZMIN*, NIKITA A SADOVSKII,
JULIA WEINSTEIN and OLEG KUTSENOK

Department of Chemistry, Moscow University, Moscow 117 234, Russia

Abstract. The formation of exciplexes (non-emitting or poorly emitting) is suggested as one of the causes for deviations of experimental data on fluorescence quenching in polar solvents from the classical model of excited-state electron transfer yielding radical ion pairs. Several evidences for the formation of such exciplexes were found for fluorescence quenching of aromatic compounds by weak electron donors and acceptors. For cyano-substituted anthracenes exciplex emission can be observed in the presence of quenchers even in polar solvents. In other systems, indirect evidences of exciplex formation were observed: nonlinear dependence of the inverse value of excited pyrene lifetime on the concentration of the quencher; very small and, in some cases, even negative experimental activation energies of pyrene fluorescence quenching, which are much less than activation energies calculated from the experimental values of the quenching rate constants etc.

The proposed model explains the difference between theoretical and experimental dependencies of $\log k_q$ vs. Gibbs energy of electron transfer ΔG_{ET} and other experimental features known for fluorescence quenching by electron donors and acceptors. This model states that the exciplex is in equilibrium with the encounter complex and apparent quenching rate constants are controlled by two main factors – the lifetime of the exciplex and the enthalpy of its formation. Experimentally observed dependence of apparent quenching rate constant on ΔG_{ET} is caused by the dependence of the exciplex formation enthalpy on ΔG_{ET} , which is quite different from the dependence of electron transfer activation energy on ΔG_{ET} predicted by the theoretical models. Simulations of the dependencies of $\log k_q$ vs. ΔG_{ET} according to the exciplex formation model confirms its agreement with the experimental data.

Electronic structure of the exciplex involved may be close to contact radical-ion pair only at $\Delta G_{ET} < 0$, when the rate of quenching is limited mainly by the diffusion, but for $\Delta G_{ET} > 0$, the structure of the exciplex should be much less polar.

Keywords. Fluorescence quenching; polar media; exciplex mechanisms; excited-state electron transfer.

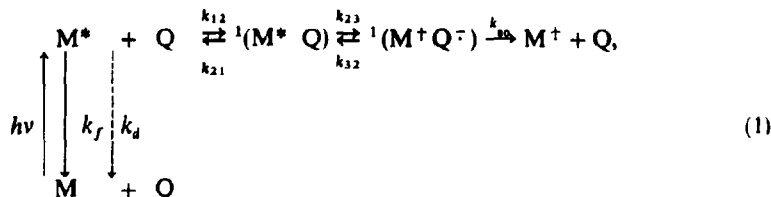
1. Introduction

Electron transfer photoreactions are very important in chemistry and biology. Excited-state electron transfer is supposed to be a general mechanism of fluorescence quenching in the absence of energy transfer and heavy atom effects. It is necessary to know the real mechanism of this process prior to the discussion of various theoretical models of electron transfer.

The classical kinetic scheme proposed by Rehm and Weller (1969, 1970) assumes

*For correspondence

that the electron transfer step yields contact radical-ion pairs which dissociate very fast in polar solvents (k_{30} is about 10^{11} s^{-1}):



$$k_0 = k_{1,2} / [1 + (1 + k_{3,2}/k_{3,0})k_{2,1}/k_{2,3}], \quad (2)$$

$$\varphi_0/\varphi = \tau_0/\tau = 1 + k_{\text{O}}\tau_0[\text{Q}], \quad (3)$$

where ϕ_0 , ϕ and τ_0 , τ are fluorescence quantum yields and lifetimes in the absence and in the presence of a quencher Q, respectively ($1/\tau_0 = k_f + k_s$).

A number of experimental investigations (Fox and Chanon 1988) showed the existence of the typical dependence of the quenching rate constants k_Q in polar solvents on the Gibbs energy of electron transfer ΔG_{ET} which has a diffusion limit for $\Delta G_{ET} \ll 0$ and kinetic limit for $\Delta G_{ET} \geq 0$. This experimental dependence is in good agreement with the kinetic scheme (1), if one assumes that activation energy of an electron transfer step depends on ΔG_{ET} according to the empirical Weller's equation (Rehm and Weller 1969, 1970).

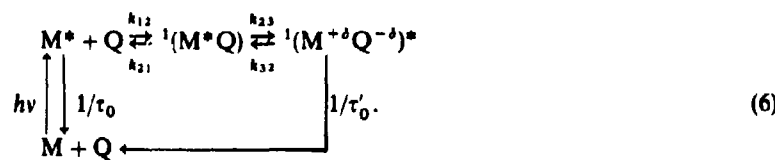
$$\Delta G_{23}^* = \Delta G_{\text{ET}}/2 + [(\Delta G_{\text{ET}}/2)^2 + (\Delta G_0^*)^2]^{1/2}, \quad (4)$$

or theoretical Marcus' equation (Marcus 1956).

$$\Delta G_{\text{23}}^* = \Delta G_0^*(1 + \Delta G_{\text{ET}}/a\Delta G_0^*)^2. \quad (5)$$

But numerous experimental data obtained in recent years for various systems (Hishimura *et al* 1977, Baggott and Pilling 1983, Kitamura *et al* 1987, Avila *et al* 1991, Carrera *et al* 1991, Neumann and Pastre 1991 etc.) have shown that such correlation is qualitative rather than quantitative. Wide scatter is observed for k_Q at $\Delta G_{ET} \geq 0$. Even values of k_Q greater than thermodynamically permitted for electron transfer were observed.

To find out the origin of these deviations we investigated fluorescence quenching kinetics and determined the activation energies of quenching from the temperature dependence of the apparent quenching constants in several systems. Fluorescence quenching of pyrene and 9-cyanoanthracene by some weak electron donors and acceptors was studied in acetonitrile ($\Delta G_{E1} \approx 0$) and in other solvents (Kuzmin and Soboleva 1986; Kuzmin *et al* 1992). We found several evidences that fluorescence quenching even in polar solvents can proceed by the formation of exciplexes rather than by direct electron transfer mechanism:



In the case of equilibrium between the excited molecules and the exciplex the value of the apparent quenching rate constant is controlled by the lifetime of the exciplex and equilibrium constant of its formation rather than by the rate constant of electron transfer.

Exciplexes are well known to be formed in electron transfer photoreactions in non-polar media (Gordon and Ware 1975). But in polar media no exciplex emission was observed in most cases and electron-transfer reactions are usually assumed to yield radical-ion pairs which dissociate very fast ($\sim 10^{-10} - 10^{-11}$ s) and produce free radical-ions.

Kinetics of exciplex formation in non-polar solvents were studied in various systems (Kuzmin and Soboleva 1986):



Fluorescence quenching follows the Stern-Volmer equation, but the observed Stern-Volmer quenching constant has completely different sense:

$$\varphi_0/\varphi = 1 + K_{SV}[Q] = 1 + k_1 \tau_0 [Q] / (1 + k_{-1} \tau'_0). \quad (8)$$

The ratio of exciplex (φ') and initial molecule (φ) fluorescence quantum yields linearly depends on the quencher concentration:

$$\varphi'/\varphi = k'_f k_1 \tau_0 [Q] / k_f (1 + k_{-1} \tau'_0). \quad (9)$$

Initial molecule fluorescence decay kinetics ($f(t)$) is biexponential and exciplex fluorescence kinetics ($f'(t)$) is the difference of the same exponents:

$$f(t) = f_0 [\alpha \exp(-t/\tau_1) + \exp(-t/\tau_2)], \quad (10)$$

$$f'(t) = f'_0 [\exp(-t/\tau_2) - \exp(-t/\tau_1)]. \quad (11)$$

Dependence of the lifetimes of these exponents on the quencher concentration, in the general case, is nonlinear and can be expressed by the following expressions:

$$\begin{aligned} 1/\tau_{1,2} &= 1/\tau_0 + k_1 [Q] + 1/\tau'_0 + k_{-1} \\ &\pm [(1/\tau_0 + k_1 [Q]) - 1/\tau'_0 - k_{-1}]^2 + 4k_1 k_{-1} [Q]]^{1/2}, \end{aligned} \quad (12)$$

$$\alpha = (1/\tau_0 + k_1 [Q] - 1/\tau_2) / (1/\tau_1 - 1/\tau_0 - k_1 [Q]). \quad (13)$$

In the case of reversible exciplex formation ($k_{-1} \gg 1/\tau'_0$, at $\tau_0 \gg \tau'_0$, the dependence of τ_0/τ_2 on $[Q]$ is sublinear (τ_1 is very short at $k_1 \tau_0 [Q] \gg 1$ and may be imperceptible)

$$\tau_0/\tau_2 \approx (1 + (\tau_0/\tau'_0) K_{Ex} [Q]) / (1 + K_{Ex} [Q]), \quad (14)$$

($K_{Ex} = k_{23}/k_{32}$ is the exciplex formation equilibrium constant), and has initial slope different from the Stern-Volmer constant for φ_0/φ and reaches the limit equal to τ_0/τ'_0 . With the increase of concentration of the quencher, the observed lifetime of M^* (which is in equilibrium with the exciplex) falls to the limit determined by the exciplex

lifetime. For $\tau_0 \ll \tau'_0$, the dependence of $1/\tau_2$ on $[Q]$ can even have a negative initial slope.

2. Evidence for exciplex formation in polar solvents

Fluorescence quenching of pyrene and 9-cyanoanthracene by some weak electron donors and acceptors in acetonitrile and other polar solvents follows the Stern-Volmer equation (figure 1)

$$\varphi_0/\varphi = 1 + K_{SV}[Q]. \quad (15)$$

A weak new emission band was observed for 9-cyanoanthracene in the presence of 1,6-dimethylnaphthalene (DMN) (figure 2) but no new emission bands were observed in the presence of the quenchers in most of the other systems investigated. This means that exciplexes have low emission rate constants or very short lifetimes. The apparent quenching rate constant according to scheme (6) can be expressed as

$$k_Q = K_{SV}/\tau_0 = k_1/(1 + k_{-1}\tau'_0). \quad (16)$$

The ratio of the emission quantum yields of 9-cyanoanthracene and its exciplex linearly depends on the concentration of DMN (figure 3) according to (9). Fluorescence decay kinetics of 9-cyanoanthracene in the presence of DMN is biexponential and fluorescence kinetics of its exciplex is the difference between the same exponents, [(10)-(11)].

Pyrene fluorescence decays monoexponentially (at least two orders of magnitude) in the absence and the presence of the quenchers but the lifetimes do not follow the

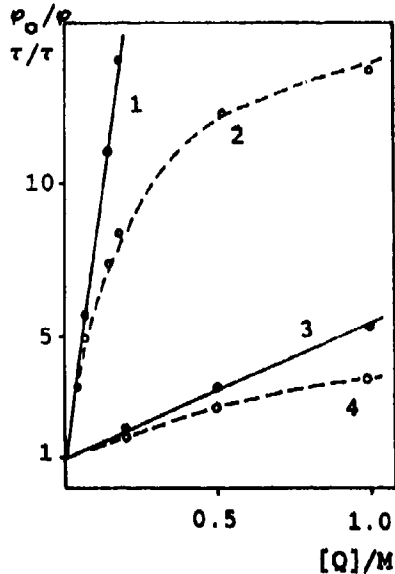


Figure 1. Plots of pyrene relative fluorescence quantum yields φ_0/φ (1, 3) and lifetimes τ_0/τ (2, 4) vs. concentration of dibutylphthalate in acetonitrile (1, 2) and in butyronitrile (3, 4).

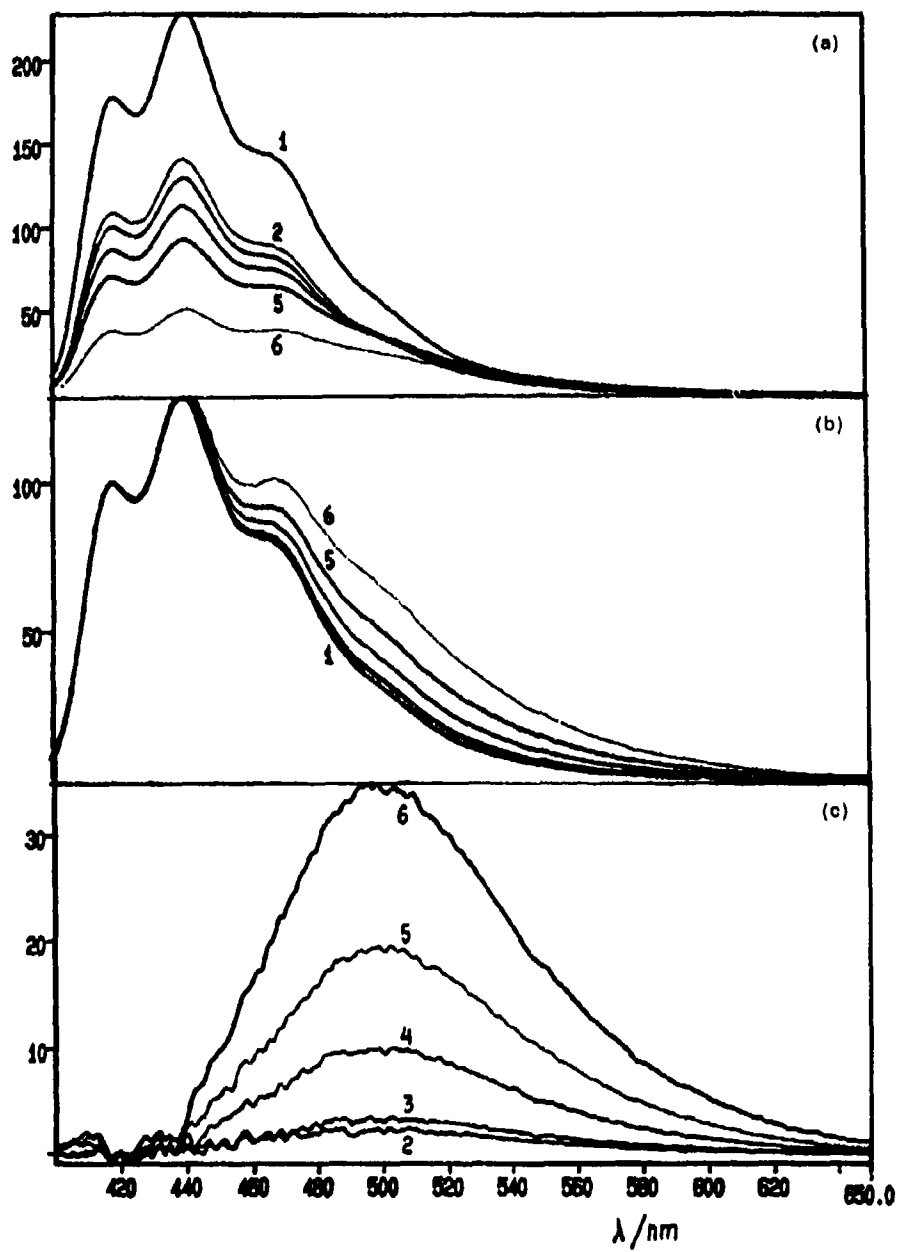


Figure 2. Uncorrected fluorescence spectra of 9-cyanoanthracene in the presence of various concentrations of 1,6-dimethylnaphthalene in acetonitrile (a) (1–6: 0, 2, 4, 9, 20, 40 mM), normalized fluorescence spectra (b) and exciplex emission spectra (extracted from overall spectra) (c).

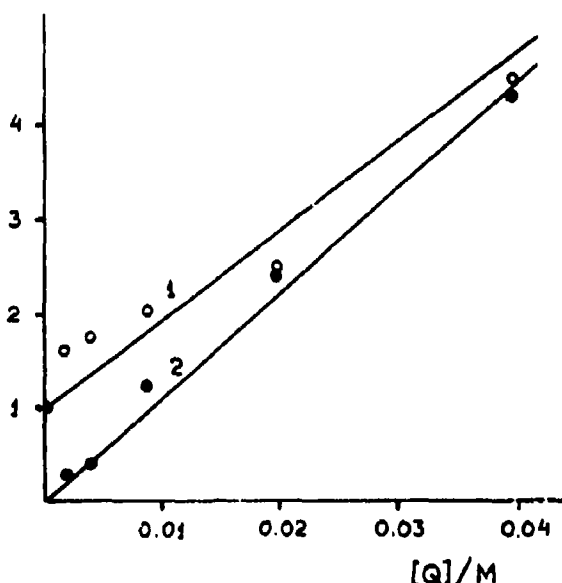


Figure 3. Plots of relative fluorescence quantum yields of 9-cyanoanthracene (φ_0 , φ , 1) and of the exciplex (φ , φ , 2) vs. concentration of 1,6-dimethylnaphthalene in acetonitrile.

Stern-Volmer equation – $1/\tau$ sublinearly depends on the quencher concentration (figure 1), which is typical for exciplex formation. (14). Plots of $[Q]/(\tau_0/\tau - 1)$ and $\varphi_0\tau/\varphi\tau_0$ vs. $[Q]$ give K_{Ex} and τ_0/τ'_0 :

$$[Q]/(\tau_0/\tau - 1) = (1/K_{Ex} + [Q])/(\tau_0/\tau'_0 - 1), \quad (17)$$

$$\varphi_0\tau/\varphi\tau_0 = 1 + K_{Ex}[Q]. \quad (18)$$

The values of K_{Ex} and τ'_0 obtained are given in table 1.

To confirm the nature of the nonlinear dependence of $1/\tau$ on $[Q]$ we studied this dependence in the presence of additional quenchers (O_2 and dimethylfumarate which quench both excited pyrene molecules and the exciplexes and change τ_0 and τ'_0) and obtained the same values of K_{Ex} . The observed difference in τ_0 and τ'_0 show that both excited pyrene molecules and exciplex are quenched by oxygen and by dimethylfumarate with diffusion rate constants. It is important that exciplex lifetimes are relatively long – from 10 to 30 ns. This means that the reason for the absence of exciplex emission for these systems is the very low value of the emission rate constant ($k_f < 10^6 s^{-1}$).

Another proof of exciplex formation is the very low (and in some cases even negative) value of experimental activation energy of quenching, determined from the temperature dependence of the apparent quenching rate constant in the range (-40) to ($+60$)°C. Apparent activation energy determined this way according to (16) is a sum of the exciplex formation enthalpy (negative) and its decay activation energy (small and positive).

Table 1. Experimental data for pyrene and 9-cyananthracene. Stern-Volmer fluorescence quenching constants K_{sv} , apparent quenching rate constants k_0 (at 298 K), experimental activation energies E_{app}^* and exciplex formation equilibrium constants K_{ex} and lifetimes τ_0 .

Quencher	Solvent	K_{sv} (M ⁻¹)	$k_0/10^7$ (M ⁻¹ s ⁻¹)	E_{app}^* (kJ/mol)	K_{ex} (M ⁻¹)	τ_0 (ns)
<i>Pyrene</i>						
DBP	MeCN	57	18	-4.6	4 ± 2	17 ± 5
	MeCN + O ₂				6 ± 2	8 ± 3
	MeCN + Q'				3 ± 2	8 ± 3
	PrCN	2.6	0.9	5.9	0.6 ± 0.4	35 ± 20
	AcOEt	2.0	0.9	5.7		
	CH ₂ Cl ₂	7.2	2.9	3.8		
	Toluene	2.3	0.8	7.1		
DEP	MeCN	57	18	-6.7		
DMB	MeCN	14	4.7	-7.0		
Et ₂ NH	MeCN	99	33	10.5		
BuNH ₂	MeCN	1.2	0.4	5.0		
<i>9-Cyananthracene</i>						
DMN	MeCN	80	490		45	260

Abbreviations: DBP = dibutylphthalate; DEP = diethylphthalate; DMB = 1,4-dimethoxybenzene; Et₂NH = diethylamine; BuNH₂ = *tert*-butylamine; Q' = dimethylfumarate; DMN = 1,6-dimethylnaphthalene; MeCN = acetonitrile; PrCN = butyronitrile; AcOEt = ethylacetate.

Formal activation energies E_{app}^* , calculated from the ratio of the diffusion rate constant in the solvent and apparent quenching rate constant at a given temperature (supposing that it is the activation enthalpy which is responsible for their difference) are about 14–26 and 20–25 kJ/mol greater than the respective experimental ones.

3. The nature of the exciplex

The electronic structure of exciplexes is usually represented by a combination of the wavefunctions of locally excited and charge transfer states (if the excited state of the quencher can be neglected owing to much higher excitation energy):

$$\Psi(AD)^* = a\Psi(A^*)\Psi(D) + b\Psi(A^-D^+). \quad (19)$$

Coefficients a and b depend on the difference of the energies of the locally excited and charge transfer states (which can be approximated by the enthalpy of an electron transfer ΔH_{ET}) and on the exchange interaction parameter β . Enthalpy of the exciplex ΔH_{ex} (neglecting the polarization of the solvent) and magnitude of electron transfer in the exciplex ${}^1(M^{-6}Q^{+6})^*$ depend on the same parameters:

$$\Delta H_{ex} \approx \Delta H_{ET}/2 - [(H_{ET}/2)^2 + \beta^2]^{1/2}, \quad (20)$$

$$\delta \approx 1/\{1 - (\Delta H_{ET}/\beta) \cdot [(1 + (\Delta H_{ET}/2\beta)^2)^{1/2} - \Delta H_{ET}/2\beta]\}. \quad (21)$$

The enthalpy of exciplex formation will be negative not only for negative ΔH_{ET} but

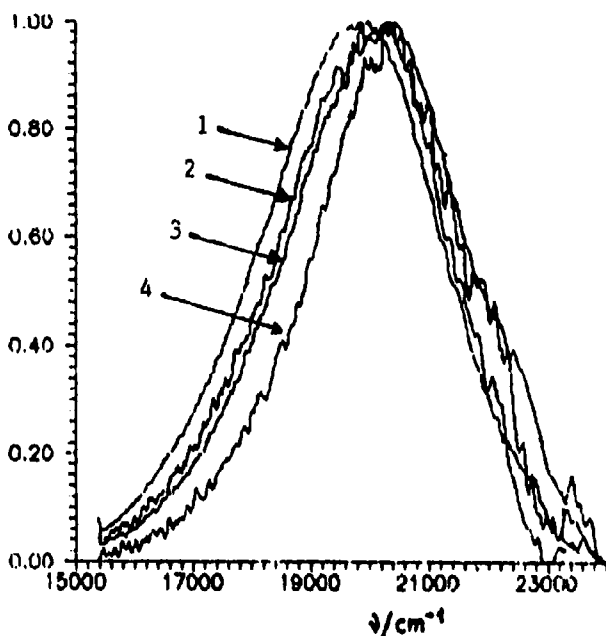


Figure 4. Corrected emission spectra of the exciplexes of 9-cyanoanthracene with 1,6-dimethylnaphthalene in acetonitrile (1), butyronitrile (2), dichloromethane (3), and toluene (4).

also for ΔH_{ET} close to zero and even positive ΔH_{ET} . For strongly negative ΔH_{ET} , $\delta \approx 1$ and ordinary polar exciplexes are formed whose structure is close to radical-ion pair. But for positive ΔH_{ET} , $\delta \ll 1$ and low polar exciplexes are formed (their electronic structure is similar to ordinary ground-state charge transfer complexes). According to (20) the smaller ΔH_{ET} , the greater the exciplex formation equilibrium constant $K_{Ex} = \exp(-\Delta G_{Ex}/RT)$. Emission maxima of the exciplex of 9-cyanoanthracene with 1,6-dimethylnaphthalene only slightly depends on the polarity of the solvent (figure 4) which confirms the low polarity of such exciplexes.

The emission bands of these low polar exciplexes can be very weak for several reasons: the low value of the equilibrium constant K_f and the low probability of radiative transition to the ground state. The emission band can also be masked by the main fluorescence band of pyrene.

Decay of the exciplex can also proceed by several ways: by internal conversion to the ground state (encounter complex M·Q), by intersystem crossing to the triplet state (triplet exciplex) and by dissociation on free radical-ions (solvated). All these processes should have sufficiently slow rates ($< 10^8 \text{ s}^{-1}$) to provide the relatively long lifetime of the exciplex ($> 10^{-8} \text{ s}$). For the latter process, this means that its activation energy is greater than 25 kJ/mol. Internal conversion and intersystem crossing can have low probability because of small values of Franck-Condon factor and spin-inversion factor respectively rather than because of high activation energy (which can be close to zero). All these four rate constants (including emission rate constant) should depend on the chemical nature of both fluorophore and quencher.

4. Simulation of the dependence of k_Q on ΔH_{ET}

We simulated the dependence of k_Q on ΔH_{ET} for both the kinetic models of fluorescence quenching, (1) and (6), using the following approximations.

Rate constants are expressed by the Arrhenius' equations

$$k_{ij} = k_{ij}^0 \cdot \exp(-E_{ij}^*/RT).$$

Encounter complex formation in acetonitrile

$$k_{12}^0 = 10^{11} \text{ M}^{-1}\text{s}^{-1}; \quad E_{12}^* = 5 \text{ kJ/mol}.$$

Equilibrium constant of encounter complex formation

$$k_{12}/k_{21} = 0.5 \text{ M}^{-1}, \quad \Delta H_{12} = 0.$$

For (1):

Electron transfer in the encounter complex

$$k_{23}^0 = 10^{11} \text{ s}^{-1}; \quad \Delta G_{23}^+ = (\Delta G_{ET}/2) + [(\Delta G_{ET}/2)^2 + (\Delta G_0^+)^2]^{1/2}, \\ \Delta G_0^+ = 10 \text{ kJ/mol}.$$

Radical-ion pair decay

$$k_{30} = 10^{11} \text{ s}^{-1}; \quad E_{30}^* = 0$$

For (6):

Exciplex formation

$$k_{23}/k_{32} = \exp(-\Delta H_{Ex}/RT); \quad k_{23}^0 = 10^{11} \text{ M}^{-1}\text{s}^{-1}; \\ \Delta H_{Ex} = (\Delta H_{ET}/2) - [(\Delta H_{ET}/2)^2 + \beta^2]^{1/2}; \quad \Delta H_{ET} \approx \Delta G_{ET}; \\ E_{23}^+ = (\Delta H_{Ex}/2) + [(\Delta H_{Ex}/2)^2 + (\Delta H_0^+)^2]^{1/2}, \quad \Delta H_0^+ = 10 \text{ kJ/mol};$$

β -variable parameter (initial value $\beta = E_F^+ - E_{Exp}^+ = -15 \text{ kJ/mol}$).

Exciplex decay

$$1/\tau'_0 = k_{30}^0 \exp(-E_{30}^*/RT)$$

$k_{30}^0 = A$ and $E_{30}^* = E$ are variable parameters.

For (6) apparent quenching rate constants k_Q were calculated from

$$k_Q = 10^{11} \exp(-5/RT) / \{1 + 2 \times 10^{11} \exp(-5/RT) / (10^{11} \exp(-E_{23}^*/RT)) \\ + 2 \times 10^{11} \exp(-5/RT) \cdot \exp(\Delta G_{Ex}/RT) / (A \cdot \exp(-E/RT))\}. \quad (22)$$

Simulated dependence of $\ln k_Q$ on ΔG_{ET} according to the classical scheme (1) (curve 1) and the exciplex scheme (6) for various values of β and τ'_0 (curves 2-9) are given in figure 5. For $\Delta G_{ET} \approx 0$, quenching rate constants according to (6) are smaller than those for (1). For $\Delta G_{ET} \gg 0$, the quenching rate constants do not depend on ΔG_{ET} and are greater than those expected according to the classical scheme (1). In this region of ΔG_{ET} values the quenching of excited molecules results from their

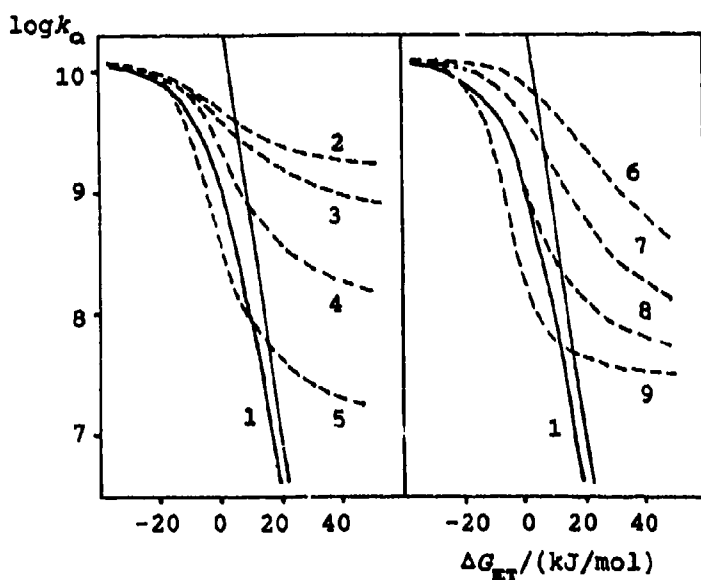


Figure 5. Plots of apparent fluorescence quenching rate constants ($\ln k_q$) on Gibbs energy of electron transfer ΔG_{ET} according to kinetic schemes (1) and (6): 1 - simulation according to scheme (1); 2-9 - simulation according to scheme (6). 2-5 - $\beta = 10 \text{ kJ/mol}$, $\tau'_0 = 0.01$, 1, 10, 100 ns; 6-9 - $\tau'_0 = 30 \text{ ns}$, $\beta = 20, 15, 10, 5 \text{ kJ/mol}$.

conversion to the exciplex. A limiting value of the apparent quenching rate constant and the slope of the plot of $\log k_q$ vs. ΔG_{ET} are functions of τ'_0 and β .

At fixed τ'_0 values, the rise of β will result in the contraction of the range of the dependence of k_q on ΔG_{ET} and increase in the limiting value of k_q (curves 2-4). At sufficiently large values of β , the quenching rate constant does not depend on ΔG_{ET} in the whole range $\Delta G_{ET} > 5 \text{ kJ/mol}$ because of the irreversibility of the exciplex formation. This exciplex decays by internal conversion and/or by intersystem crossing.

At fixed values of β , the decrease of the exciplex lifetime τ'_0 results in the increase of the quenching rate constant (curves 5-7). The greater the value of β , the greater the stability of the exciplex and the smaller the effect of τ'_0 on the apparent quenching rate constant. At sufficiently large values of β , the lifetime of the exciplex does not affect the quenching because of the irreversibility of the exciplex formation.

Activation energy of quenching can vary in wide range from negative to positive values in accordance with the parameters β , ΔG_{ET} and τ'_0 .

The exciplex scheme (6) represents quite well the experimental data for temperature-dependence of the apparent rate constant of pyrene fluorescence quenching by dibutylphthalate in acetonitrile at the following values of the parameters: $\beta = -13.5 \text{ kJ/mol}$, $A = 1.1 \times 10^9 \text{ s}^{-1}$, $E = 10 \text{ kJ/mol}$, $\Delta G_{ET} = -2 \text{ kJ/mol}$ (figure 5). In butyronitrile the best fit of the experimental data was obtained at $\beta = -10 \text{ kJ/mol}$, $A = 0.9 \times 10^9 \text{ s}^{-1}$, $E = 11 \text{ kJ/mol}$, $\Delta G_{ET} = +9 \text{ kJ/mol}$ (figure 5). At 20°C k_{30} is equal to $5 \times 10^7 \text{ M}^{-1} \text{s}^{-1}$ in acetonitrile and $3 \times 10^7 \text{ M}^{-1} \text{s}^{-1}$ in butyronitrile which are close to the values determined directly from fluorescence kinetics (table 1). In less polar butyronitrile

the value of β is slightly smaller than in acetonitrile. The values of activation energy and pre-exponential factor of exciplex decay are close in both solvents.

5. Quenching dynamics

Let us consider the nature of the potential barriers, along with the reaction coordinate in the course of fluorescence quenching, taking into account exchange interactions between reactants (coupling of locally excited and charge transfer states) in the frame of very simple approximations (figure 6).

For positive ΔG_{ET} (figure 6, top) as the reactants D^* and A approach each other, the energy decreases according with increase of the overlap of the wavefunctions of the reactants (increase of the exchange interaction energy β) and decrease of the energy (E_2) of the charge transfer state ($D^+ A^-$).

$$E \approx [(E_1 + E_2)/2] - [(E_1 - E_2)^2/4 + \beta^2]^{1/2}, \quad (23)$$

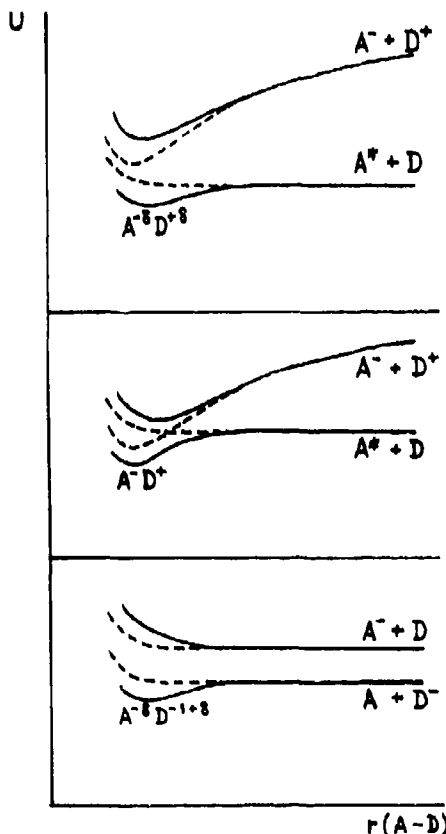


Figure 6. Potential energy curves for exciplex formation and electron transfer at $\Delta G_{ET} > 0$ (top) and at $\Delta G_{ET} < 0$ (middle) for uncharged reactants, and for an uncharged and a charged reactant (bottom).

where E_1 is the energy of the locally excited state (D^*A). An exciplex with a modest degree of electron transfer is formed. The degree of electron transfer increases gradually as reactants approach each other and solvent reorganization also gradually follows the polarization of the encounter complex.

Three potential barriers along with the reaction coordinate for the exciplex formation and subsequent complete electron transfer can arise. The first one is the diffusion barrier which has the usual activation energy in the range 5–10 kJ/mol. The second is the activation energy of exciplex formation which can be formally approximated by:

$$E_{23} = (\Delta H_{ET}/2) + [(\Delta H_{ET}/2)^2 + (\Delta H_0^+)^2]^{1/2}; \quad (24)$$

assuming $\Delta H_0^+ = 10$ kJ/mol, similar to Weller's model (this value was found to be unessential for the results of the simulations since equilibrium between the exciplex and the reactants is established at $\Delta G_{ET} > 0$).

Complete electron transfer in this exciplex needs activation energy of about $[\Delta H_{ET}^2 + 4\beta^2]^{1/2}$ and yields a contact radical-ion pair (which can dissociate on free (solvated) radical-ions). Therefore, dominant ways of decay of the exciplex formed are internal conversion, intersystem crossing and emission (which do not need substantial activation energy), rather than complete electron transfer and formation of radical-ions. The rates of the first two radiationless decay processes may be very responsive to the chemical nature of the reactants. Therefore the lifetime of the exciplex can vary in the wide range $\sim 10^{-12} - 10^{-7}$ s and may depend on the chemical nature of both excited molecule and quencher.

For negative ΔG_{ET} (middle part of figure 6), the approach of the reactants towards each other can also be followed by the gradual increase of the charge separation but (in contrast to $\Delta G_{ET} > 0$) it finally produces a radical-ion state. This is the most well-known kind of exciplex. Along with reaction coordinates, the exchange interaction and the magnitude of charge transfer increase gradually. The solvent reorganization also occurs gradually and reorganization energy is much smaller than is expected from the Marcus theory.

Completely different nature of the activation barrier can be expected for electron transfer charged and uncharged molecules (figure 6, bottom). In this case, electrostatic interaction does not exist in either the initial or the final states and the potential curves of both the states in the first approximation are parallel to each other. For exergonic ($\Delta G_{ET} < 0$) electron transfer the inclusion of exchange interactions will produce the repulsion of the potential curves (the rise of the energy of the initial state $D^* + A$ which can be expressed by the analog of (21) but with the positive sign ahead of the square root). This rise of energy will depend on the distance of electron transfer and will build up an additional potential barrier for electron transfer. Therefore, some additional contribution to the activation energy of electron transfer due to an exchange interaction between reactants must be taken into account in the models of electron transfer processes at negative ΔG_{ET} .

Conclusions

The model assuming the formation of sufficiently long-lived (up to 10–50 ns) exciplexes even in polar solvents is able to explain and quantitatively describe the experimentally observed abnormal temperature effect and lifetime dependence of fluorescence quenching

in polar solvents and also the deviations of the experimental dependence of the quenching rate constants on ΔG_{ET} from that predicted by the electron transfer theory of the quenching (especially in the kinetic region). The stabilization energy of the exciplex at positive ΔG_{ET} can arise from exchange interactions between reactants (similar to ground state CT complexes); such exciplexes may have a low contribution of charge transfer state. The radiationless decay of the exciplex does not need any activation energy. This mechanism does not suppose the necessity of complete electron transfer between reactants in the excited state. Therefore, fluorescence quenching cannot be used with confidence for the verification of the theories of electron-transfer processes and for the determination of the redox-potentials of quenchers.

The exciplex model of quenching supposes that there are two main parameters - exciplex formation equilibrium constant K_{ET} and its lifetime τ'_0 - which determine the apparent value of the fluorescence quenching rate constant. The abnormal temperature effect arises from the negative enthalpy of the exciplex formation (in contrast to the positive activation energy of electron transfer).

The correlation between quenching rate constants and the free energy of electron transfer ΔG_{ET} has different origins in the classical Weller's model, (1), and in the exciplex model, (2). In the classical model, two parameters which control the value of the quenching rate constant are the activation energy of isoergonic reaction ΔG_0^+ and the lifetime of the radical-ion pair ($1/k_{30}$). The last one was supposed to be 0.01 ns and ΔG_0^+ was found to be 10 kJ/mol (Rehm and Weller 1970). The last one, ΔG_0^+ , was assumed to be variable to explain the variations in the $\log k_Q$ vs. ΔG_{ET} relationships.

In the exciplex model (6), the dependence of apparent quenching rate constants on ΔG_{ET} arises from the dependence of the exciplex formation enthalpy on ΔG_{ET} , (20). The lifetime of the exciplex may exceed by many orders of magnitude the lifetime of radical-ion pairs in polar solvents and can vary in a very wide range, depending on the chemical structure of both the excited molecule and quencher. Positive and negative deviations from classical Weller's curve $\log k_Q$ vs. ΔG_{ET} may arise from the variations of the dependence of K_{ET} on ΔG_{ET} and from the variations of τ'_0 . In consistence with numerous experimental data the slope of $\log k_Q$ vs. ΔG_{ET} plot in the kinetic region in the frame of the exciplex model (6) as a rule is much smaller than for thermodynamic limit (which is 5.9 kJ per one logarithmic unit).

References

- Avila V, Cosa J J, Chesta C A and Previtali C M 1991 *J. Photochem. Photobiol.* **A62** 83
Baggott J E and Pilling M J 1983 *J. Chem. Soc., Faraday Trans.* **79** 221
Carrera A, Cosa J J and Previtali C M 1991 *J. Photochem. Photobiol.* **A56** 267
Fox M A and Chanon M (eds) 1988 *Photoinduced electron transfer* (Amsterdam: Elsevier) vol. A D
Gordon M and Ware W R (eds) 1975 *The exciplex* (New York: Academic Press)
Hishimura T, Nakashima N and Mataga N 1977 *Chem. Phys. Lett.* **46** 334
Kitamura N, Obata R, Kim H -B and Tazuka S 1987 *J. Phys. Chem.* **91** 2033
Kuzmin M G, Sadovskii N A, Weinstein J A and Soloveichik O M 1992 *High Energy Chem.* **26** 522 (in Russian)
Kuzmin M G and Soboleva I V 1986 *Prog. React. Kinet.* **14** 157
Neumann M G and Paatre I A 1991 *J. Photochem. Photobiol.* **61** 91
Marcus R A 1956 *J. Chem. Phys.* **24** 966
Rehm D and Weller A 1969 *Ber. Bunsenges Phys. Chem.* **73** 834
Rehm D and Weller A 1970 *Israel J. Chem.* **8** 259

The spectra, lifetime and laser activity of 2,5-bis(1-naphthyl)vinylpyrazine and 2,5-bis(2-naphthyl)vinylpyrazine

SAMY A EL-DALY¹, EL-ZEINY M EBEID^{1*},
SADIQ M EL-HAZMY², ABDALLAH S BABAQI²,
ZENAT EL-GOHARY³ and GUY DUPORTAIL⁴

¹Department of Chemistry, Faculty of Science, Tanta University, Tanta, Egypt

²Department of Chemistry, Faculty of Science, Sana'a University, Sana'a, Republic of Yemen

³Physics Department, Faculty of Science, El-Monufia University, Shebin El-Kom, Egypt

⁴Laboratoire de Biophysique, Faculté de Pharmacie de Strasbourg, Université Louis Pasteur, Strasbourg, France

Abstract. Both 2,5-bis(1-naphthyl)vinylpyrazine (BNVP) and 2,5-bis(2-naphthyl)vinylpyrazine (B2NVP) diolefinic dyes have relatively short excited-state lifetimes, high fluorescence efficiencies and low photochemical quantum yields. BNVP solutions in dimethyl formamide and methylene chloride give amplified spontaneous emission (ASE) with a maximum at 500 nm. The low solubility of B2NVP in organic solvents does not allow the measurement of ASE for this dye. The excited state absorption spectra (ESA) of BNVP show an absorption band around 525 nm which reduces dye laser efficiency.

Energy transfer from 7-diethylamino-4-methylcoumarin to BNVP and B2NVP has been studied by applying Stern-Volmer plots. The underlying mechanism is a radiative long range energy transfer.

Both BNVP and B2NVP undergo solubilization in anionic as well as cationic micelles.

Keywords. Diolefinic dyes; excited-state lifetimes; fluorescence quantum yields; amplified spontaneous emission.

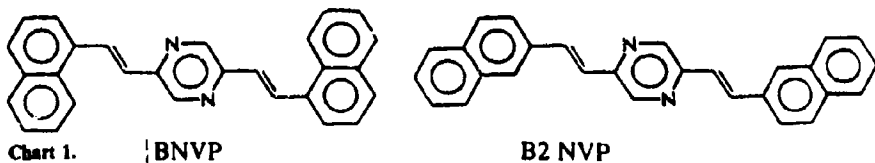
1. Introduction

Diolenic compounds containing pyrazinyl moieties have been reported as important candidates in many research areas. 2,5-Distyrylpyrazine (DSP) was the first reported derivative to undergo solid state four-centre photopolymerization giving rise to a highly crystalline polymer (Hasegawa 1982, 1983; Hasegawa *et al* 1988). Members of this family of compounds have been recently reported as organic electroluminescent crystals giving high brightness at a low DC voltage of about 10 volts (Nohara *et al* 1990).

One of the most important applications of these compounds is their use as laser dyes (Ebeid *et al* 1985, 1986; Hasegawa *et al* 1989). Dye laser emission from DSP (Ebeid *et al* 1985) and 1,4-bis(β -pyrazinyl-2-vinyl) benzene (BPVB) (Ebeid *et al* 1986) was observed upon pumping concentrated solutions of these dyes using a nitrogen laser source.

*For correspondence

In the present communication we report the emission characteristics, lifetime values and amplified spontaneous emission of BNVP and B2NVP (chart 1).



2. Experimental

BNVP and B2NVP samples were kindly provided by Professor Masaki Hasegawa of Tokyo University. The last crystallization of BNVP (m.p. 213–214.5°C) was from toluene and that of B2NVP (m.p. 319–320°C) was from xylene. Fluorescence spectra and fluorescence quantum yields (ϕ_f) were measured using a Shimadzu RF 510 spectrofluorophotometer using diphenylanthracene and quinine sulphate as reference standards (Morris *et al* 1976). Photochemical quantum yields (ϕ_c) were measured using a method that has been described earlier (Ebeid *et al* 1986). UV-visible absorption and reflectance spectra were measured using a Shimadzu UV-2100S spectrophotometer. Fluorescence lifetimes were measured using single-photon counting and phase and modulation fluorimetry. In the single-photon counting technique, fluorescence decays were recorded using an ORTEC single-photon counting apparatus equipped with a hydrogen flash lamp operating at about 15 kHz. Excitation wavelengths were selected using a Bausch and Lomb UV-Visible monochromator (type 33-80-07, 1200 grooves/mm). The emission wavelength was selected using appropriate interference filters (Schott, Mainz, Germany). The data were registered in a 400-channel analyser with a linearity of 0.174 ns/channel. The decay profiles were analysed by iterative convolution using autocorrelation and residuals criteria (Grinvald and Steinberg 1974; Demas 1983). Phase and modulation lifetimes were measured using an SLM-48000 fluorimeter. For high dye concentrations, a triangular cuvette was used to minimize reabsorption in both lifetime and fluorescence measurements. For dilute solutions a 4 mm optical length cuvette was used.

Amplified spontaneous emission (ASE) as well as excited state absorption (ESA) were kindly carried out by Professor Ewald Daltrozzo of the University of Konstanz (Germany).

Differential thermal analysis (DTA) was carried out using a Shimadzu XD-3U thermal analyser. Molecular weights of irradiated and unirradiated BNVP and B2NVP samples were monitored using a Knauer Vapour Pressure Osmometer.

3. Results and discussion

BNVP and B2NVP are of the same molecular weight, yet the reported melting point of B2NVP is nearly 100°C higher than that of BNVP. This has been confirmed by using DTA. DTA thermograms also indicate the absence of thermal processes other than melting up to $\approx 350^\circ\text{C}$. The wide difference in melting points reflects different molecular packing and interactions in crystalline samples. Excitation ageing of

crystalline BNVP and B2NVP samples results in a decrease in emission and excitation intensities indicating photochemical reactivity. This is a particularly significant phenomenon since both BNVP and B2NVP thin films have been applied (Nohara *et al* 1990) in electroluminescent devices and photochemical reactivity is an undesired phenomenon in that respect.

Reflectance spectra of BNVP and B2NVP crystals also indicate a solid state photochemical reaction in these samples. The reflectance maxima at ≈ 420 nm in BNVP and that at ≈ 400 nm in B2NVP decrease in intensity with concomitant appearance of reflectance maxima at 280 and 220 nm for BNVP and B2NVP samples, respectively. Further studies are needed to identify the photochemical product(s) that are believed to be oligomers obtained by $\pi-\pi$ addition of the olefinic double bonds as reported earlier for similar diolefinic derivatives (Hasegawa 1982, 1983).

The electronic absorption, emission and excitation spectra of BNVP and B2NVP solutions in DMSO solvent are shown in figure 1. The electronic absorption spectrum of BNVP in DMSO consists mainly of symmetrical absorption bands around

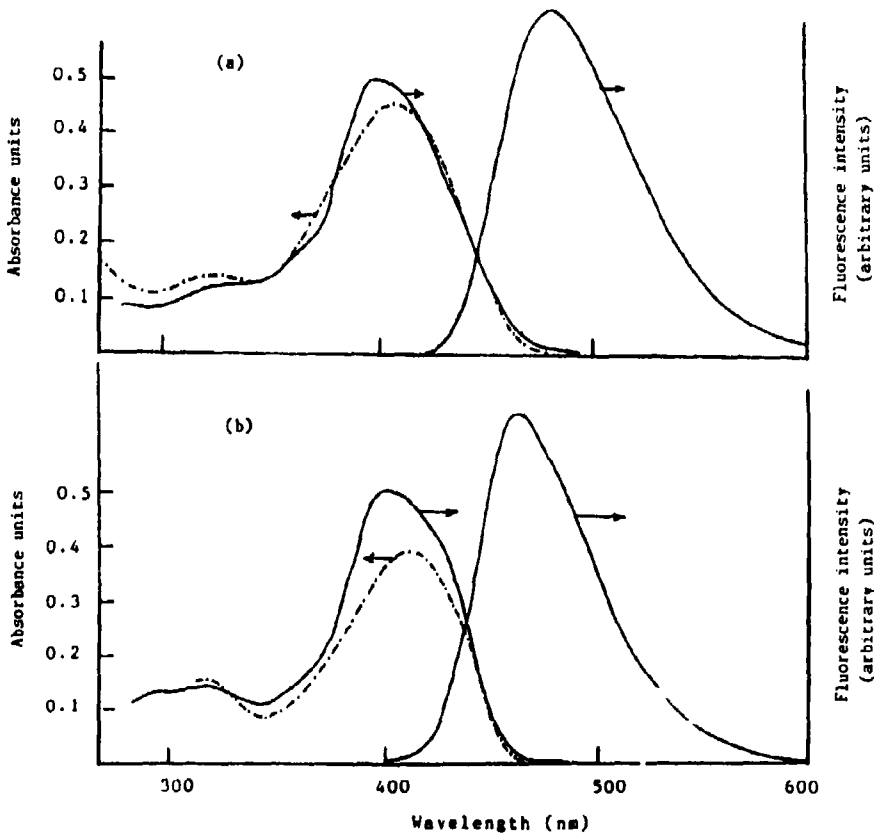


Figure 1. The emission, excitation and absorption spectra of (a) BNVP, and (b) B2NVP solutions in DMSO (10^{-3} mol dm $^{-3}$). (—) emission ($\lambda_{\text{em}} = 410$ nm) and excitation (following the respective emission maxima and (---) Absorption spectra.

≈ 405 nm with molar absorptivity $\epsilon_{\text{max}} = 45,500 \text{ dm}^3 \text{ mol}^{-1} \text{ cm}^{-1}$; the emission spectrum is unsymmetrical with a maximum at 480 nm ($\lambda_{\text{ex}} = 410$ nm).

For B2NVP both absorption and emission spectra in DMSO are unsymmetrical with an absorption maximum at 410 nm and an emission maximum at 460 nm. The emission from BNVP occurs at lower energy as compared to that from B2NVP, a phenomenon that is related to excited state solvation. The longer lifetime of BNVP as compared to that of B2NVP (*vide infra*) allows greater solvation of the BNVP excited state as compared with that of B2NVP.

The position of emission maxima for both BNVP and B2NVP is dependent upon the solvent polarity Δf , where Δf is given by the relation (Rao *et al* 1976; Brecht 1986).

$$\Delta f = \frac{(\epsilon - 1)}{(2\epsilon + 1)} - \frac{(n^2 - 1)}{(4n^2 + 2)}$$

where ϵ and n are the dielectric constant and the refractive index of the solvent respectively. A linear correlation exists between λ_{max} (emission) and Δf for both BNVP and B2NVP with λ_{max} increasing as Δf increases. The effect of medium polarity on the absorption maxima of both dyes is insignificant. These phenomena are diagnostic for excited states that are more polar than the ground state (Griffith 1976). The electronic absorption, emission and excitation spectra of BNVP and B2NVP dilute solutions ($\approx 10^{-5} \text{ mol dm}^{-3}$) undergo change upon UV-irradiation ($\lambda_{\text{ex}} = 365$ nm). The underlying photoreaction in such dilute solutions of diolefinic derivatives is thought to be a *cis-trans* photoisomerization.

The photochemical quantum yields (ϕ_f) are low and the ϕ_e and fluorescence quantum yields ϕ_f are summarized in table 1.

The effects of the medium on the spectra of BNVP and B2NVP have been further studied in relation to the acidity of the medium and the micellization phenomenon. The electronic absorption spectra of both dyes in ethanol do not change significantly on lowering the pH of the medium down to a value of 1. In 0.8 mol dm^{-3} ethanolic

Table 1. ϕ_f and ϕ_e values of BNVP and B2NVP in different media at room temperature

Dye	Medium	$\phi_f, \lambda_{\text{ex}} =$			ϕ_e
		365 nm	337 nm	$\lambda_{\text{ex}} = 365$ nm	
BNVP	EtOH	0.52	0.47	1.03×10^{-4}	
	BuOH	0.67	0.56		
	DMSO	0.72	0.64		
	Cyclohexane	0.72	0.66		
	SDS ($8 \times 10^{-3} \text{ mol dm}^{-3}$)	0.60	0.52		
	CTAC (0.1 mol dm^{-3})	0.50	0.38		
B2NVP	EtOH	0.64	0.45	2.6×10^{-4}	
	MeOH	0.65	0.42		
	BuOH	0.75	0.46		
	DMSO	0.74	0.57		
	Acetone	0.64	0.58		
	CHCl ₃	0.63	0.56		
	Ethylene glycol	0.49	0.26		

solutions of HCl, a yellow protonated product is obtained and fluorescence efficiencies of both dyes decrease substantially. The effect of acidity of the medium on the emission properties is particularly important in relation of pH-tuning in dye lasers (Weller 1961; Dienes 1975).

Both BNVP and B2NVP undergo solubilization in anionic (e.g. sodium dodecyl sulphate, SDS) and cationic (e.g. cetyltrimethylammonium chloride, CTAC) micelles. The solubilization process is associated with an increase in the fluorescence intensities. Plots of the surfactant concentrations versus fluorescence intensities of both dyes show abrupt increase in fluorescence intensities at surfactant concentrations corresponding to the critical micelle concentrations (cmc) of SDS and CTAC which is the case for many organic dyes (Muthuramu and Ramamurthy 1984).

The lifetimes of BNVP and B2NVP in DMSO are summarized in table 2.

Table 2. Lifetime values of BNVP and B2NVP in DMSO at room temperature.

Sample	Concentration (mol dm ⁻³)	λ_{ex} (nm)	λ_{em} (nm)	τ (ns)			
				Single photon	Phase + modulation	Phase only	Modulation only
BNVP	10^{-5}	405	485	1.82	1.77	1.76	1.78
	10^{-3}	365	485	2.11			
B2NVP	10^{-5}	410	481	1.38	1.32	1.31	1.34
	$\approx 10^{-4}$	365	481	1.33			

The lifetimes are short both for dilute and concentrated solutions. We found no evidence for molecular aggregation in concentrated solutions (10^{-4} mol dm⁻³) of both dyes, giving emission spectra that are slightly red-shifted compared with those of dilute dye solutions due to reabsorption. The lifetimes also reveal one decay component in both dilute and concentrated solutions. The absence of molecular aggregation is of great significance since molecular aggregation is usually associated with fluorescence quenching via excimer formation (Jones 1990; Gilbert and Baggott 1991) and is conducive to bimolecular photochemical reactions (Suzuki *et al* 1974). The lifetimes in DMF and CH₂Cl₂ are close to those in DMSO. For BNVP the lifetimes are 1.66 and 1.53 ns in DMF and CH₂Cl₂, respectively.

Solutions of BNVP in dimethyl formamide (DMF) and in methylene chloride (CH₂Cl₂) of concentration 2.98×10^{-4} mol dm⁻³ give amplified spontaneous emission (ASE) with a maximum at 500 nm. The solubility of B2NVP in both solvents was too low to allow any ASE measurements and laser emission was not observed from B2NVP solutions solely because of lack of solubility. The excited singlet-state absorption (ESA) cross-section σ_A^* of BNVP is shown in figure 2. The ground state absorption cross-section (σ_A), the emission cross-section (σ_E) as well as the effective emission cross section σ_E^* are also shown in figure 2.

The emission cross-section σ_E was calculated from the relation (Nair 1982)

$$\sigma_E(\lambda^4 E(\lambda)\phi_f)/(8\pi\tau_f cn^2),$$

where $E(\lambda)$ is the normalized fluorescence lineshape function at a certain wavelength (λ) such that

$$\int_0^\infty E(\lambda)d\lambda = \phi_f,$$

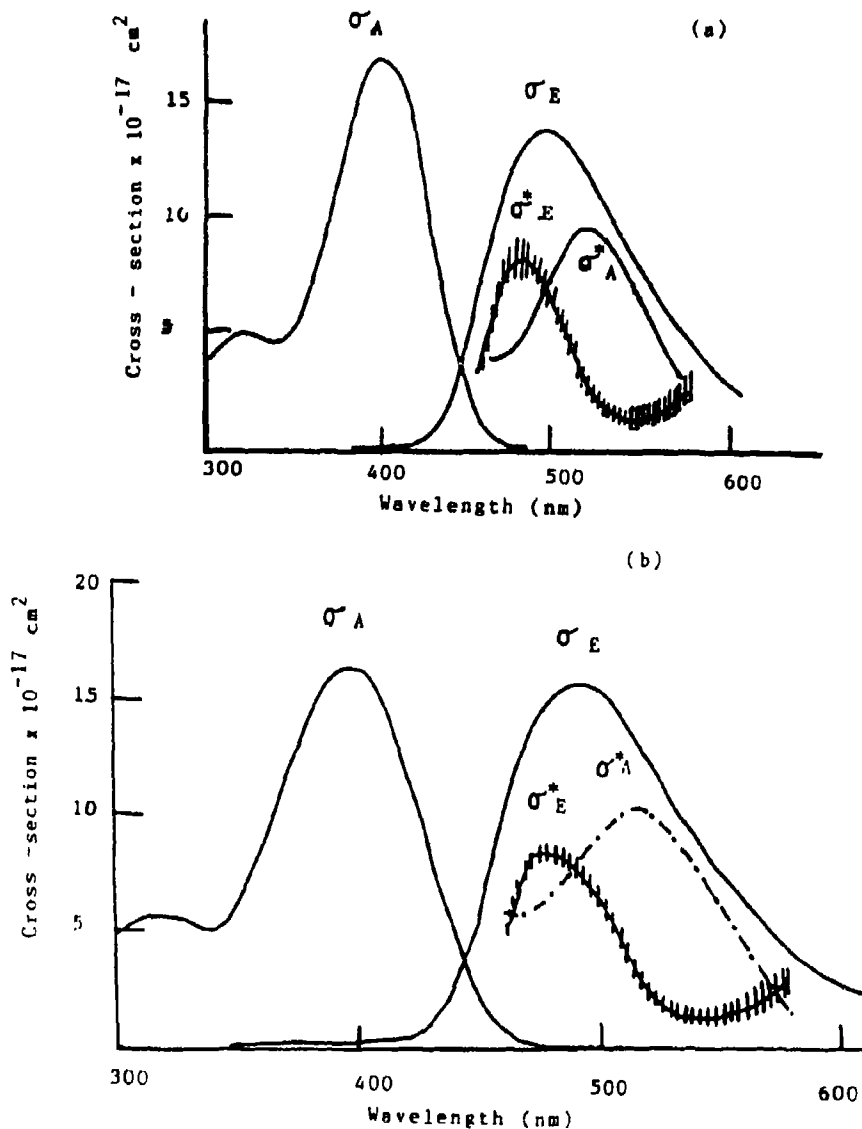


Figure 2. The cross-sections (in units of cm^2) of some processes in BNVP in (a) DMF, and (b) CH_2Cl_2 . σ_A and σ_E are the ground state absorption and emission cross-sections. σ_A^* is the excited state absorption cross-section and σ_E^* is the effective emission cross-section where $\sigma_E^* = (\sigma_E - \sigma_A^*)$.

n is the refractive index of the dye solution, τ is the fluorescence lifetime and c is the velocity of light. $E(\lambda)$ was obtained from the fluorescence spectra of dilute dye solutions to minimize reabsorption.

The ground-state absorption cross-section σ_A was calculated in terms of values of

molar absorptivities $\epsilon(\lambda)$ (Nair 1982) where

$$\sigma_A(\lambda) = 3.82 \times 10^{-21} \epsilon(\lambda).$$

Both emission and absorption cross-sections are given in units of cm^2 .

The effective emission cross section σ_E^* is given as the difference $(\sigma_E - \sigma_A^*)$. In DMF and CH_2Cl_2 , the results are similar, showing an absorption band around 525 nm in the first excited singlet state. This absorption reduces the dye laser efficiency and seems to be common for the derivatives with a central pyrazine ring system e.g. 2,5-distyryl pyrazine (DSP) and 1,4-bis(β -pyrazinyl-2-vinyl) benzene (BPVB) (El-Daly *et al* 1993). Members of the same diolefinic laser dye series containing pyridyl moieties namely 1,4-bis(β -pyridyl-2-vinyl) benzene (P2VB) and its isoelectronic dye 1,4-bis(4-pyridyl-2-vinyl)benzene (P4VB) are more efficient laser dyes as compared to BNVP, BPVB and DSP. It was shown (El-Daly *et al* 1993) that σ_E^* values in case of diolefinic dyes containing a pyrazinyl moiety are higher than those in dyes containing a pyridyl moiety. This view, however, has to be substantiated by examining more compounds.

The harvesting of BNVP and B2NVP to pump nitrogen laser photons can be improved by using mixtures of these dyes with other suitable laser dyes, e.g. 7-diethyl amino-4-methylcoumarin in the form of the energy transfer dye laser (ETDL) system.

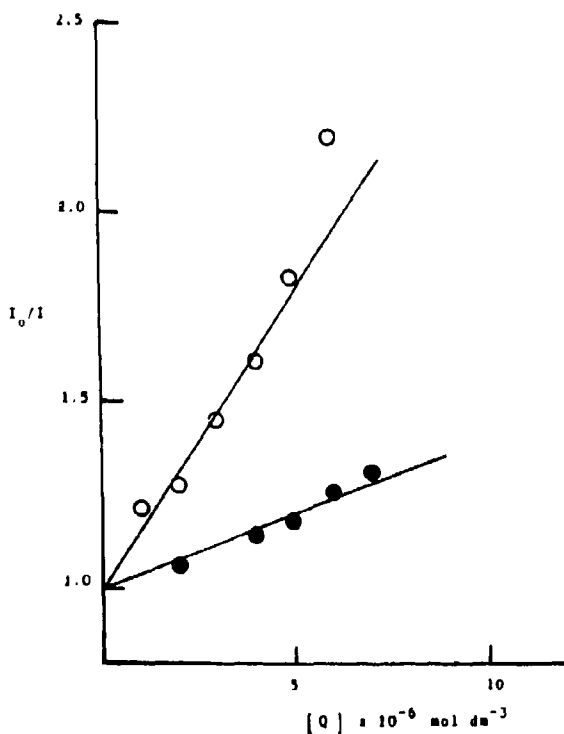


Figure 3. Stern-Volmer plots of the quenching of 7-diethylamino-4-methylcoumarin fluorescence using (●) BNVP and (○) B2NVP as quenchers in DMSO at room temperature $\lambda_{ex} = 337 \text{ nm}$ and $\lambda_{em} = 450 \text{ nm}$.

Both BNVP and B2NVP act as good photon acceptors from 7-diethylamino-4-methyl-coumarin that has maximum absorption at 373 nm in ethanol and maximum emission at 450 nm. Figure 3 shows the Stern-Volmer plots of quenching of 7-diethylamino-4-methylcoumarin fluorescence using BNVP and B2NVP as quenchers. The room temperature second-order quenching rate constants k_q in DMSO have been calculated from the slopes and the lifetime of 7-diethylamino-4-methyl coumarin of 3.6 ns (Masilamani and Sivaram 1982). The quenching rate constants (k_q) for BNVP and B2NVP in DMSO at room temperature are 1×10^{13} and $4.36 \times 10^{13} \text{ dm}^3 \text{ mol}^{-1} \text{ s}^{-1}$ respectively. These values are about three orders of magnitude higher than the diffusion rate constant (k_{diff}) in DMSO at room temperature ($= 0.37 \times 10^{10} \text{ dm}^3 \text{ mol}^{-1} \text{ s}^{-1}$). The high quenching rate constant, together with the overlap between the donor emission and the acceptor absorption, indicates a diffusionless long range radiative energy transfer mechanism.

Acknowledgements

We thank Professor Masaki Hasegawa of Tokyo University for providing BNVP and B2NVP samples. We also thank Professor Ewald Doltrozzo of Konstanz University, Germany, for measuring the ASE and ESA using apparatus not available to us.

References

- Brech E 1986 *Anal. Chem.* **58** 384
- Demas J N 1983 *Excited state lifetime measurements* (New York, London: Academic Press) chap. 6, and references therein
- Dienes A 1975 In *Laser applications to optics and spectroscopy* (eds) S Jacobs, M Sargent III, J F Scott and M O Scully (London, Tokyo: Addison-Wesley) chap. 2
- Ebeid E M, Issa R M, El-Daly S A and Sabry M M F 1986a *J. Chem. Soc., Faraday Trans. II* **82** 1981
- Ebeid E M, Issa R M, Ghoneim M M and El-Daly S A 1986b *J. Chem. Soc., Faraday Trans. I* **82** 909
- Ebeid E M, Sabry M M F and El-Daly S A 1985 *Laser Chem.* **5** 223
- El-Daly S A, Ebeid E M and Doltrozzo E 1993 (unpublished results)
- Grinvald A and Steinberg I Z 1974 *Anal. Biochem.* **59** 583
- Griffith J 1976 *Colour and constitution of organic molecules* (London: Academic Press) p. 76
- Gilbert A and Baggott J 1991 *Essentials of molecular photochemistry* (London, Paris: Blackwell Scientific Publications) p. 145
- Hasegawa M 1982 *Adv. Polym. Sci.* **42** 1
- Hasegawa M 1983 *Chem. Rev.* **83** 507
- Hasegawa M, Harashina H and Hosokawa T 1989 *Jpn. Kokai Tokkyo Koho Jap. Patent* 89-75618
- Hasegawa M, Katsumata T, Uo Y, Suigo K and Itaka Y 1988 *Macromolecules* **21** 3134
- Jones G H 1990 In *Dye laser principles with applications* (eds) F J Duarte and L W Hillman (London, New York: Academic Press) p. 301
- Masilamani V and Sivaram B M 1982 *J. Luminesc.* **27** 137
- Morris J V, Mahaney M A and Huber J R 1976 *J. Phys. Chem.* **80** 969
- Muthuramu K and Ramamurthy V 1984 *J. Photochem.* **26** 57
- Nair L G 1982 *Prog. Quant. Electron.* **7** 153
- Nohara M, Hasegawa M, Hosokawa C, Tokallin H and Kusumoto T 1990 *Chem. Lett.* **2** 189
- Rao C N R, Singh S and Senthilnathan V P 1976 *Chem. Soc. Rev.* **5** 297
- Suzuki F, Tamaki T and Hasegawa M 1974 *Bull. Chem. Soc. Jpn.* **47** 210
- Weller A 1961 In *Progress in reaction kinetics* (ed.) G Porter (London: Pergamon) vol. 1, chap. 7

Room-temperature phosphorescence of 2,2'-biquinoline in polymeric matrices

C CAZEAU-DUBROCA^{*1}, A PEIRIGUA¹, G NOUCHI¹,
M FADOUACH² and Ph CAZEAU³

¹Centre de Physique Moléculaire Optique et Hertzienne, UA 283 CNRS, Université de Bordeaux I, 351 Cours de la libération, 33405, Talence, France

²Laboratoire de Spectrométrie et Physique Appliquée, Université Mohammed V, Faculté des Sciences, Rabat, Maroc

³Laboratoire Chimie Organique du Silicium et de l'Etain, UA 35 CNRS, Université de Bordeaux I, 351 Cours de la libération, 33405, Talence, France

Abstract. An original and very strong long-lived emission of 2,2'-biquinoline is observed in hydrogen-bonded polymeric matrices only. This long-lived emission ($\tau_{ph} = 1$ s) is ascribed to room-temperature phosphorescence (RTP) because of the large value of the decay time, the temperature-dependence, and the polarization results.

The existence of hydrogen-bonded complexes in the ground state is assumed to be the origin of the RTP. They involve changes in the conformation of the 2,2'-biquinoline.

Keywords. H-bonded polymeric matrices; room-temperature phosphorescence, 2,2'-biquinoline.

1. Introduction

The photophysics and photochemistry of ligand molecules of various complexes of metals and ligands have been investigated because of their particular relevance in a large range of applications (Ohno and Kato 1974; Clarke *et al* 1980; Vinodgopal and Leenstra 1985; Yagi *et al* 1985; 1991). The double molecule 2,2'-biquinoline (2,2'-BQ) is a typical chelating agent for metal ion: with possible *cis* and *trans* conformations. Properties of the triplet state of 2,2'-BQ have been studied by various techniques: by steady state ESR (Higuchi *et al* 1980) and by Raman and ODMR techniques (Clarke *et al* 1982). Some studies on 2,2'-biquinoline complexes have stressed the close connection between the metal complex formation and the conformational changes in the ligand molecule (Klassen 1976; Frederiks *et al* 1979; Higuchi *et al* 1980, 1986).

Our interest in this molecule arises from earlier observations on other double molecules such as 1,1' and 2,2'-binaphthyl. In a previous study on the luminescence of 2,2'-binaphthyl solutions, we showed an anomalous dependence of the ratio I_{phos}/I_{flu} , versus excitation, at nitrogen liquid temperature (Fadouach *et al* 1992). This anomalous behaviour is due to the charge transfer (CT) character of highest singlet states (S^*); we assumed the existence of various conformers more or less twisted as

*For correspondence

the origin of this behaviour. These conformers seemed, to be depending on the viscosity of the environment and its ability to form hydrogen bonds. The present study on the 2,2'-BQ is now performed, largely to increase the phosphorescence (and make the phenomenon more sensitive) because the presence of the lone pair orbital of intracyclic nitrogen has to increase the intersystem crossing (and, thus the phosphorescence), due to the presence of the n,π^* states. In the present study, when including the 2,2'-BQ in various polymeric matrices, we show evidence for an original and strong room temperature phosphorescence (RTP). This RTP only appears in the case of hydrogen-bonded polymeric matrices.

In recent years the phenomenon of RTP has attracted large interest, and so also its application in spectroscopic analysis (Vo-Dinh 1984). In 1974, Winefordner and coworkers (Wellon *et al* 1974; Vo Dinh and Hooyhman 1979) established the general use of RTP as an analytical technique. Although many basic aspects of RTP remain to be explained, this phenomenon received immediate attention and rapidly found its place as a new spectrochemical technique for trace organic analysis.

2. Experimental techniques

2,2'-Biquinoline was purchased from Fluka Chemica AG, and checked for luminescent impurities by thin layer chromatography (TLC). As no impurities were observed, the compound was used without further purification. All solvents (Aldrich) used were of spectroscopic grade. Polyethylene (PE) films, of thickness about 50 and 100 μ , are commercially available. Polyvinylchloride (PVC) films were either XVPH type of thickness about 17 and 19 μ (kindly donated by Grace Society) or O'Kay type commercially available of about the same thickness. Polyvinylalcohol (PVA) films were made in the laboratory with rhodoviol pellets (Rhône-Poulenc 30S). Melamine formal (MF) was graciously provided by Polrey, SA.

2,2'-Biquinoline was introduced into the matrices by direct inclusion during film elaboration (PVA, MF) or by absorption from an *n*-hexane solution and evaporation of the solvent (PE, PVC). All the films were washed with *n*-butylchloride and dried carefully before use. All absorption spectra were recorded on a Cary 118 Varian spectrometer, and emission and excitation spectra on a Jobin-Yvon JY3CS spectrofluorimeter with a 150 W xenon lamp. 2,2'-BQ concentration in the films was of the order of 10^{-3} M.

3. Experimental results

3.1 Absorption

2,2'-Biquinoline is included in several polymeric matrices, more or less polar, able or not, to undergo hydrogen bonding: PE or PVC was the nonhydrogen-bonded matrix and MF or PVA was the hydrogen-bonded matrix. The absorption spectra in these different matrices are very similar to those in solution; the first structured band between 355 and 280 nm looks like that of quinoline (same global shape, same structure) but red-shifted (about 40 nm), involving a larger delocalization of the aromatic ring orbital. The second unstructured band presents a similar quasi red-shift

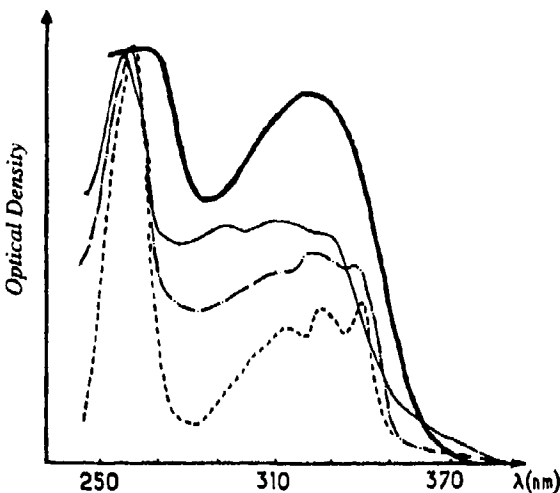


Figure 1. Absorption spectra of 2,2'-BQ in different polymeric matrices at room temperature (concentration $\approx 10^{-5}$ M), with optical density calibrated on the maximum (260 nm) of the second absorption band: — MF matrix; - - - rigid PVA matrix; - · - soft PVA matrix; ···· PVC matrix.

($\lambda_{\max} \approx 260$ nm). The increasing of the matrix polarity does not change very much with the absorption spectra (from PE to PVC), but the relative oscillator strengths of these first bands are very sensitive to increase of hydrogen bonding. Figure 1 shows the absorption spectra of the 2,2'-BQ in MF (of very strong rigidity), in PVA (rigid and soft matrix successively), and PVC. A similar effect of hydrogen bonding on the absorption spectra of 2,2'-BQ has been observed by decreasing the temperature of solutions in methylcyclohexane containing some traces of water in it, proof of stabilization of the hydrogen-bonded complexes at low temperature (unpublished results).

The relative variation of the oscillator strengths of the two first bands of 2,2'-BQ is probably due to deformation of the conformation, involving coupling of the two quinolic parts. The large flexibility of this molecule is coherent with the calculation results: very weak energetic barrier around the C₂-C_{2'} bond (about 1 kcal). A similar deforming role of hydrogen bonding has been already shown in the case of various TICT molecules (Cazeau-Dubroca 1991; Cazeau-Dubroca *et al* 1992).

3.2 Emission

In nonhydrogen-bonded polymeric matrices, only normal fluorescence is observed at room temperature. In hydrogen-bonded polymeric matrices, a very intense long-lived emission also appears (figure 2a). This emission is ascribed to room temperature phosphorescence (RTP) because of the following reasons:

- (a) the large similitude of the emission shape (same structure) to that of the one observed at liquid nitrogen temperature, in the case of solutions or polymeric matrices (figure 2b- α).

- (b) the polarization of this long-lived emission is negative, when excited by both the first bands of the absorption spectrum ($S_0 \rightarrow S_1^*$), ($S_0 \rightarrow S_2^*$), and involves the ${}^3\pi, \pi^*$ character of the emissive triplet state (figure 2b- β) at room temperature as at liquid nitrogen temperature (more negative indeed, in this last case).
- (c) the very large value of the lifetime, τ_D (decay time), in the range of about one second (figure 3a), is specific of either a phosphorescence issue to a ${}^3\pi, \pi^*$ triplet state or an α -delayed fluorescence (as in the case of DMABN in PVA at room temperature, for instance (Cazeau-Dubroca et al 1983, 1986), the emissive TICT state being populated through the highest vibrational levels of the triplet state).
- (d) the temperature dependence is specific of phosphorescence: a continuous decrease of emission intensity on increasing the temperature, from liquid nitrogen temperature to room temperature, is observed (figure 3b).

Elsewhere this RTP depends on excitation wavelength: the ratio $I_{\text{phos}}/I_{\text{flu}}$ increases on increasing the wavelength excitation; the 340 nm wavelength seems to be "optimum" for the excitation of RTP, this means a larger efficiency for the RTP owing to more "red" conformer corresponding to the less energetic spectrum. The excitation spectra of fluorescence and phosphorescence, respectively, are the same. Indeed, this RTP is very dependent on the rigidity of the matrix.

We have to note that this RTP looks like that of the quinoline (very weak, increased by heavy atoms) in a special matrix (chalk and paper) (Ford and Hurtubise 1979). The

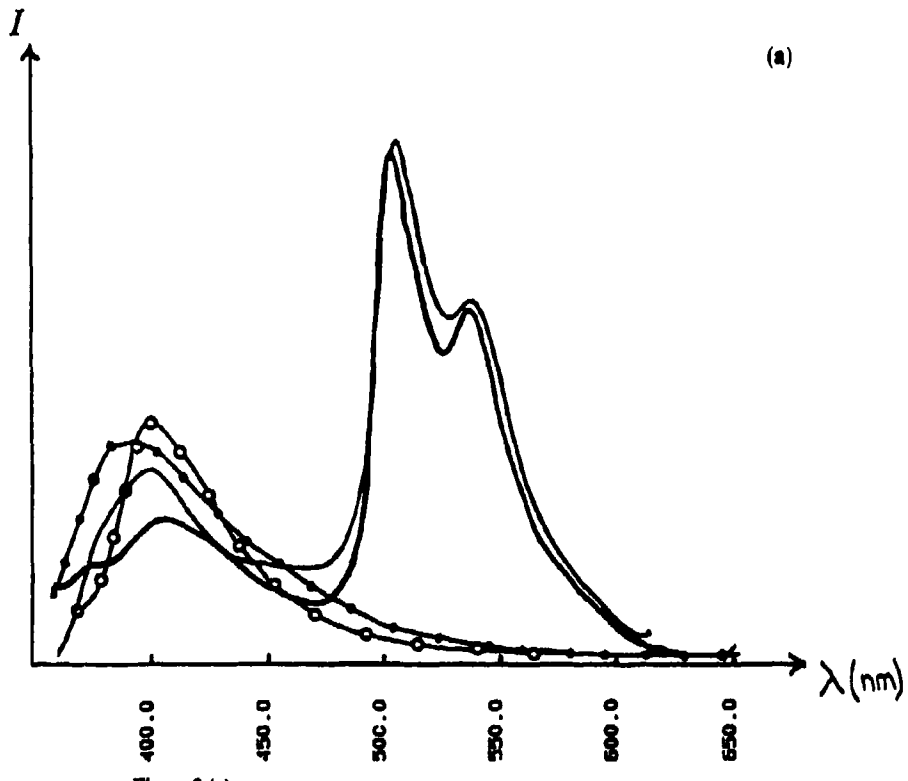


Figure 2.(a)

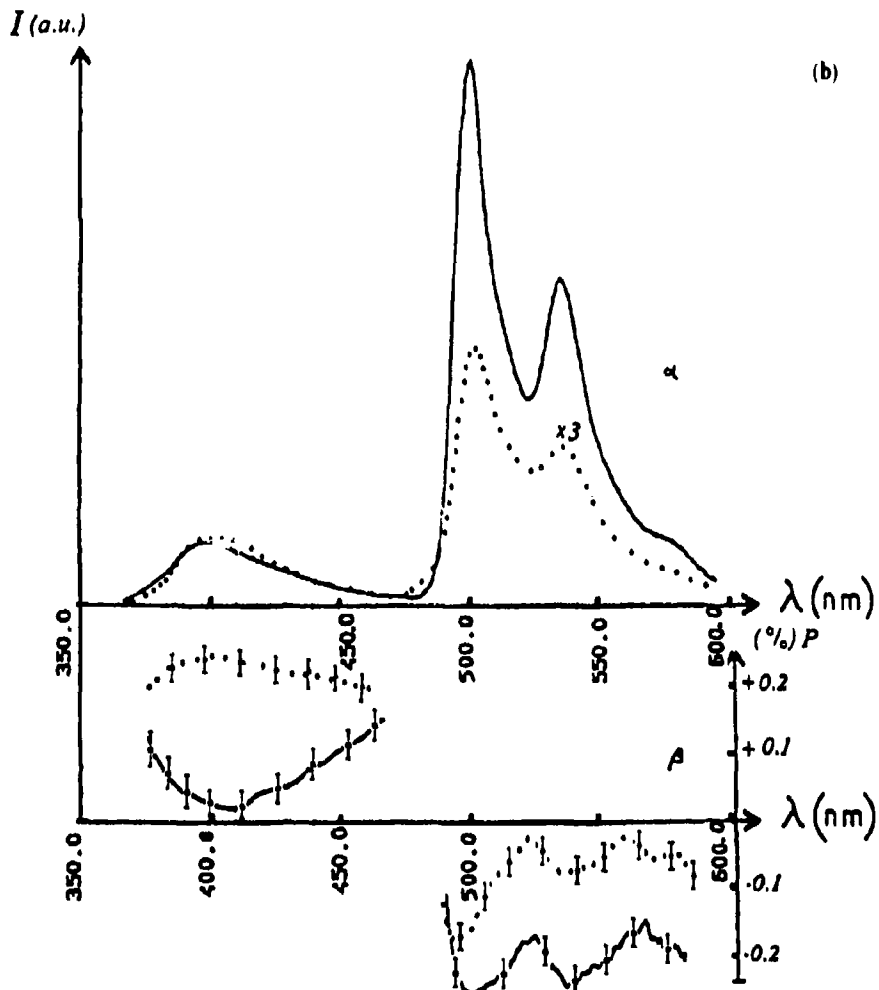


Figure 2. (a) Emission spectra of 2,2'-BQ in different polymeric matrices at room temperature (concentration $\approx 10^{-3}$ M): — MF matrix ($\lambda_{\text{exc}} \approx 340$ nm); — PVA rigid matrix ($\lambda_{\text{exc}} \approx 340$ nm); -○-○- PVA soft matrix ($\lambda_{\text{exc}} \approx 330$ nm); -●-●- PVC matrix ($\lambda_{\text{exc}} \approx 310$ nm). (b) α - Emission spectra of 2,2'-BQ in rigid PVA excited at 340 nm at room temperature (● ● ●) and at nitrogen liquid temperature (—). β - Polarization spectra of the emission of 2,2'-BQ in rigid PVA excited at 340 nm at room temperature (● ● ○ ○ ● ●) and at nitrogen liquid temperature (—).

presence of the two chromophores (two quinolines) with some special conformation with respect to each other (induced by hydrogen bonding), increases the RTP phenomenon. The hydrogen bonding stains the complex to a conformation different from that of the bare molecule. Recently, Higuchi *et al* (1980) assigned the EPR signal of 2,2'-BQ in the stretched PVA film to the *trans* conformer. Furthermore, we have

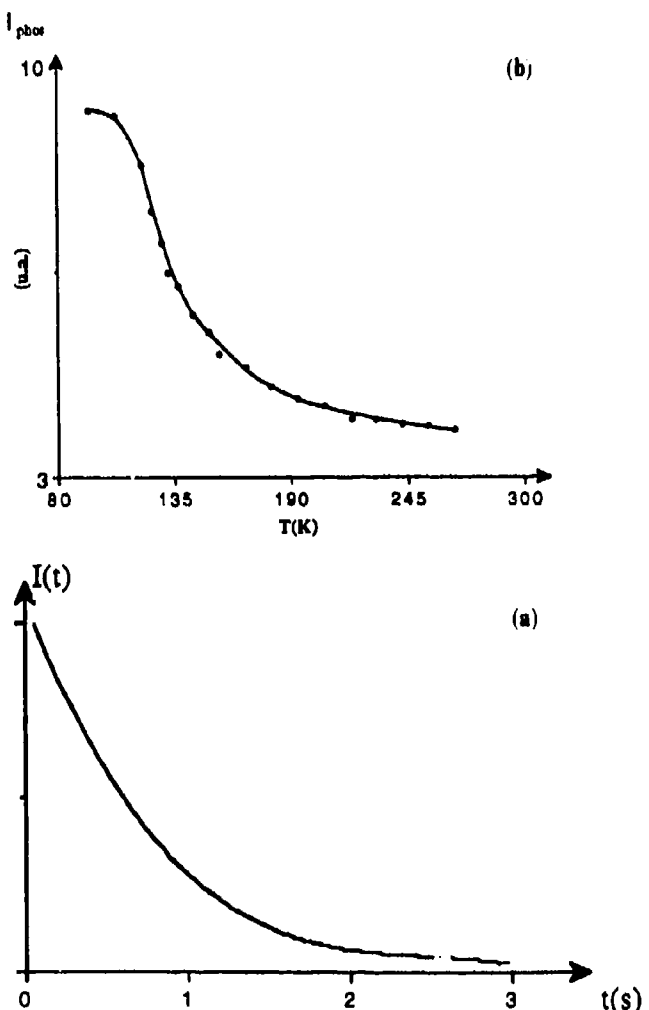


Figure 3. (a) Phosphorescence decay curve monitored at 500 nm of 2,2'-BQ in rigid PVA matrix, at room temperature, excited at 340 nm. (b) Evolution of maximum of the phosphorescence intensity ($\lambda_{\text{max}} \approx 500$ nm) against the temperature of the 2,2'-BQ in rigid PVA matrix, excited at 340 nm.

observed the absorption and luminescence spectra of 2,2'-BQ in the stretched PVA rigid film at room temperature (the stretched 250% films are obtained by a similar process as that of Higuchi *et al* 1980). Hence, the RTP, observed in hydrogen-bonded matrices, is assigned to the *cis* conformer of the molecule. The reasons for this assignment are as follows.

- In the stretched PVA rigid film, the observed absorption spectrum shows a relatively weak first band (relative to the second band) and a ratio $I_{\text{phos}}/I_{\text{fluo}}$ weaker than in unstretched PVA rigid films cf. figures 4a and b.

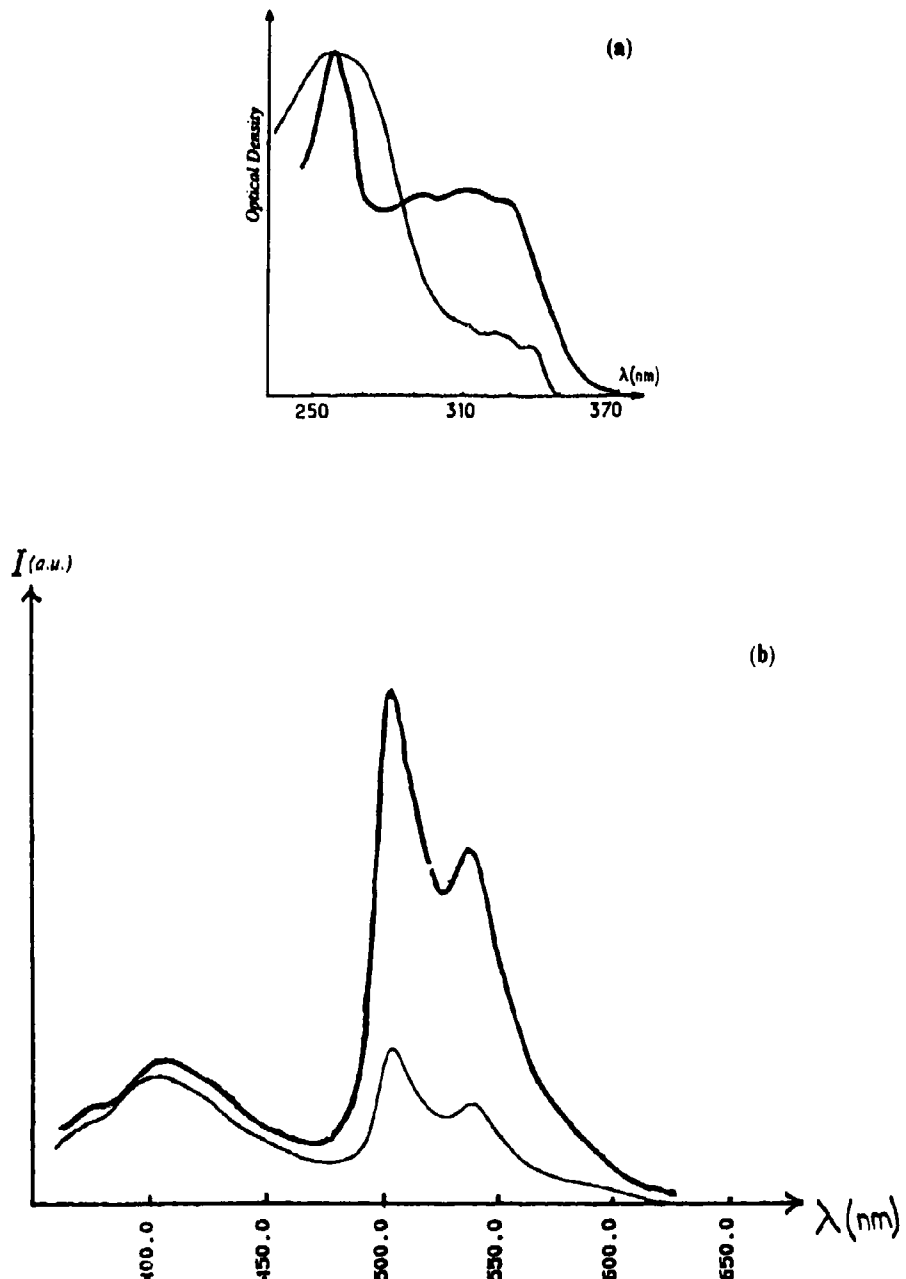


Figure 4. (a) Absorption spectra of 2,2'-BQ at room temperature (concentration $\approx 10^{-5}$ M); — in unstretched rigid PVA film; - - - in stretched rigid PVA film. (b) Emission spectra of 2,2'-BQ excited at 340 nm at room temperature: — in unstretched rigid PVA film; - - - in stretched rigid PVA film.

• Furthermore, the results of the calculated intermolecular interactions, simulating the hydrogen-bonded complex of the 2,2'-BQ, are consistent with the *cis* conformer, while the more stable conformation of the bare molecule is the *trans* one (unpublished results). Moreover, the simulated spectroscopic results, by CNDO/s are coherent with the relative variation of the oscillator strengths, for the two conformers respectively *cis* and *trans* (unpublished results). The deforming role of hydrogen bonding in the ground state has been already stressed by some of us, it seems to be a general phenomenon.

4. Conclusions

In the present study, we show a strong long-lived emission in some hydrogen-bonded polymeric matrices. This long-lived emission is ascribed to a room temperature phosphorescence issue to a $^3\pi,\pi^*$ triplet state, because its negative polarization by both excitations of the two first absorption bands. This RTP is very dependent on the temperature and on the viscosity of the matrix. Furthermore, the appearance of the RTP is correlated to the presence of hydrogen-bonded complexes in the ground state, according to the absorption spectra. We assume that these hydrogen-bonded complexes in the ground state correspond to a different conformation of the 2,2'-BQ, owing to the very large difference in the ratios of the oscillator strengths of the two first absorption bands, in comparison with that of the bare molecule (absorption in nonhydrogen-bonded matrix, for instance). A further study simulating the hydrogen bonded complex (and its probable deformation) will be presented subsequently.

References

- Cazeau-Dubroca C 1991 In *Trends in physical chemistry* (eds) Council of Scientific Research Integration (Tiruvandrum: Research Trends) 2 233
 Cazeau-Dubroca C, Perigaud A, Ait Lyazidi S and Nouchi G 1983 *Chem. Phys. Lett.* **98** 511
 Cazeau-Dubroca C, Perigaud A, Ait Lyazidi S, Nouchi G, Cazeau Ph and Lapouyade R 1986 *Chem. Phys. Lett.* **124** 110
 Cazeau-Dubroca C, Peirigaud A, Ben-Brahim M, Nouchi G and Cazeau Ph 1992 *Proc. Indian Acad. Sci. (Chem. Sci.)* **104** 209
 Clarke R H, Mitra P and Vinodgopal K 1980 *Chem. Phys. Lett.* **76** 237
 Clarke R H, Mitra P and Vinodgopal K 1982 *J. Chem. Phys.* **77** 5288
 Fadouach M, Benali M, Kadiri A, Cazeau-Dubroca C and Nouchi G 1992 *Spectrochim. Acta A* **48** 1491
 Ford C D and Hurtubise J 1979 *Anal. Chem.* **51** 659
 Frederiks S M, Luong J C and Wrighton M S 1979 *J. Am. Chem. Soc.* **101** 7415
 Higuchi J, Suzuki K, Arai H, Saitoh A and Yagi M 1986 *J. Phys. Chem.* **90** 1270
 Higuchi J, Yagi M, Iwaki T, Bunden M, Tanigaki K and Ito T 1980 *Bull. Chem. Soc. Jpn.* **53** 890
 Klassen D M 1976 *Inorg. Chem.* **15** 3166
 Ohno T and Kato S 1974 *Bull. Chem. Soc. Jpn.* **47** 2953, and references therein
 Vinodgopal K and Leenstra W R 1985 *J. Phys. Chem.* **89** 3824
 Vo-Dinh T 1984 *A series of monographs on analytical chemistry and its applications. Chemical Analysis Series*. Vol. 68 (eds) P J Elving and J D Winefordner (New York: Wiley-Interscience) p. 239
 Vo-Dinh T and Hooyhuis J R 1979 *Anal. Chem.* **51** 1915
 Wellon S L, Paynter R A and Winefordner J D 1974 *Spectrochim. Acta A* **30** 2133
 Yagi M, Makiguchi K, Ohnuki A, Suzuki K, Higuchi J and Nagase S 1985 *Bull. Chem. Soc. Jpn.* **58** 252
 Yagi M, Torii M, Yamauchi N, Kaneshima T and Higuchi J 1991 *Chem. Phys. Lett.* **187** 604

Application of the three-level model: Rise and decay kinetics of the temperature-dependent emission of metal ions with s^2 -valence electron configuration

M DIEHL*, J DEGEN and H H SCHMIDTKE

Institut für Theoretische Chemie, Heinrich-Heine Universität Düsseldorf, Universitätsstrasse 1, D-40225 Düsseldorf, Germany

Abstract. Temperature-dependent rise time and lifetime results, by measuring the photon emission in the temperature range 10–200 K, were obtained on *cis*-(NEt₄)₂[TeCl₄Br₂]²⁻(C_{2v}) and [SeCl₄]²⁻(O₄). The kinetics of excitation and relaxation are described by a three-level model containing transition rate constants which are related to different symmetry selection rules between corresponding electronic levels. The transient emission can be modified by varying the excitation pulse length. Besides a slow component in the luminescence decay-curve (0.5 ms at $T = 12$ K) a second, faster component can be detected. The amplitude ratio of these components can be increased by decreasing the excitation pulse length, which can be explained by assuming non-thermally equilibrated excited states. The results allow the assignment of the lowest levels which arise from the excited *sp* electron configuration of the central ion.

Keywords. Three-level model; temperature-dependent emission of metal ions; s^2 -valence electrons.

1. Introduction

The three-level system is well established to explain kinetic experiments (Stepanov 1968). For the general case, the nomenclature and a schematic diagram are given in figure 1. Γ_i denote terms of the s^2 and *sp* configuration. The solution for the corresponding rate equations is

$$n_i(t) = \sum_{j=1}^2 A_{ij} \exp(-t/\tau_j) + A_{i,3}, \quad i = 0, 1, 2. \quad (1)$$

A thorough treatment of the three-level system can be found in the book of Stepanov (1968), hence, no further details are given here. In this work, the model is applied to the interaction between electronically excited states and the ground state of metal complexes with s^2 -electron configuration of the central ion. The limitation of the model lies in the number of parameters (k_{ij}) which are necessary to describe the system completely. In the description of transient luminescence a total number of six rate constants are involved. There is even an unsteadiness in the two rates k_{01} and k_{02} if the whole process of excitation and relaxation is to be described. Every rate

*For correspondence

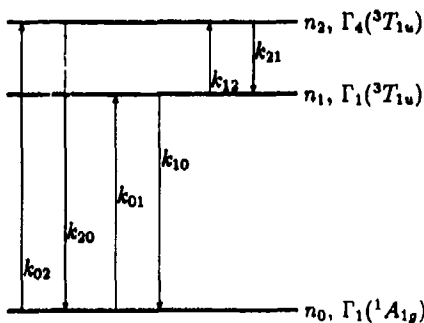


Figure 1. Three level system.

constant consists of two contributions, a radiative and a nonradiative part. Despite the fact that the magnitude of some of the rate constants can be estimated sufficiently well, e.g. there is no nonradiative excitation from the ground state and no radiative interaction between the excited states, there is still a discussion going on, on how to assign some rate constants found from kinetic experiments to the transitions in the examined systems (Hughes and Pells 1975; Meidenbauer and Gliemann 1988; Donker *et al* 1989a). There are many papers dealing with the application of the three-level model to systems with s^2 electron configuration and the energy difference ΔE between the lowest excited states (Degen and Schmidtke 1989; Donker *et al* 1989a; Schmidtke *et al* 1992). In order to be able to apply the three-level model, one has to make assumptions on these rate constants. It is common to assume that the rates which connect the two excited state are related by the Boltzmann factor as

$$k_{12} = k_{21} \exp(-\Delta E/k_B T). \quad (2)$$

This is reasonable because of the small energy difference (in the magnitude of some 100 cm^{-1}) and since there are only nonradiative contributions to these rates. On the other rate constant there are different opinions, especially whether the largest rate which can be determined from time-dependent lifetime measurements must be assigned to a radiationless deactivation (k_{20}) or is the Boltzmann rate (k_{21}). The value of ΔE , estimated from the experiment, seems to be relatively independent from the assumption for the rate constants (Meidenbauer and Gliemann 1988; Donker *et al* 1989a; Degen *et al* 1993).

2. Experimental

Excitation is achieved by an argon-ion laser (Spectra Physics 2016, 457.5 nm line), the plasma light is removed with a LASERspek III monochromator. The cw-beam is modulated by an optoacoustic modulator (Matsushita EFC-C200-P11). The pulse/pause ratio can be adjusted in a wide range, the maximum frequency with this setup is 10 MHz. Cooling of the sample is performed with a Leybold Heraeus R 219 closed-cycle cryostat (minimum temperature 12 K). The transient detection of the luminescence is done via standard single photon counting equipment which is described elsewhere (Schmidtke *et al* 1992). Sample preparation for the Te(IV)-compound is precipitation

with SnCl_4 under inert gas conditions resulting in doped crystals with 1% Te (Schmidtke *et al* 1992). The Cs_2SeCl_6 samples are used undoped (Degen and Schmidtke 1989).

3. Results

We examine the transient luminescence of *cis*- $[\text{TeCl}_4\text{Br}_2]^{2-}$ (C_{2v}) and $[\text{SeCl}_6]^{2-}$ (O_h). The shortest excitation pulse length applied is 100 ns. The longest pulse width is several milliseconds. Upon excitation with pulse widths in the order of 100 μs , both systems respond with a single exponential [$\propto 1 - \exp(-t/\tau)$ for the rise and $\propto \exp(-t/\tau)$ for the decay]. The interpretation of the time dependencies is described elsewhere (Degen and Schmidtke 1989; Donker *et al* 1989b; Schmidtke *et al* 1992; Degen *et al* 1993). If the excitation pulse length is decreased, the response changes to a transient luminescence which can no longer be fitted to a single exponential. Figure 2 shows the response of *cis*- $[\text{TeCl}_4\text{Br}_2]^{2-}$ to a 1- μs excitation pulse. It can be seen that two exponentials are necessary to fit the observed transient. The fast component is governed by the rise time of the excitation pulse which is of the order of 20 ns. By decreasing the width of the excitation pulse, the amplitude of the fast component is increased. This can be shown in a quantitative manner for the Se-compound (Degen *et al* 1993).

4. Discussion

With excitation pulse-width dependent lifetime measurements additional information about the rate constants in Tl^{+} -like systems can be obtained. Since the observed pulse width dependencies exist, the Boltzmann-related rates (k_{12} and k_{21}) cannot be

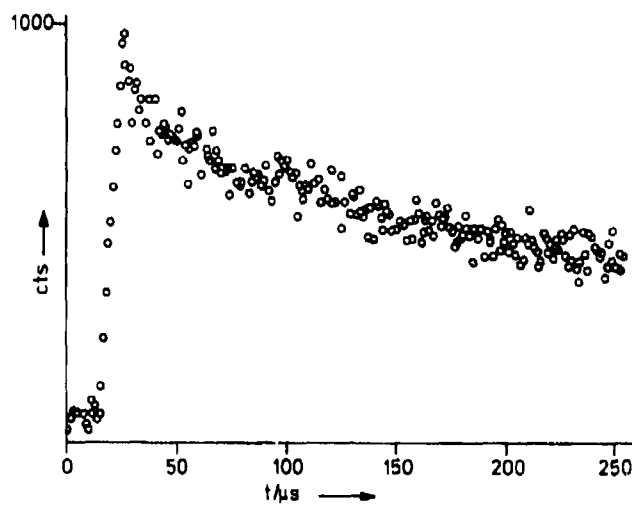


Figure 2. Transient luminescence of *cis*- $(\text{NEt}_4)_2\text{TeCl}_4\text{Br}_2$ at $15,500\text{ cm}^{-1}$ under excitation with a 1- μs laser pulse ($\lambda_{ex} = 457.5\text{ nm}$).

the rates with the greatest magnitude because thermal equilibrium would be expected even shortly (some 10 ns) after application of the excitation pulse. It can be concluded that the depopulating rate k_{20} corresponds to the observed fast decay constant. This is consistent with the dominant transition rate for $\Gamma_4 \rightarrow \Gamma_1$ (Se-compound, O_h symmetry), as deduced from selection rules (Degen and Schmidtke 1989; Donker *et al* 1989b) for molecular transitions.

References

- Degen J, Diehl M and Schmidtke H-H 1993 *Mol. Phys.* **78** 103
Degen J and Schmidtke H-H 1989 *Chem. Phys.* **129** 483
Donker H, Smit W M A and Blasse G 1989a *J. Phys. Chem. Solids* **50** 603
Donker H, van Schaik W, Smit W M A and Blasse G 1989b *Chem. Phys. Lett.* **158** 509
Hughes A E and Pella G P 1975 *Phys. Status Solidi B* **71** 707
Meidenbauer K and Gilemann G 1988 *Z. Naturforsch. A* **43** 555
Stepanov B I 1968 *Theory of luminescence* (London: Iliffe)
Schmidtke H-H, Diehl M and Degen J 1992 *J. Phys. Chem.* **96** 3605

Reflectivity as a probe for chemical reactions

M SCHUBMELL*, H R TSCHUDI, P KUHN and H RIES

Paul Scherrer Institute, CH-5232 Villigen-PSI, Switzerland

Abstract. Endothermic chemical reactions taking place at temperatures above 1000 K are candidates for the utilization of solar energy in highly concentrating solar furnaces. Special interest is focussed onto the question of whether light drives the reaction differently from heat. To observe such an effect it is important to monitor the chemical process of the sample under irradiation. In this paper we propose spectral reflectivity as a probe for chemical changes. We present laboratory measurements showing reflectivity changes associated with the oxidation of magnetite. We observed significant changes at temperatures coinciding with the oxidation temperature of magnetite. We further observed a change of the reflectivity associated with the phase transition of maghemite to hematite. Contrary to the literature, we find that this phase transition leads off at about 525 K.

Keywords. Reflectivity; chemical reaction; phase transition; solar furnace.

1. Introduction

Conversion of solar energy into chemical fuels has been a field of intense research for many years (Bolton and Archer 1991). This is usually attempted as a thermochemical reaction under highly concentrated solar irradiation, e.g. in a solar furnace. Special interest is focussed onto the question of whether concentrated light drives the reaction differently from heat. One possible effect of irradiation might be, for example, a decrease of the reaction temperature (Sizmann 1989). To observe such an influence it is important to monitor the chemical process of the sample under irradiation. In this paper we propose spectral reflectivity as a probe for chemical changes. This can be done even under intense solar irradiation by using, say, a flash of known spectral intensity. We report laboratory measurements showing the reflectivity changes associated with the thermal oxidation of magnetite. In combination with an accurate method to measure surface temperatures as proposed, for example, by Ries *et al* (1989) one should be able to quantify the influence of concentrated radiation on a chemical reaction.

2. Experimental

Thin films of powdered magnetite (iron(III)-oxide, Fe_3O_4 , 97% purity) were prepared on a 4-nm-thick circular stainless steel substrate, 3 cm in diameter, by various techniques, e.g. repeated slow drying of aqueous suspensions dripped onto the substrate or spraying of an aqueous suspension onto the hot (400–500 K) substrate. Using the

*For correspondence

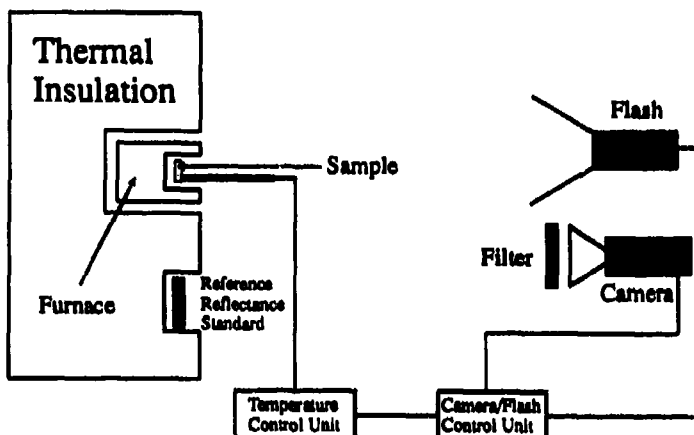


Figure 1. Experimental setup to measure reflectivities.

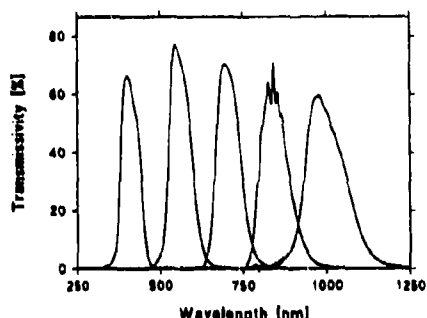


Figure 2. Transmissivity of the bandpass filters used as a function of wavelength. Peak transmittances are at 400, 550, 700, 850 and 1000 nm.

spray technique we achieved powdered thin films with a matte surface and a thickness of approximately 100 μm .

The samples were placed in a cavity-like furnace, made of stainless steel open to the atmosphere, and heated by a thermocoax wire wound around the metal block. The furnace is embedded in a block of ceramic insulation. A few centimeters away from the sample, we placed a calibrated reference reflectance standard (Spectralon). The temperature of the sample is controlled by two thermocouples slightly stuck into the substrate. The experimental setup is depicted schematically in figure 1.

To determine the reflectivity of the sample we proceeded as follows. The sample and the reference target were first illuminated with a flash (flashtime $\approx 1 \text{ ms}$) and imaged with a slow-scan high-resolution (16 bit) CCD-camera. To determine the thermal background radiation a second set of images was taken without the flash. By subtracting the images taken with and without the flash the net reflected radiation was calculated. Consequently the reflectivity can be computed by comparing the reflected radiation from the sample with that from the reference reflectance standard. The reflectivity has been measured at five wavelength bands by using bandpass filters

with peak transmittances at 400, 550, 700, 850 and 1000 nm. The transmissivity of the used filters is shown in figure 2. The FWHM-values of the filters amount to 67, 57, 80, 82 and 130 nm, respectively.

3. Results

In figure 3 we show the reflectivity of a powdered magnetite film (Fe_3O_4) heated at a rate of 8 K/min as a function of the temperature at different wavelengths. At about 475 K a gradual increase in the reflectivity can be observed at all wavelengths. We attribute this increase to the oxidation of magnetite, i.e. the reaction



From the literature it is known that magnetite is oxidized to the metastable maghemite ($\gamma\text{-Fe}_2\text{O}_3$) at low temperature. At higher temperatures the maghemite transforms irreversibly into hematite ($\alpha\text{-Fe}_2\text{O}_3$). However, a transition temperature cannot be assigned to this phase transition since it transforms gradually. Therefore it is generally believed that maghemite exists only as an intermediate product of the oxidation process from magnetite to hematite (Goto 1964; Swaddle and Oltmann 1980; Oezdemir and Banerjee 1984).

To investigate the transition of $\gamma\text{-Fe}_2\text{O}_3$ into $\alpha\text{-Fe}_2\text{O}_3$ we also measured the reflectivities of maghemite and hematite as functions of temperature. The maghemite and hematite samples were prepared by heating powdered magnetite films at 500 K and at 1170 K, respectively, for approximately 80 minutes. A subsequent X-ray diffraction analysis indicated that after this treatment the first sample consisted of $\approx 95\%$ maghemite whereas the second sample was oxidized to pure hematite. Figure 4 shows the results of the reflectivity of $\gamma\text{-Fe}_2\text{O}_3$, $\alpha\text{-Fe}_2\text{O}_3$ and Fe_3O_4 versus the temperature at 850 and 700 nm. The heating rate was again ≈ 8 K/min.

It can be seen that the reflectivity of the stable hematite continually decreases with increasing temperature as predicted by the Urbach rule (Kurik 1971). The reflectivity

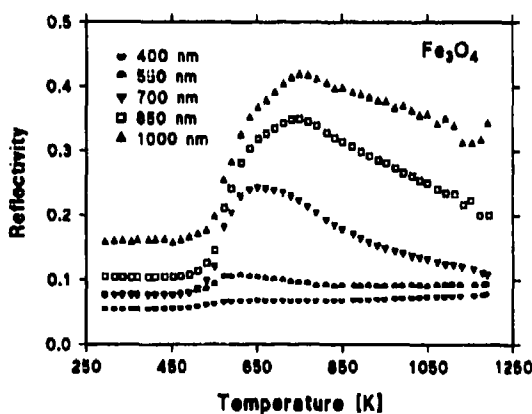


Figure 3. Reflectivity of Fe_3O_4 at different wavelengths versus temperature. Heating rate ≈ 8 K/min.

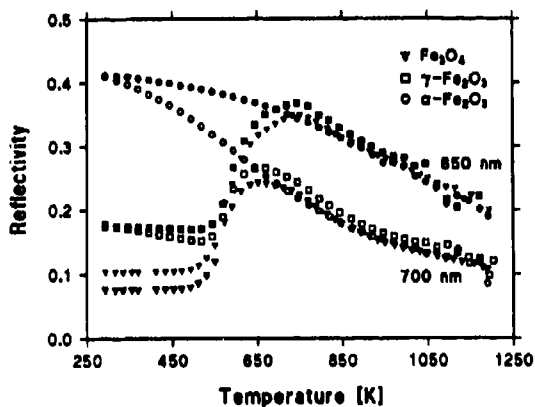


Figure 4. Temperature dependence of the reflectivity of Fe_3O_4 , $\alpha\text{-Fe}_2\text{O}_3$ and $\gamma\text{-Fe}_2\text{O}_3$ at 850 and 700 nm. Heating rate $\approx 8 \text{ K/min}$.

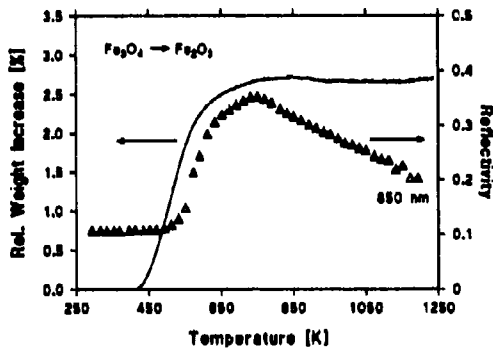


Figure 5. Thermogravimetric analysis of magnetite and reflectivity at 850 nm.

data for maghemite show that the phase transition to hematite leads off at about 525 K. This temperature is about 150 K lower than the transition temperature reported in the literature (Goto 1964). Furthermore, it is only slightly higher than the oxidation temperature of magnetite. There is evidence that the rate of phase change strongly depends on temperature (Landolt-Boernstein 1980). In our experiment the phase change seems to be over at about 1000 K. The time needed to heat up the sample from 525 to 1000 K amounts to approximately 60 min.

A similar investigation was performed by thermoanalytical methods. In figure 5 we show data of a thermogravimetric analysis (TGA) of magnetite together with reflectivity data at 850 nm.

The TGA-data show that the oxidation of Fe_3O_4 leads off at $\approx 425 \text{ K}$. The reflectivity measurements indicate a significant change in the reflectivity at a slightly higher temperature ($\approx 475 \text{ K}$). Based on the TGA-data, we estimate that at this temperature about 12% of the magnetite is oxidized to maghemite.

4. Conclusions

Using Fe_3O_4 as an example we showed that reflectivity can be an appropriate property to monitor chemical or structural changes on surfaces. We found that the oxidation of magnetite as well as the phase transition of maghemite to hematite can be observed by this method. We showed that the phase transition of maghemite to hematite leads off at $\approx 525\text{ K}$ which is about 150 K lower than the values found in the literature.

We believe that this method can be an important tool to study chemical reactions on surfaces. By using, say, a powerful flash, the reflectivity can be measured even under intense solar radiation. Therefore, in combination with accurate temperature measurement, the potential influence of concentrated solar irradiation on a chemical reaction might be observed.

Acknowledgement

This work has been supported by the Swiss Federal Office of Energy.

References

- Bolton J R and Archer M 1991 *Photoconversion of solar energy. Lecture notes* (Brigels, Switzerland: Wiley & Sons) (to be published)
Goto Y 1964 *Jpn. J. Appl. Phys.* **3** 741
Kurik M V 1971 *Phys. Status Solidi A* **8** 9
Landolt-Bornstein 1980 *Numerical data and functional relationship in science and technology* (Berlin: Springer Verlag) vol. 12b
Oezdemir O and Banerjee S K 1984 *Geophys. Res. Lett.* **11** 161
Ries H, Schubnell M and Spirkl W 1989 Simultaneous radiometric measurement of absorber temperature and irradiance. In *Clean and safe energy forever: Proc. of the ISES Solar World Congress* (Tokyo: Pergamon)
Sizmann R 1989 *Chimia* **43** 202
Swaddle T W and Oltmann P 1980 *Can. J. Chem.* **58** 1763

Intramolecular and dissociation dynamics of triatomic molecules: Some results for HCN and CO₂

JAIR BOTINA¹ and NASEEM RAHMAN^{2*}

¹Dipartimento di Scienze Chimiche dell'Università di Trieste, Piazzale Europa 1, 34100 Trieste, Italy

²International Institute for Pure and Applied Chemistry, UNIDO, Area di Ricerca, Padriciano 99, 34012 Trieste, Italy

Abstract. Intramolecular dynamics of two linear molecules HCN and CO₂ are studied by computing trajectories, plotting Poincaré sections and calculating Lyapunov exponents. The process of dissociation is then studied by the same technique for HCN in the presence of a strong CO₂ laser. Results of these preliminary calculations unequivocally show a threshold intensity for dissociation which is possible to verify experimentally.

Keywords. Intramolecular dynamics; dissociation probability; triatomic molecules; Poincaré sections; Lyapunov exponent.

1. Introduction

How much of intramolecular dynamics is understood by performing computations of trajectories integrating the Hamiltonian equation of motion? It turns out that a lot can be learned and the limitations are quite often that of not having enough computer time to carry through all that you would want to do.

In this article, we use some recently utilized and accurate model Hamiltonians for the molecules CO₂ and HCN and examine what classical mechanics can say regarding these molecules. The results are relevant for two cases. In § 2, some results of computation of trajectories in the configuration space of vibrational motion of these molecules are presented utilizing Poincaré sections. The qualitative change in the dynamics on increasing the energy of the molecules is well understood by these computations. The dynamics can thereby be related to the theory of chaos and clear transitions from periodic regular trajectories to non-periodic irregular trajectories are seen. It is difficult to accurately quantify the transition energy by computing the trajectories and examining the Poincaré sections. A much better but (computationally) quite expensive method is to calculate the Lyapunov exponents for these trajectories. The change of sign of the Lyapunov exponent with variation of the energy of the system lets one obtain more accurate values of the transition energy. The results of these are discussed in § 2.

The success of the implementation of our own routine for the computation of the trajectories induced us to consider the dynamics of dissociation of these molecules stimulated by an external electromagnetic field. The problem is discussed in § 3 where

* For correspondence

the first results of these computations are presented. This new technique has now been implemented for the first time to discuss the intramolecular dissociation dynamics as well as to obtain the dissociation probability. It appears to be a rather promising technique especially in view of the near impossibility of obtaining any accurate quantum-mechanical photodissociation probability due to the prohibitive expense of the relevant computation. The threshold field strength of dissociation for HCN has been obtained with an accuracy which should be compared both with theoretical and with eventually experimental methods.

2. Intramolecular dynamics

The Hamiltonian model for CO₂ molecule is given by:

$$H = H_1 + H_2 + H_{12}, \quad (1)$$

with

$$H_i = (P_i^2/2\mu_i) + V(R_i), \quad i = 1, 2, \quad (2a)$$

$$H_{12} = (1/m_C)P_1 P_2, \quad (2b)$$

$$V(R_i) = D(1 - \exp(-\alpha R_i))^2, \quad (2c)$$

where $D = 5.5 \text{ eV}$ and $\alpha = 3.1 \text{ \AA}^{-1}$.

In the above equation, R_i is the displacement of the CO bond from its equilibrium position, P_i is the conjugate momenta corresponding to R_i , $1/\mu_i = 1/m_C + 1/m_O$, m_C is the mass of the central atom (carbon mass), m_O is the oxygen mass and i refers to the specific bond in the molecule. These bonds are not equivalent if all the three masses are different. H_i is the Hamiltonian for the reduced mass μ_i consisting of the kinetic energy $P_i^2/2\mu_i$ and the potential $V(R_i)$ which depends only on the position R_i . The term H_{12} is the coupling between the motion of the two reduced masses (Wilson *et al* 1955). Since the molecules are linear, we assume that the angle between the two relevant bonds is 180°. Regardless of the choice of the potentials $V(R_i)$, the coupling term H_{12} is exact and plays a crucial role in our consideration. Such a model, while deficient in many respects such as absence of rotation, bending motion, Fermi resonance etc., is still capable of generating a good number of the vibrational levels of the molecule and therefore has been utilized for various studies in the literature (Buch *et al* 1982; Halonen and Child 1982; Terasaka and Matsushita 1985; Botschwina 1988; Karrlein 1991; Shi and Rabitz 1991).

For HCN, the Hamiltonian (Smith *et al* 1991) has given the same form as (1) and (2), with

$$V(R_i) = V_{i1}Z_i^2 + V_{i2}Z_i^3 + V_{i3}Z_i^4, \quad i = 1, 2, \quad (3a)$$

$$Z_i = 1 - \exp(-\alpha_i R_i), \quad (3b)$$

and the term H_{12} , however, is chosen to be

$$H_{12} = -(1/m_C)P_1 P_2 + V(R_1, R_2), \quad (3c)$$

where

$$V(R_1, R_2) = V_1 Z_1 Z_2 + V_2 Z_1^2 Z_2 + V_3 Z_2^2 Z_1. \quad (3d)$$

All the parameters are given in table 1 and the indices 1 and 2 correspond to CN and CH coordinates, respectively. These parameters approximately fit the first 40 stretching vibrational levels in the spectrum with an error of about 0.01% of the energy values and predict the two possible dissociation pathways associated with this molecule within 15% for the channel (H + CN) and within 8% for the channel (HC + N) (Smith *et al* 1991).

The Hamiltonian equations of motion along with conservation of energy, give rise to a set of three coupled equations for each of these two Hamiltonians. These are then integrated generating the trajectories and the results are plotted as Poincaré sections with the coordinate R_2 and the momentum P_2 as the variables. Figures 1 and 2 show a set of these for CO₂ and HCN respectively. These are in ascending order in energy and even a cursory perusal of them shows how the trajectories make the transition from being periodic to chaotic as the energy is increased. A more

Table 1. Parameters for the generalized Morse potential for HCN (Smith *et al* 1991).

$\alpha_{\text{CN}} = 2.306172 \text{ \AA}^{-1}$	$\alpha_{\text{CH}} = 1.847393 \text{ \AA}^{-1}$	$V_1 = 0.30763 \text{ eV}$
$V_{11} = 10.99446 \text{ eV}$	$V_{21} = 5.69714 \text{ eV}$	$V_2 = -9.425 \times 10^{-6} \text{ eV}$
$V_{12} = 0.499332 \text{ eV}$	$V_{22} = 0.47528 \text{ eV}$	$V_3 = 3.657 \times 10^{-4} \text{ eV}$
$V_{13} = 5.954 \times 10^{-3} \text{ eV}$	$V_{23} = 8.426 \times 10^{-3} \text{ eV}$	

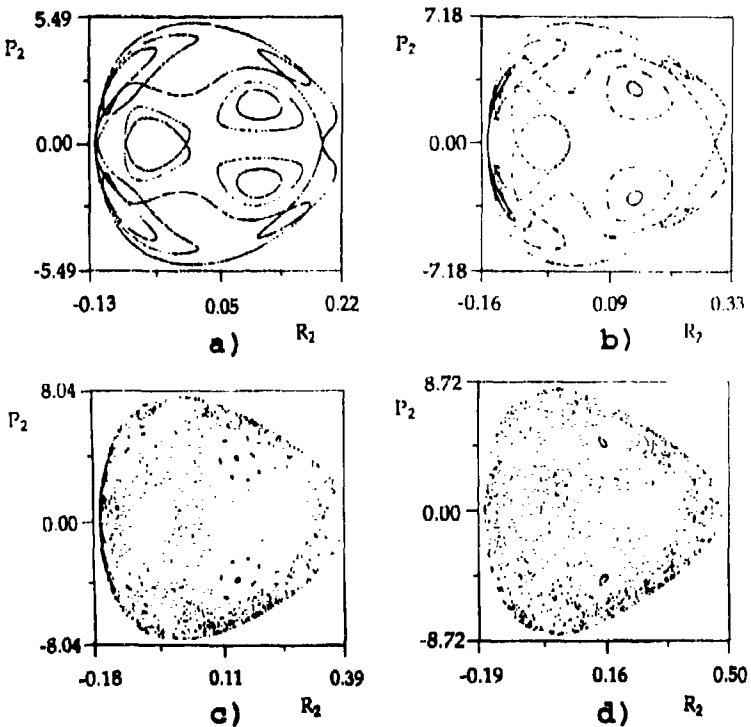


Figure 1. Poincaré section at different values of energy for the CO₂ molecule where the two atoms of oxygen are 18 amu. (a) 1.5, (b) 2.5, (c) 3.0 and (d) 3.5 eV.

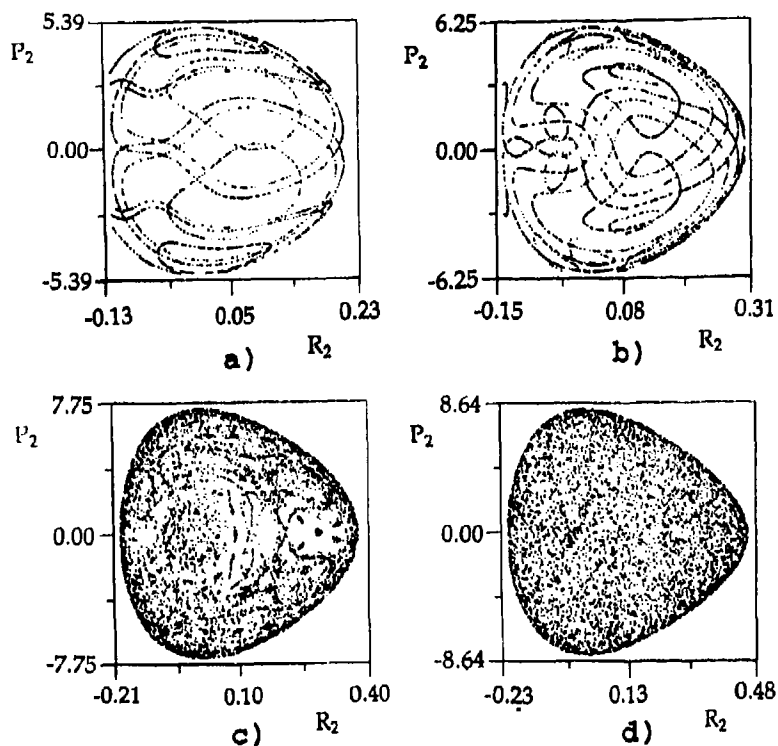


Figure 2. Poincaré section at four values of energy for the molecule DC^{16}N . (a) 2, (b) 3, (c) 4 and (d) 5 ev.

Table 2. Lyapunov exponent at different values of the energy.

	Energy (ev)	Lyapunov exponent
CO_2	2.50	-1.0
	2.76	-0.2
	3.00	0.5
HCN	2.00	-1.5
	2.80	-0.1
	2.90	0.3

quantitative estimate of the energy where such a transition occurs (threshold energy) requires rather extensive calculations involving computation of the Lyapunov exponent (Benettin *et al* 1976; Shimada and Nagashima 1979; Wolf *et al* 1985; Meyer 1986). Table 2 indicates where that occurs for $^{12}\text{C}^{16}\text{O}_2$, $^1\text{H}^{12}\text{C}^{14}\text{N}$, respectively.

There are two remarks that need to be made and which are generally applicable. First, even the simplest of couplings $-P_1 P_2/m_C$ is able to create the transition to chaos from elementary models of vibrational dynamics. Therefore, we expect, in

general, to see manifestation of transition to chaos at some energy for all polyatomic molecules in their vibrational motion. Second, chaotic dynamics is strongly and sensitively dependent on the isotopic mass chosen for the molecule (Pichierri 1992; Bonina *et al* 1993).

These computations have served as a starting point for calculation dissociation probability of HCN by intense laser fields utilizing trajectories and Poincaré sections and to investigate the relationship between the threshold energy for chaotic dynamics and the dissociation probability brought about by the external electromagnetic field.

3. Dissociation dynamics of HCN

We employed the same type of method described in the previous section to study the laser-induced dissociation of HCN molecule. The laser field is characterized by the electric field strength and frequency of the laser light. Interaction between the molecule and the laser radiation field is included through the dipole moment function. The Hamiltonian for the laser-molecule interactions is

$$H_I = E_0 \mu(\mathbf{R}) \cdot \cos(\omega t), \quad (4)$$

where E_0 is the electric field strength, μ is the dipole moment, t is the time, and ω is the frequency of the laser. The dipole function was taken as

$$\begin{aligned} \mu = (\mathbf{R}_{\text{CH}}, \mathbf{R}_{\text{CN}}) = A & [(R_{\text{CN}} + R_{\text{CN},eq}) \exp(-\beta R_{\text{CN}}) \\ & - (R_{\text{CH}} + R_{\text{CH},eq}) \exp(-\beta R_{\text{CH}})], \end{aligned} \quad (5)$$

where A is a constant proportional to the permanent dipole of the molecule in its

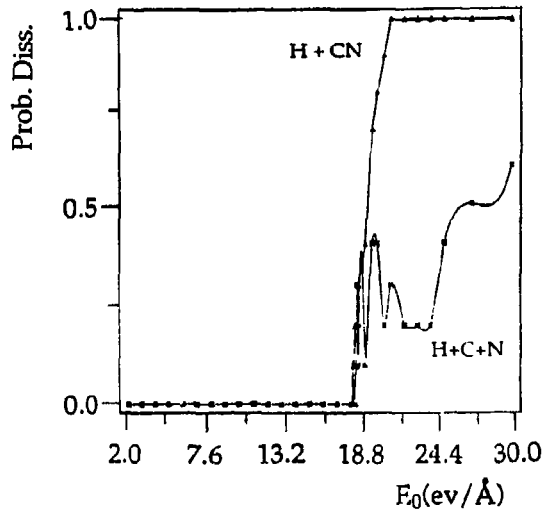


Figure 3. Classical probability of dissociation in function of the electric field strength (ev/Å) where the frequency of the laser is 114 ev. The number of initial conditions is 20.

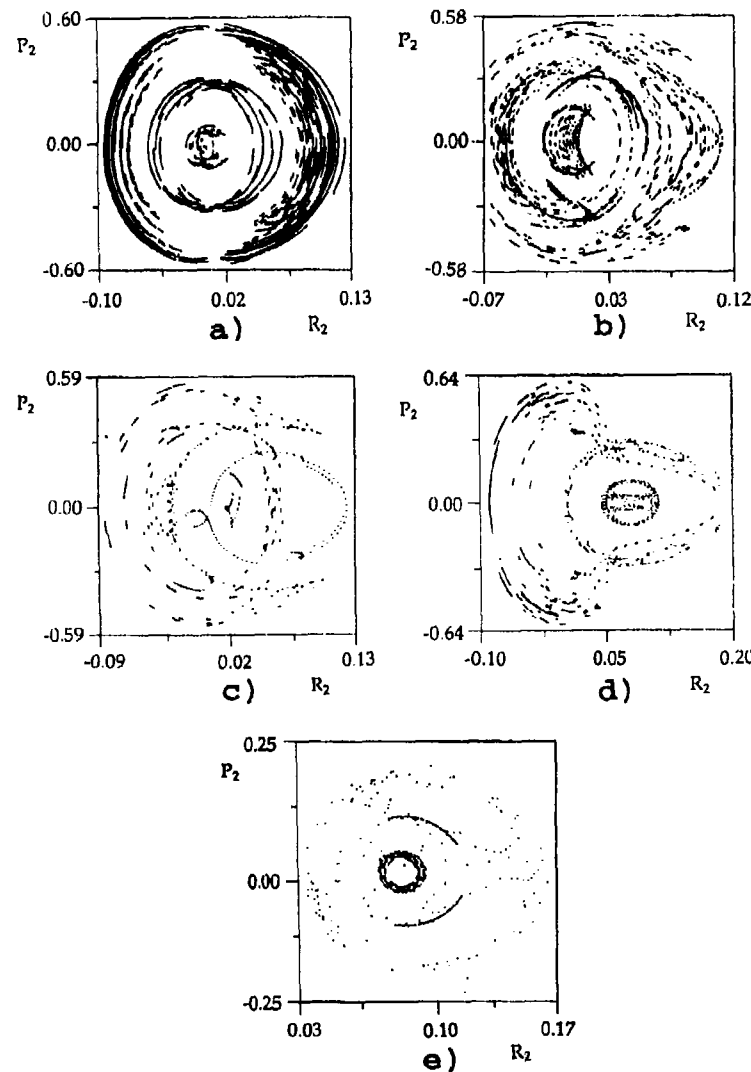


Figure 4. Poincaré section at different values of the electric field strength where the frequency of laser is 0.114 eV for the molecule of HCN. (a) 5, (b) 10, (c) 15, (d) 18 and (e) 19 eV/Å.

equilibrium, R_i is the displacement from the equilibrium position, $R_{i,eq}$, of each bond i , and β is a constant that is taken equal to one. We expect this dipole function to be a good approximation because the force constants of C-H and C-N are not very different from the corresponding force constants in HCN (Smith *et al* 1987; Botschwina 1988).

In order to study the laser-induced dissociation probability of the HCN molecule, it is necessary to calculate the classical probability of dissociation starting from a set

Table 3. Lyapunov exponent and the maximum value of energy reached at different values of the electric field strength where the frequency of laser is 0.114 ev for the molecule of HCN. At 19 ev/Å there is dissociation.

Electromagnetic strength (ev/Å)	Lyapunov exponent
5	0.0050
10	0.0224
15	0.0327
18	0.0500
19	0.2500

of initial conditions at a specific energy. The probability is given by

$$P_{\text{diss}}(R, T) = \frac{1}{N} \sum_{i=1}^N \delta(R_i(T)), \quad (6)$$

where N is the number of initial conditions, T is the optical cycle, R is the deviation of the relevant bond (CN or CH) from its equilibrium position and δ function is defined as

$$\delta(R_i) = \begin{cases} 1, & \text{if } R_i \geq R_{\text{diss}} \\ 0, & \text{if } R_i < R_{\text{diss}} \end{cases}, \quad (7)$$

and R_{diss} is taken equal to 9 Å (at this value the potential energy = 1×10^{-5} ev). The results are given in figure 3 where we show the classical probability as a function of the field strength E_0 (ev/Å) for the reactions, HCN → H + CN and H + CN → H + C + N. It is clear from figure 3 that the threshold field strength for the dissociation of HCN → H + CN has a value of 18.16 ev/Å.

In figure 4 we show the same Poincaré section (i.e. for R_2 and P_2) at different values of field strength and a frequency of 0.114 ev. These are for field strengths: (a) 5 ev/Å, (b) 10 ev/Å, (c) 15 ev/Å (d) 18 ev/Å and (e) 19 ev/Å. At the last field strength (figure 4e), we have already calculated that the dissociation probability of the molecule is equal to 0.40 for the reaction HCN → H + CN and 0.20 for the reaction H + CN → H + C + N (figure 3). From these figures, we see that at the lowest field strength i.e. at 5 ev/Å, the Poincaré section is confined to an almost circular region. With increase of field strength, qualitative changes appear; however, it is difficult to conclude much regarding dissociation from these figures.

Lyapunov exponents at different values of electromagnetic field strength are shown in table 3. At 19 ev/Å, even though the molecule dissociates, one can still calculate the Lyapunov exponent as long as the calculation is limited to not very long time periods. The values of the Lyapunov exponent jumps from 0.05 at 18 ev/Å to 0.25 for 19 ev/Å. Therefore one sees that dissociation may be related to deterministic chaos (Smith *et al* 1987; Botschwina 1988).

Acknowledgements

We wish to express our gratitude to the staff of BULL (Area di Ricerca) for a generous grant of computation time on their DPX/250 computer. Part of the computation and the graphics were performed in the Silicon Graphics workstation provided by IIC. JB wishes to thank ICS for hospitality and financial support during the course of the work.

References

- Benettin G, Galgani L and Strelcyn J M 1976 *Phys. Rev. A* **14** 2338
Botina J, Pichierri F and Rahman N 1993 *Chem. Phys. Lett.* (to be published)
Botschwina P 1988 *J. Chem. Soc. Faraday Trans.* **84** 1263
Buch V, Gerber R B and Ratner M A 1982 *J. Chem. Phys.* **76** 5397
Halonen L and Child M S 1982 *Mol. Phys.* **46** 239
Karrlein W 1991 *J. Chem. Phys.* **94** 3293
Meyer H D 1986 *J. Chem. Phys.* **84** 3147
Pichierri F 1992 *Effetti Dinamici sulle Proprietà Statistiche di Stati Vibrazionali Altamente Eccitati in Molecole Triatomiche*, thesis, Università degli Studi di Trieste
Shi S and Rabitz H 1991 *Comput. Phys. Commun.* **63** 71
Shimada I and Nagashima T 1979 *Prog. Theor. Phys.* **61** 1605
Smith A M, Jorgensen U G and Lehmann K 1987 *J. Chem. Phys.* **87** 5649
Smith A M, Klemperer W and Lehmann K 1991 *J. Chem. Phys.* **94** 5040
Terasaka T and Matsushita T 1985 *Phys. Rev. A* **32** 538
Wilson R B Jr, Decius J C and Cross P C 1955 *Molecular vibrations. The theory of infrared and Raman vibrational spectra* (New York: McGraw-Hill)
Wolf A, Swift J B, Swinney H L and Vastano J A 1985 *Physica* **D16** 285

Factors which determine the efficiency of sensitized singlet oxygen production

F WILKINSON*, D J McGARVEY and A OLEA

Department of Chemistry, Loughborough University of Technology, Loughborough,
Leicestershire, LE11 3TU, UK

Abstract. Nanosecond laser photolysis measurements of sensitized phosphorescence from oxygen have been used to obtain values for singlet oxygen formation efficiencies during oxygen quenching of excited singlet and triplet states of anthracene and naphthalene derivatives. Oxygen quenching of excited singlet states of anthracene and dicyanoanthracene in cyclohexane has been shown to lead to catalyzed production of triplet states with unit efficiency in both cases, but concurrent production of singlet oxygen only occurs in the case of 9,10-dicyanoanthracene with efficiency close to unity whereas the efficiency for singlet oxygen production due to direct oxygen quenching of excited singlet anthracene is close to zero. In contrast to these results, oxygen quenching of the triplet states of anthracene and dicyanoanthracene in cyclohexane yields singlet oxygen with unit efficiency whereas the singlet oxygen formation efficiency during oxygen quenching of triplet 1-ethynaphthalene is only 0.86 in cyclohexane and drops to 0.51 in acetonitrile. This solvent dependence demonstrates the role which charge transfer interactions play in determining singlet oxygen yields. Further information concerning the decay of excited oxygen-aromatic hydrocarbon charge-transfer complexes have been obtained from picosecond laser pump-probe studies where direct excitation is into the charge-transfer bands of oxygenated 1-ethynaphthalene. Following the excitation of the charge-transfer complex, the triplet state of 1-ethynaphthalene is rapidly produced with an efficiency which shows a marked solvent dependency, being 0.4 and 0.8 in acetonitrile and cyclohexane, respectively. The measured yields of singlet oxygen formation following excitation into 1-ethynaphthalene-oxygen charge-transfer complexes are 0.36 and 0.78 in these two solvents which is greater than that expected on the basis of the measured triplet yields. Mechanisms of quenching of excited states by oxygen which explain these results are discussed.

Keywords. Singlet oxygen yields; oxygen quenching; charge transfer absorption.

1. Introduction

It is well known that molecular oxygen is a paramagnetic molecule which is ubiquitous and efficiently quenches electronically excited states in dilute fluid solution (Birks 1970). The ground electronic state of molecular oxygen has zero angular momentum about its internuclear axis, contains two unpaired *p*-electrons and is given the group theoretical symbol $^3\Sigma_g^-$. The two electronically excited states of oxygen which arise from the same electron configuration, both with spin pairing of these two electrons, are the $^1\Delta_g$ and the $^1\Sigma_g^+$ states which lie 94 and 157 kJ mol $^{-1}$ respectively above the ground state. Oxygen is one of the most efficient quenchers of electronically excited

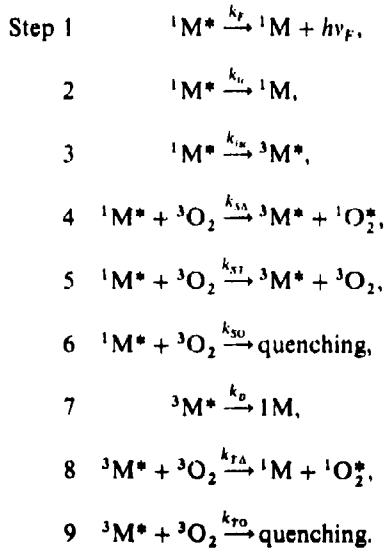
* For correspondence

states and it is often assumed that electronic excitation energy is transferred to oxygen with high efficiency when spin statistical factors are taken into account. In a set of classic studies, Gijzeman *et al* (1973) showed that the rate constants for oxygen quenching of the triplet states of several aromatic hydrocarbons are less than those expected for a diffusion-controlled reaction, being $\leq 3 \times 10^9 \text{ dm}^3 \text{ mol}^{-1} \text{ s}^{-1}$ in benzene solution at room temperature, which is about one ninth of the rate constants observed for oxygen quenching of excited singlet states of aromatic hydrocarbons (Ware 1962). However, the fractions of singlet and triplet states quenched by oxygen which produce singlet oxygen have more recently been shown to vary substantially from one compound to another. (Redmond and Braslavsky 1988a; Saltiel and Atwater 1988; McLean *et al* 1990; Wilkinson *et al* 1993). Quenching of excited singlet states by oxygen may produce singlet oxygen when the gap between the first excited singlet and triplet states of the aromatic hydrocarbon exceeds 94 kJ mol^{-1} and can, in addition, catalyse further production of triplet states (see below). This has to be taken into account when interpreting the quantum yields of singlet oxygen production measured in any experiments where there is oxygen quenching of singlet states.

The various competing reactions can be understood by considering the nine steps shown below from which it follows that

$$\Phi_F^0 = \frac{k_F}{k_F + k_{ic} + k_{isc}} \text{ and } \Phi_T^0 = \frac{k_{ic}}{k_F + k_{ic} + k_{isc}}, \quad (1)$$

where Φ_F^0 and Φ_T^0 are the quantum yields of fluorescence and of triplet state production in the absence of oxygen, respectively.



We can define the fraction of singlet states quenched by oxygen as

$$P_{\text{O}_2}^S = k_{\text{O}_2}^S [\text{O}_2]/(k_D^S + k_{\text{O}_2}^S [\text{O}_2]), \quad (2)$$

where

$$k_{O_2}^S = k_{s\Delta} + k_{sT} + k_{so} \text{ and } k_D^S = k_F + k_{lc} + k_{isc}.$$

The quantum yield of triplet production in the presence of oxygen $\phi_T^{O_2}$ is given by

$$\phi_T^{O_2} = \phi_T^0(1 - P_S^{O_2}) + f_T^{O_2}P_S^{O_2}, \quad (3)$$

where $f_T^{O_2}$ is the fraction of singlet states quenched by O_2 which yield triplet states. Note that step 6 represents quenching of the singlet state by oxygen by any mechanism which does not produce either singlet oxygen or triplet states i.e., other than those shown in steps 4 and 5. The quantum yield of singlet oxygen production by sensitization ϕ_Δ is given by the sum of the contributions due to oxygen quenching of singlet and triplet states i.e.

$$\phi_\Delta = \phi_\Delta(S_1) + \phi_\Delta(T_1). \quad (4)$$

If f_Δ^S and f_Δ^T are defined as the fractions of S_1 and T_1 states respectively quenched by oxygen which give $O_2^*(^1\Delta_g)$ it follows that

$$\phi_\Delta = f_\Delta^S P_S^{O_2} + \phi_T^0 f_\Delta^T P_T^{O_2}, \quad (5)$$

where $P_T^{O_2}$ equals that fraction of the triplet states which are quenched by oxygen, which is often close to unity because of the long lifetimes of many triplet states.

Quenching of the excited singlet state leads to a Stern-Volmer relationship between the fluorescence quantum yields in the absence and presence of oxygen as given by (6) where F^0 and F represent the fluorescent intensity of the sensitizer in the absence and presence of oxygen i.e.

$$\phi_F^0/\phi_F = F^0/F = 1 + k_{O_2}^S [O_2]/k_D^S. \quad (6)$$

When $P_T^{O_2} = 1$, combining (2), (3), (5) and (6) gives

$$\phi_\Delta(F^0/F) = (f_\Delta^S + f_T^{O_2} f_\Delta^T)[(F^0/F) - 1] + \phi_T^0 f_\Delta^T. \quad (7)$$

which can be used to obtain information concerning the crucial factors; however, one needs independent measurements of ϕ_T^0 and $f_T^{O_2}$ to determine f_Δ^S and f_Δ^T .

Alternatively one can produce the triplet states of the sensitizer with unit efficiency by energy transfer using aromatic ketones as triplet energy donors. Then (5) becomes

$$\phi_\Delta = f_\Delta^T P_T^{O_2}. \quad (8)$$

This allows values of f_Δ^T to be determined. We have recently employed this method used previously by ourselves (Garner and Wilkinson 1976) and others (Gorman *et al* 1987) to demonstrate the dependence of f_Δ^T for a series of naphthalene derivatives in benzene on the oxidation potential of the sensitizer (McGarvey *et al* 1992).

The perturbing effects of dissolved oxygen on the UV/Vis absorption spectra of organic molecules is a well-known phenomenon which was first studied in detail by Evans (1957) and subsequently discussed by Tsubomura and Mulliken (1960) and Birks (1970). The additional absorption bands observed include the lowest energy transition which corresponds to the $S_0 \rightarrow T_1$ transition of the organic molecules in intimate contact with an oxygen molecule. More intense absorption observed at

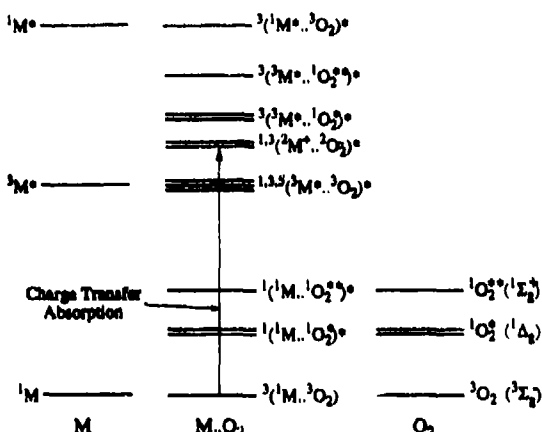


Figure 1. Schematic diagram of the lower energy levels of the $M \dots O_2$ complex between an aromatic molecule, M , and molecular oxygen, O_2 .

shorter wavelengths is often attributed to CT transitions within $^3(M \dots O_2)$ contact complexes (see figure 1) and this assignment is supported by the broad structureless appearance of the bands. In this paper, we exploit the optical absorption properties of oxygen/organic molecule contact complexes to directly populate, using both nanosecond and picosecond laser pulses, excited state complexes which may be involved in the dynamic quenching of excited states by oxygen.

2. Experimental

2.1 Materials

Anthracene (Aldrich Gold Label), naphthalene (Aldrich, scintillation grade, > 99%), 1-ethylnaphthalene (Fluka, 99%), benzophenone (BP) (Aldrich Gold Label) and *p*-methoxyacetophenone (PMAP) (Aldrich, 99%) were used as received. Acridine (Aldrich) was recrystallised from ethanol and 9,10-dicyanoanthracene (Kodak) was recrystallised from benzene. Acetonitrile (Aldrich, spectrophotometric grade) was dried by refluxing over calcium hydride. All other solvents were spectrophotometric grade from Aldrich and were used as received.

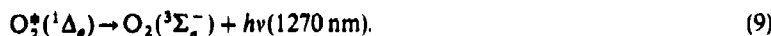
2.2 Picosecond pump-probe measurements

Solutions of 1·5 M 1-ethylnaphthalene (EN) in cyclohexane and acetonitrile were equilibrated with 2–4 atmospheres of oxygen yielding absorbances of ~ 0·3 around 355 nm compared with ~ 0·05 for air-equilibrated solutions. The absorbance due to the EN/O₂ contact complex exhibits a linear dependence on oxygen concentration under our conditions. The picosecond time-resolved absorption measurements were carried out at the Rutherford-Appleton Laboratory Laser Support Facility. The picosecond laser system was a frequency-doubled mode-locked Nd/YAG pumping a dye laser operating at 706 nm. The pump and probe wavelengths were obtained by

frequency-doubling to give 353 nm and mixing of 1064 nm and 706 nm to give 424 nm. The operating conditions were as follows: pump wavelength = 353 nm, pump energy = $4\mu\text{J}$; probe wavelengths = 424 nm and 706 nm, pulse duration = $\sim 5\text{ ps}$, irradiation area = 0.8 mm^2 . The probe wavelengths are suitable for detection of the EN triplet state (424 nm) and the EN radical cation (706 nm). We are not aware of a documented spectrum for EN^+ but expect that it will have a similar spectrum to the naphthalene radical cation which is well documented (Liu *et al* 1992). The yield of EN triplet state following CT excitation was measured by comparison of the triplet state absorption, observed at 424 nm, 400 ps after excitation with that from an identical optically-matched air-equilibrated solution containing BP or PMAP. Under our conditions ($[\text{EN}] = 1.5\text{ M}$) energy transfer is complete within 300 ps. Both ketones give the same yield of sensitised ${}^3\text{EN}^*$ demonstrating that energy transfer from the triplet state of these aromatic ketones proceeds with 100% efficiency giving an effective EN triplet state yield of unity for these solutions.

2.3 Nanosecond flash photolysis and singlet oxygen yield measurements

For nanosecond flash photolysis studies and for the singlet oxygen yield measurements the 355 nm harmonic of a Lumonics HY200 Q-switched Nd/YAG laser (8 ns, 15 mJ pulse $^{-1}$) was employed as the excitation source. Oxygen-quenching rate constants were determined by sensitising the EN triplet state with an aromatic ketone and measuring the rate of triplet decay in an air-equilibrated solution. Singlet oxygen was detected by monitoring the 0,0 vibronic band of the phosphorescence centred at 1270 nm (9) using a Judson germanium photodiode (J16-8SP-R05M, active diameter = 0.5 cm) coupled to a Judson PA100 amplifier,



The phosphorescence was detected at right angles to the exciting beam through a silicon cut-off filter. The laser energies employed did not exceed 0.7 mJ pulse $^{-1}$. Individual luminescence traces were signal-averaged and fitted using a single exponential function to yield the luminescence intensity I_0 at $t = 0$. The I_0 values were plotted against relative laser intensity to obtain plots which were linear below 0.5 mJ pulse $^{-1}$. Comparison of the slopes of these plots yielded relative singlet oxygen yields. The fluorescence measurements with anthracene and dicyanoanthracene were carried out using a Perkin-Elmer 3000 fluorimeter and the oxygen concentrations were in the range $2.4\text{--}34.6 \cdot 10^{-3}\text{ mol dm}^{-3}$.

3. Results and discussion

The singlet-triplet energy gap in the case of many aromatic hydrocarbons, e.g. anthracene, naphthalene and their derivatives, is such that it is energetically possible to produce singlet oxygen via oxygen quenching of both excited singlet and triplet states i.e. by reactions (4) and (8) given earlier. According to (7) plots of $\phi_\Delta(F^0/F)$ versus $[(F^0/F) - 1]$ should be linear and figure 2 shows that this applies to the data we obtained for anthracene and dicyanoanthracene in cyclohexane. The slopes and intercepts for these two compounds show very large differences. The slopes of these plots give values for $(f_\Delta^S + f_\Delta^T f_T^{O_2})$ of 0.91 ± 0.05 and 1.95 ± 0.05 respectively for

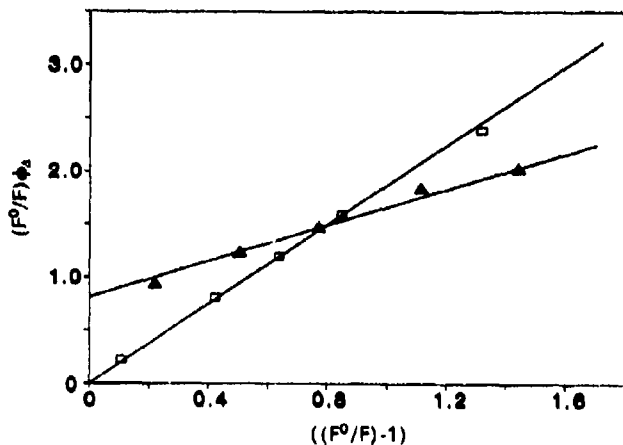


Figure 2. Plots according to (7) (see text) which illustrate the dependence of ϕ_A , the singlet oxygen yield, on the extent of fluorescence quenching by oxygen, where F^0 and F represent the fluorescence intensities in the absence and presence of oxygen, for (\blacktriangle) anthracene and (\blacksquare) dicyanoanthracene in cyclohexane.

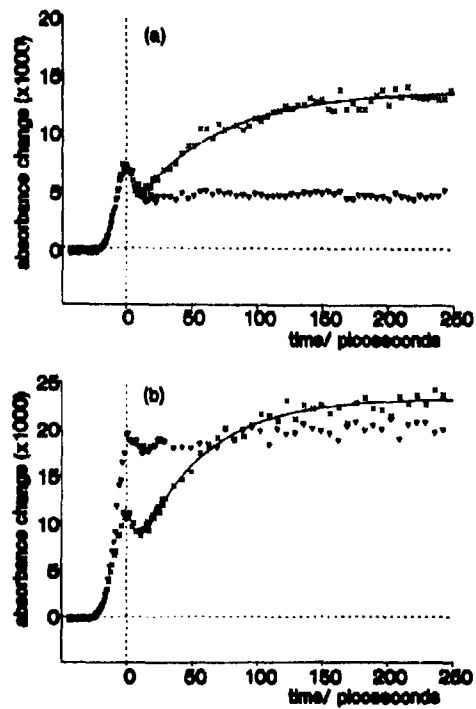


Figure 3. Picosecond absorption profiles observed for 1.5 mol dm^{-3} of 1-ethylnaphthalene in (a) acetonitrile and (b) cyclohexane; (∇) oxygenated with 3–4 atmospheres of oxygen, (\times) air-equilibrated containing benzophenone. The oxygenated and ketone-containing solutions were optically matched at the excitation wavelength (353 nm).

anthracene and dicyanoanthracene. The value for dicyanoanthracene is close to the maximum value of 2 which arises when $f_A^S = f_A^T = f_T^{O_2} = 1$ i.e. all these fractions are unity which applies when oxygen quenching is exclusively via steps 4 and 8. This is the situation for dicyanoanthracene in this solvent. Note that the intercept of the plot for dicyanoanthracene in figure 3 is 0 ± 0.05 which is consistent with $\Phi_T \approx 0$. In the case of anthracene, however, the intercept is equal to 0.77 ± 0.05 which equals $(f_A^T \Phi_T^0)$ and since the triplet yield is reported to be 0.72 ± 0.05 (Horrocks and Wilkinson 1968) these values are consistent with $f_A^T = 1.0 \pm 0.05$. Potashnik *et al* (1971) have shown that oxygen quenching of singlet anthracene does lead to enhanced triplet absorption with $f_T^{O_2} = 0.9 \pm 0.1$ in toluene and acetonitrile. It follows that f_A^S is close to zero for anthracene. The reason why f_A^S values are so different for anthracene and dicyanoanthracene is likely to be due to the same reason which causes the intersystem crossing yields of these two compounds to be so different, namely the presence or absence of an intermediate triplet state between the S_1 and T_1 states in these anthracene derivatives.

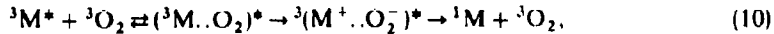
The probabilities of dissociation of collisional complexes of the type shown in figure 1 relative to the probability of internal conversion leading to energy dissipation in these complexes determines the values of f_A^S and f_A^T . In an attempt to understand such processes we have examined the singlet oxygen yields when excitation, under an elevated pressure of oxygen, was directly into the CT state (see figure 1) in comparison with the singlet oxygen yields observed via triplet sensitisation from triplet BP (or PMAP) in air-equilibrated 1.5 M EN solutions using optically matched solutions. The singlet oxygen yields from the sensitised samples were assumed to be the same as those measured by us using smaller EN concentrations (~ 0.05 M). In these measurements the standards used were acridine in acetonitrile, $\Phi_A = 0.82$ (Redmond and Braslavsky 1988b) and *p*-methoxyacetophenone/0.1 M naphthalene in cyclohexane, $\Phi_A = 0.92$ (Gorman *et al* 1991). Thus values of the singlet oxygen yields resulting from absorption to CT states of O_2/EN complexes, Φ_A^{CT} , equal to 0.36 and 0.78 were obtained in acetonitrile and cyclohexane respectively.

Using 353 nm picosecond excitation of the same solutions, a 'prompt' increase in absorption at 424 nm where triplet naphthalene absorbs was observed (figure 3), which does not significantly decay over the timescales investigated (~ 1 ns). Thus the EN triplet state is produced within a few picoseconds i.e. within the risetime of our picosecond apparatus. Superimposed upon the rise in triplet state absorption we observe a rapid symmetrical rise and fall in absorption which follows the excitation pulse. This component is present regardless of whether the solution is oxygenated or not and so is not derived from the CT state. Also this rapid component is not observed with neat acetonitrile or cyclohexane but is observed in the case of neat benzene. This feature has been observed previously (Masuhara *et al* 1981; Miyasaka *et al* 1985) in studies of multiphoton absorption by neat aromatic liquids as a rapid component absorbing around 420 nm and was attributed to electron-aromatic ion production and geminate recombination. We believe a similar process is operating when 1.5 M EN solutions are subjected to 353 nm picosecond excitation. The consequence of this multiphoton absorption is the appearance of a relatively small long-lived (> 1 ns) absorption which may be due to the excited singlet or triplet state of EN or it may be due to the EN radical cation or a combination of these. Since we do not have the facility of spectral resolution with our picosecond measurements we are presently unable to identify this weak background absorption.

Using the picosecond apparatus and probing at 706 nm for the EN radical cation we observed only very small 'prompt' absorptions ($\sim 10^{-3}$) which were not sensitive to the concentration of oxygen. This agrees with our nanosecond photolysis measurements where we also were unable to detect significant absorption in the 680–720 nm region following excitation into the CT band using either solvent. However these observations contrast with the report by Kristiansen *et al* (1991) who detected the 1-methylnaphthalene radical cation in acetonitrile following CT excitation. Unfortunately no details concerning the amounts of radical cation so produced were given. Thus it is difficult to compare results.

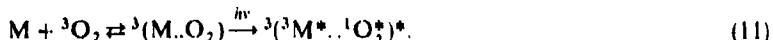
The varying efficiencies of triplet state formation (Φ_T^{CT}) as a function of solvent is apparent from the traces shown in figure 3. The triplet yield determinations derived exclusively from the picosecond pump-probe measurements of optically matched solutions are 0.40 and 0.80 in acetonitrile and cyclohexane respectively. We have determined f_A^T for EN in acetonitrile and cyclohexane using triplet ketones as triplet energy donors and the values we obtained were 0.51 and 0.86 respectively. The value of the product $f_A^T \Phi_T^{CT}$ that is equal to the amount of singlet oxygen production, which would be expected following excitation to the charge transfer state on the basis of the observed yield of triplet state production, equals 0.20 and 0.69 in acetonitrile and cyclohexane respectively, which is not equal to our measured values of Φ_A^{CT} particularly in acetonitrile. Thus more singlet oxygen is produced from the charge transfer state than can be accounted for from the amount of triplet state produced. Another interesting feature of the data is the large solvent dependence of Φ_T^{CT} . Thus in cyclohexane the triplet state production from the charge transfer state is very efficient ($\sim 80\%$) but in acetonitrile it is dramatically reduced to only 40%. This difference is clearly shown in figure 3.

In a previous paper (McGarvey *et al* 1992) we used the Rehm-Weller equation (Rehm and Weller 1970), neglecting the coulombic term, and calculated the free energy of the relaxed charge transfer states, ${}^1,{}^3(M^+..O_2^-)^*$ to be $\sim 30\text{ kJ mol}^{-1}$ below the localised triplet for EN. In acetonitrile where any coulombic correction will be small since it has a dielectric constant of 37.5 the excited complexes ${}^1,{}^3(M^+..O_2^-)^*$ are very likely to lie below the localised triplet and to be populated followed the formation of ${}^3M^*$ by energy transfer or following triplet state production following charge transfer absorption. There is a large difference between the f_A^T and k_q^T values for EN in the two solvents. In cyclohexane the values of f_A^T and k_q^T are 0.86 and $1.6 \times 10^9 \text{ l mol}^{-1} \text{ s}^{-1}$ respectively, while for acetonitrile the values are 0.51 and $3.3 \times 10^9 \text{ l mol}^{-1} \text{ s}^{-1}$. These numbers indicate that (9) is more important in acetonitrile than in cyclohexane due to the more favourable CT interactions in the more polar solvent. It is likely that this is due to the catalysed intersystem crossing via the triplet channel i.e.



which does not produce singlet oxygen. In cyclohexane which has a dielectric constant of 2.02 it is quite likely that the relaxed charge transfer states, ${}^1,{}^3(M^+..O_2^-)^*$ lie above the localised triplet and in the absence of CT-mediated quenching the triplet channel is impeded relative to the singlet channel because of poor Franck-Condon factors (Gijzeman *et al* 1973). Thus we would expect that deactivation of the initially prepared excited state complex to give ground state products would be faster in acetonitrile than in cyclohexane. This means that separation of ${}^3(M..O_2)^*$ to yield the triplet state would be more important in cyclohexane as observed.

Since the triplet energies of naphthalene and 1-methylnaphthalene are 255 and 249 kJ mol⁻¹ respectively (Murov 1973) it is likely that the energy of ${}^3({}^3\text{M}^*..{}^1\text{O}_2^*)^*$ i.e., the complex formed by association of the triplet state of EN and singlet oxygen, will be ~ 343 kJ mol⁻¹, which is slightly higher than the excitation energy used in these experiments (338 kJ mol⁻¹). In fact, Dijkgraaf and Hoijtink (1963) have reported a broad shoulder around 350 nm in oxygenated naphthalene solutions which they attribute to the simultaneous transition described by



Thus the simplest explanation for the fact that Φ_{CT}^A is higher than $f_A^T \Phi_T^{CT}$ is that excitation at 353 and 355 nm gives both ${}^3\text{M}^*$ and singlet oxygen following dissociation of ${}^3({}^3\text{M}^*..{}^1\text{O}_2^*)^*$ formed either as a result of direct absorption to this doubly excited complex or following internal conversion from the initially formed Franck-Condon charge transfer complex ${}^3(\text{M}^+..{}^1\text{O}_2)^*_{FC}$. In the case of acetonitrile and cyclohexane, respectively, this would require a quantum yield of 0.16 and 0.08 for this process in these two solvents. The fact that several organic compounds, which have energy gaps between their lowest singlet and triplet states greater than 94 kJ mol⁻¹ give singlet oxygen yields greater than one (Tsubomura and Mulliken 1960; Saltiel and Atwater 1988; Kanner and Foote 1992) when excited into their lowest singlet excited states, demonstrates that this doubly excited state dissociates to give both the triplet state and singlet oxygen when it is populated in the case of many other compounds.

4. Conclusions

We have shown how fluorescence quenching measurements combined with singlet oxygen yield measurements can be used to obtain values of f_A^S and f_A^T , the fractions of singlet oxygen formed for oxygen quenching of excited singlet and excited triplet states, respectively. The values of f_A^S for anthracene and 9,10-dicyanoanthracene are 0 and 0.95 ± 0.05 respectively. Unfortunately there are very few f_A^S values in the literature (see Saltiel and Atwater 1988 and Wilkinson *et al* 1993 and references therein). Thus it is difficult at present to speculate on the reasons for observed variations in f_A^S . By contrast, many authors have obtained values for f_A^T , and recent measurements by ourselves (McGarvey *et al* 1992) have indicated the important role charge transfer interactions play in increasing the probability of quenching by pathways which do not lead to energy transfer. We have used picosecond pump probe techniques following exclusive direct excitation of charge transfer complexes of 1-ethylnaphthalene/O₂ to probe the fate of excited charge transfer complexes. We observe a prompt production of the triplet state is less than 5 picoseconds. We have shown that the quantum yields of prompt triplet states produced are 0.4 and 0.8 in acetonitrile and cyclohexane, respectively, i.e. we have shown that the value is strongly dependent on the polarity of the solvent. The quantum yield of singlet oxygen production following charge transfer excitation is also solvent dependent; however, the values obtained for Φ_A^{CT} are 0.36 and 0.78 which are greater than one would expect on the basis of the measured triplet yields. We suggest that the excited charge transfer complex can dissociate to give both triplet states and singlet oxygen immediately following excitation.

Acknowledgements

The authors are grateful to the US Army, the Fundacion Andes and to SERC for financial support.

References

- Birks J B 1970 *Photophysics of aromatic molecules* (London: Wiley-Interscience) chap. 10, p. 492, and references therein
 Dijkgraaf C and Hoijtink G J 1963 *Tetrahedron Suppl.* 2 **19** 179
 Evans D F 1957 *J. Chem. Soc.* 1351
 Garner A and Wilkinson F 1976 *Singlet oxygen, reactions with organic compounds and polymers* (eds B Ranby and J F Rabek) (New York: John Wiley & Sons) p. 48
 Gijzeman O L J, Kaufman F and Porter G 1973 *J. Chem. Soc., Faraday Trans.* 2 **69** 708
 Gorman A A, Hamblett I, Lambert C, Prescott A L, Rodgers M A J and Spence H M 1987 *J. Am. Chem. Soc.* **109** 3091
 Gorman A A, Krusnovsky A A and Rodgers M A J 1991 *J. Phys. Chem.* **95** 598
 Horrocks A R and Wilkinson F 1968 *Proc. R. Soc. A* **306** 257
 Kanner R C and Foote C S 1992 *J. Am. Chem. Soc.* **114** 678
 Kristiansen M, Scurlock R D, Lu K-K and Ogilby P R 1991 *J. Phys. Chem.* **95** 5190
 Liu A, Sauer Jr M C, Loffredo D M and Trifunac A D 1992 *J. Photochem. Photobiol.* **A67** 197
 Masuhara H, Miyasaka H, Ikeda N, and Mataga N 1981 *Chem. Phys. Lett.* **82** 59
 McGarvey D J, Szekeres P G and Wilkinson F 1992 *Chem. Phys. Lett.* **199** 314
 McLean A J, McGarvey D J, Truscott T G, Lambert C and Land E J 1990 *J. Chem. Soc., Faraday Trans.* **86** 3075
 Miyasaka H, Masuhara H and Mataga N 1985 *J. Phys. Chem.* **89** 1631
 Mirov S L 1973 *Handbook of photochemistry* (New York: Marcel Dekker)
 Potashnik R, Goldschmidt C R and Ottolenghi M 1971 *Chem. Phys. Lett.* **9** 404
 Redmond R W and Braslavsky S E 1988a *Chem. Phys. Lett.* **148** 523
 Redmond R W and Braslavsky S E 1988b *Photo sensitisation: NATO ASI Series* (eds) G Moreno, R H Pottier and T G Truscott (Heidelberg: Springer-Verlag) vol. H15, p. 93
 Rehm D and Weller A 1970 *Z. Phys. Chem.* **69** 183
 Saltiel J and Atwater B W 1988 *Adv. Photochem.* **14** 1
 Tsubomura H and Mulliken R S 1960 *J. Am. Chem. Soc.* **82** 5966
 Ware W R 1962 *J. Phys. Chem.* **66** 455
 Wilkinson F, Helman W P and Ross A B 1993 *J. Phys. Chem., Ref. Data* **33** 001

First photothermal deflection spectroscopy set-up in Egypt

SOHAIR NEGM

Prof. Hassan Talaat Laboratory, Advanced Laser Spectroscopy Laboratory, Ain Shams University, Abbassia, Cairo, Egypt
Present address: Faculty of Engineering (Shoubra), Zagazig University (Benha), Zagazig, Egypt

Abstract. We have succeeded in carrying out some ultra-sensitive photothermal experiments, using photothermal deflection spectroscopy (PDS) (or mirage effect). We have also employed the PDS technique to study the optical and thermal properties of solid/air interfaces. The experimental set-up of the transverse PDS has been described.

The experimental results show that there is an exponential decay in PD signals with increase in the chopper frequency as well as with an increase of the phase difference. The PD signal decreases with increasing the probe beam normal offset to allow us to calculate the thermal diffusion length of the deflection medium (air in our case). We determined the thermal diffusion of air to be = 0.43 mm at the chopper frequency 50 Hz, which is in agreement with published values. Further, we employed the PD technique to obtain the spectra for two dyes [Rhodamine 6G (Rh6G) and Crystal Violet (CV)] of different optical absorption structures. The PDS shows a good resolution of the peaks of CV which are hardly separated in optical absorption measurements.

Finally, a comparison of the photoacoustic spectra (PAS) of the two dyes was carried out, which showed that PDS has better spatial spectral resolution.

Keywords. Photothermal deflection spectroscopy; properties of solid/air interfaces; optical absorption.

1. Introduction

Absorption spectroscopy is normally carried out indirectly through measurement of the incident, reflected and/or transmitted intensities, from which one can determine the absorbed intensity. Among the principal techniques to measure absorption directly are the photothermal deflection (PD) and photoacoustic (PA) spectroscopies. Both spectroscopies measure the heat deposited in the material due to the absorption of photons, either optically in the case of PD or acoustically in the case of PA. It is well known that upon the absorption of electromagnetic radiation by a given medium, a fraction or all the excitation energy is converted into thermal energy through de-excitation processes. This de-excitation mechanism has provided the physical basis for the highly sensitive PD spectroscopy. This technique was first introduced in 1980 by Boccaro *et al* (1980) and subsequently developed by Aamodt and Murphy (1981) and by Jackson *et al* (1981). PD spectroscopy is a powerful and novel experimental method in which the absorption coefficient of the sample is deduced from the measurements of the thermal gradient in the gas layer adjacent to the sample surface.

In this method, the sample is illuminated with a chopped monochromatic light "pump beam" and, when the sample absorbs any of the energy incident on it, some of the energy levels in the sample are excited and subsequently these energy levels must be de-excited. The most common mode of de-excitation is through the non-radiative or heating mode and thus the optical excitation of the sample results in a periodic heat flow from the sample to the surrounding media. This, in turn, results in a corresponding change in the index of refraction. By probing this variation of the refractive index by a second weak "probe beam", it experiences a periodic deflection synchronous with the intensity modulation. The amplitude and phase of the periodic deflection of the probe beam can be measured with a position sensor. This deflection is directly related to the optical absorption of the sample as will be shown in the next section. The positioning of the probe beam with respect to the pump beam allows for two choices in performing PDS: collinear configuration, where the gradient of the index of refraction is both created and probed within the sample, and transverse configuration, in which the index of refraction is accomplished in a thin layer adjacent to the sample surface. The latter is the case that will be discussed in this work. The photothermal technique has many advantages:

- (1) The technique could be employed for samples whose optical absorptions are difficult to obtain directly, e.g. powdered samples, as also for samples that are completely opaque to transmitted light.
- (2) It also incorporates the thermal properties of the sample and its surroundings, hence, this property, like thermal diffusivity and conductivity, could be determined.
- (3) It is an ultra-high sensitive method for probing the thermal properties of matter. The temperature rise associated with this process is of the order of 10^3 - 10^4 °C. The technique is easily used for absorption detection.
- (4) It surmounts the limitation of PA (where the sample has to be enclosed in a PA cell) and measurements may often be made in open sample configuration with substantial reduction in experimental complexity.
- (5) Acoustic shielding requirements are less stringent.
- (6) There is also no background due to window absorption.
- (7) PD works in hostile environments such as at extreme temperatures or in caustic substances.

Because of the above advantages, for the use of FDS and our experience in PAS, it was decided to construct a set-up for PDS (according to Fournier and Boccara) (Boccara *et al* 1980) measurements in air, in an on-going project to study materials whose optical absorptions are normally difficult to obtain.

In this paper, we present our initial results using the PDS set-up to determine the optical absorption of dye lasers in powder form and to compare the obtained spectra with those obtained using PAS.

2. Theory

In order to correlate the deflection signal to processes occurring at the sample surface, it is necessary to determine: (1) The temperature distribution T in the sample and the surrounding media as a function of position and time; (2) the optical beam propagation through the non-homogeneous medium; (3) the relation between the deflection and the output voltage of the position sensor.

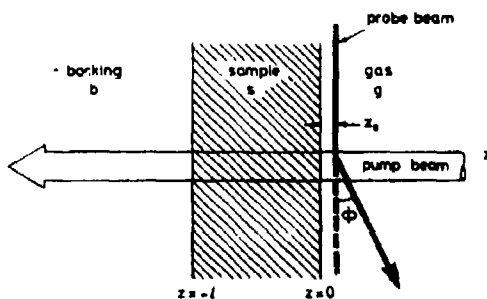


Figure 1. Geometry of the thermal field evaluation (transverse PDS).

2.1 Temperature distribution in the sample and the surrounding media

Consider the geometry as shown in figure 1; the sample is placed on a backing material and surrounded by a fluid (air in our case). The boundary planes are assumed to be parallel and infinitely extended in the radial direction. The sample is illuminated perpendicularly by a modulated laser beam or a lamp as we have used in our work. Assume that both the gas and the backing material are optically non-absorbing media. The absorbed radiation heats the sample and diffuses through the gas-sample and the backing material. The time dependent a.c. component of the temperature T satisfies the equations (Salazar *et al* 1989),

$$\nabla^2 T_g - (1/\kappa_g)(\partial T_g/\partial t) = 0, \text{ for gas,} \quad (1a)$$

$$\nabla^2 T_s - (1/\kappa_s)(\partial T_s/\partial t) = -(Q(r,t)/k_s), \text{ for sample,} \quad (1b)$$

$$\nabla^2 T_b - (1/\kappa_b)(\partial T_b/\partial t) = 0, \text{ for backing,} \quad (1c)$$

subject to the following boundary condition.

(i) Temperature continuity at the sample surface:

$$T_g|_{z=0} = T_s|_{z=0} \quad \& \quad T_s|_{z=-l} = T_b|_{z=-l}; \quad (2a)$$

(ii) Heat flow continuity at the sample surface:

$$k_g \frac{\partial T_g}{\partial z} \Big|_{z=0} = k_s \frac{\partial T_s}{\partial z} \Big|_{z=0} \quad \& \quad k_s \frac{\partial T_s}{\partial z} \Big|_{z=-l} = k_b \frac{\partial T_b}{\partial z} \Big|_{z=-l}; \quad (2b)$$

where l is the sample thickness, $k_{(i)}$ is the thermal conductivity of the material (i) (cal/cm s °C), $\rho_{(i)}$ the density of the material (i) (g/cm³), $c_{(i)}$ the specific heat of the material (i) (cal/g °C), and $\kappa_{(i)} = k_{(i)}/\rho_{(i)} \cdot c_{(i)}$, the thermal diffusivity of material (i). (i) can have subscripts s, g, b, representing sample, gas and backing material (Rossencwaig and Gersho 1976). $Q(r,t)$ is the heat deposited per unit volume oscillating with frequency ω and can be given by:

$$Q(r,t) = (P_0 \alpha / \pi a^2) \exp(\alpha z) \exp(-r^2/a^2)^{1/2} \exp(i\omega t), \quad (3)$$

where P_0 is the power of the exciting beam, α is the optical absorption coefficient of the sample and a is the beam radius defined at 1/e of the intensity.

The set of equations (1), with initial conditions (2), has been solved using the method of separation of variables in cylindrical geometry. The solutions are

$$T_g(r, z, t) = \frac{1}{2} \int_0^\infty \delta J_0(\delta r) E(\delta) \exp(-\beta_g z) \exp(i\omega t) d\delta, \quad (4)$$

$$\begin{aligned} T_s(r, z, t) = \frac{1}{2} \int_0^\infty & \delta d\delta J_0(\delta r) [\Gamma(\delta) \exp(\alpha z) + A(\delta) \exp(\beta_s z) \\ & + B(\delta) \exp(-\beta_s z)] \exp(i\omega t), \end{aligned} \quad (5)$$

$$T_b(r, z, t) = \frac{1}{2} \int_0^\infty \delta J_0(\delta r) D(\delta) \exp(\beta_b(l+z)) \exp(i\omega t) d\delta, \quad (6)$$

where $\beta_i^2 = \delta^2 + (i\omega/\kappa_i)$ ($i = g, s, b$) is the relation between the separation constants, and J_0 is the Bessel function of zero order and we have:

$$A(\delta) = -[\Gamma(\delta)/H(\delta)][(1-g)(b-P)\exp(-\alpha l) + (1+b)(g+P)\exp(\beta_s l)], \quad (7)$$

$$\begin{aligned} B(\delta) = -[\Gamma(\delta)/H(\delta)][(1+g)(b-P)\exp(-\alpha l) \\ + (1-b)(g+P)\exp(-\beta_s l)], \end{aligned} \quad (8)$$

$$D(\delta) = \Gamma(\delta) \exp(-\alpha l) + A(\delta) \exp(-\beta_s l) + B(\delta) \exp(\beta_s l), \quad (9)$$

$$E(\delta) = \Gamma(\delta) + A(\delta) + B(\delta), \quad (10)$$

$$H(\delta) = (1+g)(1+b)\exp(\beta_s l) - (1-g)(1-b)\exp(-\beta_s l). \quad (11)$$

$$g = (k_g \beta_g / k_s \beta_s), \quad (12)$$

$$b = (k_b \beta_b / k_s \beta_s), \quad (13)$$

$$P = (\alpha/\beta_s). \quad (14)$$

The physical interpretation of (4), (5) and (6) is that any temperature distribution can be decomposed into distribution of the form of

$$J_0(\delta r) \exp(-\beta_i z).$$

The distributions act independently of each other and have an effective thermal length given by

$$l_i = (1/\mathcal{M}_i(\beta_i)) = [\mathcal{M}_i(K_i^2 + \delta^2)^{1/2}]^{-1}.$$

The case of $\delta = 0$ and $i\omega/\kappa$ can be expanded to real and imaginary parts. Then $\beta = (1+i)(\omega/2\kappa_i)^{1/2}$, which is the one-dimensional solution given by Rossencraig and Gersho (1976). δ can then be expressed as a parameter to show how the heat is diffused in directions other than the z -direction.

2.2 Temperature distribution for transverse PDS

For transverse PDS, the probe beam propagates completely within the gas. The material is divided into two classes according to the optical absorption coefficient (Salazar *et al* 1989)

2.1a *Optically opaque solids ($\alpha l \gg 1$):* In these materials the optical length ($\mu\alpha = 1/\alpha$) is much smaller than the sample thickness l and (4) T_g can be expressed as:

$$T_g(r, z) = \frac{1}{2} \frac{P_0}{2\pi k_b} \int_0^\infty \delta J_0(\delta r) \exp(-\delta^2 a^2/4) \frac{1}{\beta_i} \left(\frac{1 + \exp(-2\beta_i l)}{1 - \exp(-2\beta_i l)} \right) \exp(-\beta_g z) d\delta. \quad (15)$$

2.2b *Optically transparent solids ($\alpha l \ll 1$):* The optical absorption length of these materials is much greater than the sample thickness and the temperature distribution in the gas is given by (Salazar *et al* 1989)

$$T_g(r, z) = \frac{1}{2} \frac{P_0}{2\pi k_b} \int_0^\infty \delta J_0(\delta r) \exp(-\delta^2 a^2/4) \frac{\alpha}{\beta_i^2} \exp(-\beta_g z) d\delta. \quad (16)$$

2.3 Optical beam deflection for transverse PDS

In the case of transverse PDS, the probe beam is directed parallel to and grazing the sample surface through the gas and is deflected by an amount (Salazar *et al* 1989)

$$\phi = (1/n)(dn/dT) \int_{-\infty}^{\infty} \nabla_{\perp} T_g \times dS, \quad (17)$$

where n is the gas refractive index and S is the ray path, see figure 2 where the x -axis is the probe beam direction. There are two components of the probe beam deflection: the transverse component ϕ_t and the normal component ϕ_n , where

$$\phi_t = -(1/n)(dn/dT) \int_{-\infty}^{\infty} (\partial T_g / \partial y) dx \hat{k}, \quad (18)$$

$$\phi_n = (1/n)(dn/dT) \int_{-\infty}^{\infty} (\partial T_g / \partial z) dx \hat{j}. \quad (19)$$

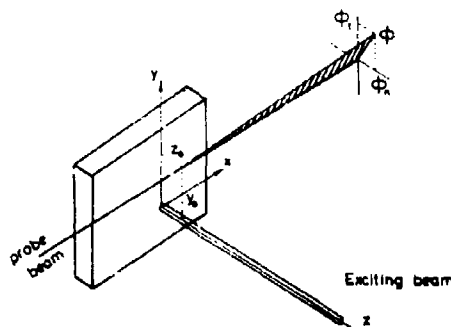


Figure 2. Geometry for the "mirage" deflection. The probe beam has a transverse offset y_0 and a normal offset z_0 .

Using (4) for T_s and taking into consideration the integral transform relation (Murphy and Aamodt 1980) one can write:

$$\phi_t = (1/n)(dn/dT) \int_0^\infty \delta \sin(\delta y) E(\delta) \exp(-\beta_s z) \exp(i\omega t) d\delta \hat{K}, \quad (20)$$

$$\phi_n = (1/n)(dn/dT) \int_0^\infty \beta_s \cos(\delta y) E(\delta) \exp(-\beta_s z) \exp(i\omega t) d\delta \hat{J}, \quad (21)$$

and by classifying the material into two parts we get the following relations.

2.3a For optically opaque solids:

$$\begin{aligned} \phi_t &= -\frac{1}{n d T} \frac{P_0}{2\pi k_s} \exp(i\omega t) \int_0^\infty \delta \sin(\delta y) \exp(-\delta^2 a^2/4) \\ &\times \frac{1}{\beta_s} \left(\frac{1 + \exp(-2\beta_s l)}{1 - \exp(-2\beta_s l)} \right) \exp(-\beta_s z) d\delta \hat{K}, \end{aligned} \quad (22a)$$

$$\begin{aligned} \phi_n &= \frac{1}{n d T} \frac{P_0}{2\pi k_s} \exp(i\omega t) \int_0^\infty \beta_s \cos(\delta y) \exp(-\delta^2 a^2/4) \\ &\times \frac{1}{\beta_s} \left(\frac{1 + \exp(-2\beta_s l)}{1 - \exp(-2\beta_s l)} \right) \exp(-\beta_s z) d\delta \hat{J}. \end{aligned} \quad (22b)$$

2.3b For optically transparent solids:

$$\phi_t = -\frac{1}{n d T} \frac{P_0}{2\pi k_s} \exp(i\omega t) \int_0^\infty \delta \sin(\delta y) \exp(-\delta^2 a^2/4) \frac{\alpha}{\beta_s} \exp(-\beta_s z) d\delta \hat{K}, \quad (23a)$$

$$\phi_n = \frac{1}{n d T} \frac{P_0}{2\pi k_s} \exp(i\omega t) \int_0^\infty \beta_s \cos(\delta y) \exp(-\delta^2 a^2/4) \frac{\alpha}{\beta_s} \exp(-\beta_s z) d\delta \hat{J}, \quad (23b)$$

where P_0 is the pump beam power, z is the normal offset, y is the transverse offset. The above two equations show that the deflection is proportional to the power of the pump beam and exponentially decays with the modulation frequency.

2.4 The relation between the deflection and the output voltage of the position sensor

The deflection of the beam due to the change in the index of refraction of the medium adjacent to the sample is detected by the position sensor with converts the deflection into an output voltage. The change of the signal ΔV above the d.c. level is calculated as shown in figure 3. Assuming a Gaussian probe beam

$$\frac{\Delta V}{V} = \frac{\Delta I}{I_0} = 4\Delta x \int_0^\infty \frac{2}{\pi \omega_2^2} \exp(-2r^2/\omega_2^2) dr = \frac{4}{(2\pi)^{1/2}} \frac{\Delta x}{\omega_2}, \quad (24)$$

since $\phi_d = \Delta x$, where d is the distance from the focal spot of the probe beam to the

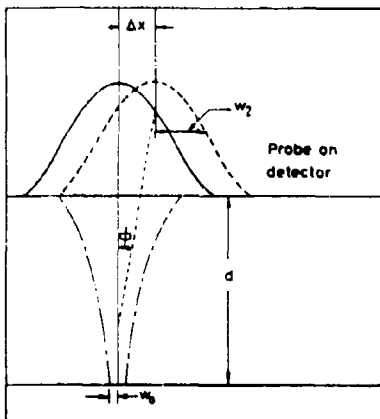


Figure 3. Probe beam on the detector.

detector, I_0 is the probe beam intensity, and ω_2 is the radius of the spot on the detector.

$$\omega_2 = \lambda d / (\pi \omega_0 n_0),$$

where ω_0 is the probe beam radius at the focal spot. Hence,

$$\Delta V = [4/(2\pi)^{1/2}] \phi(\pi \omega_0 n_0 / \lambda) V. \quad (2.5)$$

This equation shows that the output signal is independent of the distance between the sample and the detector for modulation frequency of the order of few hundred cycles per second.

3. Experimental procedure

We have carried out the transverse (PD) technique (Jackson *et al* 1981), in our work here. The set-up is shown in figure 4. A 1000 W tungsten-halogen lamp is used, with its housing cooled by water circulation and small air fan. The light from the lamp is focussed by a glass lens L_1 into the entrance slit of the monochromator (Carl Zeiss Jena, 287804) to provide a tunable light source. A mechanical chopper (variable speed) [15 Hz-10 kHz light chopper, Noise Interference Type Boston Electronic (617) 566-382] is located in front of the entrance slit of the monochromator. Its purpose is to chop (interrupt) the light beam and to provide the reference signal for detection. The monochromator is motorized to allow for accurate scan of the wavelength. The output light was focussed on the sample by using camera lens L_2 . An He-Ne laser (high pointing stability 0.5 mW laser uniphase 1101 power supply Model 1201 (408) 434-1800) with output wavelength 6328 Å served as the optical probe beam. This beam is focussed by a convex lens L_3 with focal length 10 cm. The deflection of the probe was monitored by a position sensor (split photo diode) detector low noise preamplifier (Ithaco Model 1202 (607) 272-7640 at 60 cm from the sample. The output of the position sensor amplifier was fed into a synchro-He⁺ lock-in amplifier (Princeton Applied Research Model 186A) (Murphy and Aamodt 1980).

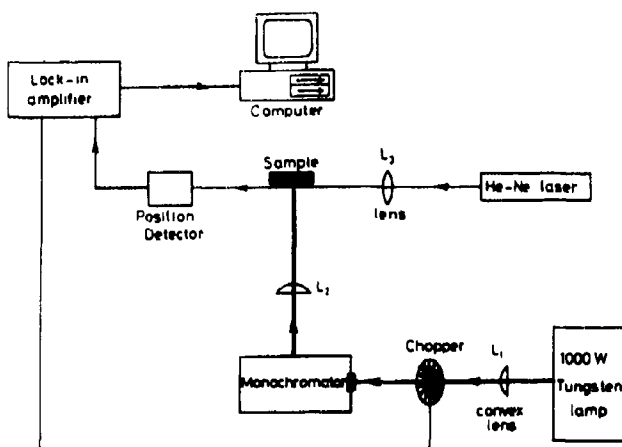


Figure 4. Experimental set-up of the transverse (PDS) technique.

The square-wave output signal generated by the chopper is applied to the reference signal input of the lock-in amplifier. The output from the lock-in amplifier is connected to an $x - y$ recorder or a personal computer. In order to isolate the set-up from possible laboratory vibrations that can prove to have a very destructive effect on the PDS signal, a specially designed sand box was used to avoid these vibrations. The PDS components were also held to a heavy iron plate that was placed on the sand box. This design was very effective in reducing possible vibrations leading to a noisy signal. Under these conditions, maximum deflection and good transverse resolution across the heated region were achieved.

4. Results and discussions

4.1 The dependence of the amplitude and the phase of the signal on the chopper frequency at constant value of the normal offset z_0

To check the correspondence of the change of the signal amplitude and phase with the chopper frequency, and to see how it follows the theory, the dependence of the amplitude and the phase of the signal were determined as the frequency of the chopper was changed (at constant value of normal offset z_0). The experimental results of PD signal of the carbon black sample versus the chopper frequency (ω) are shown in figure 5. The plots show that the PD signal amplitude falls off as $1/\omega$. This is in agreement with theory, (22), and the literature (Jackson *et al* 1981). This result was repeated for three values of the probe beam offset z_0 . Further, by comparing these results for the three normal offset values of z_0 , one can see that the signal amplitude decreases as the probe beam offset increases. From both these observations, one can conclude that there is a strong dependence of the signal on the modulated frequency and also on the probe beam offset z_0 as indicated by theory (Aamodt and Murphy 1981). Since the main source of the PD signal is the sample surface temperature, each component (spatial frequency) has different effective thermal diffusion length. The high spatial terms contribute to the rapidly varying temperature profile, while the low

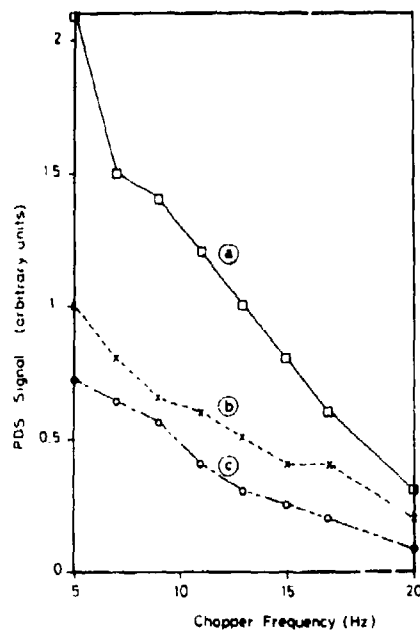


Figure 5. The transverse PDS vs. the chopper frequency at probe beam normal offset $z_0 = 250 \mu\text{m}$ (a), $500 \mu\text{m}$ (b), $750 \mu\text{m}$ (c).

spatial frequency terms determine a slowly varying coarser feature. Since the thermal diffusion length is a measure of how far diffusing from a heat source can travel and remain coherent with the excitation source modulation, and since each spectral component has its own effective thermal diffusion length, the sample volume contributing to the surface temperature will be different for each component. Since $\mu_i = (2k_i/\omega)^{1/2}$ where μ_i is the thermal diffusion length of material i , for high modulation frequency the thermal diffusion length of the sample will be small and the contribution comes only from a small volume. On the other hand, for low spatial frequency, μ_i is larger and the contribution comes from a big volume, thus the coarser features are determined. Figure 6 shows the increase in the phase difference of the PDS signal as the chopping frequency increases. The phase difference is a function of the diffusion length of the sample, and it indicates that there is a time delay between the excitation of the sample and subsequent deflection of the beam.

4.2 The dependence of the signal on the normal offset z_0 at constant modulation frequency

In this part, as can be seen from figure 7, the effect on the PDS signal of varying the value of the normal probe beam offset z_0 . In this case again, the sample was standard Carbon Black sample. There is an exponential increase of the signal as the probe beam approaches the sample surface. The exponential dependence which is illustrated in (22a) where $\phi \propto \exp(-z_0/l_g)$ and $l_g = (2k_g/\omega)^{1/2}$. We can see that there is also a strong dependence of the PDS signal on the probe beam offset z_0 . The exponential

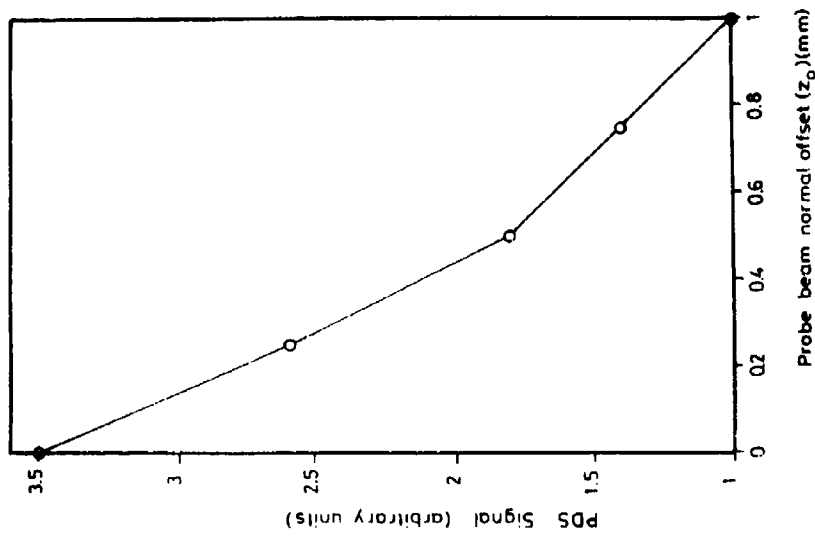


Figure 7. The transverse PDS signal amplitude vs the probe beam normal offset z_0 at chopper frequency 15 Hz.

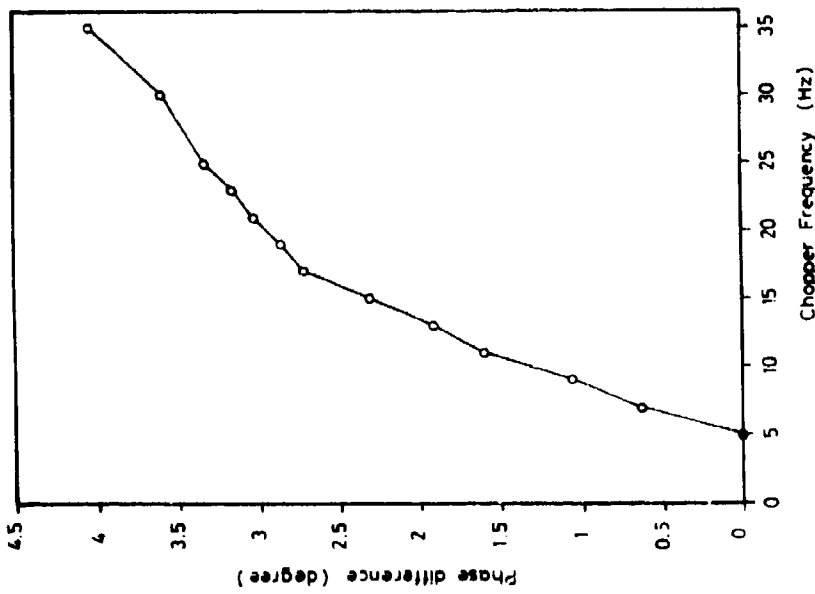


Figure 6. The phase difference vs the chopper frequency.

decrease of the signal with the increasing values of z_0 can be used to determine the diffusivity of the deflecting medium (air). By taking the logarithm of both sides of ($\phi \propto \exp(-z_0/H_g)$) we get

$$\ln \phi = k - (\omega/2k_g)^{1/2} z_0,$$

which is a straight line whose slope is $(\omega/2k_g)^{1/2}$; this gives the value of the thermal diffusion length (l_g) of the air to be ≈ 0.438 mm at 50 Hz. This is in agreement with the published value given by Boccaro *et al* (1983).

4.3 Spectral results

We also employed the PD technique to investigate photothermal signal resolution of the absorption bands of two dyes with differing absorption bands. These dyes are: Rhodamine 6G (Rh6G) and Crystal Violet (CV) which has two overlapping bands at 550 nm and 580 nm which could hardly be separated optically. The normalized PDS spectra of the two dyes are shown in figure 8. One can observe from the figures that the PDS spectrum for Rh6G exhibits a peak at ≈ 530 nm while in the case of CV it shows a peak at ≈ 560 nm.

As mentioned earlier, the transverse PDS has spatial resolution on the sample surface. We have measured three spectra for Crystal Violet dye (CV) at different values of the probe beam normal offset z_0 . These spectra are shown in figure 9. It can be seen from the figures that for large values of z_0 the spectrum is wide and

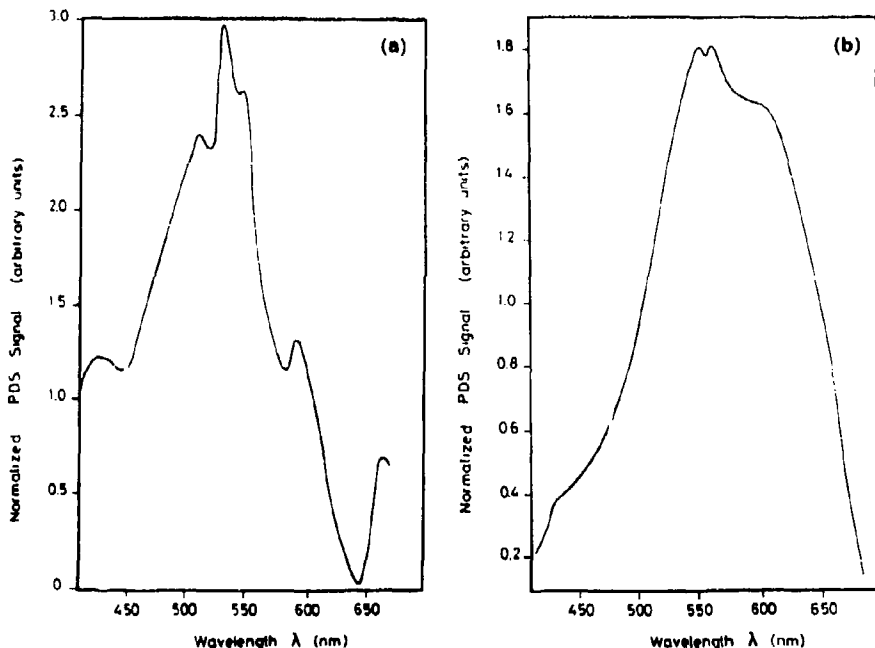


Figure 8. The normalized PD spectra of Rh6G (a) and CV (as powder) (b) at chopper frequency 14 Hz.

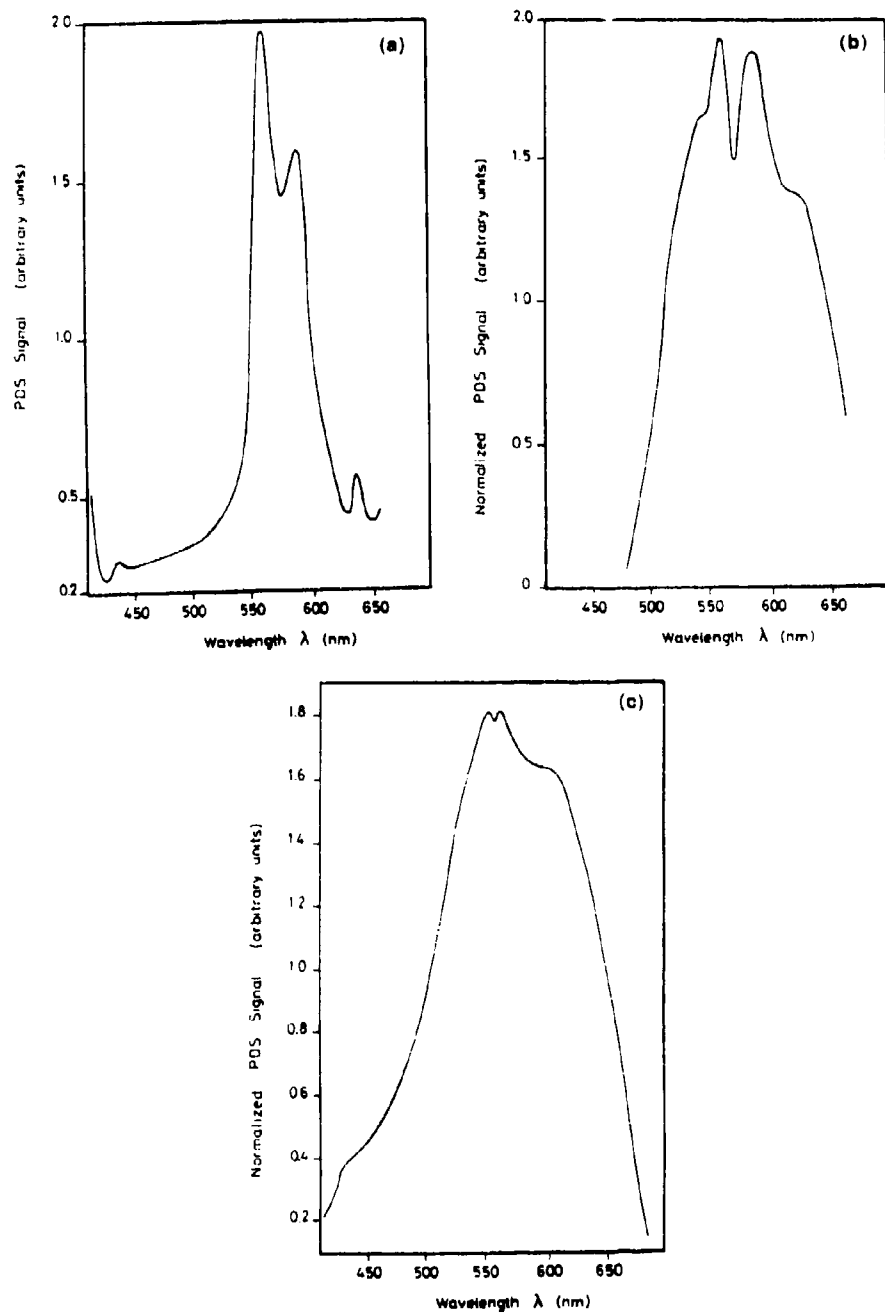


Figure 9. The normalized spectra of CV at chopper frequency 14 Hz. The probe beam normal offset: $z_0 \approx 85 \mu\text{m}$ (a), $125 \mu\text{m}$ (b), $175 \mu\text{m}$ (c).

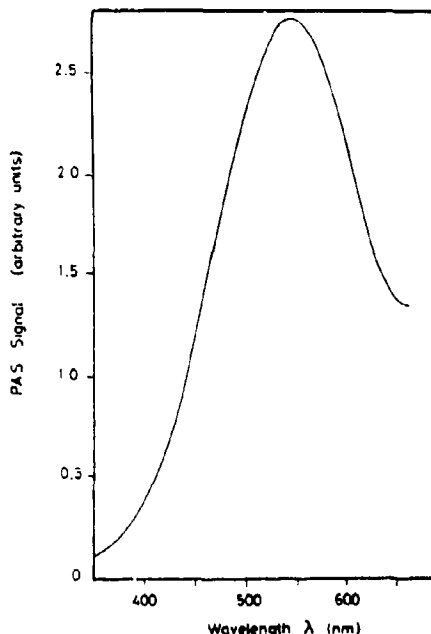


Figure 10. Normalized PAS of Rh6G (solid) at chopper frequency 14 Hz.

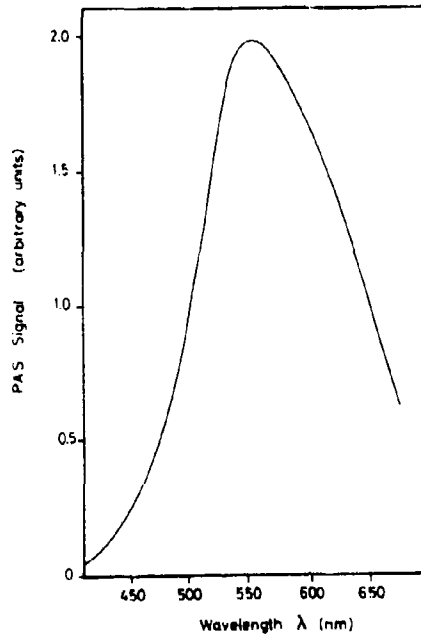


Figure 11. Normalized PAS of CV (solid) at chopper frequency 14 Hz.

smooth and there is a complete masking of the much sharper peaks of CV. This is because at large values of z_0 ($z_0 = 175 \mu\text{m}$), the observed spectrum is a collection of the average values of the contributions of all points of the inhomogeneous sample surface. For the smaller value of z_0 we can see that the spectrum is much narrower and noiser. The two peaks, seen at wavelengths 550 and 580 nm, became regular. For the smallest value of z_0 used ($85 \mu\text{m}$), the two peaks become very narrow and are well-resolved. This shows that the PDS has much better resolution than regular optical absorption. Using PDS we are able to resolve the two peaks that normally overlap.

4.4 Comparison with photoacoustic spectroscopy

Since PDS and PA detection provide similar experimental information, a comparison of these two methods is of interest. We compared our experimental PD spectra with the PA spectra for the same two dye materials (Rh6G and CV). The figures 10, 11 show the normalized PA spectra of the two dyes. We observe from these figures and from figure 8 that the PA spectra of both Rh6G and CV are broader and form smoother bands than that of the corresponding PD spectra even at large values of the probe beam offset z_0 .

5. Conclusion

As we have seen, we have succeeded in designing, building and calibrating a complete set-up for a newly developed spectroscopic technique in our laboratory in Egypt, namely *Transverse Photothermal Deflection Spectroscopy*. Though the technique seemed at times during development to be hard, difficult and prone to noise caused by vibration, particularly at the point of detection, the ease of application of the technique to the study of both the thermal and optical properties for solid interfaces finally justified such efforts.

We have also carried out a comparative study of the PDS and the photoacoustic PA spectra for the two dyes (Rh6G and CV) under the same conditions. The PD spectra were recorded at different normal offset distances from the samples and then compared to the PA spectra which showed that PDS was able to resolve the two peaks of CV, which are hardly resolved by either optical or PA measurements. The PDS proved to be superior to the PA due to its higher capability in spatial and spectral resolutions. These are initial results and we plan future work along these lines.

Acknowledgement

I would like to express my sincere gratitude to my professor Dr. Hassan Talaat for his guidance, encouragement and enriching discussions throughout this work.

References

- Aamodt L C and Murphy J C 1981 *J. Appl. Phys.* **52** 4903
- Boccara A C, Fournier D and Bodz J 1980 *Appl. Phys. Lett.* **36** 130
- Jackson W B, Amer N A, Boccara A C and Fournier D 1981 *Appl. Opt.* **20** 1333
- Murphy J C and Aamodt L C 1980 *J. Appl. Phys.* **51** 4580
- Rosenzwaig A and Gershoff A 1976 *J. Appl. Phys.* **47** 64
- Salazar A, Sanchez A -L and Fernandez J 1989 *J. Appl. Phys.* **65** 4150

Pulsed-laser ablation and deposition of superconducting BiSrCaCuO thin films

A GIARDINI-GUIDONI¹, T M DI PALMA², V MAROTTA²,
R MARTINO², A MORONE², G P PARISI² and S ORLANDO²

¹ Università degli Studi "La Sapienza", P le A Moro, 5 Roma, Italy

² Istituto per i Materiali Speciali- C N R, Zona Industriale di Tito Scalo, P O Box 27 Tito Scalo (Pz), Italy

Abstract. The present work reports some results obtained using the laser deposition technique to produce superconducting thin films. *In situ* analysis of transients formed in the plume and surface diagnostics of deposited Bi-Sr-Ca-Cu-O (BSCCO) thin films have been performed. It has been ascertained that mixed-oxide cluster ions are produced in the plume, together with neutral and ionized atoms of the constituent material. The effect of annealing parameters on the structure and quality of pellets and deposited thin films of BSCCO are reported and discussed.

Keywords. Pulsed-laser ablation; BiSrCaCuO thin films; thin-film deposition, superconducting thin films.

1. Introduction

The discovery of a superconducting phase in LaBaCuO compounds constituted a breakthrough in the search for superconducting materials with high transition temperatures (Bednorz and Muller 1986). The worldwide effort has lead to the production of a number of superconductors mainly formed of ceramic composite materials, whose common structural feature is the presence of CuO₂ planes in which the copper atoms form a square lattice with the oxygen placed between nearest-neighbour copper atoms (Maeda *et al* 1988). The production of high-quality powder and superconducting thin films from these materials is very important for practical applications as well as for basic studies. The fabrication of high-quality thin films by the pulsed-laser deposition technique (PLD), successfully demonstrated in the late eighties (Venkatesan *et al* 1988), has recently experienced an explosive growth (Beech and Boyd 1992). The advantage of this technique over other deposition methods such as sputtering or molecular beam epitaxy, is the simplicity of the deposition scheme, since the laser source is placed outside the vacuum deposition chamber. Laser rays enter through a window into a vacuum chamber and impinge on the material to be deposited. Laser removal of matter produces a plume in which electrons, ions and neutral species are present. The ablated material can be collected on a substrate placed at a suitable distance. After appropriate heat treatment, the thin films deposited (of BSCCO material)

*For correspondence

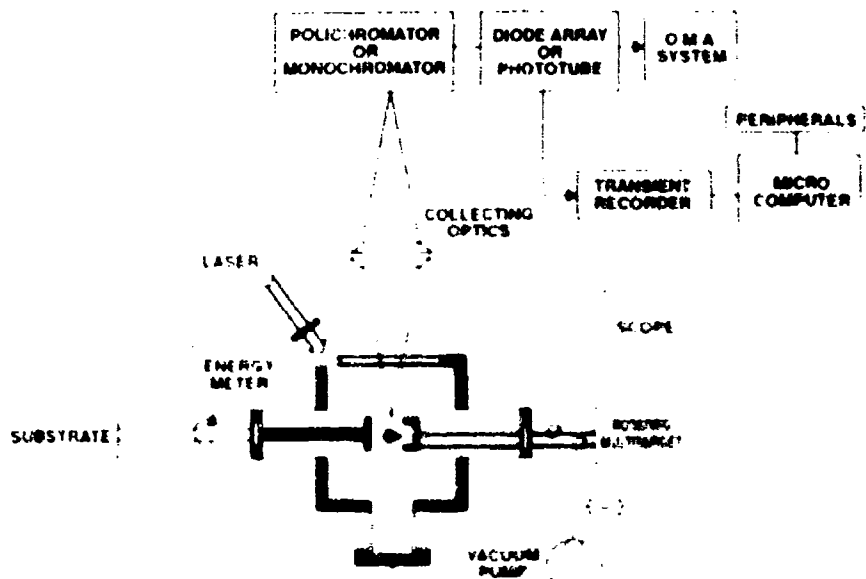


Figure 1. Experimental apparatus.

become superconducting. The main interest was focused on studies aimed at understanding the interrelationship between the chemistry, laser ablation processes and the resulting microstructural properties of the thin films deposited. Initially, in our laboratory, we were interested in elucidating the interaction between laser beams and matter (Giardini-Guidoni et al. 1990). Measurements of space- and time-dependent emission spectra of the species present in the plume provide a key to understanding the dynamics and reactivity of the ablated materials in the gas phase (Giardini-Guidoni et al. 1990). Evidence of chemical reactions in the plume has been ascertained; in particular, it has been shown that the copper ion reacts with second-group oxides (CaO , BaO , SrO) leading to the formation of mixed ions at the expense of pure oxide clusters (Mele et al. 1989). Studies aimed at clarifying the role played by the annealing parameters in the structure and quality of deposited thin films are reported here. Some information on pellet sintering is also given. A schematic of the deposition apparatus is shown in figure 1.

2. Experimental

The laser system is a frequency-doubled ($\lambda = 510\text{ nm}$, pulse duration 10 ns) or quadrupled ($\lambda = 266\text{ nm}$) Nd-YAG laser (Quantel 541). The vacuum chamber for ablation and deposition already described (Giardini-Guidoni et al. 1990) is equipped with a quartz laser entrance window and with a rotatable multi-target support and a substrate holder. The pressure in the chamber is kept at 3×10^{-6} torr during the ablation process. The laser energy is about $2.5 - 3.0\text{ J/cm}^2$ the incidence angle with respect to

the target surface is 45°. The ablated material originates a luminous plume which extends about 2.5 cm from the surface. Time-of-flight mass spectrometry and luminescence measurements have already been employed to obtain information on the intermediate species, neutral and ionized, present in the plume and the results (Giardini Giudoni et al 1990, Mele et al 1990) are only summarized here. Sr, Bi, Ca, Cu and simple oxide ions predominated in the mass spectrum and masses of simple and mixed positive cluster oxide ions were present. The mass spectrometric plume analysis was performed in the region near the laser spot on the surface, so it does not exclude heavier aggregates being formed at a greater distance from the target. They could in the end reach the substrate and initiate film growth. In the total emission of the plume, taken at a distance of 0.5 mm from the target, atom and ion emissions were strongly predominant. Very weak emission features attributable to CuO, CaO and SrO molecules were also observed. Time-resolved spectrum measurements for most of the emission lines show a prompt and delayed emission, which has already been attributed to laser and collisional excitation of ablated species, respectively (Saenger

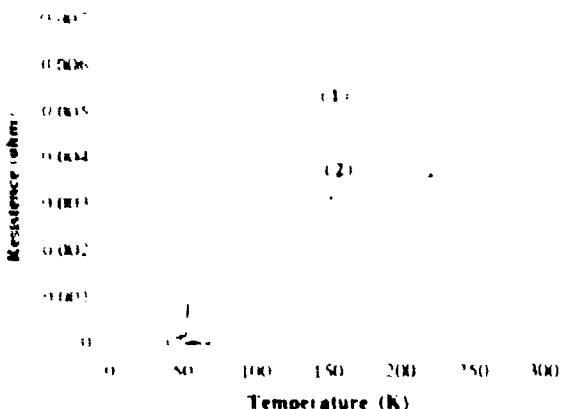


Figure 2. Temperature dependence of electrical resistivities of two samples sintered in air at 845°C for two different periods of time: sample 1 = 30 h and sample 2 = 100 h.

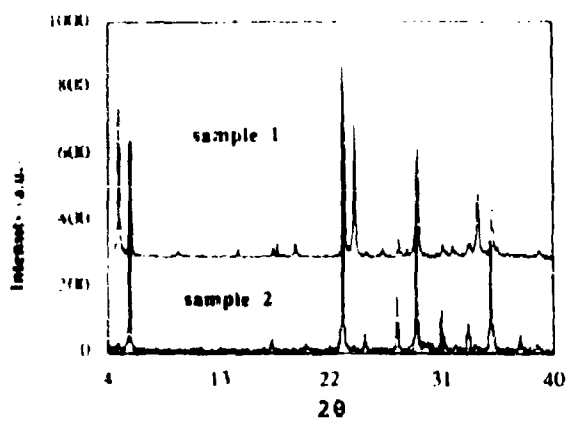


Figure 3. X-ray CuKa pellet diffraction patterns of samples 1 and 2.

et al 1989). On the holder, different substrates glued by silver paint can be positioned in front of the target, at a distance of 2.5 cm. Thin films were deposited on SrTiO₃ (100) or MgO (200) substrates by laser ablation of sintered BSCCO pellets obtained by calcining mixtures of Bi₂O₃, CaCO₃, SrCO₃ and CuO, doped with lead in some cases. Initial attempts to form the superconducting phases, although following the standard fabrication route of sintering in air at 845 °C after repeated cycles of grinding and pelletizing, failed to obtain good quality pellets. This could be attributed to segregation of molten material during the calcination stage. The effects of the calcination and sintering time in the furnace are shown, as an example, in figures 2 and 3, where the temperature dependence of electric resistivity and X-ray diffraction spectra of two typical samples are reported.

3. Results and discussion

The data show that superconducting phases are obtained after a longer sintering time (figure 2). The X-ray diffraction pattern confirms this behaviour. In fact, at a longer sintering time (100 h) the 4.8° peak related to the 2223 phase increases with respect to the 5.7° peak related to the 2212 phase (Hitoshi *et al* 1988). The presence of both these peaks indicates that multiphase pellets are formed. Thin-film deposits were produced by laser ablation of multiphase superconducting pellets. A deposition rate of 0.19 mm/s has been measured. The thickness of thin films, measured with an x-step profilometer, was typically 1 μm after 2 hours of irradiation. The deposited films were annealed in air in the temperature range between 840 and 880 °C, for different durations. Analysis of standard pellets and the thin films produced either "as deposited" or after annealing was performed by scanning electron microscopy (SEM), X-ray photoelectron spectroscopy (XPS) and X-ray diffraction. XPS surface analysis of films deposited by a superconducting target confirmed the presence of all the constituent elements. Moreover, the analysis of the Cu_{2p} region of the target and deposited film showed that the copper valence is restored after the annealing treatment in the presence of oxygen (Giardini Guidoni *et al* 1990). Annealing duration and temperature affect the quality of the deposited thin films. In table 1 results obtained on some samples originating from a superconducting BSCCO target in different annealing conditions are reported. Resistance vs temperature characteristics of the samples of table 1 are plotted in figure 4.

It can be seen that a long annealing time (sample a) appears to deteriorate the quality of the film. A higher annealing temperature produces similar behaviour (sample b), as can be observed in the resistance measurements. X-ray diffraction

Table 1. Results obtained on samples under different annealing conditions.

Sample	Deposition (time) (h)	T _c (K)	Annealing temperature	Annealing time	Predominant phase
a	1	45	855	12 h	2212
b	3	65	880	12 h	2201
c	3	65	855	6 h	2212
d	2	73	855	2 h	2212

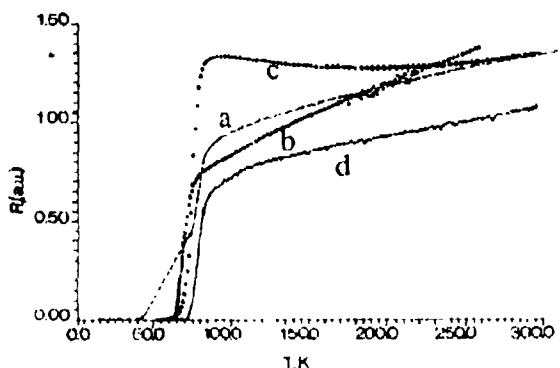


Figure 4. Electrical resistivity vs temperature of four thin films annealed in different conditions as reported in the table 1.

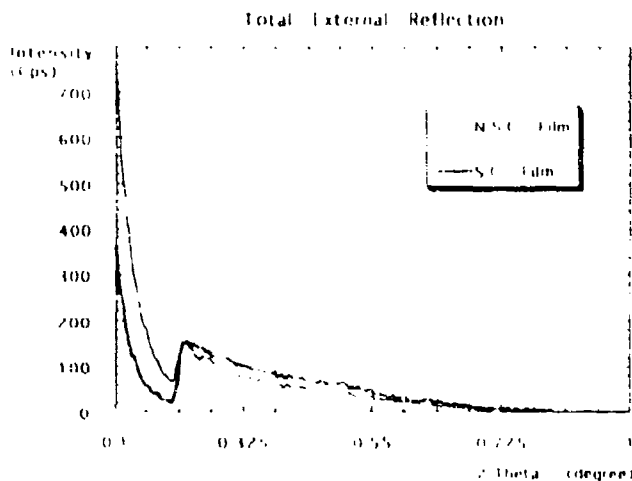


Figure 5. Total external reflection of superconducting and nonsuperconducting films measured by the high-resolution synchrotron radiation powder diffraction station at Adone.

patterns of the samples, not reported here for the sake of brevity, were performed by a Siemens diffractometer D5000 and by a high-resolution powder diffractometer mounted on a beam line of the Adone storage ring (Burattini *et al.* 1992).

In these spectra, peaks were observed at $2\Theta = 5.47^\circ$, 29.3° and 35.3° . These peaks are considered to correspond to (001) series of unit cell with its long axis perpendicular to the substrate. The observed peaks are related to the 2:2:1:2 phase ($T_c = 85\text{ K}$). However, the spectra indicate that the films are polycrystalline with only a slight preferential c-axis orientation of the grains. When the BSCCO thin film was annealed near its melting point, 880°C , the presence of the $2\Theta = 7.2^\circ$ and 21.9° peaks indicated a phase change from 2:2:1:2 to 2:2:0:1. Figure 5 shows the total external reflection of nonsuperconducting and superconducting thin films obtained by synchrotron radiation at the Adone storage ring in the range $0.1 - 1^\circ$ (2Θ).

These measurements will permit some information to be obtained on the physical properties of the thin films, such as refractive index, density and thickness. In conclusion, the present investigation clearly demonstrates that the plume of evaporated material is mainly formed by atoms, ions and a few oxide clusters. Its composition does not always appear to be representative of target composition; however, the net result of deposition is stoichiometric. To obtain high-quality thin films, not only a suitable target but also a good choice of post-annealing treatment is required.

Acknowledgements

The authors gratefully acknowledge Dr U Gambardella, Dr C Alvani and Dr M Penna for valuable discussions and constructive criticism.

References

- Beech I and Boyd J W 1992 *Photochemical processing of electronic materials* (London: Academic Press) p. 387
Bednorz J G and Muller K B 1986 *Z. Phys.* **B64** 189
Burattin F, Simeoni S, Cappuccio G and Mainielli P 1992 *Rev. Sci. Instrum.* **63** 1002
Giardini Guidoni A, Desimoni E, Salvi A M, Leghi R, Ambroto M, Morone A, Piccirillo S and Snels M 1990a *Proc. Int. Conf. Lasers* p. 331
Giardini Guidoni A, Morone A, Snels M, Desimoni E, Salvi A M, Fanton R, Berden W C M and Giorgi M 1990b *Appl. Surf. Sci.* **46** 321
Girault C, Dumini D, Aubretton J and Catherinot A 1989 *Appl. Phys. Lett.* **55** 2
Hitoshi N, Kazuharu S, Yukishige K and Tomoi K 1988 *Jpn. J. Appl. Phys.* **27** 1864
Maeda H, Tamaka Y, Fukutomi M and Asano T 1988 *Jpn. J. Appl. Phys.* **27** 1209
Mele A, Consalvo D, Stranges D and Giardini-Guidoni A 1990 *Int. J. Mass Spectrom. Ion Process.* **98** 159
Saenger K L 1989 *J. Appl. Phys.* **66** 4435
Venkatesan T, Wu X D, Inam A and Wachtmeister B 1988 *Appl. Phys. Lett.* **52** 2293

Laser ablation of inorganic and organic materials

A MELE*, A GIARDINI-GUIDONI and R TEGHIL[†]

Dipartimento di Chimica, Università "La Sapienza" P.le A Moro 5, Rome, Italy

[†]Dipartimento di Chimica, Università della Basilicata, Via N. Sauro 85, 85100 Potenza, Italy

Abstract. An intense photon flux impinging on a solid target induces the ejection of material. In a dynamic regime, the cloud may be collected on an appropriate substrate to provide the growth of solid films. Thin layer deposition of refractory semi-conductor materials, high T_c superconductors and diamond-like (DLC) films have been obtained by pulsed laser evaporation of suitable targets. The plume which is explosively emitted from the target is formed of atoms, ions, molecules and clusters. A study of laser-induced products of various solid targets by time-of-flight mass spectrometry and luminescence analysis has shown some of the chemical pathways which follow laser evaporation and lead to nucleation and growth processes for thin film formation. Simple and complex oxides, carbon with metals, and finally graphite or organic compounds, are the materials employed as sources to grow thin film deposits. The reactivity of oxide ions formed by ablation of mixtures of simple oxides has been investigated. Metal oxide reduction during laser ablation and reaction with graphite yields carbide cluster ions presaging the structure of solid carbide lattices. Laser ablation of a number of organic materials has been investigated to determine the effectiveness of these targets in the formation of DLC films.

Keywords. Lasers, ablation, clusters, thin film deposition

1. Introduction

Laser-induced ablation, also denoted as laser sputtering, describes the process of material removal under the action of short high intensity laser pulses. The extremely high power density that can be obtained by a sharply focused pulsed laser makes it possible to evaporate virtually every material. Ruby lasers (694 nm) and Nd: YAG lasers ($\lambda = 266, 355, 532, 1064$ nm) have all been used to vaporize a variety of material from rubber to platinum to tungsten.

There are excellent reviews on this subject (Novak *et al* 19⁸, Srinivasan and Brazen 1989), so that this report will concentrate mostly, but not exclusively, on studies carried out in the photochemistry laboratory at the University of Rome and will be related mainly with the chemical and physical aspects of this phenomenon.

2. Laser-solid interaction

In the first age, only the thermal effect of the coherent radiation was taken into account to model the energy conversion concerning laser-material interaction with

*For correspondence

Table 1. Thermal vs. non-thermal processes.

Photothermal
<i>Very low laser power:</i> below 10^4 W/cm^2
Heated surface
Thermal ejection of volatile species
<i>Low laser power:</i> from 100 MW/cm^2
Long wavelengths (IR)
Long pulselengths $\geq 10\text{ ns}$
Lack of photoionization, electron impact ionization, removal of isolated atoms, molecules (neutral)
Photochemical
<i>Moderate laser power:</i> from 200 to 500 MW cm^{-2}
Short wavelengths
Short pulselengths (Multiphoton ionization within the plume)
<i>High laser power:</i> $\geq 500 \text{ MW cm}^{-2}$
Short wavelengths
Short pulselengths (inelastic photon-electron loss)
<i>Very high laser power:</i> $\sim 500 \text{ MW cm}^{-2}$
Vaporization atomization
The plume becomes an opaque plasma

solids. With the advent of suitable *Q*-switched pulsed lasers, delivering high power laser pulses (short duration in the nanosecond range) the interaction was also described by photochemical models. Table 1 shows results for thermal and non-thermal processes on varying the laser characteristics (Srinivasan 1986; Dijkkamp *et al* 1987; Kuper and Stuke 1987). Photothermal laser ablation concerns the fundamental mechanism of interaction between laser rays and the solid, and the time scale for the thermalization of the excitation energy. If laser ablation is thermally activated, it can be described by the temperature and total energy change. Photochemical laser ablation is determined by the degree of selective excitation. In other words, thermal ablation refers to a mechanism in which phonons generated as a result of non-radiative transition or of electron-lattice interactions are accumulated leading to partial emission of material by vibrational motion. In electronically induced laser ablation, an accumulation of electronic excitation leads directly to bond breaking.

3. Analysis of laser-induced vapour plume

The luminous ejection of neutral and charged particles formed by the laser interaction with a solid surface, the so-called plume, is schematically shown in figure 1. The plume of evaporated material is cone-shaped, characterized by a highly forward peaked distribution of the components of the target. This distribution is $\cos^n\Theta$ with $1 < n < 12$, where the angle is measured with respect to the target normal (Kelly and Rothenberg 1985; Singh and Narayan 1990). This is in contrast to what one expects from a purely thermal expansion characterized by a $\cos\Theta$ distribution of the first order. This angular distribution indicates that material removal is a combination of different mechanisms. In addition to a change in angular distribution there is also a

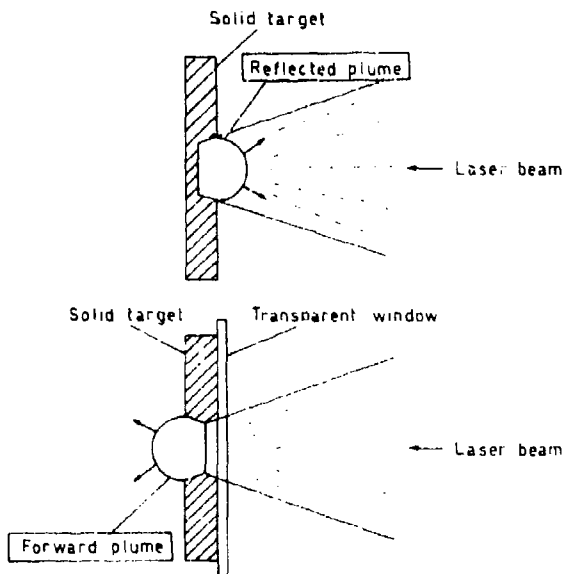


Figure 1. Schematic of the plume formed by two different configurations of laser-solid interaction.

Table 2. Angular distribution of components.

Incongruent ablation	
Non-stoichiometric components	Low laser intensity
Broad distribution	
$\cos \Theta$ distribution	
Congruent ablation	
Stoichiometric components	High laser intensity
Forward directed component	Short pulses
$\cos^n \Theta$ distribution, $n > 1$	

variation in the composition of the evaporated material as a function of the angle of ejection. The sharp forward-peaked distribution has the same stoichiometry as the target, while the broad distribution is non-stoichiometric (table 2).

The laser energy density is critical in determining the composition of the ablated material. High laser density and short pulse lead to stoichiometric ablation. In contrast, the stoichiometry is not maintained at low laser density. A difficult process to characterize is the expansion of the plasma as it continues to interact with the laser and the ambient. This problem is especially complex for multicomponent material expanding into a reactive region.

Many spectroscopic techniques have been used to characterize the composition of the evaporated material. These techniques include emission, absorption, laser-induced fluorescence (LIF) and resonance-enhanced multiphoton ionization (REMPI). Of these, dispersed plume emission has been used most extensively to identify species in the vapour and it has provided much of the early plume characterization data.

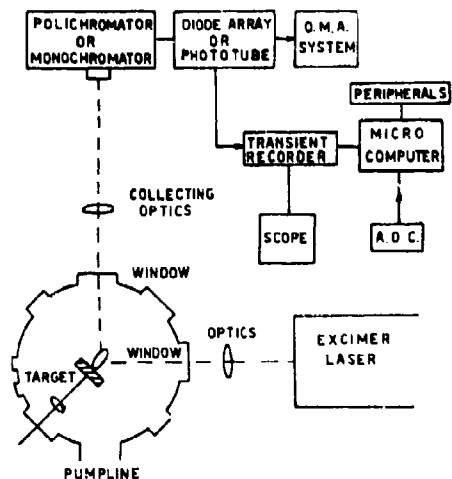


Figure 2. Optical multichannel analyser experimental arrangement for the plume analysis.

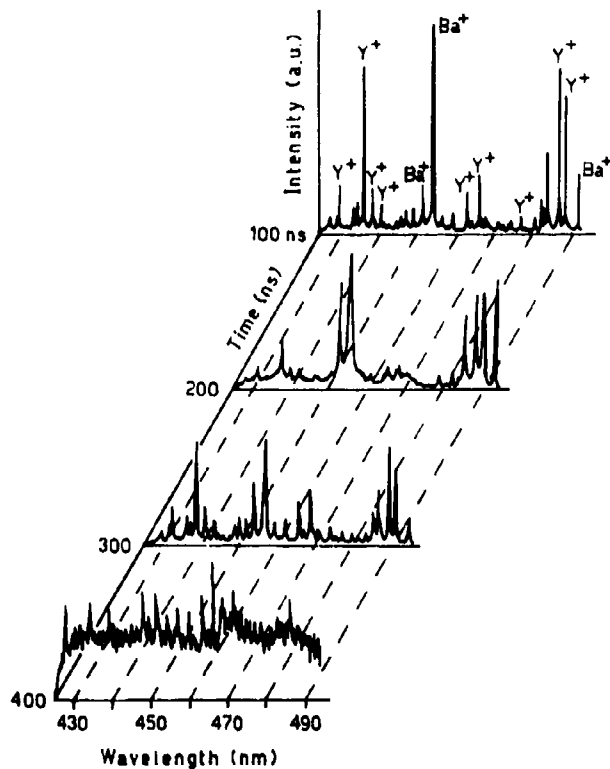


Figure 3. Time-resolved plume emission from a YBCO target.

However, the emission monitors only the electronically excited species with measurable quantum yields for fluorescence. A schematic of an apparatus to measure luminescence from the plume is shown in figure 2 (Giardini-Guidoni and Mele 1991). Effective particle velocity has been obtained from time dependence of the optical emission intensity. Data have been collected on several emission lines for a variety of neutral and ionic species. The results indicate most probable velocities of about 5×10^5 cm/s for neutral species and 2×10^6 cm/s for ions. An example of dispersed plume emission from a superconductor is shown in figure 3.

Mass spectrometry is also largely used to identify the species generated by the laser target interaction: ions and neutrals. Time-of-flight measurements yield important information on the dynamical behaviour of the laser-produced plume. In conclusion, the objective in making these measurements has been to describe both temporal and angular dependence of the desorbed species in terms of the laser and target characteristics.

4. Cluster production and studies

Clusters can be defined as an assembly of atoms and molecules sometimes attached to ions whose structure originates from different types of forces linking the atoms and molecules (Giardini-Guidoni and Mele 1991). Observation of gas-phase clusters has been made by several techniques. Among them, laser ablation proved to be quite successful. The variety of molecules studied is enormous. It is impossible to predict the results which are obtained, since the precise mechanism of the laser-induced plume and the subsequent processes are not completely understood.

Figure 4 shows a schematic of the laser vaporization cluster source used for cluster experiments. A pulsed laser is directed at the surface of a solid rod of the material to be studied. A high density helium flow (2–3 atm) over the target serves as a buffer gas in which clusters of the target material form, thermalize to near-room temperature, and then cool to near 0 K in the subsequent supersonic expansion. The content of this cluster beam can be probed by matrix isolation spectroscopy or laser-induced fluorescence, or examined by mass spectrometry of the ions formed as shown in figure 4. In other experiments, the whole material ejected from a solid target hit by the laser is analysed at each pulse by a time-of-flight mass spectrometer. This simple method of laser evaporation and ionization, shown in figure 5, leads directly to the formation of clusters with intensity and distribution which in many cases may be compared with the results obtained by the method of evaporation and subsequent supersonic expansion.

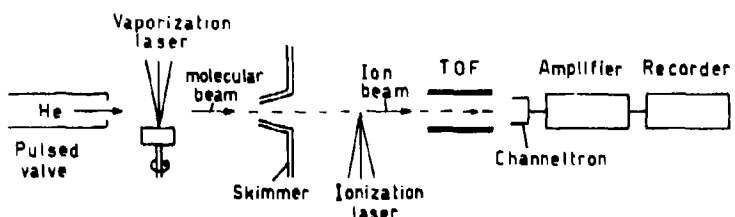


Figure 4. Laser vaporisation cluster source combined with a schematic of the TOF mass spectrometer.

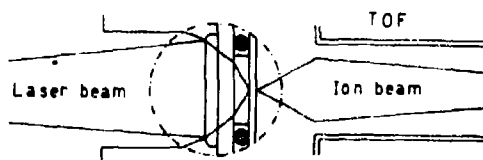


Figure 5. Sampling and grid assembling for direct laser ablation and TOF mass analysis.

Table 3. Positive ions formed by laser ablation of simple oxides

Oxide	Homologous series of cluster ions	M_nO_x $n(\max)$	Valence	Fragment ions ^a
ZrO ₂	$[(ZrO_2)_n]^+$ $[ZrO(ZrO_2)_n]^+$	5	4	$Zr^+(vs); ZrO^+(es)$ $ZrO^{+2}(s)$
CeO	$[Ce(CeO_2)_n]^+$ $[CeO(CeO_2)_n]^+$	4	4	$Ce^{+3}(s); CeO^+(es)$
SnO ₂	$Sn_1^+; Sn_2O^+; [SnO]_n]^+$ $[Sn(SnO)]_n]^+$	3	2	$Sn^+(s); SnO^+(s)$
Al ₂ O ₃	$Al_1^+; Al_2O^+$	2	—	$Al^+(es); AlO^+$
Y ₂ O ₃	$Y_2O^+; [(YO)_n(Y_2O_3)_m]^+$	7	3	$Y^+(s); YO^+(vs); YO^{+2}$
La ₂ O ₃	$[(LaO)(La_2O_3)]^+$	15	3	$La^+(s); LaO^+(es)$
MgO	$Mg_1^+; Mg_2O^+; Mg_3O^+$	2	—	$Mg^+(es); MgO^+$
CaO	$Ca_1O^+(vs); [(CaO)_n]^{+2}$ $[Ca(CaO)]_n]^+$	7	2	$Ca^+(s); CaO^+(es)$
SrO	$[(SrO)_n]^+; [Sr(SrO)]_n]^+$	7	2	$Sr^+(es); SrO^+(s)$
BaO	$[(BaO)_n]^+; [Ba(BaO)]_n]^+$	3	2	$Ba^+(s); BaO^+(s)$
SnO	$Sn_1^+; Sn_2O^+; [SnO]_n]^+$ $[Sn(SnO)]_n]^+$	3	2	$Sn^+(s); SnO^+(s)$
SiO ₂	$Si_1O_2^+(s); Si_2O_3^+(s)$ $[(SiO_2)_n]^+; [Si(SiO)]_n]^+$ $[SiO(SiO_2)]_n]^+$	11	4	$Si^+(s); SiO^+(s)$
GeO ₂	$Ge^+(s); Ge_2^+(s)$ $[(GeO)_n]^+$	3	2	$Ge^+(es); GeO^+(s)$
PbO	$Pb_1O^+; Pb_2O_2^+; Pb_2O_6^+$	2	—	$Pb^+; PbO^+; PbO_4^{+2}$ $PbO^{+2}(vs)$
As ₂ O ₃	$As_1^+; As_2^+; [(AsO)_n]^+$ $[As(AsO)]_n]^+; (AsO)nO^+$	6	2	$AsO^{+2}(vs)$
Bi ₂ O ₃	$Bi_1^+; [(BiO)_n]^+$ $[Bi(BiO)]_n]^+$	4	2	$Bi^+(es); BiO^+(es)$
CuO	$[Cu]_n^+; Cu_2O^+$	6	1	$Cu^+(vs); CuO^+$

^aIons with $n = 1$; (s); strong; (vs) very strong.

Ionic clusters are formed by laser ablation of simple and complex solid oxides and their mixtures. In table 3, the positive ions observed in the mass spectra of a few oxides studied among others are reported (Consalvo *et al* 1989; Mele *et al* 1989). These oxides are quite important *per se* and for the implications as precursors of high temperature superconducting materials as for instance Y_2O_3 , La_2O_3 , CaO , SrO and CuO . From table 3 the formation of homologous sequences of cluster ions for all oxides reported can be observed. Furthermore the mass spectrum of each oxide shows alternation, the so-called magic numbers, that is, higher ion intensities alternate with lower ones indicating preferred composition based on more stable structures.

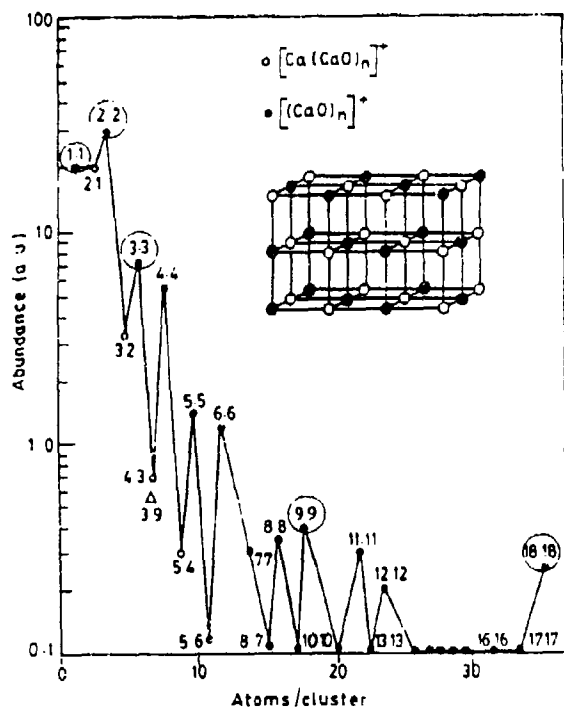


Figure 6. Positive cluster ions produced by direct laser evaporation technique of calcium oxide

Typically the data of calcium oxide show one series (figure 6) corresponding to the stoichiometry of the solid oxide target $(\text{CaO})_n^+$ together with another sequence of metal rich oxide (sequence $\text{Ca}(\text{CaO})_n^+$). This behaviour is characteristic of other II-group oxides, Mg, Sr, Ba and of yttrium and lanthanum oxide. The intensity anomalies or magic cluster numbers are easy to understand by assuming an ionic potential (Martin 1983) between Ca^{+2} and O^{-2} ions which leads to a closed-shell structure.

The abundance maxima observed in the series are explained as arising from the exceptional stability of compact cubic structures that are essentially pieces of the face centred cubic (*fcc*) metal oxide crystal lattice. The series corresponding to metal-rich oxide $\text{Me}(\text{MeO})_n$ can refer to an ionic model leading to abundance maxima when n is one less than the maxima of the stoichiometric cluster. In fact, in the cubic structure the excess electron from the extra metal atom could be localized in an anion vacancy in the lattice analogously to a solid state *F* center (Giardini-Guidoni and Mele 1991). The ions named 'fragment ions' in the table 3 are usually much more abundant than the cluster ions. The hypothesis is that they are produced in a very hot region of the plume by a process of fragmentation of the bulk material or of larger oxide clusters. The mass spectrum of figure 7 shows the sequences found by laser-evaporating Y_2O_3 . Complexes and mixed oxides, which are precursors of superconductors, yield binary and ternary oxide clusters. The spectra shown in figure 8 refer to ablation of mixtures

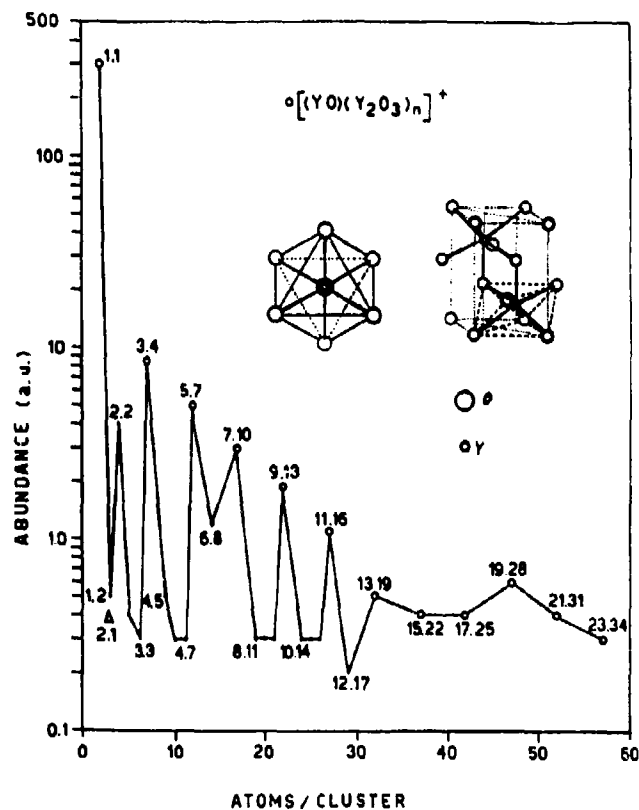


Figure 7. Positive cluster ions produced by direct laser evaporation technique of yttrium oxide.

of lanthanum, strontium and copper oxide and of a mixture of 4 components. These results simply prove that by ablation it is possible to produce copper-based complex oxides. Furthermore, it has been found that in the dynamics of the process leading to thin film deposition, the composition of the target plays an important role.

Carbon clusters have been produced by laser vaporization of a graphite rod in helium beam and probed downstream by UV laser photoionization and time-of-flight (TOF) mass analysis (figure 5) (Rohlfing *et al.* 1984). Carbon cluster mass spectra from graphite have been also studied by direct laser evaporation and TOF detection. Both experiments, detecting positive ions, showed an even/odd intensity alternation among carbon clusters C_n with the maximum occurring for odd n . The interpretation proposed for this effect was based on extended Hückel calculations which showed for linear chains, odd clusters to be more stable than even clusters (Pitzer and Clementi 1959; Hoffmann 1966).

Carbon clusters are also formed by photodecomposition of polynuclear aromatic hydrocarbons. As in graphite ablation, the peaks present in the mass spectra, shown in figure 9 for chrysene, exhibit carbon cluster C_n with n up to 600 with intensity alternations analogous to graphite. Some magic numbers, C_{60} , C_{70} , related to

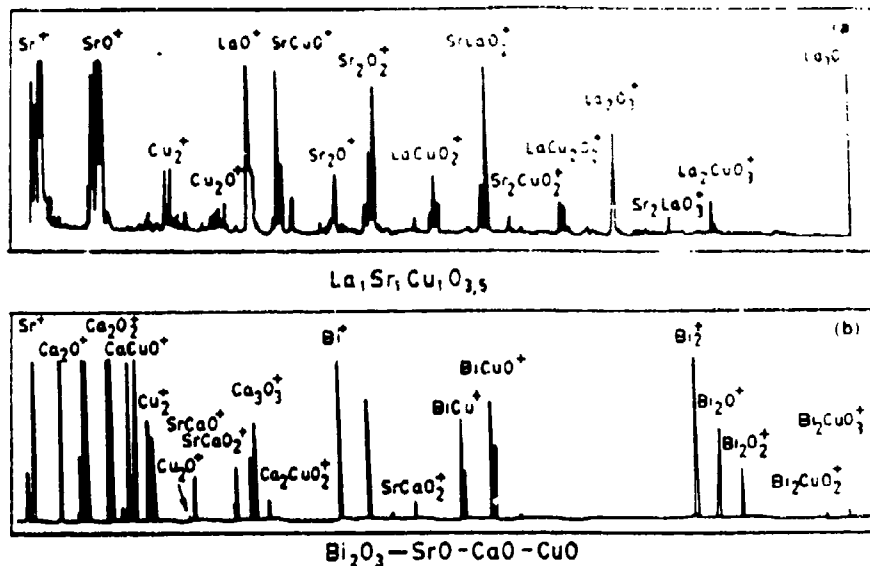


Figure 8. Positive cluster ions formed by direct laser evaporation: (a) mixture of $\text{La}_{1.5}\text{Sr}_1\text{Cu}_1\text{O}_{3.5}$, (b) $\text{Bi}_2\text{O}_3\text{-SrO-CaO-CuO}$.

fullerene structures are also seen. It is well known that most of these aromatic hydrocarbons are noxious materials. They all have strong carcinogenic action. The use of a high power beam to decompose these materials into non-dangerous substances has been suggested. The results of laser ablation are important for the waste treatment of these substances and also for DLC thin film deposition (Giardini-Guidoni *et al* 1989; Lineman *et al* 1989).

5. Ablation and reactivity

The advent of the laser vaporization technique provides a useful mean to study reaction kinetics of isolated atoms and clusters. Unpublished results obtained long ago by simply laser-ablating a zirconium rod in presence of a flow of molecular oxygen are shown in figure 10. Several zirconium oxide ions are observed in this mass spectrum, indicating that zirconium reacts with oxygen and can make clusters of various Zr/O ratios (Giardini-Guidoni *et al* 1991).

Another simple laser ablation experiment concerns reactions of metal oxides with graphite. Ablation of a finely ground mixture of these two compounds produces carbide cluster ions. Formation takes place through a series of chemical reactions in the surrounding area hit by the laser beam. The scheme of these reactions is shown in figure 11 together with the mass spectra of the ions produced by reactions of lanthanum oxide and graphite (Consalvo *et al* 1989; Teghil *et al* 1990). Two extreme cases have been observed in the formation of lanthanum carbide clusters and others. In one case the mass spectra show the main sequence $(\text{MeC}_2)_x^+$ together with a carbide cluster of a more general formula $(\text{Me}_n\text{C}_m)_x^+$ with a ratio of carbon to metal greater

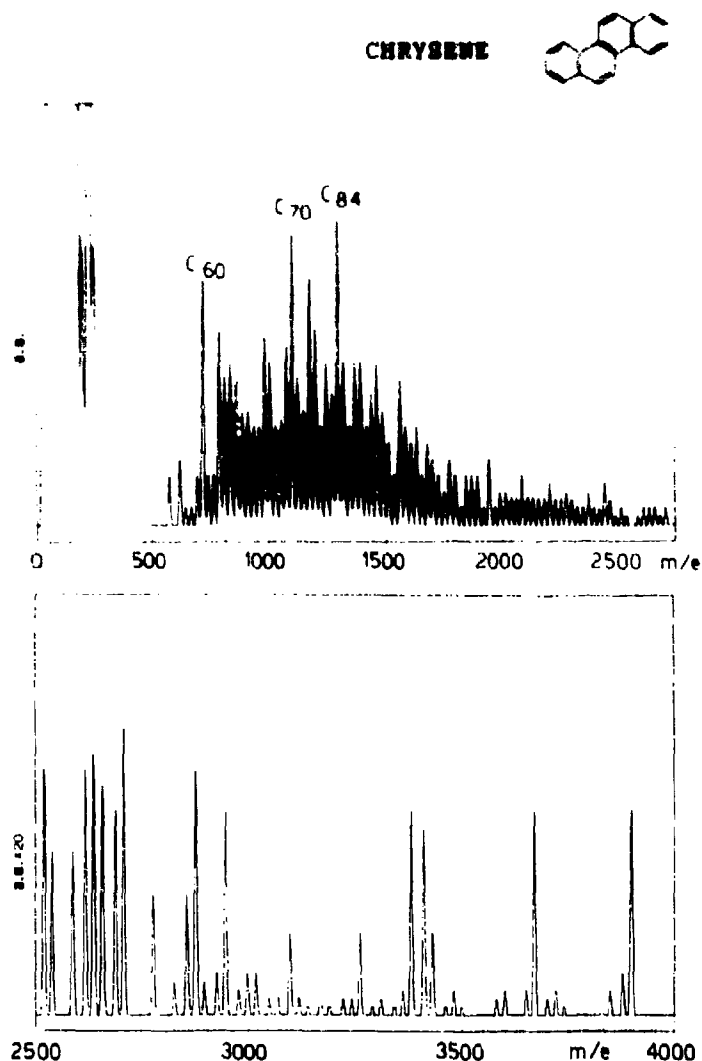


Figure 9. Positive ion TOF mass spectra obtained by direct laser evaporation of a chrysene sample (Giardini-Guidoni *et al.* 1990).

than 2. This behaviour is probably due to the effect of the carbon atom density in the reaction region. In the other case, the spectra contains the $(\text{MeC}_2)_x^+$ sequence together with peaks corresponding to unreacted metal oxide MeO and metal oxycarbide $\text{Me}_x\text{O}_y\text{C}_z$ cluster ions. The most typical trend is shown in the same figure 11 for a 1:1 mixture of lanthanum oxide and graphite. The even-odd alternation for these small carbide clusters may again be explained according to Clementi (Pitzer and Clementi 1959) in terms of a simple molecular-orbital theory. Neutral and positively charged odd species have a molecular orbital completely filled and are more stable than the even species with only half-filled orbitals.

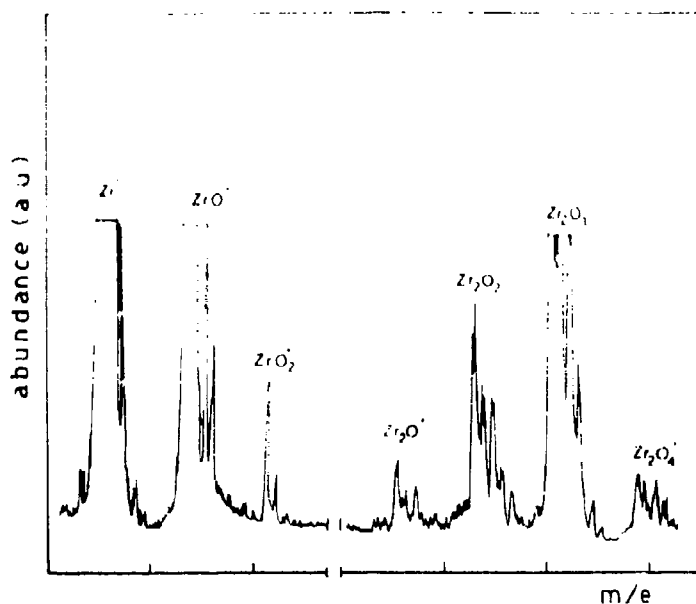


Figure 10. Positive ion TOF mass spectra formed by direct laser evaporation of a zirconium rod in an oxygen flow.

Other applications of laser ablation in this field deal with the study of reactions of metal clusters with various substances. The reactivity of clusters of metal atoms is of interest since enhanced reaction rates and new reaction pathways may result from unique cluster size, geometries and electronic structures. Additionally reactivity studies on clusters may also throw some light on the nature of cluster bonding. Metal clusters are generated by laser vaporization of a solid rod in a pulse of helium as shown in figure 4. The clusters are then expanded into a fast flow reactor where a pulse of reactant gas mixture crosses the metal cluster beam.

Reactions of niobium clusters with benzene derivatives and a few unsaturated non-aromatic reagents have been investigated (Song *et al* 1990). Other studies concern reactions of vanadium clusters with propene and halopropene (St. Pierre *et al* 1987). New reaction pathways and chemical reactivities of metal clusters as a function of cluster size have been determined. The reaction probability was found to depend on the size of niobium clusters as well as on the structure and stability of the organic molecule. The importance of the changes in cluster geometry in determining both ionization potentials and reactivity was also studied in the reactions of iron, cobalt and nickel clusters with ammonia and water by the Riley group (Winter *et al* 1991). The dependence of these properties on cluster size indicates that the clusters grow with icosahedral packing. However, in many cases there is not a unique structure for a given cluster. Smalley created a sample of Nb₁₉⁺ charged clusters and measured how quickly they reacted with hydrogen (Chesnowsky *et al* 1990). He found that some of the clusters ignored the hydrogen altogether, while others grabbed the hydrogen molecule whenever they came in contact with it. This difference in reactivity was attributed to different structures. The 19 atoms in the cluster can arrange

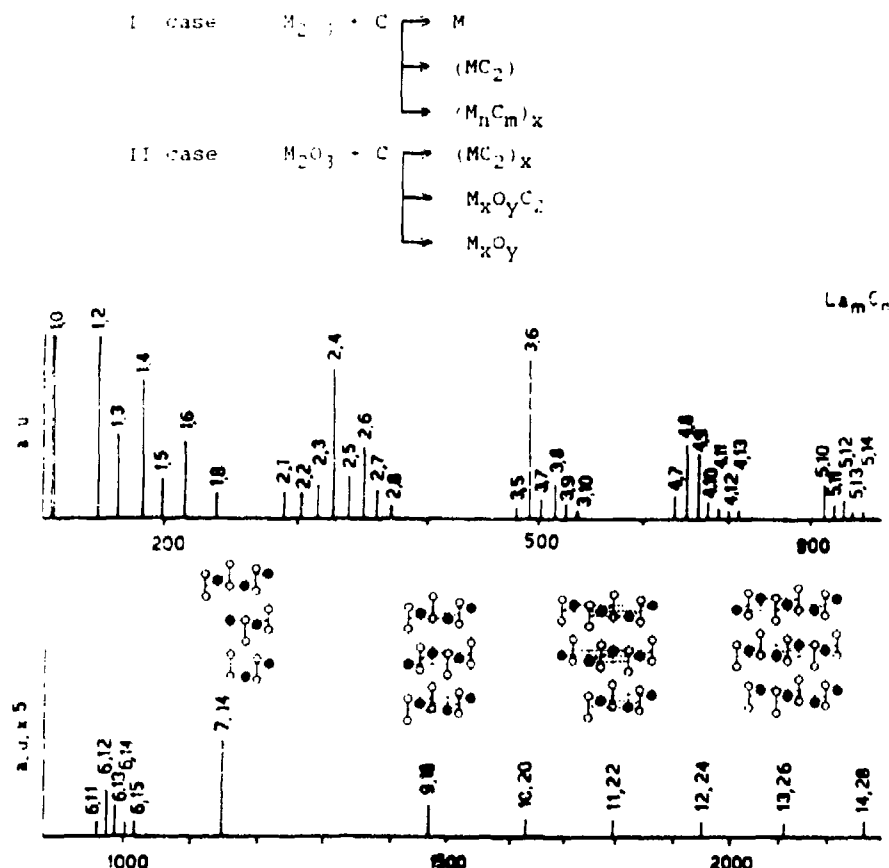


Figure 11. Schematic of the two reaction pathways determined by laser evaporation of oxides and graphite mixtures. Positive cluster ion spectra obtained by laser evaporation of a mixture of La_2O_3 and graphite.

themselves either in an eight-sided double pyramid or in a "capped icosahedron". The double pyramid has flat sides and a flat surface and reacts very poorly with hydrogen molecules. The capped icosahedron has bumpy sides and many sites for reaction with hydrogen.

Laser ablation has been applied with success to the field of organic photochemistry. The combination of laser ablation and TOF mass spectrometry has been used to determine products formed from organic compounds. The study of triazines may typically depict chemical reactions occurring during laser ablation. Triazine molecules strongly absorb in the UV regions 272 and 222 nm with assignments $n \rightarrow \pi^*$ and $\pi \rightarrow \pi^*$ transitions. The wavelength of a frequency quadrupled Nd-YAG laser falls in this region and therefore a photochemical process is feasible (Giardini-Guidoni *et al* 1989; Mele *et al* 1992). A schematic of the process is shown in figure 12 for a typical triazine where two different reaction pathways have been observed for all triazines examined. A retro Diels-Alder ring opening process and a cluster ion formation

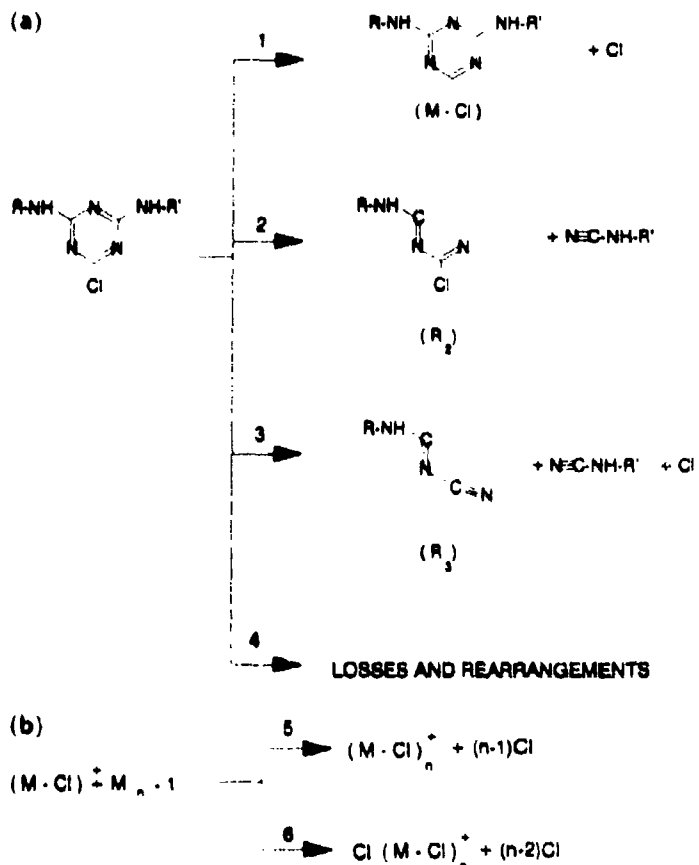


Figure 12. Schematic of the processes induced by laser ablation of triazines. (a) retro Diels-Alder ring opening; (b) cluster ion formation.

pathway (Giardini-Guidoni *et al.* 1991) can be seen. Aggregation occurs in the dark region, fragmentation in the hot central zone of the plume.

6. Laser ablation and deposition

Laser ablation has received much attention in the preparation of thin film deposits. Semiconductors, metals, superconductors and dielectric films have been grown by a variety of processes involving photochemical or thermal reactions induced by pulsed-laser ablation. Although dating back to more than 20 years, this technique only recently attracted much interest particularly in the field of high temperature superconductors. The advantages of the pulsed-laser ablation approach for depositing high quality thin films for electronic device applications begin with the simplicity of the experimental setup (figure 13). All that is required is a pulsed laser, a vacuum chamber, a heated substrate holder and a target. A copper grid and a gas nozzle can

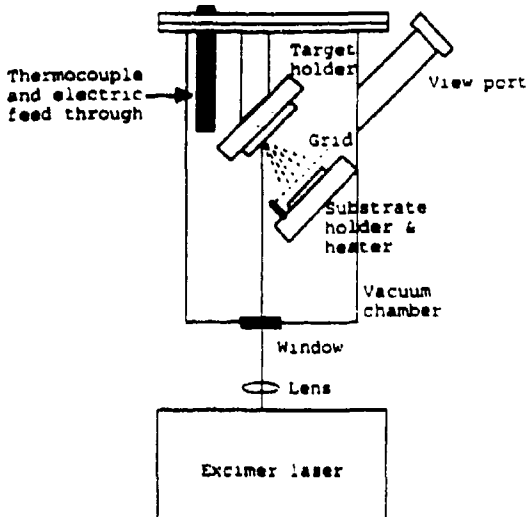


Figure 13. Schematic diagram of the apparatus used in the reflected plume experiments for thin film deposition.

also be placed. A positive or negative voltage can be applied to the grid. A buffer gas may be introduced through a gas nozzle. It has been found that for DLC deposition the voltage plays a relevant role. It is important in these experiments that the result of the evaporation yields a congruent deposition in terms of rate, composition, thickness and quality. The main objective of these studies is to understand the correlation between the target properties, the chemistry of the ablation and the resulting microstructures of the film deposited. The measurements of space- and time-dependent emission spectra of the species present in the plume provide a key to understand the dynamics and reactivity of the ablated material in the gas phase. It is fairly well established that the nucleation phenomena occur mainly at the edge of the plume and heavier aggregates are formed at a larger distance from the target. These aggregates then reach the substrate and initiate the film growth.

High T_c thin films may be obtained from a superconducting target and laser ablation is thus the means to produce thin films. Deposition may also be obtained by direct laser ablation of a stoichiometric mixture. At present it is controversial whether a target obtained from a simple stoichiometric mixture may produce the same high quality superconducting material.

Thin film formation takes place through various stages. It starts with the neutral and ionic species being deposited on a suitable substrate and it ends with the formation of a continuous crystalline layer. It is clear that the deposition parameters play an important role in the growing process. The nucleation frequency and the coalescence process, the two most important processes, depend strongly on the deposition rate and the substrate temperature. Of course thin film preparation by laser ablation is followed by analysis of the properties of the material. In the case of superconducting materials, scanning electron microscopy examines the morphology of the film, X-ray diffraction determines the proper condition of epitaxial growth and finally electrical

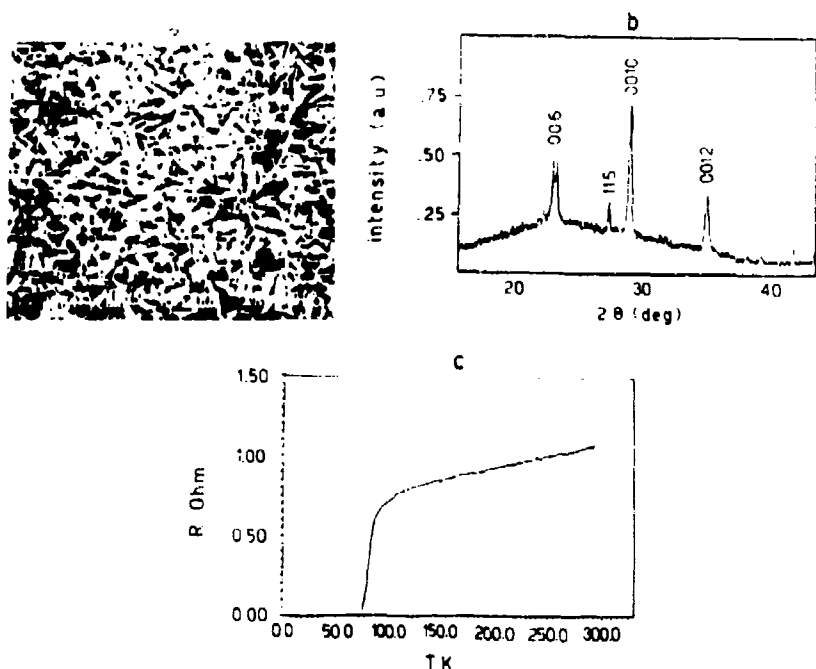


Figure 14. Techniques used for characterisation of thin film deposits: (a) SEM micrograph of a laser-ablated BiSrCaCuO film; (b) X-ray diffraction of a BSCCO thin film made by laser ablation of a BSCC sample on $\text{SrTiO}_3(100)$; (c) Transition resistivity curve of BSCCO thin film deposited on SrTiO_3 .

resistivity provides an indication of the effectiveness of the whole ablation deposition process. A few examples of these measurements are shown in figures 14 a,b,c.

Several interesting aspects are associated with laser-ablation deposition of the semiconductor, cadmium telluride (CdTe) (Cheung and Santur 1992). A comparison of the mass spectra of the species from the bulk by evaporative heating and by pulsed-laser ablation is shown in figure 15. It can be seen that while Cd ions are present in both cases, the Te_2^+ species is present in the thermal vapour obtained from the bulk at 650°C . This fact disturbs the homoepitaxial growth kinetics of the cadmium telluride thin film on the 111 crystallographic face. On the contrary, laser ablation provides the proper conditions for epitaxial growth. The rapid response time in pulsed-laser evaporation is another important factor and can be used for fast modulation of evaporating flux intensity. Modulation time constant is an order of magnitude greater than obtained by changing the crucible temperature in thermal evaporation, as for example in molecular beam epitaxy. There are two ways of flux modulation. One approach is to change laser power density, but a more practical approach is to change the laser repetition rate as shown in figure 16. In one case, relative evaporation rate depends exponentially on the surface temperature and its dependence on power density is also exponential. In the second case the relationship between the evaporation rate and the repetition rate is linear (Cheung and Santur 1992).

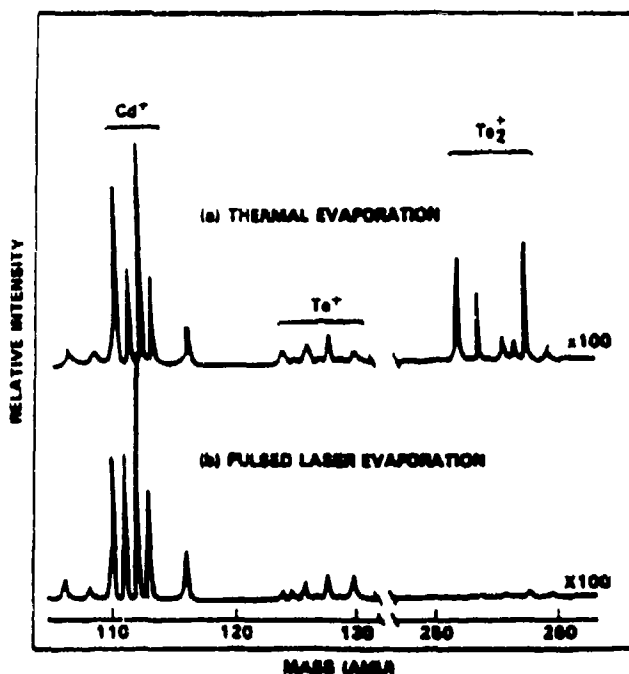


Figure 15. Mass spectra of CdTe evaporated (Cheung and Santur 1992).

Another very interesting application of laser ablation concerns the deposition of diamond-like carbon (DLC) films (Sato *et al* 1988). Diamond is the stablest form of carbon at high temperature and high pressure and, therefore, at first the idea was to convert graphite directly into diamond. More recently the synthesis of metastable diamond at low pressure was also explored. A high activation energy between stable and metastable states may provide a barrier to interconversion. DLC refers to this product which is synthesized not in the diamond stable region but under metastable conditions, that is, in the graphite region. Various products have been utilized as targets to deposit DLC thin films. These substances are shown in table 4. The deposited film exhibited properties characteristic of DLC material, as confirmed by high electrical resistivity, optical transparency in the infrared, chemical inertness and mechanical hardness with high refractive index (Athwal *et al* 1992). In figure 17 plots of the DLC film thickness of the various substances studied as a function of the number of laser pulses is shown. From the slope of each line, deposition rates between 3.4 to 27.4 Å/pulse have been calculated. Deposition from graphite is much slower. The data on the hybridization and structure of the various compounds used as target for DLC deposition are shown in table 5. The diamond structure is also reported. It can be seen that in moving from planar or purely aromatic structures to fullerene or fullerene shells, the main change is due to a different carbon atom configuration which exhibits varying degrees of strain or a tendential $C\ sp^2 \rightarrow C\ sp^3$ hybridization. The mechanism by which carbon atoms can rearrange themselves is not straightforward. There is an ordering process that takes place during ablation and condensation of

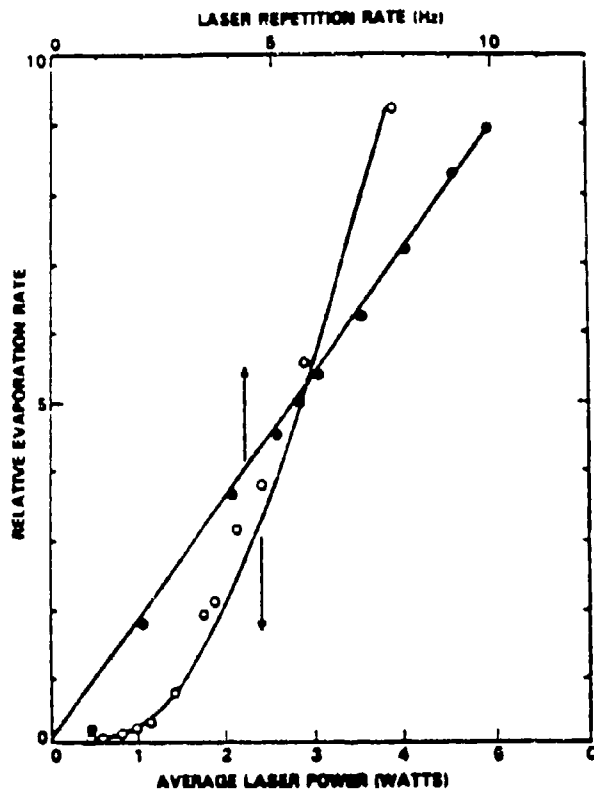


Figure 16. Evaporation rate modulation by changing the laser power density and changing the repetition rate (Cheung and Santur 1992).

Table 4. Targets used for DLC thin film deposition

Graphite
PMMA (polymethylmethacrylate, $C_8H_{16}O_2$)
Chrysene ($C_{16}H_{12}$)
Violanthrone ($C_{34}H_{16}O_2$)
Fullerene (C_{60})

carbon vapour. Diamond stability is about only 10 meV lower than that of graphite. Laser ablation produces necessarily both $C\ sp^2$ and $C\ sp^3$ configuration in different ratios. The shock wave formed in the expansion of the vapour and the high temperature may both favour a $C\ sp^3$ configuration in the deposition process.

7. Conclusions

In this review, the process of laser ablation has been very briefly described. A simple outline of the perceived mechanism in terms of energy deposition on the target,

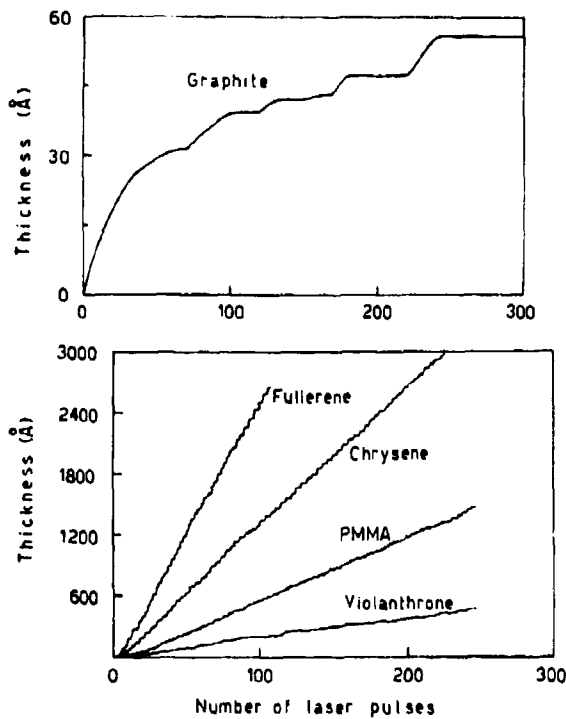


Figure 17. DLC film thickness versus number of laser pulses for various solid targets.

Table 5. Schematic of structures and hybridization of substances used as targets for DCL thin film deposition.

Compound	Hybridization	Structure
Graphite	$sp^2 + \pi$	
Aromatic polycyclic	$sp^2 + \pi$	
Fullerene	bonding $sp^2 + \pi$ possibly sp^3	
Carbon anions	$sp^2 + \pi$	
Diamond	sp^3	

*vdW—van der Waal

particle ejection and plume dynamics has been presented here. Laser ablation has tremendous exciting potential and offers many advantages over traditional methods in a variety of fields, ranging from spectroscopy and reactivity to thin film deposition, as seen from the few examples shown.

Acknowledgement

This work was partly supported by CNR project "chimica fine".

References

- Athwal I S, Mele A and Ogryzlo E A 1992 *Diamond and related material* **1** 731
Cheshnovsky O, Taylor K J, Conceicao J and Smalley R E 1990 *Phys. Rev. Lett.* **64** 1785
Cheung J T and Santur H 1992 *Laser Ablation of electronic materials* (eds) E Fogarassy and S Lazon (Amsterdam: North Holland) p. 325
Consalvo D, Mele A, Stranges D, Giardini-Guidoni A and Teghil R 1989 *Int. J. Mass Spectrom. Ion Process.* **91** 319
Dijkkamp D, Gorda A S and Venkatesan T 1987 *Phys. Rev. Lett.* **58** 2142
Giardini-Guidoni A and Mele A 1991 *Laser Chem.* **11** 205
Giardini-Guidoni A, Mele A, Pizzella G, Fantoni R, Luzic V, Moliterni A C G and Snels M 1991 *Proceed. Int. Conf. on "Laser 91"*, p. 821
Giardini-Guidoni A, Meroni A, Snels M, De Simone E, Salvi A M, Fantoni R, Berden W C M and Giorgi M 1990 *Appl. Surf. Sci.* **46** 321
Giardini-Guidoni A, Teghil R, Moroni A, Snels M, Mele A, Letardi T and Di Lazzaro P 1989 *Proc. Int. Conf. on Lasers* **89** 731
Hoffmann R 1966 *Tetrahedron* **22** 539
Kelly R and Rothenberg E 1985 *Phys. Rev.* **B7/8** 755 and reference therein
Kuper S and Stuke M 1987 *Appl. Phys.* **B44** 199
Lineman D N, Viswanadham S K, Sharkey A C and Hercules A M 1989 *Microbeam analysis* (ed.) D E Russell (San Francisco: San Francisco Press) p. 297
Martin T P 1983 *Phys. Rep.* **98** 167
Mele A, Consalvo D, Stranges D, Giardini-Guidoni A and Teghil R 1989 *Appl. Surf. Sci.* **43** 398
Mele A, Giardini-Guidoni A, Teghil R, Pizzella G and Letardi T 1992 *Mol. Cryst. Liq. Cryst.* **219** 193
Novak F P, Balasanmugam K, Viswanadham K, Parker C D, Wilk Z A, Mattern D and Hercules D M 1983 *Int. J. Mass Spectrom. Ion Phys.* **53** 135
Pitzer K S and Clementi E 1959 *J. Am. Chem. Soc.* **81** 4477
Rohlfing E A, Cox D M and Kaldor A 1984 *J. Chem. Phys.* **81** 3322
Sato T, Furano S, Iguchi S and Hanabusa M 1988 *Appl. Phys.* **A45** 355
Singh R K and Narayan J 1990 *Phys. Rev.* **B41** 8843
Song L, Freitas J E and El-Sayed M A 1990 *J. Phys. Chem.* **94** 1604
St. Pierre R J, Chronister E L and El-Sayed M A 1987 *J. Phys. Chem.* **91** 5228
Srinivasan R 1986 *Science* **234** 559
Srinivasan R and Brazen B 1989 *Chem. Rev.* **89** 1303
Teghil R, Giardini-Guidoni A, Piccirillo S, Mele A and Polla-Mattiot F 1990 *Appl. Surf. Sci.* **46** 220
Winter B J, Klots T D, Parks E K and Riley S J 1991 *Z. Phys.* **D19** 375

Laser degradation of pollutants: Polychlorobiphenyls, triazines and polycyclic aromatic hydrocarbons

R FANTONI¹, A GIARDINI-GUIDONI, A MELE*,
G PIZZELLA and R TEGHIL²

Dipartimento di Chimica, Università "La Sapienza," P.le A Moro 5, Rome, Italy

¹ENEA, AREA INN, Dip. SVIL CP 65, Frascati, Italy

²Dipartimento di Chimica, Università di Basilicata, Via N. Sauro 85, Potenza, Italy

Abstract. Visible and UV radiations have been widely used to induce chemical reactions in gases, liquids and heterogeneous systems before the development of commercial lasers for use in these regions. The availability of laser sources has allowed extensive studies on chemical reactions and time-resolved techniques to investigate the mechanism of excitation and relaxation of organic molecules in gaseous and condensed phases.

A very important field recently investigated is the laser-induced decomposition of organic molecules, present either as gas or as major constituents of or traces in solutions, with the aim of removing toxic species from chemically hazardous wastes. An investigation of laser-induced decomposition of important categories of pollutants such as polychlorobiphenyls, herbicides (triazines) and polycyclic aromatic hydrocarbons will be reported here. The experiments demonstrate the effectiveness of laser-induced techniques for the decomposition of these compounds. In most cases photofragmentation leads to the formation of non-toxic products in very high yields.

Keywords. Laser; degradation; ablation; polychlorobiphenyl; triazine; polycyclic aromatic hydrocarbons.

1. Introduction

In the past years there has been a very strong interest in developing new technologies to monitor the environment and to reduce the level of pollutants. Different types of laser sources ranging from IR to UV have been employed to induce reactions in gases, liquids and heterogeneous systems. Degradation of organic pollutants has also been studied to determine the various products obtained by irradiation and to establish the mechanism of the dissociation process. Chemical reactors equipped for irradiation of solid, liquid and gas phase systems have been built. On-line diagnostic techniques such as laser-induced fluorescence (LIF), coherent anti-Stokes Raman scattering (CARS), luminescence and time-of-flight (TOF) mass spectrometry have been developed and utilized to detect transient reaction intermediates. Final products have been analysed by gas chromatography, HPLC and XPS spectroscopy.

This report will deal with an experimental investigation on the laser-induced degradation of three important pollutants, namely polychlorobiphenyls (PCB),

*For correspondence

herbicides (triazines) and polycyclic aromatic hydrocarbons (PAH). The aim of these studies was to obtain a quantitative laser-induced decomposition of these compounds by employing radiation from different lasers. Excimer lasers ($\lambda = 308, 248$ and 193 nm), frequency quadrupled Nd-YAG laser ($\lambda = 266$ nm), were utilized to remove these toxic products and to establish the condition for drastically reducing chemical hazards, so that the harmless wastes can be either reused or released without danger to the environment.

2. Polychlorobiphenyls

The molecular structures of all PCB are similar to that of diphenyl, which is known to be formed by two phenyl rings lying in 45° rotated planes. Because of partial conjugation between the two aromatic π systems, the biphenyl molecules show a fairly strong $\pi \rightarrow \pi^*$ UV absorption peaked at 249 nm (Dyke *et al* 1971).

The occurrence of UV absorption resonant with available excimer laser radiation suggested the PCB photodecomposition experiments here reported. The laser irradiation of PCBs in the liquid phase was performed by excimer lasers at $308, 248$ and 193 nm with a pulse length of $10\text{--}15$ ns according to the laser mixture and total pressure. A commercial mixture of PCBs (Aroclor 1254) in *n*-hexane and in methanol were used.

Quantitative analyses of the irradiated products were carried out by means of gas-liquid chromatography. The chromatograph had both pulsed electron capture detector and flame ionization detector capabilities. It is worth recalling that the electron capture detector (ECD) is sensitive only to electronegative atoms, mostly to chlorine and other halogens and less to oxygen. The flame ionization detector (FID) counts all the positive ions generated in the combustion of the organic molecule, i.e. it registers peaks due to non-substituted hydrocarbons.

The energetics of the bond-breaking processes (Guggenheim and Prue 1964) which correlate to the energy of the excimer lasers employed, strongly supports single-photon absorption for direct dissociation of PCB. In fact the XeCl laser should induce only dechlorination on some heavy PCB, whereas the KrF laser is expected to break the biphenyl bond; the complete rupture of all the aromatic rings could be achieved by the ArF laser provided that all congeners in the mixtures absorb this radiation. Irradiation of $250\text{ }\mu\text{g/ml}$ of Aroclor 1254 in *n*-hexane (1 h, 2 Hz) using the XeCl (75 mJ), KrF (40 mJ) and ArF (4 mJ) lasers have fully confirmed these simple predictions. As expected, after XeCl laser irradiation the gas chromatographic analysis (ECD detector) showed the occurrence of dechlorination and isomerization with disappearance of a few heavy PCB and the formation of lighter homologues. Neither the effective destruction of the pollutant or complete dechlorination was achieved due to the fact that not all the PCB in the Aroclor 1254 mixture contribute to the UV absorption band at 320 nm. Much lighter species, corresponding to biphenyl and aromatic bond rupture were produced by irradiation with the ArF laser. Nevertheless only some of the heavy PCB congeners were dissociated and the process was ineffective for the destruction of the whole family of pollutants. This should be related to the bad matching between the laser emission wavelength and the overall absorption spectrum of the mixture. Complete destruction of the PCB was observed after irradiation of the Aroclor 1254 with KrF accompanied by the formation of light hydrocarbons.

The data in figure 1 show that all PCB in Aroclor 1254 have been completely destroyed and no chlorinated or oxidized products are formed. The data in figure 2

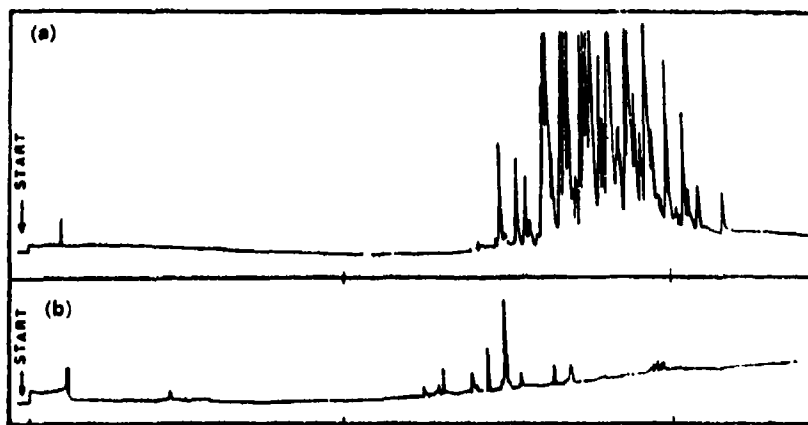


Figure 1. Gas chromatograms of $187 \mu\text{g/ml}$ Aroclor 1254 in *n*-hexane, measured using an FID detector: (a) before irradiation, (b) after irradiation with a KrF laser at the same conditions as above.

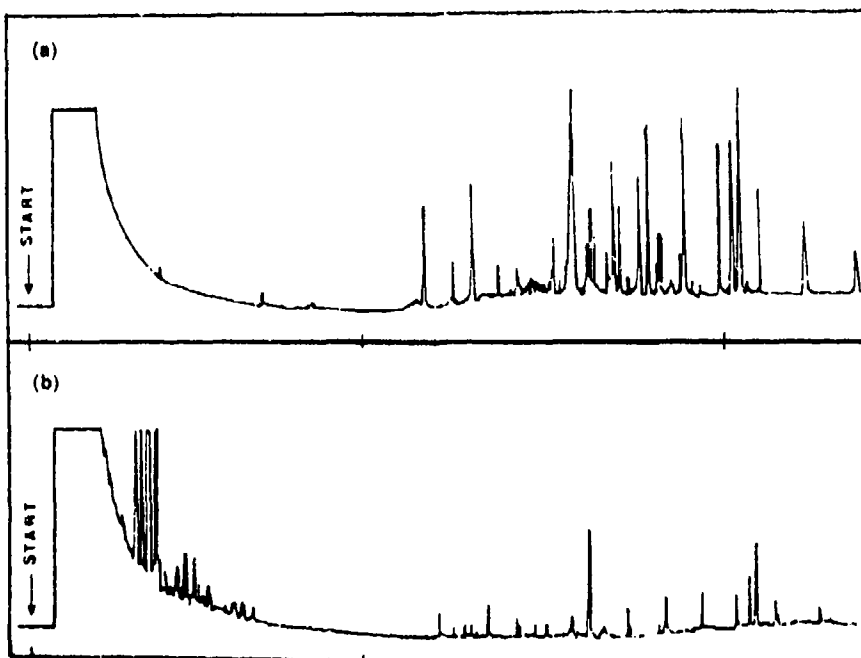


Figure 2. Gas chromatograms of $187 \mu\text{g/ml}$ Aroclor 1254 in *n*-hexane, measured using ECD detector: (a) before irradiation, (b) after 60 min of irradiation, 40 mJ KrF laser at 2 Hz.

confirm the complete PCB destruction, only traces of heavy species are detected which appear to correspond to molecules containing condensed aromatic rings. Since C-H bond rupture is the second threshold for PCB dissociation and it is also accessible energetically, HCl should be the main chlorinated product. HCl traces were indeed

found in the solution containing the final products after extraction with distilled water and ion chromatography.

3. Polycyclic aromatic hydrocarbons

It is well known that many noxious organic compounds found in the ambient particulate originate from anthropogenic sources (Hruday *et al* 1974). The attention in environmental research has been focussed on polycyclic aromatic hydrocarbons (PAH), which have strong carcinogenic action. Recently, PAH have been identified in the fly ash from municipal incinerators together with polychlorodibenzo-*p*-dioxins (PCDDs) and polychlorodibenzofurans (PCDF) which are formed by pyrolysis of polychlorobenzenes (PCBz) and polychlorophenols (PCP) (Buser 1979).

The investigation of the ablative photodecomposition of these organic materials has been performed with both a pulsed TEA CO₂ laser and a frequency quadrupled Nd-YAG laser. Ablation by a CO₂ laser operating on the 10 μ P20 line was performed on a solid target irradiated at normal incidence. The ablated material originates a luminous plume of 1 cm height. Emission has been collected and qualitatively analysed as a function of wavelength by an optical multichannel analyser system (OMA). The laser-ablated solid was deposited on a substrate and analysed by ESCA. ESCA analysis of the thin film resulting from anthracene ablation is reported in figure 3 for the C_{1s} region. It can be seen that it qualitatively corresponds to the graphite peak confirming that most of the ablated anthracene gives rise to carbon. The spectral analysis of the plume by OMA shows that emission is mainly due to hydrogen and the minor peaks are assigned to C⁺, C₂, C₃ as reported in figure 4. These results, indicate that the energy deposited in the solid by the laser initiates a process which leads to total degradation and graphitisation of the pollutant.

Ions resulting from the ablation process by means of the Nd:YAG laser were analysed by a time-of-flight mass spectrometer. Both positive and negative ions have been detected and mass analysed. One striking feature of the abundances for both

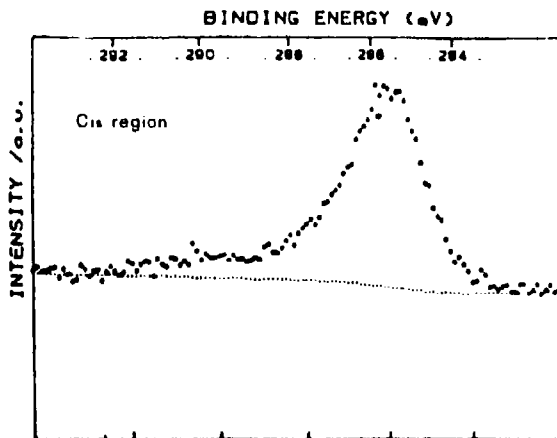


Figure 3. ESCA spectrum of a thin film deposit from anthracene ablation by means of CO₂ laser.

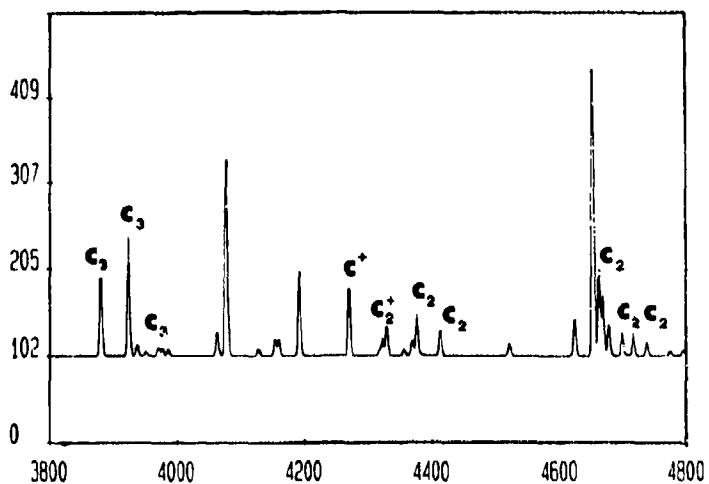


Figure 4. OMA spectral analysis of the plume from anthracene.

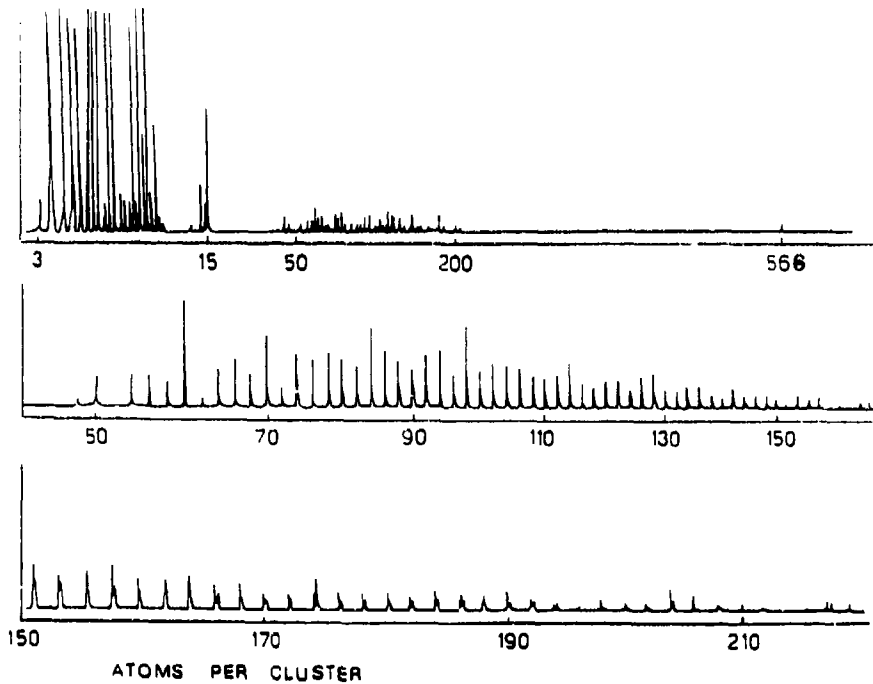


Figure 5. Mass spectra of chrysene.

positive and negative ions is the fact that at masses higher than those corresponding to C_{48} , the spectrum is the same for all the PAH studied (Linemann *et al* 1989; Mele *et al* 1989). Similar mass spectra have been observed in laser ablation of pure graphite (Pradel *et al* 1989).

In figure 5, the mass spectrum of positive ions observed in chrysene is shown. Although relative intensities depend on experimental conditions, some magic cluster sizes C_{60} , C_{70} , C_{84} have been observed in agreement with previous data (Rohlfing *et al* 1984). Recent results on photofragmentation of carbon cluster ions show that in the decomposition process the C_2 loss dominates. The negative ion mass spectra indicate the presence of clusterization yielding C_n cluster ions up to $n = 700$. At mass lower than the parent peak, all the hydrocarbons studied show the presence of C_n^- , C_nH^- .

These results strongly indicate a general tendency of aromatic compounds to produce fragmentation. This is shown from the large number of C_n^\pm ions obtained from all hydrocarbons irradiated. The similarity of the aromatic hydrocarbons and of graphite mass spectra supports the hypothesis that ion formation is governed by the same mechanism which produces ablation and chemical reactions in the highly dense cloud of material. Cluster ion formation is, therefore, the ultimate process yielding graphitization. These results are of great relevance in the treatment of wastes of aromatic products. The development of a large-scale plant that uses laser sources may be particularly appropriate for this purpose.

4. Triazines

4,6-Aminosubstituted azines are commonly used as herbicides. Their classification depends on the composition of the amino chains ($R-NH-$) bound to the triazine aromatic ring and on the nature of the other substituent in position 2, which is usually $-Cl$, $-O-CH_3$ or $-S-CH_3$. In spite of their low toxicity with respect to pesticides, their large use in agriculture makes them major pollutants in the soil and in drinking water sources.

The electronic transitions of these molecules, the $n \rightarrow \pi$ and the $\pi \rightarrow \pi^*$, are centred around 272 and 222 nm respectively in pyridine; the wavelength shifts towards the visible as the molecular complexity increases, e.g. at 323 and 372 nm in pyrazine (Tomer *et al* 1988). Photoablation experiments on solid aminotriazines either under vacuum or in the presence of a buffer gas were developed to study the mechanism of decomposition of this important class of pollutants in an attempt to produce non-hazardous species. Laser ablation experiments for optical diagnosis of the plume

Table 1. Solid targets used in laser ablation experiments.

Common name	IUPAC name
Cyanuric acid	2,4,6-Triazinetriol
Melamine	2,4,6-Triamino-s-triazine
	2-Chloro-4,6-diamino-s-triazine
Simazine	2-Chloro-4,6-bis(ethylamino)-s-triazine
Atrazine	2-Chloro-4-ethylamino-6-isopropylamino-s-triazine
Propazine	2-Chloro-4,6-bis(isopropylamino)-s-triazine
Ametryne	2-Methylthio-4-ethylamino-6-isopropylamino-s-triazine
Prometryne	2-Methylthio-4,6-bis(isopropylamino)-s-triazine
Atraton	2-Methoxy-4-ethylamino-6-isopropylamino-s-triazine
	2,6-Dichloropyrazine

from 4,6-aminosubstituted triazines has been performed at 308 (XeCl) nm and 248 nm (KrF) (Mele *et al* 1990; Giardini-Guidoni *et al* 1991). Some simpler systems, belonging to the family of melamines and pyrazines, have been also irradiated for comparison. The compounds studied are listed in table 1. The mechanism of photodecomposition has been studied by directly detecting the ions formed by coupling a time-of-flight mass spectrometer with a frequency quadrupled Nd:YAG laser ($\lambda = 266$ nm) (Giardini-Guidoni *et al* 1991).

4.1 Optical diagnosis

Laser ablation experiments of solid triazine samples have been carried out under vacuum (10^{-6} torr background pressure). A luminous plume, with a bright blue-green emission visible to the unaided eye, is seen in all UV laser ablation experiments. According to a recent classification (Ito *et al* 1989), the laser energy focussed on the sample (60 mJ) was in the middle fluence region (4×10^8 W/cm²) where absorption occurs both from the solid and the first-vaporized gas. Emission spectra of electronically excited fragments have been detected by an Optical Multichannel Analyser as a function of the delay from the laser pulse at different gate widths (≥ 100 ns). Space-resolved measurements along the luminescent plume axis have been performed by fine adjustment of focussing and collecting optics. All emission spectra of the plume obtained by ablation of different substituted-azines at the two wavelengths used are quite similar. Several ions, atoms and diatomic molecular fragments in electronically excited states have been detected. The strongest near-UV visible emission lines are mostly due to CN (violet system with tail bands, from 350 to 425 nm), C₂ (Swan's system with high pressure band, from 435 nm to 565 nm), CH (4300 Å system, around 431 nm), NH (3350 Å system, around 336 nm), H (Balmer series) and C⁺ (at 426.7 nm). Overview spectra at 308 nm, showing the most intense fragment bands, are shown in figure 6. In ametryne and prometryne atomic sulphur emission appears near 420 nm. In atraton atomic oxygen emission has been detected at 394.73 nm. Weak atomic chlorine lines have been observed in all the chlorinated samples near 481 nm. The intense CN⁺ band around 320 nm (3185 Å system at 326.33 and 318.51 nm) has been observed at short time delay in laser ablation of 2,6-dichloropyrazine, which conversely

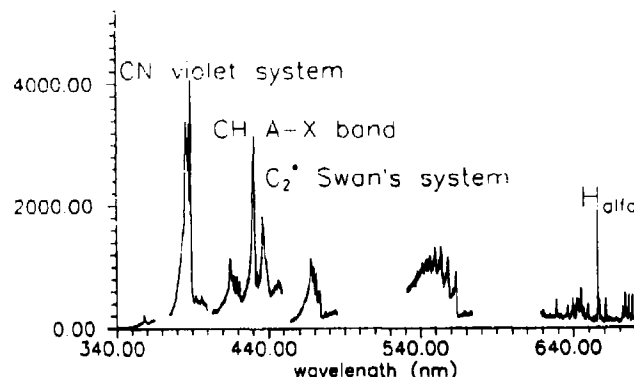


Figure 6. Overview spectrum (most intense portion) during atrazine laser ablation at 308 nm ($d = 2$ mm), no gate.

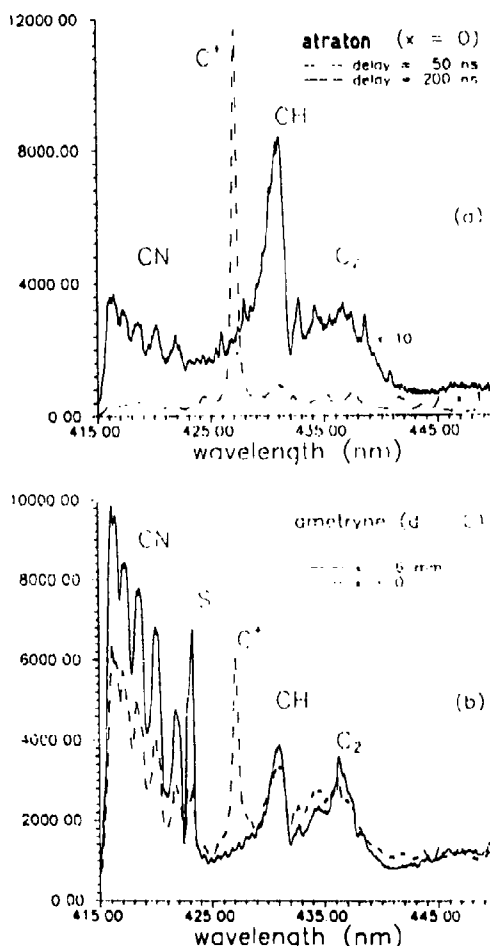


Figure 7. Selected portions of optical emission spectra during laser ablation of different substituted triazines at 308 nm: (a) Atraton, spectra measured at different delay times from the laser pulse (100 ns gate); (b) Ametryne, spectra measured at different focal distances from the surface (no gate).

did not show any CH emission. Highly excited atoms and ions are detected very close to the ablated surface and at very short time delay with respect to the laser pulse. Their lifetime, monitored by 100 ns time resolution, appears to be unaffected by the addition of a buffer gas. Emission from highly excited atomic fragments, however, tend to be localised closer to the sample surface as the buffer pressure is increased. Emission from excited molecular fragments comes later in time and is more diffuse in space, as shown by the typical results obtained (figure 7), where significant portions of emission spectra of atraton (a) and ametryne (b) are reported as functions of time delay from the laser pulse and of the focal distance from the surface, respectively. The relaxation of small fragments (CH^+) is observed at the plume border,

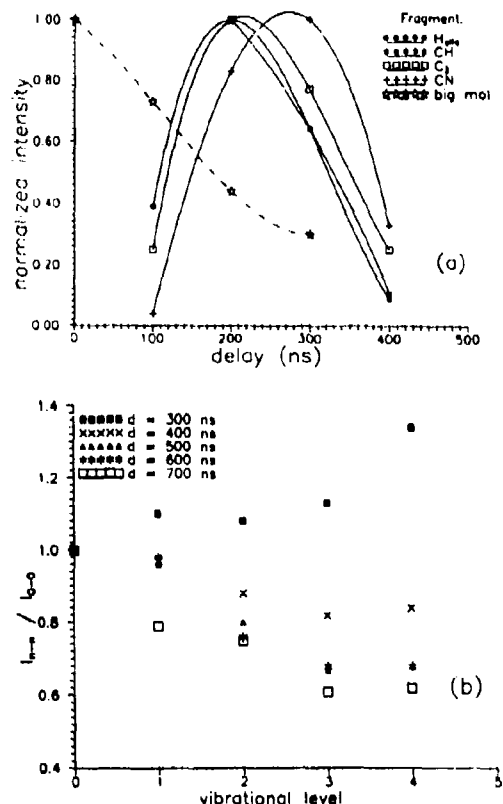


Figure 8. Time evolution of fragment emission during laser ablation of propazine at 248 nm, gate width = 100 ns. (a) Integrated band intensity for different fragments; ablation 2 mm from the surface, no buffer. (b) Relative intensity of $v - v = 0$ emission lines detected in the violet system; ablation at the surface, 10 torr N₂ added.

and it has been found that this takes place also upon addition of a buffer gas. A typical time-resolved fragment distribution obtained by laser ablation of propazine at 248 nm is shown in figure 8a. The vibrational distribution of most abundant electronically excited molecular fragments detected in emission, e.g. CN (violet band), C₂ (Swan's system) and CH (A-X band), gives indications of preferential reaction patterns and of secondary fragmentation. Details of the time behaviour of CN emission in different vibrationally excited levels are reported in figure 8b. In the case of N₂ addition to propazine (10, 30 and 80 torr), CH emission disappears and H is observed only very close to the surface. Duration of emission from other molecules and delay for maximum fluorescence intensity increase with buffer pressure.

4.2 Mass spectrometric analysis

The ionic species produced by laser ablation of solid triazine were mass analyzed by a time-of-flight mass spectrometer. The apparatus and procedure have been previously

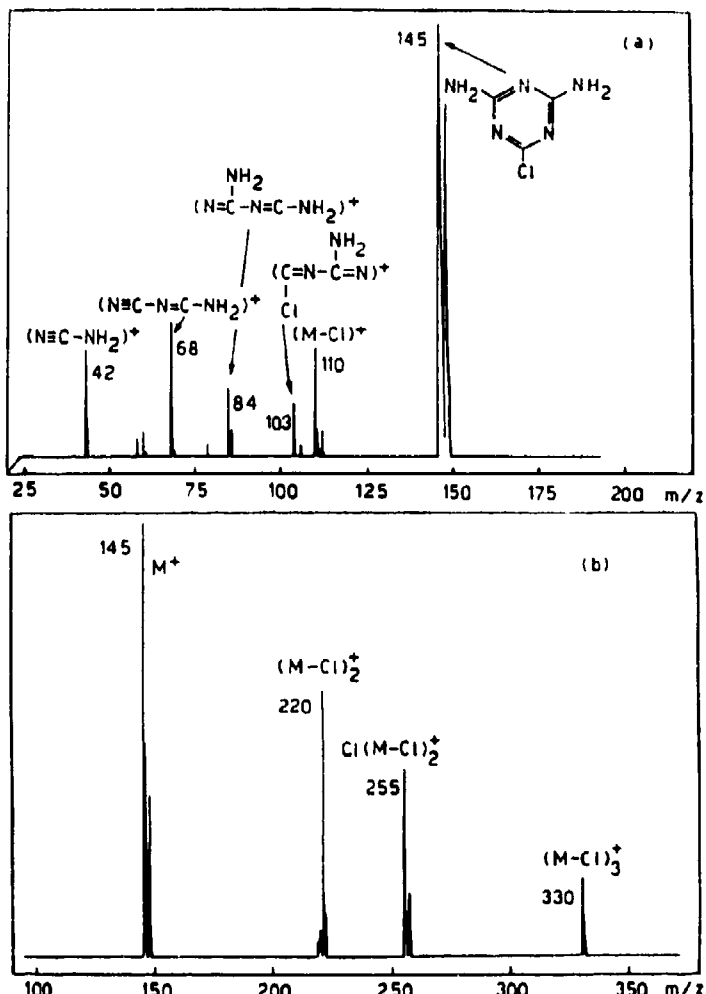


Figure 9. Positive ion mass spectrum of 2-chloro-4,6-diamino-s-triazine: (a) fragmentation mass spectrum; (b) cluster ion formation.

described (Mele *et al* 1992). The solid samples were prepared from ground powders, spread on a grid and directly irradiated by a pulsed-frequency quadrupled Nd:YAG laser ($\lambda = 266$ nm). Both positive and negative ions have been detected and identified.

A typical mass spectrum of a triazine is shown in figure 9: (a) ions at m/e lower than the parent; (b) ions at m/e larger than the parent ion. The ions in figure 9 are produced from fragmentation of the molecular solid. In the higher mass range in figure 9b, two aggregation processes are identified. Clusters of dehalogenated parent molecules of formula $(M-Cl)_n$ and clusters of chlorine atoms with dehalogenated molecules of formula $Cl(M-Cl)_n$ are observed. It can be noted from the fragments in figure 9a that a Diels-Alder ring-opening process takes place i.e. a 4 + 2 bond rupture occurs. Analogous fragmentation processes are observed for other triazines.

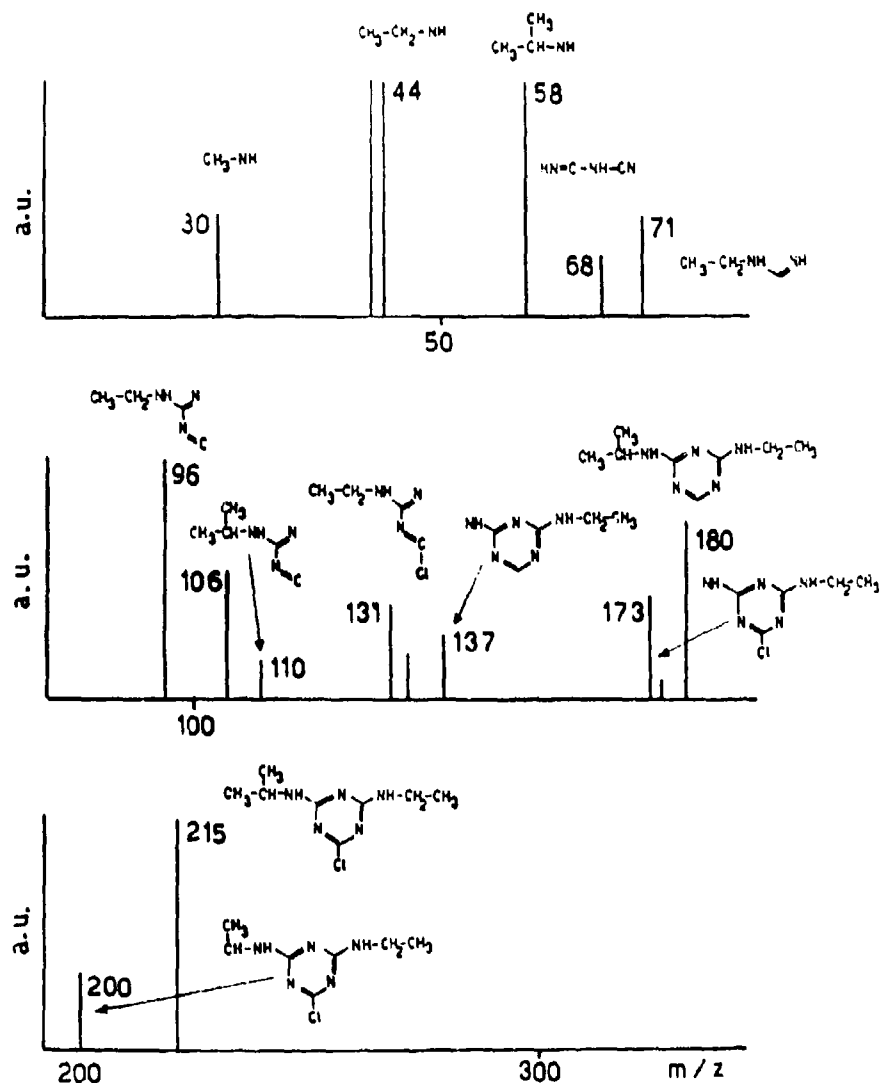
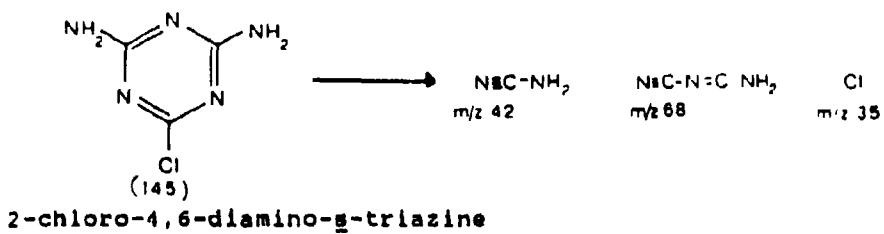


Figure 10. TOF fragmentation mass spectrum of atrazine at 266 nm: positive ions.



The mass spectra of atrazine in figure 10 shows the various fragments of degradation of the product.

A possible ring opening process is typically the following (Mele *et al* 1992).

5. Conclusions

The results of the present investigation have shown that laser photolysis may be usefully applied to the treatment of dangerous material which has to be rejected. Serious problems have been faced by municipalities in getting rid of substances which can neither be treated by heat nor left in the ground. Among other pollutants PCB are well known as precursors of polychlorodibenzodioxines (PCDA) and polychlorodibenzofuranes (PCDF) (Eiceman *et al* 1979). Polycyclic hydrocarbons are also very noxious substances which cannot be easily destroyed. The laser treatment in solution or by laser ablation of the pollutants have shown the effectiveness of the method to obtain non-toxic substances by simple degradation. Investigations have to be made to determine suitable pathways to obtain inert derivatives from such pollutants. Degradation of PCB and PAH has been particularly successful. In both cases, laser-induced decomposition processes lead to very high yields of non-toxic materials: PCB produce low molecular weight compounds; a process of graphitisation takes place by laser irradiation of all PAH examined. The results obtained by ablation of triazines have shown that the laser treatment is not exhaustive. Irradiation leaves behind some amounts of cyanides and polycyanides formed by ring opening and cleavage of triazines. This may be typical of any compound containing the C-N bond in its structure. A higher laser fluence will probably provide a more extensive degradation process.

References

- Buser H R 1979 *Chemosphere* **8** 415
 Dyke S F, Floyd A J, Sainsbury M and Theobald R S 1971 *Organic spectroscopy. An introduction*. (Harmondsworth: Penguin)
 Eiceman G A, Clement E E and Karasek F W 1979 *Anal. Chem.* **51** 2343
 Giardini-Guidoni A, Mele A, Pizzella G, Fantoni R, Lazić V, Moliterni A G G and Snels M 1991a *Proc. Int. Conf. Lasers* **91** 821
 Giardini-Guidoni A, Mele A, Pizzella G and Teghil R 1991b *Org. Mass Spectrosc.* **26** 779
 Guggenheim E A and Prue J E 1964 *Physicochemical calculation* (Amsterdam: North-Holland)
 Hrudey S E, Perry R and Willings R A 1974 *Environ. Res.* **7** 294
 Ito H, Ozaki Y, Suzuki K, Kondow T and Kuchitsy K 1989 *J. Mol. Spectrosc.* **127** 283
 Linemann D N, Viswanadham S K, Sharkey A G and Hercules D M 1989 *Microbeam analysis* (ed.) P E Russell (San Francisco: San Francisco Press) p. 297
 Mele A, Giardini-Guidoni A, Pizzella G, Teghil R and Barbini R 1990 *Proc. Int. Conf. on Lasers* p. 799
 Mele A, Giardini-Guidoni A and Teghil R 1989 *Proc. XIV Atomic and Molecular Physics*, Riva del Garda, Italy
 Mele A, Giardini-Guidoni A, Teghil R, Pizzella G and Letardi T 1992 *Mol. Cryst. Liq. Cryst.*, **219** 193
 Pradel P, Monchicourt P, Lancagne J J, Pedrix M and Watel G 1989 *Chem. Phys. Lett.* **158** 412
 Rohlfing E A, Cox D M and Kaldor A 1984 *J. Chem. Phys.* **81** 3322
 Tomer J L, Holtzclaw K W, Pratt D W and Spangler L H 1988 *J. Chem. Phys.* **88** 1528

Hydrogen-atom and proton-induced electron transfer reactions via triplet exciplexes

HARUO SHIZUKA* and MINORU YAMAJI

Department of Chemistry, Gunma University, Kiryu, Gunma 376, Japan

Abstract. It has been shown by means of laser flash photolysis at 355 nm that (1) hydrogen atom transfer (HT) from triplet naphthalene derivatives (produced by the triplet sensitization of benzophenone (BP)) to BP occurs via a triplet exciplex having a weak charge-transfer structure; (2) in the presence of protons, HT is enhanced in the naphthol-BP system via a protonated triplet exciplex whereas in the naphthylammonium ion-BP system, markedly reduced; (3) in the methoxynaphthalene-BP system, proton-induced electron transfer (ET) takes place via a protonated triplet exciplex, and (4) these triplet exciplexes have sandwich-like structures on the basis of experiments for intramolecular HT and ET of the methylene bridged compounds.

Keywords. Laser flash photolysis; hydrogen-atom transfer; proton-induced electron transfer; triplet exciplexes; triplet naphthalene derivatives.

1. Introduction

Acid-base reactions in the excited states of aromatic compounds have been extensively studied since they are elementary processes in both chemistry and biochemistry (Förster 1950; Weller 1952, 1956, 1961; Beens *et al* 1965; Wehry and Rogers 1966; Van der Donckt 1970; Ireland and Wyatt 1976; Schulman 1976, 1977; Klopffer 1977). In this decade, there has been considerable interest in photochemical and photophysical properties of aromatic compounds in the presence of protons (Shizuka 1985); proton transfer reactions in the excited state and proton-induced quenching (Tsutsumi and Shizuka 1977, 1978; Shizuka and Tobita 1982; Shizuka *et al* 1988), a one-way proton transfer reaction in the excited state of hydrogen-bonded complexes (Shizuka *et al* 1985, 1986; Shizuka and Serizawa 1986) and examples for the absence of excited-state prototropic equilibrium (Shizuka *et al* 1985d).

On the other hand, hydrogen atom transfer reactions in the triplet state of carbonyl compounds from a variety of substrates, such as alcohols, hydrocarbons and amines, are well-known. The reaction proceeds by either hydrogen atom transfer or electron transfer followed by proton transfer. A large number of studies on intermolecular and intramolecular hydrogen atom transfer reactions of carbonyl triplets have been reported upon direct excitation (Wagner and Hammond 1968; Dalton and Turro 1970; Wagner 1971, 1976; Turro *et al* 1972; Cohen *et al* 1973; Scaiano 1973/1974; Formoshinho 1976, 1978; Arimitsu *et al* 1975; Turro 1978; Okada *et al* 1980, 1982; Peters *et al* 1980, 1982; Simon and Peters 1981, 1982, 1984; Manring and Peters 1983;

*For correspondence

Hoshino *et al* 1986; Wagner *et al* 1986; Hoshino and Shizuka 1987, 1988, 1993; Devadoss and Fessenden 1990, 1991; Miyasaka *et al* 1991). However, until recently, little attention has been paid to hydrogen-atom and electron-transfer reactions from triplet aromatic compounds produced by triplet sensitization of carbonyl compounds to carbonyl compounds (Shizuka and Fukushima 1983; Shizuka *et al* 1985a, b; Kohno *et al* 1991; Yamaji *et al* 1992; Kaneko *et al* 1993; Sekiguchi *et al* 1993).

By means of laser flash photolysis with third harmonics (355 nm) from a nanosecond Nd³⁺:YAG laser, kinetic studies on the hydrogen atom (HT) and proton-induced electron transfer (*p* - eT) reactions from triplet naphthalene derivatives (produced by the triplet sensitization of benzophenone) to benzophenone have been carried out. It is revealed that the HT and *p* - eT reactions proceed via the triplet exciplexes having a sandwich-like structure with weak charge-transfer interaction. The proton effects on the rate constants for the HT and *p* - eT reactions have been also investigated. The reaction mechanisms are illustrated.

2. Results and discussion

2.1 The hydrogen atom transfer reaction of triplet naphthylammonium ion to benzophenone (Kohno *et al* 1991)

The excited singlet state of benzophenone (¹BP*) is initially produced upon 355-nm laser excitation in the naphthylammonium ion (RNH₃⁺)-benzophenone (BP) system since only BP has absorbance at 355 nm in the present system. According to the El-Sayed rule (1962-1964), the triplet benzophenone (³BP*) was formed via fast intersystem crossing at picosecond time scale (Anderson *et al* 1974; Damschen *et al* 1978).

Since the triplet energies of BP and RNH₃⁺ are 69.2 (Murov 1973) and 60.9 kcal/mol (Shizuka and Fukushima 1983), respectively, the ET reaction occurs from ³BP* to RNH₃⁺ in the nanosecond time scale, competing with hydrogen abstraction of ³BP* from RNH₃⁺ or solvent molecules.

Figure 1 shows the time-resolved transient absorption spectra obtained after a 355-nm laser pulse in the RNH₃⁺ (3.0×10^{-3} M)-BP (1.12×10^{-2} M) system in the presence of [H₂SO₄] = 0.015 M (a) and 0.5 M (b) in methanol-water (9:1 v/v) at 290 K. The absorption band at 410 nm in figure 1a or 415 nm in figure 2b is the triplet-triplet (*T*-*T*) absorption of RNH₃⁺ produced by triplet energy transfer (ET) from triplet benzophenone (³BP*). On the microsecond time scale, the *T*-*T* absorption of RNH₃⁺ decreases, and absorption bands with peaks at 510 and 545 nm appear in intensity with an isosbestic point at 455 nm. The 510- and 545-nm bands correspond to the absorption spectra of the naphthylamine cation radical (RNH₂⁺) and the benzophenone ketyl radical (>COH) (Land 1968) respectively. The first-order rate constants (*k*_{obsd}) for the decay of triplet naphthylammonium ion (³RNH₃⁺*) observed at 410 nm and 415 nm are 2.4×10^6 s⁻¹ and 2.0×10^5 s⁻¹ for the present systems with [H₂SO₄] = 0.015 M and 0.5 M, respectively. On the other hand, both the rate constants for the rises of RNH₂⁺ at 510 and >COH at 545 nm are consistent with those for the decay of ³RNH₃⁺* in both cases. Therefore, it is concluded that the hydrogen atom transfer (HT) reaction from ³RNH₃⁺* to BP occurs effectively to yield RNH₂⁺ and >COH regardless of the concentration of the acid used. However, the *k*_{obsd} value for the HT of ³RNH₃⁺* is strongly affected and is reduced by the acid

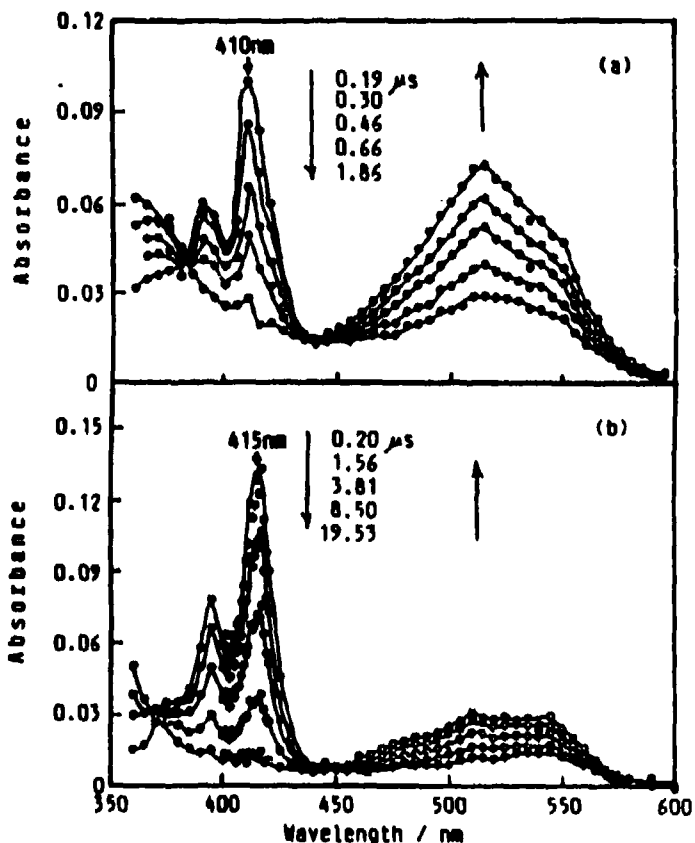


Figure 1. Time-resolved transient absorption spectra of the RNH_3^+ (3.0×10^{-3} M)-BP (1.12×10^{-3} M) systems on the microsecond time scale in the presence of $[\text{H}_2\text{SO}_4] = 0.015$ M (a) and 0.5 M (b) in MeOH-water (9:1 v/v) at 290 K obtained after laser photolysis at 355 nm (Kohno *et al.* 1991).

concentration. The efficiencies (ϕ_{HT}) of the HT reaction from ${}^3\text{RNH}_3^{+*}$ to BP are 0.95 and 0.31 for the present systems with $[\text{H}_2\text{SO}_4] = 0.015$ M and 0.5 M, respectively. It is obvious that the ϕ_{HT} value as well as that of k_{obsd} is affected considerably by addition of acids.

In order to study the reaction mechanism for the HT reaction from ${}^3\text{RNH}_3^{+*}$ to BP in the presence of protons, the concentration effects of BP and acids are investigated by nanosecond laser flash photolysis.

Figure 2 shows the plots of k_{obsd} vs [BP] in the presence of $[\text{H}_2\text{SO}_4] = 0.015$ M (a), 0.05 M (b) and 0.5 M (c). The value of k_{obsd} increases with increase of [BP], while it decreases with increase of $[\text{H}_2\text{SO}_4]$. However, there is a leveling off at higher [BP], especially at lower $[\text{H}_2\text{SO}_4]$ ($\lesssim 0.05$ M), which indicates an equilibrium in the excited state such as a triplet exciplex. On the other hand, figure 3 shows the plots of k_{obsd} vs [acid] in order to study the proton effect on the HT reaction of RNH_3^+ -BP systems at various [acid] with H_2SO_4 and HClO_4 as proton sources. The value of

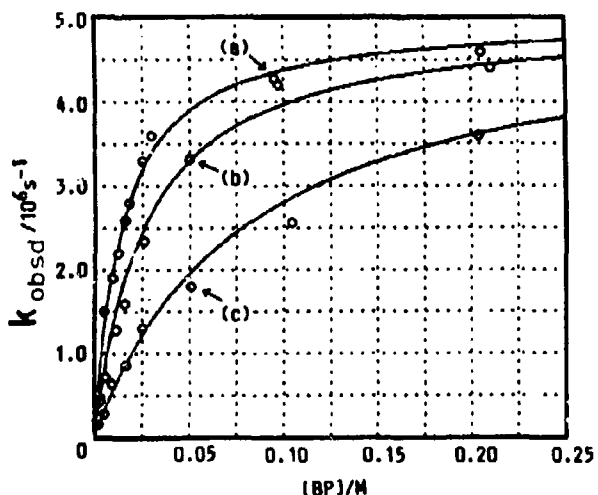


Figure 2. Plots of the decay rate constant (k_{obsd}) of ${}^3\text{RNH}_2^{+*}$ as a function of [BP] monitored at 410 nm in the presence of $[\text{H}_2\text{SO}_4] = 0.015 \text{ M}$ (a), 0.05 M (b) and 0.2 M (c). The solid curve denotes the calculated value of k_{obsd} by using (1) (Kohno *et al* 1991).

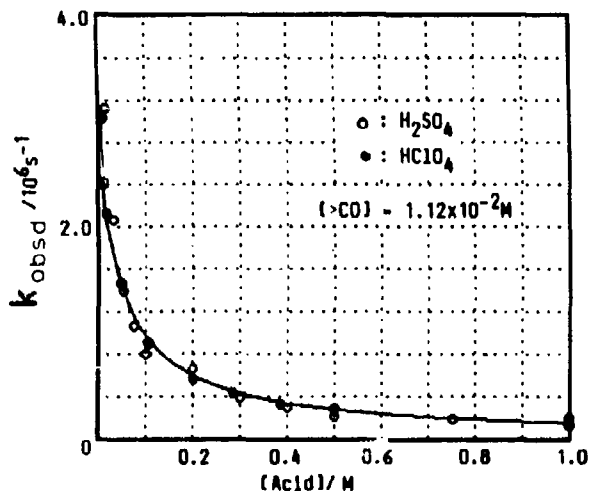
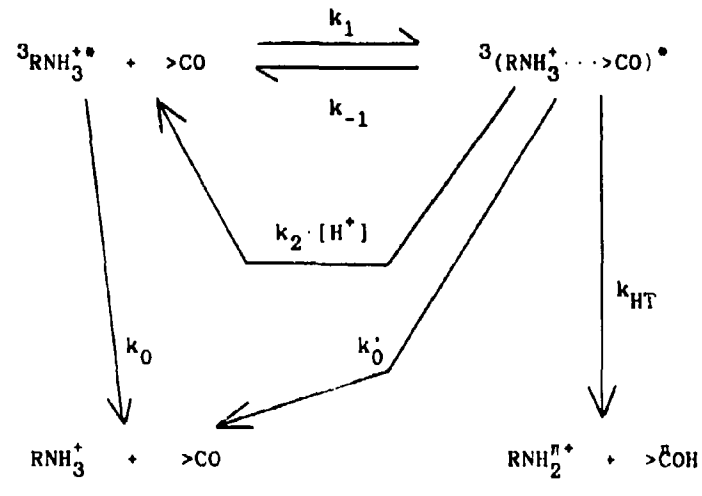


Figure 3. Plots of the decay rate constant (k_{obsd}) of ${}^3\text{RNH}_2^{+*}$ as a function of acid $[\text{H}_2\text{SO}_4]$ (○), HClO_4 (●) in the presence of $[\text{BP}] = 1.12 \times 10^{-2} \text{ M}$. The solid curve denotes the calculated values of k_{obsd} by using (1) (Kohno *et al* 1991).

k_{obsd} drastically decreases with an increase of [acid]. The k_{obsd} value obtained in the HClO_4 system agrees with that in the H_2SO_4 system as shown in figure 3. H_2SO_4 is known to behave almost as a monoprotic acid even in dilute solution (Cox and Yates 1978).



Scheme 1.

From the above results, the mechanism of the HT reaction is accounted for by scheme 1, where the triplet exciplex, $^3(\text{RNH}_3^{+} \cdots \text{BP})^*$ formed between $^3\text{RNH}_3^{+*}$ and BP with 1:1 ratio, k_1 and k_{-1} are the rate constants for formation and decomposition of $^3(\text{RNH}_3^{+} \cdots \text{BP})^*$, respectively, k_0 and k'_0 the decay rate constants of $^3\text{RNH}_3^{+*}$ and $^3(\text{RNH}_3^{+} \cdots \text{BP})^*$ to the ground state ($\text{RNH}_3^{+} + \text{BP}$), respectively, k_{HT} the rate constant for HT via $^3(\text{RNH}_3^{+} \cdots \text{BP})^*$ and k_d denotes the decay rate constant of $^3(\text{RNH}_3^{+} \cdots \text{BP})^*$ by protonation, resulting in the reproduction of $^3\text{RNH}_3^{+*} + \text{BP}$ due to the Coulombic repulsion in the protonated triplet exciplex, $^3(\text{RNH}_3^{+} \cdots \text{COH})^*$. That is, the concentration of free $^3\text{RNH}_3^{+*}$ increases with increase of $[\text{H}_2\text{SO}_4]$. Therefore, the vibrational structures of the T-T absorption spectrum of $^3\text{RNH}_3^{+*}$ at 415 nm with $[\text{H}_2\text{SO}_4] = 0.5 \text{ M}$ are sharper than that of $^3(\text{RNH}_3^{+} \cdots \text{BP})^*$ at 410 nm with $[\text{H}_2\text{SO}_4] = 0.015 \text{ M}$ as shown in figure 1.

According to scheme 1, k_{obsd} is expressed by

$$k_{\text{obsd}} = \{k_0 + K_1 \cdot [\text{BP}] \cdot k_{\text{ex}} \cdot (1 + [\text{H}_2\text{SO}_4] \cdot k'_2 / k_{-1})^{-1}\} \cdot \{1 + K_1 \cdot [\text{BP}] \cdot (1 + [\text{H}_2\text{SO}_4] \cdot k'_2 / k_{-1})^{-1}\}^{-1}, \quad (1)$$

where we use $k'_2 \cdot [\text{H}_2\text{SO}_4]$ instead of $k_2 \cdot [\text{H}^+]$. When the kinetic parameters in scheme 1 are $K_1 (= k_1 / k_{-1}) = 110 \text{ M}^{-1}$, $k'_2 / k_{-1} = 40 \text{ M}^{-1}$, $k_0 = 1 \times 10^4 \text{ s}^{-1}$ and $k_{\text{ex}} (= k'_0 + k_{HT}) = 5 \times 10^6 \text{ s}^{-1}$, the calculated values of k_{obsd} from (1) shown as solid curves in figures 2 and 3 are in good agreement with the experimental ones.

2.2 The hydrogen atom transfer reaction from triplet naphthol to BP

When the naphthol (ROH)-BP system is employed under 355-nm laser pulsing, the ET reaction occurs in the nanosecond time scale from $^3\text{BP}^*$ to ROH competing with

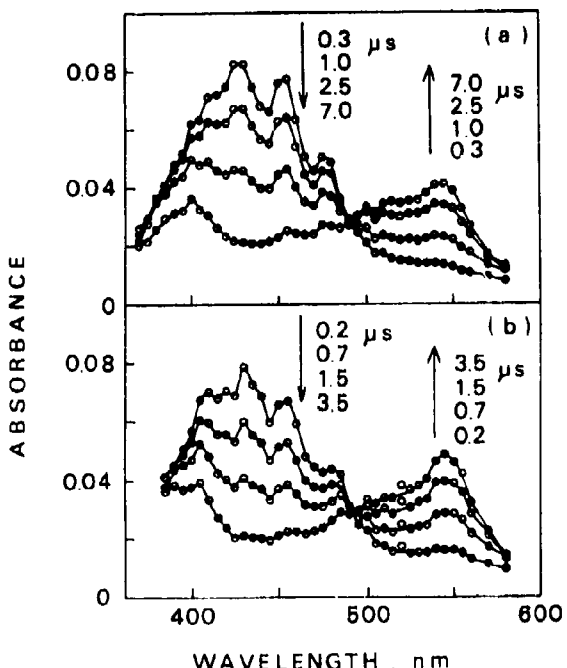


Figure 4. Time-resolved transient absorption spectra of the ROH (3.0×10^{-3} M)-BP (6.7×10^{-3} M) system in acetonitrile-water (4:1 v/v) in a microsecond region for $[H_2SO_4] = 0$ M (a) and 0.5 M (b) observed after 355-nm laser pulsing at 290 K (Kaneko *et al.* 1993).

hydrogen abstraction from ROH and deactivation of $^3\text{BP}^*$ by ROH. The triplet energies of BP and ROH are known to be 69.2 and 58.6 kcal mol $^{-1}$, respectively, in a polar solvent (Murov 1973).

In order to elucidate the HT reaction from $^3\text{ROH}^*$ to BP with $[H_2SO_4] = 0$ and 0.5 M, transient absorption spectra were analyzed on a microsecond time scale. Figure 4 shows the typical transient absorption spectra observed at 0.2–7 μ s after laser pulsing in ROH (3.0×10^{-3} M)-BP (6.7×10^{-3} M) systems containing (a) $[H_2SO_4] = 0$ and (b) 0.5 M in acetonitrile-water (4:1 v/v) at 290 K. In both spectra (a) and (b), the 430-nm band for triplet naphthol ($^3\text{ROH}^*$) decreases with an isosbestic point at 490 nm, accompanying an increase in intensities of the 545-nm and the 400-nm bands for the benzophenone ketyl radical ($>\dot{\text{C}}\text{OH}$) and the 1-naphthoxy radical ($\text{R}\dot{\text{O}}$), respectively.

Figure 5 shows the time traces of the transient absorbance changes observed at 430 nm ((a) and (c)) for $^3\text{ROH}^*$ and 545 nm ((b) and (d)) for $>\dot{\text{C}}\text{OH}$ after laser pulsing in ROH (3.0×10^{-3} M)-BP (6.7×10^{-3} M) systems with $[H_2SO_4] = 0$ ((a) and (b)) and 0.5 M ((c) and (d)) in acetonitrile-water (4:1 v/v) at 290 K. The rate constants (k_{obsd}) of the decay for $^3\text{ROH}^*$ are $2.8 (\pm 0.2) \times 10^5 \text{ s}^{-1}$ for $[H_2SO_4] = 0$ M and $7.4 (\pm 0.3) \times 10^5 \text{ s}^{-1}$ for $[H_2SO_4] = 0.5$ M, respectively. The rate constant for the decay of $^3\text{ROH}^*$ is almost identical with that for the rise of $>\dot{\text{C}}\text{OH}$ within experimental error (10 %) showing that the HT reaction takes place from $^3\text{ROH}^*$ to BP. On the other hand, the k_{obsd} value at 430 or 545 nm in the system with

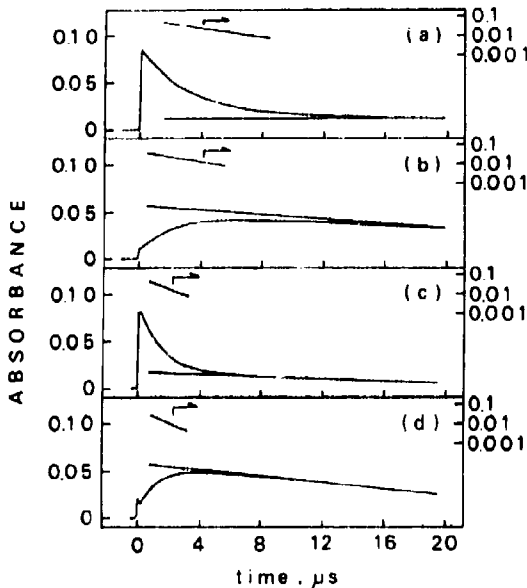


Figure 5. Time traces of the absorbance changes for transient species observed at 430 nm (a) and 545 nm (b) for $[H_2SO_4] = 0\text{ M}$ and at 430 nm (c) and 545 nm (d) for $[H_2SO_4] = 0.5\text{ M}$ after a 355-nm laser pulse in the ROH ($3.0 \times 10^{-3}\text{ M}$)-BP ($6.7 \times 10^{-3}\text{ M}$) system in acetonitrile-water (4:1 v/v) at 290 K (Kaneko *et al.* 1993).

$[H_2SO_4] = 0.5\text{ M}$ is 2.6 times greater than that in the system without H_2SO_4 . This indicates that k_{obsd} at 430 or 545 nm is obviously enhanced by protons. The efficiency (ϕ_{HT}) for the HT reaction from $^3\text{ROH}^*$ to BP are 0.73 and 0.85 for ROH ($3.0 \times 10^{-3}\text{ M}$)-BP ($6.7 \times 10^{-3}\text{ M}$) systems with $[H_2SO_4] = 0\text{ M}$ and 0.5 M , respectively. These results show that the value of ϕ_{HT} is enhanced by protons as well as that of k_{obsd} . These findings imply that the HT reaction from $^3\text{ROH}^*$ to BP is enhanced by protons in contrast to the case of RNH_3^+ (Kohno *et al.* 1991). In order to elucidate the effect of protons on the HT reaction, laser photolysis at 355 nm was carried out in the ROH-BP system at various concentrations of H_2SO_4 .

Figure 6 shows the plots of the decay rate constant (k_{obsd}) of $^3\text{ROH}^*$ at 430 nm vs $[H_2SO_4]$ ($\leq 1.0\text{ M}$) obtained by laser photolysis in ROH ($3.0 \times 10^{-3}\text{ M}$)-BP (0.1 M) systems containing various $[H_2SO_4]$ in acetonitrile-water (4:1 v/v) at 290 K. The k_{obsd} value linearly increases with an increase of $[H_2SO_4]$. Therefore, k_{obsd} is formulated as

$$k_{\text{obsd}} = k_1 + k_2 \cdot [H_2SO_4], \quad (2)$$

where k_1 and k_2 are the quenching rate constant by H_2SO_4 and the decay rate constant of $^3\text{ROH}^*$ for the ROH ($3.0 \times 10^{-3}\text{ M}$)-BP (0.1 M) system without H_2SO_4 , respectively. From the slope and intercept of the line, we have $k_1 = 4.8 \times 10^6 \text{ M}^{-1} \text{ s}^{-1}$ and $k_2 = 3.5 \times 10^6 \text{ s}^{-1}$.

Figure 7 shows the plots of k_{obsd} at 430 nm as a function of [BP] ($\leq 2.0 \times 10^{-1}\text{ M}$) obtained by laser photolysis at 355 nm in ROH ($3.0 \times 10^{-3}\text{ M}$)-BP systems containing $[H_2SO_4] = 0, 0.5$ and 1.0 M in acetonitrile-water (4:1 v/v) at 290 K. The value of

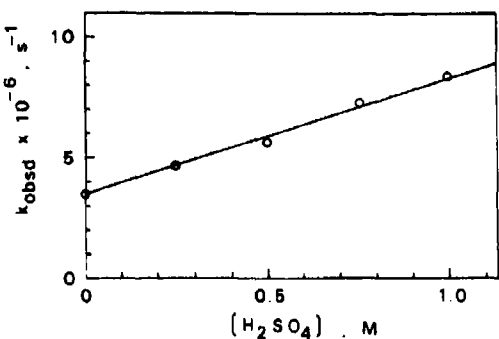


Figure 6. Plots of the decay rate constant (k_{obsd}) of ${}^3\text{ROH}^*$ as a function of $[\text{H}_2\text{SO}_4]$ observed at 430 nm after laser pulsing at 355 nm in the ROH (3.0×10^{-3} M)-BP (0.1 M) system in acetonitrile-water (4:1 v/v) at 290 K (Kaneko *et al.* 1993).

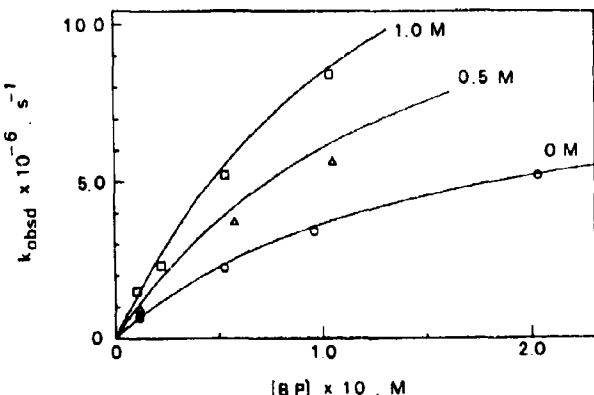
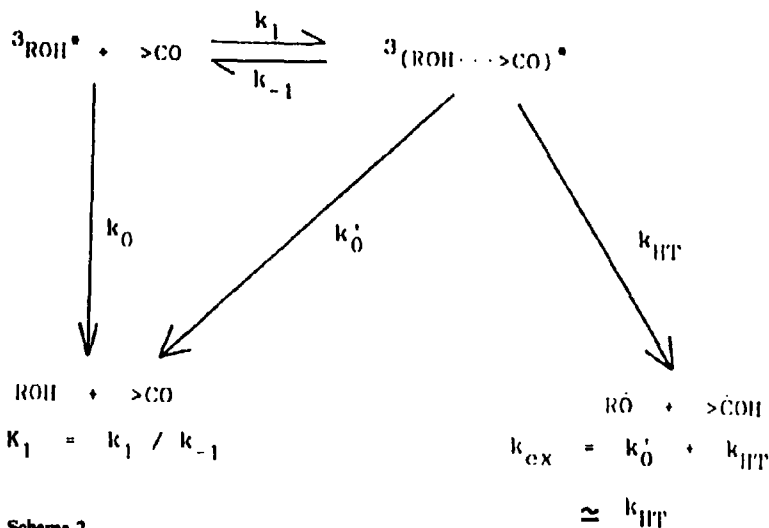


Figure 7. Plots of the decay rate constant (k_{obsd}) of ${}^3\text{ROH}^*$ as a function of [BP] observed at 430 nm after laser pulsing in the ROH (3.0×10^{-3} M)-BP system with $[\text{H}_2\text{SO}_4] = 0$ (○), 0.5 (△) and 1.0 M (×) in acetonitrile-water (4:1 v/v) at 290 K. The solid curves are calculated by (7) (Kaneko *et al.* 1993).

k_{obsd} increases considerably, though not linearly, with an increase of [BP] at each $[\text{H}_2\text{SO}_4]$. These plots imply the formation of the triplet exciplex, ${}^3(\text{ROH} \cdots > \text{CO})^*$, which is considered to have a weak charge-transfer interaction from ROH to BP since no difference in the T-T absorption spectrum between ${}^3\text{ROH}^*$ and ${}^3(\text{ROH} \cdots > \text{CO})^*$ is observed.

In order to explain the above results, a reaction mechanism is suggested for the ROH-BP system without protons in scheme 2, where k_0 , k'_0 and k_{HT} are the decay rate constants for ${}^3\text{ROH}^*$ in the absence of BP, ${}^3(\text{ROH} \cdots > \text{CO})^*$ to ROH plus BP in the ground state and ${}^3(\text{ROH} \cdots > \text{CO})^*$ to the production of $>\dot{\text{C}}\text{OH}$ and $\text{R}\dot{\text{O}}$ (i.e., the HT rate constant), respectively, k_+ and k_- the rate constants for the formation and the dissociation of ${}^3(\text{ROH} \cdots > \text{CO})^*$, respectively. A fast equilibrium between $({}^3\text{ROH}^* + > \text{CO})$ and ${}^3(\text{ROH} \cdots > \text{CO})^*$ with an equilibrium constant (K_1) is supposed. According to scheme 2, the observed rate constant (k_{obsd}) for the decay of



Scheme 2.

³ROH* is formulated as follows.

$$k_{\text{obsd}} = (k_0 + k_{\text{ex}} \cdot K_1 \cdot [\text{BP}]) \cdot (1 + K_1 \cdot [\text{BP}])^{-1}, \quad (3)$$

where $K_1 = k_1/k_{-1}$ and $k_{ex} = k'_0 + k_{HT}$. On the assumption that the value of k_0 is negligible compared to those of the competitive processes, i.e., $k_0 \ll k_{ex}, K_1$, [BP], (3) can be transformed as

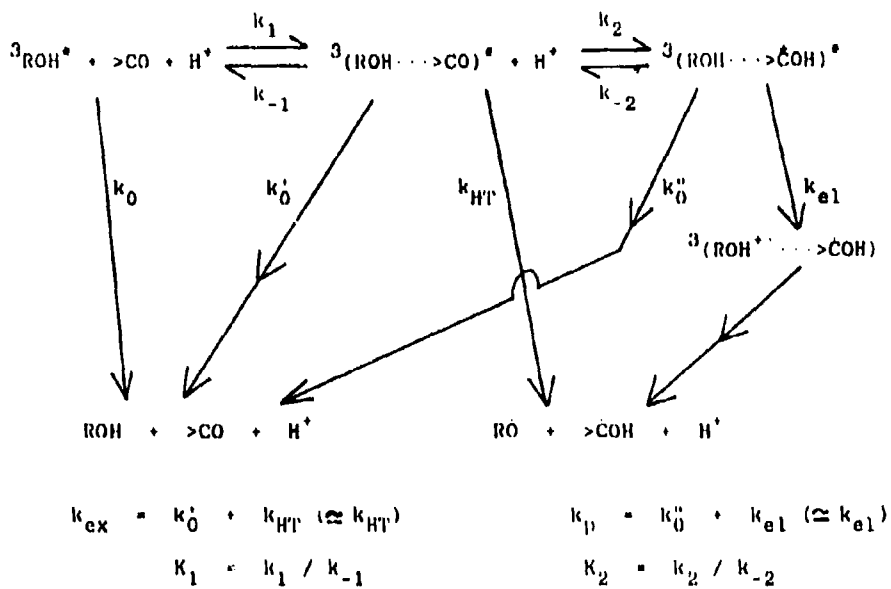
$$k_{\text{obsd}}^{-1} = k_{\text{ex}}^{-1} + (k_{\text{ex}} \cdot K_1)^{-1} \cdot [\text{BP}]^{-1}. \quad (4)$$

By the use of the experimental values of k_{obsd} obtained in acetonitrile–water (4:1 v/v), plots of k_{obsd}^{-1} vs $[\text{BP}]^{-1}$ gave a straight line. From the slope and the intercept of the line, we obtained $k_{\text{ex}} = 9.1 \times 10^6 \text{ s}^{-1}$ and $K_1 = 6.7 \text{ M}^{-1}$. Since $k_0 = 1.4 \times 10^5 \text{ s}^{-1}$ (Shizuka *et al* 1985a) the assumption of $k_0 \ll k_{\text{ex}}, K_1, [\text{BP}]$ is proper in the range $[\text{BP}] > 0.02 \text{ M}$. The solid curve for $[\text{H}_2\text{SO}_4] = 0 \text{ M}$ in figure 7 was calculated from (3) using the determined values of k_{ex} and K_1 in acetonitrile–water (4:1 v/v) at 290 K. Since the experimental values of k_{obsd} are in good agreement with those calculated, the proposed mechanism is appropriate for the HT reaction from ${}^3\text{ROH}^*$ to BP without acid.

For the $\text{ROH} (3.0 \times 10^{-3} \text{ M})-\text{BP} (6.7 \times 10^{-3} \text{ M})$ system without acid, the efficiency of the HT reaction (ϕ_{HT}^0) was 0.73 in acetonitrile-water (4:1 v/v) at 290 K. According to scheme 2, ϕ_{HT}^0 can be expressed as

$$\phi_{HT}^0 = k_{HT} \cdot K_1 \cdot [BP] \cdot (k_0 + k_{HT} \cdot K_1 \cdot [BP])^{-1}. \quad (5)$$

By the use of $k_0 = 1.4 \times 10^5 \text{ s}^{-1}$ (Shizuka *et al* 1985a) and the determined values of k_{ex} and K_1 , we obtained $k_{\text{HT}} = 8.9 \times 10^6 \text{ s}^{-1}$. From the value of k_{HT} , we have estimated the ratio of the HT reaction to the deactivation processes of the triplet exciplex ${}^3(\text{ROH} \cdots > \text{CO})^*$ as $k_{\text{HT}}/k_{\text{ex}} = 0.98$. Therefore, once ${}^3(\text{ROH} \cdots > \text{CO})^*$ is produced, it is fated to undergo the HT reaction very effectively.



Scheme 3.

The mechanism in scheme 2 is extended to the ROH-BP system in the presence of protons as shown in scheme 3 considering the protonated triplet exciplex $^3(\text{ROH} \cdots > \text{COH})^*$. In the presence of protons, $^3(\text{ROH} \cdots > \text{CO})^*$ forms the protonated triplet exciplex $^3(\text{ROH}^+ \cdots > \text{COH})^*$ with an equilibrium constant ($K_2 = k_2 / k_{-2}$). Here, k_2 and k_{-2} are the rate constants for protonation of $^3(\text{ROH} \cdots > \text{CO})^*$ and deprotonation of $^3(\text{ROH} \cdots > \text{COH})^*$, respectively. The protonated triplet exciplex $^3(\text{ROH}^+ \cdots > \text{COH})^*$ decays to $\text{ROH} + > \text{CO} + \text{H}^+$ in the ground state with the rate constant (k'_0) or undergoes the intraexciplex electron transfer reaction with the rate constant (k_{el}) to produce the triplet radical pair $^3(\text{ROH}^+ \cdots > \text{COH})$. The radical pair rapidly transforms $\text{RO} + > \text{COH} + \text{H}^+$. The decay rate constant of $^3(\text{ROH}^+ \cdots > \text{COH})^*$ is denoted as k_p ($= k'_0 + k_{\text{el}}$). As stated above, the triplet exciplex $^3(\text{ROH} \cdots > \text{CO})^*$ has a weak charge transfer structure from ROH to BP. Accordingly, protonation of the benzophenone site ($> \text{CO}$) of $^3(\text{ROH} \cdots > \text{CO})^*$ may occur to produce $^3(\text{ROH}^+ \cdots > \text{COH})^*$. According to scheme 3, k_{obsd} is formulated as

$$k_{\text{obsd}} = (k_0 + k_{\text{ex}} \cdot K_1 \cdot [\text{BP}] + k_p \cdot K_1 \cdot K_2 \cdot [\text{BP}] \cdot [\text{H}^+]) \cdot (1 + K_1 \cdot [\text{BP}] + K_1 \cdot K_2 \cdot [\text{BP}] \cdot [\text{H}^+])^{-1}. \quad (6)$$

Since the activity of H_2SO_4 in acetonitrile-water (4:1 v/v) is unknown, we denote K'_2 and $[\text{H}_2\text{SO}_4]$ for K_2 and $[\text{H}^+]$, respectively. Thus, we obtain

$$k_{\text{obsd}} = (k_0 + k_{\text{ex}} \cdot K_1 \cdot [\text{BP}] + k_p \cdot K_1 \cdot K'_2 \cdot [\text{BP}] \cdot [\text{H}_2\text{SO}_4]) \cdot (1 + K_1 \cdot [\text{BP}] + K_1 \cdot K'_2 \cdot [\text{BP}] \cdot [\text{H}_2\text{SO}_4])^{-1}. \quad (6')$$

If it is assumed that $1 + K_1 \cdot [\text{BP}] \gg K_1 \cdot K'_2 \cdot [\text{BP}] \cdot [\text{H}_2\text{SO}_4]$, (6') is rewritten as

$$\begin{aligned} k_{\text{obsed}} &= (k_0 + k_{\text{ex}} \cdot K_1 \cdot [\text{BP}]) \cdot (1 + K_1 \cdot [\text{BP}])^{-1} \\ &\quad + (k_p \cdot K_1 \cdot K'_2 \cdot [\text{BP}]) \cdot (1 + K_1 \cdot [\text{BP}])^{-1} \cdot [\text{H}_2\text{SO}_4]. \end{aligned} \quad (7)$$

Comparing (2) with (7), we have

$$\begin{aligned} k_t &= (k_p \cdot K_1 \cdot K'_2 \cdot [\text{BP}]) \cdot (1 + K_1 \cdot [\text{BP}])^{-1} \\ &= 4.8 \times 10^6 \text{ s}^{-1}, \end{aligned} \quad (8)$$

and

$$k_d = (k_0 + k_{\text{ex}} \cdot K_1 \cdot [\text{BP}]) \cdot (1 + K_1 \cdot [\text{BP}])^{-1}. \quad (9)$$

When $[\text{BP}] = 0.1 \text{ M}$ and $K_1 = 6.7 \text{ M}^{-1}$ are substituted into (8), we obtain $k_p \cdot K'_2 = 1.2 \times 10^7 \text{ M}^{-1} \text{ s}^{-1}$. We calculated the values of k_d as $3.7 \times 10^6 \text{ s}^{-1}$, with the values obtained of k_0 , k_{ex} , K_1 and $[\text{BP}] = 0.1 \text{ M}$. This value agrees well with the experimental value ($3.5 \times 10^6 \text{ s}^{-1}$) for $[\text{BP}] = 0.1 \text{ M}$ obtained in figure 3 within experimental error (10%).

The solid curves for $[\text{H}_2\text{SO}_4] = 0.5$ and 1.0 M in figure 7 are calculated from (6') by using the determined values of k_0 , k_{ex} , K_1 and $k_p \cdot K'_2$. The calculated values are consistent with experimental ones.

For the ROH ($3.0 \times 10^{-3} \text{ M}$)-BP ($6.7 \times 10^{-3} \text{ M}$) system with $[\text{H}_2\text{SO}_4] = 0.5 \text{ M}$, the total efficiency (ϕ_{HT}^p) of the HT reaction in the presence of protons was obtained as 0.85. According to scheme 3, ϕ_{HT}^p is formulated as

$$\begin{aligned} \phi_{\text{HT}}^p &= (k_{\text{HT}} \cdot K_1 \cdot [\text{BP}] + k_{\text{ex}} \cdot K_1 \cdot K'_2 \cdot [\text{BP}] \cdot [\text{H}_2\text{SO}_4]) \cdot \\ &\quad (k_0 + k_{\text{ex}} \cdot K_1 \cdot [\text{BP}] + k_p \cdot K_1 \cdot K'_2 \cdot [\text{BP}] \cdot [\text{H}_2\text{SO}_4])^{-1}. \end{aligned} \quad (10)$$

When we introduce into (10) the ratio of γ which is defined as $\gamma = k_{\text{ex}}/k_p$, and use the determined values of k_0 , k_{HT} ($\approx k_{\text{ex}}$), $k_p \cdot K'_2$, $[\text{BP}] = 6.7 \times 10^{-3} \text{ M}$ and $[\text{H}_2\text{SO}_4] = 0.5 \text{ M}$, we have $\gamma = 1.1$. Considering the experimental error (10%) in determining ϕ_{HT}^p , k_p can be regarded as k_{ex} (i.e., $k_{\text{ex}} \gg k'_0$). Therefore, ${}^3(\text{ROH})^+ \rightarrow \text{COH}$ produced by the intraexciplex electron transfer reaction dissociates into ROH^+ and COH effectively without the back-electron transfer reaction. The deprotonation of ROH^+ rapidly occurs to produce RO plus H^+ since ROH^+ seems to be very acidic.

2.3 Proton-induced electron transfer reaction from triplet methoxynaphthalene to BP (Yamaji *et al* 1992)

When the ROH of an ROH-BP system is replaced by methoxynaphthalene (ROMe) in the absence of protons, no reaction occurs owing to the triplet methoxynaphthalene (${}^3\text{ROMe}^*$) produced by triplet sensitization of BP. However, in the presence of protons in the ROMe-BP system, proton-assisted photoionization (*p*-ion) reaction of ${}^3\text{ROMe}^*$ produced by triplet sensitization of BP effectively occurs to produce the metoxy naphthalene cation radical ($\text{ROMe}^{+\cdot}$) and COH (Shizuka *et al* 1985b).

Figure 8a shows the transient absorption spectra on a microsecond time scale for the 1 ROMe ($3.0 \times 10^{-3} \text{ M}$)-BP ($6.7 \times 10^{-3} \text{ M}$)- H_2SO_4 (1.0 M) system in acetonitrile-water (4:1 *v/v*) at 290 K. The $T_1 \leftarrow T_1$ absorption of BP at 525 nm disappears within 100 ns after laser pulsing, resulting in the formation of a transient peak at 435 nm.

The transient spectrum at 435 nm was assigned to the $T_1 \leftarrow T_0$ absorption of ${}^1\text{ROMe}$. At 500 ns after laser pulsing, new transient peaks at 380, 545, and 650 nm appear with a decrease of the 435-nm peak for ${}^3\text{ROMe}^*$ with an isosbestic point at 490 nm. The 545-nm transient is known as $>\text{COH}$ (Land 1968). Both transient peaks at 380 and 650 nm are ascribable to the 1-methoxynaphthalene cation radical, ${}^1\text{ROMe}^+$. The reference spectra of ${}^3\text{ROMe}^*$, $>\text{COH}$, and ${}^1\text{ROMe}^+$ are depicted in figure 8b. The molar absorption coefficient of ${}^1\text{ROMe}^+$ can be readily determined from spectral analysis since the rate constant for the formation of ${}^1\text{ROMe}^+$ is the same as that of $>\text{COH}$. The rate constants for the rise of both transient peaks at 545 nm for $>\text{COH}$ and 650 nm for ${}^1\text{ROMe}^+$ were the same as that for the decay, $k_{\text{obsd}} = 8.9 \times 10^5 \text{ s}^{-1}$ observed at 435 nm for ${}^3\text{ROMe}^*$ within 5% experimental error, as shown in figure 8c. In the absence of protons, no photoionization takes place in the ${}^1\text{ROMe-BP}$ system upon 355 nm excitation. These results show that the ionization of ${}^3\text{ROMe}^*$ is assisted by both protons and BP, leading to the production of ${}^1\text{ROMe}^+$ and $>\text{COH}$.

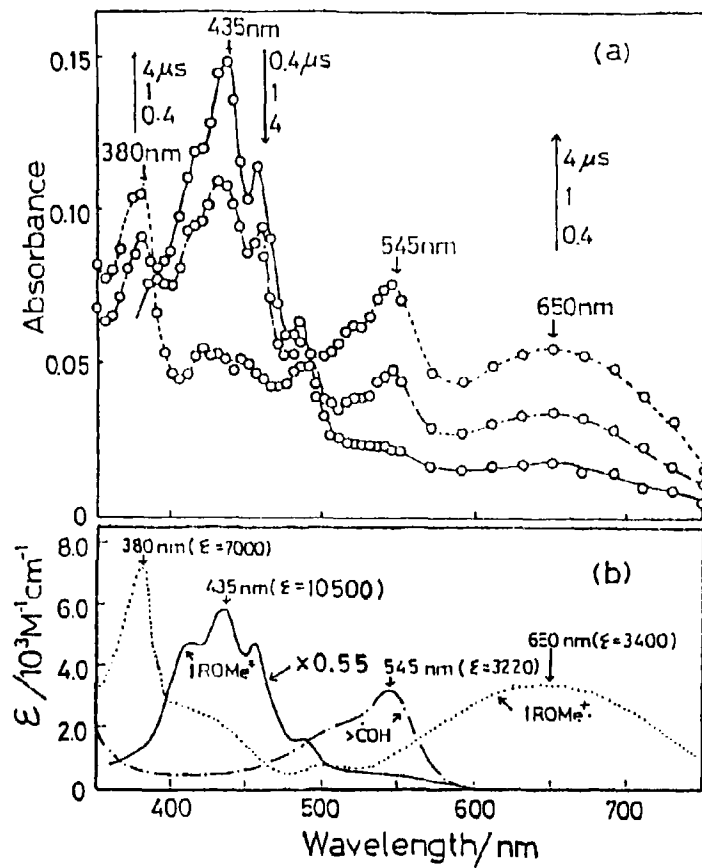


Figure 8. (a) & (b).

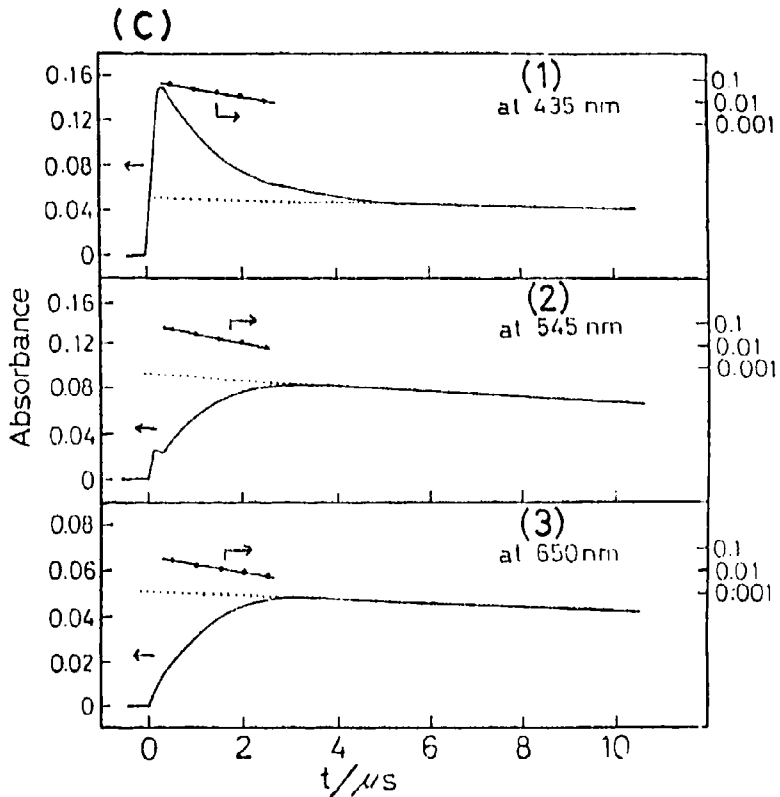


Figure 8. (a) Time-resolved transient absorption spectra in a microsecond time scale for the 1 ROMe ($3.0 \times 10^{-3}\text{ M}$)– BP ($6.7 \times 10^{-3}\text{ M}$)– H_2SO_4 (1.0 M) system in acetonitrile–water (4:1 v/v) observed after 355-nm laser pulsing at 290 K (Yamaji *et al.* 1992). (b) Reference absorption spectra for the transient species (${}^3\text{1 ROMe}^*$, $>\text{COH}$ and 1 ROMe^+) (Yamaji *et al.* 1992). (c) Time traces of the absorbance changes for transient species monitored at 435 nm (${}^3\text{1 ROMe}^*$) (1), at 545 nm ($>\text{COH}$) (2) and at 650 nm (1 ROMe^+) (3) after a 355-nm laser pulse to the 1 ROMe ($3.0 \times 10^{-3}\text{ M}$)– BP ($6.7 \times 10^{-3}\text{ M}$)– H_2SO_4 (1.0 M) system in acetonitrile–water (4:1 v/v) at 290 K (Yamaji *et al.* 1992).

Similar transient spectra of ${}^3\text{2 ROMe}^*$ were obtained in the 2 ROMe ($3.0 \times 10^{-3}\text{ M}$)– BP ($6.7 \times 10^{-3}\text{ M}$) system containing $[\text{H}_2\text{SO}_4] = 1.0\text{ M}$ by laser flash photolysis at 355 nm as shown in figure 9a. The transient absorption at 430 nm for ${}^3\text{2 ROMe}^*$ ($\epsilon = 14,700\text{ M}^{-1}\text{ cm}^{-1}$) (Yamaji *et al.* 1992) produced by triplet sensitization of BP decreases with increase of the new absorption peaks 545 nm for $>\text{COH}$ ($\epsilon = 3220\text{ M}^{-1}\text{ cm}^{-1}$) (Land 1968), 380 and 600 nm ($\epsilon = 6500\text{ M}^{-1}\text{ cm}^{-1}$) for 2 ROMe^+ . The decay rate constant, $k_{\text{obsd}} = 1.0 \times 10^3\text{ s}^{-1}$ at 290 K observed at 430 nm for ${}^3\text{2 ROMe}^*$ was the same as the rise rate at 545 nm for $>\text{COH}$ or 600 nm for 2 ROMe^+ . The reference spectra of the transients are also shown in figure 9b. These observations demonstrate that in the presence of protons, the ionization of ${}^3\text{2 ROMe}^*$ occurs to produce the 2-methoxynaphthalene cation radical, 2 ROMe^+ , and the

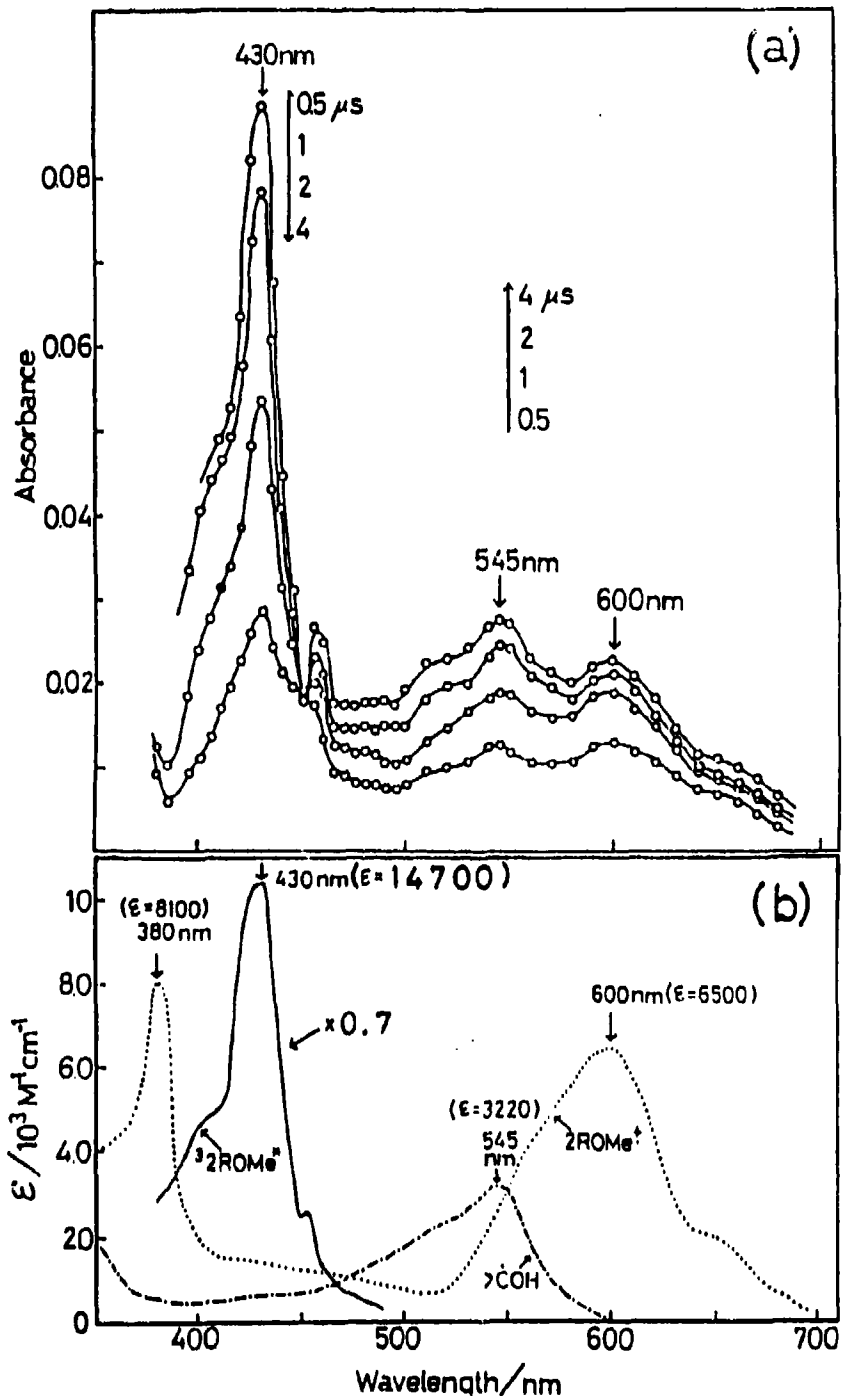
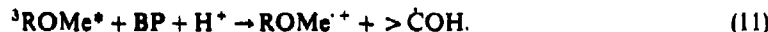


Figure 9. (a) Time-resolved transient absorption spectra in a microsecond time scale for the 2ROMe (3.0×10^{-3} M)-BP (6.7×10^{-3} M)- H_2SO_4 (1.0 M) system in acetonitrile-water (4:1 v/v) observed after 355-nm laser pulsing at 290 K (Yamaji *et al.* 1992). (b) Reference absorption spectra for the transient species (${}^3\text{2ROMe}^*$, $>\text{COH}$ and ${}^2\text{ROMe}^+$) (Yamaji *et al.* 1992).

benzophenone ketyl radical, $>\text{COH}$. No photoionization upon 355 nm excitation was observed for the 2 ROMe-BP system in the absence of protons.

From these results, the ionization of ${}^3\text{ROMe}^*$ can be expressed as



The ionization potentials of 1 ROMe and 2 ROMe are known to be 179.4 and 182.6 kcal mol⁻¹, respectively (Shizuka and Tobita 1982). However, the proton-assisted photoionization of ROMe occurs with lower triplet energies (1 ROMe: 59.7 kcal mol⁻¹, Murov 1973; 2 ROMe: 61.9 kcal mol⁻¹, Yamaji *et al* 1992).

The efficiencies (ϕ_{ion}) for the ionization of ROMe are evaluated as 0.84 for the 1 ROMe (3.0×10^{-3} M)-BP (6.7×10^{-3} M)- H_2SO_4 (1.0 M) system and 0.29 for the 2 ROMe (3.0×10^{-3} M)-BP (6.7×10^{-3} M)- H_2SO_4 (1.0 M) system.

The deactivation processes of ${}^3\text{ROMe}^*$ produced by the triplet sensitization of BP have been studied in the ROMe-BP- H_2SO_4 system under various concentrations of BP and H_2SO_4 at 290 K.

Upon laser excitation at 355 nm in the 1 ROMe (3.0×10^{-3} M)-BP (≤ 0.2 M) systems with $[\text{H}_2\text{SO}_4] = 0$, 0.5 and 1.0 M at 290 K, the decay rate constants, k_{obsd} of ${}^3\text{1 ROMe}^*$ at 435 nm were measured. The k_{obsd} value corresponds to the decay rate constant of ${}^3\text{ROMe}^*$ which is equal to the rise rate constant of $\text{ROMe}^{+\cdot}$ or $>\text{COH}$ as described above. Figure 10 shows the plots of k_{obsd} vs [BP] obtained after laser pulsing to 1 ROMe-BP- H_2SO_4 systems. The value of k_{obsd} increases with increase of [BP] and $[\text{H}_2\text{SO}_4]$ though not linearly. Especially in the system with $[\text{H}_2\text{SO}_4] = 0$, a leveling-off is expected at higher [BP] (≥ 0.2 M). Similar results were obtained in the 2 ROMe (3.0×10^{-3} M)-BP (≤ 0.2 M) systems with $[\text{H}_2\text{SO}_4] = 0$, 0.1 and 1.0 M at 290 K as

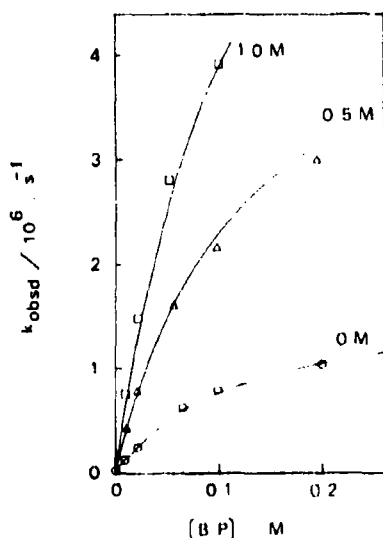


Figure 10. Plots of the decay rate constant (k_{obsd}) of ${}^3\text{1 ROMe}^*$ as a function of [BP] observed at 435 nm after laser pulsing at 355 nm in the 1 ROMe (3.0×10^{-3} M)-BP systems with $[\text{H}_2\text{SO}_4] = 0$ (○), 0.5 (△) and 1.0 (×) in acetonitrile-water (4:1 v/v) at 290 K. The solid lines are calculated using (16) (Yamaji *et al* 1992).

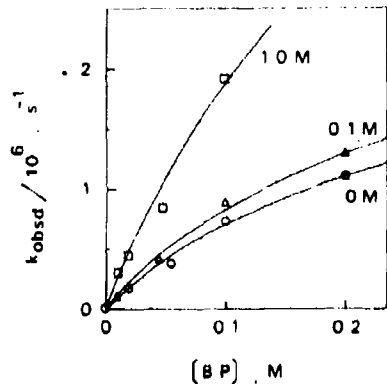
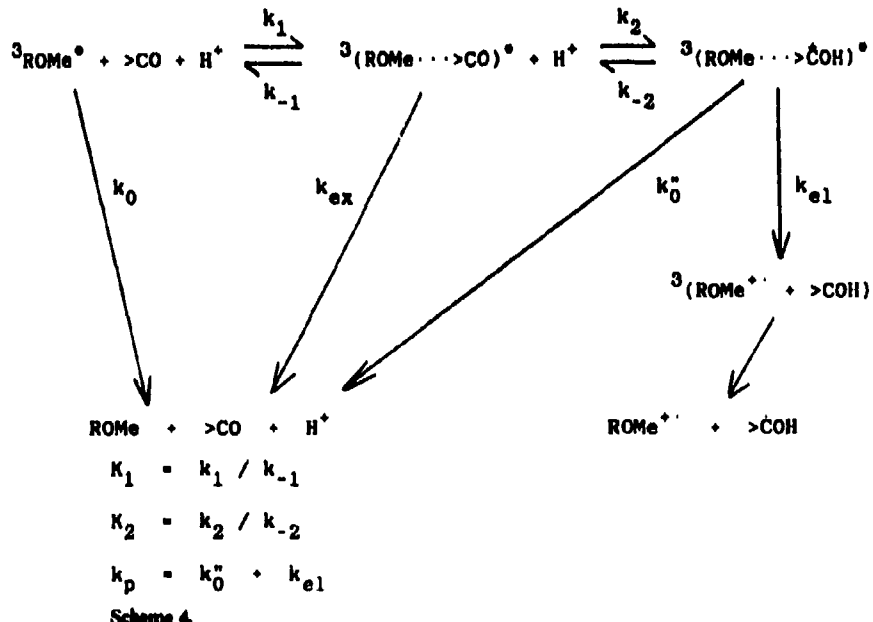


Figure 11. Plots of the decay rate constant (k_{obsd}) of ${}^3\text{ROMe}^*$ as a function of [BP] observed at 430 nm after laser pulsing at 355 nm in the 2 ROMe (3.0×10^{-3} M)-BP systems with $[\text{H}_2\text{SO}_4] = 0$ (○), 0.1 (△) and 1.0 M (×) in acetonitrile-water (4:1 v/v) at 290 K. The solid lines are calculated using (16) (Yamaji *et al.* 1992).



shown in figure 11. Such a nonlinear quenching of ${}^3\text{ROMe}^*$, as shown in figures 10 and 11, cannot be explained by a simple quenching mechanism, and implies the existence of the triplet exciplex, ${}^3(\text{ROMe} \cdots >\text{CO})^*$. In order to account for these experimental results, we propose the proton-assisted photoionization mechanism shown in scheme 4, where ${}^3\text{ROMe}^*$, ${}^3(\text{ROMe} \cdots >\text{CO})^*$ and ${}^3(\text{ROH} \cdots >\dot{\text{C}}\text{OH})^*$ denote the triplet ROMe, the 1:1 triplet exciplex and the protonated triplet exciplex, respectively, k_0 , k_{ex} and k''_0 the decay rate constants of ${}^3\text{ROMe}^*$, ${}^3(\text{ROMe} \cdots >\text{CO})^*$

and ${}^3(\text{ROMe} \cdots > \dot{\text{C}}\text{OH})^*$, respectively, to the ground state, K_1 and K_2 the corresponding equilibrium constants for complex formations, and k_{ex} the rate constant for the intraexciplex electron transfer reaction of ${}^3(\text{ROMe} \cdots > \dot{\text{C}}\text{OH})^*$. Spectral changes in the $T_a \leftarrow T_1$ absorptions among ${}^3\text{ROMe}^*$, ${}^3(\text{ROMe} \cdots > \text{CO})^*$ and ${}^3(\text{ROMe} \cdots > \dot{\text{C}}\text{OH})^*$ were scarcely observed, suggesting that these triplet exciplexes have weak charge-transfer structures. The acid-base reactions of ${}^3\text{BP}^*$ are known to be very fast, their equilibria are established within 20 ns after laser pulsing (Hoshi and Shizuka 1986). In scheme 4, we neglected the proton-induced quenching of ${}^3\text{ROMe}^*$ considering the following reason; as $[\text{BP}]$ approaches 0 M, the values of k_{obsd} at each $[\text{H}_2\text{SO}_4]$ in figures 10 and 11 become close to the same. On the assumption that both equilibria for the formation of ${}^3(\text{ROMe} \cdots > \text{CO})^*$ and ${}^3(\text{ROMe} \cdots > \dot{\text{C}}\text{OH})^*$ are attained within 200 ns, the following equation for the observed decay rate, k_{obsd} observed at 435 nm for ${}^3\text{1 ROMe}^*$ and at 430 nm for ${}^3\text{2 ROMe}^*$ can be derived,

$$k_{\text{obsd}} = (k_0 + K_1 \cdot [\text{BP}] \cdot k_{\text{ex}} + K_1 \cdot K_2 \cdot [\text{BP}] \cdot [\text{H}^+] \cdot k_p) \cdot (1 + K_1 \cdot [\text{BP}] + K_1 \cdot K_2 \cdot [\text{BP}] \cdot [\text{H}^+])^{-1}, \quad (12)$$

where $k_p = k_{\text{ex}} + k_0'$. Since there is no information about the activity of H_2SO_4 in acetonitrile-water (4:1 v/v), we use K_2' and $[\text{H}_2\text{SO}_4]$ instead of K_2 and $[\text{H}^+]$, respectively. Therefore, (12) is reformed as

$$k_{\text{obsd}} = (k_0 + K_1 \cdot [\text{BP}] \cdot k_{\text{ex}} + K_1 \cdot K_2' \cdot [\text{BP}] \cdot [\text{H}_2\text{SO}_4] \cdot k_p) \cdot (1 + K_1 \cdot [\text{BP}] + K_1 \cdot K_2' \cdot [\text{BP}] \cdot [\text{H}_2\text{SO}_4])^{-1}. \quad (12')$$

At first, we consider the simplest case of the 1 ROMe (3.0×10^{-3} M)-BP (≤ 0.2 M) and the 2 ROMe (3.0×10^{-3} M)-BP (≤ 0.2 M) systems in the absence of H_2SO_4 . For these cases, (12') can be simplified as

$$k_{\text{obsd}} = (k_0 + K_1 \cdot [\text{BP}] \cdot k_{\text{ex}}) \cdot (1 + K_1 \cdot [\text{BP}])^{-1}. \quad (13)$$

On the assumption that the value of k_0 is small enough to be negligible, i.e., $k_0 \ll K_1 \cdot [\text{BP}] \cdot k_{\text{ex}}$ in the $[\text{BP}]$ range studied (10^{-2} M $\leq [\text{BP}] \leq 0.2$ M), (13) can be transformed as

$$k_{\text{obsd}}^{-1} = k_{\text{ex}}^{-1} + (K_1 \cdot k_{\text{ex}})^{-1} \cdot [\text{BP}]^{-1}. \quad (14)$$

By the use of the experimental values of k_{obsd} obtained for 1 ROMe and 2 ROMe, plots of k_{obsd}^{-1} vs $[\text{BP}]^{-1}$ gave a straight line. From the slope and the intercept of the line, we obtained the values of k_{ex} and K_1 as $1.6 \times 10^6 \text{ s}^{-1}$ and 10.1 M^{-1} for 1 ROMe, $2.5 \times 10^6 \text{ s}^{-1}$ and 4.0 M^{-1} for 2 ROMe, respectively. Since we experimentally obtained the values of k_0 as $6.8 \times 10^4 \text{ s}^{-1}$ and $5.4 \times 10^4 \text{ s}^{-1}$ for 1 ROMe and 2 ROMe, respectively, upon 266-nm laser excitation to ROMe in acetonitrile-water (4:1 v/v) at 290 K, the assumption of $k_0 \ll K_1 \cdot [\text{BP}] \cdot k_{\text{ex}}$ is proper in the range $[\text{BP}] \geq 10^{-2}$ M. The solid curves for $[\text{H}_2\text{SO}_4] = 0$ M in figures 10 and 11 are, respectively, calculated by (13) and the determined values of k_{ex} and K_1 . The calculated values are in good agreement with those measured in both 1 ROMe-BP and 2 ROMe-BP systems.

For the next step, in order to determine the values of k_p and K_2' for the ROMe-BP system in the presence of protons, we have measured the k_{obsd} values for the ROMe-BP system with various $[\text{H}_2\text{SO}_4]$ in acetonitrile-water (4:1 v/v) at 290 K.

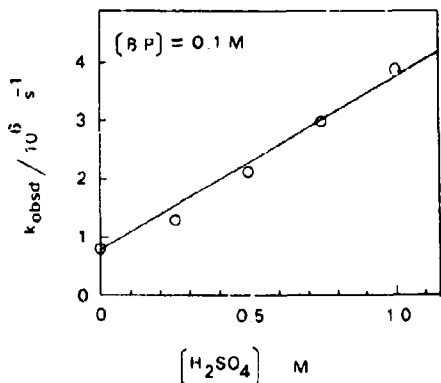


Figure 12. Plots of the decay rate constant (k_{obsd}) of ${}^3\text{I}\text{ROMe}^*$ as a function of $[\text{H}_2\text{SO}_4]$ observed at 435 nm after laser pulsing at 355 nm in the 1 ROMe (3.0×10^{-3} M)-BP (6.7×10^{-3} M)- H_2SO_4 (1.0 M) system in acetonitrile-water (4:1 v/v) at 290 K (Yamaji *et al.* 1992).

Figures 12 and 13 show the plots of k_{obsd} vs. $[\text{H}_2\text{SO}_4]$ observed for 1 ROMe (3.0×10^{-3} M)-BP (1.0×10^{-1} M) and 2 ROMe (3.0×10^{-3} M)-BP (1.0×10^{-1} M) systems, respectively. In both systems, plots show a straight line. Therefore, we can express k_{obsd} as a function of $[\text{H}_2\text{SO}_4]$ as follows

$$k_{\text{obsd}} = k_d + k_s [\text{H}_2\text{SO}_4]. \quad (15)$$

From the intercept and the slope of the line, we obtained the values of k_d and k_s as $8.0 \times 10^5 \text{ s}^{-1}$ and $3.0 \times 10^6 \text{ M}^{-1} \text{ s}^{-1}$ for 1 ROMe, $7.5 \times 10^5 \text{ s}^{-1}$ and $1.2 \times 10^6 \text{ M}^{-1} \text{ s}^{-1}$ for 2 ROMe, respectively. When we assume $1 + K_1 \cdot [\text{BP}] \gg K_1 \cdot K'_2 \cdot [\text{BP}] \cdot [\text{H}_2\text{SO}_4]$ in the range studied ($10^{-2} \text{ M} \leq [\text{BP}] \leq 0.2 \text{ M}$ and $[\text{H}_2\text{SO}_4] \leq 1.0 \text{ M}$), (12') is written as

$$\begin{aligned} k_{\text{obsd}} = & (k_0 + K_1 \cdot [\text{BP}] \cdot k_{\text{ex}}) \cdot (1 + K_1 \cdot [\text{BP}])^{-1} + \\ & K_1 \cdot K'_2 \cdot [\text{BP}] \cdot k_p \cdot (1 + K_1 \cdot [\text{BP}])^{-1} \cdot [\text{H}_2\text{SO}_4]. \end{aligned} \quad (16)$$

Comparing (15) with (16), we have

$$k_d = (k_0 + K_1 \cdot [\text{BP}] \cdot k_{\text{ex}}) \cdot (1 + K_1 \cdot [\text{BP}])^{-1}, \quad (17)$$

$$k_s = K_1 \cdot K'_2 \cdot [\text{BP}] \cdot k_p \cdot (1 + K_1 \cdot [\text{BP}])^{-1}. \quad (18)$$

When we use $[\text{BP}] = 0.1 \text{ M}$ and the determined values of K_1 and k_s in (18), the values of $K'_2 \cdot k_p$ are obtained as $6.4 \times 10^6 \text{ M}^{-1} \text{ s}^{-1}$ and $4.2 \times 10^6 \text{ M}^{-1} \text{ s}^{-1}$ for 1 ROMe-BP and 2 ROMe-BP systems, respectively. According to (17), we calculated the values k_d with the determined values of k_0 , k_{ex} , K_1 and $[\text{BP}] = 0.1 \text{ M}$ to be $8.6 \times 10^5 \text{ s}^{-1}$ and $7.7 \times 10^5 \text{ s}^{-1}$ for 1 ROMe-BP and 2 ROMe-BP systems, respectively, which correspond to those obtained above within 10% experimental error.

The solid curves for the 1 ROMe-BP system with $[\text{H}_2\text{SO}_4] = 0.5$ and 1.0 M in figure 10 and for the 2 ROMe-BP system with $[\text{H}_2\text{SO}_4] = 0.1$ and 1.0 M in figure 11 are calculated by (16) with $[\text{BP}] = 6.7 \times 10^{-3} \text{ M}$ and the determined values of k_0 ,

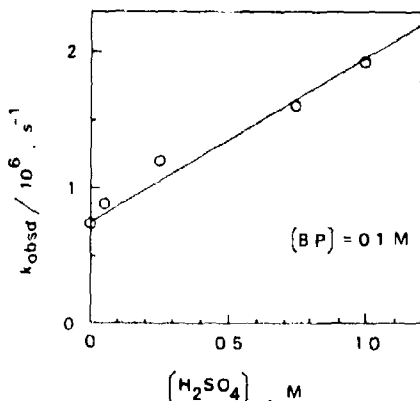


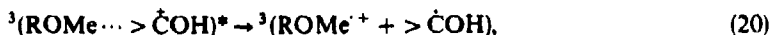
Figure 13. Plots of the decay rate constant (k_{absd}) of ${}^3\text{2ROMe}^*$ as a function of $[\text{H}_2\text{SO}_4]$ observed at 430 nm after laser pulsing at 355 nm in the 2ROMe (3.0×10^{-3} M)-BP (6.7×10^{-3} M)- H_2SO_4 (1.0 M) system in acetonitrile-water (4:1 v/v) at 290 K (Yamaji *et al.* 1992).

k_{ex} , K_1 and $K'_2 \cdot k_p$. The calculated values are consistent with those obtained experimentally within 10% error. This fact suggests that (12') is available for the kinetic analysis of the present system.

According to scheme 4, ϕ_{ion} is formulated as

$$\phi_{\text{ion}} = (K_1 \cdot K'_2 \cdot [\text{BP}] \cdot [\text{H}_2\text{SO}_4] \cdot k_{\text{el}}) \cdot (k_0 + K_1 \cdot [\text{BP}] \cdot k_{\text{ex}} + K_1 \cdot K'_2 \cdot [\text{BP}] \cdot [\text{H}_2\text{SO}_4] \cdot k_p)^{-1}. \quad (19)$$

When we define the ratio, $\gamma = k_{\text{el}}/k_p$ and put into (19) the determined values of k_0 , k_{ex} , K_1 , $K'_2 \cdot k_p$, $[\text{BP}] = 6.7 \times 10^{-3}$ M and $[\text{H}_2\text{SO}_4] = 1.0$ M, we have $\gamma = 1.0$ and 0.60 for 1 ROMe and 2 ROMe systems, respectively. These values indicate that the intraexciplex electron transfer reaction effectively occurs to yield ROMe^+ and $>\text{COH}$. This reason is considered as follows. By the intraexciplex electron transfer in ${}^3(\text{ROMe} \cdots >\text{COH})^*$, the triplet radical pair may be initially produced in a solvent cage according to the spin conservation rule.

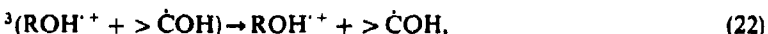
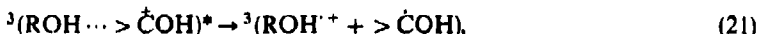


where ${}^3(\text{ROMe}^+ + >\text{COH})$ represents the triplet radical pair in a solvent cage. Hence, the geminate recombination between the triplet radicals is impossible without spin inversion, and the radicals can escape from the solvent cage without the back-electron transfer. In other words, once intraexciplex electron transfer occurs, the triplet radical pair, ${}^3(\text{ROMe}^+ + >\text{COH})$ readily dissociates into ROMe^+ and $>\text{COH}$ with high efficiency.

It should be noted that the pK_a value in the ground state of BP has a large negative value (-5.7) (Bonner and Phillips 1966), and no protonation to BP occurs in the ground state under the experimental conditions. On the other hand, protonation to the triplet exciplex, ${}^3(\text{ROMe} \cdots >\text{CO})^*$ takes place. In ${}^3(\text{ROMe} \cdots >\text{CO})^*$, slight electron migration may occur from ${}^3\text{ROMe}^*$ to BP since ${}^3(\text{ROMe} \cdots >\text{CO})^*$ has

weak charge-transfer character. At higher acid concentrations, the protonated exciplex, ${}^3(\text{ROMe} \cdots > \dot{\text{C}}\text{OH})^*$ is, therefore, produced by protonation to ${}^3(\text{ROMe} \cdots > \text{CO})^*$. The electron affinity of the protonated BP($> \dot{\text{C}}\text{OH}$) in the exciplex may become large compared to that of BP resulting in the intraexciplex electron transfer.

When 1-naphthol (ROH) is used instead of 1 ROMe, the proton-enhanced hydrogen atom transfer reaction occurs via the intracomplex electron transfer reaction as follows.



where ${}^3(\text{ROH}^+ + > \dot{\text{C}}\text{OH})$ represents the triplet radical pair in a solvent cage. The 1-naphthol cation radical (ROH^+) could not be detected experimentally (Kaneko *et al* 1993). The result shows that ROH^+ dissociates very rapidly into the 1-naphthoxy radical, $\text{R}\dot{\text{O}}$ and H^+ , since the pK_a value of ROH^+ is considered to be very negative. Comparing (20) with (21), the present study strongly supports the mechanism on the proton-enhanced hydrogen atom transfer reaction.

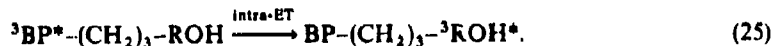
2.4 The intramolecular hydrogen atom transfer reaction of $\text{BP}-(\text{CH}_2)_3-\text{ROH}$ and proton-induced electron transfer of $\text{BP}-(\text{CH}_2)_3-\text{ROMe}$ in the triplet state (Sekiguchi *et al* 1993)

As to the structures of ${}^3(\text{ROH} \cdots > \text{CO})^*$ and ${}^3(\text{ROMe} \cdots > \text{CO})^*$, it is considered to have a sandwich-like structure which is locally excited because the triplet-triplet absorption spectra of ${}^3\text{ROH}^*$ and ${}^3\text{ROMe}^*$ are similar to those of ${}^3(\text{ROH} \cdots > \text{CO})^*$ and ${}^3(\text{ROMe} \cdots > \text{CO})^*$, respectively. However, little information on structures of triplet exciplexes has been obtained though it is of great interest to reveal the conformations of triplet exciplexes for HT and ionization reactions.

One of the most useful methods for the study of chromophore interactions is to link the chromophore with a nematicine chain $-(-\text{CH}_2)_n-$ to restrict their conformation. According to Hirayama's "n = rule" (Hirayama 1965), it is known that the two chromophores linked by $-(-\text{CH}_2)_3-$ must be situated face-to-face upon their interaction. Thus, the problem on the structures of ${}^3(\text{ROH} \cdots > \text{CO})^*$ and ${}^3(\text{ROMe} \cdots > \text{CO})^*$ for HT and ionization will be answered by using the linked molecular systems of hydroxynaphthylpropylbenzophenone ($\text{BP}-(\text{CH}_2)_3-\text{ROH}$) and methoxynaphthylpropylbenzophenone ($\text{BP}-(\text{CH}_2)_3-\text{ROMe}$), respectively.

2.4a The intramolecular hydrogen atom transfer reaction in the triplet state of $\text{BP}-(\text{CH}_2)_3-\text{ROH}$: The intramolecular HT reaction in the triplet state of $\text{BP}-(\text{CH}_2)_3-\text{ROH}$ has been revealed. After 355-nm laser excitation of $\text{BP}-(\text{CH}_2)_3-\text{ROH}$, intramolecular triplet energy transfer (intra-ET) from the triplet benzophenone moiety (${}^3\text{BP}^*$) to the naphthol moiety ($-\text{ROH}$) occurs to produce the triplet naphthol moiety (${}^3\text{ROH}^*$) within 100 ps as well as the case of the naphthalene-BP system (Lamola *et al* 1965). The transient absorption spectra have been observed after a 355-nm laser pulse to $\text{BP}-(\text{CH}_2)_3-\text{ROH}$ (3.0×10^{-3} M) in acetonitrile-water (4:1 v/v) at 295 K. At 25 ns after a pulse, the transient absorption spectrum has the 430-nm band which resembles the triplet-triplet ($T-T$) absorption of 1-naphthol (Shizuka

et al 1985a; Kaneko *et al* 1993; Yamaji *et al* 1993). Therefore, in the present system of BP-(CH₂)₃-ROH, we can conclude that the intra-ET from ³BP*- to -ROH occurs within laser pulse duration, resulting in BP-(CH₂)₃-³ROH*.



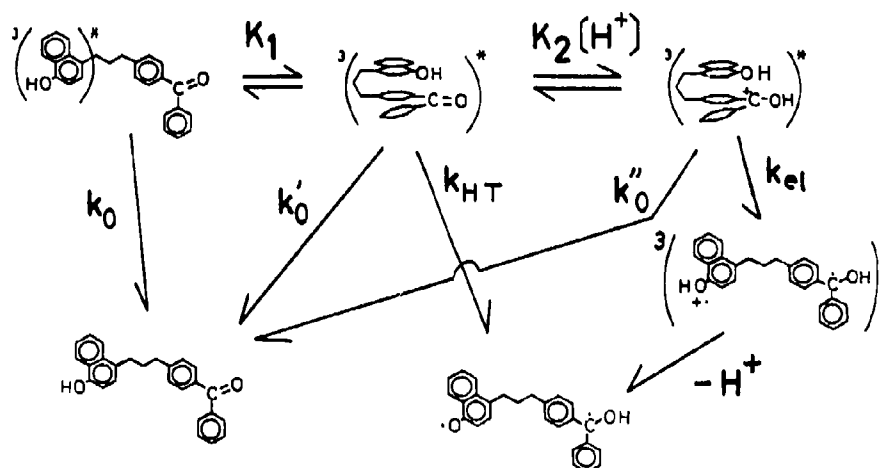
After the intra-ET reaction of BP-(CH₂)₃-ROH, with a lapse of time, the 430-nm band of BP-(CH₂)₃-³ROH* decreases in intensity with an isosbestic point, accompanying an increase in intensities of the 550-nm and the 400-nm bands for the benzo-phenone ketyl radical moiety (>COH-) and the naphthoxy radical moiety (-RO), respectively (Shizuka *et al* 1985a; Kaneko *et al* 1993). The time traces of the transient absorbance changes have been observed at 430 nm for ³ROH* and 550 nm for >COH- after laser pulsing to BP-(CH₂)₃-ROH (3.0×10^{-3} M) in acetonitrile-water (4:1 v/v) at 295 K. The first-order rate constant (k_{obsd}) for the decay at 430 nm is almost identical with that for the rise at 550 nm ($9.8 \times 10^6 \text{ s}^{-1}$) within experimental error (10%), indicating that the HT reaction occurs from ³ROH* to BP-. Since the k_{obsd} value ($9.8 \times 10^6 \text{ s}^{-1}$) is independent of [BP-(CH₂)₃-ROH] ($\leq 6.0 \times 10^{-3}$ M), it is concluded that the HT reaction is an intramolecular one (intra-HT) of BP-(CH₂)₃-³ROH* to produce >COH-(CH₂)₃-RO with rate constant ($9.8 \times 10^6 \text{ s}^{-1}$) in the range of [BP-(CH₂)₃-ROH] studied. The efficiency (ϕ_{HT}) for the intra-HT reaction is 1.0 for BP-(CH₂)₃-ROH in acetonitrile-water (4:1 v/v). This ϕ_{HT} value implies that the intra-HT reaction of BP-(CH₂)₃-ROH occurs very efficiently.

The plots of the rate constant (k_{obsd}) for intra-HT vs $[\text{H}_2\text{SO}_4]$ (≤ 0.5 M) have been obtained after a laser pulse to BP-(CH₂)₃-ROH (3.0×10^{-3} M) in acetonitrile-water (4:1 v/v). The k_{obsd} value increases linearly with increase of $[\text{H}_2\text{SO}_4]$. Therefore, k_{obsd} is also represented as

$$k_{\text{obsd}} = k_4 + k_5 \cdot [\text{H}_2\text{SO}_4]. \quad (26)$$

From the slope and the intercept of the line, we have $k_4 = 3.3 \times 10^6 \text{ M}^{-1} \text{ s}^{-1}$ and $k_5 = 9.8 \times 10^5 \text{ s}^{-1}$. On the other hand, the efficiency of intra-HT (ϕ_{HT}) was 1.0 in the range of $[\text{H}_2\text{SO}_4]$ (≤ 0.5 M) studied as mentioned above. As a result, for the proton effect on intra-HT of BP-(CH₂)₃-ROH, only the rate constant for intra-HT is enhanced by protons.

In order to account for the results obtained on intra-HT of BP-(CH₂)₃-ROH, we propose the intra-HT mechanism as shown in scheme 5 analogous to that for inter-HT of the ROH-BP system (Kaneko *et al* 1993), where ³(BP-(CH₂)₃-ROH)*, ³(>COH-(CH₂)₃-ROH)* and ³(>COH-(CH₂)₃-ROH⁺) denote the intramolecular triplet exciplex with a sandwich-like structure, the protonated intramolecular triplet exciplex and the triplet radical pair produced by the intraexciplex electron transfer (intra-el), respectively. k_0 , k'_0 and k''_0 are the corresponding decay rate constants of BP-(CH₂)₃-³ROH*, ³(BP-(CH₂)₃-ROH)* and ³(>COH-(CH₂)₃-ROH)* to the ground BP-(CH₂)₃-ROH, respectively, k_{HT} and k_{el} the rate constants for intra-HT of ³(BP-(CH₂)₃-ROH)* to >COH-(CH₂)₃-RO and intra-el of ³(>COH-(CH₂)₃-ROH)* to ³(>COH-(CH₂)₃-ROH⁺), respectively, and K_1 and K_2 the corresponding equilibrium constants of formation of the triplet exciplex and the protonation of the triplet exciplex, respectively.

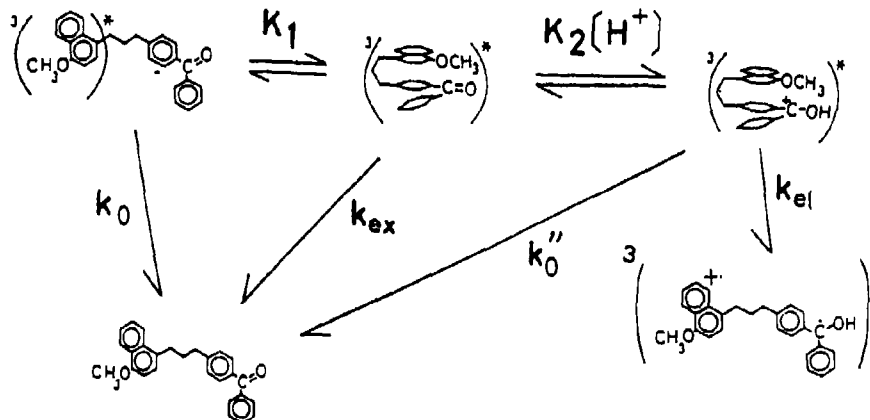


Scheme 5.

2.4b The intramolecular proton-induced electron transfer in the triplet state of $\text{BP}-(\text{CH}_2)_3-\text{ROMe}$: The intramolecular $p\text{-}\epsilon\text{T}$ reaction of $\text{BP}-(\text{CH}_2)_3-\text{ROMe}$ in the triplet state is as follows: After 355-nm laser excitation of $\text{BP}-(\text{CH}_2)_3-\text{ROMe}$, the intra-ET from ${}^3\text{BP}^*$ to the methoxynaphthalene moiety ($-\text{ROMe}$) occurs to produce the triplet methoxynaphthalene moiety ($-{}^3\text{ROMe}^*$) as well as in the case of $\text{BP}-(\text{CH}_2)_3-\text{ROH}$. The transient absorption spectra have been observed after 355-nm laser pulsing to $\text{BP}-(\text{CH}_2)_3-\text{ROMe}$ (3.0×10^{-3} M) in acetonitrile–water (4:1 v/v) at 295 K with $[\text{H}_2\text{SO}_4] = 0, 0.005$ and 0.5 M. The transient spectrum observed at 400 ns after laser pulsing in $\text{BP}-(\text{CH}_2)_3-\text{ROMe}$ without H_2SO_4 shows the 435-nm band which resembles $T-T$ absorption of 1-ROMe (Shizuka *et al.* 1985b; Yamaji *et al.* 1992). The 435-nm band decays with the first order rate constant ($1.8 \times 10^5 \text{ s}^{-1}$) in the absence of protons. However, in the presence of protons, with lapse of time, the 550-nm band for $>\text{COH}^-$ and the 380- and 650-nm bands for the methoxynaphthalene cation radical moiety ($-\text{ROMe}^+$) (Shizuka *et al.* 1985b; Yamaji *et al.* 1992) increase in intensity with isosbestic points, while the 435-nm band decreases.

The time traces of the transient absorbance changes have been observed at 435 nm for $-{}^3\text{ROMe}^*$, 550 nm for $>\text{COH}^-$ and 650 nm for $-\text{ROMe}^+$ after laser pulsing to $\text{BP}-(\text{CH}_2)_3-\text{ROMe}$ (3.0×10^{-3} M) in acetonitrile–water (4:1 v/v) with $[\text{H}_2\text{SO}_4] = 0.5$ M at 295 K. The first-order rate constant ($k_{\text{obs}} = 6.8 \times 10^6 \text{ s}^{-1}$) for the decay at 435 nm was the same as those for the rises of $>\text{COH}^-$ at 550 nm and $-\text{ROMe}^+$ at 650 nm within experimental error (10%), and independent of $[\text{BP}-(\text{CH}_2)_3-\text{ROMe}] (\leq 6.0 \times 10^{-3}$ M) in acetonitrile–water (4:1 v/v) with $[\text{H}_2\text{SO}_4] = 0.5$ M at 295 K. From the above results, the ionization of $\text{BP}-(\text{CH}_2)_3-{}^3\text{ROMe}^*$ is concluded to occur only in the presence of protons to produce $>\text{COH}-(\text{CH}_2)_3-\text{ROMe}^+$ by intra-el.

The efficiencies (ϕ_{ion}) of the ionization for $>\text{COH}-(\text{CH}_2)_3-\text{ROMe}^+$ are 0.3 and 1.0 for $\text{BP}-(\text{CH}_2)_3-\text{ROMe}$ in acetonitrile–water (4:1 v/v) with $[\text{H}_2\text{SO}_4] = 0.005$ and 0.5 M, respectively. These values of ϕ_{ion} show that protons promote the ionization efficiency for $\text{BP}-(\text{CH}_2)_3-\text{ROMe}$ as well as for intermolecular ROMe–BP systems (Yamaji *et al.* 1992).



Scheme 6.

We also investigated the proton effect on the rate constant (k_{obsd}) for intra-*p*-ion of $\text{BP}-(\text{CH}_2)_3-\text{ROMe}$. The plots of k_{obsd} vs $[\text{H}_2\text{SO}_4]$ ($\leq 1.0 \text{ M}$) have been obtained after laser pulsing of $\text{BP}-(\text{CH}_2)_3-\text{ROMe}$ ($3.0 \times 10^{-3} \text{ M}$) in acetonitrile–water (4:1 *v/v*). The k_{obsd} value increases linearly, proportional to $[\text{H}_2\text{SO}_4]$. Therefore, k_{obsd} is reexpressed with the use of (26). From the slope and the intercept of the line, we have $k_s = 1.6 \times 10^7 \text{ M}^{-1} \text{s}^{-1}$ and $k_d = 1.8 \times 10^5 \text{ s}^{-1}$ for the intra-*p*-ion of $\text{BP}-(\text{CH}_2)_3-\text{ROMe}$.

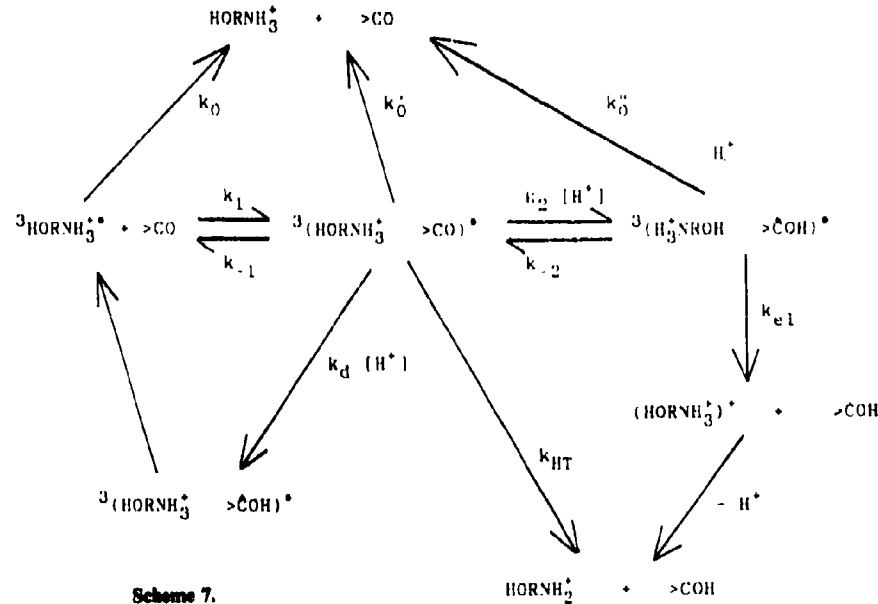
The intra-*p*-ion mechanism for $\text{BP}-(\text{CH}_2)_3-\text{ROMe}$ is proposed as shown in scheme 6, referring to those of the ROMe-BP systems (Yamaji *et al.* 1992) and intra-HT, where ${}^3(\text{BP}-(\text{CH}_2)_3-\text{ROMe})^*$, ${}^3(>\text{COH}-(\text{CH}_2)_3-\text{ROMe})^*$ and ${}^3(>\text{COH}-(\text{CH}_2)_3-\text{ROMe}^{\cdot+})$ denote the corresponding intramolecular triplet exciplex with a sandwich-like structure, the protonated intramolecular triplet exciplex and the intramolecular triplet radical pair produced by intra-el, respectively. k_0 , k_{ss} and k''_0 are the decay rate constants of $\text{BP}-(\text{CH}_2)_3-\text{ROMe}^*$, ${}^3(\text{BP}-(\text{CH}_2)_3-\text{ROMe})^*$ and ${}^3(>\text{COH}-(\text{CH}_2)_3-\text{ROMe})^*$ to the ground $\text{BP}-(\text{CH}_2)_3-\text{ROMe}$, respectively, k_{el} the rate constant for intra-el of ${}^3(>\text{COH}-(\text{CH}_2)_3-\text{ROMe})^*$ to ${}^3(>\text{COH}-(\text{CH}_2)_3-\text{ROMe}^{\cdot+})$, and K_1 and K_2 the corresponding equilibrium constants for formation of the triplet exciplex and protonation of the triplet exciplex, respectively.

2.4c Conformation of triplet exciplexes: As mentioned above, it has been observed that intra-HT and intra-*p*-ion of $\text{BP}-(\text{CH}_2)_3-\text{ROH}$ and $\text{BP}-(\text{CH}_2)_3-\text{ROMe}$ take place as well as the intermolecular ones of the ROH-BP and ROMe-BP systems, respectively. For both intermolecular and intramolecular reactions, the mechanisms can be explained considering the triplet exciplex and the protonated triplet exciplex. When the chromophores are linked with $-(\text{CH}_2)_3-$, it is enabled to take a stacked configuration of chromophores, which has a weak charge-transfer interaction. Therefore, it can be concluded that the structures of the triplet exciplex and the protonated triplet exciplex for intra-HT and intra-*p*-ion are sandwich-like as illustrated in schemes 5 and 6, respectively.

2.5 The hydrogen-atom transfer reaction of triplet hydroxynaphthylammonium ion to benzophenone

The HT reaction of triplet naphthalene derivative with both the groups, $-\text{NH}_3^+$ and $-\text{OH}$, of the hydroxynaphthylammonium ion (HORNH_3^+) has been investigated in order to elucidate the reactivity of the substituent group for HT and its mechanism.

The transient absorption spectra have been observed after a laser pulse at 355 nm in the HORNH_3^+ (8.0×10^{-3} M)-BP (1.2×10^{-3} M) systems with $[\text{H}_2\text{SO}_4] = 0.015$ M and 0.5 M, respectively, in MeOH-water (9:1 v/v) at 290 K. While the 430-nm band for triplet HORNH_3^+ (${}^3\text{HORNH}_3^+*$) decreases with isosbestic points at 490 and 610 nm, new transient absorption bands appear at 455, 545 and 800 nm with lapse of time. The 545-nm band is known to be $>\text{COH}$ with its molar absorption coefficient $\epsilon = 3220 \text{ M}^{-1} \text{ cm}^{-1}$ at 545 nm (Land 1968). The transient absorption bands at 455 and 800 nm are ascribed to the 5-hydroxy-1-naphthylamine cation radical (HORNH_2^+) since they are similar to the absorption spectrum of HORNH_2^+ obtained after γ -radiolysis of HORNH_2 in PVC film (unpublished data). The change from the absorption spectrum of triplet HORNH_3^+ , ${}^3(\text{HORNH}_3^+*)$ to that of the hydroxynaphthylamine cation radical (HORNH_2^+) demonstrates that the $-\text{NH}_3^+$ group is more reactive for HT of the HORNH_3^+ -BP system than the $-\text{OH}$ group. The rate constant for HT increases with an increase of [BP] showing a leveling-off at higher [BP] while it decreases with increase of acid concentration. However, at higher acid concentrations, the rate constant shows a leveling off. Therefore, it is impossible to explain the above experimental results by the simple mechanism for the RNH_3^+ -BP system (Kohno *et al* 1991). The hybrid mechanism from those for the RNH_3^+ -BP (Kohno *et al* 1991) and ROH-BP (Kaneko *et al* 1993) systems has been proposed for the HT reaction of the HORNH_3^+ -BP system as shown in scheme 7. It has been concluded that the more protic hydrogen atom is the more reactive in HT.



Scheme 7.

3. Conclusion

After 355-nm laser pulsing in the naphthalene derivative (RNH_3^+ , ROH, ROMe and HORNH_3^+)-BP systems, the ET from ${}^3\text{BP}^*$ occurs to naphthalene derivatives in the nanosecond time scale.

It has been shown that the HT and $p-eT$ reactions from triplet naphthalene derivatives (${}^3\text{RNH}_3^+$, ${}^3\text{ROH}^*$, ${}^3\text{ROMe}^*$ and ${}^3\text{HORNH}_3^+{}^*$) take place to BP via triplet exciplexes, intermolecularly and intramolecularly, on a microsecond time scale. It has been shown that the triplet exciplexes have a sandwich-like structure with weak CT character. There are proton effects on the above HT and $p-eT$ reactions originating from the protonated triplet exciplexes.

Acknowledgement

This work was supported partially by a Scientific Research Grant-in-Aid from the Ministry of Education, Science and Culture of Japan.

References

- Anderson R W Jr, Hochstrasser R M, Lutz H and Scott G W 1974 *J. Chem. Phys.* **61** 2500
Arimitsu S, Masuhara H and Tsubomura H 1975 *J. Phys. Chem.* **79** 1255
Beens H, Grellmann K H, Gurr M and Weller A 1965 *Discuss. Faraday Soc.* **98** 183
Bonner T G and Phillips J 1966 *J. Chem. Soc. B* 650
Cohen S G, Parola A and Parsons G H Jr 1973 *Chem. Rev.* **73** 141
Cox R A and Yates K 1978 *J. Am. Chem. Soc.* **100** 3861
Dalton J C and Turro N 1970 *J. Annu. Rev. Phys. Chem.* **21** 499
Damshen D E, Merritt C D, Perry D L, Scott G W and Talley L D 1978 *J. Phys. Chem.* **82** 2268
Devadoss C and Fessenden R W 1990 *J. Phys. Chem.* **94** 4540
Devadoss C and Fessenden R W 1991 *J. Phys. Chem.* **95** 7253
El-Sayed M A 1962 *J. Chem. Phys.* **36** 573
El-Sayed M A 1963 *J. Chem. Phys.* **38** 2834
El-Sayed M A 1964 *J. Chem. Phys.* **41** 24
Formoshinho S J 1976 *J. Chem. Soc., Faraday Trans. 2* **72** 1913
Formoshinho S J 1978 *J. Chem. Soc., Faraday Trans. 2* **74** 1978
Förster Th 1950 *Z. Elektrochem. Angew. Phys. Chem.* **54** 42, 531
Hirayama F 1965 *J. Phys. Chem.* **69** 3163
Hoshino M and Shizuka H 1986 *Bull. Chem. Soc. Jpn.* **61** 2711
Hoshino M and Shizuka H 1987 *J. Phys. Chem.* **91** 714
Hoshino M and Shizuka H 1988 In *Photo-induced electron transfer* (eds) M A Fox and N Chanon (Amsterdam: Elsevier) part C, p. 313
Hoshino M and Shizuka H 1993 In *New aspects of radiation curing in polymer science and technology* (eds) J P Fouassier and J F Rabek (London: Elsevier) Vol. 2 (in press)
Hoshino M, Seki H, Kaneko M, Kinoshita K and Shizuka H 1986 *Chem. Phys. Lett.* **132** 209
Ireland J F and Wyatt P A H 1976 *Adv. Phys. Org. Chem.* **12** 131, and a number of references therein
Kaneko S, Yamani M, Hoshino M and Shizuka H 1993 *J. Phys. Chem.* (submitted)
Klopffer W 1977 *Adv. Photochem.* **10** 311
Kohno S, Hoshino M and Shizuka H 1991 *J. Phys. Chem.* **86** 1297
Lamola A A, Leermakers P A, Byers G W and Hammond G S 1965 *J. Am. Chem. Soc.* **87** 2322
Land E J 1968 *Proc. R. Soc. London A* **303** 457
Manring L E and Peters K S 1983 *J. Am. Chem. Soc.* **105** 5708
Miyasaka H, Morita K, Kamada K, Nagata T, Kiri M and Mataga N 1991 *Bull. Chem. Soc. Jpn.* **64** 3229

- Murov S L 1973 *Handbook of photochemistry* (New York: Marcel Dekker)
Okada T, Karaki T and Mataga N 1982 *J. Am. Chem. Soc.* **104** 7191
Okada T, Tashita N and Mataga N 1980 *Chem. Phys. Lett.* **75** 220
Peters K S, Freilich S C and Shafer C G 1980 *J. Am. Chem. Soc.* **102** 5701
Peters K S, Pang E and Rudzki J 1982 *J. Am. Chem. Soc.* **104** 5535
Scalano J C 1973/1974 *J. Photochem.* **2** 81
Schulman S G 1976 In *Modern fluorescence spectroscopy* (ed.) E L Wehrly (New York: Plenum) vol. 2
Schulman S G 1977 In *Fluorescence and phosphorescence spectroscopy* (Oxford: Pergamon)
Sekiguchi T, Yamaji M, Tatemitsu H, Sakata Y and Shizuka H 1993 *J. Phys. Chem.* **97** 7003
Shizuka H 1985 *Acc. Chem. Res.* **18** 141, and references cited therein
Shizuka H and Fukushima M 1983 *Chem. Phys. Lett.* **101** 598
Shizuka H, Hagiwara H and Fukushima M 1985a *J. Am. Chem. Soc.* **107** 7816
Shizuka H, Hagiwara H, Satoh H and Fukushima M 1985b *J. Chem. Soc., Chem. Commun.* 1454
Shizuka H, Kameta K and Shinozaki T 1985c *J. Am. Chem. Soc.* **107** 3956
Shizuka H, Ogiwara T and Kimura E 1985d *J. Phys. Chem.* **89** 4302
Shizuka H and Serizawa M 1986 *J. Phys. Chem.* **90** 4573
Shizuka H, Serizawa M, Kobayashi H, Kameta K, Sugiyama H, Matsuura T and Saito I 1988a *J. Am. Chem. Soc.* **110** 1726
Shizuka H, Serizawa M, Okazaki K and Shioya S 1986 *J. Phys. Chem.* **90** 4694
Shizuka H, Serizawa M, Shimo T, Saito I and Matsuura T 1988b *J. Am. Chem. Soc.* **110** 1930
Shizuka H and Tobita S 1982 *J. Am. Chem. Soc.* **104** 6919, and references cited therein
Simon J D and Peters K S 1981 *J. Am. Chem. Soc.* **103** 6403
Simon J D and Peters K S 1982 *J. Am. Chem. Soc.* **104** 6542
Simon J D and Peters K S 1984 *Acc. Chem. Res.* **17** 277
Tsutsumi K and Shizuka H 1977 *Chem. Phys. Lett.* **52** 485
Tsutsumi K and Shizuka H 1978 *Z. Phys. Chem. (Wiesbaden)* **111** 129
Turro N J 1978 *Modern molecular photochemistry* (Menlo Park, CA: Benjamin/Cummings)
Turro N J, Dalton J C, Dawes K, Farrington G, Hautala R, Morton D, Niemczyk M and Schore N 1972
Acc. Chem. Res. **5** 92
Van der Donckt E 1970 *Prog. React. Kinet.* **5** 273
Wagner P J 1971 *Acc. Chem. Res.* **4** 168
Wagner P J 1976 *Top. Curr. Chem.* **66** 1
Wagner P J and Hammond G S 1968 *Adv. Photochem.* **5** 21
Wagner P J, Truman R J, Puchalski A E and Wake R 1986 *J. Am. Chem. Soc.* **108** 7727
Wehrly E L and Rogers L B 1966 In *Fluorescence and phosphorescence analyses* (ed.) D M Hercules (New York: Wiley-Interscience) p. 125
Weller A 1952 *Ber. Bunsenges. Phys. Chem.* **56** 662
Weller A 1956 *Ber. Bunsenges. Phys. Chem.* **60** 1144
Weller A 1961 *Proc. React. Kinet.* **1** 189
Yamaji M, Sekiguchi T, Hoshino M and Shizuka H 1992 *J. Phys. Chem.* **96** 9353
Yamaji M, Tanaka T and Shizuka H 1993 *Chem. Phys. Lett.* (in press)

Resonant two-photon ionization processes of van der Waals adducts: Spectroscopy and reactivity of styrenes clustered with various molecules

A GIARDINI-GUIDONI^a, A MELE^a, S PICCIRILLO^a, M CORENO^a,
and M SNELS^{b*}

^a Università degli Studi di Roma "La Sapienza", Dipartimento di Chimica, P.le A Moro,
5, I-00185 Rome, Italy

^b Istituto Materiali Speciali, CNR Tito Scalo (Pz), Italy

Abstract. Research on the formation and properties of clusters of aromatic molecules bonded to numerous solvents is rapidly expanding. Recently much attention has been paid to these adduct species with the objective of clarifying nucleation phenomena. Photophysical and photochemical studies of these clusters give information on solvent effects, intraccluster reactions and charge-transfer processes. Model calculations of potential surfaces of vdW adducts have provided knowledge of the intraccluster binding energy and vdW vibrational modes in a few systems. Here, data are reported on resonant two-photon ionization R2PI mass spectra and on spectroscopic shifts of styrenes clustered with various atoms and molecules.

Keywords. Two-photon ionization; van der Waals adducts; styrene clusters.

1. Introduction

The importance of van der Waals (vdW) interactions in the study of aromatic systems bonded to solvent molecules has been amply recognized (Bernstein 1990; Even *et al* 1990). Studies on clusters of these compounds by reactive and unreactive moieties are particularly valuable in understanding condensation and nucleation phenomena, energetics of inter- and intramolecular modes and finally kinetics of reactive processes (Brutschy 1990; Keese and Castleman 1990).

Production of these adducts can be achieved by adiabatic expansion in vacuum through a nozzle of solute–solvent mixtures. By varying the pressure and temperature at the nozzle, it is possible to change the size distribution of clusters formed in the expansion. The clusters are usually analysed by laser-induced fluorescence (LIF), IR spectroscopy or mass spectrometry. Resonance enhanced two-photon ionization (R2PI) combined with time-of-flight (TOF) detection of the adducts has been demonstrated to be a powerful technique suitable for both spectroscopy and reactivity studies (Breen *et al* 1989; Brutschy 1990).

*For correspondence

Spectroscopic studies allow us to probe the solvent environment and how it affects the solute electronic structure. In particular, the evolution of the solute absorption spectrum, as a function of the increasing number of solvent molecules, can be related to a coalescence process leading to the condensed phase. Another important aspect is the identification through mass spectrometric analysis of the solute-solvent intra-cluster reaction which can take place within a very short time after ionization.

In this paper, results are reported on the spectroscopy and reaction dynamics of styrene (STY) and 4-fluorostyrene (4FSTY) clustered with noble gases and several substances. These aromatic molecules are sensitive probes of the molecular interaction with solvent media. Their choice has been dictated also by the fact that the first excited state S_1 is for both approximately half way with respect to the ionization continuum. The cluster ions produced in the R2PI process have little excess energy and it may be assumed that fragmentation plays a minor role. A comparison between the spectroscopy and the reactivity of these two systems, with respect to the solvent molecules, is reported here.

2. Experimental methods

The experimental apparatus used to produce supersonic molecular beams of clusters, shown in figure 1 together with the ionization laser and TOF mass spectrometer, has been already described (Giardini Guidoni *et al* 1993) and will be only briefly summarized here.

The system consists of two independently pumped vacuum chambers, separated by a skimmer of 1 mm inner diameter. The clusters are formed in a supersonic expansion of He, seeded with the aromatic system, either pure or mixed with solvent molecules in a suitable ratio. The stagnation pressure can be varied between 0.5 and

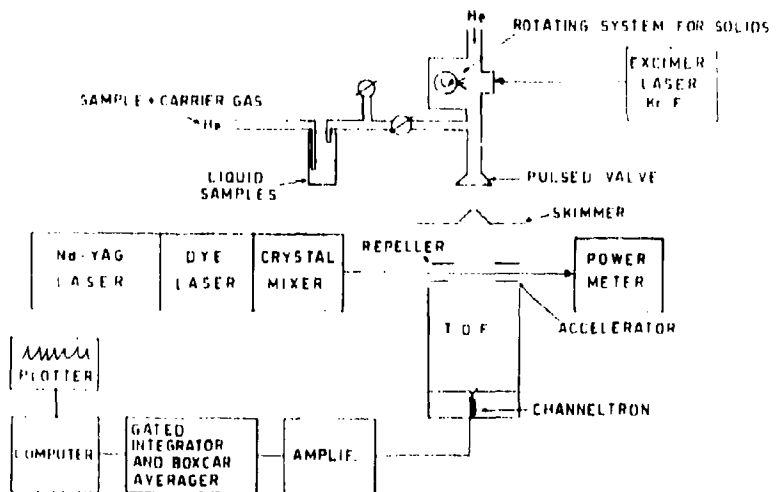


Figure 1. Schematic of the experimental apparatus for the production and detection of clusters.

4 bar. The expansion in the first chamber is obtained through a pulsed valve (General Valve) with a nozzle of 400 μm inner diameter and aperture time up to 600 μs . The repetition rate is 10 Hz. The pressure in the first chamber is kept around 10^{-5} torr. The skimmed beam is crossed perpendicularly by the ionization laser 30 cm downstream between the first two acceleration plates of a Wiley-McLaren TOF mass spectrometer. The resolving power of the TOF is 1 mass unit at m/e 200. The clusters are ionized by one colour R2PI process by using a frequency doubled dye laser pumped by an Nd: YAG (Quantel model 710). The relative intensity of the ion signal depends on the expansion conditions: stagnation pressure, time lag between the dye laser pulse relative to the gas pulse and laser wavelength.

The compounds studied are STY and 4FSTY, pure or mixed with Ar, CCl_4 , NH_3 , $\text{C}_2\text{H}_5\text{NH}_2$ (MEA) and $(\text{C}_2\text{H}_5)_2\text{NH}$ (DEA). STY and 4FSTY are used as supplied by Aldrich Chemicals without any further purification.

3. Spectroscopy

Spectroscopy of STY and 4FSTY, either pure or bound to reactive or non-reactive systems, deals mainly with 0_0^0 transitions from the ground state S_0 to the lowest singlet excited state S_1 . The spectral shift near the vibronic origin of this $\pi \rightarrow \pi^*$ transition occurs in various chromophore solvent adducts as largely reported in the literature (Bernstein 1990, and references therein). The spectral shift of a given electronic transition with respect to the isolated molecule is a measure of the relative energy difference between the lower and upper electronic states induced by aggregation. The magnitude and direction of the electronic shift is strongly related to the nature of the interaction between the chromophore which is the solute and the solvent. Of course, a red shift indicates a smaller energy difference between the ground and the excited states in the adduct, a blue shift a larger difference.

The spectra of STY-Ar_n clusters are reported in figure 2, together with the spectrum of pure STY. As shown, the structure of STY-Ar and STY-Ar₂ have sharp origins and exhibit features due to vdW modes. The STY-Ar 0_0^0 transition is shifted by 32 cm^{-1} with respect to pure STY spectrum, confirming previous measurements (Dimopoulou-Rademann *et al* 1988). The STY-Ar₂ spectral shift is 63 cm^{-1} , almost twice that of STY-Ar. This behaviour is analogous to what was found for other aromatic systems (Bernstein 1990). It is explained by the presence of two equivalent sites for the Ar atoms, one above and the other below the aromatic ring. The STY-Ar₃ exhibits complex features due to the more numerous intramolecular vdW modes and eventually to the presence of isomeric structures (Hermine *et al* 1992). Analogous data have been obtained in the case of 4FSTY-Ar clusters (Piccirillo *et al* 1993).

Spectra of some STY-(CCl_4)_n complexes are reported in figure 3. The red shift for the 0_0^0 transition of the STY- CCl_4 adduct is 89 cm^{-1} , much larger than that found for STY-Ar. This fact can be explained by the much larger polarizability of the CCl_4 molecule with respect to Ar. As the cluster size increases to n values larger than 2, both broad and sharp components are observed in the spectra. The shift of the band maxima as a function of the n solvent molecules shows an evolution toward the red with respect to the 0_0^0 transition of the bare STY molecule. The large bandwidth can be attributed to the presence of interaction between the chromophore and the solvent molecules leading to the formation of different isomers (Even *et al* 1990). The UV

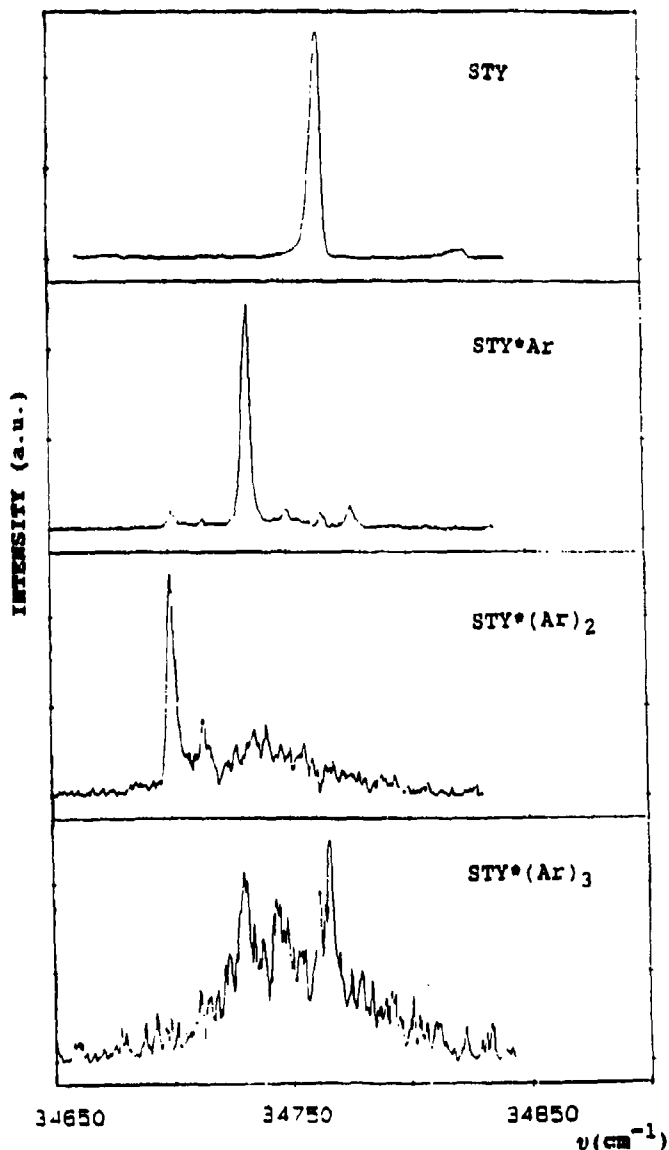


Figure 2. The mass resolved R2PI spectra of styrene clustered by Ar atoms. The spectral shift scale is relative to the S_1 electronic origin of styrene.

absorption band of STY in CCl_4 solution (insert in figure 3) has a maximum centred at $34,180 \text{ cm}^{-1}$. The resulting red shift of 580 cm^{-1} with respect to pure STY in the gas phase can be the tendencial value of $\text{STY}(\text{CCl}_4)_n$ for very large n , indicating that these aggregates represent the first building blocks of a solute molecule in CCl_4 solution.

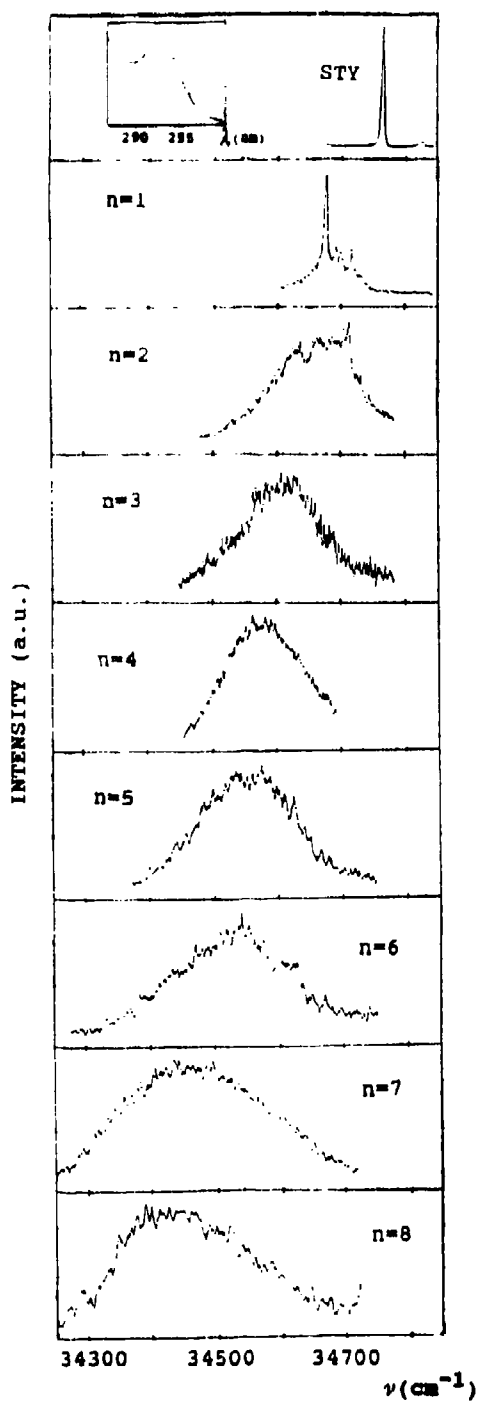
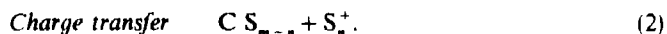


Figure 3. The mass resolved R2PI spectra of styrene clustered by CCl_4 molecules. The spectral shift scale is relative to the S_1 electronic origin of styrene.

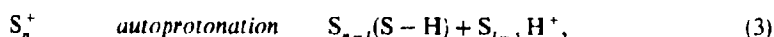
4. Reactivity

It is well known that, following R2PI ionization, reactions can take place within the cluster. Resonant two-photon ionization can lead to introcluster processes where the chromophore solute reacts with the solvent either by nucleophilic substitution or by charge or proton transfer reaction (Breen *et al* 1989; Brutschy 1990).

The following scheme represents possible introcluster solvent (S) and chromophore (C) reactions:



Cluster ions S_n^+ from solvent molecules having a dual character may lead to autoprotection:



where C - H and S - H stands for an H lost.

In styrenes complexed with amines we have found the occurrence of internal ion-molecule reactions which lead to the formation of protonated species. Typical

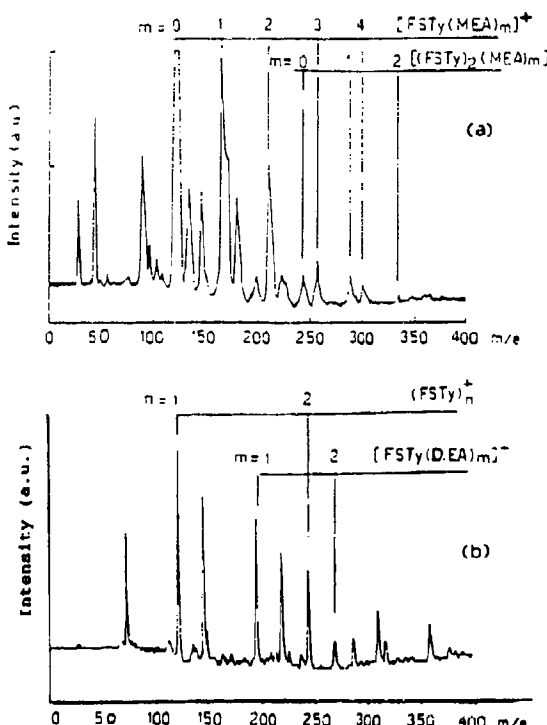


Figure 4. Mass spectra of a mixture of 4FSTY with MEA (a) and DEA (b), taken at a laser frequency of $34,350\text{ cm}^{-1}$ (292 nm).

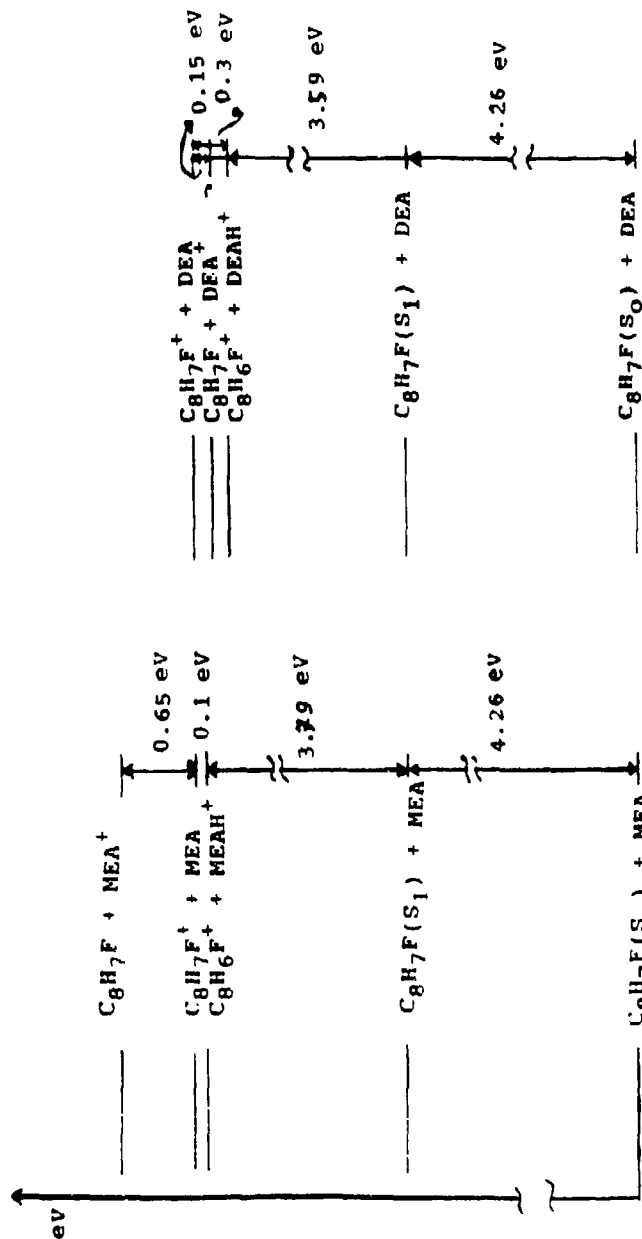


Figure 5. Energies of the charge transfer and protonation processes in 4FSTY-MEA and 4FSTY-DEA systems.

mass spectra of 4FSTY·MEA and 4FSTY·DEA taken at $34,250\text{ cm}^{-1}$ are reported in figure 4.

In the spectra of 4FSTY and MEA mixtures (figure 4a), besides the main cluster sequences, $4\text{FSTY}\cdot(\text{MEA})_m^+$ and $(4\text{FSTY})_2\cdot(\text{MEA})_m^+$, several peaks can be observed.

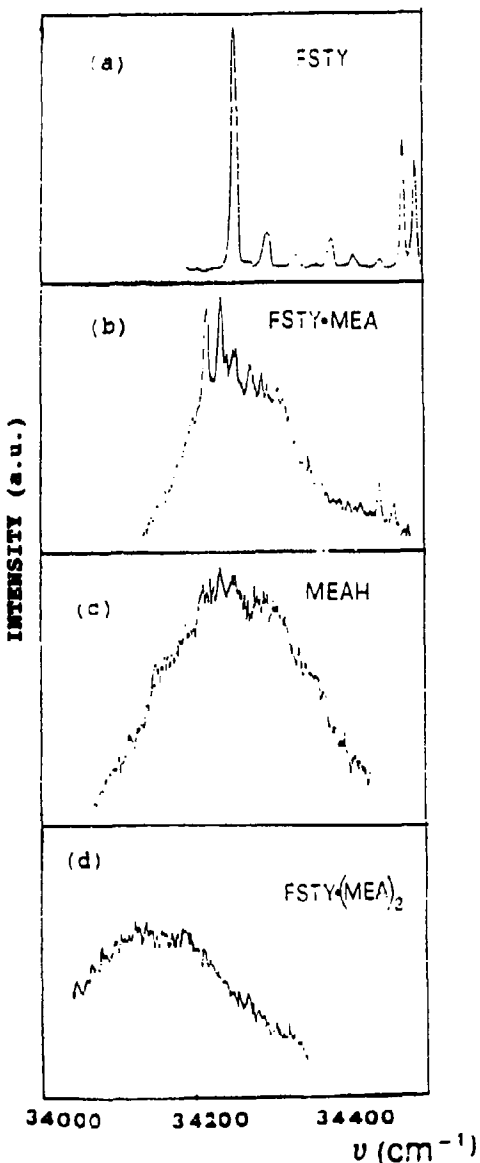


Figure 6. Wavelength dependence of 4FSTY^+ (a), $(4\text{FSTY}\cdot\text{MEA})^+$ (b), MEAH^+ (c) and $[4\text{FSTY}\cdot(\text{MEA})_2]^+$ (d).

These peaks have been assigned to $(MEA)_m^+$, $MEAH^+$ and protonated $(MEA)_nH^+$ clusters. Other peaks attributed to fragmentation are also observed. 4FSTY and DEA mixtures (figure 4b) behave similarly and the spectra are characterized by main cluster sequences. Other peaks have been assigned to intracluster charge transfer products. Addition of NH_3 to the 4FSTY beam also produces cluster sequences but only at very high ratios of $NH_3/4FSTY$ are intracluster reactions observed.

With reference to the transfer reaction scheme, a diagram of the energetics has been plotted in figure 5 for 4FSTY with MEA, and DEA, using literature data (Lias *et al* 1984; Brutschy 1990) and not accounting for the cluster binding energy.

From the energetics values reported in figure 5, the proton transfer reaction in the MEA adduct appears to be slightly exothermic (0.1 eV) and the charge transfer process endothermic by about 0.65 eV. This fact supports the hypothesis that $MEAH^+$ is formed mainly by direct intracluster proton transfer from 4FSTY to solvent. The data obtained on a single mass selected in the TOF spectrum as a function of laser frequency are reported in figure 6 (c) at m/e 46 for $MEAH^+$, (a) at m/e 122 for $FSTY^+$, (b) at m/e 167 for $(4FSTY \cdot MEA)^+$ and (d) at m/e 212 for $(4FSTY \cdot (MEA)_2)^+$. The wavelength dependence of $MEAH^+$, though less structured, has the same trend of $4FSTY \cdot MEA^+$. This confirms the hypothesis that the former ion is a product of the direct intracluster proton transfer (1). It can be noted that the absorption spectrum of 4FSTY is characterized by sharp peaks attributed to the vibronic levels of the $S_1 \leftarrow S_0$ electronic transition. Wavelength excitation of the $4FSTY \cdot MEA$ cluster shows, on the top of a broad continuum, a fine structure related to vdW and vibronic modes. Some intensity contribution towards the red of the wavelength in $MEAH^+$ spectrum is observed. This feature may arise from the contribution of other processes yielding $MEAH^+$. In particular, dissociative charge transfer followed by autoprotection (3) of higher cluster ions $[4FSTY \cdot (MEA)_m]^+$ should be taken into account. Typically $4FSTY \cdot (MEA)_2$ absorption is shifted further toward the red with respect to pure 4FSTY (figure 6). This would justify a contribution to the spectrum of $MEAH^+$ in the red region.

In the case of the 4FSTY·DEA adduct, both charge and proton transfer reactions are exothermic by 0.15 and 0.3 eV, respectively. As already hypothesized (Brutschy 1990; Keese and Castleman 1990), if energetically allowed, charge transfer processes always dominate other competing processes. In the TOF mass spectrum, peaks corresponding to $(DEA)_n^+$ cluster ions appear to be asymmetrically broadened; the presence of this tail can be ascribed to the proton transfer pathway leading to $(DEA)_nH^+$ formation.

Acknowledgements

This work is partly supported by the National Research Council (CNR) of Italy under Progetto Finalizzato "Electro-optical Technologies" and "Chimica Fine".

References

- Bernstein E R (ed.) 1990 In *Atomic and molecular clusters* (Amsterdam: Elsevier) p. 551
Breen J J, Kilgore K, Tzeng W B, Keese R G and Castleman A W Jr 1989 *J. Chem. Phys.* **90** 11
Brutschy B 1990 *J. Phys. Chem.* **94** 8637

- Dimopoulou-Rademann O, Even U, Amirav A and Jortner J 1988 *J. Phys. Chem.* **92** 5371
Even U, Ben Horin N and Jortner J 1990 *J. Chem. Phys. Lett.* **180** 138
Giardini Guidoni A, Piccirillo S, Coreno M, Snels M, Morone A and Teghil R 1993 *Appl. Surf. Sci.* **69** 340
Hermine P, Coutant B, Amar F G and Brechignac Ph 1992 *Z. Phys. D* **22** 529
Keese R G and Castleman A W Jr 1990 In *Atomic and molecular clusters* (ed.) E R Bernstein (Amsterdam: Elsevier) p. 507
Lias S G, Liebman J F and Levin R D 1984 *J. Phys. Chem. Ref. Data* **13** 693
Piccirillo S, Coreno M, Giardini Guidoni A, Pizzella G, Snels M and Teghil R 1993 *J. Mol. Struct.* (to be published)

Primary photophysical processes in *J*-aggregates of spectral sensitizers

K KEMNITZ^{*1}, K YOSHIHARA², T SUZUMOTO³, T TANI³
M LINDRUM⁴, J MOLL⁵ and S DAEHNE⁵

¹ BioQuant Ltd., Rudower Chaussee 6, D(O)-1199 Berlin, Germany

² Institute for Molecular Science, Myodaiji, Okazaki 444, Japan

³ Fuji Photo Film Co., Ltd., Ashigara Research Laboratories, Minami-Ashigara, Kanagawa 250-01, Japan

⁴ Free University of Berlin, Institute of Experimental Physics, Arnimallee 14, D(W)-1000 Berlin 33, Germany

⁵ Federal Institute for Materials Research and Testing, Laboratory of Time-Resolved Spectroscopy, Rudower Chaussee 5, D(O)-1199 Berlin, Germany

Abstract. We present temperature-dependent superradiant fluorescence decays and relative quantum yields in *J*-aggregates formed by two carbocyanine dyes, and compare homogeneous with heterogeneous systems. It will be shown that a generalisation of the results obtained in case of pseudoisocyanine is not appropriate, since each dye aggregate displays its own photophysical behaviour that has to be investigated individually. The exciton in the present systems seems to be coupled to an acoustic mode rather than to an optical mode, as had been found in case of pseudoisocyanine in ethylene glycol matrix. In addition, as a second novel feature, global analysis of the temperature-dependent, nonexponential fluorescence decays revealed the presence of an excited-state reaction, both in heterogeneous and homogeneous systems.

Keywords. *J*-aggregate; superradiance; spectral sensitisation.

1. Introduction

Excitonic energy transfer within *J*-aggregates of pseudoisocyanine (PIC) at very low temperatures is well established, and had been demonstrated by hole burning (De Boer *et al* 1987; Hirschmann and Friedrich 1989), photon echo (De Boer *et al* 1987; De Boer and Wiersma 1987, 1990), and time-resolved fluorescence (Fidder *et al* 1991b) techniques. Recent theories discuss, parallel to experiment, the nature of relaxation channels that are in competition with exciton migration (Spano and Mukamel 1989; Fidder *et al* 1991a). Superradiant fluorescence decays (Dorn and Müller 1987; De Boer and Wiersma 1990; Spano *et al* 1990) that become faster at low temperatures are a hallmark of coherence effects in *J*-aggregates, as is the decrease of the fluorescence lifetime with increasing aggregate size (Kemnitz *et al* 1990; Muenter *et al* 1992; Tani *et al* 1992).

Superradiant fluorescence decay is in competition with electron transfer in the photographic sensitisation process (figure 1). Since the main competitors, i.e., electron

* For correspondence

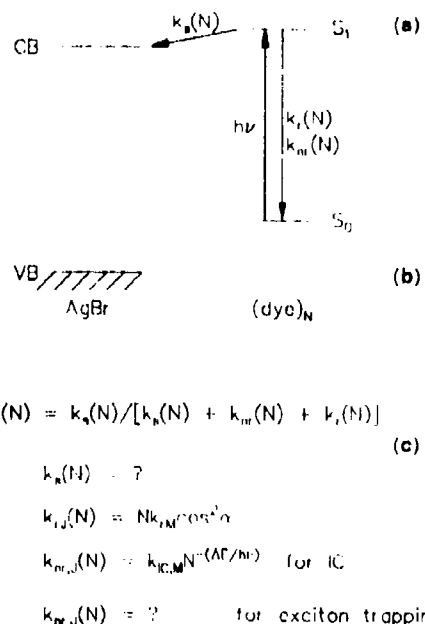


Figure 1. Simplified representation of spectral sensitisation with the competitive processes of: (a) electron injection into the conduction band of AgBr, $k_s(N)$, (b) superradiant decay, $k_r(N)$, and (c) nonradiative decay, $k_{nr}(N)$, where each process is a function of aggregate coherence size, N .

transfer, k_s , radiative decay, k_r , and nonradiative decay, k_{nr} , are all dependent on aggregate size, N , it is of great interest to establish the individual dependencies, with the ultimate goal of optimising the yield of sensitisation, $\Phi_R(N)$. Figure 2a shows the size dependence of k_s and that of the sum of radiative and nonradiative rate constant, k_L , obtained from fluorescence kinetics and sensitisation yields of *J*-aggregates adsorbed on AgBr (Tani *et al* 1992). The increase of k_L with increasing aggregate size is thought to be due to coherence effects. Figure 2b shows the size-dependent absorption spectra of the *J*-aggregates on AgBr, where the band maximum shifts to the red and the half width decreases with increasing aggregate size.

The decrease of k_s with increasing size in figure 2a is not well understood, at present. To improve the fundamental understanding of the electron transfer step involved in the above complex reaction scheme (figure 1), we investigated a series of dyes, shown in a classical Marcus representation in figure 3 (Tani *et al* 1992), with a prominent steep increase of the rate constant of electron transfer, as measured by the yield of sensitisation, Φ_R , with increasing half-wave reduction potential, E_R , of the dyes. Such steep increase in the normal region is caused by a very small reorientation energy, $\lambda = 0.05$ eV, typical of a solvent-free system (Kemnitz *et al* 1988). The behaviour in the inverted region (dashed), however, is unknown as yet, and new dyes will have to be used to explore this important region that will yield additional parameters, important for the complete characterisation of electron transfer in photographic systems. Once the basic parameters like intramolecular and external reorientation

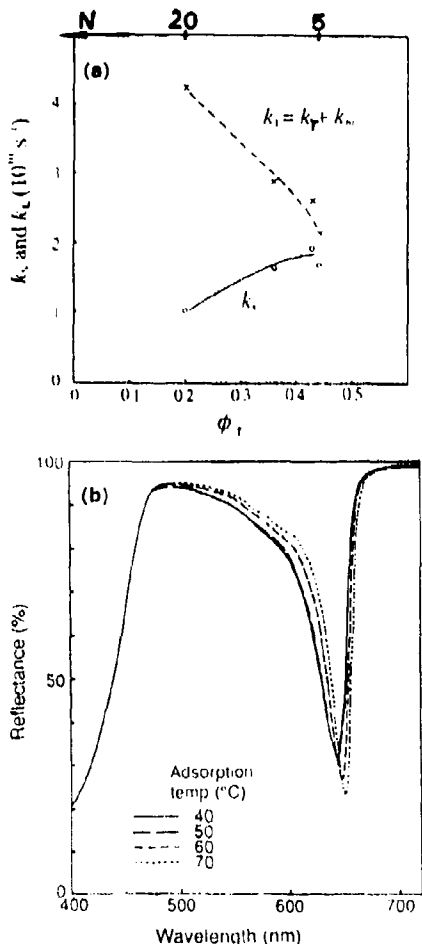


Figure 2. (a) Dependence of the electron injection rate constant, k_e , and of the sum of radiative and nonradiative rate constants, k_t , on aggregate size that relates inversely to the efficiency of sensitisation, Φ , (after Tani *et al* 1992). (b) Reflectance spectra of film samples of DCTC adsorbed on AgBr depending on aggregate size. With increasing aggregate size, N , the maxima shift to the red and the bandwidth decreases (after Tani *et al* 1992).

energy and electron-exchange matrix element are known, it might be possible, in a second step, to extract the size dependencies of these parameters that govern electron transfer in photographic sensitisation.

An alternative path of separating the individual decay processes in the sensitisation process was followed in the development of reference systems without electron transfer, i.e., J-aggregates adsorbed on SiO_2 (Kemnitz *et al* 1990) and KBr, where KBr was chosen in order to create an inert surface more similar to that of AgBr. These systems are, analogous to the homogeneous counterpart, i.e., liquid or glassy mixtures of ethylene glycol/water(EG) (Lindrum *et al* 1993), very sensitive towards changes in environment, and both heterogeneous and homogeneous systems are thus well suited

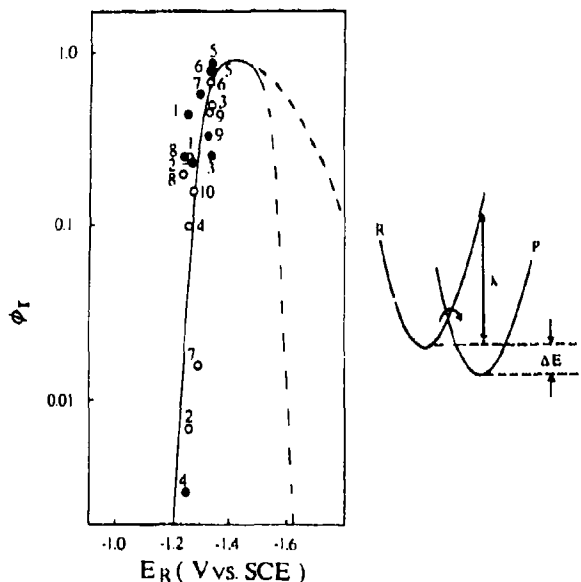


Figure 3. Simple Marcus representation of the rate constant of electron injection, as measured by the efficiency of photosensitization, Φ_r , and the reduction potential of various cyanine dyes, E_R (after Tani *et al* 1992). The reorientation energy, λ , of the solvent-free system is very small, i.e., about 0.05 eV.

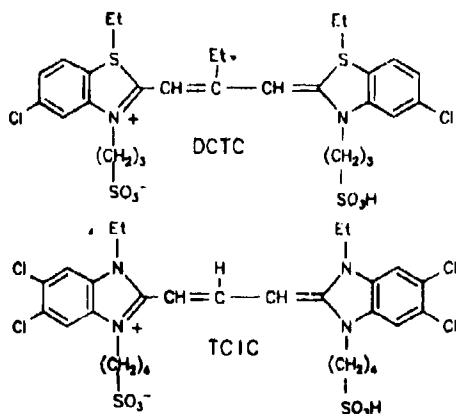


Figure 4. The chemical structures of 5,5'-dichloro-9-ethyl-benzthia-carbocyanine (DCTC) and 5,5',6,6'-tetrachloro-benzimidido-carbocyanine (TCIC).

for the fundamental study of environmental effects on exciton-phonon coupling, and helpful in the eventual understanding of the individual size dependencies of all the processes involved.

We present fluorescence decays and relative quantum yields of *J*-aggregates formed by 5,5'-dichloro-9-ethyl-benzthia-carbocyanine (DCTC, figure 4) on KBr (Kemnitz 1993) and by 5,5',6,6'-tetrachloro-benzimidido-carbocyanine (TCIC, figure 4) in

ethylene glycol/H₂O (4:1) matrix (Lindrum *et al.* 1993), in the temperature range 293–4 K. Both systems display enhanced fluorescence decays at low temperature, accompanied by an increase of relative fluorescence quantum yield, clearly indicating an increase of the radiative rate constants at low temperatures.

As a novel feature, the presence of an excited-state reaction was revealed by global analysis of fluorescence decays, acquired at up to 12 different temperatures (Kemnitz 1993). Various physical models to account for the complex fluorescence decay features have been tested and compared.

The individual decay characteristics depend on environment, i.e., on the substrate in case of heterogeneous systems. Figures 5a and 6 display the temperature behaviour of J-aggregates of DCTC, adsorbed on SiO₂ and KBr, respectively, and the opposite temperature-dependence is obvious. In case of the homogeneous systems, the fluorescence

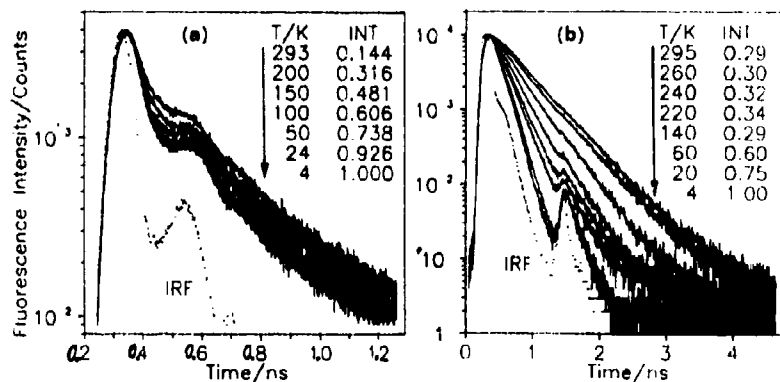


Figure 5. Temperature-dependent fluorescence kinetics and relative fluorescence quantum yields of (a) DCTC adsorbed on KBr, and (b) TCIC in fluid and solid matrix of ethylene glycol/H₂O (4:1).

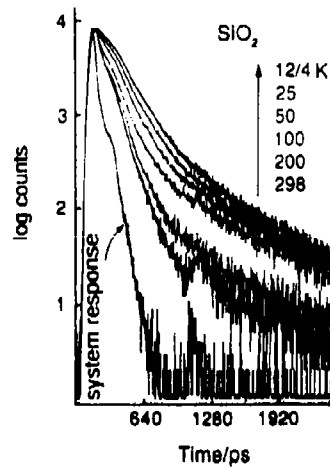


Figure 6. Environmental effect in case of DCTC/SiO₂. The fluorescence decays slow down at reduced temperature in contrast to DCTC/KBr in figure 5a.

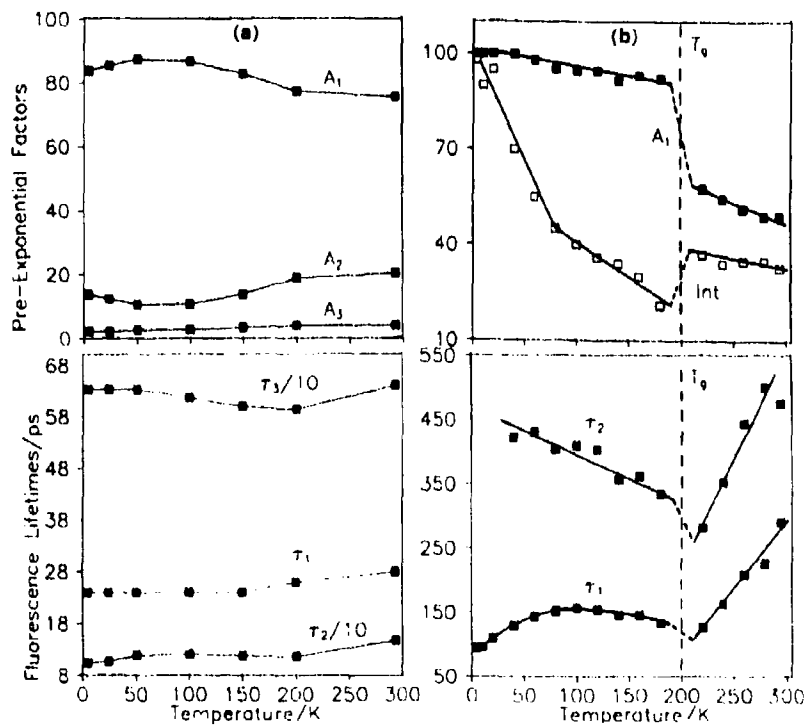


Figure 7. (a) Three-exponential analysis of the nonexponential fluorescence decays of DCTC/KBr, and (b) two-exponential analysis of TCIC in ethylene glycol/H₂O.

dynamics depend on solvent composition, i.e., on the amount of H₂O in the EG systems (Lindrum *et al* 1993), and on the phase, i.e., on the fluid or the solid properties of the matrix (figure 7b).

2. Experimental

The time-correlated single photon counting systems (Kemnitz *et al* 1990; Rempel *et al* 1990) as well as the preparation of the heterogeneous film samples (Kemnitz *et al* 1990; Tani *et al* 1992) and that of the homogeneous EG samples (Lindrum *et al* 1993) were described previously. Excitation wavelengths were 620 and 580 nm and the emission was observed at 630 and 590 nm for DCTC and TCIC, respectively. Heterogeneous and homogeneous samples were excited at low-photon density and observed under front-face geometry. Global analysis software was from Globals Unlimited. Application and advantages of global fluorescence decay analysis are well documented in literature (Beechem *et al* 1989; Rumbles *et al* 1991; Kemnitz and Sakaguchi 1992; Boens *et al* 1992).

3. Results and discussion

3.1 Temperature-dependence of superradiant fluorescence decay

Figure 5 shows the temperature-dependent, nonexponential fluorescence decays and the relative fluorescence intensities of (a) the heterogeneous DCTC/KBr system, and of (b) TCIC in the macroscopically homogeneous EG/H₂O matrix. Both systems display enhanced fluorescence decays at reduced temperatures, accompanied by a strong increase of fluorescence intensity, thus clearly demonstrating the increase of the radiative rate constant at low temperatures. The fluorescence decays are complex and can phenomenologically be fitted by a multi-exponential function of up to three exponents. The degree of non-exponentiality varies with temperature and phase. This effect can most clearly be seen in case of TCIC in figure 7b, where the fluid phase from 293–220 K can roughly be fitted by two exponents, whereas the rigid matrix shows a smooth transition from three-exponential decay at 180 K to strictly single-exponentiality at 4 K. The heterogeneous system of DCTC/KBr in figure 7a needs three exponents within the whole temperature range, in contrast. The fluorescence lifetimes in this system are almost independent of temperature, with a slight tendency towards shorter lifetimes at lower temperatures (τ_1, τ_2). The most conspicuous feature, however, is the variation of the pre-exponential factor of the fast component, A_1 , in figure 7a (top). Global three-exponential analysis at 7 temperatures, at varying degrees of parameter-linkage, clearly shows that it is mainly the increase of A_1 at low temperatures that is responsible for the enhancement of the fluorescence decay at reduced temperatures in figure 5a. Analogously, the increase of A_1 in case of TCIC in figure 7b (top) could be shown to be an essential feature of the temperature-dependent fluorescence decays in figure 5b. Thus, any physical model has to accommodate the increase of the pre-exponential factor of the fast component, next to the decrease of the fluorescence lifetimes at low temperatures, and, of course, the pronounced increase of fluorescence intensity.

3.2 Excited-state reaction

Global analysis, employing complex excited-state schemes with numerous fit parameters, is no simple task, because there exist many local and even global minima in the multidimensional error surface, yielding mostly nonphysical fit parameters. The challenge is to locate the global minima of physical significance. Such systems turn out to be rare and highly restricted, fortunately, so that it is possible to suggest and discuss a limited number of physical models. By applying global analysis, we were able to test and compare the physical models that are displayed in figure 8. The quality of the individual models is judged by their global χ^2 , where three-exponential, unrestricted fitting is taken as ultimate quality standard. The integrity of all the present models discussed was confirmed by kinetic simulations and reanalyses of the artificial decays, convoluted with a real system response function.

The transition, mentioned above, from three- to single-exponentiality in case of TCIC upon reduction of temperature, clearly points to the existence of an excited-state reaction. The primarily excited, superradiant state relaxes, in a temperature-dependent reaction, k_{12} , towards a weakly emitting "trap"-state of longer fluorescence lifetime (figure 8c). At 4 K, the transition k_{12} is completely frozen and a single-exponential

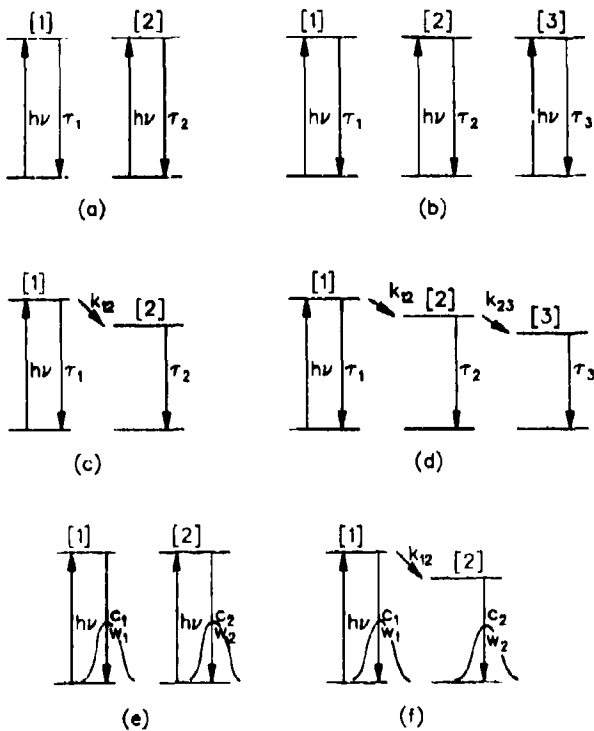


Figure 8. Various reaction schemes that have been tested and compared by global analysis: (a) two-exponential decay caused by two S_0 species, (b) three-exponential decay caused by three S_0 species, (c) excited-state two-level scheme, (d) excited-state three-level scheme, (e) two distributed (Gaussian) S_0 species, and (f) distributed (Gaussian) excited-state two-level scheme.

decay can be observed. Scheme (c) in figure 8 can roughly fit the observed decays of the solid domain below 200 K in figure 5b, but a perfect fit is obtained only for the Gaussian-distributed analogue. Scheme (f), yielding a global χ^2 -equal to that of three-exponential fitting. The distributed fit replaces a discrete fluorescence lifetime by a distribution of lifetimes whose pre-exponential factors are determined by a Gaussian envelope. Figure 9b shows the decrease of centre wavelength, C_1 , from about 130 to 90 ps at lower temperature, accompanied by a reduction of the half width, W_1 , from 90 to about 4 ps. The slow component, caused by the emission of the product-state, can be modelled by $C_2 = 725$ ps and $W_2 = 660$ ps, independent of temperature. The interconverting rate constant, k_{12} , decreases from 1/4 to 1/400 ns and is responsible, together with the decrease of W_1 , for the transition from three- to one-exponentiality at 4 K. The increase of the fluorescence intensity at low temperatures is reflected in an increase of the species-associated spectra (SAS_i). The SAS represent the intrinsic fluorescence bands of both excited-state species and are proportional to fluorescence quantum yield. Both species display increasing SAS, in case of the superradiant state due to an increase of the radiative rate constant, and in case of the trap-state, probably due to the decrease of the nonradiative decay at low temperatures. Two candidates

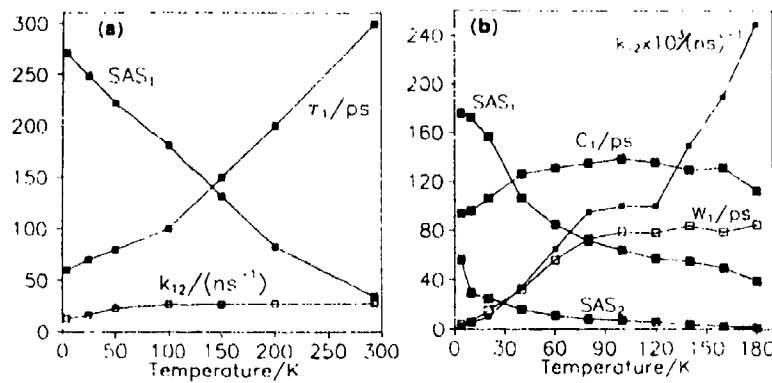


Figure 9. Best fits combining fluorescence decay and quantum yield data of figure 5. (a) In case of DCTC, a three-level excited-state scheme is discussed. (b) TCIC in solid matrix can best be fitted by a distributed two-level excited-state scheme.

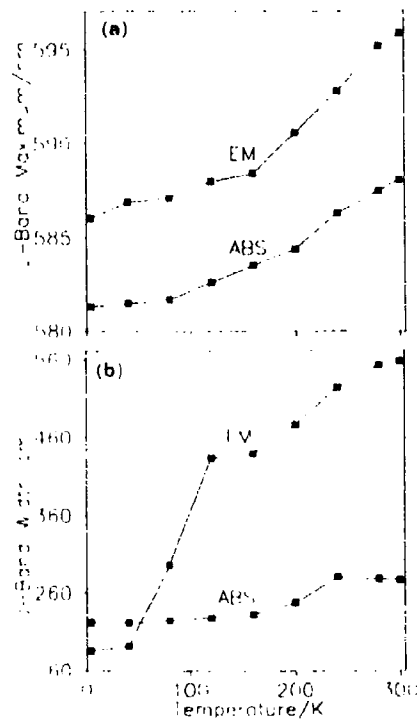


Figure 10. Temperature-dependent maximum (a) and bandwidth (b) of absorption and fluorescence spectra of TCIC/EG.

for a weakly emissive trap state were proposed recently: (a) a structural irregularity within the aggregate, i.e., a small section forming a nonfluorescent H-dimer (Muenter *et al.* 1992) and (b) thermally activated, subradiant states within the exciton band (Spano *et al.* 1991).

Figure 10 shows the temperature-dependence of the maximum (a) and bandwidth (b) of absorption and fluorescence spectra of TCIC/EG (Moll *et al* 1993). The parallel blueshift of absorption and fluorescence spectra at lower temperatures in figure 10a have also been observed in case of PIC/EG and can be understood in terms of exciton coupling to low-frequency phonons (Fidder *et al* 1991b). Figure 10b displays the decrease of the fluorescence bandwidth at reduced temperatures, which is much larger than that of the absorption spectrum. In addition, the fluorescence bandwidth at room temperature is about twice the absorption bandwidth. We take this behaviour as support for our notion from above that the emission of trap states, responsible for the broadened emission band at 293 K, is reduced at lower temperatures due to reduced k_{12} .

The combination of decreasing τ_1 and of decreasing k_{12} at reduced temperatures leads to an observed lifetime, τ_{obs} , e.g., in two-exponential analysis, that is only weakly dependent on temperature. τ_1 in figures 7a and b decreases by less than 20 and 50%, at 4 K, respectively, whereas the intensity increases 7 and 5 times within the same temperature range. The variation of fluorescence intensity with temperature was corrected for the shift of absorption and fluorescence bands (figure 10a). The increase of the extinction coefficient at reduced temperature was roughly cancelled by the decrease of fluorescence intensity, since excitation was at the high-energy side of the absorption band, whereas the fluorescence was observed at the low-energy side of the emission band.

In case of the heterogeneous system, the distributed two-level excited-state scheme from above is not sufficient to fit the data, and a third excited-state level has to be introduced, scheme (d) in figure 8. The parameters describing the third component, i.e., the rate constant of interconversion, k_{23} , SAS₃, and fluorescence lifetime, τ_3 , are of secondary importance only and are very approximate. Figure 9a shows the temperature dependence of the more important parameters, i.e., the decrease of k_{12} , the increase of SAS₁, and a decrease of τ_1 from 300 to 60 ps at 4 K. This behaviour is strictly analogous to that of the homogeneous system described in figure 9b. The

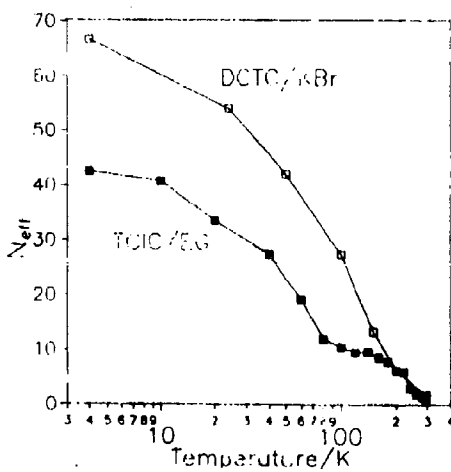


Figure 11. Temperature dependence of the coherence size, N_{eff} , of DCTC/KBr and TCIC/EG.

core of both the homogeneous and heterogeneous model is an excited-state reaction, characterised by decreasing rate constant of interconversion, k_{12} , from a superradiant to a weakly emitting state, increasing SAS_1 , and decreasing superradiant lifetime, τ_1 , at reduced temperatures. The radiative lifetime, $1/k_r(T)$, can be calculated from $SAS_1(T)$ and $\tau_1(T)$, both obtained from scheme 8(d) or (f): $1/k_r(T) = \tau_1(T)/SAS_1(T)$, under the assumption that $SAS_1(4\text{ K}) = \Phi_f(4\text{ K}) = 1$. Figure 11 displays the coherence length, N_{eff} , of TCIC/EG and DCTC/KBr, calculated according to $N_{\text{eff}} = k_r(J)/k_r(M)$, with $k_r(M) = 1/(4\text{ ns})$. Whereas N_{eff} in case of PIC in EG/H₂O is absolutely independent of temperature between 4 and 50 K, we observe a change in N_{eff} of about 100% in case of both carbocyanines in this temperature range.

Two physical models that cannot be distinguished at the current level of precision are present in case of the liquid phase. The first model is a variant of the excited-state schemes described above. As already seen from the parameters obtained by two-exponential fitting in figure 7b (bottom), both fluorescence lifetimes, τ_1 and τ_2 , decrease at low temperatures, and we have to assume that two superradiant states are involved in this particular case. The second model, based on a Gaussian ground-state distribution of fluorescence lifetimes, does not involve an excited-state reaction, and is based on a single fluorescent state. Both models will be compared and discussed in a future paper (Kemnitz 1993) and will be contrasted by a different approach (Lindrum *et al* 1993).

Two potential alternatives for the explanation of temperature-dependent pre-exponential factors, (a) that of two emitting ground-state populations (figure 8a or 8e), where the slower decaying and more weakly emitting species would have to stop emitting at 4 K, and (b) that of a temperature-dependent ground-state equilibrium between two distributions, are inconceivable in the present systems and were discarded.

3.3 Theoretical considerations

Figure 12 displays the main results of the theory of exciton-phonon coupling, as developed by Spano *et al* (1990), and shows the dependence of coherence size, N_{eff} , on temperature, T , and on the physical aggregate size, N . Figure 12a represents the case of an optical phonon and contains the qualitative behaviour of the system of PIC in EG/H₂O by De Boers and Wiersma (1990) as bold line. They observed strictly temperature-independent behaviour below 50 K and a linear decrease of N_{eff} , by a large factor of about 50, with increasing temperature. The detailed analysis yielded the following parameters: $N = 75$, exciton-phonon coupling strength, $F_{\text{op}} = 210\text{ cm}^{-1}$, and the optical mode, $\Omega_{\text{op}} = 240\text{ cm}^{-1}$, using the nearest-neighbour dipole-dipole interaction energy, $V = 600\text{ cm}^{-1}$. The analysis was based on the experimental observation of a decrease of the fluorescence decay time by about 10 times, when the temperature was lowered from 200 to 50 K, accompanied by a change in quantum yield of less than 25%.

The experimental observations in the present carbocyanine dye systems differ in several ways from that of PIC described above: (1) complex, non-exponential fluorescence decays, as opposed to one-exponentiality, (2) relatively small changes of fluorescence lifetimes in two- or three-exponential analyses, i.e., a decrease of less than 1.5 times, when going from 293 to 4 K, with a major part of the change occurring below 50 K, (3) a strong increase of relative fluorescence quantum yield, i.e., an increase by up to

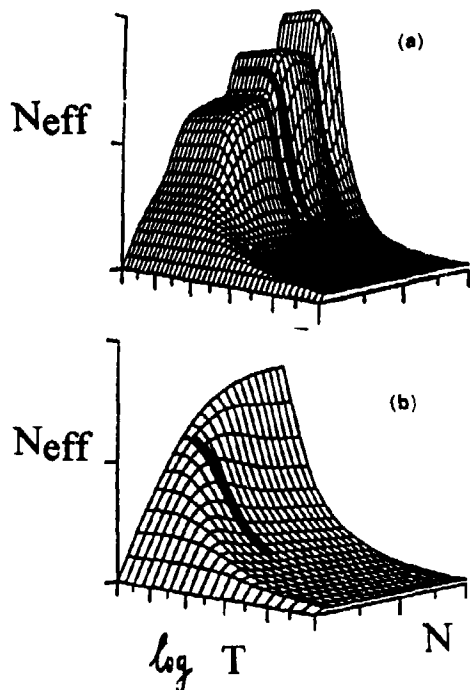


Figure 12. Theory of exciton-phonon coupling after Spano *et al* (1990), with the dependence of coherence size, N_{eff} , on temperature, T , and physical aggregate size, N . (a) Optical mode, containing the qualitative behaviour of the data on PIC by De Boer and Wiersma (1990) as bold line. (b) Acoustic mode with qualitative temperature dependence of N_{eff} of the present data as bold line.

7 times in the same temperature region, and (4) the existence of an excited-state reaction, manifest in a temperature-dependent degree of non-exponentiality, i.e., temperature-dependent pre-exponential factors obtained in multi-exponential fluorescence decay analysis.

Figure 12b shows the exciton-phonon coupling in case of an acoustic mode and displays the qualitative behaviour of the present systems of figure 11 as bold line. The increase of N_{eff} , even at very low temperatures, is typical for acoustic modes (moderate size aggregates) and is in contrast to the behaviour of optical modes in figure 12a.

It appears that the temperature dependence of N_{eff} of the present systems in figure 11 is in qualitative accord with the assumption of coupling to an acoustic mode. Coupling to low-frequency acoustic modes ($\Omega_{\text{ac}} < 30 \text{ cm}^{-1}$) had recently been suggested by Muenter *et al* (1992) to control the weakly temperature-dependent fluorescence dynamics of PIC J-aggregates adsorbed on AgBr.

4. Conclusions

Our investigations of the temperature-dependent superradiant fluorescence dynamics of J-aggregates of carbocyanine dyes in heterogeneous and homogeneous environments

led to several novel features not observed in case of PIC: (1) individual temperature behaviour, demonstrating a varying degree of exciton-phonon coupling, (2) dependence on environment, (3) coupling to an acoustic mode, and (4) the existence of an excited-state reaction.

By applying global analysis, we were able to elucidate several models of physical significance from the complex fluorescence decay behaviour. In one of the models discussed, we postulate a slight quenching of the superradiant state by weakly emitting trap states, with the trapping rate constant decreasing at reduced temperatures. The nature of the trap is unknown as yet, but its emission spectrum is currently being investigated by temperature- and emission-resolved ps spectroscopy.

The application of ground- and excited-state distributions (Gaussian or other) in fitting fluorescence dynamics of (micro)-heterogeneous systems is a very promising tool for the design of kinetic models. The conspicuous reduction at low temperatures of the Gaussian half-width in one of our kinetic models is a very attractive feature and deserves further investigation.

Acknowledgements

Three of us (ML, JM, SD) wish to thank Professors D Stehlik and C v Borczyskowski for helpful discussions and support and the Deutsche Forschungsgemeinschaft as well as the Fonds der Chemischen Industrie for financial support.

References

- Beechem J M, Gratton E, Ameloot M, Knutson J R and Brand L 1989 In *Fluorescence spectroscopy* (ed.) J R Lakowicz (New York: Plenum) vol. 1
Boens N, Andriessen R, Ameloot M, Van Dommelen L and DeSchryver F C 1992 *J. Phys. Chem.* **96** 6331
De Boer S, Vink K J and Wiersma D A 1987 *Chem. Phys. Lett.* **137** 99
De Boer S and Wiersma D A 1990 *Chem. Phys. Lett.* **165** 45
Dorn H -P and Müller A 1987 *Appl. Phys.* **B43** 167
Fidder H, Knoester J and Wiersma D A 1991a *J. Chem. Phys.* **95** 7880
Fidder H, Terpstra J and Wiersma D A 1991b *J. Chem. Phys.* **94** 6895
Hirschmann R and Friedrich J 1989 *J. Chem. Phys.* **91** 7988
Kemnitz K 1993 (to be submitted)
Kemnitz K, Nakashima N and Yoshihara K 1988 *J. Phys. Chem.* **92** 3915
Kemnitz K and Sakaguchi T 1992 *Chem. Phys. Lett.* **196** 497
Kemnitz K, Yoshihara K and Tani T 1990 *J. Phys. Chem.* **94** 3099
Lindrum M, Moll J, Glismann A and Daehne S 1993 (to be submitted)
Moll J, Daehne S and Lindrum M 1993 (to be submitted)
Muenter A A, Brumbaugh D V, Apolito J, Horn L A, Spano F C and Mukamel S 1992 *J. Phys. Chem.* **96** 2783
Rempel U, v. Maltzan B and v. Borczyskowski C 1990 *Chem. Phys. Lett.* **169** 347
Rumbles G, Brown A J and Phillips D 1991 *J. Chem. Soc., Faraday Trans.* **87** 825
Spano F C, Kuklinski J R and Mukamel S 1990 *Phys. Rev. Lett.* **65** 211
Spano F C, Kuklinski J R and Mukamel S 1991 *J. Chem. Phys.* **94** 7534
Spano F C and Mukamel S 1989 *J. Chem. Phys.* **91** 683
Tani T, Suzumoto T, Kemnitz K and Yoshihara K 1992 *J. Phys. Chem.* **96** 2778

Photochemical reaction of [6]-1,4-cyclophaneanthraquinone

SADAO MIKI*, F M ABDEL-LATIF, TOSHIHIRO NAKAYAMA
and KUMAO HAMANOUE

Department of Chemistry, Kyoto Institute of Technology, Matsugasaki, Sakyo-ku, Kyoto
606, Japan

Abstract. [6]-1,4-Cyclophaneanthraquinone (CHAQ) has been synthesized and its photochemical reaction is studied. Nanosecond laser photolysis of CHAQ in EPA at room temperature reveals that both the lowest excited singlet and triplet states of CHAQ cause the intramolecular hydrogen-atom abstraction yielding the 1,4-biradical, i.e., the hydrogen-atom abstraction by the carbonyl oxygen from the benzylic methylene of the cyclophane bridge. Since steady-state photolysis of CHAQ in EPA at 77 K reveals the formation of cyclophane-9-hydroxy-1,10-anthraquinone-1-methide (2), the results obtained by steady-state photolysis at room temperature are interpreted as follows: (1) In benzene, 2 changes to a naphthaloquinone derivative (6). (2) In EPA, 2 yields its ethanol adduct (3) and there exists an equilibrium between 3 (major) and 6 (minor). (3) By a dark reaction, 3 and/or 6 revert very slowly to CHAQ.

Keywords. Cyclophaneanthraquinone, intramolecular hydrogen-atom abstraction.

1. Introduction

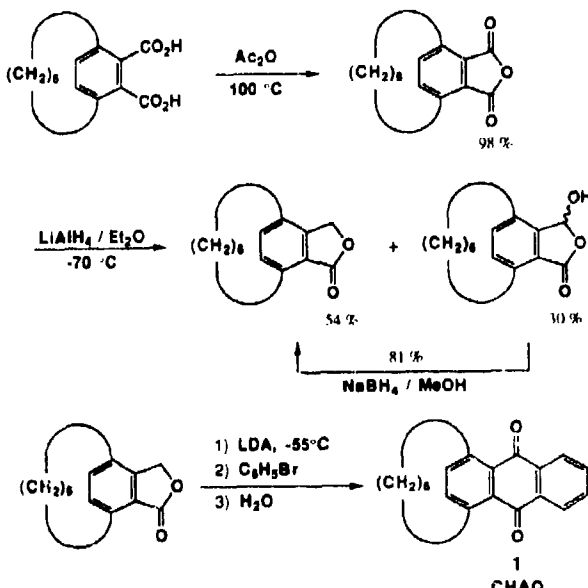
Pairs of isomeric molecules undergoing photochemical interconversion have been studied recently in an attempt to search for solar energy storage systems as well as molecular memory devices. We have thus been studying the photophysics and photochemistry of sterically strained polyacenequinone derivatives focusing on their photovalence isomerization (Nakayama *et al* 1988; Miki *et al* 1988, 1992b). Since [6]-1,4-cyclophaneanthraquinone (CHAQ) has a methylene bridge and one of the benzene rings is deformed to a boat form, it is expected that this compound can undergo photoisomerization yielding a hemi-Dewar type isomer. From these points of view, we have already prepared CHAQ and identified the final photoproduct to be cyclophane-hemi-Dewar-anthraquinone (Miki *et al* 1992c). Recently, however, we have found that this identification is incorrect owing to a low resolution of a ¹H NMR spectrometer (90 MHz). Hence, this review deals with results of our recent reinvestigation (Miki *et al* 1992a).

Although photochemistry of strain-free anthraquinones with a benzylic methylene has already been reported by Gritsan *et al* (1990, 1991), we believe that CHAQ is still an interesting compound because of its novel photochemical reaction which is different from that of several strain-free anthraquinones.

*For correspondence

2. Nanosecond laser photolysis of CHAQ in EPA (diethylether/isopentane/ethanol = 5:5:2 volume ratio) at room temperature

Starting from [6]-3,6-cyclophaneephthalic acid prepared following the method by Liebe *et al* (1985), the title compound (CHAQ) is synthesized according to scheme 1; the final step is a modification of the method reported by Sammes and Dodsworth (1979).



Scheme 1.

Figure 1 shows the transient absorption spectra obtained by nanosecond laser photolysis of CHAQ in EPA at room temperature. In comparison with the spectrum obtained at the end of nanosecond pulse excitation (40 ns delay), those obtained at longer delay times have a weak absorption band at $\lambda_{\text{max}} = 385 \text{ nm}$ compared with that at $\lambda_{\text{max}} = 490 \text{ nm}$. As shown in figure 2, the transient absorption monitored at 490 nm appears within the duration of the nanosecond pulse excitation (FWHM = 20 ns) and then grows further in following a single-exponential function with a rise time of 0.42 μs . In contrast, the transient absorption monitored at 385 nm decreases following a single-exponential function with lifetime equal to the rise time obtained for the 490-nm absorption. Hence, we have concluded that the transient absorption (with $\lambda_{\text{max}} = 490 \text{ nm}$), which appeared within the duration of the nanosecond pulse excitation, is the absorption of the 1,4-biradical produced by the intramolecular hydrogen-atom abstraction at the lowest excited singlet of CHAQ and that the slow rise of the 490-nm absorption is due to the formation of the 1,4-biradical produced by the intramolecular hydrogen-atom abstraction at the lowest excited triplet state of CHAQ with an absorption maximum at 385 nm; the 1,4-biradical is produced by the hydrogen-atom abstraction of the carbonyl oxygen from the benzylic methylene.

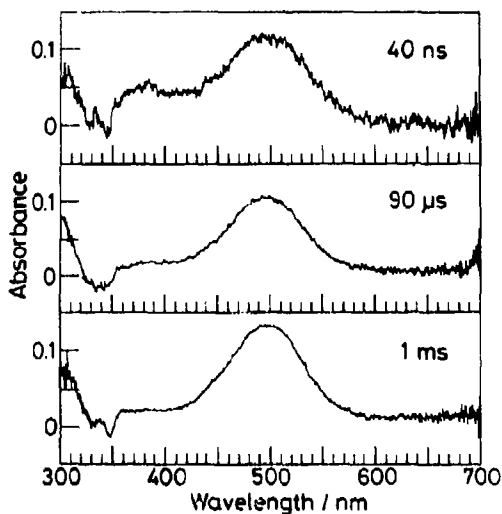


Figure 1. Transient absorption spectra obtained by nanosecond laser photolysis of CHAQ in EPA at room temperature.

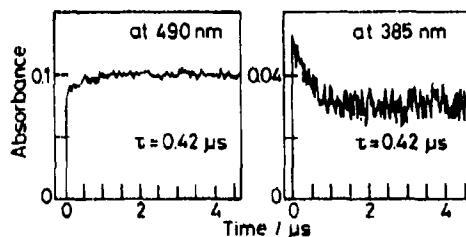


Figure 2. Single-exponential rise (at 490 nm) and decay (at 385 nm) of transient absorptions obtained by nanosecond laser photolysis of CHAQ in EPA at room temperature.

3. Steady-state photolysis of CHAQ in EPA at 77 K and at room temperature

Figure 3 shows the absorption spectral change caused by 405-nm steady-state photolysis of CHAQ in EPA at 77 K (cf. full lines). With the spectral decrement due to the reactant absorption, a new absorption band with $\lambda_{\text{max}} = 542 \text{ nm}$ as well as that at 300–400 nm grows up. One can clearly observe two isosbestic points at 476 and 466 nm. In comparison with the absorption spectra of 9-hydroxy-1,10-anthraquinone-1-methide and its derivatives as reported by Gritsan *et al.* (1990, 1991), we propose that the product obtained at 77 K is cyclophane-9-hydroxy-1,10-anthraquinone-1-methide (2 in scheme 2) produced via the 1,4-biradical.

After steady-state photolysis at 77 K, the sample warming up to room temperature gives rise to the disappearance of the 542-nm band and the appearance of another new band at $\sim 340 \text{ nm}$ as well as that of the reactant (CHAQ) (cf. dotted line). After this, a 1-day dark reaction causes the spectral change from the dotted to the dashed spectra, indicating that a shoulder at longer wavelengths decreases with accompanying increase of the absorption due to the reactant (CHAQ). These results indicate that

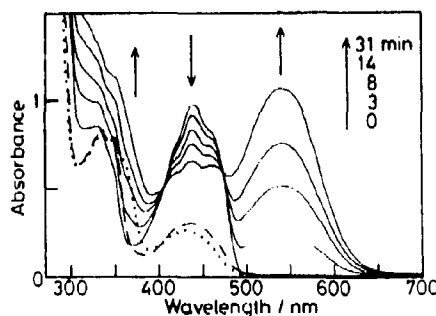
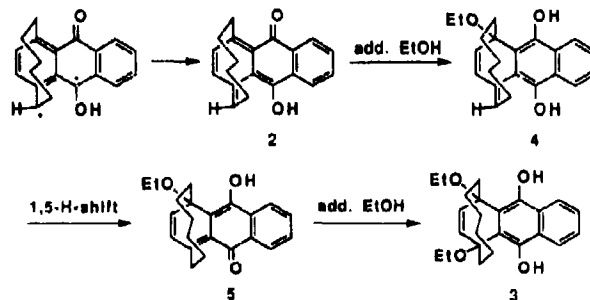


Figure 3. Spectral change caused by 405-nm steady-state photolysis of CHAQ in EPA at 77 K (full lines). By warming the sample solution up to room temperature after photolysis, the dotted spectrum is obtained and a further 1-day dark reaction gives the dashed spectrum.



Scheme 2.

2 produced at 77 K (with an absorption maximum at 542 nm) is a precursor of at least two compounds (with absorption bands at 300–370 nm) which can exist at room temperature.

We believe that steady-state photolysis of CHAQ in EPA at room temperature mainly gives rise to the formation of two compounds based on the fact that the dotted spectrum shown in figure 3 is rather similar to the spectra obtained by room-temperature photolysis of CHAQ as shown by full lines in figure 4 and the dashed spectrum shown in figure 3 is similar to that shown in figure 4. Since it is well known that almost all of the strain-free 9-hydroxy-1,10-anthraquinone-1-methides isomerize easily to the corresponding anthraquinones via the reverse intramolecular hydrogen-atom transfer, it can be concluded that one of the striking features of cyclophane-9-hydroxy-1,10-anthraquinone-1-methide (**2**) is its almost negligible reversion to the reactant (CHAQ). Owing to the lack of co-planarity of the π -moiety caused by the methylene bridge, the reverse hydrogen-atom transfer for **2** may require a much higher activation energy than those for the strain-free planar compounds.

Changing the solvent from EPA to [^2H] chloroform *in vacuo*, analysis of the photoproducts has been performed using a ^1H NMR spectrometer (300 MHz). Although the NMR signals obtained are very complicated, the formation of **3** (cf. scheme 2) as the main product is really confirmed; 8.55 ppm (s, 2H, OH) and 5.97 ppm (s, 2H, olefin); 3.94 ppm (dq, 2H) and 3.51 ppm (dq, 2H) for the diastereotopic methylene

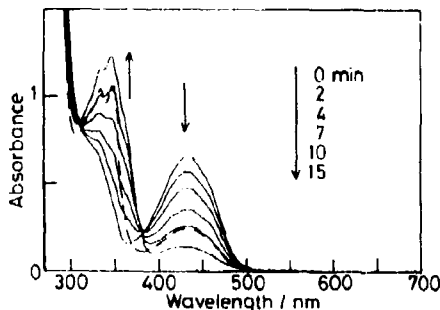


Figure 4. Spectral change caused by 405-nm steady-state photolysis of CHAQ in EPA at room temperature (full lines). By a 2-day dark reaction after photolysis, the dashed spectrum is obtained.

protons of the ethoxy groups. We thus suppose that **3** is formed from **2** following the mechanism shown by scheme 2. Since the highly strained enone part of **2** is expected to be very reactive, addition of ethanol to this compound may give rise to the formation of **4**, releasing the strain of the exomethylene group followed by the 1,5-hydrogen-atom shift finally yielding **5**. After this, addition of ethanol to **5** may produce strain-free **3**. Based on the well-known fact that anthrahydroquinone and its derivatives are fluorescent, we have assigned the dashed spectrum shown in figure 2 or **3** to the absorption of **3** because its fluorescence excitation spectrum is identical with the absorption spectra shown by the dashed lines in figures 2 and 3.

On keeping the sample solution in the dark for a long time, the NMR signals due to **3** disappear with the accompanying appearance of not only the signals due to ethanol but also those due to recovered CHAQ. This thermal reversion may be interpreted in terms of ethanol elimination from **3**.

4. Steady-state photolysis of CHAQ in benzene at room temperature

As shown in figure 5, 405-nm steady-state photolysis of CHAQ in benzene at room temperature reveals the spectral change somewhat different in form from that obtained in EPA at room temperature (cf. figure 4). After photolysis, a 1-day dark reaction causes spectral decrement and increment due to the product and the reactant, respectively (cf. dashed line). In [$^2\text{H}_6$] benzene, photolysis of CHAQ is also performed and then the results of ^1H NMR analysis obtained are as follows: 6.51 ppm (*d*, 1H, *J* = 9.9 Hz), 5.50 ppm (*d*, 1H, *J* = 9.9 Hz) and 5.03 ppm (*dd*, 1H, *J* = 5.4 and 11.7 Hz). Although product identification based on the NMR signals alone is not satisfactory enough, we believe that at least a methylene cyclohexene moiety really exists. We thus tentatively propose that **6** is produced via **2**.

Since similar NMR signals are observed even in EPA, **6** in this solvent may be a minor product. This is supported by the following facts: (1) The dotted spectrum shown in figure 2 can be interpreted in terms of the superposition of the absorption due to **3** on that due to **6**. (2) The photochemistry of CHAQ at room temperature in EPA is found to be identical to that in ethanol. After photolysis in ethanol, we thus have changed the solvent to benzene and found that the absorption spectrum of **3** changes very slowly to that of **6** and reverted CHAQ.

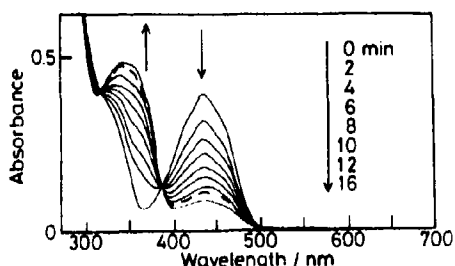
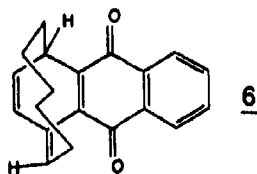


Figure 5. Spectral change caused by 405-nm steady-state photolysis of CHAQ in benzene at room temperature (full lines). By a 1-day dark reaction after photolysis, the dashed spectrum is obtained.



5. Conclusions

Although [6]-1,4-cyclophaneanthraquinone (CHAQ) is a sterically strained compound, the photoinduced intramolecular hydrogen-atom abstraction is identical with that of several strain-free anthraquinones with a benzylic methylene (Gritsan *et al* 1990, 1991). In the latter cases, however, 9-hydroxy-1,10-anthaquinone-1-methides produced via the 1,4-biradicals easily revert to the original anthraquinones. In this sense, we believe that the photochemistry of CHAQ presented here is very unique and interesting.

Acknowledgement

We acknowledge the generous financial support of Nagase Science and Technology Foundation.

References

- Gritsan N P, Khmelinski I V and Usov O M 1991 *J. Am. Chem. Soc.* **113** 9615
- Gritsan N P, Shvartsberg E M, Russikh V V and Khmelinski I V 1990 *Russ. J. Phys. Chem.* **64** 1660
- Liebe J, Wolf C, Krieger C, Weis J and Tochtermann W 1985 *Chem. Ber.* **118** 4144
- Miki S, Abdel-Latif F M, Nakayama T and Hamanoue K 1992a *Abstr. Symp. Photochem. Jpn.*, p. 337
- Miki S, Kagawa H, Matsuo K, Kobayashi O, Yoshida M and Yoshida Z 1992b *Tetrahedron* **48** 1567
- Miki S, Matsuo K, Yoshida M and Yoshida Z 1988 *Tetrahedron Lett.* **29** 2211
- Miki S, Shimizu R and Nakatsuji H 1992c *Tetrahedron Lett.* **33** 953
- Nakayama T, Yamaguchi T, Ushida K, Hamanoue K, Miki S, Matsuo K and Yoshida Z 1988 *Chem. Phys. Lett.* **148** 259
- Sammes P G and Dodsworth D J 1979 *J. Chem. Soc., Chem. Commun.* 33

SUBJECT INDEX

AMI	
AMI heats of formation for the reaction of alcohols with a series of β -lactams and aza- β -lactams: Design of novel β -lactamase inactivators	131
Ablation	
Laser ablation of inorganic and organic materials	715
Laser degradation of pollutants: Polychlorobiphenyls, triazines and polycyclic aromatic hydrocarbons	735
Acetonitrile	
Near infrared spectral studies on interactions of CH_3 groups with halide ions	71
Acid-alkaline transition in heme proteins	
Circular dichroism studies of acid=alkaline transition in heme proteins	167
Alkyl group lability	
Comparison of alkyl group labilities in O- and N-alkylated DNA bases: A semiempirical molecular orbital study	253
Alkylated DNA bases	
Comparison of alkyl group labilities in O- and N-alkylated DNA bases: A semiempirical molecular orbital study	253
Amine-assisted triplet formation of haloanthracenes	
Amine-assisted photochemical dehalogenation of haloanthracenes (9-halo and 9,10-dihalo compounds) and their triplet formation	747
Amine-mediated proton shift	
Photocyclization of arylethylenes: Mechanism and scope of the reactions	603
Amino acids	
Formation constants of ternary complexes of Cu(II), Ni(II), Co(II), Mn(II) and Zn(II) with phenylhydrazones and amino acids	219
Ammonium aryldithiocarbamate	
A convenient preparation of 2-thioxo-4(3 <i>H</i>)-quinazolinones	11
Amplified spontaneous emission	
The spectral, lifetime and laser activity of 2,5-bis(1-naphthyl)vinylpyrazine and 2,5-bis(2-naphthyl)vinylpyrazine	651
Anion-molecular interactions	
Near infrared spectral studies on interactions of CH_3 groups with halide ions	71
Anisotropy	
Studies on mixed mesomorphism: Determination of latent transition temperature (LTT) by extrapolation	209
Anthranilic acid	
A convenient preparation of 2-thioxo-4(3 <i>H</i>)-	
quiazolinones	11
Antimicrobial activity	
Synthesis and antimicrobial activity of 1-benzamido-5-hydroxyindole derivatives	189
Aquatic	
Kinetics of sunlight photodegradation of 2,3,4,7,8-pentachlorodibenzofuran in natural water	399
Aromatic sulphoxides	
Pulse radiolytic of some aromatic sulphoxides in aqueous solutions	141
Artificial photosynthesis	
Strategies for solar fuel generation	315
Aryl phenylsulfonylacetone	
Preparation of some organic precursors via photolytic demetallation of their iron complexes	575
Arylethylenes	
Photocyclization of arylethylenes: Mechanism and scope of the reactions	603
Asymmetric induction	
Light-induced cycloadditions of captodative alkenes	583
Au electrode	
Investigations on adsorption of paraquat radical cations on gold electrodes by voltammetry coupled with laser Raman spectroscopy	287
Aza-β-lactam	
AMI heats of formation for the reaction of alcohols with a series of β -lactams and aza- β -lactams: Design of novel β -lactamase inactivators	131
1-Benzamido-5-hydroxyindole derivatives	
Synthesis and antimicrobial activity of 1-benzamido-5-hydroxyindole derivatives	189
Benzocyclobutene	
Sunlight-initiated cycloaddition reactions of the benzene ring	555
Benzooquinone	
Time-domain electron-spin-resonance studies on hydrogen atom transfer to photoexcited quinones	273
2,2'-Biquinoline	
Room temperature phosphorescence of 2,2'-biquinoline in polymeric matrices	659
BiSrCaCuO thin films	
Pulsed-laser ablation and deposition of superconducting BiSrCaCuO thin films	709
Bimetallic cluster	
Gold-platinum bimetallic cluster catalysts for visible light-induced hydrogen production from water	343

Binding	
Binding of rose bengal onto bovine serum albumin	279
Binuclear species	
Kinetics and mechanism of the reversible formation of the binuclear species between pyridine-2-carboxylato(pentaammine) cobalt(III) and cobalt(II) in aqueous solution	245
Biologically active	
Studies on organometallic compounds: An approach towards characterization of structure and activity of triorganostannylyl 2-(aryloazo)-benzenecarboxylates in relation to the bacterial cell wall	183
Biologically active substances	
Syntheses of substituted isoxazolines using Vilsmeier Haack reagent	19
2,2'-Bipyridyl	
Spectral and thermal studies on mixed ligand complexes of zinc(II) and cadmium(II) with diethyldithiocarbamate and 2,2'-bipyridyl/1,10-phenanthroline	87
Biradical	
Is tetramethyleneethane a ground state triplet?	53
Birch reduction	
Investigations on C ₇₀ H ₃₀ obtained by the Birch reduction of C ₇₀	303
Bivalent metal ions	
Chelation behaviour of biologically active <i>o</i> -hydroxy naphthaldehyde derivatives with bivalent metal ions in different solvents: A potentiometric study	103
Bovine serum albumin	
Binding of rose bengal onto bovine serum albumin	279
Bromamine-T	
Kinetics of oxidation of glycylglycine by bromamine-T in acid medium	63
Bromate driven oscillations	
New uncatalysed bromate-driven oscillators: The Rhodamine B base/Rhodamine B-BrO ₃ -H ₂ SO ₄ system	125
Bulk reactions	
Study of interaction between microclusters of silver and arsenious trisulphide	25
CIDEP	
Time-domain electron-spin-resonance studies on hydrogen atom transfer to photoexcited quinones	273
CIDNP	
Electron-nuclear cross-relaxation effect on the photochemical reaction of benzaldehyde as studied by CIDNP and DNP	629
CIDNP detected ESR	
Electron-nuclear cross-relaxation effect on the	
photochemical reaction of benzaldehyde as studied by CIDNP and DNP	629
CPK space-filling models	
Studies on organometallic compounds: An approach towards characterisation of structure and activity of triorganostannylyl 2-(aryloazo)-benzenecarboxylates in relation to the bacterial cell wall	183
C₇₀	
Investigations on C ₇₀ H ₃₀ obtained by the Birch reduction of C ₇₀	303
C₇₀H₃₀	
Investigations on C ₇₀ H ₃₀ obtained by the Birch reduction of C ₇₀	303
Cadmium(II)	
Spectral and thermal studies on mixed ligand complexes of zinc(II) and cadmium(II) with diethyldithiocarbamate and 2,2'-bipyridyl/1,10-phenanthroline	87
Carbondioxide	
Kinetics of the reversible uptake of carbon dioxide and sulphur dioxide by the <i>cis</i> -(hydroxo)(imidazole)bis(ethylenediamine)cobalt(III) ion in aqueous medium. A comparative study	225
Catalysts	
Gold-platinum bimetallic cluster catalysts for visible light-induced hydrogen production from water	343
CdS	
Photoinduced charge transfer processes in ultra-small semiconductor clusters. Photophysical properties of CdS clusters in nafion membrane	505
Centralized electrolytic generation	
Strategies for solar generation	315
Charge separation	
Photoinduced charge separation by ruthenium(II) photosensitizers	487
Charge-transfer	
Cis-trans photoisomerization of 1,2-diarylethylenes: Effect of charge transfer interactions	475
Charge transfer absorption	
Factors which determine the efficiency of sensitized singlet oxygen production	685
Charge-transfer complexes	
Graph-theoretical calculation of products of eigen coefficients: Some application to charge-transfer complexes	111
Charge-transfer interactions	
Molecular structure of electron donor-acceptor complexes of metallotetr phenylporphyrins with trinitrobenzene	161
Chemical reaction	
Momentum space investigation of C _{2e} dissociation of water	149
Chemical reaction	
Reflectivity as a probe for chemical reactions	671

Chemisorption	
Study of interaction between microclusters of silver and arsenious trisulphide	25
Circular dichroism	
Circular dichroism studies of acid=alkaline transition in hemoproteins	167
Cis-(hydroxo) (imidazole)bis(ethylenediamine)	
Cobalt(II)	
Kinetics of the reversible uptake of carbon dioxide and sulphur dioxide by the <i>cis</i> -(hydroxo) (imidazole)bis(ethylenediamine)cobalt(III) ion in aqueous medium. A comparative study	225
Closed-shell metal ion	
Spectroscopic and magnetic studies of mixed-ligand complexes of zinc(II)	611
Clusters	
Study of interaction between microclusters of silver and arsenious trisulphide	25
Laser ablation of inorganic and organic materials	715
Cobalt(II)	
Kinetics and mechanism of the reversible formation of the binuclear species between pyridine-2-carboxylato(pentaammine) cobalt(III) and cobalt(II) in aqueous solution	245
Cobalt(III)-dioximes	
Iron(II) reduction of halogenopyridinecarboxylatocobalt(III)-dioxide complexes: Kinetics and mechanism	95
Computer molecular model	
Studies on organometallic compounds: An approach towards characterisation of structure and activity of triorganostannyl 2-(arylazo)benzenecarboxylates in relation to the bacterial cell wall	183
Conformational changes	
Binding of rose bengal onto bovine serum albumin	279
Coordinated picolinate	
Kinetics and mechanism of the reversible formation of the binuclear species between pyridine-2-carboxylato(pentaammine)cobalt(III) and cobalt(II) in aqueous solution	245
Critical points	
Momentum space investigation of C_2 , dissociation of water	149
Cross relaxation	
Electron-nuclear cross-relaxation effect on the photochemical reaction of benzaldehyde as studied by CIDNP and DNP	629
Cross-linking	
Emission characteristics of laser dyes C1 and Rh6G in cross-linked polyvinyl alcohol solutions	47
Curtius reaction	
Complexes of N,S donor ligands. Co ^{II} , Co ^{III} , Mn ^{III} , Fe ^{III} and Pd ^{II} complexes of 1,2-di(<i>p</i> -amino-	
phenylthio)ethane: Synthesis, characterisation and reactions	1
Cyclodextrin complexes	
Photosensitizing properties of squaraine dyes	513
Cyclic voltammetry	
Investigations on adsorption of paraquat radical cations on gold electrodes by voltammetry coupled with laser Raman spectroscopy	287
Cyclophenanthraquinone	
Photochemical reaction of [6]-1,4-cyclophenanthraquinone	797
DNP	
Electron-nuclear cross-relaxation effect on the photochemical reaction of benzaldehyde as studied by CIDNP and DNP	629
Damage to photoocured surfaces	
Applied photochemistry in dental science	405
Degradation	
Purification of drinking water by irradiation: A review	373
Laser degradation of pollutants. Polychlorobiphenyls triazines and polycyclic aromatic hydrocarbons	735
Dense dipolar liquids	
Dielectric friction and solvation dynamics: Novel results on relaxation in dipolar liquids	79
Dental materials	
Applied photochemistry in dental science	405
Diamino-dithioether	
Complexes of N,S donor ligands. Co ^{II} , Co ^{III} , Mn ^{III} , Fe ^{III} and Pd ^{II} complexes of 1,2-di(<i>p</i> -amino-phenylthio)ethane: Synthesis, characterisation and reactions	1
Diarylethylenes	
Cis-trans photoisomerization of 1,2-diarylethylenes: Effect of charge transfer interactions	475
Dichlorobenzoquinone	
Studies of photochemical reaction by CIDNP-detected ESR spectrum	619
Diethylidithiocarbamate	
Spectral and thermal studies on mixed ligand complexes of zinc(II) and cadmium(II) with diethylidithiocarbamate and 2,2-biphenyl-1,10-phenanthroline	87
Diglycine	
Kinetics of oxidation of glycylglycine by bromamine-T in acid medium	63
9,10-Dihalo and 9-halo compounds	
Amine-assisted photochemical dehalogenation of haloanthracenes (9-halo and 9,10-dihalo compounds) and their triplet formation	567
1,4-Dihydro-1,4-ethanonaphthalenes	
Light induced cycloadditions of captodative alkenes	583

Dimethyl sulphoxide	
Near infrared spectral studies on interactions of CH ₃ groups with halide ions	71
Diolefinic dyes	
The spectral, lifetime and laser activity of 2,5-bis(1-naphthyl)vinylpyrazine and 2,5-bis(2-naphthyl)vinylpyrazine	651
Dipolar liquids	
Molecular theory of ion solvation dynamics in water, acetonitrile and methanol: A unified microscopic description of collective dynamics in dipolar liquids	295
Disproportionation mechanism	
Electron transfer through vesicle membranes: Mechanistic ambiguities	539
Dissociation probability	
Intramolecular and dissociation dynamics of triatomic molecules: Some results for HCN and CO ₂	677
Distannanes	
Applied photochemistry for free radical organic synthesis by means of distannane reagents	591
Donor-acceptor linked compound	
Photoinduced ET and back ET in bimetalated compounds of Ru(II)-Rh(III) and Ru(II)-Co(III)	495
Dynamic nuclear polarization	
Studies of photochemical reaction by CIDNP-detected ESR spectrum	619
Eigen coefficients	
Graph-theoretical calculation of products of eigen coefficients: Some application to charge-transfer complexes	111
Electron diffraction	
Study of interaction between microclusters of silver and arsenious trisulphide	25
Electron donor-acceptor complexes	
Molecular structure of electron donor-acceptor complexes of metallo-tetraphenylporphyrins with trinitrobenzene	161
Electron momentum density	
Momentum space investigation of C ₂ , dissociation of water	149
Electron relays	
Light-induced hydrogen production using waste compounds as sacrificial electron donors	353
Electron spin polarization	
Time-domain electron-spin-resonance studies on hydrogen atom transfer to photoexcited quinones	273
Electron transfer	
Gold-platinum bimetallic cluster catalysts for visible light-induced hydrogen production from water	343
Light-induced hydrogen production using waste compounds as sacrificial electron donors	353
Light-induced electron transfer in simple and supramolecular Ru-polypyridine complexes	435
Photoinduced charge separation by ruthenium(II) photosensitizers	487
Photoinduced ET and back ET in bimetalated compounds of Ru(II)-Rh(III) and Ru(II)-Co(III)	495
Electron transfer through vesicle membranes: Mechanistic ambiguities	539
Synthetic chemistry via radicals generated by photoinduced electron transfer	563
Electronic structure	
Is tetramethyleneethane a ground state triplet?	53
Emission lifetimes	
Photoinduced charge transfer processes in ultra-small semiconductor clusters. Photophysical properties of CdS clusters in nafion membranes	505
Enzyme inhibitor	
AM1 heats of formation for the reaction of alcohols with a series of β -lactams and azu- β -lactams: Design of novel β -lactamase inactivators	131
Ethyl arylcyanoacetate	
Preparation of some organic precursors via photolytic demetallation of their iron complexes	575
Exciplex mechanisms	
Exciplex mechanism of fluorescence quenching in polar media	637
Excited state basicities	
Basicity of some proto-typical carbonyls in the ground and some low-lying excited states: Application of the orthogonal gradient method of orbital optimization in an INDO-MC SCF framework - I	195
Excited-state electron transfer	
Exciplex mechanism of fluorescence quenching in polar media	637
Excited-state lifetimes	
The spectral, lifetime and laser activity of 2,5-bis(1-naphthyl)vinylpyrazine and 2,5-bis(2-naphthyl)vinylpyrazine	651
Exposed residues	
Binding of rose bengal onto bovine serum albumin	279
Fenton reaction	
Heterogeneous and homogeneous photoassisted wastewater treatment	393
Fermi correlation	
Basicity of some proto-typical carbonyls in the ground and some low-lying excited states: Application of the orthogonal gradient method of orbital optimization in an INDO-MC-SCF framework - I	195

Fluorescence	
Emission characteristics of laser dyes C1 and RhG in cross-linked polyvinyl alcohol solutions	47
Fluorescence quenching	
Exciplex mechanism of fluorescence quenching in polar media	637
Fluorescence quantum yields	
The spectral, lifetime and laser activity of 2,5-bis(1-naphthyl)vinylpyrazine and 2,5-bis(2-naphthyl)vinylpyrazine	651
Free radical synthesis	
Applied photochemistry for free radical organic synthesis by means of distannane reagents	591
Fullerene	
Investigations on $C_{70}H_{30}$ obtained by the Birch reduction of C_{70}	303
Graphs	
Graph-theoretical calculation of products of eigen coefficients: Some application to charge-transfer complexes	111
Ground state interactions	
Photophysics of pyrene-substituted oligosilanes	451
H-bonded polymeric matrices	
Room temperature phosphorescence of 2,2'-biquinoline in polymeric matrices	659
Halanthracene radical anions	
Amine-assisted photochemical dehalogenation of halanthracenes (9-halo and 9,10-dihalo compounds) and their triplet formation	567
Hydrogen	
Photobiotechnology: Application of photosynthesis to the production of renewable fuels and chemicals	333
Hydrogen atom transfer	
Hydrogen atom and proton-induced electron transfer reactions via triplet exciplexes	747
$H_2^{18}O$ production	
Gold-platinum bimetallic cluster catalysts for visible light-induced hydrogen production from water	343
Hydroxyalkyl radical	
Time-domain electron-spin-resonance studies on hydrogen atom transfer to photoexcited quinones	273
Hydroxyl radicals	
Heterogeneous and homogeneous photoassisted wastewater treatment	393
α-Hydroxy naphthaldehyde derivatives	
Chelation behaviour of biologically active α -hydroxy naphthaldehyde derivatives with bivalent metal ions in different solvents: A potentiometric study	103
Intercalation	
Studies on organometallic compounds: An approach towards characterisation of structure and activity of (norganostannyl 2-(arylazo)benzenecarboxylates in relation to the bacterial cell wall	183
Intramolecular dynamics	
Intramolecular and dissociation dynamics of triatomic molecules. Some results for HCN and CO ₂	677
Intramolecular hydrogen-atom abstraction	
Photochemical reaction of [6]-1,4-cyclophenanthraquinone	797
Ion solvation dynamics	
Molecular theory of ion solvation dynamics in water, acetonitrile and methanol. A unified microscopic description of collective dynamics in dipolar liquids	295
Ionic mobility	
Dielectric friction and solvation dynamics. Novel results on relaxation in dipolar liquids	79
Iron(II) reduction	
Iron(II) reduction of halogenopyridinecarboxylato cobalt(III)-dioxime complexes: Kinetics and mechanism	95
Isoniazide	
Synthesis and structural investigation of some mixed-ligand selenito complexes of cobalt(II)	173
Isoxazolines	
Syntheses of substituted isoxazolines using Vilsmeier-Haack reagent	19
J-aggregate	
Primary photophysical processes in J-aggregates of spectral sensitizers	783
Kinetics	
Kinetics of oxidation of glycylglycine by bromamind-T in acid medium	53
Kinetics of the reversible uptake of carbon dioxide and sulphur dioxide by the cis-(hydroxo)(imidazole)bis(ethylenediamine)cobalt(III) ion in aqueous medium. A comparative study	225
Kinetics and mechanism of the reversible formation of the binuclear species between pyridine-2-carboxylato(pentaammine)cobalt(III) and cobalt(II) in aqueous solution	245
Kinetics of charge transfer reactions in photoelectrochemical cells	463
β-Lactamase	
AM1 heats of formation for the reaction of alcohols with a series of β -lactams and aza- β -lactams: Design of novel β -lactamase inactivators	131

- Langmuir-Blodgett assemblies**
 Photoinduced electron transfer reactions of *trans*-stilbene surfactants in Langmuir-Blodgett assemblies and phospholipid bilayers 327
- Laser degradation**
 Laser degradation of pollutants. Polychlorophenyl triazines and polycyclic aromatic hydrocarbons 715
- Laser dye**
 Emission characteristics of laser dyes Cl⁺ and Rh6G in cross-linked polyvinyl alcohol solutions 47
- Laser flash photolysis**
 Hydrogen atom and proton-induced electron transfer reactions via triplet exciplexes 242
- Laser Raman spectroscopy**
 Investigations on adsorption of paraquat radical cations on gold electrodes by voltammetry coupled with laser Raman spectroscopy 287
- Lasers**
 Laser ablation of inorganic and organic materials 715
- Lattice contraction**
 Study of interaction between microclusters of silver and arsenous tri sulphide 25
- Ligand-ligand charge-transfer state**
 Spectroscopic and magnetic studies of mixed ligand complexes of zinc(II) 611
- Liquid crystal**
 Studies on mixed mesomorphism. Determination of latent transition temperature (LTT) by extrapolation 299
- U(III) aminopolycarboxylate-resorcinol orcinol phloroglucinol**
 Periodicity in the formation constant values of lanthanide(III)aminopolycarboxylateresorcinol orcinol phloroglucinol mixed ligand complexes 185
- Local modes**
 Near infrared spectral studies on interactions of CH₃ groups with halide ions 71
- Lyapunov exponent**
 Intramolecular and dissociation dynamics of triatomic molecules. Some results for HCN and CO₂ 677
- MNDO**
 Investigations on C₆₀H₆₀ obtained by the Birch reduction of C₆₀ 401
- MO calculations**
 Is tetramethyleneethane a ground state triplet? 53
- Macrocyclic cryptand**
 Template synthesis of a macrocyclic cryptand having mixed cations via [2+1] Schiff base condensation 215
- Macrocycle**
 Complexes of N,S donor ligands. Cu^{II}, Co^{II}, Mn^{II}, Fe^{II} and Pd^{II} complexes of 1,2-diaminophenylmethane. Synthesis, characterization and reactions 1
- Maleic acid derivatives**
 Formation of phosphoranes from methyl maleanilates and related substrates with triphenylphosphine and their Wittig olefinations with aromatic aldehydes 265
- Mass spectra**
 Synthesis and antimicrobial activity of 1-benzamido-5-hydroxyindole derivatives 189
- Membrane**
 Electron transfer through vesicle membranes. Mechanistic ambiguities 510
- Mesogen**
 Studies on mixed mesomorphism. Determination of latent transition temperature (LTT) by extrapolation 299
- Metallo-tetraphenylporphyrins**
 Molecular structure of electron donor-acceptor complexes of metallo-tetraphenylporphyrins with trinitrobenzene 361
- Methyl iodide**
 Near infrared spectral studies on interactions of CH₃ groups with halide ions 71
- Microscopic theory of solvation dynamics**
 Molecular theory of ion solvation dynamics in water, acetonitrile and methanol. A unified microscopic description of collective dynamics in dipolar liquids 295
- Mixed ligand complexes**
 Spectral and thermal studies on mixed ligand complexes of zinc(II) and cadmium(II) with diethylthiocarbamate and 2,2'-bipyridyl 1,10-phenanthroline 67
- Formation constants of ternary complexes of Cu(II), Ni(II), Co(II), Mn(II) and Zn(II) with phenylhydrazines and amino acids 219
- Mixed mesomorphism**
 Studies on mixed mesomorphism. Determination of latent transition temperature (LTT) by extrapolation 299
- Mixed-ligand cobalt-complexes**
 Synthesis and structural investigation of some mixed-ligand clathro complexes of cobalt(II) 173
- Molecular devices**
 Supramolecular photochemistry. Luminescent and redox active dendritic polynuclear metal complexes 423
- Molecular orbital calculations**
 Comparison of alkyl group labilities in O- and N-alkylated DNA bases. A semiempirical molecular orbital study 251

Momentum space		
Momentum space investigation of C_{1s} dissociation of water	149	
Monotropy		
Studies on based monomorphism Determination of latent transition temperature (LTT) by extrapolation	209	
NMR spectroscopy		
Circular dichroism studies of acid-base-alanine transition in hemoproteins	161	
$\pi\pi^*$ states of carbonyl		
Basicity of some proto-typical carbonyls in the ground and some low-lying excited states		
Application of the orthogonal gradient method of orbital optimization in an INDO-MC-SCF framework	195	
Nafion		
Photoinduced charge transfer processes in ultra-small semiconductor clusters. Photophysical properties of CdS clusters in nafion membranes	405	
Near-UV CD		
Binding of <i>cocc</i> bengal onto bovine serum albumin	279	
Nitromethane		
Near infrared spectral studies on interactions of CH_3 groups with halide ions	71	
Nuclear tunnelling		
Photoinduced ET and back-ET in bimetalated compounds of Ru(II)-Rh(II) and Ru(II)-Co(II)	495	
π -ZnO semiconductor		
Photoelectrochemistry of ZnO thin film electrode sensitized by an oxouranium (VI) complex in an acetonitrile photocell	235	
Optical absorption		
First photothermal deflection spectroscopy set-up in Egypt	695	
Optically-detected magnetic-resonance method		
Spectroscopic and magnetic studies of mixed-ligand complexes of zinc(II)	611	
Organometallics		
Studies on organometallic compounds: An approach towards characterisation of structure and activity of inorganostannyl 2-(aryloxy)benzenecarboxylates in relation to the bacterial cell wall	183	
Orthogonal gradient method		
Basicity of some proto-typical carbonyls in the ground and some low-lying excited states: Application of the orthogonal gradient method of orbital optimization in an INDO-MC-SCF framework	195	
Overtone spectra		
Near infrared spectral studies on interactions of		
CH ₃ groups with halide ions	71	
Oxidation		
Kinetics of oxidation of glycylglycine by bromine monoxide in acidic medium	63	
Oxygen		
Photobiotechnology: Application of photosynthesis to the production of renewable fuels and chemicals	313	
Oxygen quenching		
Factors which determine the efficiency of sensitized singlet oxygen production	485	
PEC cell		
Photoelectrochemistry of ZnO thin film electrode sensitized by an oxouranium (VI) complex in an acetonitrile photocell	235	
Paracetamol		
Investigations on adsorption of paracetamol radical cations on gold electrodes by voltammetry coupled with laser Raman spectroscopy	287	
Percus-Yevick (PY) and hypernetted-chain (HNC) closures		
SSOZ-HNC and SSOZ-PY integral equation studies of the structure of three-site polar fluids	31	
Periodicity in formation constants		
Periodicity in the formation constant values of lanthanide(III)aminopolycarboxylateresorcinol acetol phloroglucinol mixed ligand complexes	155	
Phase transition		
Reflectivity as a probe for chemical reactions	671	
1,10-phenanthroline		
Spectral and thermal studies on mixed ligand complexes of zinc(II) and cadmium(II) with diethylthiocarbamate and 2,2'-bipyridyl/1,10-phenanthroline	87	
Phenylhydrazones		
Formation constants of ternary complexes of Cu(II), Ni(II), Co(II), Mn(II) and Zn(II) with phenylhydrazones and amino acids	219	
Phospholipid bilayers		
Photoinduced electron transfer reactions of <i>trans</i> -stilbene surfactants in Langmuir-Blodgett assemblies and phospholipid bilayers	527	
Phosphorescence		
Spectroscopic and magnetic studies of mixed-ligand complexes of zinc(II)	611	
Photo-induced hydrogen production		
Light-induced hydrogen production using waste compounds as sacrificial electron donors	353	
Photobiotechnology		
Photobiotechnology: Application of photosynthesis to the production of renewable fuels and chemicals	343	

Photochemical dehalogenation of haloanthracenes by amines	
Amine-assisted photochemical dehalogenation of haloanthracenes (9-halo and 9,10-dihalo compounds) and their triplet formation	567
Photochemistry	
Supramolecular photochemistry. Luminescent and redox active dendritic polynuclear metal complexes	421
Photoproduced charge separation by ruthenium(II) photosensitizers	487
Synthetic chemistry via radicals generated by photoproduced electron transfer	563
Photochemistry of squaraine dyes	
Photosensitizing properties of squaraine dyes	513
Photocuring of polymeric materials	
Applied photochemistry in dental science	405
Photocyclization	
Photocyclization of arylethylenes. Mechanism and scope of the reactions	603
Photocycloaddition	
Sunlight-initiated cycloaddition reactions of the benzene ring	555
Light-induced cycloadditions of captodative alkenes	583
Photodegradation	
Kinetics of sunlight photodegradation of 2,3,4,7,8-pentachlorodibenzofuran in natural water	399
Photoinduced electron transfer	
Photoinduced electron transfer reactions of <i>trans</i>-stilbene surfactants in Langmuir-Blodgett assemblies and phospholipid bilayers	527
Photoinitiating system	
Applied photochemistry in dental science	405
Photoisomerization	
Cis-trans photoisomerization of 1,2-diarylethylenes: Effect of charge transfer interactions	475
Photolysis	
Purification of drinking water by irradiation. A review	373
Preparation of some organic precursors via photolytic demetallation of their iron complexes	575
Photooxidation	
Heterogeneous and homogeneous photoassisted wastewater treatment	393
Photophysics	
Supramolecular photochemistry. Luminescent and redox active dendritic polynuclear metal complexes	421
Photosensitization	
Photoelectrochemistry of ZnO thin film electrode sensitized by an oxouranium(IV) complex in an acetonitrile photocell	235
Photosensitizers	
Photoinduced charge separation by ruthenium(II) photosensitizers	487
Photosynthesis	
Photobiotechnology: Application of photosynthesis to the production of renewable fuels and chemicals	333
Photothermal deflection spectroscopy	
First photothermal deflection spectroscopy set-up in Egypt	695
Photovoltaic energy	
Strategies for solar fuel generation	315
Platinized chloroplasts	
Photobiotechnology: Application of photosynthesis to the production of renewable fuels and chemicals	333
Platinum	
Gold-platinum bimetallic cluster catalysts for visible light-induced hydrogen production from water	343
Poincaré sections	
Intramolecular and dissociation dynamics of triatomic molecules. Some results for HCN and CO₂	677
Polar media	
Exciplex mechanism of fluorescence quenching in polar media	637
Pollutants	
Purification of drinking water by irradiation. A review	373
Poly(4-vinylpyridine) complexes	
Photosensitizing properties of squaraine dyes	513
Polychlorinated dibenzofurans	
Kinetics of sunlight photodegradation of 2,3,4,7,8-pentachlorodibenzofuran in natural water	399
Polychlorobiphenyl	
Laser degradation of pollutants: Polychlorobiphenyls, triazines and polycyclic aromatic hydrocarbons	735
Polycyclic aromatic hydrocarbons	
Photocyclization of arylethylenes. Mechanism and scope of the reactions	603
Laser degradation of pollutants: Polychlorobiphenyls, triazines and polycyclic aromatic hydrocarbons	735
Polystyrene-supported distannane	
Applied photochemistry for free radical organic synthesis by means of distannane reagents	591
Polyvinyl alcohol	
Emission characteristics of laser dyes C1 and Rh6G in cross-linked polyvinyl alcohol solutions	47
Propan-1-one derivatives	
Syntheses of substituted isoxazolines using Vilsmeyer-Haack reagent	19
Properties of solid/air interfaces	
First photothermal deflection spectroscopy set-up in Egypt	695
Proton-induced electron transfer	
Hydrogen atom and proton-induced electron	

transfer reactions via triplet exciplexes	747	Ruthenium (II) complexes	
Pulse radiolysis		Photoinduced charge separation by ruthenium(II)	
Pulse radiolysis of some aromatic sulphoxides in aqueous solutions	141	photosensitizers	487
Pulsed-laser ablation		S _n Ar	
Pulsed-laser ablation and deposition of superconducting BiSrCaCuO thin films	709	Preparation of some organic precursors via photolytic demetallation of their iron complexes	575
Pyrene substituted oligosilanes		s ² -valence electrons	
Photophysics of pyrene substituted oligosilanes	451	Application of the three-level model: Rise and decay kinetics of the temperature-dependent emission of metal ions with s ² -valence electron configuration	667
Pyridinecarboxylic acids		Selenito	
Iron(II) reduction of halogenopyridinecarboxylato cobalt(III)-dioxime complexes: Kinetics and mechanism	95	Synthesis and structural investigation of some mixed-ligand selenito complexes of cobalt(II)	173
Quadricyclane		Semiconductor clusters	
Studies of photochemical reaction by CIDNP-detected ESR spectrum	619	Photoinduced charge transfer processes in ultrasmall semiconductor clusters. Photophysical properties of CdS clusters in nafion membrane	505
Radical cation		Semiconductor-electrodes	
Investigations on adsorption of paraquat radical cations on gold electrodes by voltammetry coupled with laser Raman spectroscopy	287	Kinetics of charge transfer reactions in photo-electrochemical cells	463
Radical ions		Semiconductor-particles	
Cis-trans photoisomerization of 1,2-diarylethylenes. Effect of charge transfer interactions	475	Kinetics of charge transfer reactions in photo-electrochemical cells	463
Radicals		Semiquinone radical	
Light-induced hydrogen production using waste compounds as sacrificial electron donors	353	Time-domain electron-spin-resonance studies on hydrogen atom transfer to photoexcited quinones	273
Synthetic chemistry via radicals generated by photoinduced electron transfer	563	Silicon-bridged compounds	
Radiolysis		Photophysics of pyrene substituted oligosilanes	451
Purification of drinking water by irradiation: A review	373	Singlet oxygen yields	
Reactive polymers		Factors which determine the efficiency of sensitized singlet oxygen production	35
Applied photochemistry for free radical organic synthesis by means of distannane reagents	591	Singlet-triplet gap	
Rearrangement energy		Is tetramethyleneethane a ground state triplet?	53
Photoproduced ET and back-ET in bimetalated compounds of Ru(II)-Rh(III) and Ru(II)-Co(III)	495	Site-site Ornstein-Zernike (SSOZ) equation	
Reflectivity		SSOZ-HNC and SSOZ-PY integral equation studies of the structure of three-site polar fluids	31
Reflectivity as a probe for chemical reactions	671	Site-site distribution functions	
Relay sensitizer		SSOZ-HNC and SSOZ-PY integral equation studies of the structure of three-site polar fluids	31
Light-induced hydrogen production using waste compounds as sacrificial electron donors	353	Size quantization effect	
Rhodamine B base-BrO ₃ ⁻ -H ₂ SO ₄		Photoinduced charge transfer processes in ultrasmall semiconductor clusters. Photophysical properties of CdS clusters in nafion membrane	505
New uncatalysed bromate-driven oscillators: The Rhodamine B base/Rhodamine B-BrO ₃ ⁻ -H ₂ SO ₄ system	125	Solar electrochemical generation	
Room-temperature phosphorescence		Strategies for solar fuel generation	315
Room temperature phosphorescence of 2,2'-biquinoline in polymeric matrices	659		
Rose bengal			
Binding of rose bengal onto bovine serum albumin	279		

Solar energy storage		
Gold-platinum bimetallic cluster catalysts for visible light-induced hydrogen production from water	343	
Solar fuel generation		
Strategies for solar fuel generation	315	
Solar furnace		
Reflectivity as a probe for chemical reactions	671	
Solvation dynamics		
Dielectric friction and solvation dynamics: Novel results on relaxation in dipolar liquids	79	
Solvation time correlation function		
Molecular theory of ion solvation dynamics in water, acetonitrile and methanol: A unified microscopic description of collective dynamics in dipolar liquids	295	
Space-resolved phototransformation		
What is new in stereophotolithography?	359	
Spectral sensitisation		
Primary photophysical processes in <i>J</i> -aggregates of spectral sensitizers	783	
Stabilised phosphoranes		
Formation of phosphoranes from methyl maleimides and related substrates with triphenylphosphine and their Wittig olefinations with aromatic aldehydes	265	
Stability constants		
Chelation behaviour of biologically active <i>o</i> -hydroxy naphthaldehyde derivatives with bivalent metal ions in different solvents. A potentiometric study	103	
Stannyl radicals		
Applied photochemistry for free radical organic synthesis by means of distannane reagents	591	
Stereophotolithography		
What is new in stereophotolithography?	359	
Structural parameters		
Molecular structure of electron donor-acceptor complexes of metallotetraphenylporphyrins with trinitrobenzene	161	
Structure factors		
SSO ₂ -HNC and SSO ₂ -PY integral equation studies of the structure of three-site polar fluids	31	
Styrene clusters		
Resonant two-photon ionization process of van der Waals adducts: Spectroscopy and reactivity of styrenes clustered with various molecules	773	
Sulphur dioxide		
Kinetics of the reversible uptake of carbon dioxide and sulphur dioxide by the <i>cis</i> -(hydroxol imidazole)bis(ethylenediamine)cobalt(III) ion in aqueous medium. A comparative study	225	
Sunlight		
Kinetics of sunlight photodegradation of 2,3,4,7,8-pentachlorodibenzofuran in natural water	399	
	Sunlight-initiated cycloaddition reactions of the benzene ring	555
Superconducting thin films		
Pulsed-laser ablation and deposition of superconducting BiSrCaCuO thin films	709	
Supermolecules		
Supramolecular photochemistry. Luminescent and redox active dendritic polynuclear metal complexes	421	
Superradiance		
Primary photophysical processes in <i>J</i> -aggregates of spectral sensitizers	783	
Supramolecular photochemistry		
Light-induced electron transfer in simple and supramolecular Ru-polypyridine complexes	435	
Supramolecular Ru-polypyridine complexes		
Light-induced electron transfer in simple and supramolecular Ru-polypyridine complexes	435	
Temperature-dependence of ET rate		
Photoinduced ET and back-ET in bimetalated compounds of Ru(II)-Rh(III) and Ru(II)-Co(III)	495	
Temperature-dependent emission of metal ions		
Application of the three-level model. Rise and decay kinetics of the temperature-dependent emission of metal ions with π^2 -valence electron configuration	667	
Template synthesis		
Template synthesis of a macrobicyclic cryptand having mixed donors via [2+1] Schiff base condensation	215	
Ternary complexes		
Formation constants of ternary complexes of Cu(II), Ni(II), Co(II), Mn(II) and Zn(II) with phenylhydrazones and amino acids	219	
Tetrahydrocyclobuta[<i>u</i>]naphthalenes		
Light-induced cycloadditions of captodative alkenes	583	
Tetramethyleneethane		
Is tetramethyleneethane a ground state triplet?	53	
Theoretical proton affinities		
Basicity of some proto-typical carbonyls in the ground and some low-lying excited states		
Application of the orthogonal gradient method of orbital optimization in an INDO MC SCF framework	195	
Thin film		
Photoelectrochemistry of ZnO thin film electrode sensitized by an oxouranium (VI) complex in an acetonitrile photocell	235	
Thin film deposition		
Laser ablation of inorganic and organic materials	715	

- Thin-film deposition**
 Pulsed-laser ablation and deposition of superconducting BiSrCaCuO thin films 709
- 2-Thioxo-4(3*H*)-quinazolinone**
 A convenient preparation of 2-thioxo-4(3*H*)-quinazolinones 11
- Three-level model**
 Application of the three-level model: Rise and decay kinetics of the temperature-dependent emission of metal ions with s^2 -valence electron configuration 667
- TiO₂-photosensitization**
 Photosensitizing properties of squaraine dyes 513
- Time domain ESR**
 Time-domain electron-spin-resonance studies on hydrogen atom transfer to photoexcited quinones 273
- Titanium dioxide**
 Heterogeneous and homogeneous photoassisted wastewater treatment 393
- Topography**
 Momentum space investigation of C₂, dissociation of water 149
- Transients**
 Pulse radiolysis of some aromatic sulphoxides in aqueous solutions 141
- Transition metal cryptates**
 Template synthesis of a macrobicyclic cryptand having mixed donors via [2 + 3] Schiff base condensation 215
- Trans-stilbene surfactants**
 Photoinduced electron transfer reactions of trans-stilbene surfactants in Langmuir-Blodgett assemblies and phospholipid bilayers 527
- Tri-*n*-butyl-tinnyl carboxylates**
 Studies on organometallic compounds: An approach towards characterisation of structure and activity of triorganostannyll 2-(arylazo)benzenecarboxylates in relation to the bacterial cell wall 183
- Triatomic molecules**
 Intramolecular and dissociation dynamics of triatomic molecules. Some results for HCN and CO₂ 677
- Triazine**
 Laser degradation of pollutants. Polychlorobiphenyls, triazines and polycyclic aromatic hydrocarbons 735
- Triethylammonium arylidithiocarbamate**
 A convenient preparation of 2-thioxo-4(3*H*)-quinazolinones 11
- Trinitrobenzene acceptor**
 Molecular structure of electron donor-acceptor complexes of metallophenylporphyrins with trinitrobenzene 161
- Triorganostannyl 2-(arylazo)benzenecarboxylates**
 Studies on organometallic compounds: An approach towards characterisation of structure and activity of triorganostannyll 2-(arylazo)benzenecarboxylates in relation to the bacterial cell wall 183
- Triplet exciplexes**
 Hydrogen atom and proton-induced electron transfer reactions via triplet exciplexes 747
- Triplet excited state**
 Light induced cycloadditions of captodative alkenes 583
- Triplet induction**
 Cis-trans photoisomerization of 1,2-diarylethylenes: Effect of charge transfer interactions 475
- Triplet naphthalene derivatives**
 Hydrogen atom and proton-induced electron transfer reactions via triplet exciplexes 747
- Triquinane**
 Sunlight-initiated cycloaddition reactions of the benzene ring 555
- Two-photon ionization**
 Resonant two-photon ionization process of van der Waals adducts: Spectroscopy and reactivity of styrenes clustered with various molecules 773
- Uncatalysed oscillation**
 New uncatalysed bromate-driven oscillators. The Rhodamine B base/Rhodamine B, BrO₃, H₂SO₄ system 125
- van der Waals adducts**
 Resonant two-photon ionization process of van der Waals adducts. Spectroscopy and reactivity of styrenes clustered with various molecules 771
- Viologen**
 Electron transfer through vesicle membranes 539
- Mechanistic ambiguities** 539
- Wastewater treatment**
 Heterogeneous and homogeneous photoassisted wastewater treatment 393
- Water purification**
 Purification of drinking water by irradiation. A review 373
- Water splitting**
 Photobiotechnology: Application of photosynthesis to the production of renewable fuels and chemicals 333
- Weighted least squares method**
 Cation behaviour of biologically active α -hydroxy naphthaldehyde derivatives with bivalent metal ions in different solvents: A potentiometric study 103

Wittig reactions	Zinc (II)
Formation of phosphoranes from methyl maleanilates and related substrates with triphenylphosphine and their Wittig olefinations with aromatic aldehydes	Spectral and thermal studies on mixed ligand complexes of zinc(II) and cadmium(II) with diethyldithiocarbamate and 2,2'-bipyridyl/1,10-phenanthroline
265	87
Zero-field splittings	Zinc(II) mixed-ligand complexes
Spectroscopic and magnetic studies of mixed-ligand complexes of zinc(II)	Spectroscopic and magnetic studies of mixed-ligand complexes of zinc(II)
611	611

AUTHOR INDEX

- Abd-El-Aziz Alaa S
Preparation of some organic precursors via photolytic demetallation of their ion complexes 575
- Abdel-Latif F M
see Miki Sadao 797
- Abdel Mottaleb M S A
Foreword 311
- Abdulkhadar M
Study of interaction between microclusters of silver and arsenious trisulphide 25
- Acharya A N
*Kinetics of the reversible uptake of carbon dioxide and sulphur dioxide by the *cis*-(hydroxo)(imidazole)*bis*(ethylenediamine)cobalt(III) ions in aqueous medium. A comparative study* 225
- Aizawa T
see Meng Q 619
- Al-Qaradawi S Y
Sunlight-initiated cycloaddition reactions of the benzene ring 555
- Albert I D L
see Chakrabarti Aparna 53
- Albini A
Synthetic chemistry via radicals generated by photoinduced electron transfer 563
- Ali Sameh Saad
see Yamakage Yuzuru 629
- Almgren Mats
see Hammarstrom Leif 539
- Aloisi G G
see Mazzucato U 475
- Andre J C
What is new in stereolithography? 359
- Avasthi B N
see Srivastava P K 125
- Azumi T
see Meng Q 619
- see* Yamakage Yuzuru 629
- see* Yamamoto S 611
- Babaqui Abdallah S
see El-Daly Samy A 651
- Babar S M
see Balasubramaniyan V 265
- Babu C Sathesan
see Madhusoodanan M 31
- Bagchi Biman
see Roy Srabani 79, 295
- Balan T P
see Priyadarshini K I 47
- Balasubramaniyan V
Formation of phosphoranes from methylmaleanilates and related substrates with triphenylphosphine and their Wittig olefinations with aromatic aldehydes 265
- Balzani Vincenzo
Supramolecular photochemistry. Luminescent and redox active dendritic polynuclear metal complexes 421
- Banerjee Asok
see Maji B B 183
- Bauer R
see Ruppert G 393
see Königstein Christian 353
- Behere D V
see Modi S 167
- Bharadwaj Parimal K
see Raghunathan Kaliappa G 215
- Bhattacharyya S P
see Medhi Chitrani 195
- Biswas G
see Maji B B 183
- Blakemore D C
see Al-Qaradawi S Y 555
- Borsman Stefan
see Dürr Heinz 435
- Botina Jair
Intramolecular and dissociation dynamics of triatomic molecules: Some results for HCN and CO₂ 677
- Bredehorn J
see Döpp D 583
- Campagna Sebastiano
see Balzani Vincenzo 421
- Cazeau Ph
see Cazeau-Dubroca C 659
- Cazeau-Dubroca C
Room temperature phosphorescence of 2,2'-biquinoline in polymeric matrices 659
- Chakrabarti Aparna
Is tetramethyleneethane a ground state triplet? 53
- Chandrasekhar J
see Chakrabarti Aparna 53
- see* Govindaraj A 303
- Chourasia P
Synthesis and structural investigation of some mixed-ligand selenito complexes of cobalt(II) 173

- Corbel S
see Andre J C 359
- Coren M
see Giardini Guidoni A 773
- Crosby G A
see Yamamoto S 611
- Daehne S
see Kemnitz K 783
- Das Debes K
see Mukherjee Asok K 111
- Das Nigamananda
 Kinetics and mechanism of the reversible formation of the binuclear species between pyridine-2-carboxylato(pentaammine)cobalt(III) and cobalt(II) in aqueous solution 245
- Das Ranjan
 Time-domain electron-spin-resonance studies on hydrogen atom transfer to photoexcited quinones 273
- Das Suresh
 Photosensitizing properties of squaraine dyes 513
- Dash A C
see Acharya A N 225
- Dayalan A
 Iron(II) reduction of halogenopyridinecarboxylatocobalt(III)-dioxime complexes: Kinetics and mechanism 95
- De Denus Christine R
see Abd-El-Aziz Alaa S 575
- De Schryver F C
see Declercq D 451
- Declercq D
 Photophysics of pyrene substituted oligosilanes 451
- Degen J
see Diehl M 667
- Denti Gianfranco
see Balzani Vincenzo 421
- Dey G R
see Kishore K 141
- Dey K
see Mukherjee G 1
- Di Palma T M
see Giardini-Guidoni A 709
- Diehl M
 Application of the three-level model: Rise and decay kinetics of the temperature-dependent emission of metal ions with s^2 -valence electron configuration 667
- Döpp D
 Light-induced cycloadditions of captodative alkenes 583
- Doshi A V
see Lohar J M 209
- Duncan Lyngdoh R H
 Comparison of alkyl group labilities of O- and N-alkylated DNA bases: A semiempirical molecular orbital study 253
- Dupontail Guy
see El-Daly Samy A 651
- Dürr Heinz
 Light-induced electron transfer in simple and supramolecular Ru-polypyridine complexes 435
- Ebeid El-Zeiny M
see El-Daly Samy A 651
- El-Daly Samy A
 The spectral, lifetime and laser activity of 2,5-bis-2(1-naphthyl)vinylpyrazine and 2,5-bis-2(2-naphthyl)vinylpyrazine 651
- El-Gohary Zenat
see El-Daly Samy A 651
- El-Hazmy Sadiq M
see El-Daly Samy A 651
- El-Sayed Mostafa
 Foreword 311
- Elisei F
see Mazzucato U 475
- Eriant A W
see Döpp D 583
- Fadouach M
see Cazeau-Dubroca C 659
- Fantoni R
 Laser degradation of pollutants: Polychlorobiphenyls, triazines and polycyclic aromatic hydrocarbons 735
- Fasani E
see Albini A 563
- Foga Myrosia M
see Friesen Ken J 399
- Freccero M
see Albini A 563
- Friesen Ken J
 Kinetics of sunlight photogradation of 2,3,4,7,8-pentachlorodibenzofuran in natural water 399
- Furman Inna
see Whitten David G 527
- Gadaginamat G S
see Kamat A G 189
- Gadre Shridhar R
 Momentum space investigation of C_{2v} dissociation of water 149
- Ganguly S N
see Maji B B 183
- Garg B S
 Investigation of the adsorption of paraquat radical cations on gold electrodes by voltammetry coupled with laser Raman spectroscopy 287

Geiger Cristina <i>see</i> Whitten David G	527	Hussain Reddy K Spectral and thermal studies on mixed ligand complexes of zinc(II) and cadmium(II) with diethyldithiocarbamate and 2,2'-bipyridyl/1,10-phenanthroline	87
George K C <i>see</i> Abdulkhadar M	25		
George M V <i>see</i> Das Suresh	513		
Getoff Nikolai Purification of drinking water by irradiation. A review	373	Ibuki Kazuyasu <i>see</i> Nakayama Toshihiro	567
Ghatak K L <i>see</i> Maji B B	183	Ikeda S <i>see</i> Yamamoto S	611
Giardini-Guidoni A <i>see</i> Fantoni R	735	Iyengar T Asha Kinetics of oxidation of glycylglycine by bromamine-T in acid medium	63
<i>see</i> Male A	715		
Pulsed-laser ablation and deposition of superconducting BiSrCaCuO thin films	709	Jayaraj A F Near infrared spectral studies on interactions of CH ₃ groups with halide ions	71
Resonant two-photon ionization process of van der Waals adducts: Spectroscopy and reactivity of styrenes clustered with various molecules	773	Jezequel J Y <i>see</i> Andre J C	359
Gilbert A <i>see</i> Al-Qaradawi S Y	555	Joshi R G <i>see</i> Kamat A G	189
Gopidas K R Photoinduced charge transfer processes in ultrasmall semiconductor clusters. Photophysical properties of CdS clusters in nafion membranes	505	Junggebauer J <i>see</i> Neumann W P	591
Gopinathan C <i>see</i> Priyadarshini K I	47	Juris Alberto <i>see</i> Balzani Vincenzo	421
Gosavi S S <i>see</i> Balasubramanyan V	265	Kamat A G Synthesis and antimicrobial activity of 1-benzamido-5-hydroxyindole derivatives	189
Govindaraj A Investigations on C ₇₀ H ₃₀ obtained by the Birch reduction of C ₇₀	303	Kamat P V <i>see</i> Gopidas K R	505
Greenbaum E Photobiotechnology: Application of photosynthesis to the production of renewable fuels and chemicals	333	<i>see</i> Das Suresh	513
Hamanoue Kumao <i>see</i> Miki Sadao	797	Kemnitz K Primary photophysical processes in J-aggregates of spectral sensitizers	783
<i>see</i> Nakayama Toshihiro	567	Kishore K Pulse radiolysis of some aromatic sulphoxides in aqueous solutions	141
Hammarström Leif Electron transfer through vesicle membranes: Mechanistic ambiguities	539	Kishore S Binding of rose bengal onto bovine serum albumin	279
Harendza M <i>see</i> Neumann W P	591	Komath Snehasudha <i>see</i> Roy Srabani	79
Heppe Giseler <i>see</i> Dürr Heinz	435	Königstein Christian Light-induced hydrogen production using waste compounds as sacrificial electron donors	353
Heisler G <i>see</i> Ruppert G	393	Krishnan V <i>see</i> Padmanabhan M	161
Hermans E <i>see</i> Declercq D	451	Kuhn P <i>see</i> Schubnell M	671
Hoffman Morton Z <i>see</i> Sun Hai	487	Kulkarni S A <i>see</i> Gadre Shridhar R	149
Hofstädler K <i>see</i> Ruppert G	393	Kutsenok Oleg <i>see</i> Kuzmin Michael G	637
		Kuzmin Michael G Exciplex mechanism of fluorescence quenching in polar media	637

- Lakhan Ram
*A convenient preparation of 2-thioxo-4(3*H*)-quiazolinones* 11
- Lal Bahadur
Photoelectrochemistry of ZnO thin film electrode sensitized by an oxouranium (VI) complex in an acetonitrile photocell 235
- Lalitha S
see Chakrabarti Aparna 53
- Lanfermann Ajung H
see Döpp D 583
- Lapouyade R
Photocyclization of arylethylenes: Mechanism and scope of the reactions 603
- Lessmann K
see Neumann W P 591
- Lezynska Krystyna
see Abd-El-Aziz Alaa S 575
- Limaye S N
see Verma Sangeeta 155
- Linden Lars-Åke
Applied photochemistry in dental science 405
- Lindrum M
see Kemnitz K 783
- Lingappa Y
see Hussain Reddy K 87
- Lohar J M
Studies on mixed mesomorphism: Determination of latent transition temperature (LTT) by extrapolation 209
- Madan A
see Modi S 167
- Madhusoodanan M
SSOZ-HNC and SSOZ-PY integral equation studies of the structure of three-site polar fluids 31
- Maeda K
see Meng Q 619
see Yamakage Yuzuru 629
- Mahadevappa D S
see Iyengar T Asha 63
- Maji B B
Studies on organometallic compounds: An approach towards characterization of structure and activity of triorganotannyl 2-(arylazo)benzenecarboxylates in relation to the bacterial cell wall 183
- Marotta V
see Giardini-Guidoni A 709
- Martino R
see Giardini-Guidoni A 709
- Maruthamuthu Meenakshi
see Kishore S 279
- Mazzucato U
Cis-trans photoisomerization of 1,2-diarylethylenes: Effect of charge transfer interactions 475
- McGarvey D J
see Wilkinson F 685
- Medhi Chitrani
Basicity of some proto-typical carbonyls in the ground and some low-lying excited states: Application of the orthogonal gradient method of orbital optimization in an INDO-MC-SCF framework - I 195
- Mele A
see Fantoni R 735
see Giardini-Guidoni A 773
Laser ablation of inorganic and organic material 715
- Mella M
see Albini A 563
- Memarian H R
see Döpp D 583
- Memming R
Kinetics of charge transfer reactions in photo-electrochemical cells 463
- Meng Q
Studies of photochemical reaction by CIDNP-detected ESR spectrum 619
see Yamakage Yuzuru 629
- Miki Sadao
Photochemical reaction of [6]-1,4-cyclophenanthraquinone 797
- Miller R D
see Declercq D 451
- Mishra A P
see Chourasia P 173
- Mitra S
see Modi S 167
- Modi S
Circular dichroism studies of acid=alkaline transition in heme proteins 167
- Moll J
see Kemnitz K 783
- Moorthy P N
see Kishore K 141
- Morone A
see Giardini-Guidoni A 704
- Mukherjee Asok K
Graph-theoretical calculation of products of eigen coefficients: Some application to charge-transfer complexes 111
- Mukherjee G
*Complexes of N,S donor ligands, Co^{II}, Co^{III}, Mn^{III}, Fe^{III} and Pd^{II} complexes of 1,2-di-(*o*-aminophenylthio)ethane: Synthesis, characterization and reactions* 1
- Naidu Raghava
see Rao E Nagewara 219
- Nakayama Toshihiro
Amine-assisted photochemical dehalogenation of halonanthracenes (9-halo and 9,10-dihalo com-

- pounds) and their triplet formation 567
see Miki Sadao 757
- Nangia A
AM1 heats of formation for the reaction of alcohols with a series of β -lactams and aza- β -lactams: Design of novel β -lactamase inactivators 131
- Negm Sohair
First photothermal deflection spectroscopy set-up in Egypt 695
- Neumann W P
Applied photochemistry for free radical organic synthesis by means of distannane reagents 591
- Nouchi G
see Cazeau-Dubroca C 659
- Nozaki K
Photoinduced ET and back-ET in bimetalated compounds of Ru(II)-Rh(III) and Ru(II)-Co(III) 495
- Ohno T
see Nozaki K 495
- Olea A
see Wilkinson F 685
- Orlando S
see Giardini-Guidoni A 709
- Padmanabhan M
Molecular structure of electron donor-acceptor complexes of metallocryptophenylporphyrins with trinitrobenzene 161
- Pain S
see Maji B B 183
- Pal S
see Mukherjee G 1
- Pandey J P
see Lal Bahadur 235
- Parddeep N
see Garg B S 287
- Parisi G P
see Giardini-Guidoni A 709
- Peirigua A
see Cazeau-Dubroca C 659
- Perumal Paramasivam T
see Venugopal Murugapillai 19
- Piccirillo S
see Giardini-Guidoni A 773
- Pics M
see Döpp D 583
- Pizzella G
see Fantoni R 735
- Poddar S N
see Mukherjee G 1
- Poojari M Damodara
see Padmanabhan M 161
- Priyadarshini K I
Emission characteristics of laser dyes Cl and Rh6G in cross-linked polyvinyl alcohol solutions 47
- Radha P K
see Das Ranjan 273
- Raghunathan Kaliappa G
Template synthesis of a macrobicyclic cryptand having mixed donors via [2+3] Schiff base condensation 215
- Rahman Nasreen
see Botina Jair 677
- Ramasetha S
see Chakrabarti Aparna 53
- Rao C N R
see Govindaraj A 303
- Rao E Nageswara
Formation constants of ternary complexes of Cu(II), Ni(II), Co(II), Mn(II) and Zn(II) with phenylhydrazones and amino acids 219
- Rao Tata N
see Lal Bahadur 235
- Rathna A
see Govindaraj A 303
- Ricevuto Vittorio
see Balzani Vincenzo 421
- Richard Wanda
see Whitten David G 527
- Ries H
see Schubnell M 671
- Roy Srabani
Dielectric friction and solvation dynamics: Novel results on relaxation in dipolar liquids 79
Molecular theory of ion solvation dynamics in water, acetonitrile and methanol: A unified microscopic description of collective dynamics in dipolar liquids 295
- Ruppert G
Heterogeneous and homogeneous photoassisted wastewater treatment 393
- Sadovskii Nikita A
see Kuzmin Michael G 637
- Sahadev
Chelation behaviour of biologically active α -hydroxy naphthaldehyde derivatives with bivalent metal ions in different solvents: A potentiometric study 103
- Saxena M C
see Verma Sangeeta 155
- Schmidtko H H
see Diehl M 667
- Schubnell M
Reflectivity as a probe for chemical reactions 671

Schwarz Ralph <i>see</i> Dürr Heinz	435	visible light-induced hydrogen production from water	343
Serroni Scolastica <i>see</i> Balzani Vincenzo	421	Tributsch Helmut Strategies for solar fuel generation	315
Sharma R K <i>see</i> Sahadev	103	Trierweiler Hans-Peter <i>see</i> Dürr Heinz	435
Shizuka Haruo Hydrogen atom and proton-induced electron transfer reactions via triplet exciplexes	747	Tschudi H R <i>see</i> Schubnell M	671
Sindhwan S K <i>see</i> Sahadev	103	Venkataraman Balu <i>see</i> Das Ranjan	273
Singh Surjit <i>see</i> Jayaraj A F	71	Venugopal Murugapillai Syntheses of substituted isoxazolines using Vilsmeier-Haack reagent	19
Snels M <i>see</i> Giardini Guidoni A	773	Verma Sangeeta Periodicity in the formation constant values of lanthanide(III)aminopoly-carboxylateresorcinol/orcinol/phloroglucinol mixed ligand complexes	155
Spooner Susan P <i>see</i> Whitten David G	527	Vijayaraghavan V R <i>see</i> Dayalan A	95
Srivastava Madhu <i>see</i> Lakhani Ram	11	Weinstein Julia <i>see</i> Kuzmin Michael G	637
Srivastava P K New uncatalysed bromate-driven oscillators: The Rhodamine B base/Rhodamine B-BrO ₃ ⁻ H ₂ SO ₄ systems	125	Whitten David G Photoinduced electron transfer reactions of <i>trans</i> -stilbene surfactants in Langmuir-Blodgett assemblies and phospholipid bilayers	513
Sun Hai Photoinduced charge separation by ruthenium(II) photosensitizers	487	Wilkinson F Factors which determine the efficiency of sensitized singlet oxygen production	685
Suryesh K K <i>see</i> Chourasia P	173	Yamaji Minoru <i>see</i> Shizuka Haruo	747
Suzumoto T <i>see</i> Kemnitz K	783	Yamakage Y Electron-nuclear cross-relaxation effect on the photochemical reaction of benzaldehyde as studied by CIDNP and DNP	629
Tini T <i>see</i> Kemnitz K	783	<i>see</i> Meng Q	619
Teghil R <i>see</i> Fantoni R	735	Yamamoto S Spectroscopic and magnetic studies of mixed-ligand complex of zinc(II)	611
<i>see</i> Mele A	715	Yonezawa Tetsu <i>see</i> Toshima Naoki	343
Tembe B L <i>see</i> Madhusoodanan M	31	Yoshihara K <i>see</i> Kemnitz K	783
Tews H <i>see</i> Neumann W P	591	Yoshimura A <i>see</i> Nozaki K	495
Thiery Urs <i>see</i> Dürr Heinz	435		
Thomas K George <i>see</i> Das Suresh	513		
Tongare D B <i>see</i> Balasubramanyan V	265		
Toshima Naoki Gold-platinum bimetallic cluster catalysts for			

**Proceedings of the Indian Academy of Sciences
Chemical Sciences**

**Volume 105
1993**

**Published by the Indian Academy of Sciences
Bangalore 560 080**

Proceedings of the Indian Academy of Sciences

Chemical Sciences

Editor

V Krishnan
Indian Institute of Science, Bangalore

Associate Editor
S Chandrasekaran
Indian Institute of Science, Bangalore

Editorial Board

J Chandrasekhar, Indian Institute of Science, Bangalore
N Chandrakumar, Central Leather Research Institute, Madras
M K Chaudhuri, North-Eastern Hill University, Shillong
M Chowdhury, Indian Association for the Cultivation of Science, Calcutta
B M Deb, Panjab University, Chandigarh
G R Desiraju, University of Hyderabad, Hyderabad
K N Ganesh, National Chemical Laboratory, Pune
A K Lala, Indian Institute of Technology, Bombay
J P Mittal, Bhabha Atomic Research Centre, Bombay
A S N Murthy, Indian Institute of Technology, New Delhi
V N R Pillai, Mahatma Gandhi University, Kottayam
C N R Rao, Indian Institute of Science, Bangalore
S Ramakrishnan, Indian Institute of Science, Bangalore
N Sathyamurthy, Indian Institute of Technology, Kanpur
R P Sharma, Central Institute of Medicinal and Aromatic Plants, Lucknow

Editor of Publications of the Academy
G Srinivasan
Raman Research Institute, Bangalore

Subscription Rates (Effective from 1989)

All countries except India (Price includes AIR MAIL charges)	1 year US\$125	3 years \$340	5 years \$500
India	1 year Rs. 75	10 years Rs. 400	

All correspondence regarding subscription should be addressed to The Circulation Department of the Academy.

Editorial Office:

Indian Academy of Sciences, C V Raman Avenue
Sadarhivinagar, P.B. No. 8005
Bangalore 560080

Telephone: (080) 342546
Telex: 0845-2178 ACAD IN
Telefax: 91-80-346094

© 1993 by the Indian Academy of Sciences. All rights reserved.

"Notes on the preparation of papers" are printed in the last issue of every volume.

Proceedings (Chemical Sciences)

Volume 105, 1993

CONTENTS

Inorganic and Analytical

Complexes of N, S donor ligands. Co ^{II} , Co ^{III} , Mn ^{III} , Fe ^{III} and Pd ^{II} complexes of 1,2-di-(<i>o</i> -aminophenylthio)ethane: Synthesis, characterisation and reactions <i>G Mukherjee, S Pal, S N Poddar and K Dey</i>	1-9
Spectral and thermal studies on mixed ligand complexes of Zinc(II) and cadmium(II) with diethyldithiocarbamate and 2,2'-bipyridyl/1,10-phenanthroline <i>K Hussain Reddy and Y Lingappa</i>	87-94
Iron(II) reduction of halogenopyridinecarboxylatocobalt(III)-dioxime complexes: Kinetics and mechanism <i>A Dayalan and V R Vijayaraghavan</i>	95-101
Chelation behaviour of biologically active <i>o</i> -hydroxy naphthaldehyde derivative with bivalent metal ions in different solvents: A potentiometric study <i>Sahadev, R K Sharma and S K Sindhwani</i>	103-110
Periodicity in the formation constant values of lanthanide(III), aminopolycarboxylate, resorcinol/orcinol/phloroglucinol mixed ligand complexes <i>Sangeeta Verma, S N Limaye and M C Saxena</i>	155-160
Molecular structure of electron donor-acceptor complexes of metallo-tetraphenylporphyrins with trinitrobenzene <i>M Padmanabhan, M Damodara Poojari and V Krishnan</i>	161-165
Circular dichroism study of acid=alkaline transition in hemeproteins <i>S Modi, A Madan, D V Behere and S Mitra</i>	167-172
Synthesis and structural investigation of some mixed-ligand selenito complexes of cobalt(II) <i>P Chourasia, K K Suryesh and A P Mishra</i>	173-181
Studies on organometallic compounds: An approach towards characterisation of structure and activity of triorganostannyl 2-(arylazo)benzene-carboxylates in relation to the bacterial cell wall <i>B B Maji, S Pain, G Biswas, K L Ghatak, S N Ganguly and Asok Banerjee</i>	183-187
Formation constants of ternary complexes of Cu(II), Ni(II), Co(II), Mn(II) and Zn(II) with phenylhydrazones and amino acids <i>E Nageswara Rao and R Raghava Naidu</i>	219-224
Kinetics of the reversible uptake of carbon dioxide and sulphur dioxide by the <i>cis</i> -(hydroxo)(imidazole) bis(ethylenediamine) cobalt(III) ion in	

ii *Volume contents*

aqueous medium. A comparative study	<i>A N Acharya and A C Dash</i>	225-233
Photoelectrochemistry of ZnO thin film electrode sensitized by an oxouranium(VI) complex in an acetonitrile photocell	<i>Lal Bahadur, J P Pandey and Tata N Rao</i>	235-243
Kinetics and mechanism of the reversible formation of the binuclear species between pyridine-2-carboxylato(pentaammine)cobalt(III) and cobalt(II) in aqueous solution	<i>Nigamananda Das</i>	245-252

Organic

A convenient preparation of 2-thioxo-4(3 <i>H</i>)-quinazolinones	<i>Ram Lakan and Madhu Srivastava</i>	11-17
Syntheses of substituted isoxazolines using Vilsmeier-Haack reagent	<i>Murugapillai Venugopal and Paramasivam T Perumal</i>	19-23
Synthesis and antimicrobial activity of 1-benzamido-5-hydroxyindole derivatives	<i>A G Kamat, R G Joshi and G S Gadaginamath</i>	189-193
Comparison of alkyl group labilities of O- and N-alkylated DNA bases: A semiempirical molecular orbital study	<i>R H Duncan Lyngdoh</i>	253-263
Formation of phosphoranes from methyl malcanilates and related substrates with triphenylphosphine and their Wittig olefinations with aromatic aldehydes	<i>V Balasubramaniyan, D B Tongare, S S Gosavi and S M Babar</i>	265-271

Physical and Theoretical

Study of interaction between microclusters of silver and arsenious trisulphide	<i>M Abdulkhadar and K C George</i>	25-29
SSOZ-HNC and SSOZ-PY integral equation studies of the structure of three-site polar fluids	<i>M Madhusoodanan, C Satheesan Babu and B L Tembe</i>	31-45
Emission characteristics of laser dyes C1 and Rh6G in cross-linked polyvinyl alcohol solutions	<i>K I Priyadarshini, T P Balan and C Gopinathan</i>	47-52
Is tetramethyleneethane a ground state triplet?	<i>Aparna Chakrabarti, I D L Albert, S Ramasesha, S Lalitha and Jayaraman Chandrasekhar</i>	53-62
Kinetics of oxidation of glycylglycine by bromamine-T in acid medium	<i>T Asha Iyengar and D S Mahadevappa</i>	63-70
Near infrared spectral studies on interactions of CH ₃ groups with halide ions	<i>A F Jayaraj and Surjit Singh</i>	71-78

Graph-theoretical calculation of products of eigen coefficients: Some application to charge-transfer complexes	Asok K Mukherjee and Debes K Das	111-123
New uncatalysed bromate-driven oscillators: The Rhodamine B base/Rhodamine B-BrO ₃ ⁻ -H ₂ SO ₄ systems	P K Srivastava and B N Avasthi	125-130
AM1 heats of formation for the reaction of alcohols with a series of β -lactams and aza- β -lactams: Design of novel β -lactamase inactivators	A Nangia	131-139
Pulse radiolysis of some aromatic sulphoxides in aqueous solutions	K Kishore, G R Dey and P N Moorthy	141-147
Basicity of some proto-typical carbonyls in the ground and some low-lying excited states: Application of the orthogonal gradient method of orbital optimization in an INDO-MC SCF framework - I	Chitrani Medhi and S P Bhattacharyya	195-208
Studies on mixed mesomorphism: Determination of latent transition temperature (LTT) by extrapolation	J M Lohar and A V Doshi	209-214
Time-domain electron-spin-resonance studies on hydrogen atom transfer to photoexcited quinones	Ranjan Das, P K Radha and Balu Venkataraman	273-277
Binding of rose bengal onto bovine serum albumin	S Kishore and Meenakshi Maruthamuthu	279-285
Investigations on adsorption of paraquat radical cations on gold electrodes by voltammetry coupled with laser Raman spectroscopy	B S Gary and N Pardeep	287-294

Rapid Communication

Dielectric friction and solvation dynamics: Novel results on relaxation in dipolar liquids	Srabani Roy, Snehasudha Komath and Biman Bagchi	79-85
Momentum space investigation of C _{2v} dissociation of water	Shridhar R Gadre and Sudhir A Kulkarni	149-153
Template synthesis of a macrobicyclic cryptand having mixed donors via [2 + 3] Schiff base condensation	Kallappa G Ragunathan and Parimal K Bharadwaj	215-217
Molecular theory of ion solvation dynamics in water, acetonitrile and methanol: A unified microscopic description of collective dynamics in dipolar liquids	Srabani Roy and Biman Bagchi	295-301
Investigations on C ₇₀ H ₃₀ obtained by the Birch reduction of C ₇₀	A Govindaraj, A Rathna, J Chandrasekhar and C N R Rao	303-309

Special Issue on Solar Energy Storage and Applied Photochemistry

Editor's note	311
Foreword	<i>M S A Abdel-Mottaleb and M A El-Sayed</i> 313
Strategies for solar fuel generation	<i>H Tributsch</i> 315–331
Photobiotechnology: Application of photosynthesis to the production of renewable fuels and chemicals	<i>E Greenbaum</i> 333–342
Gold-platinum bimetallic cluster catalysts for visible light-induced hydrogen production from water	<i>N Toshima and T Yonezawa</i> 343–352
Light-induced hydrogen production using waste compounds as sacrificial electron donors	<i>C Königstein and R Bauer</i> 353–358
What new in stereolithography?	<i>J C Andre, S Corbel, and J Y Jezequel</i> 359–371
Purification of drinking water by irradiation. A review	<i>N Getoff</i> 373–391
Heterogeneous and homogeneous photoassisted wastewater treatment	<i>G Ruppert, K Hofstädler, R Bauer and G Heisler</i> 393–397
Kinetics of sunlight photodegradation of 2, 3, 4, 7, 8-pentachlorodibenzofuran in natural water	<i>Ken J Friesen and M M Fogal</i> 399–403
Applied photochemistry in dental science	<i>L-Å Lindén</i> 405–419
Supramolecular photochemistry. Luminescent and redox active dendritic polynuclear metal complexes	<i>V Balzani, G Denti, S Serroni, S Campagna, V Ricevuto and A Juris</i> 421–434
Light-induced electron transfer in simple and supramolecular Ru-poly-pyridine-complexes	<i>H Dürr, S Boßmann, G Heppe, R Schwarz, U Thiery and H-P Trierweiler</i> 435–450
Photophysics of pyrene substituted oligosilanes	<i>D Declercq, Hermans, F C De Schryver and R D Miller</i> 451–461
Kinetics of charge trans-	tions in photoelectrochemical cells
	<i>R Memming</i> 463–474
Cis-trans photoisomerization of 1,2-diarylethylenes: Effect of charge transfer interactions	<i>U Mazzucato, G G Aloisi and F Elisei</i> 475–486
Photoinduced charge separation by ruthenium(II) photosensitizers	<i>Hai Sun and M Z Hoffman</i> 487–494
Photoinduced ET and back-ET in bimetalated compounds of Ru(II)-Rh(III) and Ru(II)-Co(III)	<i>K Nozaki, A Yoshimura and T Ohno</i> 495–503

Photoinduced charge transfer processes in ultrasmall semiconductor clusters. Photophysical properties of CdS clusters in nafion membrane K R Gopidas and P V Kamat	505-512
Photosensitizing properties of squaraine dyes S Das, K G Thomas, P V Kamat and M V George	513-525
Photoinduced electron transfer reactions of <i>trans</i> -stilbene surfactants in Langmuir-Blodgett assemblies and phospholipid bilayers D G Whitten, I Furman, C Geiger, W Richard and S P Spooner	527-538
Electron transfer through vesicle membranes: Mechanistic ambiguities L Hammarström and M Almgren	539-554
Sunlight-initiated cycloaddition reactions of the benzene ring S Y Al-Qaradawi, D C Blakemore and A Gilbert	555-562
Synthetic chemistry via radicals generated by photoinduced electron transfer A Albini, E Fasani, M Mella and M Freccero	563-566
Amine-assisted photochemical dehalogenation of haloanthracenes (9-halo and 9,10-dihalo compounds) and their triplet formation T Nakayama, K Ibuki and K Hamanoue	567-574
Preparation of some organic precursors via photolytic demetallation of their iron complexes A S Abd-El-Aziz, C R De Denus and K Lezynska	575-581
Lightinduced cycloadditions of captodative alkenes D Döpp, J Bredehorn, A W Erian, A Jung, H Lanfermann, H-R Memarian, B Mühlbacher and M Pies	583-589
Applied photochemistry for free radical organic synthesis by means of distannane reagents W P Neumann, M Harendza, J Junggebauer, K Lessmann and H Tews	591-601
Photocyclization of arylethylenes. Mechanism and scope of the reactions R Lapouyade	603-610
Spectroscopic and magnetic studies of mixed-ligand complexes of Zn(II) S Yamamoto, S Ikeda, T Azumi and G A Crosby	611-617
Studies of photochemical reaction by CIDNP-detected ESR spectrum Q Meng, Y Yamakage, T Aizawa, K Maeda and T Azumi	619-628
Electron-nuclear cross-relaxation effect on the photochemical reaction of benzaldehyde as studied by CIDNP and DNP Y Yamakage, Q Meng, S S Ali, K Maeda and T Azumi	629-636
Exciplex mechanism of fluorescence quenching in polar media M G Kuzmin, N A Sadovskii, J Weinstein and O Kutsenok	637-649
The spectra, lifetime and laser activity of 2,5-bis-2(1-naphthyl) vinylpyrazine and 2,5-bis-2(2-naphthyl) vinylpyrazine S A El-Daly, E M Ebeld, S M El-Hazmy, A S Babaqi, Z El-Gohary and G Duportail	651-658

Room-temperature phosphorescence of 2,2'-biquinoline in polymeric matrices C Cazeau-Dubroca, A Peirigua, G Nouchi, M Fadouach and Ph Cazeau	659-666
Application of the three-level model: Rise and decay kinetics of the temperature-dependent emission of metal ions with s^2 -valence electron configuration M Diehl, J Degen and H-H Schmidtke	667-670
Reflectivity as a probe for chemical reactions H R Tschudi, P Kuhn and H Ries	671-675
Intramolecular and dissociation dynamics of triatomic molecules: Some results for HCN and CO ₂ J Botina and N Rahman	677-684
Factors which determine the efficiency of sensitized singlet oxygen production F Wilkinson, D J McGarvey and A Olea	685-694
First photothermal deflection spectroscopy set-up in Egypt S Negm	695-708
Pulsed laser ablation and deposition of superconducting BiSrCaCuO thin films A Giardini-Guidoni, T M Di Palma, V Marotta, R Martino, A Morone, G P Parisi and S Orlando	709-714
Laser ablation of inorganic and organic materials A Mele, A Giardini-Guidoni and R Teghil	715-733
Laser degradation of pollutants: Polychlorobiphenyls, triazines and polycyclic aromatic hydrocarbons R Fantoni, A Giardini-Guidoni, A Mele, G Pizzella and R Teghil	735-746
Hydrogen-atom and proton-induced electron transfer reactions via triplet exciplexes H Shizuka and M Yamaji	747-772
Resonant two-photon ionization processes of van der Waals adducts: Spectroscopy and reactivity of styrenes clustered with various molecules A Giardini-Guidoni, A Mele, S Piccirillo, M Coreno and M Snels	773-782
Primary photophysical processes in J-aggregates of spectral sensitizers K Kemnitz, K Yoshihara, T Suzumoto, T Tani, M Lindrum, J Moll and S Daehne	783-795
Photochemical reactions of [6]-1,4-cyclophaneanthraquinone S Miki, F M Abdel-Latif, T Nakayama and K Hamanoue	797-802
Subject Index	803-814
Author Index	815-820

Proceedings (Chemical Sciences)

Notes on the preparation of papers

Authors wishing to have papers published in the *Proceedings* should send them to the Editorial Office.

Four sets (one original and 3 copies) of the paper must be submitted.

The papers must normally present results of original work. Critical reviews of important fields will also be considered for publication. Submission of the script will be held to imply that it has not been previously published and is not under consideration for publication elsewhere; and further that, if accepted, it will not be published elsewhere.

Typecript

Papers should be typed double spaced with ample margin on all sides on white bond paper 280 x 215 mm. This also applies to the abstract, tables, figure captions and the list of references which are to be typed on separate sheets.

Title page

- (1) The title of the paper must be short and contain words useful for indexing.
- (2) The names with initials of authors and the name and address of the institution where the work was done must be given.
- (3) An *abbreviated running title* of not more than 50 letters and spaces must also be given.

Abstract

All papers must have an abstract of not more than 200 words of the significant results reported in the paper. Presentation of numerical results should be avoided as far as possible in the abstract.

Keywords

Between 3 and 6 keywords must be provided for indexing and information retrieval.

The Text

The paper must be divided into sections starting preferably with 'Introduction' and ending with

'Conclusions'. The main sections should be numbered 1, 2, etc., sub-sections 1.1, 1.2, etc. and further sub-sections (if necessary) 1.1a, 1.1b, etc.

Tables

All tables must be numbered consecutively in arabic numerals in the order of appearance in the text. The tables should be self-contained and have a descriptive title.

Figures

All figures including photographs should be numbered consecutively in arabic numerals in the order of appearance in the text. Figure captions must be typed on a separate sheet.

Line drawings must be in India ink on good quality tracing paper or on white card of a size smaller than that of text paper. Structural formulae of compounds must be drawn in India ink on tracing paper. Lines must be drawn sufficiently thick for reduction to a half or third of the original size (0.3 mm for axes and 0.6 mm for curves are suggested).

Symbols and Mathematical Material

Handwritten symbols and equations should be avoided as far as possible. Where unavoidable, identify each symbol by spelling it out in the margin in pencil or on a separate sheet of paper. Distinguish between typewritten symbols likely to cause confusion e.g. 'one' and lowercase 'ell'; Caps or lower case 'Oh' and 'Zero'; 'Kappa', caps and i.e. 'kay' etc.

Equations must be clearly written, each on its own line, well away from the text. All equations must be numbered consecutively in arabic numerals with the number in parentheses near the right hand margin. Indices or superscripts must be indicated in pencil with a V sign and subscripts with a ^ sign. Single or double underlining in colour should be used to denote lower case and capital letters respectively. The following colour scheme should be used to denote different characters—blue for Greek, red for German (gothic), green for script and brown for bold face types. Authors must indicate wherever special characters (Greek, German, script, scalar, vector, tensor, matrix, etc.) are required. All other letters will be set in italic types. Vectors must be underlined by a wavy line and tensors by two wavy lines. The SI system of units and symbols is recommended.

References

References should be cited in the text by author and year. If there are more than two authors, reference should be to the first author followed by *et al* in the text. References at the end of the paper should be listed alphabetically by authors names, followed by initials, year of publication, name of the journal (abbreviated according to the World List of Scientific Periodicals, Butterworths, London), volume number, and number of the first page. References to books should include: name(s) of author(s), initials, year of publication, title of the book, edition if not the first, initials and name(s) of editor(s), if any, preceded by ed(s), place of publication, publisher and chapter or pages referred to. References to theses must include the year, the title of the thesis, the degree for which submitted and the University. References to reports and unpublished conference proceedings should include the title of the report/paper.

but when necessary should be numbered consecutively, and typed on a separate sheet.

Appendices

All appendices should be numbered consecutively in arabic numerals.

Proofs

Authors are requested to prepare the manuscript carefully before submitting it for publication to minimise corrections and alterations in the proof stage which increase publication costs. The proofs sent to the authors together with the reprint order form must be returned to the editorial office *within two days of their receipt*.

Reprints

50 reprints of each article will be supplied free of charge.

Footnotes

Footnotes to the text should be avoided if possible

(Continued from back page)

Resonant two-photon ionization processes of van der Waals adducts: Spectroscopy and reactivity of styrenes clustered with various molecules A Giardini-Guidoni, A Mele, S Piccirillo, M Coreno and M Snel	773
Primary photophysical processes in J-aggregates of spectral sensitizers K Kemnitz, K Yoshihara, T Suzumoto, T Tani, M Lindrum, J Moll and S Daehne	783
Photochemical reactions of [6]-1,4-cyclophaneanthraquinone S Miki, F M Abdel-Latif, T Nakayama and K Hamanoue	797
Subject Index	803
Author Index	815
Volume Contents	i

(Continued from inside back cover)

Photocyclization of arylethylenes. Mechanism and scope of the reactions	R Lapouyade	603
Spectroscopic and magnetic studies of mixed-ligand complexes of Zn(II)	S Yamamoto, S Ikeda, T Azumi and G A Crosby	611
Studies of photochemical reaction by CIDNP-detected ESR spectrum	Q Meng, Y Yamakage, T Aizawa, K Maeda and T Azumi	619
Electron-nuclear cross-relaxation effect on the photochemical reaction of benzaldehyde as studied by CIDNP and DNP	Y Yamakage, Q Meng, S S Ali, K Maeda and T Azumi	629
Exciplex mechanism of fluorescence quenching in polar media	M G Kuzmin, N A Sadovskii, J Weinstein and O Kutsenok	637
The spectra, lifetime and laser activity of 2,5-bis-2(1-naphthyl) vinylpyrazine and 2,5-bis-2(2-naphthyl) vinylpyrazine	S A El-Daly, E M Ebeid, S M El-Hazmy, A S Babaqi, Z El-Gohary and G Duportail	651
Room-temperature phosphorescence of 2,2'-biquinoline in polymeric matrices	C Cazeau-Dubroca, A Peirlgua, G Nouchi, M Fadouach and Ph Cazeau	659
Application of the three-level model: Rise and decay kinetics of the temperature-dependent emission of metal ions with s^2 -valence electron configuration....	M Diehl, J Degen and H-H Schmidtke	667
Reflectivity as a probe for chemical reactions	M Schubnell, H R Tschudi, P Kuhn and H Ries	671
Intramolecular and dissociation dynamics of triatomic molecules: Some results for HCN and CO ₂	J Botina and N Rahman	677
Factors which determine the efficiency of sensitized singlet oxygen production	F Wilkinson, D J McGarvey and A Olea	685
First photothermal deflection spectroscopy set-up in Egypt	S Negm	695
Pulsed laser ablation and deposition of superconducting BiSrCaCuO thin films	A Giardini-Guidoni, T M Di Polma, V Marotta, R Martino, A Morone, G P Parisi and S Orlando	709
Laser ablation of inorganic and organic materials	A Mele, A Giardini-Guidoni and R Teghil	715
Laser degradation of pollutants: Polychlorobiphenyls, triazines and polycyclic aromatic hydrocarbons	R Fantoni, A Giardini-Guidoni, A Mele, G Pizzella and R Teghil	735
Hydrogen-atom and proton-induced electron transfer reactions via triplet exciplexes	H Shizuka and M Yamaji	747

(Continued on previous page)

(Continued from back cover)

Light-induced electron transfer in simple and supramolecular Ru-polyppyridine-complexes	H Dürr, S Boßmann, G Heppe, R Schwarz, U Thiery and H-P Trierweiler	435
Photophysics of pyrene substituted oligosilanes	D Declercq, E Hermans, F C De Schryver and R D Miller	451
Kinetics of charge transfer reactions in photoelectrochemical cells	R Memming	463
Cis-trans photoisomerization of 1,2-diarylethylenes: Effect of charge transfer interactions	U Mazzucato, G G Aloisi and F Elisei	475
Photoinduced charge separation by ruthenium(II) photosensitizers	Hai Sun and M Z Hoffman	487
Photoinduced ET and back-ET in bimetallated compounds of Ru(II)-Rh(III) and Ru(II)-Co(III).....	K Nozaki, A Yoshimura and T Ohno	495
Photoinduced charge transfer processes in ultrasmall semiconductor clusters. Photophysical properties of CdS clusters in nafion membrane	K R Gopidas and P V Kamat	505
Photosensitizing properties of squaraine dyes	S Das, K G Thomas, P V Kamat and M V George	513
Photoinduced electron transfer reactions of trans-stilbene surfactants in Langmuir-Blodgett assemblies and phospholipid bilayers	D G Whitten, I Furman, C Geiger, W Richard and S P Spooner	527
Electron transfer through vesicle membranes: Mechanistic ambiguities	L Hammarström and M Almgren	539
Sunlight-initiated cycloaddition reactions of the benzene ring	S Y Al-Qaradawi, D C Blakemore and A Gilbert	555
Synthetic chemistry via radicals generated by photoinduced electron transfer	A Albini, E Fusani, M Mella and M Freccero	563
Amine-assisted photochemical dehalogenation of haloanthracenes (9-halo and 9,10-dihalo compounds) and their triplet formation	T Nakayama, K Ibuki and K Hamanoue	567
Preparation of some organic precursors via photolytic demetallation of their iron complexes	A S Abd-El-Aziz, C R De Denus and K Lezynska	575
Lightinduced cycloadditions of captodative alkenes	D Döpp, J Bredehorn, A W Erian, A Jung, H Lanfermann, H-R Memarian, B Mühlbacher and M Pies	583
Applied photochemistry for free radical organic synthesis by means of distannane reagents	W P Neumann, M Harendza, J Junggebauer, K Lessmann and H Tews	591

(Continued on last page)

Vol. 105, No. 6, December 1993

Proceedings of the Indian Academy of Sciences — Chemical Sciences

Proceedings of the Second International Conference on Solar Energy Storage and Applied Photochemistry, Cairo, January 1993

CONTENTS

Editor's note.....	311
Foreword <i>M S A Abdel-Mottaleb and M A El-Sayed</i>	313
Strategies for solar fuel generation..... <i>H Tributsch</i>	315
Photobiotechnology: Application of photosynthesis to the production of renewable fuels and chemicals <i>E Greenbaum</i>	333
Gold-platinum bimetallic cluster catalysts for visible light-induced hydrogen production from water <i>N Toshima and T Yonezawa</i>	343
Light-induced hydrogen production using waste compounds as sacrificial electron donors <i>C Königstein and R Bauer</i>	353
What new in stereolithography? <i>J C Andre, S Corbel, and J Y Jezequel</i>	359
Purification of drinking water by irradiation. A review <i>N Getoff</i>	373
Heterogeneous and homogeneous photoassisted wastewater treatment <i>G Ruppert, K Hofstädler, R Bauer and G Heisler</i>	393
Kinetics of sunlight photodegradation of 2, 3, 4, 7, 8-pentachlorodibenzofuran in natural water..... <i>Ken J Friesen and M M Fogar</i>	399
Applied photochemistry in dental science <i>L-Å Lindén</i>	405
Supramolecular photochemistry. Luminescent and redox active dendritic polynuclear metal complexes..... <i>V Balzani, G Denti, S Serroni, S Campagna, V Ricevuto and A Juris</i>	421

(Continued on inside back cover)

Indexed in CURRENT CONTENTS

Edited and published by G Srinivasan for the Indian Academy of Sciences, Bangalore 560 080.
Typeset at Thomson Press (I) Ltd., New Delhi 110001 and printed at Macmillan India Press, Madras 600 041.